Origin and evolution of atmospheric xenon and other noble gases : geodynamical and atmospheric implications

Guillaume Avice




Université de Lorraine

École doctorale R.P.2.E

Centre de Recherches Pétrographiques et Géochimiques

Thèse de doctorat présentée et soutenue publiquement pour l'obtention du titre de
Docteur de l'Université de Lorraine (Spécialité: Géosciences)

par Guillaume Avice

Origin and evolution of atmospheric xenon and other noble gases: geodynamical and atmospheric implications

Origine et évolution du xénon et des autres gaz rares atmosphériques: implications géodynamiques et atmosphériques

---

Soutenance publique le 18 Mars 2016 à 14h dans l'amphithéâtre du CRPG
devant le jury composé de MM.

Directeur de thèse:
Pr. Bernard Marty, Centre de Recherches Pétrographiques et Géochimiques (Nancy, France)

Co-directeur de thèse:
Pr. Ray Burgess, School of Earth, Atmospheric and Environmental Sciences, University of Manchester (UK)

Rapporteurs:
Pr. Nick Arndt, Université Joseph Fourier / Institut des Sciences de la Terre (Grenoble, France)
Pr. Chris Ballentine, Department of Earth Sciences, University of Oxford (UK)

Examinateurs:
Dr. Marc Chaussidon, Institut de Physique du Globe de Paris (France)
Dr. Yves Marrocchi, Centre de Recherches Pétrographiques et Géochimiques (Nancy, France)

Centre de Recherches Pétrographiques et Géochimiques, 15 rue Notre-Dame des Pauvres,
54500 Vandoeuvre-lès-Nancy, France

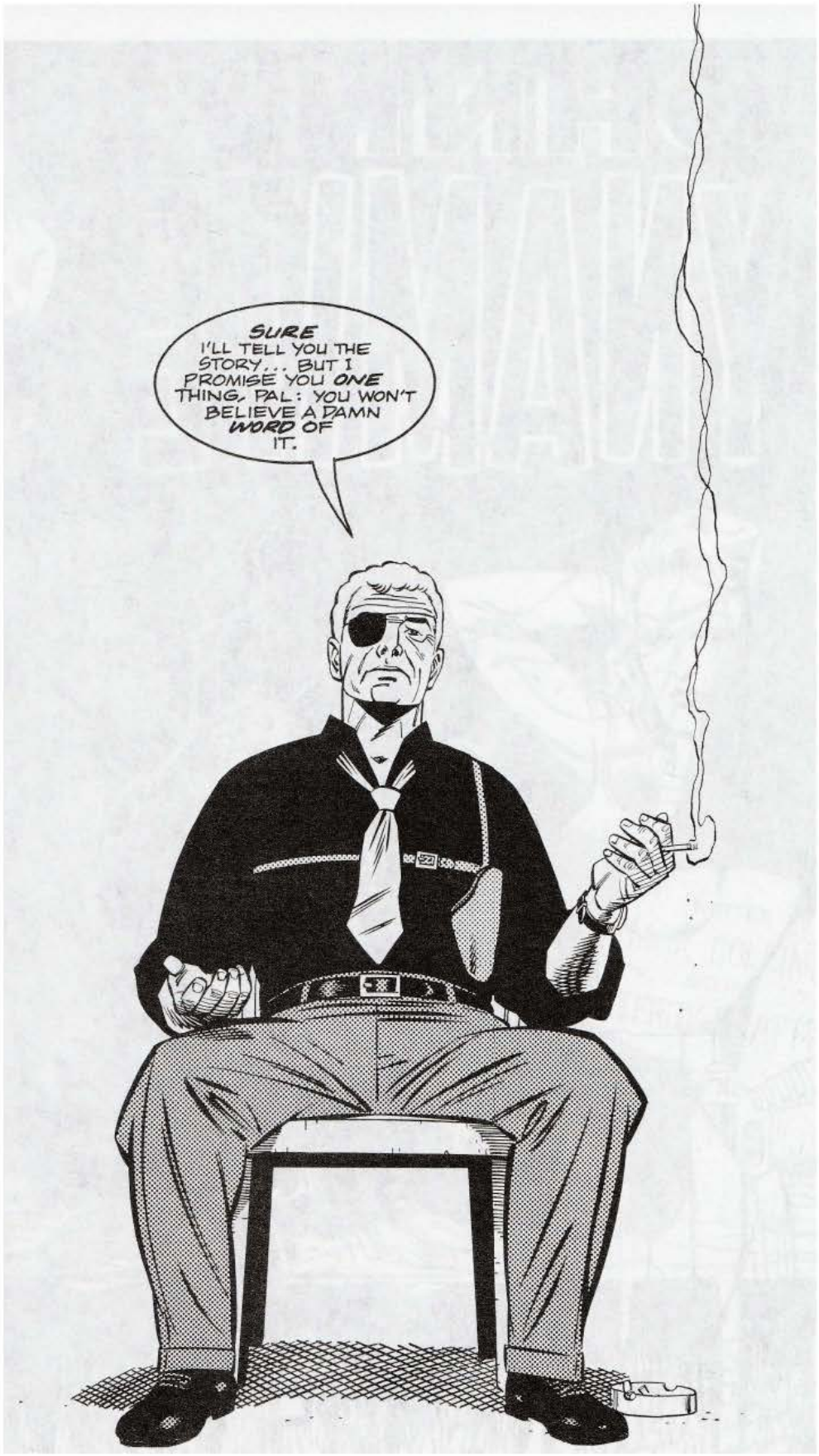

Johnny Dynamite, K. Fitch and P. Morisi

Il n'y a qu'un pas du plus sublime enthousiasme au ridicule, de même que de la plus profonde sagesse à la plus stupide bêtise.

Franz Schubert

Remerciements

C'est le moment de remercier toutes les personnes m'ayant soutenu, supporté dans tous les sens du terme et/ou contribué de près ou de loin à ces travaux de thèse et la tâche est ardue tant elles sont nombreuses.

La première personne que je tiens à remercier chaleureusement est, bien entendu, Bernard Marty mon directeur de thèse. Merci Bernard pour ton encadrement pendant cette thèse. Tu as toujours su être présent aux moments cruciaux tout en me laissant libre de collaborer avec d'autres chercheurs et d'explorer des pistes aux issues parfois plus qu'incertaines. Grâce à cela je sais désormais que le xénon contenu dans les lampes de cinéma n'est pas fractionné... Probablement sans t'en douter, tu formes tes étudiants selon le précepte de Benjamin Franklin (rien que ça !) à savoir: "Dis-moi et je l'oublierai. Enseigne-moi et je me souviendrai. Implique-moi et j'apprendrai". Cette thèse sous ta direction était scientifiquement et humainement très enrichissante. Je n'oublierai jamais nos discussions, plus ou moins sérieuses, et ne portant pas toujours sur le xénon comme on pourrait pourtant le croire.

J'ai passé de très bons moments à l'université de Manchester, sous la co-direction de Ray Burgess pour effectuer les analyses Ar-Ar. Je tiens donc à te remercier Ray pour ton accueil, tes conseils et ton expertise sur le légendaire MS1 ainsi que toute l'équipe de Manchester pour son aide, les (trop ?) nombreuses pintes de bière le vendredi soir et pour avoir moqué mon "so frenchy accent".

Je tiens également à remercier sincèrement les membres du jury, Chris Ballentine, Nick Arndt, Marc Chaussidon et Yves Marrocchi pour avoir accepté d'évaluer ce travail et pour nos échanges scientifiques au cours de cette thèse.

Il faudrait presque faire la liste de tous les membres du CRPG pour se rendre compte à quel point il fait bon faire une thèse dans ce laboratoire. On prend vraiment bien soin de nous. Merci à Raph' d'être un directeur à l'écoute des étudiants et toujours ouvert au dialogue. Je tiens tout particulièrement à remercier l'équipe administrative exceptionnelle (Isabelle, Aurélie, Cati, Martine et cie) qui m'a souvent aiguillé dans les dédales de l'administration et qui fait preuve d'un grand savoir-faire et d'une efficacité redoutable. Bruno et Yannick du service général sont toujours là pour nous épauler et répondre à nos demandes (toujours) urgentes. Pierrot de l'atelier est un véritable magicien du métal et j'ai bien conscience qu'aucun des résultats de cette thèse n'aurait été obtenu sans sa contribution.

Bien entendu, je tiens à remercier tout particulièrement les ermites du laboratoire gaz rares et en tout premier Laurent Zimmermann ("Zim") forcément. Merci Laurent pour tout ce que tu m'as appris, pour ta bonne humeur, tes blagues plus ou moins douteuses et surtout pour ne jamais me prendre au sérieux même le peu de fois où je le suis. Merci également à Bouch pour son aide et ses conseils. De nombreux étudiants s'agitent autour des spectros du deuxième étage pour faire croire qu'ils fonctionnent vraiment, un grand merci à Maïa, Ptit Ju (Amalpartout), Sarah, Christine, Rémi (Alain)Delon, Gaëlle (Maîtresse Gaga), Thomas D. etc... Je n'oublie pas que PH, fin psychologue, a été le premier à m'accueillir en stage au CRPG il y a six ans, merci beaucoup ! Merci à Evelyn pour ses conseils, sa gentillesse et les chocolats. Merci à David Bécar-Foul pour m'avoir appris à apprendre, je te souhaite bon vent, plein de musique et de science, pour la réussite je ne m'en fais pas trop. Merci à Doug H. pour ce merveilleux spectro. Enfin, et c'est le plus difficile, merci à Pete qui nous manque énormément. Ton départ prématuré laisse un ultra-vide au labo qui, pour une fois, n'a rien de bon.

Merci aussi à Antonio Caracausi pour sa bienveillance et cette belle collaboration. A très bientôt autour d'un verre de Ben Rye !

Ma vie au CRPG ne s'est pas cantonnée au labo gaz rares. Merci aux compagnons de pause "oxygène", François, Lydéric, Camille et Martin, Jesse, Guillaume C. et Guillaume M. Merci à Gaston pour les cafés du matin et les histoires de pierres précieuses. La cafèt' du CRPG a également été l'occasion d'échanger,

rarement sérieusement, avec Julien C., Jérôme, Etienne, CFL, Thomas R., Nordine, Johan, Larry, Tix, Christophe etc.

Je tiens à remercier chaleureusement Matthias MMMM... Meier et Rainer Wieler pour m'avoir embarqué dans l'aventure Hypatia.

Merci Yves pour ton amitié et ton expertise sur le xénon. Les moments passés chez toi à te battre aux fléchettes de manière éhontée, un verre de Suze à la main, en dissertant sur l'origine de la phase Q et de la droite de Pantin, resteront gravés dans ma mémoire. Merci également à Anne pour nous supporter dans ces moments et à Georges Lynx pour sa bonne humeur.

Même si j'ai passé pas mal de temps aux gaz rares, j'ai fait quelques séjours intensifs dans notre bureau du mythique et inégalable quatrième étage. Merci à Romain Ismaël, Léo Célestin Martin et Rémi pour ces fabuleux moments partagés à raconter et faire n'importe quoi la plupart du temps et à s'entraider de temps en temps.

Merci à tous les copains: Matthieu et Benji, Marion et Tom, Xavier, Fred, Pierre et Mathieu. Merci également aux nouveaux lorrains Pauline et Nico et à la famille Lamoureux dans son ensemble.

Deux personnes ont énormément contribué à cette thèse, peut-être même sans vraiment s'en douter. Merci à Raphaël Taillardat pour m'avoir intéressé aux sciences naturelles et m'avoir si bien orienté il y a presque dix ans. Merci à Emilienne pour toute cette musique magnifique qui m'accompagne depuis tant d'années et pour tout le reste.

Merci à Guimou pour ces trois années de (presque) concubinage. Mon amitié pour toi n'a probablement d'égal que ta causticité légendaire.

Je suis extrêmement reconnaissant à ma famille pour son soutien indéfectible malgré quelques interrogations sur l'utilité du xénon pour contraindre le changement climatique. Mes parents ont absolument toujours été là pour m'aider, m'encourager, me conseiller et n'ont jamais souhaité autre chose pour moi que de réussir dans ce qui me plaît. Alors merci papa et maman pour votre soutien. Merci à ma soeurette, Anne-Laure, pour plein de choses et surtout pour ton écoute et ta prévenance. Ne t'inquiète pas je vais bien ;-)

Et enfin merci à toi Dorine pour ton soutien sans faille, ton rire, ta compréhension, ta patience, ta confiance et ton amour. Se lancer dans une thèse c'est aussi un peu embarquer ses proches malgré eux et dans cette aventure tu as été, et tu l'es toujours, formidable. Je te dois énormément.

Je souhaite dédier cette thèse à ma grand-mère (Mamie) qui avait peut-être raison: "Vu tous les engins qu'ils envoient dans l'espace, faut pas s'étonner que le temps soit tout détraqué".

Résumé

L'un des enjeux majeurs de la géochimie est de contraindre l'origine et l'évolution des éléments volatils terrestres (eau, azote et gaz rares (He, Ne, Ar, Kr, Xe)) (Marty, 2012). L'atmosphère moderne est issue de l'intégration de nombreux phénomènes tels que les contributions tardives de matière extraterrestre (météorites, comètes), le dégazage mantellique, le retour de gaz rares atmosphériques dans le manteau par subduction de matériel crustal riche en éléments volatils, les fuites thermiques et non-thermiques de l'atmosphère dans l'espace etc. Les gaz rares, chimiquement inertes, sont ici d'excellents traceurs permettant de remonter à l'origine de l'atmosphère et de suivre son évolution au cours du temps (Ozima and Podosek, 2002). Les compositions isotopiques de l'azote et de l'eau contenus dans l'atmosphère terrestre sont très proches de celles mesurées dans les météorites primitives appelées les chondrites. L'origine des gaz rares sur Terre est, elle, plus mystérieuse. Pour le manteau terrestre, une contribution de gaz d'originaire solaire semble incontournable pour l'helium (He) et probable pour le néon (Ne) (Honda et al., 1987; Yokochi and Marty, 2004). Les gaz rares plus lourds, l'argon (Ar) et le krypton (Kr) ont quant à eux une signature isotopique probablement dérivée de celle des chondrites (Holland et al., 2009; Ballentine and Holland, 2008) tandis que l'origine du xénon (Xe) mantellique reste inconnue à ce jour.

Le xénon (Xe), gaz rare stable le plus lourd, possède 9 isotopes stables (^{124,126,128,129,130,131,132,134,136}Xe) faisant de ce gaz rare un puissant traceur des phénomènes de fractionnement isotopique dépendant de la masse. Certains de ces isotopes ont également été produits par décroissance radioactive. Par exemple une partie du ^{129}Xe sur Terre a été produit par décroissance radioactive du ^{129}I ($t_{1/2}$ = 15,7 Ma) éteint aujourd'hui. Les isotopes ^{131,132,134,136}Xe ont, quant à eux, été produits en partie par fission spontanée de ^{244}Pu ($t_{1/2}$ = 82 Ma) et de ^{238}U ($t_{1/2}$ = 4.45 Ga). Le xénon est donc également très utile pour dater des évènements ayant eu lieu tout au long de l'histoire géologique de notre planète grâce à ces contributions radioactives à court (^{129}I), moyen (^{244}Pu) et long terme (^{238}U).

Le xénon atmosphérique terrestre présente des caractéristiques uniques par rapport aux autres composantes du système solaire. Premièrement, il est appauvri d'un facteur 20 environ par rapport à l'abondance attendue si celle-ci suivait le même schéma d'appauvrissement que les chondrites par rapport à un gaz de composition solaire. Il s'agit du problème du "xénon manquant". De plus, le Xe atmosphérique est fractionné isotopiquement (entre 30 et 40 ‰.u^{-1}, calculé pour les isotopes légers $^{124-130}$Xe) par rapport aux compositions isotopiques mesurées dans les chondrites ou dans le gaz solaire. Ces deux caractéristiques, l'appauvrissement élémentaire et le fractionnement isotopique, forment le paradoxe du xénon (Ozima and Podosek, 2002). Une autre caractéristique du xénon atmospherique est qu'il ne peut être directement issu

du fractionnement isotopique d'une composante chondritique ou solaire. Une fois corrigée du fractionnement isotopique, la composition de départ, nommée U-Xe (Pepin, 1991), présente un appauvrissement en ^{134}Xe et ^{136}Xe. Le problème ici est que cette composition isotopique de départ demeure énigmatique puisqu'elle n'a jamais été mesurée dans aucun échantillon terrestre ou extraterrestre disponible.

Les modèles existant à ce jour pour expliquer le paradoxe du xénon font appel à des épisodes précoces de fuite hydrodynamique des gaz rares atmosphériques pendant les cent premiers millions d'années de l'histoire de la Terre (Pepin, 1991; Tolstikhin and O'Nions, 1994). Ces fuites sont suivies d'un dégazage mantellique de Ne, Ar et Kr avec rétention préférentielle du xénon dans le manteau terrestre. D'autres modèles favorisent une fuite similaire mais suivie cette fois ci d'une contribution cométaire appauvrie en xénon (Dauphas, 2003).

Des études précédentes ont démontré que le xénon contenu dans les inclusions fluides d'échantillons archéens présente une composition, pour les isotopes légers, intermédiaire entre les composantes primordiales du système solaire (Soleil et chondrites) et l'atmosphère actuelle (e.g. Pujol et al. (2009, 2011); Holland et al. (2013)). Ce résultat a été interprété comme étant le fruit d'une perte prolongée du xénon depuis l'atmosphère vers l'espace, accompagnée d'un fractionnement isotopique (Marty, 2012; Hébrard and Marty, 2014). Une telle perte, encore opérante à l'Archéen (3.5 - 2.9 Ga), permettrait d'expliquer le paradoxe du xénon et réfuterait les modèles précédents proposant un fractionnement isotopique très précoce du Xe.

Ces travaux de thèse ont visé à caractériser précisément l'évolution du fractionnement isotopique du xénon atmosphérique au cours des temps géologiques avec pour objectifs finaux de contraindre l'origine des éléments volatils sur Terre et de suivre l'évolution des réservoirs terrestres superficiels (océan et atmosphère) depuis l'Archéen jusqu'à aujourd'hui. Dans ce but, des échantillons d'âges variés, susceptibles d'avoir enregistré la composition de l'atmosphère au cours du temps, ont été sélectionnés et analysés. Une réflexion sur l'origine du Xe contenu dans des gaz d'origine magmatique a également été entreprise pour contraindre l'origine du Xe dans le manteau et comprendre les intéractions manteau-atmosphère au cours du temps.

L'analyse précise de la composition isotopique du Xe contenu dans les gaz riches en CO_2 émis dans la région magmatique de l'Eifel (Allemagne) (voir Figure A(a)) a permis de déterminer quelle était la composante primordiale du Xe dans le manteau terrestre. La corrélation définie par les échantillons pointe vers une source chondritique (météroritique) pour le xénon contenu dans le manteau terrestre (Figure A(b)). De plus, la déconvolution du spectre isotopique obtenu (Figure A(a)) permet d'estimer les différentes contributions fissiogéniques ($^{136}Xe_{Pu}$, $^{136}Xe_{U}$) et radiogéniques ($^{129}Xe_{I}$). Un rapport $\frac{^{136}Xe_{Pu}}{^{136}Xe_{Pu}+^{136}Xe_{U}}$ entre 0.8 et 1.0 démontre la forte contribution de la fission du plutonium au Xe de l'Eifel par rapport à la contribution de l'uranium. Ceci indique que ce gaz est issu du manteau inférieur et que celui-ci est resté isolé pendant les derniers 4.45 Ga. Une dichotomie entre le manteau supérieur et le manteau inférieur s'est établie à cette époque. En effet, le manteau supérieur présente des rapports I (réfractaire) / Pu (volatil) plus élevés que le manteau profond ce qui suggère une augmentation

de la contribution de corps riches en éléments volatils à ce réservoir au fur et à mesure de l'accrétion terrestre.

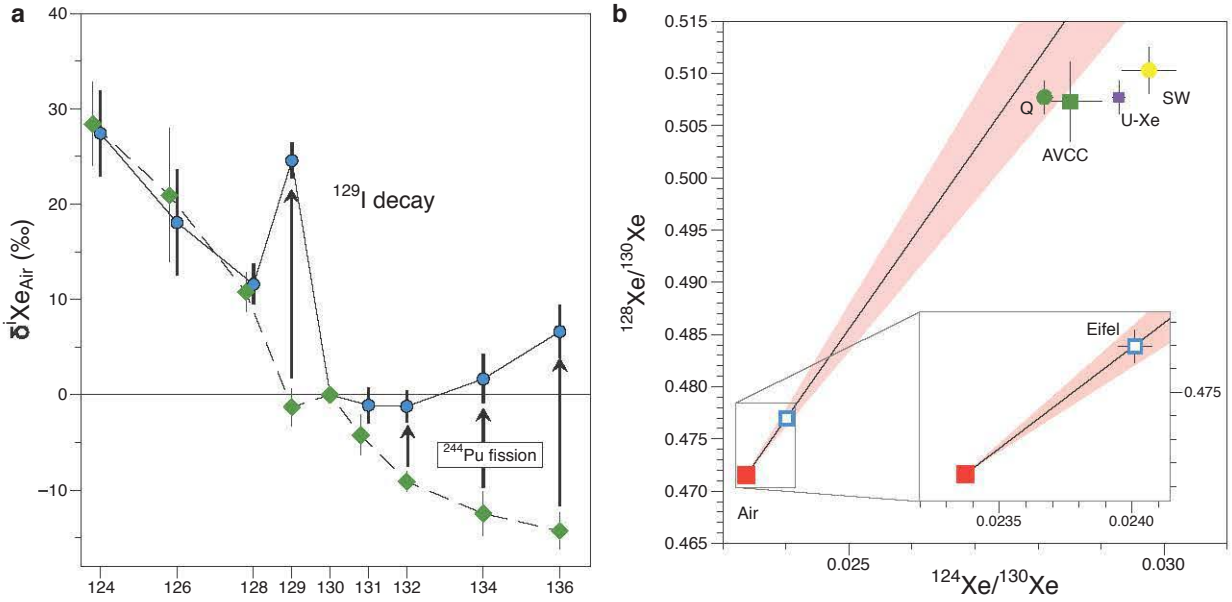

Figure A: Résultats d'analyse du xénon contenu dans les gaz riches en CO_2 émis dans la région magmatique de l'Eifel (Allemagne). (a) Spectre isotopique du Xe mesuré (points bleus) comparé à un mélange Air+chondritique (en vert) (b) Diagramme à trois isotopes démontrant la corrélation établie par le Xe de l'Eifel entre l'atmosphère terrestre et les composantes chondritiques (AVCC, Q). Une origine solaire (SW) ou similaire au U-Xe peut désormais être exclue pour le xénon mantellique.

Le échantillons archéens de la ceinture de roche verte de Barberton en Afrique du Sud (3.2 Ga) et du bassin de Hamersley en Australie (2.7 Ga) contiennent du xénon présentant une composition isotopique intermédiaire entre les composantes primordiales du système solaire et l'atmosphère moderne. Le fractionnement isotopique par rapport à l'atmosphère moderne est identique pour les deux âges avec des valeurs aux alentours de 13 ‰.u^{-1}. La determination précise (au ‰) de la composition isotopique du xénon contenu dans les quartz de Barberton permet de calculer quelle était la composition isotopique de départ de l'atmosphère terrestre. Cette composition isotopique est similaire au U-Xe (cf. figure B).

Cette composante primordiale était jusqu'à présent théorique, calculée pour reproduire la composition isotopique de l'atmosphère moderne après fractionnement isotopique dépendant de la masse, et n'avait jamais été mesurée dans aucun échantillon terrestre ou extraterrestre. Ce résultat démontre l'existence d'une dichotomie pour l'origine du xénon terrestre avec une composition de départ chondritique pour le manteau et similaire au U-Xe pour l'atmosphère. Une telle composition isotopique de départ pour le xénon atmosphérique, différente de la composition solaire, suggère une origine très primitive. Les comètes sont parmi les objets les plus primitifs du système solaire et pourraient avoir apporté cette composition isotopique de départ à l'atmosphère terrestre et ainsi contribué au moins en partie au bilan des éléments volatils terrestres et notamment à celui des gaz rares. Par exemple, si les comètes représentaient une fraction significative ($\simeq$10 %) de la matière apportée lors des épisodes d'accrétion tardive, l'ensemble de l'argon

atmosphérique sur Terre pourrait être d'origine cométaire (Marty et al., 2016). Malheureusement, même si cette estimation est robuste pour l'argon, le manque de mesures d'abondance de Xe et Kr dans les comètes ne permet pas de trancher si ces gaz rares lourds peuvent également avoir été apportés par des corps cométaires.

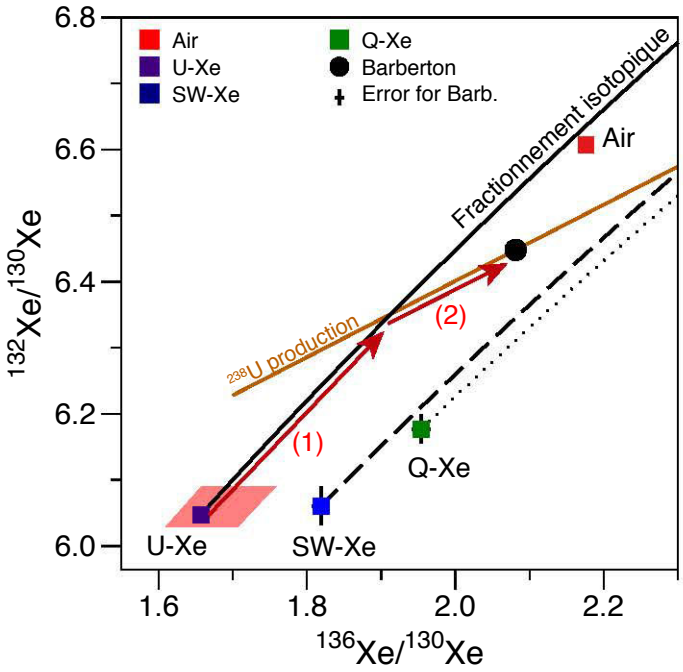

Figure B: Diagramme à trois isotopes du Xe démontrant que seul le U-Xe comme composition isotopique de départ peut expliquer la composition isotopique du xénon mesuré dans les roches archéennes (Barberton, point noir). Les flèches rouges symbolisent l'effet du fractionnement isotopique à partir du U-Xe (1) et de la contribution en ^{132}Xe et ^{136}Xe par la fission spontanée du ^{238}U (2).

Pour le xénon analysé dans les échantillons de Barberton, un excès de ^{129}Xe d'environ 6 %, inférieur à celui mesuré dans l'atmosphère actuelle (6.8 %) permet de calculer un taux de dégazage de 9 $\pm$ 5 mol.a^{-1} pour le ^{129}Xe issu de la décroissance radioactive de ^{129}I dégazé par le manteau. Ce taux de dégazage est au moins un ordre de grandeur au-dessus des taux de dégazage actuels calculés pour le gaz émis à l'aplomb des rides médio-océaniques (0.45 mol.a^{-1}) (Bianchi et al., 2010). Une telle différence pourrait s'expliquer par un dégazage mantellique important de la Terre primitive, entretenu par la chaleur conséquente produite par les radioactivités très actives au début de l'histoire de la Terre (Korenaga, 2008).

Les compositions isotopiques de l'azote et de l'argon ont également été mesurées dans les échantillons de Barberton (3.2 Ga). L'atmosphère a cette époque comportait une pression partielle d'azote similaire ou inférieure à l'actuelle. L'azote ne pouvait donc contribuer à l'augmentation de l'effet de serre à cette époque (Marty et al., 2013) comme cela avait été proposé dans des études précédentes (Goldblatt et al., 2009) pour résoudre le paradoxe du soleil jeune. De plus, la composition isotopique de l'azote était similaire à l'actuelle démontrant indirectement la présence d'un champ magnétique suffisamment puissant pour empêcher la fuite de l'azote dans l'espace et son fractionnement isotopique. Enfin, un rapport atmosphérique ^{40}Ar/^{36}Ar d'environ 200 il y a 3.2 Ga est en accord avec les modèles d'extraction crustale intensive au cours de l'Archéen

(Pujol et al., 2013b).

L'analyse isotopique à haute précision du xénon contenu dans des échantillons d'âges variés (de 3.2 Ga à 500 Ma) a permis de construire la courbe de l'évolution de la composition isotopique du xénon atmosphérique au cours des temps géologiques (Figure C). La composition isotopique du xénon atmosphérique à 3.2 et 2.7 Ga est désormais connue avec une précision de l'ordre du pour mille. Le fractionnement isotopique du xénon semble s'être arrêté pendant 400 Ma (entre 3.2 et 2.7 Ga) pour se terminer aux alentours de 2 Ga. C'est à ce moment que la composition isotopique de l'atmosphère moderne s'est établie.

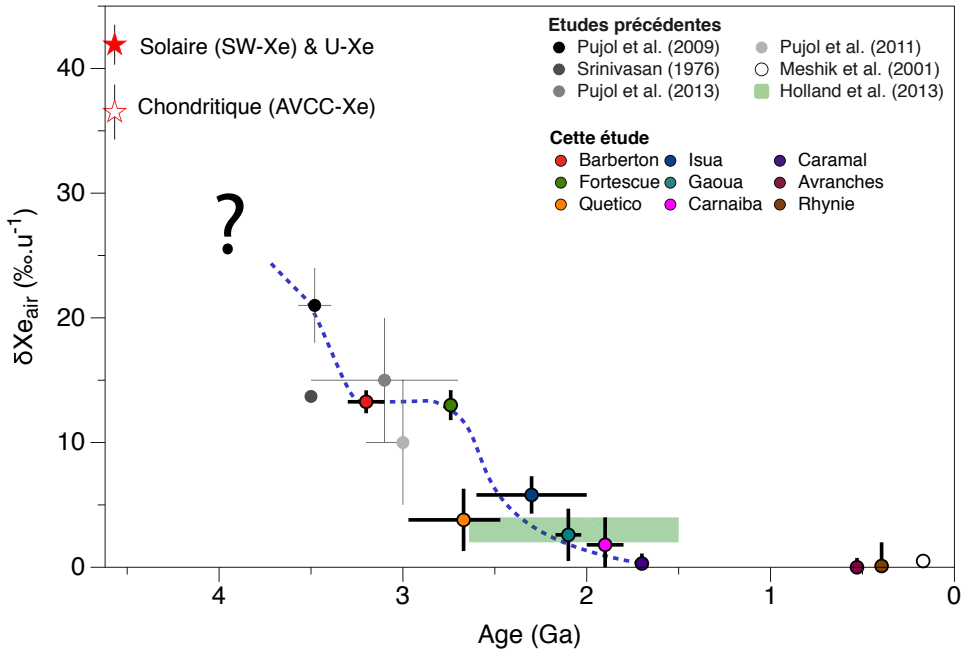

Figure C: Evolution du fractionnement isotopique du xénon atmosphérique au cours du temps déterminé au cours de cette étude. Les valeurs de la littérature sont indiquées par des cercles noirs à gris. La courbe bleue représente l'évolution possible du fractionnement isotopique. Le fractionnement isotopique semble avoir marqué un arrêt entre 3.2 et 2.7 Ga et s'être terminé aux alentours de 2 Ga. Le mode de passage d'une composition solaire, U-Xe ou chondritique à une composition fractionnée il y a 3.5 Ga reste inconnu.

Ces résultats démontrent que le fractionnement isotopique du xénon atmosphérique a eu lieu pendant plus de 2.5 Ga. Ce n'est donc pas un fractionnement élémentaire et isotopique établi pendant les cent premiers millions d'années de la Terre comme proposé dans des études précédentes (Pepin, 1991; Tolstikhin and O'Nions, 1994). Une analogie possible pour l'évolution progressive de la composition isotopique du xénon est une distillation de Rayleigh. Dans ce modèle le xénon fuit progressivement de l'atmosphère terrestre tout en étant fractionné isotopiquement. Une contrainte importante de ce modèle est que les autres gaz rares, plus légers, ne présentent pas de perte ni de fractionnement isotopique de cette ampleur. L' ionisation du xénon dans l'atmosphère par les rayons ultraviolets intenses du Soleil jeune (Claire et al., 2012) et l'intéraction éventuelle de ces ions avec la matière organique sont susceptibles d'induire un fractionnement isotopique

instantané d'environ 1 %.u^{-1} (Kuga et al., 2015; Marrocchi et al., 2011). Reste alors à trouver un processus pour faire fuire le Xe. La fuite hydrodynamique des ions de Xe entraînés par les ions hydrogène est une possibilité de mécanisme sélectif pour la fuite du Xe (Zahnle, 2015). La présence d'un champ magnétique comparable à l'actuel à l'Archéen, un flux UV intense et une ionisation préférentielle du xénon sont des paramètres en faveur de ce modèle de fuite. Une modélisation précise de ce mécanisme de fuite est tout de même nécessaire pour évaluer sa capacité à faire fuire le xénon pendant plusieurs milliards d'années.

Le développement d'un modèle numérique de dégazage et de perte sélective du xénon selon une distillation de Rayleigh permet également de corriger les intervalles de formation de l'atmosphère calculés dans des travaux précédents (e.g. Porcelli and Ballentine (2002)). Ce modèle permet d'estimer les quantités de xénon radiogénique et fissiogénique dans l'atmosphère avant la fuite préferentielle du xénon. Après correction, l'intervalle de formation de l'atmosphère passe de 100 - 110 Ma à 40^{+20}_{-10} Ma après la formation du système solaire et pourrait correspondre au dernier impact géant à l'origine de la formation de la Lune (Avice and Marty, 2014). Les résultats obtenus dans une phase plus avancée de cette étude, tels que la dichotomie manteau/atmosphère pour l'origine du xénon ou encore l'arrêt du fractionnement isotopique du Xe et donc de sa fuite pendant 400 Ma rendent nécessaire une révision de ce modèle même si la correction de ces âges pour la perte du xénon reste pertinente.

Les résultats obtenus dans cette étude permettent de construire un scénario cohérent pour l'origine et l'évolution du xénon terrestre. La terre silicatée a incorporé du xénon chondritique au cours de son accrétion. Même si une partie de ce xénon primordial et du xénon radiogénique a ensuite été dégazé, la persistence d'anomalies en $^{129}Xe_I$ et en $^{136}Xe_{Pu}$ dans le manteau inférieur démontre un isolement précoce, il y a environ 4.45 Ga, de ce réservoir terrestre. Après cet isolement, un fractionnement chimique entre le manteau supérieur et le manteau inférieur s'est établi avec une plus grande contribution au manteau supérieur de corps riches en éléments volatils pendant les dernières phases de l'accrétion terrestre. Le xénon atmosphérique présente quant à lui une composition isotopique de départ différente de celle des météorites ou du gaz solaire. Cette composition isotopique de départ, le U-Xe, pourrait avoir été apportée par des corps cométaires. Les comètes présentent des rapports gaz rares vs. eau très élevés. A tel point que 10 % de corps cométaires dans les derniers épisodes d'accrétion sont suffisants pour expliquer tout le budget d'argon atmosphérique (Marty et al., 2016). Des mesures supplémentaires de l'abondance en gaz rares et de la composition isotopique du xénon des comètes sont nécessaires pour trancher si un apport cométaire du xénon terrestre est réaliste. Enfin, l'évolution de la composition isotopique du xénon atmosphérique au cours du temps implique une fuite du xénon atmosphérique vers l'espace pendant plusieurs milliards d'années résolvant ainsi le paradoxe du xénon. Le développement de modèles numériques de fuite de xénon et d'hydrogène ionisés le long des lignes ouvertes du champ magnétique terrestre est une nécessité pour déterminer si ce mécanisme est viable pour expliquer la fuite sur le long terme du xénon atmosphérique.

Abstract

The origin of volatile elements on Earth remains poorly understood. The elemental and isotopic composition of the Earth's atmosphere has been shaped by numerous events in the history of our planet such as extraterrestrial chondritic or cometary contributions, mantle degassing, atmospheric escape etc., preventing any straightforward identification of cosmochemical ancestors. Among the noble gases, xenon (Xe) in the Earth's atmosphere is even more enigmatic. It does not appear to be genetically derived from either the protosolar nebula, or from inner solar system bodies (meteorites). Furthermore, atmospheric Xe is elementally depleted relative to other noble gases (Ne, Ar and Kr) when compared to their abundances in meteorites. It is also strongly isotopically fractionated, enriched in heavy isotopes and depleted in light isotopes, compared to other known solar system components. These two features form the "xenon paradox" (Ozima and Podosek, 2002). For the Earth's mantle, the starting isotopic composition of Xe remains unknown preventing a clear determination of mantle-atmosphere interactions with time. Recent studies of the atmosphere trapped in ancient samples (e.g. Pujol et al. (2009, 2011)) already shed some light on the xenon paradox by demonstrating that Xe in the Archean atmosphere had an isotopic composition intermediate between the potential primordial components and the modern atmosphere. These preliminary results suggested a long-term evolution of the isotopic composition of atmospheric Xe linked to unknown atmospheric escape processes.

During this study, analyses of noble gases and nitrogen were performed on ancient quartz samples of various ages (3.2 Ga to 500 Ma) in order to follow the evolution of the elemental and isotopic composition of the Earth's atmosphere with time. In particular, high-precision analysis of xenon isotopic ratios has been developed in in an attempt to decipher the origin of atmospheric Xe, to document precisely the evolution of its isotopic fractionation with time and to better understand the physico-chemical processes(s) behind this evolution. Other noble gases (Ne, Ar, Kr) and nitrogen were also analyzed to characterize the elemental and isotopic composition of the 3.2 Ga-old atmosphere. Finally, isotope systematics on Xe contained in mantle-derived gases permitted to put constraints on the origin of Xe in the Earth's mantle and to study mantle-atmosphere interactions.

Results of this PhD work are presented in this manuscript composed of four main chapters plus one additional chapter of Annexes containing co-authored papers.

The first chapter consists in a general introduction to this study. It starts with a brief description of the history of Earth's accretion and a review on the state of knowledge on the origins of terrestrial volatile elements. Important atmospheric and geodynamical features of the early Earth are then introduced. The second part of this Chapter is dedicated to an introduction to *Xenology*, the study of Xe, as isotope systematics of this noble gas is the major tool used in this study. Recent advances on the study of Archean Xe are then presented. The end of this chapter presents the main questions that guided this study.

The second chapter describes the geological settings of the samples analyzed in this study as well as

the analytical methods and developments that were applied to measure the abundances and the isotopic composition of noble gases and nitrogen contained in these samples.

The third chapter is composed of four papers presenting results and interpretations of this study and organized following a logical order with respect to the Earth's accretion and evolution.

The first paper, in revision in the *Nature* journal, presents the results of a collaboration with Dr. A. Caracausi (INGV, Italy) and researchers from CRPG (Nancy, France). It deals with the origin of Xe in the Earth's mantle. It also put constraints on the time of closure of mantle reservoirs and on the nature of the dichotomy between the upper and lower mantle reservoirs.

The second paper, in preparation for a submission, deals with the potential cometary origin of the atmospheric Xe inferred from high-precision analysis of isotopic ratios of Xe in 3.2 Ga-old samples. Results also permit to compute the degassing rate of the Earth during the last 3.2 Ga.

The third paper, in preparation for a submission, presents the evolution of the isotopic composition of atmospheric Xe with time. High-precision data permit to better understand the processes behind this progressive fractionation. It also constrains the elemental and isotopic composition of noble gases and nitrogen in the 3.2 Ga-old atmosphere.

The fourth paper, published in *Philosophical Transactions of the Royal Society A* (Avice and Marty, 2014), describes the results obtained from a numerical model that takes into account the selective escape and isotopic fractionation of atmospheric Xe. Closure ages for the atmosphere can thus be corrected for this long-term escape leading to new estimates of the age of the Moon-forming event.

The final chapter summarizes the main results obtained during this study. The potential cometary contribution to the Earth's atmosphere is then explored through description of the main results of a co-authored publication (Marty et al., 2016). Finally, a scenario for the origin and evolution of Earth's Xe is proposed in an attempt to bring altogether results from recent studies and those obtained during this PhD work.

Table Of Contents

Chapter 1

Introduction

This first chapter presents the context of this study i.e. the current views and possibilities for the origins and evolution of the Earth's atmosphere. Another goal of this chapter is also to present the scientific framework, specially regarding *Xenology*, necessary for understanding the present study and not always detailed in papers presented in Chapter 3 (Results and Implications). The main questions that orientated this study are presented at the end of this chapter.

Contents

1.1 Context of the study

Searching for the origins of the Earth's atmosphere and, particularly, atmospheric noble gases requires to go back to the early chaotic times of the beginning of the Solar System when the terrestrial accretion remained to be achieved and when the structure of our solar system was very different from its present state. This section is divided in two parts. The first part deals with Earth's formation and the potential relationships between volatile elements on Earth and other major reservoirs of volatile elements in the solar system (the Sun, chondrites, comets). The second part concerns the state of the Earth during the Hadean and Archean epochs. It is focused on the features of the Archean (4.5 to 3.5 Ga) atmosphere since a major part of this study was focused on studying ancient atmospheres trapped in Archean samples. It also presents what is the current state of knowledge on the evolution of the atmosphere from the Archean to Present and, particularly, on the progressive oxidation of superficial reservoirs with time.

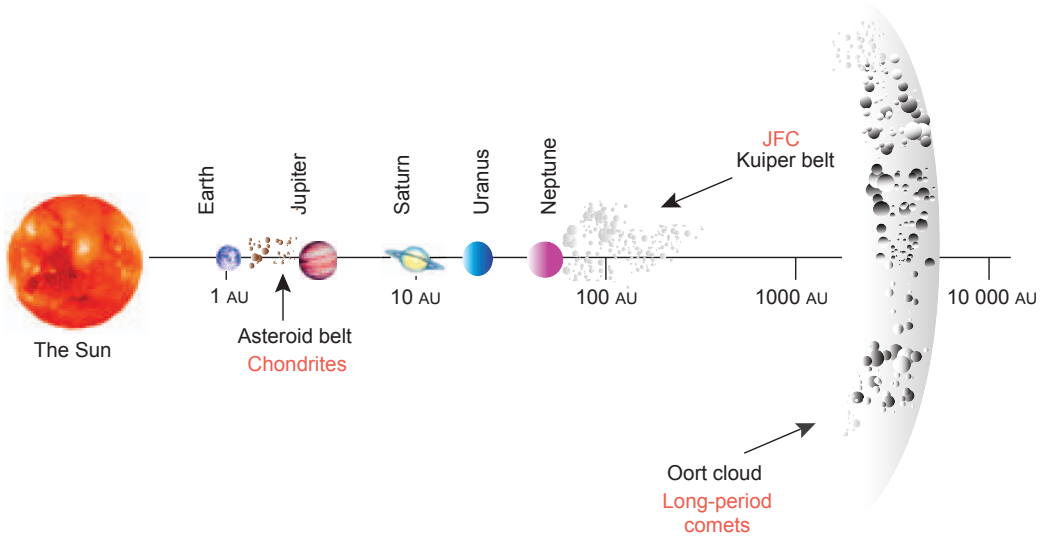

Fig. 1.1: Schematic view of the current structure of our Solar System with major reservoirs of volatile-rich bodies that may have contributed to the budget of volatile elements on Earth. JFC is for "Jupiter Family Comets". Mercury, Venus and Mars are not displayed here. Distances from the Sun are in astronomical units (AU). After Gounelle (2011).

1.1.1 Earth's accretion and the potential origins of its volatile elements

The current models for the Earth's formation and the potential origins of volatile elements present on our planet are described in this section. Before to detail the steps of Earth's accretion starting from a disk of dust, it is necessary to present briefly what is the modern structure of the Solar System i.e. to list what are the objects which may have contributed to the budget of volatile elements on Earth and what are their current locations. Major reservoirs of volatile elements in the Solar System are the Sun (99.8 % of the mass of the Solar System), meteorites (some of them, the carbonaceous chondrites, are volatile-rich), and comets. Comets are usually divided in two families: the long-period comets coming from the Oort cloud and the Jupiter Family comets (JFC) stored in the Kuiper belt beyond the orbit of Neptune. Figure 1.1 depicts the modern structure of the Solar System with its major reservoirs of volatile-rich bodies. The distinction, originally based on astronomical features, between comets and some chondrites seems more and more tenuous since recent studies revealed features that are shared by both types of objects (Gounelle, 2011).

Terrestrial accretion

It is beyond the scope of this study to present a detailed view of the mechanisms of terrestrial accretion but some key steps and observations are presented in this section since the origins of volatile elements on Earth are intimately linked to these mechanisms and to the composition of the building blocks of the Earth. Details on the scenario of terrestrial planet formation are still debated, for example concerning ways to accrete a low-mass Mars (Chambers, 2014). However there is a consensus (see a recent review by Dauphas and Morbidelli (2014)) on three major steps during terrestrial accretion:

- collision and sticking of dust grains by electrostatic and magnetic forces until the formation of mm- to cm-sized aggregates. Once formed these aggregates migrated and reached the median part of the disk to form planetesimals;
- oligarchic growth of planetesimals into planetary embryos during which bigger embryos grow faster than lighter ones;

- collisions of planetary embryos ending with the formation of terrestrial planets.

Recently, Morbidelli et al. (2015) demonstrated that the accretion disk inside of Jupiter's orbit remained dry i.e. depleted in volatile elements (H, N, noble gases) during accretion episodes because Jupiter intercepted ice-rich particles. In that case, Jupiter acted as a "fossilizing agent" for the snow line and prevented water deposition in the inner parts of the disk. During all the three steps described above, the position of the forming Earth was thus inside the limits defined by the fossilized snow line preventing the condensation of volatile elements from the solar gas on the forming Earth (Pinti, 2005) or only in minor amounts (Marty, 2012).

Most of volatile elements on Earth were thus either already contained in planetary embryos that collided when forming the proto-Earth (e.g. Theia the last embryo that contributed to the Earth and also the Moon-forming impactor) or delivered to the Earth during late addition of volatile-rich material originating from the outer regions of the Solar System. Scrutinizing the elemental and isotopic compositions of these volatile elements in Earth's modern and ancient atmosphere and in its silicate parts is a key to decipher their potential origins (see next section).

Elemental and isotopic compositions of volatile elements on Earth

Isotopic compositions of volatile elements on Earth are great tools to estimate what could be the nature of objects that brought volatile elements to the Earth. For example, hydrogen and nitrogen isotope ratios are useful because of the wide range of isotopic compositions of known terrestrial and extraterrestrial materials. Among meteorites, most of carbonaceous and enstatite chondrites have D/H and $^{15}N/^{14}N$ ratios that are similar to the Earth's atmosphere (Fig. 1.2) and have often been considered to be the carrier phases of these volatile elements to the Earth (e.g. Marty (2012)).

For water and nitrogen, comets are poor candidates for supplying volatile elements to the Earth because these objects usually present too high $^{15}N/^{14}N$ and D/H ratios (Fig. 1.2). The recent measurement of a D/H similar to the terrestrial value in comet 103P/Hartley2 (Hartogh et al., 2011) challenged these conclusions. However, the $^{15}N/^{14}N$ ratio of 6.46 x 10^{-3} (Meech et al., 2011) measured in the same comet is much higher than the terrestrial value (3.68 x 10^{-3}) (Fig. 1.2) and prevents any major contribution to the terrestrial budget of N (Hutsemékers et al., 2009) and H from this type of short-period comets. Recent measurements of the isotopic composition of hydrogen in comet 67P/Churyumov-Gerasimenko (labeled "67P/C-G" hereafter) by the Rosetta space probe gave a D/H value of (5.3 ± 0.7) x 10^{-4} for comet 67P/C-G confirming that terrestrial water cannot originate from these objects (Altwegg et al., 2015). It is worth noting here that abundances of noble gases, especially Kr and Xe, relative to those of other volatile elements (H, C, N) in comets are poorly known. This means that even if comets alone cannot have contributed to a significant part of water (H) and nitrogen on Earth, a contribution from these objects to the budget of terrestrial noble gases cannot be excluded based on these measurements.

If terrestrial hydrogen and nitrogen have isotopic compositions close to chondritic values, the origin of terrestrial noble gases, in the atmosphere and in Earth's mantle, remains debated. Some isotopic constraints for each noble gas are listed below. The case of atmospheric xenon is detailed in section 1.2 of this first chapter.

Helium: Honda et al. (1987) analyzed terrestrial diamonds and measured $^{3}He/^{4}He$ ratios close to the solar value of 3.6×10^{-4} (Ott, 2014) demonstrating that the lightest noble gas may have a solar origin in the Earth's mantle possibly from condensation of some nebular gas on the Earth during the early stages of planetary accretion.

Neon: If helium in the Earth's interior clearly carries a solar-like signature, mantle neon has still a debated

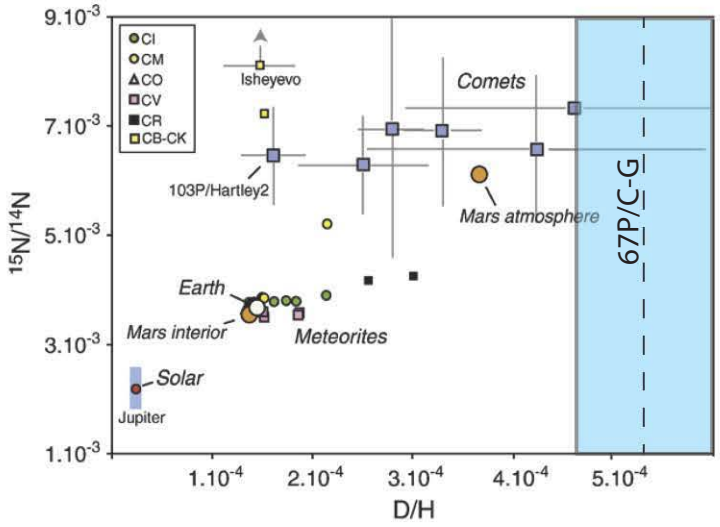

Fig. 1.2: D/H and $^{15}N/^{14}N$ isotopic ratios of solar system reservoirs and objects. Meteorites are the best candidates for supplying nitrogen and hydrogen (i.e. water (H_2O)) to the Earth as these objects have N and H isotopic compositions similar to the Earth. Comets have too high $^{15}N/^{14}N$ and D/H ratios to be the unique sources of these elements on Earth. Figure and references from Marty (2012) and from Altwegg et al. (2015) for the D/H ratio of 67P/C-G (blue range at 1σ).

origin. Pristine neon isotopic ratios in mantle-derived samples have been altered by air contamination and by crustal production of $^{20,21,22}Ne$ by diverse nucleogenic routes (Ballentine and Burnard, 2002). Figure 1.3 illustrates that the convective mantle (sampled by Mid Ocean Ridge Basalts, MORBs) and a more primitive mantle (sampled by plume magmas and gases) have distinct Ne signatures (see review by White (2015) and refs. therein). Ballentine et al. (2005) demonstrated that CO_2-rich crustal gases define a correlation pointing toward a solar-wind implanted component ($^{20}Ne/^{22}Ne \simeq 12.5$) for the primitive end-member of the air-MORB mixing line.

However, Yokochi and Marty (2004) and Honda et al. (1991) measured very high $^{20}Ne/^{22}Ne$ ratios up to 13.0 ± 0.2 close to the solar values (> 13.4) in plume-influenced rocks and in basalts, respectively. Recently, Moreira and Charnoz (2015) demonstrated that implantation, coupled with sputtering, of solar Ne on dust particles in the accretion disk leads to an enrichment in heavy isotopes because of higher penetration depths for heavy isotopes due to higher kinetic energies. The $^{20}Ne/^{22}Ne$ ratio, when a steady-state is reached, attains a value of 12.7 compatible with the ratio measured in mantle-derived rocks (12.5 - 12.9). However, the 12.7 value is lower than some values measured by Yokochi and Marty (2004) (up to 13.0 ± 0.2). Moreira and Charnoz (2015) advocated that such high values are possible if the steady-state during irradiation was not achieved i.e. various isotopic ratios are reflecting various times of irradiation in the disk. However, if this model is correct, the deep mantle would have a minimum value of 13 and lower values for the $^{20}Ne/^{22}Ne$ ratio would be due to air contamination since it is hard to imagine how the deep mantle source would have remained heterogeneous for neon isotopic ratios. This model of implantation and sputtering producing a wide range of $^{20}Ne/^{22}Ne$ values incorporated into the Earth's mantle demonstrates that Ne isotopic systematics alone cannot easily decipher between solar and solar-wind implanted (on meteorites) signatures.

Atmospheric Neon has a much lower $^{20}Ne/^{22}Ne$ ratio of 9.77 (Ozima and Podosek, 2002) compared to cosmochemical components (Solar/Chondritic) presented above. This feature is often considered as the result of an isotopic fractionation during early hydrodynamic escape (e.g. Pepin (1991)). However, Marty (2012) noticed that the isotopic $^{20}Ne/^{22}Ne$ and the elemental $^{36}Ar/^{22}Ne$ ratios best correspond to a mixing between a solar and a "planetary" chondritic component (Fig. 1.4) rather than to kinetic fractionation induced by hydrodynamic escape.

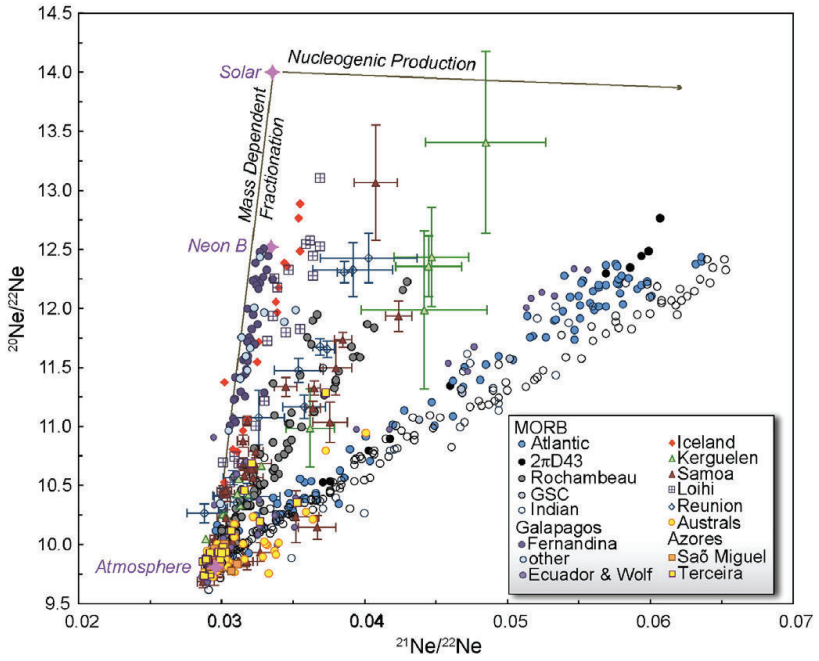

Fig. 1.3: Three-isotope plot of Neon in mantle-derived rocks showing the MORB-Atmosphere correlation together with Ne data for plume-derived samples. Only few values are higher than the Neon B components measured in meteorites. Adapted from White (2015), see refs. therein.

These observations tend to show that neon isotopic systematics might not be the best tool to distinguish between potential sources for the origins of noble gases on Earth since isotopic ratios may have been easily modified by several processes: air contamination, crustal contributions, pre-irradiation of dusts in the disk etc.

Argon: The isotopic composition of argon in Earth's interior was a subject of debate for a long time (recently reviewed by Moreira (2013)). Valbracht et al. (1997) claimed to have discovered sub-solar values for the $^{38}Ar/^{36}Ar$ ratio measured in rims of pillow basalts from Hawaii. However, Moreira (2013) considers these results as doubtful because of difficulties met during gas purification. Subsequent studies (Kunz, 1999; Raquin and Moreira, 2009; Holland and Ballentine, 2006) demonstrated that the $^{38}Ar/^{36}Ar$ ratio in Earth's interior is indistinguishable (Fig. 1.5) from the atmospheric value (0.188, Ozima and Podosek (2002)). Marty (2012) argued that the $^{38}Ar/^{36}Ar$ ratio of the Earth's atmosphere (0.188) is in the range of chondritic values (Ott, 2014) and different from the solar value (0.189, Heber et al. (2009)). However, Dauphas and Morbidelli (2014) noticed that the atmospheric $^{38}Ar/^{36}Ar$ ratio is slightly isotopically fractionated relative to chondrites (6 $‰.u^{-1}$) leaving space for some modifications of the original chondritic $^{38}Ar/^{36}Ar$ ratio by early episodes of hydrodynamic escape.

Krypton: Holland et al. (2009) analyzed mantle-derived CO_2-rich gases and demonstrated that krypton in the Earth's mantle has a Chondritic rather than Solar origin (Fig. 1.6). Despite high-precision analyses, they could not distinguish between a Solar or Chondritic origin of Xe in the same samples. Chondritic Kr and solar He, and perhaps Ne, in the Earth's mantle mean that light and heavy noble gases in the silicate Earth have been contributed by distinct cosmochemical sources.

Xenon: Xe is the rarest noble gas on Earth and is thus often found in minute quantities in mantle-derived rocks. CO_2-rich gases (e.g. Caffee et al. (1999)) are in unlimited amount and are thus often the best available samples because they provide sufficient Xe quantities to precisely study Xe isotope systematics. Furthermore, xenon isotope systematics can provide several constraints such as estimate of amounts of air recycling in

2.4. Cometary shower during the Late Heavy Bombardment ?

A cometary contribution to the terrestrial inventory of volatile elements appears limited from D/H (Dauphas et al., 2000; however, as noted above, this argument may weaken if further cometary D/H measurements confirm Earth-like compositions) and $^{15}N/^{14}N$ systematics (Jehin et al., 2009; Marty and Yokochi, 2006) The lunar surface bears

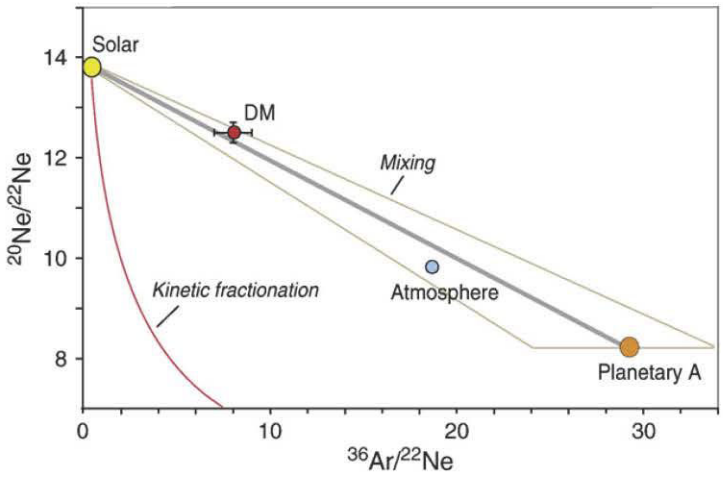

Fig. 3. Mixing diagram between Solar and the Planetary-A component of Black (1971) and Mazor et al. (1970), defined by the lower boundary of the envelope delimiting carbonaceous chondrite data. "DM" is defined by the mean of the $^{36}Ar/^{22}Ne$ ratios of the Popping rock (Moreira et al., 1998) and the CO_2 well gases from Ballentine et al. (2005) on one hand, and the highest end-member $^{20}Ne/^{22}Ne$ ratio of MORBs (Hiyoff et al., 2000). For comparison, the evolution of a solar composition upon kinetic fractionation (Rayleigh distillation, where the fractionation factor is the square root of masses) is represented by the curve at the left hand side. Neither the atmosphere nor the DM compositions fit this evolution trend.

Fig. 1.4: Neon-mixing diagram. The grey line represents the potential mixing between solar and planetary-A end-members. Isotopic composition and elemental ratios (Ar/Ne) of the Earth's atmosphere are compatible with such a mixing. Kinetic fractionation (for example during atmospheric escape) is unable to reproduce both the isotopic and elemental compositions of atmospheric neon. DM corresponds to the depleted mantle source. Figure and references from Marty (2012).

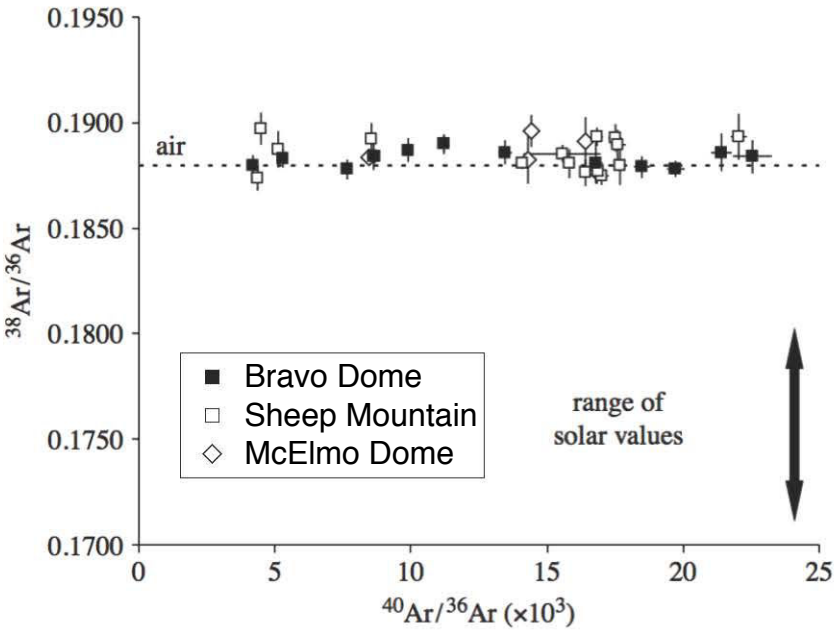

Fig. 1.5: CO_2-rich gases $^{38}Ar/^{36}Ar$ vs. $^{40}Ar/^{36}Ar$. Data are from Holland and Ballentine (2006) and figure adapted from Ballentine and Holland (2008). Mantle-derived gases have $^{38}Ar/^{36}Ar$ ratios indistinguishable from the atmospheric ratio (dashed line).

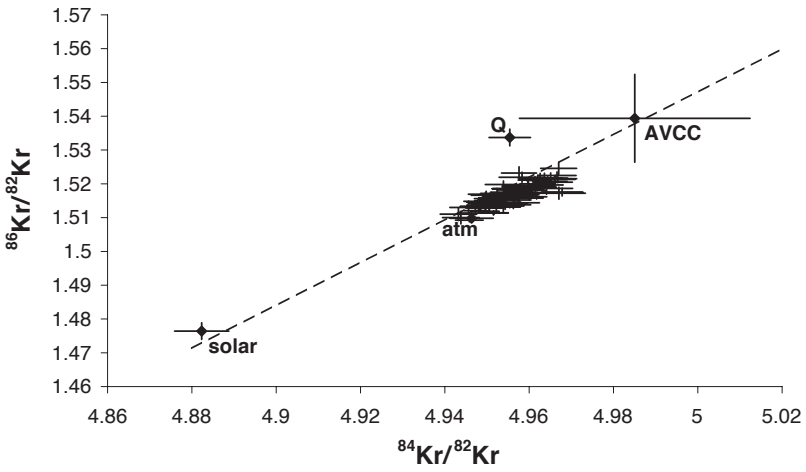

Fig. 1.6: Three-isotope plot of Kr isotopes analyzed in CO_2-rich gases. The correlation points toward a chondritic (Q-Kr or AVCC-Kr) rather than Solar ancestor for mantle Kr. Adapted from Holland et al. (2009).

the Earth's mantle (Holland and Ballentine, 2006) as well as extent and timing of mantle degassing (see Ballentine and Holland (2008) and refs. therein). However the cosmochemical origin, Solar or Chondritic, of Xe in the silicate Earth remains uncertain (Holland et al., 2009) and is of major importance to constrain degassing history and closure times of different reservoirs in the mantle (Parai and Mukhopadhyay, 2015). The correlation between air and primordial components defined by mantle-derived gases analyzed so far for light Xe isotopes (^{124,128,130}Xe) is shown in Fig. 1.7. Analyses of mantle-derived Xe always reveal the dominant presence of an atmospheric component (usually more than 90 % of the Xe signal). This atmospheric component, due to air subduction or shallow-level air contamination, in the Earth's mantle prevents the determination of the primordial end-member: Chondritic or Solar? Some decisive samples showing lower contribution from atmospheric-derived Xe and high-precision analyses are thus required to decipher between these primordial components and to build a precise picture of the history of mantle degassing.

Dynamical and elemental constraints on the origin of volatile elements on Earth

N-body simulations are currently the best numerical tools to understand how the terrestrial planets formed from a given starting distribution of planetesimals. State-of-the art numerical models comprise a significant step that is the inward and outward migration of the giant planets Jupiter and Saturn: the so-called "Grand Tack" event (Walsh et al., 2011). It caused a truncation of the disk of planetesimals and embryos with all the mass in the terrestrial planet region concentrated between 0.7 and 1.0 AU. This truncation around 1.0 AU appears necessary to form small Mars analogs. In this model the inward and then outward migration of the giant planets has also severe implications on the distribution of planetesimals. Figure 1.8 depicts the effect of this "Grand Tack" on planetesimals initially located between 0.3 and 3 AU (red dots), between giant planets orbits (light blue dots) and in more external regions of the solar system (dark blue dots). The inward migration of Jupiter scatters planetesimals originally inside the giant planets orbits toward outer regions of the solar system. The outward migration of Jupiter, captured by Saturn, repopulates the inner asteroid belt with these objects but also with objects that were originally beyond the orbits of giant planets. At the end, the inner asteroid belt is mainly constituted by planetesimals originally located inside giant planets orbits but it also contains some planetesimals originally formed in the outer regions of the solar system (blue dots in the last panel in Fig. 1.8). These objects formed in cold regions of the solar system and are thus potentially volatile-rich. Their presence in the inner asteroid belt at the end of the Grand Tack and their later disturbance during the Late Heavy Bombardment (Gomes et al., 2005)

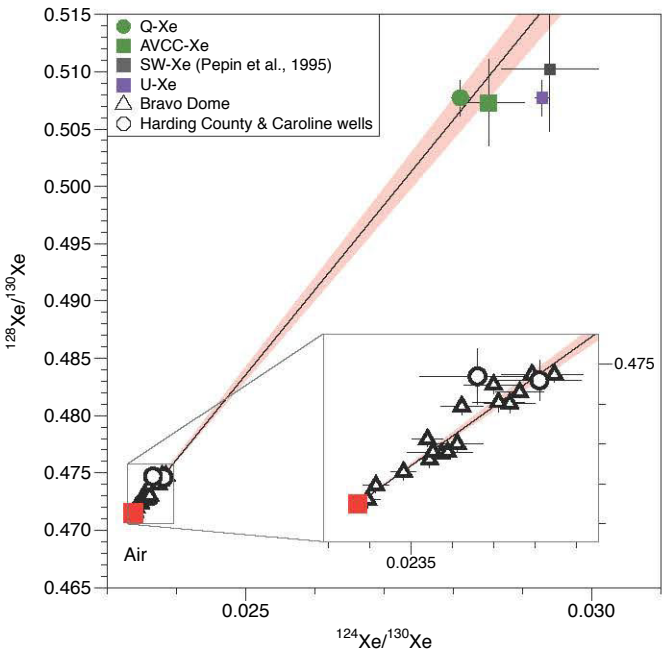

Fig. 1.7: Three-isotope plot of light Xe isotopes analyzed in mantle-derived gases (Bravo Dome, black triangles; Harding County and Caroline, open circles). See Holland et al. (2009) and Caffee et al. (1999) for data. The best fit line obtained for the whole dataset cannot decipher bewteen a chondritic or a solar origin for mantle Xe.

are probably keys to bring volatile-rich bodies in the Earth's originally dry area.

A volatile-rich contribution to the Earth during the late stages of terrestrial accretion and inferred from modeling work is also proposed by geochemical studies (Marty, 2012; Halliday, 2013). For example, Marty (2012) pointed out that a contribution of 1-3 % of volatile-rich material (carbonaceous chondrites) to an originally dry proto-Earth well explains the abundances of terrestrial water, carbon and noble gases (except for Xe, see section 1.2.4).

Volatile delivery versus atmospheric loss during impacts

Whatever the provenance of impactors that may have supplied volatile elements to the originally "dry" proto-Earth, special attention must be paid to the mass balance of atmospheric escape versus volatile delivery when objects were impacting the growing Earth. The simplest assumption that impacts were conservative with no loss of volatile elements from the target or from the impactor during an impact event is probably wrong when one considers the high energy delivered by giant impacts (Genda and Abe, 2005). There are numerous parameters governing the amount of atmospheric escape during an impact such as the size of impacting bodies, their velocity, atmospheric entry angles, the presence of an ocean on the proto-Earth etc. Impacts do not always imply a total loss of atmospheric volatile elements. de Niem et al. (2012) already demonstrated that accumulation of volatile elements probably dominates over atmospheric erosion during a heavy bombardment. For example for a late heavy bombardment of 2×10^{23} g containing between 10 % and 90 % of comet-like objects, the initial pressure of the atmosphere would have been multiplied by 2.5 to 6 demonstrating that impacts can efficiently deliver volatile elements to the growing Earth (Fig. 1.9). Similarly, Schlichting et al. (2015) demonstrated that the Earth's atmosphere reflects the equilibrium between atmospheric erosion and volatile delivery from impactors.

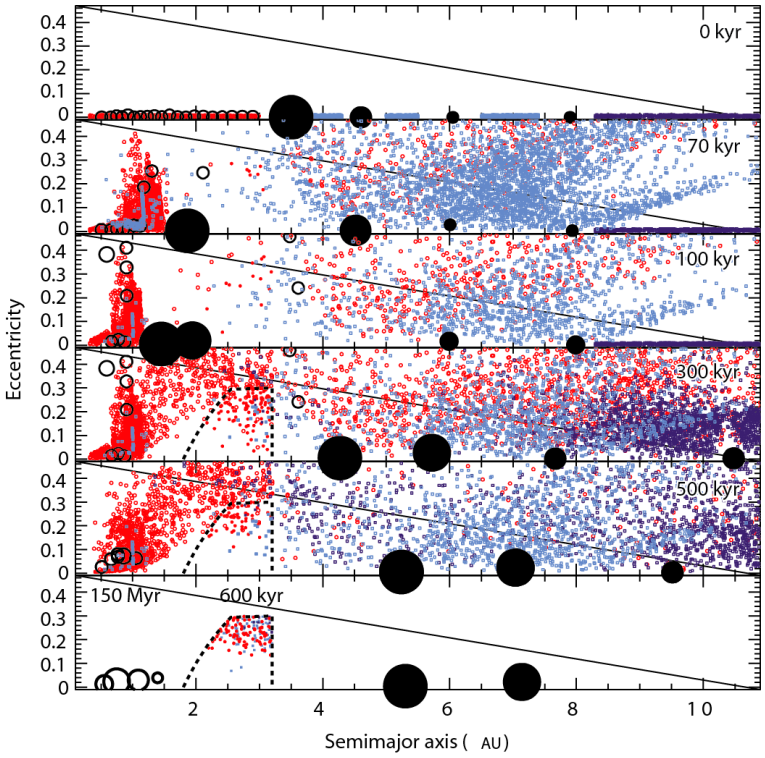

Fig. 1.8: Evolution of the small-body populations (eccentricity vs. semi-major axis) during the growth and migration of the giant planets. Jupiter, Saturn, Uranus and Neptune are represented with black-filled circles. Planetary embryos are represented with large empty circles. The dashed curves represent the boundaries of the main belt. Red dots, light blue dots and dark blue dots are planetesimals originally inside 3 AU, between giant planets orbits and in the outer solar system, respectively. Figure from Walsh et al. (2011).

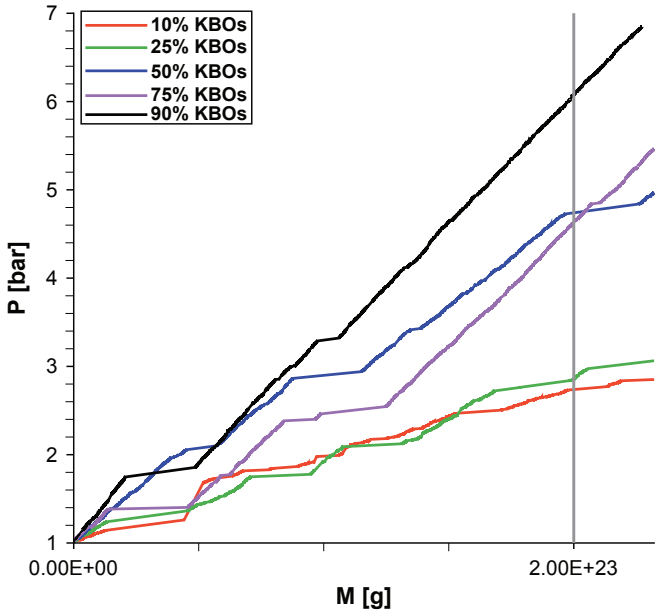

Fig. 1.9: Evolution of the terrestrial atmospheric pressure during heavy bombardment vs. the total impactor mass. Colors represent different mass contribution to the late heavy bombardment from Kuiper Belt (cometary) Objects (KBOs). The vertical grey line represents the mass of the terrestrial late heavy bombardment (2×10^{23} g) taken by Marty and Meibom (2007) to estimate the potential contribution of comets to the budget of terrestrial volatiles. Modified after de Niem et al. (2012).

The potential contribution from comets to the budget of volatile elements on Earth during final stages of Earth's accretion

A potential contribution from comets to the budget of volatile elements and organics on terrestrial planets and specially on Earth has often been advocated mainly based on elemental ratios of volatile elements in the Earth's atmosphere (Owen et al., 1992; Dauphas, 2003; Hartogh et al., 2011; Marty and Meibom, 2007). However, knowing the isotopic composition of noble gases, and specially Xe, in comets is of primordial importance here to precisely estimate their potential contribution to the budget of volatile elements on Earth. Analyses of samples from comet 81P/Wild 2 returned by the Stardust NASA mission already revealed the presence of chondritic gases ("Q" gases) in cometary grains sampled by the Stardust spacecraft (Marty et al., 2008). However there is, up to now, no in-situ measurement of the isotopic composition of heavier noble gases (Kr, Xe) in such objects.

Recently, Kramers et al. (2013) analyzed noble gases contained in an unusual diamond-rich pebble found in SW Egypt and called "Hypatia". Among other results, Kramers et al. (2013) found that Ne, Kr and Xe isotopic ratios were tending toward the G component. This component is believed to carry nucleosynthetic anomalies and to be very primitive in the history of our solar system (Ott, 2014). The authors interpreted the presence of this component as an evidence that Hypatia was originating from a cometary object that exploded when penetrating in the Earth's atmosphere, causing an outburst responsible for the formation of the Libyan Desert Glass. However, this interpretation was subsequently criticized (Reimold and Koeberl, 2014). During this study, an international collaboration has been conducted in order to measure abundances and isotopic compositions of nitrogen and noble gases in this unusual stone. Indeed, if Kramers et al. (2013) were right, Hypatia was an unique opportunity to measure the isotopic composition of N and noble gases (specially Xe) in cometary matter with very precise laboratory equipments. Results and interpretations are presented and discussed in a recent publication (Avice et al. (2015), see Annexe 5.1 for the full edited paper). Unfortunately, this study does not confirm the presence of the G component and thus does not confirm the cometary nature of the parent body of Hypatia. However the presence of Q gases (see section 1.2.3), of ^{129}Xe excess due to the decay of extinct ^{129}I (Fig. 1.10a) and of a major component released at high temperature with a δ^{15}N value of -110 ‰(Fig. 1.10b) make this extraterrestrial material unique among other known groups of meteorites. Analyses of noble gases and nitrogen contained in a graphite nodule from the Canyon Diablo iron meteorite are planned in the near future in order to make a comparison with Hypatia. Furthermore this study demonstrates another time the ubiquitous presence of Q gases in primitive and differentiated meteorites even if its origin remains unknown.

All results presented in this section call for a contribution of volatile-rich bodies to the budget of volatile elements on Earth. However, the exact contribution of comets in this late addition remains unknown.

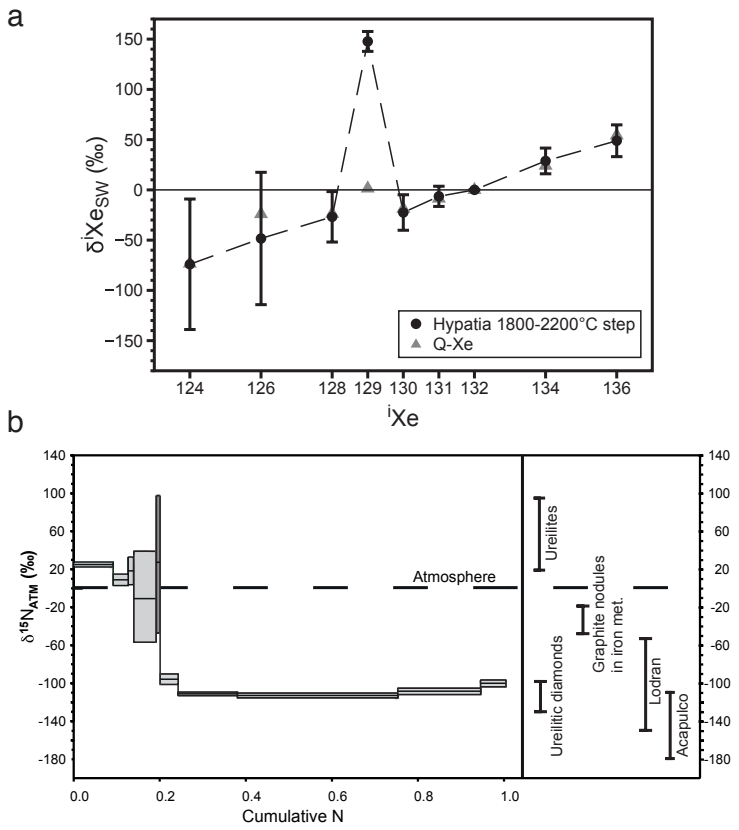

Fig. 1.10: Xe and N isotope data obtained from step-heating experiment on Hypatia samples. (a) Release of Q gases together with a ^{129}Xe excess du to the decay of extinct ^{129}I. (b) Isotopic composition of nitrogen released upon step-heating. A major light isotopic component was released with a δ^{15}N value of -110 ‰.

1.1.2 The early Earth: from the Hadean to the Archean

The Hadean is the first geological age of our planet and covers 600 Ma, from ≃4.5-4.6 to 4.0 Ga. It started after the last giant impact, probably the Moon-forming event, whose precise age is still debated and that probably melted a significant part of the Earth's mantle. Most of the rocky remnants of the first 600 Ma of our planet are zircon crystals contained in younger sedimentary rocks of the Jack Hills (Australia) geological area. However, numerous studies permitted to put constraints on this epoch by applying diverse analytical techniques to these crystals (Harrison, 2009). One major implication of these studies is that the oxygen isotope systematics applied to these crystals demonstrates that the protolith of these grains contained ^{18}O-rich clay minerals formed by interaction with liquid water (Mojzsis et al., 2001). This observation and other arguments reviewed by Harrison (2009) imply the presence of liquid water at the Earth's surface around 4.3 Ga and that this water was already acting as a weathering agent. Another implication of the presence of Jack Hills zircons is that they come from granites that constitute the upper crust. Measurements of initial ^{176}Hf/^{177}Hf ratios in these crystals are compatible with an early extraction of the continental crust during the Hadean (e.g. Blichert-Toft and Albarède (2008)). However, the crustal volumes at this time remain debated (e.g. Kemp et al. (2015)).

The Hadean was also the time for large-scale differentiation of the Earth's mantle. For example, Touboul et al. (2012) measured ^{182}W anomalies in Kostomushka komatiites signing the persistence, at least 2.8 Ga ago, of a reservoir that isolated from the whole mantle during the first tens of Ma of Solar System history. Anomalies are also found in Sm-Nd isotope systematics with a Sm/Nd fractionation occurring no later than 100 Ma after Solar System formation (Caro et al., 2003). Finally, noble gas studies of mantle-derived samples demonstrated the existence of an undegassed reservoir in the mantle with high Xe/I, Ar/K and He/(U+Th) ratios which has been isolated from whole mantle convection within the first 100 Ma of Solar System history (e.g. Marty (1989); Mukhopadhyay (2012)).

Even if Jack Hills zircons sign the presence of water on the surface, only little is known on the composition of the atmosphere during the Hadean and up to the early Archean. CO_2 and N_2 were probably dominating the budget of atmospheric gases as CH_4 released from meteoritical impacts would have been dissipated by photolysis within several tens of Ma (Kasting, 2014). The end of the Hadean (4.0 Ga) is often described as the epoch when the Earth looked much as it is today. However, the next section will demonstrate that the Earth had still very different geological and atmospheric features.

The Archean

The Archean spans a long period of 1.5 Ga of Earth's history (4.0 Ga to 2.5 Ga). This epoch is fundamental in Earth's geological history since life probably emerged at this epoch (Mojzsis et al., 1996). One remarkable feature of the Earth system during the Archean is that the Earth's mantle was probably hotter than today. Several observations and considerations argue in favor of higher temperatures for the mantle in the past. First, the whole budget of heat production was higher due to very active radioactivities, ongoing core crystallization, residual heat released during accretion. For example, Korenaga (2008) computed an internal heat flux up to 4 times higher than the modern one (around 10 TW) for the Earth 3.5 Ga ago. The widespread presence of komatiites during the Archean is probably a direct evidence that the mantle was hotter than today (Arndt and Nisbet, 2012). A somehow rough conclusion would be that, at this time, the Earth was very active and that the mantle presented a high degassing rate of its volatile elements due to a very active convection regime. However, this not clear how the high internal heat flux translated in terms of tectonics mode and extent of mantle convection (Arndt and Nisbet, 2012).

The Archean atmosphere

Despite the fact that the Archean covers one third of our planet's history, data about the composition

of Earth's atmosphere during this period are scarce due to the lack of an extended and well preserved geological record. The transition between the Archean and the Proterozoic (2.5 Ga to 0.542 Ga) is marked by an evolution of the atmosphere from an anoxic to an oxic state. In this section, key points on the Archean atmosphere and on main causes and consequences of the oxygenation of this atmosphere are presented and discussed in order to build a coherent framework for the interpretation of the results obtained during this study.

A low oxygen level in the Archean atmosphere

There are several lines of evidence for low levels of 0_2 ($< 10^{-5}$ PAL (Present Atmospheric Level)) in the Archean atmosphere from 3.9 to 2.2 Ga (Holland, 2006). This subject has been recently critically reviewed by Ohmoto et al. (2014) and some of the arguments for an O_2-poor Archean atmosphere are listed below:

- Absence of red beds usually formed by oxidation by O_2-rich water of Fe^{II} originally in biotites or hornblendes;
- Presence of detrital grains of uraninite or pyrite very labile in O_2-rich conditions;
- Presence of banded iron formations (BIFs) of Lake Superior type due to the abundance of Fe^{II} in deep oceans;
- Absence of Mo enrichment and isotopic fractionation in black shales (Anbar et al., 2007);

Mass-independent fractionation (MIF) of sulfur isotopes recorded in Archean sediments (Fig. 1.11) are one of the most clear evidence that oxygen atmospheric levels remained very low ($< 10^{-5}$ PAL) during the Archean (Farquhar and Wing, 2003). Photochemistry in the atmosphere under UV photons is the only known process able to produce significant S-MIF during photolysis of SO_2 and SO (Farquhar et al., 2001). Furthermore conservation of S-MIF signals is possible uniquely if products of UV-photolysis in the atmosphere, that are carrying $\Delta^{33}S$ with opposite signs, are separated in two categories: one with polymerized elemental S and another with sulfates produced by oxidation of elemental sulfur by CO_2 and H_2O. These two products then rain out and remain segregated in the rock record. Even if the mechanisms behind UV photolysis and conservation of the S-MIF signature in rocks are still not fully understood, production of mass-independent isotopic fractionation signatures in the past required: i) the presence of methane (CH_4), the reducing agent responsible for formation of polymers of elemental S; ii) very low levels of O_2 to ensure the formation of both sulfates and elemental sulfur carrying different $\Delta^{33}S$ signatures and to prevent any absorption of shortwave photons by tropospheric ozone (O_3); iii) a sufficient input of sulfur-bearing species to the atmosphere by abiotic or biogenic processes (Catling (2014) and refs. therein).

The faint young Sun paradox: how to warm the early Earth?

One major motivation for determining the molecular composition of the Archean atmosphere is based on one question: how to warm the early Earth sufficiently despite a faint young Sun? It has long been recognized that the Sun's luminosity is not constant and evolved from the Sun's formation to Present. Models of stellar evolution and measurements of solar analogs of different ages demonstrate that the solar energy input was around 25 % lower than today during the Archean (Sagan and Chyba, 1997). In these conditions, a modern-like composition for the Archean atmosphere would have led to a snowball Earth because modern abundances of greenhouse warming gases would not have been sufficient to compensate such a lower luminosity. However, there are several lines of evidence for the presence of liquid water at this time (Feulner, 2012; Mojzsis et al., 2001). The composition of the Archean atmosphere was thus probably different from Present times. Feulner (2012) reviewed ways to warm the early Earth with enhanced greenhouse warming driven by higher atmospheric concentrations of NH_3, CH_4 and CO_2 and pointed out the need for geochemical constraints on

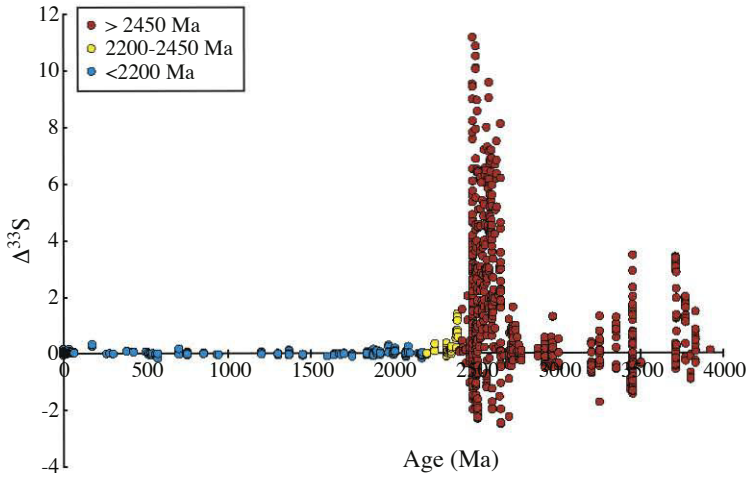

Fig. 1.11: Mass-independent fractionation of S (represented by $\Delta^{33}S$) in the geological record versus age. Adapted from Johnston (2011).

the abundances of these molecules in the ancient atmosphere. Goldblatt et al. (2009) proposed another way to solve the faint young Sun paradox. N_2 is not a greenhouse gas by itself but a higher partial pressure of this gas in the past would have amplified the greenhouse impact of other gases by broadening absorption lines. Doubling the partial pressure of nitrogen would thus have led to a global warming of 4.4 °C. However, Marty et al. (2013) demonstrated by using Ar-N_2 correlations on fluids contained in Archean samples that the atmospheric end-member presented a modern-like $N_2/^{36}Ar$ ratio corresponding to a modern-like partial pressure of nitrogen (p_{N_2}).

Studying fluids trapped in ancient samples has thus the potential to constrain the elemental composition of the ancient atmosphere and to follow its evolution with time.

Evolution of the atmosphere: When did O_2 rise in the atmosphere?

One of the major question regarding the features of the surface environments of the early Earth and thus the possibility for the emergence of aerobic life is when did O_2 become a major gas in the Earth's atmosphere? The modern concentration of O_2 is 21% by volume whereas the partial pressure during the major part of the Archean (3.5 - 2.45 Ga), inferred from S-MIF (see section 1.1.2) was probably lower than 10^{-5} PAL (Present Atmospheric Level) (Farquhar and Wing, 2003). The transition from a past reducing atmosphere to a modern-like O-rich environment is still ambiguous as a direct measurement of the p_{O_2} in ancient rocks is impossible due to the high reactivity of O_2. Estimations of the evolution of the quantity of oxygen in the Earth's atmosphere are thus based on direct geochemical proxies such as S, U, Mo. Even if some debates remain on the ability of these tools to track the evolution of the Earth's oxygenation (e.g. Domagal-Goldman et al. (2008) for the interpretation of S isotopic data), a big picture is emerging (Fig. 1.12) (Lyons et al., 2015).

S-MIF recorded in Archean sediments is a strong indication that p_{O_2} was very low at least until 3.0 Ga ago. Between 3.0 and 2.5 Ga ago the decrease in the extent of the S-MIF argues in favour of a slightly higher partial pressure (maybe 10^{-2} PAL, Farquhar and Wing (2003)) or to some episodes of so-called "whiffs" of oxygen schematically represented by the blue arrows in Fig. 1.12 (Anbar et al., 2007). The transition, between 2.5 and 2.0 Ga, to an oxygenated atmosphere (the so-called Great Oxidation Event) is well documented even if the exact mechanisms and the actors of this major change are still debated. Recently, Catling (2014) reviewed the source and sinks of oxygen for the early and modern Earth. The

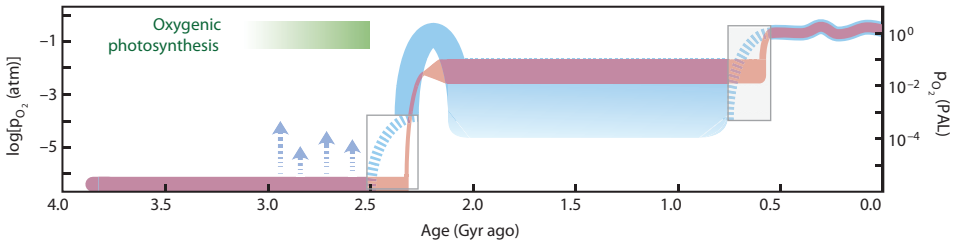

Fig. 1.12: Evolution of the partial pressure of O_2 in the Earth's atmosphere with time. The blue range denotes uncertainties on the mode of changing of the p_{O_2}. Adapted from Lyons et al. (2015).

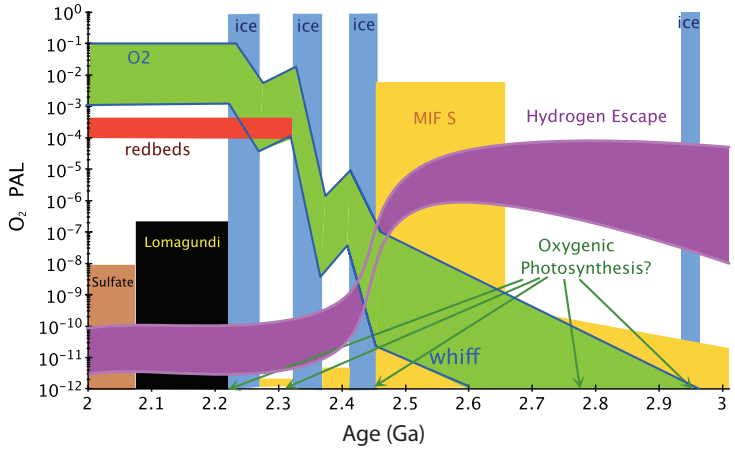

Fig. 1.13: Schematic view of the Great Oxidation Event and its relation with hydrogen escape. Hydrogen escape trend is only indicative. Modified after Zahnle et al. (2013).

author pointed out the major role played by hydrogen escape as an indirect source of oxygen through the simplified equation 1.1:

$$2H_2O \rightarrow 4H(\uparrow space) + O_2 \tag{1.1}$$

Even if this source of oxygen is limited today compared to other geological processes such as carbon or pyrite burial, hydrogen escape was much more vigorous in the past particularly because of an enhanced EUV flux from the young Sun (Claire et al., 2012). Zahnle et al. (2013) argued that past hydrogen escape was a major actor of the progressive oxidation of the Earth's surface (Fig. 1.13). In this model, onset of oxygenic photosynthesis was not sufficient to switch from a reduced to an oxidized atmosphere because O_2 produced py photosynthesis was not stable in a reduced atmosphere. Hydrogen escape appears thus necessary to make the transition from a reduced to a more oxidized atmosphere leaving abundances of O_2, produced by photosynthesis, going up.

It must be noticed here that hydrogen escape to space is not the unique hypothesis for driving Earth's oxygenation. For example, Gaillard et al. (2011) and Ciborowski and Kerr (2016) proposed that peaks of sub-aerial volcanism around 2.45 Ga released large amounts of sulphate to the oceans. Subsequent reduction of this sulphate released significant amounts of oxygen ending up in the atmosphere and driving the Great Oxidation Event.

All observations presented above suggest a very different state of the Archean Earth compared to the modern one. The major change in the Earth's atmosphere happened at the end of the Archean at ca. 2.45 Ga when the Earth surface reservoirs became oxygenated.

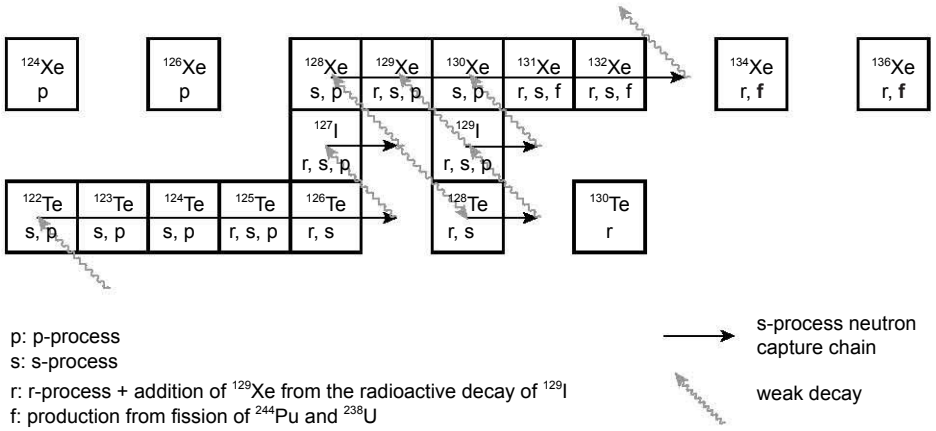

Fig. 1.14: Positions of the stable isotopes of xenon ($^{124-136}$Xe) in the chart of nuclides. Nucleosynthetic productions pathways are indicated with letters below each isotope. Modified after Clayton and Ward (1978)

1.2 Introduction to *Xenology*: principles and applications

The physical and chemical features of xenon and its nine isotopes are described in this part. The relationships between the xenon components in the solar system are also presented as well as key points on I-Pu-Xe systematics. Finally, the two major issues regarding the origin and evolution of atmospheric xenon are described as well as their potential ways of resolution.

1.2.1 Isotopic structure of Xenon and physico-chemical caracteristics

Xenon (Z=54) belongs to the family of elements "heavier than iron" and its isotopes (9) were thus produced by particular nucleosynthetic processes occurring mainly during supernovae events (Heymann and Dziczkaniec, 1979). The position of Xe in the chart of nuclides appears in Fig. 1.14. Three main nucleosynthetic processes are involved in the production of xenon isotopes (Clayton and Ward, 1978) (Fig. 1.14):

- p-process: proton capture reaction, ^{124}Xe and ^{126}Xe are the two rarest Xe isotopes and are only produced by this process;
- s-process: slow-neutron capture process where the neutron capture rate is small compared to the beta decay of the unstable nuclides (Schatz, 1986);
- r-process: rapid neutron capture process. ^{124,126,128,130}Xe isotopes are not produced through this process because they are shielded by the corresponding stable Te isotopes (Fig. 1.14).

Xenon isotopic compositions measured for components of the modern solar system are thus reflecting the nucleosynthetic mix of p-, s- and r-processes present at the time of Solar System formation ca. 4.57 Ga ago (Patterson, 1956). It is worth noting here that there are numerous different Xe components defined from analyses of meteorites (Ott, 2014). Some of them, for example the G-Xe, present nucleosynthetic anomalies (Lewis et al., 1994) demonstrating a certain level of heterogeneity in the nucleosynthetic mix of xenon in the early Solar System.

Among other noble gases, Xe is not only contributed by various nucleosynthetic pathways but it also presents unique physico-chemical features. First, its ionization potential ($\simeq$ 12.13 V corresponding to $\simeq$ 102.2 nm) is the lowest among noble gases and is also lower than the ionization potential of hydrogen (13.6 eV). Furthermore, xenon presents an extended photo-absorption cross section up to 150 nm in the VUV spectrum region. Fig. 1.15 depicts the photo-ionization and photo-absorption of xenon for wavelengths

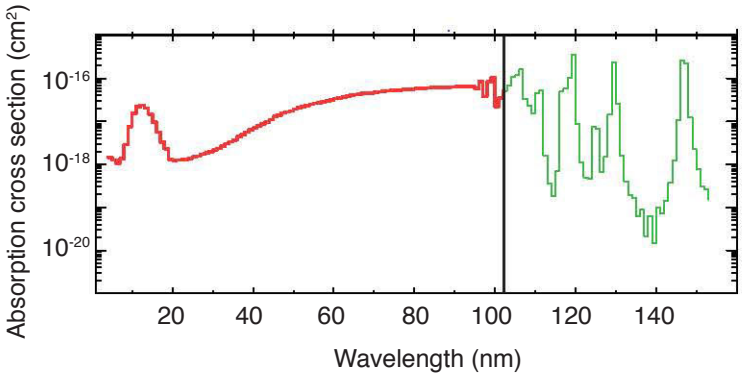

Fig. 1.15: Photo-absorption (green line) and photo-ionization (red line) cross sections of Xe. The wavelength for ionization of Xe is indicated with the vertical black line at 102 nm. Modified from Hébrard and Marty (2014). Data are from Chan et al. (1992).

between 0 and 160 nm. The two features presented above make xenon prone to absorb photons and to be ionized by these particles (Hébrard and Marty, 2014).

The electronic properties of Xe atoms make also this noble gas prone to react with other atoms and to form stable compounds such as Xe oxides (Haner and Schrobilgen, 2015). Xenon could also enter in the framework of rock-forming minerals such as perovskite (Britvin et al., 2015).

1.2.2 I-Pu-Xe systematics and the dating of reservoirs closure

In addition to nucleosynthetic processes, radioactive decay of extinct ^{129}I (β^-, $t_{1/2}$=16 Ma) and spontaneous fissions of extinct ^{244}Pu ($t_{1/2}$=82 Ma) and extant ^{238}U ($t_{1/2}$=4.46 Ga) have produced several Xe isotopes (^{129,131,132,134,136}Xe). These different modes of decay and variable half-lives led to the building of useful chronometers able to put constraints on the time of closure of reservoirs (atmosphere, mantle) during the final stages Earth's accretion (I-Xe) or later on (I-Pu-Xe). Theoretical principles on Xe chronology are also described in the introduction of the paper presented in section 3.4 of Chapter 3 and in the paper dealing with the origin of mantle Xe (section 3.1 of Chapter 3) but some of the key features are presented here as well as recent studies shedding light on the early evolution of the terrestrial mantle and atmosphere.

^{129}I decays into ^{129}Xe with a half-life of 15.7 Ma (Katcoff et al., 1951). Whatever their starting isotopic compositions, both the atmosphere and the mantle contain ^{129}Xe excesses attributed to the decay of extinct ^{129}I (Reynolds, 1960; Staudacher and Allegre, 1982). These observations demonstrate that the Earth formed and differentiated while ^{129}I decay was still ongoing i.e. during the first tens of million years after the solar system formation.

Compared to the straightforward deduction of atmospheric and mantle ^{129}Xe excesses from the decay of extinct ^{129}I (Caffee et al., 1999; Porcelli and Ballentine, 2002), deconvolution of $^{131-136}$Xe excesses coming from spontaneous fissions of ^{238}U or ^{244}Pu in mantle-derived rock or in the atmosphere is sometimes difficult due to the lack of knowledge on starting primordial compositions for the Earth's mantle or the atmosphere (see section 1.2.4). Furthermore, fission spectra of Xe isotopes produced by spontaneous fissions of ^{238}U and ^{244}Pu are also very similar (Kunz et al., 1998) except for the ^{132}Xe/^{136}Xe ratio which is often discriminant (Fig. 1.16). Parai and Mukhopadhyay (2015) recently used new analyses and literature data on mantle-derived samples (MORB samples from the upper mantle or plume-derived samples from the lower mantle) to run a numerical model which estimates the proportions of air, primordial, radiogenic and fissiogenic components for each magmatic source. This model is able to compute $^{136}Xe_{Pu}/^{136}Xe_{Pu+U}$ (Fig. 1.17(a)) and $^{129}Xe^*/^{136}Xe_{Pu}$ (Fig. 1.17(b)) ratios for each possible primordial composition. The two major outcomes of this study are:

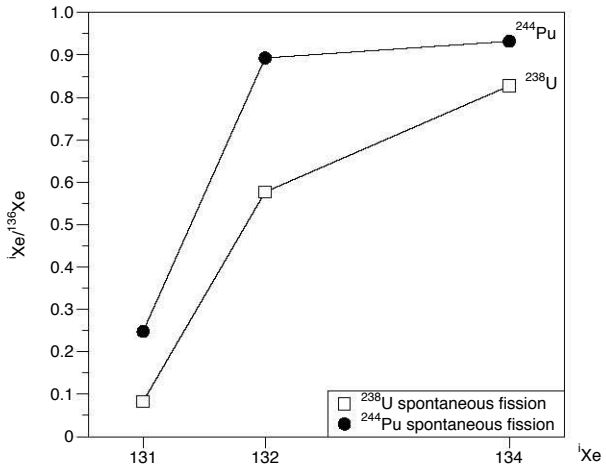

Fig. 1.16: Fission spectra for spontaneous fission of ^{238}U and ^{244}Pu normalized to ^{136}Xe. Data are from Ragettli et al. (1994).

- Lower mantle (plume-influenced) samples have higher $^{136}Xe_{Pu}/^{136}Xe_{Pu+U}$ ratios than samples derived from upper-mantle sources demonstrating that the lower mantle is less degassed (more plutogenic) than the upper-mantle;

- Samples from the upper mantle show higher $^{129}Xe^{*}/^{136}Xe_{Pu}$ ratios than those from the lower mantle. This is paradoxical since, in the case of a homogeneous initial $^{129}I/^{244}Pu$ ratios in the silicate Earth, this observation would require an earlier closure time for the upper mantle than for the lower mantle. To circumvent this paradox, Marty (1989) and Mukhopadhyay (2012) suggested an inhomogeneous accretion with a higher contribution of volatile-rich (and thus iodine-rich) bodies to the upper-mantle during the final stages of terrestrial accretion.

Xenology applied to the Earth's mantle or atmosphere requires thus the knowledge of the starting composition of xenon accreted on Earth in order to constrain the degassing history of our planet. Differences between the possible cosmochemical ancestors of Earth's xenon are presented in section 1.2.3.

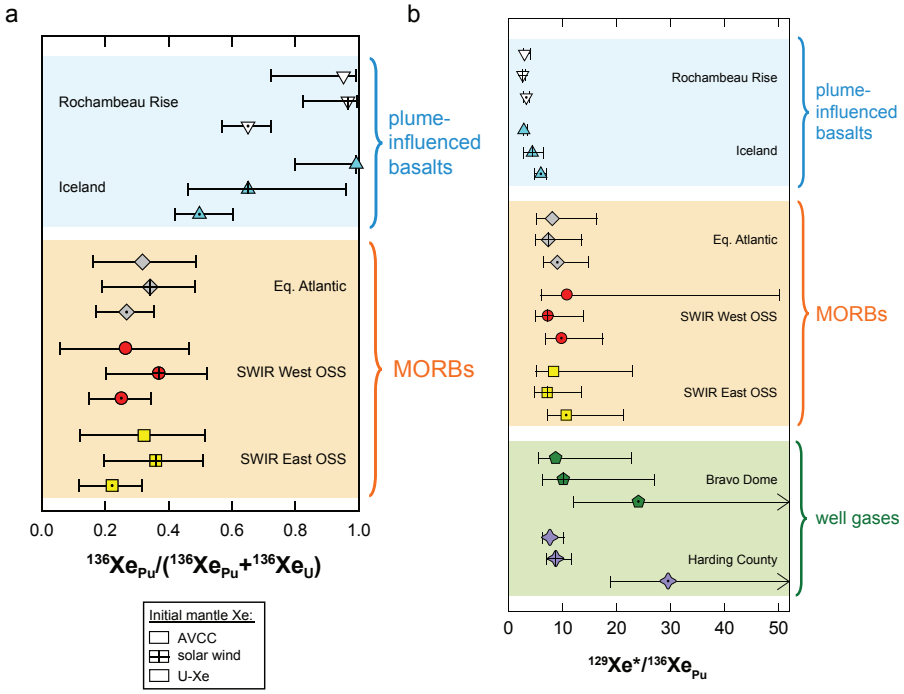

Fig. 1.17: Deconvolution of radiogenic and fissiogenic (from spontaneous fission of ^{238}U or ^{244}Pu) xenon in mantle-derived sampes. (a) $^{136}Xe_{Pu}/^{136}Xe_{Pu+U}$ ratios are diagnostic of the extent of degassing of the source. (b) $^{129}Xe^*/^{136}Xe_{Pu}$ ratios suggest a more important contribution of wet-rich (I-rich) bodies to the upper mantle. Figure adapted from Parai and Mukhopadhyay (2015).

1.2.3 Relations between solar system components

The study of xenon contained in a great variety of solar system materials and extracted by different techniques (bulk heating, step-heating, crushing, chemical separation) led to the definition of an extended *menagerie* of Xe components defined by different isotopic compositions, release temperatures etc. (Ott, 2014). Isotopic compositions of Xe components relevant to this study and discussed in this section are listed in Table 1.1. The following sections are focused on the potential relationships between solar (SW-Xe), meteoritic (Q-Xe) and atmospheric Xe.

Table 1.1: Isotopic composition of Xe (normalized to ^{130}Xe=1) for different solar system components. Error at 1σ.

Component	^{124}Xe	±	^{126}Xe	±	^{128}Xe	±	^{129}Xe	±	^{131}Xe	±	^{132}Xe	±	^{134}Xe	±	^{136}Xe	±
								^{130}Xe = 1								
Air[a]	0.0234	0.0001	0.0218	0.0002	0.4715	0.0014	6.496	0.019	5.213	0.017	6.607	0.010	2.563	0.009	2.176	0.006
Q-Xe[b]	0.0281	0.0003	0.0251	0.0002	0.5077	0.0031	6.436	0.034	5.056	0.022	6.177	0.023	2.335	0.016	1.954	0.014
SW-Xe[c]	0.0298	0.0009	0.0252	0.0011	0.5103	0.0044	6.306	0.033	5.004	0.028	6.061	0.029	2.237	0.014	1.819	0.011
U-Xe[d]	0.0293	0.0001	0.0253	0.0001	0.5083	0.0006	6.286	0.006	4.996	0.006	6.047	0.006	2.126	0.004	1.657	0.003
NEA-Xe[d]	0.0234	0.0001	0.0218	0.0002	0.4715	0.0014	6.053	0.029	5.187	0.007	6.518	0.013	2.47	0.013	2.075	0.013
Mars-Xe[e]	0.0246	0.0013	0.0214	0.0013	0.4763	0.006	15.55	0.16	5.139	0.035	6.481	0.038	2.597	0.018	2.277	0.016

[a]Basford et al. (1973)
[b]Busemann et al. (2000)
[c]Meshik et al. (2014)
[d]Pepin (1991)
[e]Swindle (2002)

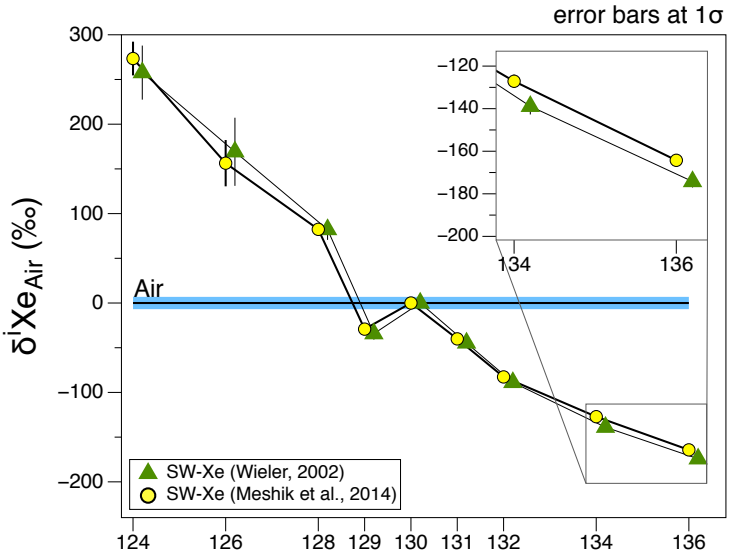

Fig. 1.18: Isotopic spectrum of Solar Wind Xe compared to the Earth's atmosphere and expressed with the delta notation (Eqn. 1.2). The new values by Meshik et al. (2014) are very similar to those from Wieler (2002) except for ^{134}Xe and ^{136}Xe that are slightly enriched in the new isotopic composition.

Solar Xe

Because the Sun hosts the major part of the mass of the solar system ($>$ 99 %), knowing the isotopic composition of xenon of this major reservoir is a major question in Xenology. First results of the solar composition were obtained by analyzing Al-foils exposed to the Solar Wind (SW) impacting the surface of the Moon during Apollo missions as well as recovered lunar soil samples (see Wieler (2002) and refs. therein). Even if these preliminary analyses were successful in defining SW-Xe (Fig. 1.18), the recent Genesis mission, launched by NASA, collected the Solar Wind directly in space and provided similar but more precise data (Meshik et al., 2014) (Fig. 1.18). For Genesis results, the isotopic composition of Xe is very similar to the one determined previously excepted for a slight depletion on ^{134,136}Xe (cf. magnification in Fig.1.18). This depletion may reflect the presence of some ^{134,136}Xe excesses in lunar samples due to the spontaneous fission of ^{244}Pu ($t_{1/2}$ = 82 Ma) for example. Recently, Marti and Mathew (2015) defined a solar component labeled "Sol-Xe" very similar to the SW-Xe defined by Meshik et al. (2014). In this study, we will adopt the values defined by Meshik et al. (2014). It must be noted here that there is no certainty that the SW-Xe sampled by the Genesis mission properly reflects the solar composition as the ejection of the Solar Wind from the Sun may induced an isotopic fractionation of Xe such as the fractionation observed for He, Ne and Ar isotopes (Heber et al., 2012). A correction based on fractionation factors computed for He is tentative. However, there is no certainty on the linear behavior of the isotopic fractionation during ejection of the Solar Wind from the outer layers of the Sun.

The enigmatic Q component

For Ar, Kr and Xe, one component is dominating the noble gas budget of primitive meteorites: the Q component (Ott, 2014). Xenon in this Q component (Q-Xe) presents an isotopic composition very different from the solar composition defined above except for ^{126}Xe/^{130}Xe and ^{128}Xe/^{130}Xe ratios that are indistinguishable from SW-Xe. This isotopic composition is represented in Fig. 1.19 in delta notation relative to

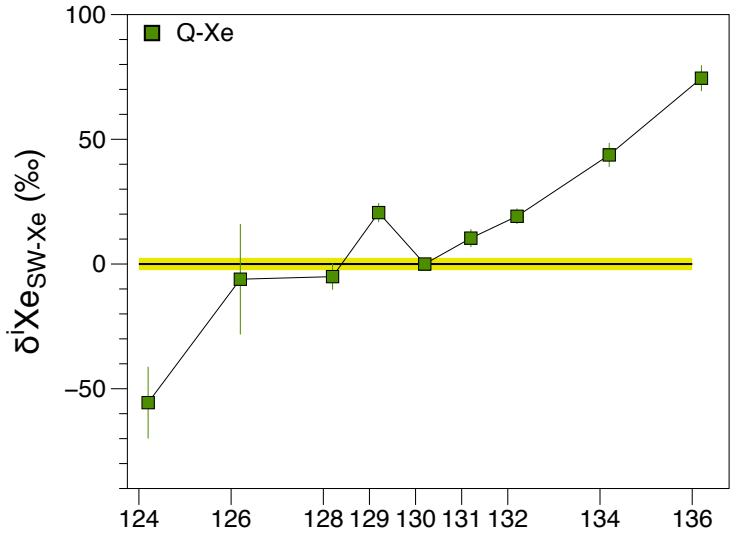

Fig. 1.19: Isotopic compositions of Q-Xe normalized to ^{130}Xe and to the solar composition (SW-Xe) and expressed with the delta notation. See Table 1.1 and refs. therein for the isotopic compositions of these components.

the isotopic composition of SW-Xe (Eqn. 1.2):

$$\delta^i Xe = [\frac{(\frac{^iXe}{^{130}Xe})_{Q-Xe}}{(\frac{^iXe}{^{130}Xe})_{SW-Xe}} - 1] \times 1000 \quad (1.2)$$

Q-Xe presents a well-resolved ^{129}Xe excess attributed to the decay of extinct ^{129}I ($t_{1/2}$ = 15.7 Ma). A depletion in ^{124}Xe and $^{131-136}$Xe excesses are obvious even if their origins remain debated (see next section).

The nature of phase Q is, up to now, only "operational" i.e. this component is isolated by chemical treatment and its main chemical characteristics are: resistance to HF + HCl and degassing when oxidation by HNO_3 (Busemann et al., 2000). Because the residue obtained after these chemical treatments is enriched in carbon, a carbonaceous nature for phase Q has often been advocated (Ott et al., 1981). However, one study demonstrated that, sometimes, releases of carbon and of noble gases do not occur over the same temperature range upon combustion (Verchovsky et al., 2012). In this study, carbon was released at 500°C whereas Xe was released for temperatures higher than 1000°C. This observation leaves space for other carriers of phase Q that are sulfides. Meteoritic sulfides are commonly found in meteorites and a preliminary study already demonstrated the presence of Q gases in sulfides located around chondrules (Vogel et al., 2004).

During this study, the potential sulfurous nature of phase Q has been analytically and theoretically explored. This work led to the publication of a paper in *Geophysical Research Letters* (Marrocchi et al., 2015) (a complete edited version of the paper is placed in Annexe 5.2). In this study, experimental work demonstrates that noble gases trapped within meteoritic sulfides have chemical and thermal behaviors similar to Q gases. Furthermore, we demonstrate that the isotopic composition of Q-Xe can be reproduced by a mass-dependent isotopic fractionation of SW-Xe together with the addition of ^{129}Xe from the decay of extinct ^{129}I with iodine abundances compatible with those reported for meteoritic sulfides (Fig. 1.20). However, U contents required to explain $^{131-136}$Xe excesses reach 50 ppm. This value appears unusually high compared to abundances of uranium measured in terrestrial sulfides (in the ppb range) but more analyses of uranium abundances in extraterrestrial sulfides are required. Elemental and isotopic analyses of noble gases in extraterrestrial sulfides are also required to decide whether or not sulfides are possible carriers

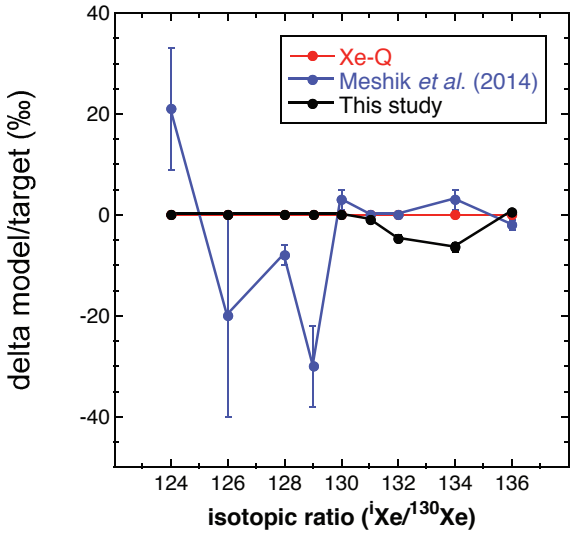

Fig. 1.20: Modeled isotopic composition of Q-Xe corrected for the radiogenic (0.21 ppm ^{129}I) and fissiogenic (9.63 ppm ^{238}U) contributions. The model is compared to a recent model based on the mixing of fractionated SW-Xe with HL-Xe and S-Xe (Meshik et al., 2014). Adapted from Marrocchi et al. (2015).

of the phase Q.

Relations between Solar Sytem Xe components

The "classical" view of the relationship between Q-Xe and SW-Xe is that Q-Xe originated from mass-fractionation of SW-Xe accompanied by the addition of diverse nucleosynthetic anomalies (S-Xe, HL-Xe) and/or products ($^{131-136}$Xe) of the spontaneous fission of ^{238}U and ^{244}Pu and by the presence of ^{129}Xe excess due to the decay of extinct ^{129}I (Ott, 2014; Marrocchi et al., 2015; Meshik et al., 2014; Crowther and Gilmour, 2013). However, when looking precisely to the isotopic structure of these two cosmochemical components (Fig. 1.19) and thanks to the precise determination of the isotopic composition of SW-Xe (Meshik et al., 2014), the difference between SW-Xe and Q-Xe on light isotopes is mainly due to the depletion of ^{124}Xe for Q-Xe relative to SW-Xe (Fig. 1.19). This observation means that the mass-dependent fractionation advocated to explain the difference between Q-Xe and SW-Xe may not be so obvious even if such an enrichment in heavy isotopes and depletion in light isotopes is now easily reproduced in laboratory experiments when Xe ions are in contact with organic matter (Kuga et al., 2015; Marrocchi et al., 2011). If ionization and isotopic fractionation in contact with organic matter are the correct processes transforming SW-Xe into Q-Xe with a mass fractionation measured on ^{124}Xe, a way to produce ^{126}Xe and ^{128}Xe excesses relative to the isotopic fractionation remains to be found.

1.2.4 Atmospheric Xenon: paradox, plausible explanations and implications

Atmospheric xenon presents striking features. It is elementally depleted and isotopically fractionated relative to potential cosmochemical ancestors. Furthermore, even after correction for this strong isotopic fractionation of unknown origin, it does not seem to be directly related to the cosmochemical precursors presented in the previous section. One major goal of this study was to understand these features that are described in this section.

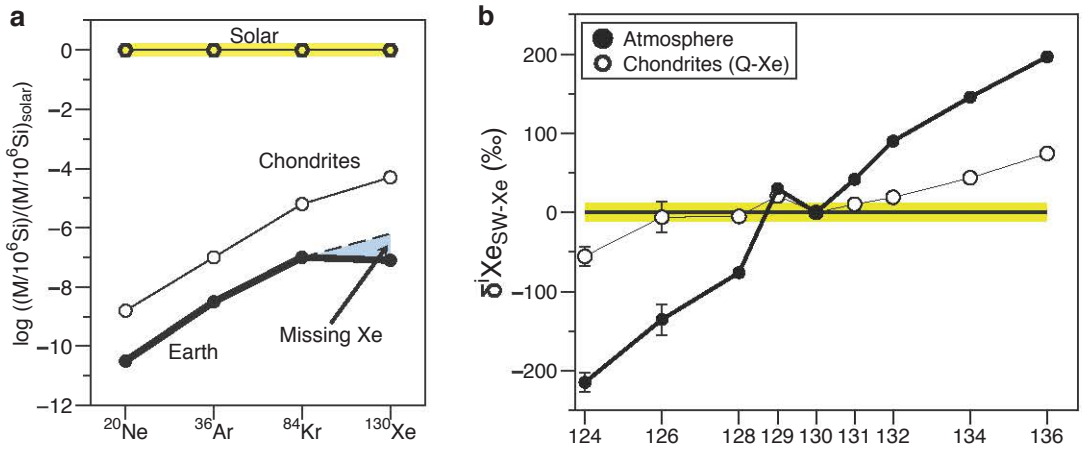

Fig. 1.21: Illustration of the xenon paradox. (a) Abundance plot showing the abundances of noble gases (Ne, Ar, Kr, Xe) on Earth and in chondrites normalized to the abundance of Silicium and to the solar composition (adapted from Porcelli and Ballentine (2002)). (b) Isotopic compositions of xenon measured in meteorites and in the Earth's atmosphere normalized to the solar composition. Isotopic compositions are from Table 1.1. Atmospheric xenon is enriched in heavy isotopes and depleted in light isotopes compared to chondritic or solar compositions.

The xenon paradox: elemental depletion and isotopic fractionation

Nobles gases on Earth and in chondritic meteorites are depleted relative to the solar composition (Fig. 1.21(a)) (Porcelli and Ballentine, 2002). For Ne, Ar and Kr the Earth follows globally the same depletion pattern than chondrites but the case of xenon is different. Atmospheric xenon is depleted in the Earth's atmosphere by a factor of 20 compared to what one would expect if the Earth was following the same depletion pattern than chondrites. This is the first feature of the xenon paradox, there is a "missing xenon" on Earth (Krummenacher et al., 1962).

The second feature of the xenon paradox is displayed in Fig. 1.21(b). Atmospheric xenon is enriched in heavy isotopes and depleted in light isotopes compared to both chondritic or solar compositions. The corresponding isotopic fractionation reaches 30-40 ‰.u^{-1}. The depleted abundance together with the isotopic fractionation of atmospheric xenon are the two features of the so-called "xenon paradox". It must be noticed here that, under the goal of parsimony, any explanation proposed for one of the two features must also consider the other feature as the depletion and the isotopic fractionation might be closely related.

The need for U-Xe to build the atmosphere?

Atmospheric xenon presents another striking feature regarding its origin. Even if analyses of mantle-derived samples demonstrated the existence of solar Ne (Honda et al., 1987) and chondritic heavy noble gases (Holland et al., 2009) incorporated into the Earth's mantle during accretion, atmospheric Xe cannot be simply derived from these known cosmochemical components by mass-dependent isotopic fractionation. Indeed, it has been recognized for several decades that solar (SW-Xe) and chondritic (Q-Xe or AVCC-Xe) are far too enriched in heavy xenon isotopes (particularly ^{134}Xe and ^{134}Xe) to match, after mass-dependent isotopic fractionation, a potential non-radiogenic/fissiogenic primitive component (NEA-Xe, Table 1.1) for the Earth's atmosphere (Igarashi, 1995; Pepin, 1991). This feature is shown in Fig. 1.22 where the isotopic composition of the modern atmosphere falls systematically at the left-side of the curves of the mass-dependent isotopic fractionation of SW-Xe or Q-Xe. Because there is no known specific process able to remove only ^{136}Xe from the atmosphere, the starting isotopic composition, after correction for isotopic fractionation, must present a deficit in ^{136}Xe relative to other potential primordial components (SW-Xe or Q-Xe).

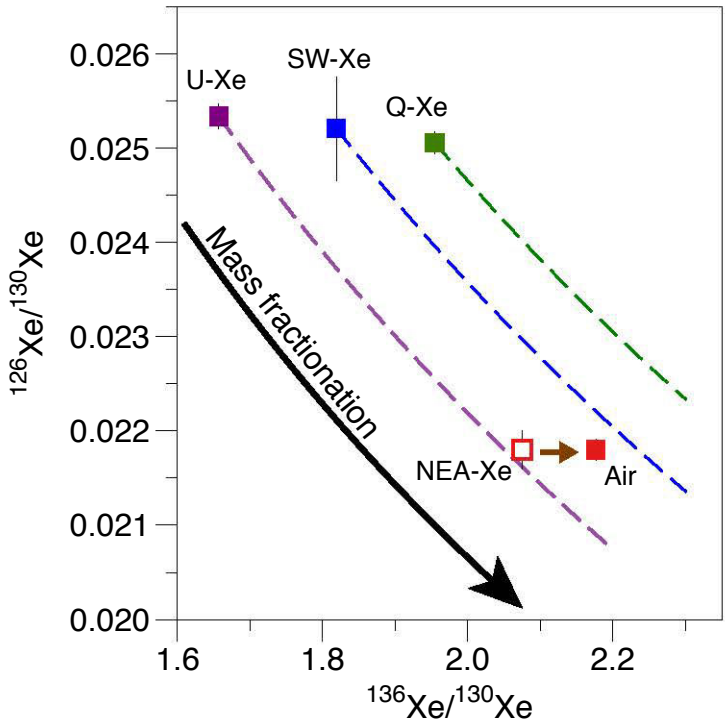

Fig. 1.22: Three-isotope plot showing the primordial components of the solar system Q-Xe, SW-Xe, U-Xe (isotopic ratios and errors (2σ) are from table 1.1). Only the mass-dependent isotopic fractionation (see thick black arrow) of U-Xe is able to lead to a non-radiogenic atmospheric xenon (NEA-Xe) that subsequently moves toward the modern atmosphere with addition of ^{244}Pu-derived fissiogenic Xe (Pepin, 1991).

Several studies (Pepin, 1991; Takaoka, 1972) tried to address this fundamental problem by statistically analyzing the interception in isotopic hyperplanes (7 dimensions) between the isotopic composition of xenon in the atmosphere, in bulk chondrites and in the Sun. These theoretical studies determined an isotopic composition labeled U-Xe (see Table 1.1) or Primitive Xe in the case of (Takaoka, 1972). "U" is here for "Ur" meaning "Primitive" not "Uranium". This component, almost identical in both studies, was interpreted as a possible primitive composition of Xe for the terrestrial atmosphere. The isotopic composition of the U-Xe component (Fig. 1.23) is almost similar to SW-Xe except for the heavy isotopes ^{134}Xe and ^{136}Xe that are depleted by 5 and 9 % respectively (Table 1.1). This depletion, of unknown origin, is the key to explain why U-Xe is a tentative primordial component for the Earth's atmosphere. Indeed after mass-dependent isotopic fractionation, $^{131-136}$Xe isotopes remain depleted relative to the modern atmosphere leaving space for some addition by the spontaneous fission of ^{244}Pu and/or ^{238}U. Recently, Meshik et al. (2015) proposed that U-Xe is not a real existing component but rather than the starting isotopic composition for the Earth's atmosphere is a slightly mass-fractionated SW-Xe. This primitive composition has to have been subsequently mass-fractionated to a higher level in order to match light isotopes of the modern atmosphere. The point here would be that Xe produced from fission of ^{244}Pu was depleted in $^{131-134}$Xe (and thus relatively enriched in ^{136}Xe) in the early atmosphere due to "chemical separation" of radioactive precursors in a similar manner to what was measured in samples from the natural Oklo nuclear reactor (Meshik et al., 2000). A major part of this early atmosphere would have been subsequently lost leaving a terrestrial fission Xe enriched in $^{131-134}$Xe, matching fission Xe for the modern atmosphere computed by Igarashi (1995). The potential problem of this theory is that, whatever the nature of the fission component, the isotopic fractionation of SW-Xe required to match the isotopic composition of light Xe isotopes (i.e. $^{124-128}$Xe/^{130}Xe) still leads to a ^{136}Xe excess relative to the modern atmosphere (Fig. 1.22) and this observation is valid whatever the yield of the fission component (enriched or depleted in ^{136}Xe) subsequently degassed by the mantle into the

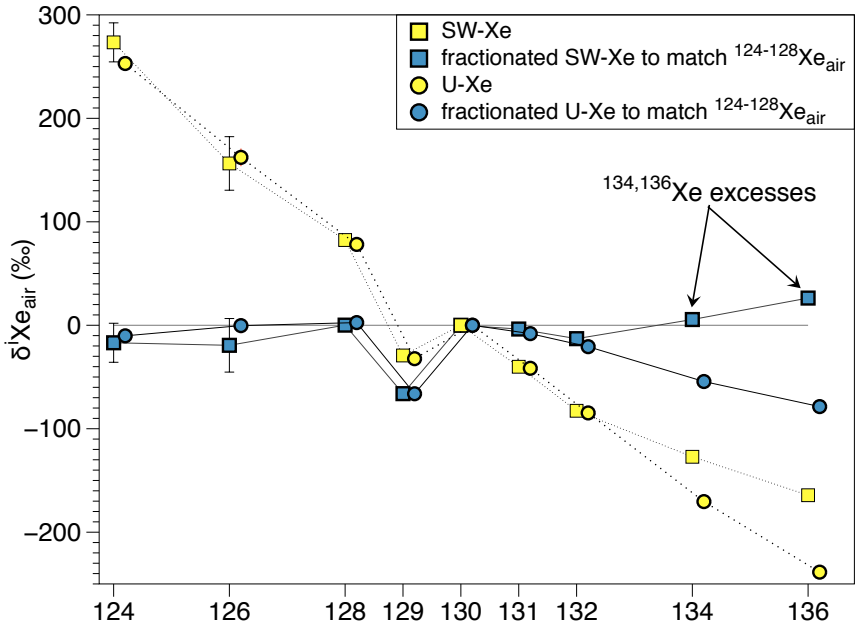

Fig. 1.23: Isotopic spectra of SW-Xe and U-Xe (before and after mass-dependent isotopic mass fractionation) relative to the isotopic composition of atmospheric Xe. Error bars at 1σ and are usually smaller than the symbols for $^{129-136}$Xe. This plot, adapted from Pepin and Porcelli (2002), demonstrates that only U-Xe is a potential primordial component for the Earth's atmosphere as fractionation of SW-Xe leads to $^{134-136}$Xe excesses. The situation is even worse for Q-Xe that already carries ^{134,136}Xe excesses (Busemann et al., 2000).

atmosphere (Ballentine and Burnard, 2002).

Whatever its nature and mode of formation U-Xe seems necessary to build the terrestrial atmosphere (Avice and Marty, 2014; Pepin, 1991) and despite an active search it has never been undoubtedly found in any extraterrestrial material (Pepin, 1994). Only one step-heating experiment on the Tatahouine diogenite probably coming from the upper crust of the Vesta asteroid leads to results with a xenon isotopically similar to U-Xe for the 1000 and 1200°C steps (Michel and Eugster, 1994). However the isotopic composition is also very similar to SW-Xe at the 2σ level where only a slight ^{136}Xe deficit might still be present.

Previous attempts to solve the Xe paradox

Dauphas and Morbidelli (2014) recently reviewed previous theoretical models that tempted to explain the xenon paradox (elemental depletion and isotopic fractionation) by using a combination of hydrodynamic escape episodes and storage of noble gases (and specially Xe) in the Earth's mantle or early preferential degassing of xenon (Pepin, 1991, 1997; Tolstikhin and O'Nions, 1994).

Pepin (1991) proposed a model to solve the xenon paradox. This model is described in Fig. 1.24 modified after Dauphas and Morbidelli (2014). Abundances of noble gases are normalized to the solar composition and expressed in log units. Numbers close to dots correspond to the fractionation factors (in permil per atomic mass unit, ‰.u^{-1}) defined by Dauphas and Morbidelli (2014). For example, for xenon it corresponds to

$$F_{Xe} = \frac{\left(\frac{(^{128}Xe/^{130}Xe)_{\text{reservoir}}}{(^{128}Xe/^{130}Xe)_{\text{Solar}}} - 1\right) \times 1000}{128 - 130}$$

The first step of this model (Fig. 1.24 (a)) is the elemental and isotopic fractionation (red circles) of atmospheric noble gases, originally having solar isotopic compositions (white circles), by giant impact-driven

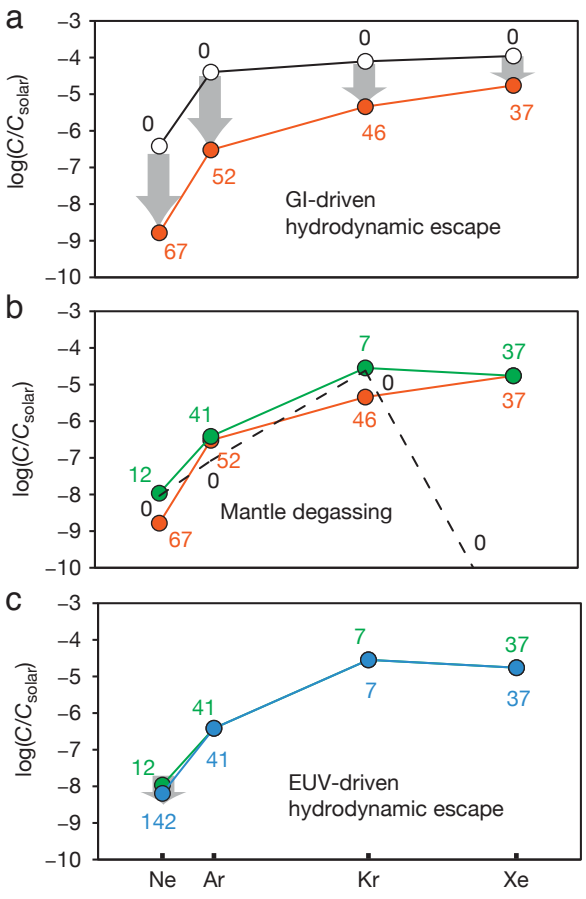

Fig. 1.24: Hydrodynamic escape and preferential Xe retention model for the origin of Earth's noble gases proposed by Pepin (1991). (a) Early hydrodynamic escape of all noble gases (b) Mantle degassing with preferential retention of Xe in the Earth's mantle (c) Last episode of EUV-driven escape to match the abundance and isotopic composition of atmospheric Ne. See text for details on the steps. Figure adapted from Dauphas and Morbidelli (2014).

hydrodynamic escape. Light noble gases are more depleted and isotopically fractionated than heavy ones during this escape episode. The second step (b) is the subsequent degassing of solar Ne, Ar and Kr originally stored in Earth's mantle. This degassing replenished the atmosphere with solar Ne, Ar and Kr and thus decreased their isotopic fractionations. During this degassing episode, Xe remained stored in the Earth's mantle. This preferential storage permitted the persistence of highly fractionated Xe in the atmosphere (37 $‰.u^{-1}$). A last EUV-driven hydrodynamic escape episode was necessary to fractionate Ne isotopes (c). The major difficulty of this model is that xenon had to have been quantitatively retained in Earth's mantle or core during episodes of mantle degassing (b). Recently, Zhu et al. (2014) proposed that the inner and outer parts of the Earth's core may store significant amounts of Xe under the forms of stable $XeNi_3$ and $XeFe_3$. These compounds appear to be stable at the temperatures and pressures met in the core. However, this study is based on first-principles calculations and no experimental study has yet explored if Xe is effectively trapped in such compounds. Storage of Xenon in the silicate Earth has also been advocated. Sanloup et al. (2005) demonstrated that Xe can be stored in SiO_2 compounds under P-T conditions corresponding to the lower continental crust. Even if the formation enthalpy is higher for XeO_2 than for SiO_2 at room conditions. The melting of Xe occurring at 5 GPa and 1500 K induces a larger Xe molar volume contributing to the reduction of free enthalpy. In these conditions, substitution of Si by Xe in the crystal network becomes possible. After a return to room temperatures and pressures, only 5 % of Xe (mainly in bubbles) remains in the crystal. Contrary to that, other experimental studies demonstrate that Xe is one order of magnitude less soluble than Ar in perovskite at 25 Gpa and 1600-1800°C (Shcheka and Keppler, 2012). These results raise doubt on the possibility to quantitatively store Xe in the Earth's mantle during early episodes of intensive degassing.

Tolstikhin and O'Nions (1994) proposed a different model based on the low solubility of Xe in silicate melts relative to other noble gases (e.g. Shcheka and Keppler (2012)). In this model, Xe was preferentially lost from the magma ocean, for example in the aftermaths of the Moon-forming impact, and isotopically fractionated by hydrodynamic escape. Remaining noble gases were then subsequently degassed and lost to space. Preferential retention of He, Ne, Ar and Kr in perovskite crystallized from solidification of the magma ocean argues in favor of this model (Shcheka and Keppler, 2012). However, the depletion and isotopic fractionation of Xe must have happened very early in Earth's history since after solidification of the magma ocean, intensive mantle degassing induced by the onset of mantle convection would have replenished the atmosphere in He, Ne and Ar.

Dauphas (2003) proposed an alternative model involving a cometary contribution to the Earth's atmosphere (Marty and Meibom, 2007). In this model, an initial atmosphere with a solar abundance pattern (depleted by a factor of 10^3) and solar isotopic compositions was lost by hydrodynamic escape. A second cometary contribution with no Ne and low Xe abundances, as measured in amorphous ices experiments (Bar-Nun and Owen, 1998), replenished the atmosphere in Ar and Kr and modified their isotopic compositions toward less fractionated values. In this model, atmospheric Xe was kept under-abundant and highly fractionated.

It must be noticed here that all types of models presented above require an early hydrodynamic escape and isotopic fractionation of the atmosphere and that these models rely on still poorly constrained parameters (differential solubility of noble gases in the early magma ocean, extent of hydrodynamic escape, abundances of Xe in cometary ices). One common outcome of these models is that the two features of atmospheric Xe (depletion and the isotopic fractionation) would have been acquired early in Earth's history i.e. during the first hundreds of Ma after solar system formation.

Archean Xe: the key to solve the xenon paradox?

The first discovery of past-atmospheric xenon isotopically fractionated happened during analyses of 3.5 Ga-old archean barite ($BaSO_4$) samples from North Pole (Australia). During total extraction experiments at 1650°C, Srinivasan (1976) demonstrated the presence in these samples of a trapped mass-dependently fractionated xenon mainly revealed by a depletion in ^{134,136}Xe isotopes relative to the modern atmosphere. Excesses on light isotopes produced by this mass-dependent fractionation were masked by various excesses due to neutron-capture and spallation effects. The extent for the mass fractionation can be estimated at 17‰.u^{-1}. A recent study analyzed similar barite samples from North Pole (Pujol et al., 2009). The isotopic spectrum of xenon trapped in the barite crystal lattice and extracted at 1650°C from these samples carried the signature of several isotopic effects:

- mass-dependent isotopic fractionation of 21 ± 3 ‰.u^{-1} originally interpreted as resulting from mutual diffusion together with Rayleigh's distillation during hydrothermal liquid-gas interactions when barites formed;
- ^{130}Xe excess due to the weak decay of ^{130}Ba that permitted to define the half-life of ^{130}Ba ($t_{1/2}$=6.10^{20}a);
- $^{131-136}$Xe excesses due to the spontaneous fission of ^{238}U that permitted to compute a formation age of 3.5 Ga for these barite samples.

Meshik et al. (2001) analyzed recent barite samples (134 Ma) and demonstrated, after corrections for decay of ^{130}Ba, that xenon trapped in these samples had an isotopic composition similar to the modern atmosphere. This study is thus confirming that there is no isotopic fractionation of Xe during barite formation. Studies described above demonstrate the great potential of barites for recording isotopic compositions of Xe at the time of their formation. Furthermore, the presence of Xe isotopes produced by the spontaneous fission of ^{238}U ensures a direct dating of any mass fractionation of Xe isotopes detected in such samples. However, the large quantities of sulfur released when heating barite samples is problematic as the required purification is fastidious (Pujol et al., 2009), risky for the mass-spectrometers and still requires analytical developments.

More recently, Pujol et al. (2011) demonstrated that xenon trapped in fluid inclusions in quartz samples from the Barberton Greenstone Belt was also isotopically intermediate between a Solar or Chondritic isotopic composition and the modern atmosphere (Fig. 1.25). The use of the Ar-Ar dating method permitted to get an age of 3.0 Ga for the time of fluid entrapment. Even if it was argued that this isotopic signal signal might reflect a mixing between a *normal* (i.e. unfractionated) atmospheric component and a mantle-derived end-member with an isotopic composition similar to U-Xe (Pepin, 2013), Pujol et al. (2013a) demonstrated that this explanation is unrealistic based on crustal-like neon isotopic ratios in these samples and the absence of ^{129}Xe excess produced by the decay of extinct ^{129}I in the Earth's mantle. Such excess would be expected if any mixing between a primitive mantle and an atmospheric end-members took place (Caffee et al., 1999). The isotopic composition of Xe recorded in these quartz, once corrected for contributions from spontaneous fission of ^{238}U, is thus probably reflecting the isotopic composition of the atmosphere 3.0 Ga ago. This isotopic composition is enriched in light isotopes and depleted in heavy isotopes (Fig. 1.25) corresponding to a mass-dependent fractionation of 10±5‰.u^{-1} (1σ). These conclusions led the authors to revisit the previous conclusion about a mass-dependent effect induced by hydrothermal circulations explaining the mass fractionation of 21±3‰.u^{-1} measured in Archean barites (Pujol et al., 2009). They favored the hypothesis that this isotopic fractionation also represents the isotopic composition of the atmosphere 3.5 Ga ago.

In a recent work, Holland et al. (2013) analyzed the isotopic composition of xenon dissolved in ancient free fluids from the Canadian Precambrian shield. They found excesses of light isotopes of Xe and computed

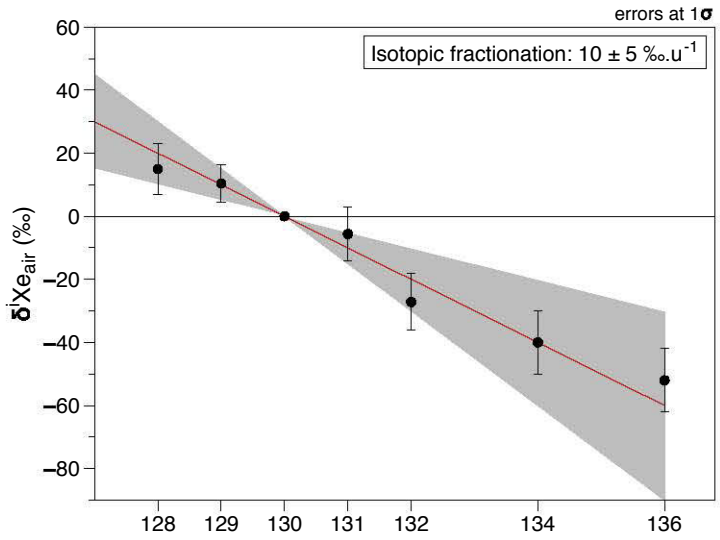

Fig. 1.25: Isotopic composition of Xe in North Pole fluid inclusions once corrected for $^{130,131-136}$Xe excesses. After correction, a mass-dependent fractionation of 10±5‰.u^{-1} is still present and reflect the isotopic composition of xenon in the Archean atmosphere. Adapted from Pujol et al. (2011).

an isotopic fractionation of Xe of 3±1 ‰.u^{-1} (1σ) and used a preliminary curve of the evolution of the isotopic composition of atmospheric Xe with time (Marty, 2012) to date these fluids. It must be noticed here that the use of this preliminary curve was somehow premature because no data points existed for the period of time considered here (1.5 to 2.7 Ga inferred from radiogenic isotope excesses). Indeed, the mechanism behind the progressive isotopic fractionation of Xe remains largely unknown and there is no certainty on the mode of evolution of the isotopic composition of atmospheric Xe as well as on the parameters governing this evolution. This study is thus confirming the existence of past-atmospheric Xe with an isotopic composition intermediate between primordial Xe and the modern atmosphere but the age of this fractionation remains hard to establish (see the range in Fig. 1.26).

A compilation of the existing data on the evolution of the isotopic composition of atmospheric Xe is listed in Table 1.2 and displayed in Fig. 1.26. Results for fluids from the Canadian Precambrian shield are represented here with ages spanning 1.5 Ga to 2.7 Ga (Holland et al., 2013). The isotopic fractionation seems to decrease from primordial values of 30-40‰.u^{-1} (depending on the starting isotopic composition, Solar, Chondritic or U-Xe) toward lower values in the Archean and finally reaching the isotopic composition of the modern atmosphere. An isotopic evolution of atmospheric Xe through time, still ongoing at least 2.7 Ga ago, demonstrates that previous models built to explain the xenon paradox (elemental depletion and isotopic fractionation) with an early hydrodynamic escape and, in some case, storage of Xe in the Earth's mantle (Pepin, 1991; Tolstikhin and O'Nions, 1994) and presented in section 1.2.4 need to be revisited. Naturally, more data are needed to confirm these preliminary results and to search for the possible physico-chemical mechanisms behind this long-term isotopic evolution of atmospheric Xe.

Long-term escape and isotopic fractionation of Xe

The progressive evolution of the isotopic composition of atmospheric Xe (see section 1.2.4) has been interpreted as evidence for progressive escape of Xe atoms from the atmosphere to the outer space (Pujol et al., 2011; Marty, 2012) accompanied by an instantaneous isotopic fractionation when Xe is ionized in presence of organic haze (Hébrard and Marty, 2014). Hébrard and Marty (2014) used a photo-chemical

Table 1.2: Compilation of the existing results on the isotopic composition of atmospheric Xe. n.d. is for not determined.

Geological Area (Country)	Lithology	Age (Ga)	±	Isotopic fractionation (‰.amu^{-1})	±	MSWD	Used Xe isotopes ($/^{130}$Xe)	Reference
Previous studies								
North Pole (Australia)	barites	3.48	0.09	21	3	n.d.	129,132,136	Pujol et al., 2009
North Pole (Australia)	barites	3.5	n.d.	13.7	n.d.	n.d.	134, 136	Srinivasan, 1976
North Pole (Australia)	quartz	3.1	0.4	15	5	n.d.	128,129,132,134,136	Pujol et al., 2013
North Pole (Australia)	quartz	3.0	+0.2	10	5	n.d.	128,129,131	Pujol et al., 2011
Timmins (Canada)	fluids	see text	-	3	1	0.067	124,126,128,130	Holland et al., 2013
Belorechenskoe (Russia)	barites	0.170	0.015	0.5	n.d.	n.d.	124,126,128,129	Meshik et al. 2001

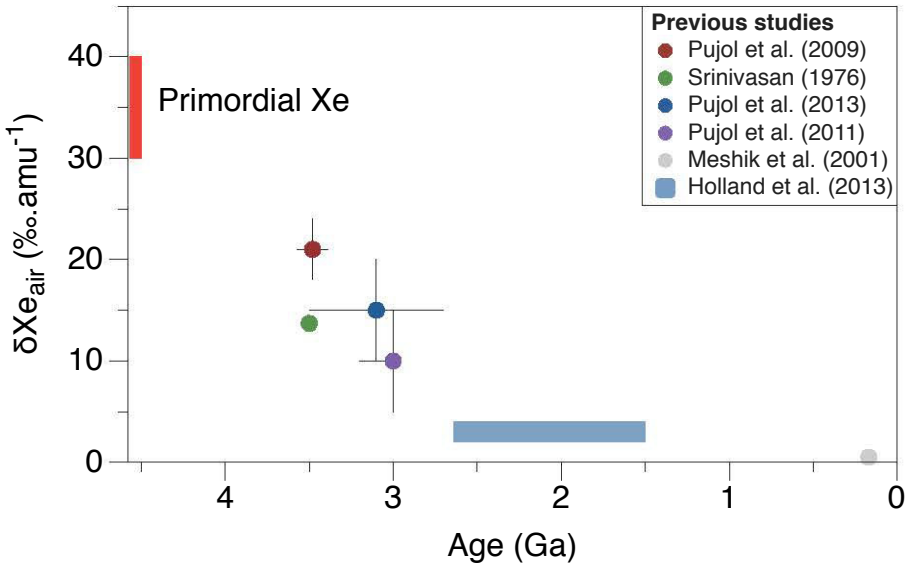

Fig. 1.26: Evolution of the isotopic composition of atmospheric xenon with time in notation δXe (‰.u^{-1}) relative to the isotopic composition of the modern atmosphere. The starting isotopic composition is either Solar or Chondritic (cf. Table 1.1). Data are from Table 1.2.

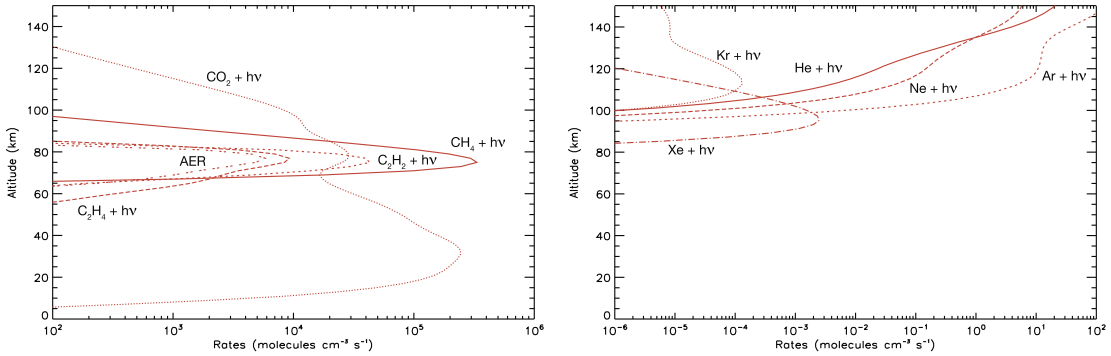

Fig. 1.27: Results of the photochemical model presented in Hébrard and Marty (2014). Production of organic aerosols (AER in the left panel) and ionization of Xe (Xe + hv in the right panel) occurred at similars altitudes 3.5 Ga ago.

model to explore several parameters controlling Xe trapping and isotopic fractionation in organic haze and escape of the remaining fraction from the Archean atmosphere to the outer space.

Firstly, there is no isotopic fractionation of neutral Xe upon adsorption (Marrocchi and Marty, 2013) but some isotopic fractionation around $1‰.u^{-1}$ occurs when Xe is ionized and in presence of organic matter (Kuga et al., 2015; Marrocchi et al., 2011). This feature requires an enhanced EUV flux from the young Sun in order to achieve ionization of Xe in the Archean atmosphere before its trapping in organic hazes. Observation of the luminosity of other stars similar but younger than our Sun already demonstrated that, indeed, the incoming EUV flux at the top of the atmosphere was higher 3.5 Ga ago (Ribas et al., 2005). It must be noticed here that a higher EUV flux during the Archean eon is also maybe required to explain mass-independent fractionation of sulfur isotopes recorded in ancient sediments (Farquhar and Wing, 2003).

Secondly, the presence of organic matter in the form of hydrocarbon aerosols ("hazes") in the Archean atmosphere is possible when starting with an atmosphere with a high CH_4/CO_2 ratio. Such a highly-reduced atmosphere during the Archean has indeed often been advocated (see Shaw (2014) and refs. therein). One of the major results presented by Hébrard and Marty (2014) is that the production of organic hazes and the ionization of Xe happened at similar altitudes in their modeled 1D Archean atmosphere (Fig. 1.27) and that the ionization and trapping of Xe occurred more frequently due to an enhanced production rate of aerosols and an easy ionization. This model is thus able to reproduce the depletion together with the isotopic fractionation of Xe. Because the presence of organic hazes is necessary to trap ionized Xe and if this model is correct, the modern isotopic composition of atmospheric Xe should have been established before the global oxygenation of the Earth's atmosphere. After this event, the presence of O_2 in the atmosphere prevented stabilization of organic hazes and thus the reservoir necessary to trap and fractionate Xe isotopes did not exist anymore. Furthermore the progressive establishment of and ozone-rich (O_3) layer in the upper atmosphere acted as a protection against the EUV flux and prevent any efficient ionization of Xe atoms in the atmosphere.

1.2.5 The case of Mars-Xe: a similar story?

Even if space missions are still helping to put constraints on the isotopic composition of noble gases and nitrogen in the Martian atmosphere (e.g. Wong et al. (2013)), studies of noble gases and nitrogen trapped in Martian meteorites give the most precise results so far on the isotopic composition of volatiles in the Martian atmosphere and in Mars interior (see Swindle (2002); Bogard et al. (2001) for comprehensive reviews).

SNC (*S*hergotty, *N*akhla, *C*hassigny) meteorites are thought to originate from asteroidal impacts on Mars (Treiman et al., 2000). During the impact, fragments of the Martian crust were ejected in space.

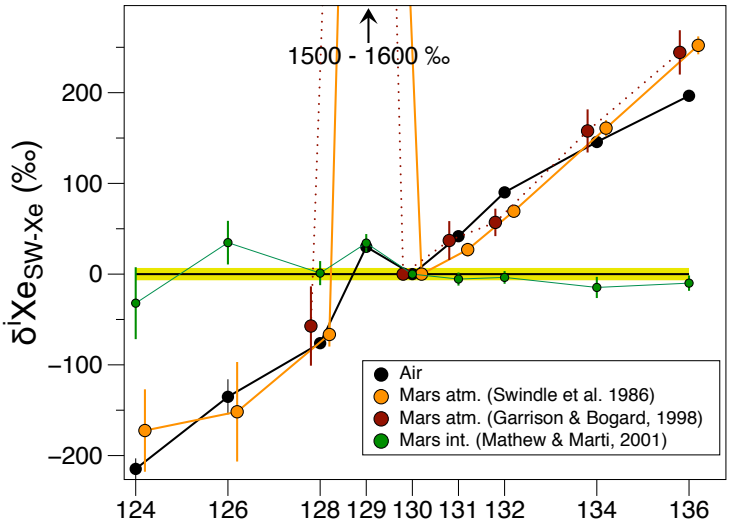

Fig. 1.28: Isotopic compositions of xenon in the Martian atmosphere and interior in notation $\delta^i Xe$ (‰.u^{-1}) relative to the isotopic composition of the Solar Wind (Meshik et al., 2014). Data are from Table 1.1 and from Swindle et al. (1986); Mathew and Marti (2001).

After several million years the parent-body of the SNC meteorites was disturbed by impacts and fragments finally collided with Earth. During the impact on Mars, portions of the Martian crust melted and trapped Martian atmospheric gases (Wiens et al., 1986). Analyses of these glass fragments in the Antarctic meteorite EETA79001 (Swindle et al., 1986) helped to define the isotopic composition of Xe in the Martian atmosphere while analyses of Xe trapped in the Chassigny meteorite provided information on the isotopic composition of Xe in Mars interior (Mathew and Marti, 2001). These isotopic compositions are reported in Fig. 1.28.

The isotopic composition of Xe in the Martian atmosphere appears broadly similar to the isotopic composition of the Earth's atmosphere except for a large ^{129}Xe excess due to extinct ^{129}I. Contrary to terrestrial Xe that seems derived from a U-Xe like composition (see section 1.2.4), Mars-Xe may be directly linked to SW-Xe by an isotopic fractionation of 31±4 ‰.u^{-1} (1σ). The fact that both Earth and Mars share a comparable isotopic fractionation of Xe together with similar ^{84}Kr/^{132}Xe ratios ($\simeq 1/20$) is intriguing because the two planets have very different geological histories (Dauphas and Pourmand, 2011) and "astronomical" features (distance from the Sun, mass, solar flux etc).

At the beginning of this study, analyses of argon and nitrogen isotopes in a freshly found Martian meteorite named "Tissint" that fell in the Moroccan desert have been published in a contribution in the journal *Science* (Aoudjehane et al., 2012). This paper is placed in Annexe 5.3. Nitrogen and argon abundances and isotopic compositions measured in glass fragments of the Tissint meteorite define a linear correlation from the Earth's atmospheric composition toward values for the Martian atmosphere measured by the Viking spacecraft (NASA mission) (Owen et al., 1977). The $\delta^{15}N$ value around 620 ‰ for the Martian atmosphere has often been interpreted as the evidence of strong photochemical escape events accompanied by Solar Wind sputtering events (Jakosky and Pepin, 1994).

1.3 Questions and research opportunities

This Chapter demonstrated that the origin of volatile elements in the terrestrial mantle and atmosphere is still a debated question. The origin of Xe on Earth is even more enigmatic due to the striking features of atmospheric Xe forming the "xenon paradox" and to the lack of uncontaminated samples to determine

the starting isotopic composition of mantle Xe necessary to track the interactions between the mantle and the atmosphere. Furthermore, knowing the elemental composition of the Archean atmosphere is a key to understand how to keep a warm early atmosphere (+ ocean) in which early forms of life emerged. The sulfur isotope composition of ancient sediments suggest also major changes in the Earth atmosphere linked to its progressive oxidation. An evolution of the isotopic composition of atmospheric Xe might help to constrain these changes. The main questions that orientated this study are:

- **What is/are the origin(s) of Xe on Earth?** Even if the origin of mantle Xe remains enigmatic, krypton in the Earth's mantle has probably a chondritic origin whereas theoretical studies suggested that atmospheric Xe cannot be directly derived from Chondritic or Solar sources. One part of this study was dedicated to the analysis and interpretations of results obtained on mantle-derived gases from the Eifel magmatic region (Germany) to search for the origin of Xe in the deep mantle. Xe in quartz samples recovered from the Barberton Greenstone Belt area was also analyzed at high precision in order to constrain the origin of atmospheric xenon.

- **What is the elemental and isotopic composition of the ancient atmosphere and what is the evolution of the isotopic composition of atmospheric Xe with time?** Results from previous studies presented in section 1.2.4 demonstrates that the isotopic composition of Archean atmospheric Xe was different from the modern one and that such results might be keys to understand the xenon paradox. However, more precise results are necessary to confirm this isotopic fractionation of atmospheric Xe in the past and to understand what are the processes that were involved in this progressive isotopic fractionation. Part of this work was dedicated to the careful selection and analysis of samples in order to complete the curve of the evolution of the isotopic composition of Xe (Fig. 1.26) from the Archean to Present and to further characterize the isotopic composition of the Archean atmosphere.

Samples and analytical tools used to answer these questions are summarized in Chapter 2. Results and their implications are described in papers (published or in preparation) listed in Chapter 3. Chapter 4 provides an additional discussion as well as the conclusions and perspectives of this study.

Chapter 2

Samples Characterization and Analytical Methods

This chapter contains descriptions of the geological setting of samples analyzed during this study as well as details on the analytical techniques used to measure the abundance and isotope composition of noble gases and nitrogen contained in these rocks. Some additional informations are also present in papers compiled in the next chapter (Chapter 3, Results and Implications).

Contents

2.1 Geological setting of the samples

The diverse geological contexts (lithologies, ages, metamorphic and resetting events ...) of samples analyzed during this study are described in this section. Particular attention is paid to samples from the Barberton Greenstone Belt (South Africa) and the Hamersley Basin (Australia) as their extensive analyses gave particularly precise and interesting results (chap. 3).

2.1.1 The Barberton greenstone belt (South Africa)

The Barberton Greenstone Belt (BGB hereafter) is located in the southeastern edge of the Kaapvaal craton, NE South Africa. It is made up of a succession of supracrustal rocks that dip in the N-E/S-W direction and that form the *Swaziland Supergroup*. These rocks are overlaid and intruded by magmatic rocks (e.g. TTG-type intrusions) (Hofmann and Harris, 2008).The *Swaziland Supergroup* is subdivided in three lithological groups (the Onverwacht, the Fig Tree and the Moodies Groups) (Fig. 2.1).

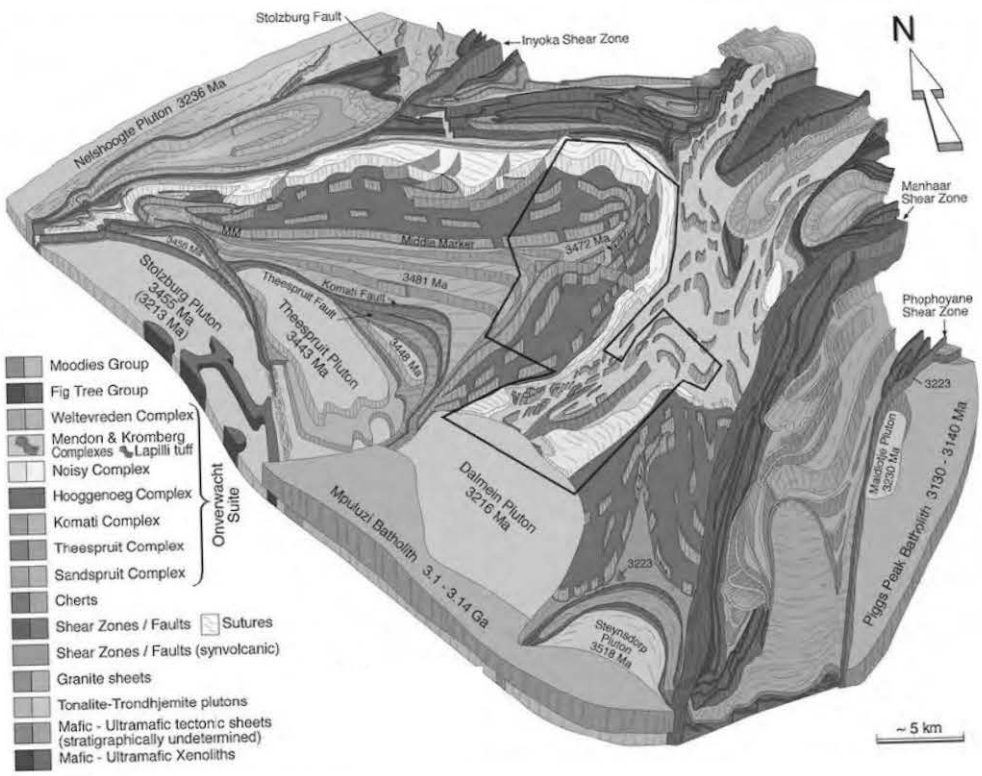

Fig. 2.1: 3D schematic map showing the structural relationships between the main petrographic units of the Barberton Greenstone Belt. Ages of the main intrusive units are also shown. Adapted from de Wit et al. (2011).

The Barberton Greenstone Belt underwent only low-grade post-depositional alterations with a peak metamorphism up to the greenschist facies (Tice et al., 2004) and is thus often considered as the best preserved 3.0-3.5 Ga-old rock sequence worldwide (Hofmann, 2005).

Description of the BARB3 core samples

Five cores were drilled in the BGB as part of the ICDP project "Peering into the Cradle of Life" (PI: N. Arndt). The five sites chosen for drilling operations were located in very different geological parts of the BGB in order to drill cores that cross-cutted several formations and lithologies (Fig. 2.2):

- BARB 1,2 "Tjakastad Komatiites", ultramafic rocks (komatiites, basalts);
- **BARB 3 "Buck Reef Chert", cherts intercalated with mafic rocks;**
- BARB 4 "Mendon Formation", shales and Banded Iron Formations (BIFs);
- BARB 5 "Barite Valley", shales and Banded Iron Formations (BIFs).

Samples were collected for all of the cores presented above, but the main results of this work were obtained by analyzing samples from the BARB 3 core. The BARB 3 core was drilled in rocks of the Kromberg Formation (>3.33 Ga). The Kromberg formation consists in pillowed and massive basalt, komatiites, cherts and some later ultramafic sills (Fig. 2.3). The ages of the Kromberg volcanic rocks are not well known but must be older than 3.352 Ga, which is the age of one of the gabbroic intrusions cutting the lavas (Furnes et al., 2013; Kamo and Davis, 1994). Unfortunately, the mafic nature of most of the Barberton lavas prevents any simple recovering of zircons and, thus, straightforward dating.

Localization of collected samples in the BARB3 core are indicated in Fig. 2.3. Samples are mainly from macro-crystalline quartz veins intruded in cherts or mafic lavas of the Kromberg formation (Fig. 2.4). It

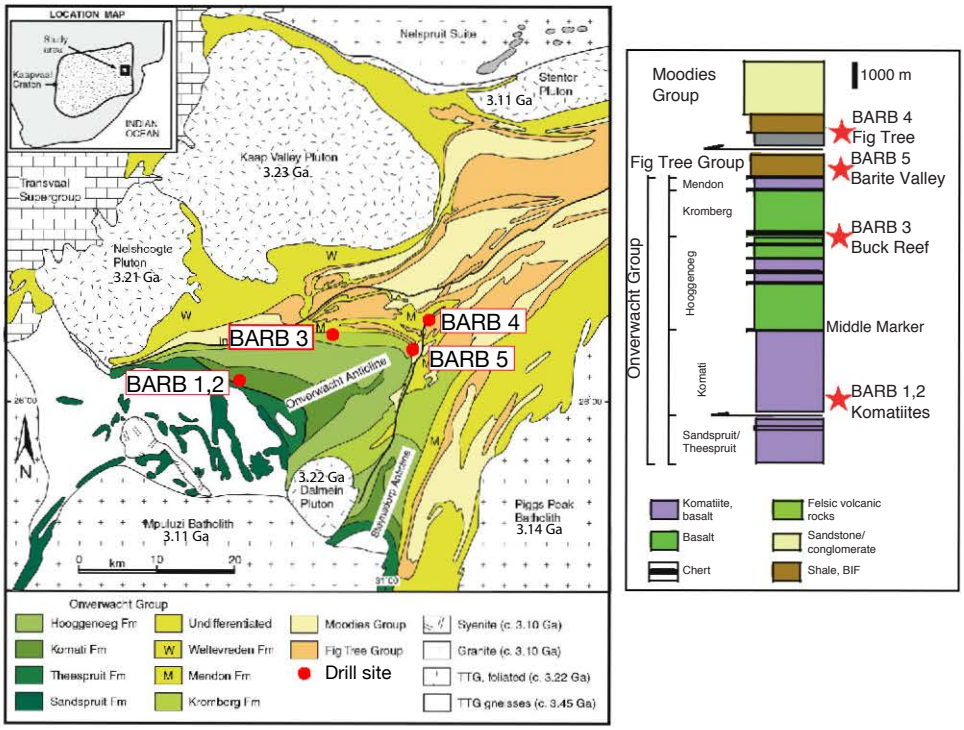

Fig. 2.2: Simplified geological map of the Barberton area with localisations of the drill sites and ages of the various plutons intruded in the vicinity. Right: schematic log of the formations sampled during the drilling operations (courtesy: N. Arndt). Map modified after Hofmann et al. (2014). Age data are from Kamo and Davis (1994).

may appear strange to sample and analyze volatile elements in fluid inclusions contained in these lithologies since the cross-cutting nature of veins demonstrates that they were derived from secondary fluid circulation events in rocks from the Kromberg formation. However, collected quartz crystals contain numerous fluid inclusions potentially rich in xenon (Böhlke and Irwin, 1992). Furthermore, application of the Ar-Ar dating technique to these quartz samples has the potential to reveal the age of fluid entrapment. See, for example, the work by Kendrick et al. (2006) on Proterozoic quartz crystals.

Preliminary microscopic observations show that quartz samples are rich in fluid inclusions (Fig. 2.5(a)). Some inclusions are of primary origin (Fig. 2.5(c)), but most of them have a secondary origin as demonstrated by their locations in trails whose orientations are parallel to the vein orientation (Fig. 2.5(a,b)). Primary and secondary inclusions have comparable sizes ($\simeq 10\mu$m) and carry 2 phases: liquid + vapor (Fig. 2.5(c)). It would be very interesting to conduct a comprehensive study of these inclusions since it could permit to put constraints on pressure and temperature conditions of quartz formation even if lot of care is necessary when studying fluid inclusions located in metamorphosed rocks (Touret, 2001). It is worth noting that the lack of knowledge on the origin and conditions of formation of these fluid inclusions is not too much of a problem for searching ancient atmospheric xenon signatures since crustal non-radiogenic/non-fissiogenic noble gases are dominated by the atmospheric signature ($>$ 99.8 %, Drescher et al. (1998)). Fluid inclusions in quartz samples have thus the potential to record the isotopic composition of the atmosphere. It is evidently necessary to get constraints on the age of fluid inclusions and fluid entrapments, which can be obtained by the Ar-Ar method.

After crushing for noble gas experiment (see section 2.2.1), oxygen isotopes analyses were carried out on quartz powder at the stable isotopes laboratory (CRPG, France). $\delta^{18}O_{quartz}$ values (Table 2.1.1) range from 11.3 to 21 ‰. These results correspond to temperatures between 93°C and 190°C during silica pre-

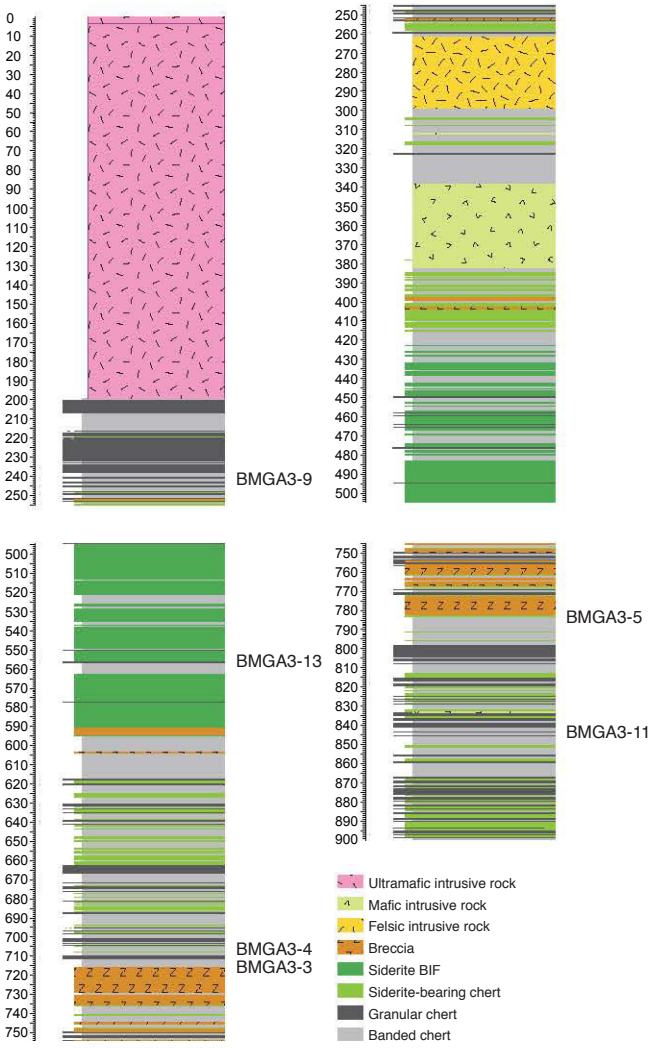

Fig. 2.3: Stratigraphic log identifying lithologies cutted by the BARB 3 core and localization of collected samples. Courtesy: A. Hofmann.

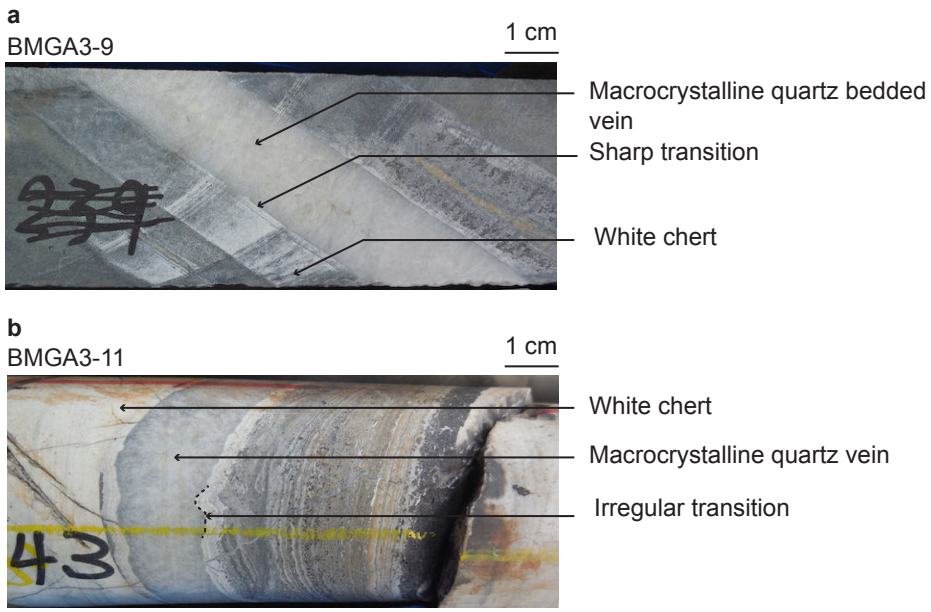

Fig. 2.4: Photographies of two samples from the BARB3 core. (a) Sample BMGA3-9 is from a vein, filled with macro-crystalline quartz crystals, cross-cutting white chert. The transition between the two lithologies is sharp with two parallels straight lines. (b) Sample BMGA3-11 is a macro-crystalline quartz vein intruded in a lithology dominated by white chert and an alternance of black and white chert. The transition between the vein and the intruded rock is sharp but irregular.

Table 2.1: Isotopic composition of oxygen in Barberton quartz samples expressed with the δ notation relative to the SMOW standard. Typical error is 0.2 ‰.

Sample	$\delta^{18}O_{SMOW}$ (‰)
BMGA 3-4	11.3
BMGA 3-9	21.0
BMGA 3-9	20.3
BMGA 3-11	18.2
BMGA 3-11	18.1
BMGA 3-13	12.5
BMGA 3-13	12.2

cipitation (Clayton et al., 1972), if the Archean seawater had an oxygen isotope composition close to the modern ocean but slightly depleted in ^{18}O because of the absence of ice caps (Robert and Chaussidon, 2006) ($\delta^{18}O_{arch.seawater}$ = -1 ‰).

Even if metamorphism in the BGB area remained limited and reached only the lower greenschist facies, pervasive fluid circulation events occurred in all rocks of the BGB resulting in silicification of sediments and K-metasomatism (Hofmann, 2005). Toulkeridis et al. (2015) applied the Rb-Sr, Sm-Nd and Pb-Pb isotopic systems on shales from the BGB and demonstrated that even if some fluids circulated in the samples until 2.2 Ga ago, fluid circulations events were not sufficient to reset all isotopic systems. This observation argues in favor of a possible preservation of an atmospheric Xe signal in quartz collected in the BGB area.

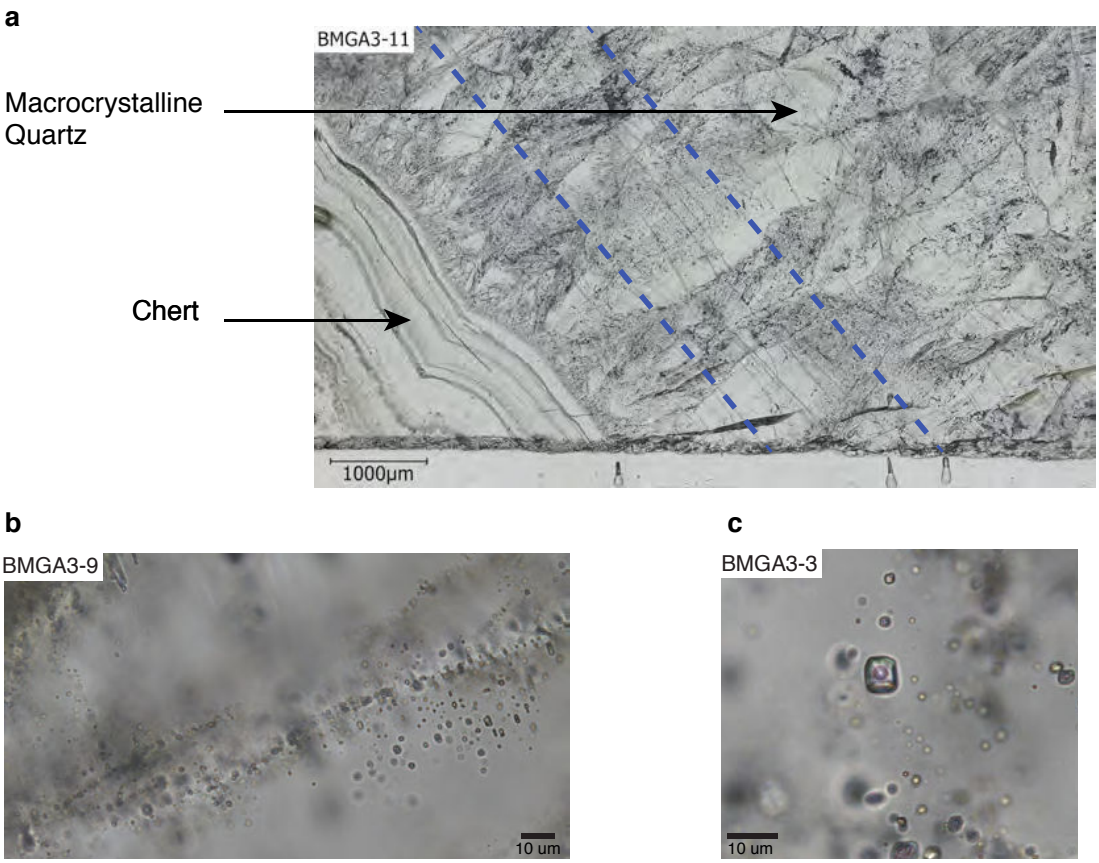

Fig. 2.5: Microphotography of fluid inclusions in Barberton quartz samples. (a) Photography of a large portion of the thick section of BMGA3-11 sample. Macrocrystalline quartz is in the middle of the vein delimited by cherty lithology (lower left). Trails of fluid inclusions are visible in the middle of the large quartz crystals. The preferential orientation of trails is indicated by the dashed blue lines. (b) Microphotography of a trail of fluid inclusions in sample BMGA3-9. (c) Microphotography of a two-phases (L+V) fluid inclusion in sample BMGA3-3.

Recent advance on the study of silicified rocks from the Barberton Greenstone Belt relevant to this study

Recently, Farber et al. (2015) analyzed cherts and quartz veins in silicified komatiites and sediments of the Mendon Formation (3.33 - 3.245 Ga), which is overlaying the Kromberg Formation. Oxygen isotope ratios of both lithologies are compatible with silica precipitation during low-temperature (< 100 °C) hydrothermal processes ($\delta^{18}O$ = 18 - 21 ‰). Numerous secondary fluid inclusions in macrocrystalline quartz are similar to the few clustered primary inclusions (2 phases L+V) and have homogenization temperatures of 150-200 °C. The authors of this study consider that the fluid entrapment occurred during a late metamorphic overprint consistent with regional deformation and regional-scale metamorphism at 3.23 Ga. Farber et al. (2015) pointed out that halogens ratios, measured by the crush-leach technique, do not reflect directly the halogen composition of the Archean seawater since fluids identified in fluid inclusions in these quartz crystals have been modified during hydrothermal circulations. Samples analyzed in this study are very similar to those analyzed by Farber et al. (2015) and may thus share a common origin.

2.1.2 The Hamersley Basin and the Fortescue Group (Australia)

Some of the oldest (3.5 Ga) rocks on Earth are located in the Pilbara craton (Australia). Pujol et al. (2009, 2011) already measured Xe in rocks from this geological area and these previous results are described in section 1.2.4. Part of this PhD study was focused on younger rocks from the regional Hamersley basin located in the southern part of the Pilbara craton (Fig. 2.6).

The Hamersley basin is located in the southern part of the Pilbara Craton. It is a volcano-sedimentary basin stratigraphically defined as the Mt Bruce Supergroup (2.78 to <2.45 Ga). The Mt Bruce Supergroup is divided in three components: The Fortescue Group (2.78 - 2.68 Ga) (Arndt et al., 1991) that unconformably overlies granite-greenstones of the Pilbara Craton, the Hamersley Group containing Banded Iron Formations (BIFs) (2.63 - 2.45 Ga) and the Turee Creek Group (< 2.45 Ga). Samples analyzed in this work are from the Fortescue Group. It is a sequence of mafic and felsic volcanic rocks with their associated sedimentary rocks covering 40,000 km^2 (Thorne and Trendall, 2001; Philippot et al., 2009)

Description of the samples

Samples analyzed in this study are labeled Pi03-17 and Pi03-44 and were kindly provided by P. Philippot (IPGP, Paris). They are from the 2.745-2.73 Ga old Boongal formation and from the Maddina formation (2.718 - 2.715 Ga), respectively (Trendall et al., 2004). These formations belong to the Fortescue Group.

The Boongal formation consists mainly of basalt flows and pillow lava basalts. Subaerial basaltic lavas usually contain spherical amygdales filled with quartz. Sample Pi03-17 is one example of these amygdales (called quartz pods hereafter). The Maddina formation also contains these amygdaloidal flows with cavities up to 30 mm large filled with quartz. These quartz-filled amygdales are quite similar to other quartz pods located in older (3.5 Ga) rocks and described and analyzed by Pujol et al. (2011). These 3.5 Ga-old quartz pods are usually interpreted as the result of hydrothermal circulation events driven by the hot basaltic lavas (Buick and Dunlop, 1990). If quartz samples from the Fortescue Group were deposited in a similar setting, their age is probably close to the age of the lava emission i.e. 2.7 Ga (Trendall et al., 2004). Quartz pods have two main lithologies (Fig. 2.7): microcrystalline quartz in the outer part of the pod and columnar quartz crystals in the inner portions of the pod. Interestingly, such textures are similar to those of quartz veins associated with cherts from the Barberton Greenstone Belt (Marin-Carbonne et al., 2013).

As for samples from the Barberton Greenstone Belt, oxygen isotopes analyses were carried out on quartz powder at the stable isotopes laboratory (CRPG, France). $\delta^{18}O_{quartz}$ values (Table 2.1.2) range from 11.5

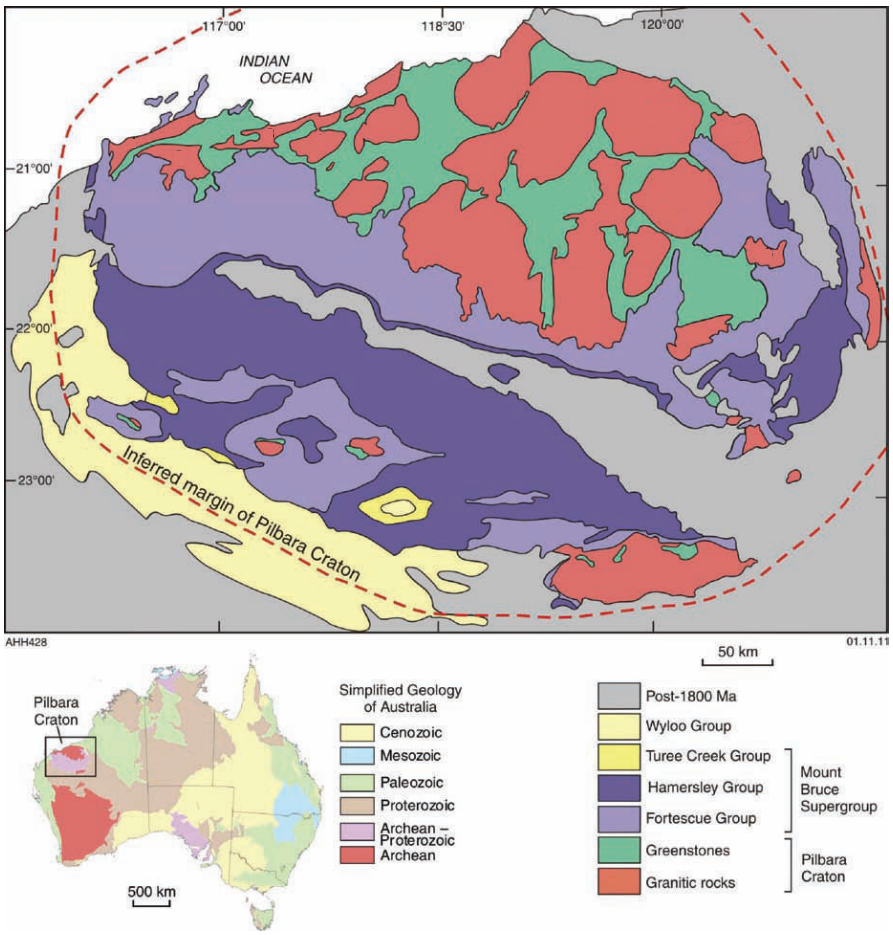

Fig. 2.6: Location and simplified geological map of the Pilbara craton and the associated Hamersley basin. Modified after Hickman and van Kranendonk (2012).

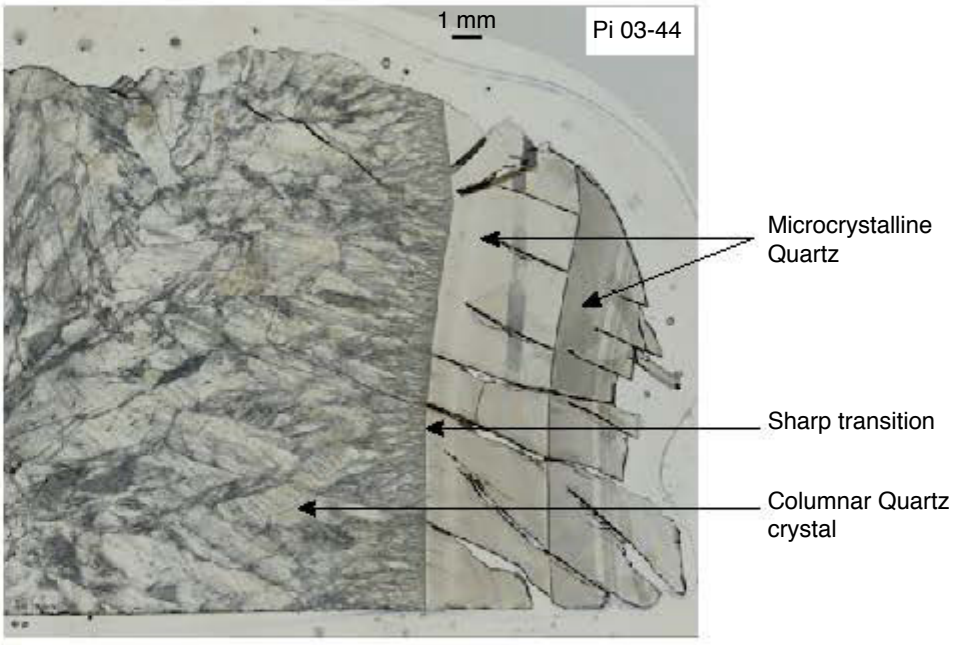

Fig. 2.7: Microphotography of a thick section of sample Pi03-44. There is an evolution in crystal nature and size from the external part (right) to the internal part (left) of the quartz pod. Small columnar quartz crystals initially formed on the sharp transition with chert. The size of columnar crystals increases with the distance from the chert.

Table 2.2: Isotopic composition of oxygen in Fortescue Group quartz samples expressed with the δ notation relative to the SMOW standard. Typical error is 0.2 ‰.

Sample	$\delta^{18}O_{SMOW}$ (‰)
Pi03-17-1	11.5
Pi03-17-2	11.5
Pi03-44-1	17.8
Pi03-44-2	18.6

to 18.6 ‰ and correspond to temperatures between 110°C and 190°C during precipitation of silica (Clayton et al., 1972).

2.1.3 Other studied geological areas

In order to track the evolution of the isotopic composition of atmospheric Xe with time, other samples of various ages have been collected during this study. Locations of these samples are summarized in Fig. 2.8. Even if it was not the purpose of this study to do a comprehensive geological/geochemical survey of these areas, some of their key features are presented in this section. Similar but shorter descriptions appear in the paper presented in section 3.3 of Chapter 3 (Results and Implications).

The Isua Greenstone Belt (Greenland)

Some rocks from the Isua greenstone belt (West Greenland) are thought to be up to 3.8 Ga-old (Nutman and Friend, 2009). Samples analyzed in this study were collected in the southern part of the belt (65° 5'29.00"N, 50° 8'11.00"W) and consisted of quartz crystals mixed with carbonates, possibly of metasomatic origin and labelled "metacarbonates" (Rose et al., 1996; Dauphas et al., 2007). Approximate location of the samples is given in the simplified geological map of the southern part of the greenstone belt (Myers, 2001) in

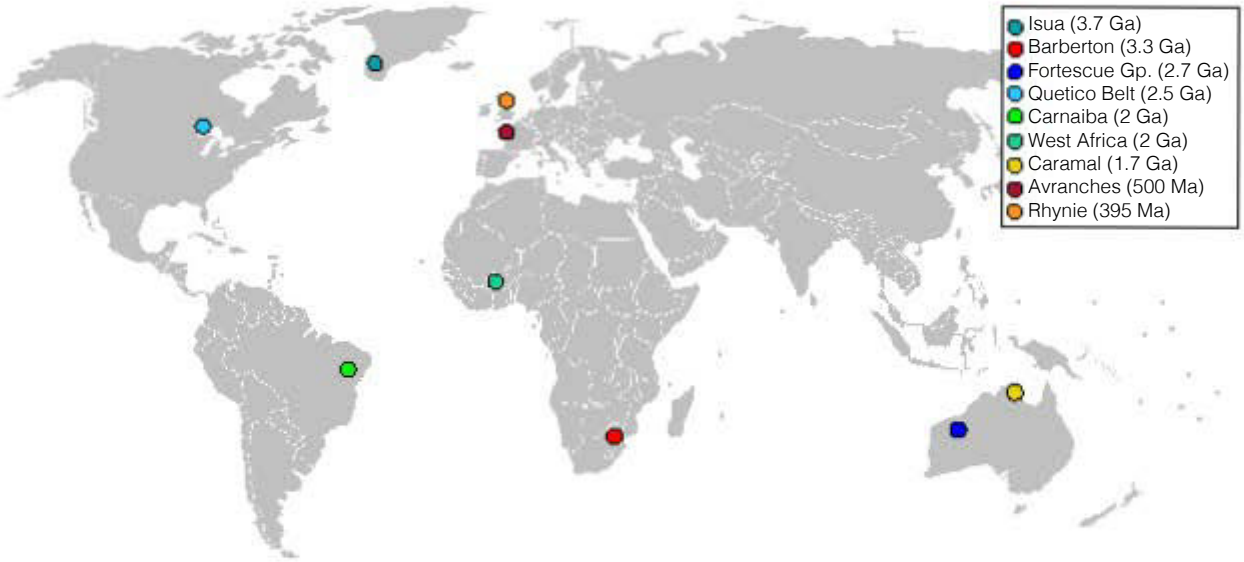

Fig. 2.8: Localisations of the samples analysed during this PhD thesis.

Fig. 2.9. After having been initially considered as sediments deposited in a shallow marine environment, these rocks are now believed to have formed by circulation of high-temperature fluids that leached surrounding ultramafic rocks (Rosing et al., 1996). An early Archean age for fluid circulation is thus doubtful and the widespread resetting event at 2.3 ± 0.2 Ga identified by Sm-Nd dating on metamorphic garnets from the same area (Blichert-Toft and Frei, 2001) is a more plausible age for the fluid circulation in these lithologies. To get insight into their chronology, these samples have been irradiated in a nuclear reactor in order to apply the extended Ar-Ar method. Experiments will be conducted in the near future.

The Quetico Belt (Canada)

Quartz samples from the Quetico Belt were kindly provided by S. Shirey (Carnegie Institute, USA). These samples are from veins intruded in metagreywackes dated at ca. 2.72 Ga (Davis et al., 1990). Younger cross-cutting granitic rocks intruding these lithologies have been dated at 2.69 Ga (Davis et al., 1990). Although these quartz crystals are younger than 2.72 Ga, the true age of the veins is unknown and could be 2.65 Ga, the age of the metamorphism almost synchronous to the onset of late plutonic intrusions (Card, 1990). It could also be as young as 2.58 Ga, the age of fluid circulations linked to the onset of gold-bearing quartz veins in the nearby Abitibi area (Hanes et al., 1992).

Carnaíba (Brazil)

Samples from Carnaíba (Brazil) are quartz crystals from emerald-hosting veins linked to the intrusion of Proterozoic leucogranites in volcano-sedimentary sequences (Giuliani et al., 1990). They were kindly provided by G. Giuliani (CRPG, Nancy). The age of the mineralization is bracketed between 1.98 Ga and 1.93 Ga based on Ar-Ar experiments on associated phlogopites (Cheilletz et al., 1993).

Gaoua mine district (Burkina Faso)

Samples from the Gaoua mine district (Burkina Faso) are the same samples than those analyzed by Le Mignot et al. (2014) for Re-Os dating of pyrite crystals. They were kindly provided by E. Le Mignot. The Gaoua mine district is located in the southern part of the Boromo-Goren greenstone belt that aggregated between 2.25 and 2.15 Ga (Baratoux et al., 2015). The gold mineralization associated with quartz samples

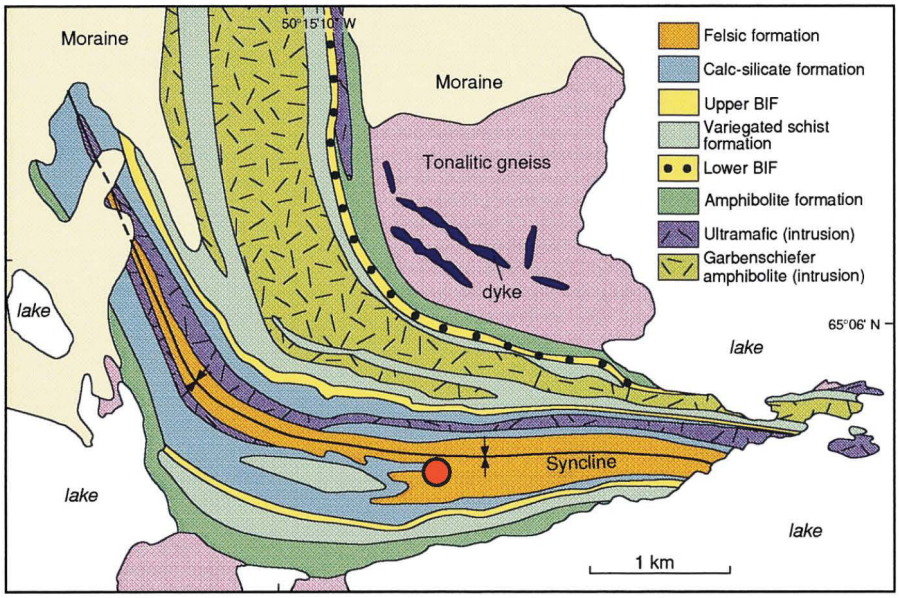

Fig. 2.9: Simplified geological map of the southern part of the Isua greenstone belt (after Myers (2001)). The red dot represents the approximative location of our sample (in the calc-silicate formation).

analyzed in this study is associated to a second episode of deformation with fluid circulations and formation of the quartz veins. Quartz crystals contain solid-free dominated inclusions with relatively low homogenization temperatures (120-200°C). Le Mignot et al. (2014) obtained ages between 2.10 ± 0.07 Ga and 2.16 ± 0.02 Ga for two generations of pyrites by using the Re-Os dating method.

Caramal (Australia)

Samples from Caramal (Australia) are from quartz breccia zones located in the basal 1.8-1.7 Ga-old Kombolgie sandstones that belong to the Kombolgie basin located in the northern part of the larger McArthur basin (Derome et al., 2003). They were kindly provided by A. Richard (Géoressources, Nancy). The main identified metamorphic event in this area is linked to the Barramundi orogen that occurred between 1.89 and 1.87 Ga, that is before deposition of rocks from the Kombolgie basin. Formation of these quartz crystals is probably linked to shallow circulation of fluids during the emplacement of mafic intrusions (Kyser et al., 2000). These intrusions in the Kombolgie basin have been dated at 1648 ± 29 Ma (Page, 1988). Quartz formed later than illites dated at 1650 ± 80 Ma with the Ar-Ar method (Kyser et al. (2000) and refs. therein).

Avranches (France)

Samples from Avranches (France) are from quartz veins intruded in the western part of the Mancellian batholith. They were kindly provided by F. Avice. The Mancellian batholith belongs to the Cadomian domain thought to have been originally located in the northern border of Gondwana before its dislocation by Paleozoic orogenies. The Mancellian batholith is one of the plutons associated with the Cadomian orogeny. Plutons in this geological area have been dated between 615 and 480 Ma. Sampled from quartz veins were probably intruded in the pluton during the late stages of cooling and hydrothermal activities. Radiometric dating results in the sampling area permit to estimate an age of 530 ± 10 Ma (1σ) for these samples (see Chantraine et al. (1994) and refs. therein).

Rhynie chert (Scotland)

The Rhynie chert (Scotland) was formed by hydrothermal circulation of meteoritic fluids that leached the crustal basement. Samples were provided by C. Rice (University of Aberdeen, UK). The Rhynie chert has been extensively studied since it contains early traces of micro-fauna dated at 396 ± 12 Ma Rice et al. (1995). The Rhynie chert also records the isotopic composition of the ancient atmosphere with a trapped $^{40}Ar/^{36}Ar$ ratio of 294.1 ± 1.5 (Cadogan, 1977) (re-normalized, Pujol et al. (2013b)) lower than the modern atmosphere (298.56, Lee et al. (2006)). These samples are thus ideal to track the isotopic composition of Xe in the Cambrian atmosphere.

2.2 Analytical methods

Analytical methods used during this study are described in this section. The basic principles as well as some key points are briefly explained but detailed descriptions also appear in "Methods" sections in the second and third papers presented in Chapter 3.

2.2.1 Noble gas mass spectrometry

Basis of the noble gas mass spectrometry rely on three major steps that are the extraction, purification and analysis of the noble gases. A great variety of extraction techniques and apparatus exist such as crushing, step-heating by conduction or induction, laser heating, laser ablation etc. In this study new crushers have been developed to release xenon (and other noble gases plus nitrogen) trapped in fluid inclusions. Purification is often based on home-made purification systems and procedures (Zimmermann et al., 2015) adapted for each experiment. Abundances and isotopic compositions of noble gases and nitrogen are then measured with noble gas mass spectrometers (Wieler, 2014).

Analytical improvements for extraction and purification of gases

Two major analytical improvements were necessary to analyze Xe contained in fluid inclusions in quartz samples. The first improvement concerns the crushing apparatus used in this study. Large amounts of samples (1-2 g) had to be loaded in the crushers because low Xe abundances ($\simeq 10^{-16}$ mol.g^{-1} of ^{130}Xe). Classical crushers used at CRPG (Nancy) consist in stainless tubes containing a magnetically-driven iron stick. However, only up to 500 mg of samples can be loaded in such crushers and Xe blank are sometimes very high ($>10^{-17}$ mol) due to the friction of the iron piston on the walls of the stainless tube. A new type of crusher has thus been developed. It consists in a modified VAT valve (Fig. 2.10) where the below is replaced by a stainless tube crushing the sample when the modified valve is closed. These new crushers are very efficient to release gas contained in fluid inclusions. Furthermore Xe blanks are very low ($\simeq 10^{-19}$ mol of ^{130}Xe) because of the absence of friction of the tube on crusher's walls.

The second analytical improvement concerns the purification of gas released from fluid inclusions. Fluid from inclusions is dominated by water. To purify the gas, high purity Ti-sponge is usually placed in one-end tubes connected to the line (called "getters") that are usually operated at 500-600°C and then at room temperature in order to decompose water at high temperatures (HT) and to trap produced hydrogen at low temperature (LT). In our case, these simple tubes were not sufficient to remove all the water released from fluid inclusions. Gas pressures in the purification line remained very high, up to 10^{-4} mbar, even after several cycles of purification (HT/LT). An "online getter" has thus been developed. It consists in a two-end tube containing Ti-sponge heated at 750°C. The crusher is placed at one end and the other end is connected to the rest of the purification line. This analytical assembly ensures that gas extracted from quartz samples and recovered in the purification line passes through the whole getter (10 cm) and, thus, that all water

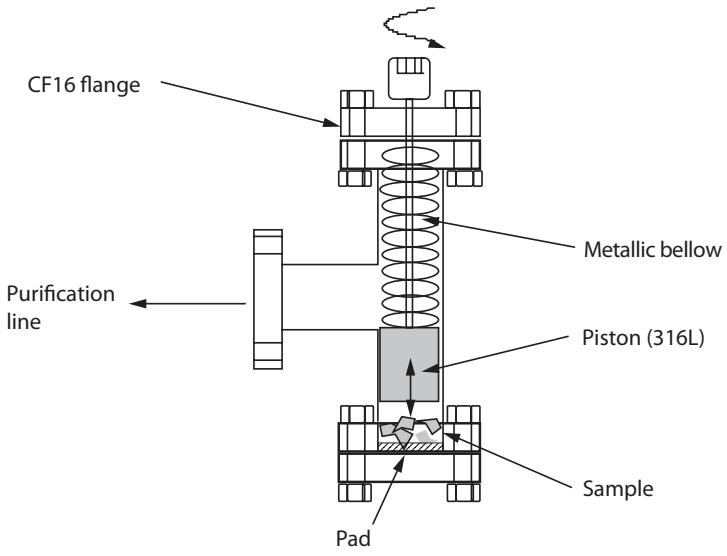

Fig. 2.10: Crushers developed during this study and used to release Xe trapped in fluid inclusions in quartz samples. Adapted from Zimmermann (2014).

molecules interact with the Ti-sponge. It is very efficient to remove water with pressures in the line down to 10^{-8} mbar, which is within the range of the nominal pressure measured when standard aliquots made from purified air are inserted in the purification line for calibration of the mass spectrometer.

The remaining part of the purification procedure, before introduction into the mass spectrometer, is more classical. Xenon and a fraction of the krypton were condensed during 20 mn on a quartz tube held at liquid nitrogen temperature (77 K). This adsorption on the walls of the glass tube is unlikely to induce any isotopic fractionation (Marrocchi and Marty, 2013). Gas in the remaining parts of the line was then pumped out. Archean quartz crystals usually contain ^{40}Ar excess (Pujol et al., 2013b), so that the remaining fraction of argon in the glass tube was often so high that, during preliminary experiments, its presence prevented an efficient ionization of Xe and thus reduced the sensitivity of the mass spectrometer for Xe. Ten dilutions of the volume of glass tube (20 cm^3) into the whole line (1500 cm^3) dramatically decreased, by a factor of 750, the residual Ar partial pressure. Xe- and Kr-rich gas fractions were subsequently released and purified with three Ti-sponge getters held at 550 °C during 5 mn and at room temperature during 5 mn before introduction of the gas aliquot in the mass spectrometer.

High-precision isotopic analysis of Xenon

We received a new multicollector mass spectrometer (Helix MC Plus by Thermofisher Scientific, HMC+ hereafter) in May 2013 at CRPG. This new machine has a very high resolution (>750) permitting to separate hydrocarbon from Xe on mass spectra and is also very stable compared to older models.

Tuning of the source For Xe and Kr analyses, the source of the HMC+ was tuned to find the equilibrium between sufficient sensitivity and acceptable peak shape i.e. a well-defined and large plateau. Source parameters are listed in Table 2.3. An example of a peak shape for ^{132}Xe is displayed in Fig. 2.11.

Gas introduction The total volume of the mass spectrometer (mass spectrometer + two getters) was higher (4100 cm^3) than the volume of the purification line (around 1000 cm^3). For this reason, the equilibration time of the partial pressure of gas into the mass spec was large. Two minutes were needed to reach the equilibrium as shown in Fig. 2.12.

Table 2.3: Source conditions for precise measurement of Xe and Kr with the HMC+ mass spectrometer.

Source Parameter	Value	Unit
Acceleration Voltage	9.9	kV
Trap Current	310	μA
Trap Voltage	13.11	V
Ion Repeller	-1.98	V
Electron Energy	79.37	eV
Extraction Focus	16	%
Extraction Lens	76.89	%
Extraction Symmetry	31.04	%
Horizontal Symmetry	46.23	%
Flatapole	0	V
Rotation Quad	-5	%
Vertical Deflection N	55	V
Vertical Deflection S	120	V

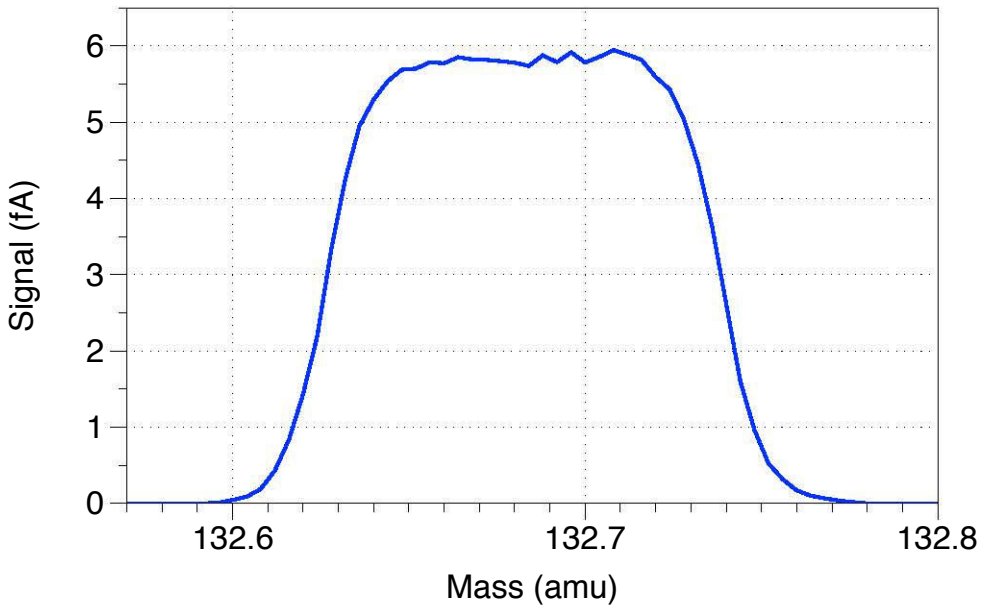

Fig. 2.11: Mass scan for ^{132}Xe with the source conditions listed in Table 2.3. The variations on the peak plateau are due to a low integration time of the signal. The plateau is large (0.07 amu) allowing a straightforward peak centering and limited variations of isotopic ratios even if the magnet is not stable.

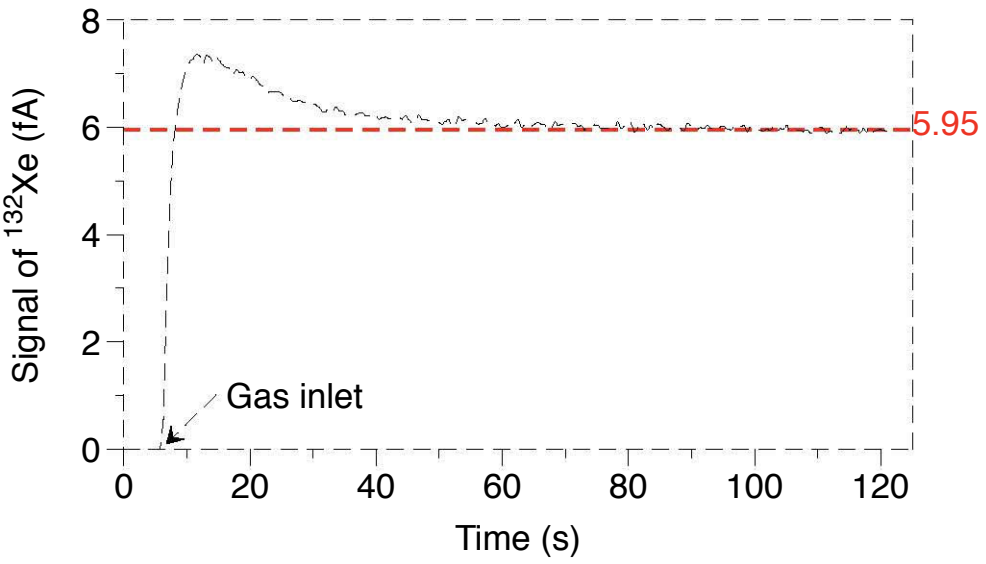

Fig. 2.12: Signal of ^{132}Xe with time after gas introduction into the HMC+ mass spectrometer. The equilibrium was reached after 2 minutes.

Table 2.4: Analytical procedure used to measure Xe isotopes in peak jumping mode with the HMC+ mass spectrometrer.

Number of cycles:	**22**	**Manual peak centering**		
Isotope	Mass (on AX) amu	Collector	Settling time (ms)	Integration time (s)
^{124}Xe	124.996	AX CDD*	5000	8.39
^{126}Xe	126.95	AX CDD	600	8.39
^{128}Xe	128.89	AX CDD	600	4.19
^{129}Xe	129.86	AX CDD	600	4.19
^{130}Xe	130.89	AX CDD	600	4.19
^{131}Xe	131.94	AX CDD	600	4.19
^{132}Xe	132.96	AX CDD	600	4.19
^{134}Xe	134.95	AX CDD	600	4.19
^{136}Xe	136.9	AX CDD	600	4.19

*CDD : "Compact Discrete Dynode" electron multiplier

Analytical procedure The analytical procedure is described in Table 2.4. The nine xenon isotopes were analyzed in peak jumping mode from ^{124}Xe to ^{124}Xe repeatedly during 22 cycles. The progressive increase of the mass during each cycle guaranteed the stability of the magnet and prevented potential hysteresis issues. A manual peak centering procedure preceded each measurement. This manual centering permitted to center Xe peaks even during blank procedure during which low Xe signals usually prevent the automated centering procedure to work efficiently. The first measurement for ^{124}Xe was preceded by a long settling time of 5 s in order to ensure the stabilization of the magnet after moving from mass 136 to mass 124. For peak jumping on following Xe isotopes ($^{126-136}$Xe), the settling time was set to 600 ms. The integration time of the signal was set to 8.39 s for rare Xe isotopes (^{124,126}Xe) and to 4.19 s for other Xe isotopes (^{128,136}Xe). In total, the analytical procedure lasted 20 mn. During the procedure, the ion consumption was quite large (38 % of the initial Xe amount, Fig. 2.13) because of the high trap current of 310 µA (Table 2.3).

Fig. 2.14 illustrates the stability of the mass spectrometer for the ^{129}Xe/^{132}Xe ratio over one month of

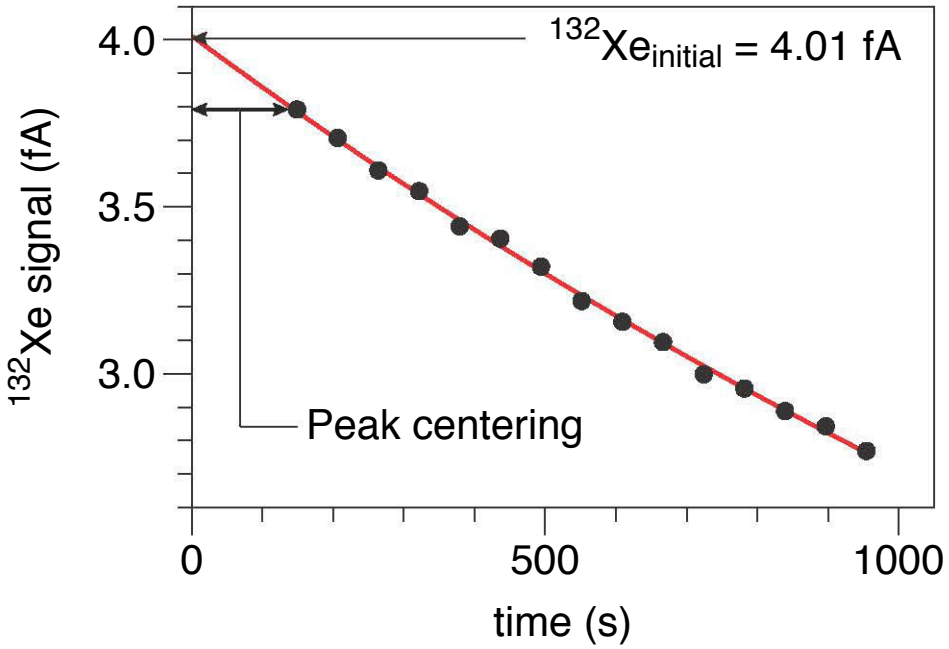

Fig. 2.13: Decrease of the ^{132}Xe signal over one analysis of a standard aliquot. After 20 mn, there is only 62 % of the initial signal. The red curve depicts the exponential fitting applied to compute the initial ^{132}Xe after equilibrium and before peak centering.

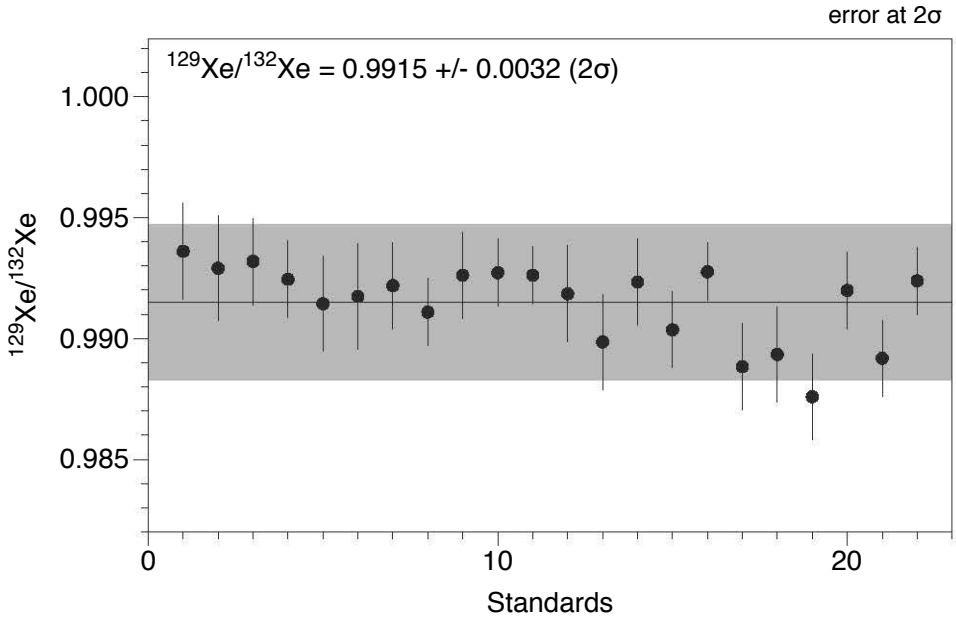

Fig. 2.14: Reproducibility of the Helix MC Plus mass spectrometer during one month of analyzes (30 standards) for the ^{129}Xe/^{132}Xe ratio. Error bars and range at 2σ.

Table 2.5: Reproducibility (standard deviation / mean) for each isotopic ratio of Xe normalized to ^{130}Xe. Reproducibility down to 0.9 ‰ was achieved for the ^{131}Xe/^{130}Xe ratio.

Isotope	^{124}Xe	^{126}Xe	^{128}Xe	^{129}Xe	^{130}Xe	^{131}Xe	^{134}Xe	^{136}Xe
Reproducibility (%)	0.64	0.75	0.43	0.15	0.24	0.09	0.12	0.24

analyses.

Combination of analytical improvements described in the previous section, fine tuning of the ion source of the Helix MC Plus and optimization of the procedure of measurement permitted to achieve a permil precision for the determination of some isotopic ratios of Xe (Table 2.2.1).

For each measured isotopic ratio of noble gases, it was necessary to correct results for blank contribution and mass-fractionation inside the mass spectrometer. These corrections were applied by using isotopic ratios rather than isotope abundances because isotopic ratios are usually more precisely determined by using mass spectrometry techniques. The diverse corrections were done by using Equation 2.1 (with the example of xenon):

$$R^i = (\frac{^iXe}{^{130}Xe})_{corr} = \frac{^{130}Xe_{mes} \times (\frac{^iXe}{^{130}Xe})_{mes} - {}^{130}Xe_{blk} \times (\frac{^iXe}{^{130}Xe})_{blk}}{^{130}Xe_{mes} - {}^{130}Xe_{blk}} \times \frac{(\frac{^iXe}{^{130}Xe})_{atm}}{(\frac{^iXe}{^{130}Xe})_{std}} \quad (2.1)$$

where i=124-136, ^{130}Xe is the isotope used to compute isotopic ratios and subscripts corr, mes, blk, atm, std are for corrected, measured, blank, atmospheric and standard, respectively. The error on each isotopic ratio was then computed by propagation of the error on each term of equation 2.1 by using Equation 2.2:

$$\sigma_{R^i} = \sqrt{\sum_j (\frac{\partial R^i}{\partial X_j} \times \sigma_{X_j})^2} \quad (2.2)$$

where X_j and σ_{X_j} correspond to the value and associated error for each term of equation 2.1.

Isotopic analysis of krypton

The priority of this study was to obtain high-precision isotopic ratios of Xe contained in samples of various ages. It is difficult to properly separate Kr from Xe because these two noble gases condensed at close temperatures. Krypton was thus analyzed most of the time after Xe but on the same gas fraction. The problem with this analytical method is that jumping from mass 130 to mass 84 induces a large instability of the HMC+ mass spectrometer and that Kr measurements had to begin 25 mn after gas inlet. This is too long to expect a good Kr signal and to extrapolate this signal to the time of gas introduction in the mass spectrometer. Krypton results were thus obtained with a lower precision than those of Xe. To check that the isotopic fractionation measured for Xe (see results in the next chapter) did not also occur on Kr, separated samples of the same rocks were analyzed with a reversed procedure where Kr was the first noble gas to be analyzed and Xe was analyzed afterwards. This procedure ensured a good precision on isotopic ratios of Kr.

Another issue with krypton results is that our standard bottle is not calibrated for Kr abundances. It is thus not possible to give results with Kr abundances for the moment. A calibration is planned in the near future. Correction of results should be straightforward because there is just a rule of three to apply.

2.2.2 Ar-Ar extended method: Ar-Ar ages and halogens (I, Cl, Br) abundances

The Ar-Ar extended method

Some collected samples were also analyzed following the Ar-Ar extended method (Turner and Bannon, 1992). This methods consists in irradiating the samples in a nuclear reactor before analysis by crushing and step-heating extraction techniques. During irradiation, samples were exposed to a high neutron flux producing nucleogenic noble gas isotopes with abundances proportional to those of the parent nuclides Cl, Br, I, K, and Ca (Table 2.6). The advantage of this technique is that information about the K(^{39}Ar)-Ar age of the samples together with data on the halogen and U, Ca, Ba abundances are obtained at the same time. Furthermore this method is able to detect very low quantities of iodine (at the ppb level) compared to conventional crush-leach techniques. Details on the irradiation are present in the supplementary material of paper in section 3.3 of Chapter 3.

Table 2.6: Nuclear reactions producing noble gas isotopes from neutron captures on halogens. Adapted from Kendrick (2012).

Parent element	Nuclear reaction	Proxy isotope
K	^{39}K(n, p)^{39}Ar	$^{39}Ar_K$
Cl	^{37}Cl(n, γ)^{38}Cl(β)^{38}Ar	$^{38}Ar_{Cl}$
Br	^{79}Br(n, γ)^{80}Br(γ)^{80}Kr	$^{80}Kr_{Br}$
I	^{127}I(n, γ)^{128}I(β)^{128}Xe	$^{128}Xe_I$
Ca	^{40}Ca(n, α)^{37}Ar	$^{37}Ar_{Ca}$

Extraction techniques and mass spectrometry

After irradiation and subsequent cooling, samples were step-crushed by using modified Nupro valves in order to release gases trapped in the largest fluid inclusions. Powders were then step-heated up to 1600°C in a Mo-crucible in order to release gases from tiny fluid inclusions and sited in the mineral lattice. Extracted gases were purified on Ti-sponge getters to remove all reactive species. Noble gases (Ar, Kr, Xe) were then condensed during 15 mn on a charcoal placed close to the source of the mass spectrometer (MS1) and held at liquid nitrogen (77K). Noble gases were finally released into the mass spectrometer by heating the charcoal at 100°C.

All data were corrected for mass fractionation in the mass spectrometer, blank contribution, atmospheric contamination, interferences and short-term radioactive decays following the irradiation. Correction and error propagations are identical to those made by Burgess et al. (2002).

Correction of the results: the problem of ^{40}Ar excess

The Ar-Ar method applied to K-poor samples often faces the problem of ^{40}Ar excess ($^{40}Ar_E$ hereafter) (see review by Kelley (2002)). $^{40}Ar_E$ represents the quantity of ^{40}Ar in excess compared to atmospheric argon trapped in the sample during its crystallization (or from atmospheric contamination), and to ^{40}Ar produced in-situ by the decay of ^{40}K. If $^{40}Ar_E$ remains uncorrected, ages obtained by the Ar-Ar method have no significance (Fig. 2.15) since they often exceed the age of the solar system for rocks that cannot be older than 3.4 Ga.

Kelley et al. (1986) demonstrated that, in some samples, $^{40}Ar_E$ is correlated to the chlorine (Cl) content of analyzed samples. This correlation is visible in a ^{40}Ar/^{36}Ar vs. Cl/^{36}Ar plot (Fig. 2.16) where the slope

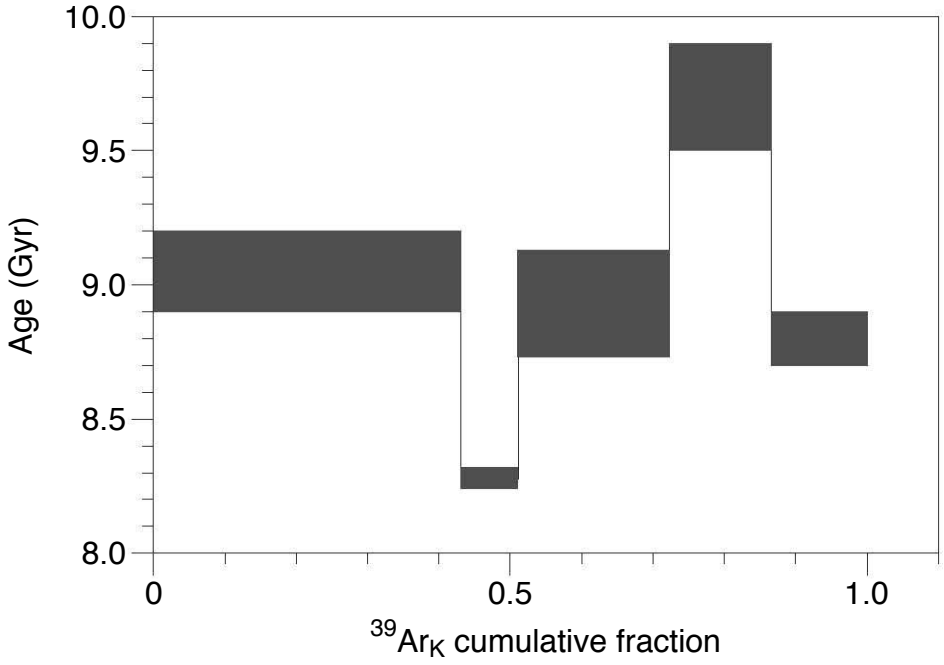

Fig. 2.15: Meaningless ages (> 4.5 Ga) obtained for sample BMGA3-9 without correcting for $^{40}Ar_E$.

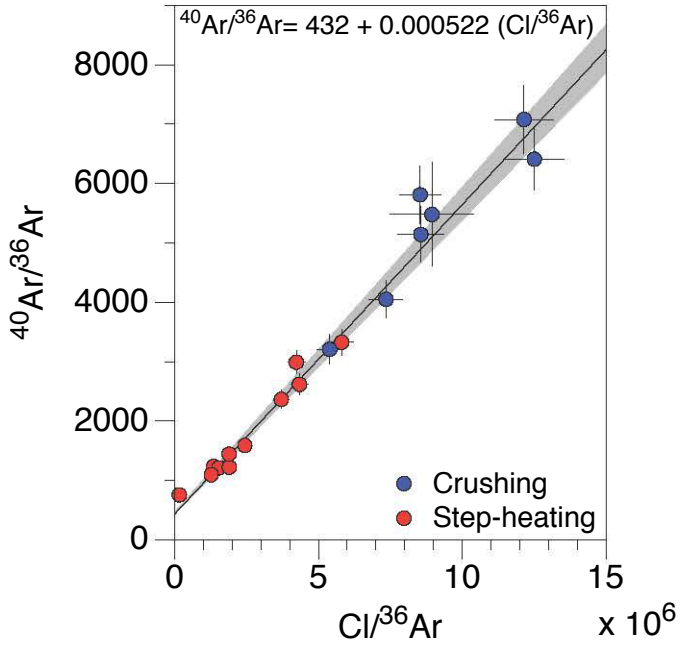

Fig. 2.16: Example of a correlation between $^{40}Ar_E$ and the chlorine content for crushing and step-heating data obtained on irradiated quartz from the Barberton Greenstone Belt. An initial ratio higher than the modern atmosphere is probably due to some $^{40}Ar_E$ uncorrelated with the chlorine content.

gives the correlation between $^{40}Ar_E$ and the chlorine content of the sample. To correct for $^{40}Ar_E$, a 3D correction method can thus be applied with a $^{40}Ar/^{36}Ar$ ratio that follows equation 2.3

$$(\frac{^{40}Ar}{^{36}Ar})_{total} = (\frac{^{40}Ar}{^{36}Ar})_0 + B \times (\frac{Cl}{^{36}Ar}) + C \times (\frac{K}{^{36}Ar}) \quad (2.3)$$

where $(\frac{^{40}Ar}{^{36}Ar})_0$ is the initial atmospheric ratio trapped in the sample and B and C the parameters for a plane in the ^{40}Ar-K-Cl space. Projection of the plane in the 2D ^{40}Ar-K space permits to define an age for the sample. Least squares optimization with removal of outliers (Strutz, 2010) is then used to find what is the best plane passing through crushing and step-heating data is applied. A Monte-Carlo method approach is used to compute error bars on each parameter of the plane in order to have an estimation of the error on each age determined by using this method (see the paper in section 3.2 of Chapter 3 for results of the 3D method).

Another step-by-step correction method was also applied on some samples similarly to what has been done by Pujol et al. (2013b). It consists in correcting results for the hydrothermal component ($^{40}Ar_E$) and testing possible initial $^{40}Ar/^{36}Ar$ ratios and ages. The best fit is obtained when coherent plateau ages are obtained by using the Isoplot software (Ludwig, 1991) and when the Mean Standard Weighted Deviation (MSWD) is close to 1 i.e. when the error on the age is representative of the variability of the dataset.

2.2.3 Analyses of other noble gases (Ne, Ar) and nitrogen

Duplicates of the samples analyzed for Xe and Kr isotopic compositions were also crushed for neon, argon, nitrogen isotopic composition and abundances measurements. Samples were crushed in the same crushers as those presented above. Crushers were directly in contact with a double-walled glass tube system plunged in liquid nitrogen in order to condense water and a major part of other reactive gases (but not nitrogen) on the walls of the tube. After waiting for gas equilibration, the original aliquot was divided in two sub-aliquots by closing a valve. One aliquot was dedicated to Ne-Ar measurements and the other aliquot to N_2 measurement. In the first aliquot, Ar was trapped on a charcoal held at liquid nitrogen temperature (77 K) ensuring no trapping of Ne. Neon was then analyzed on a VG 5400 mass spectrometer. Ar was subsequently released from the charcoal and analyzed in a different run. Separation and purification of nitrogen were made following Zimmermann et al. (2009).

Chapter 3

Results and Implications

Results obtained during this PhD study are presented in this Chapter in the form of accepted articles, publications submitted to peer-reviewed journals or in preparation for a submission. This chapter is divided in sections (one for each paper) organized following a logical progression i.e. following the main stages of Earth's accretion and evolution and thus it does not respect dates of publication. When necessary, a small discussion at the end of each section/paper presents key points, updates or some additional comments.

The first paper concerns results obtained from isotopic analyses of Xe in a CO_2-rich gas emitted in the Eifel magmatic region (Germany). This collaboration with researchers from CRPG (Nancy) and A. Caracausi (INGV, Italy) leads to the demonstration that chondritic (and not Solar) Xe has been isolated in the non-convective mantle for 4.45 Ga and that the Earth's mantle presents a chemical heterogeneity. My contribution to this collaborative work was technical assistance for analyzing the samples, treatment and interpretation of the results, participation in the redaction of the paper presented here.

The second manuscript is on the origins of volatile elements in the Earth's atmosphere inferred from isotopic measurements of xenon trapped in fluid inclusions of quartz samples from the Barberton Greenstone belt (3.2 Ga).

The third paper deals with the evolution of the isotopic composition of atmospheric Xe with time. Analyses of Xe trapped in samples of various ages demonstrates that the isotopic composition of atmospheric Xe evolved over ca. 2.5 Ga (from 4.5 to 2.0 Ga). The elemental and isotopic composition of other noble gases (Ne, Ar, Kr) and nitrogen in the Archean atmosphere is also discussed.

The fourth paper presents corrections applied to the I-Pu-Xe chronometers of the Earth's atmosphere in order to take into account the progressive escape and isotopic fractionation of atmospheric Xe. The age of the Earth's atmosphere is then computed.

Contents

3.1 Article Chondritic Xenon in the Earth's Mantle

The paper presented in this section is the result of a collaboration with A. Caracausi (INGV, Italy). It has been published in the *Nature* journal. This paper explores the isotope systematics of xenon contained in CO_2-rich gases emitted in the Eifel magmatic region (Germany) in order to constrain the origin of Xe in the Earth's mantle and to study global-scale Earth's geodynamics.

LETTER

doi:10.1038/nature17434

Chondritic xenon in the Earth's mantle

Antonio Caracausi[1,2], Guillaume Avice[2], Peter G. Burnard[2]‡, Evelyn Füri[2] & Bernard Marty[2]

Noble gas isotopes are powerful tracers of the origins of planetary volatiles, and the accretion and evolution of the Earth. The compositions of magmatic gases provide insights into the evolution of the Earth's mantle and atmosphere[1–7]. Despite recent analytical progress in the study of planetary materials[8,9] and mantle-derived gases[2–7], the possible dual origin[1,10] of the planetary gases in the mantle and the atmosphere remains unconstrained. Evidence relating to the relationship between the volatiles within our planet and the potential cosmochemical end-members is scarce[5]. Here we show, using high-precision analysis of magmatic gas from the Eifel volcanic area (in Germany), that the light xenon isotopes identify a chondritic primordial component that differs from the precursor of atmospheric xenon. This is consistent with an asteroidal origin for the volatiles in the Earth's mantle, and indicates that the volatiles in the atmosphere and mantle originated from distinct cosmochemical sources. Furthermore, our data are consistent with the origin of Eifel magmatism being a deep mantle plume. The corresponding mantle source has been isolated from the convective mantle since about 4.45 billion years ago, in agreement with models that predict the early isolation of mantle domains[11]. Xenon isotope systematics support a clear distinction between mid-ocean-ridge and continental or oceanic plume sources[6], with chemical heterogeneities dating back to the Earth's accretion[1,7]. The deep reservoir now sampled by the Eifel gas had a lower volatile/refractory (iodine/plutonium) composition than the shallower mantle sampled by mid-ocean-ridge volcanism, highlighting the increasing contribution of volatile-rich material during the first tens of millions of years of terrestrial accretion.

Owing to their inertness, low abundances and the presence of several different radioactive chronometers in their isotope systematics, the noble gases are excellent geochemical tracers of the formation and subsequent evolution of the Earth[1–7]. However, the origin of terrestrial noble gases is not fully understood. The isotopic composition of atmospheric xenon (Xe) is particularly puzzling because it appears to be strongly isotopically fractionated with respect to solar (derived from the protosolar nebula gas and represented by the solar wind composition) and chondritic (derived from an asteroid-like reservoir) components (see, for example, ref. 12). This feature could be a result of ancient atmospheric escape processes, but even after correction for mass-dependent isotope fractionation the isotope composition of atmospheric Xe cannot easily be related to a chondritic or solar origin[12]. One way to investigate the origin of terrestrial volatiles is to precisely document the compositions of noble gases that have been stored in the terrestrial mantle, presumably since the formation of the Earth.

Mantle-derived CO_2-rich gases are particularly powerful resources for investigating mantle-derived noble gases because the large quantities of sample material available make high-precision measurements possible[2–5,13]. Here we report Xe isotopic measurements in gases from a CO_2-rich well (Victoriaquelle) in the Eifel volcanic region (Germany). Geophysical and geochemical evidence suggests that the Eifel volcanism, which took place from 700 kyr ago to 11 kyr ago, was related to continental rifting and large-scale mantle upwelling[14–17]. The Victoriaquelle well, in the southwest of the Eifel region, emits CO_2-dominated gases (99.7%–99.8% CO_2) with helium isotope ratios of 4.2–4.5 Ra (where Ra is the helium isotope signature of the Earth's atmosphere) and $^{40}Ar/^{36}Ar$ ratios of up to 2,690 (ref. 18), consistent with low levels of atmospheric contamination and predominantly mantle-derived volatile emissions[18].

Our Xe isotope data (normalized to ^{130}Xe; Fig. 1, Extended Data Table 1) demonstrate that there is a mantle-derived component to this noble gas, marked by a 2.45% excess (relative to air) of ^{129}Xe from the decay of extinct ^{129}I (half-life of 16 Myr). The dataset also highlights an excess of the lightest isotopes ($^{124–128}Xe$) relative to air Xe. Because the light Xe isotopes are not affected by radiogenic or fissiogenic production, this excess $^{124–128}Xe$ must represent a primordial Xe component. Excesses of light Xe isotopes have already been recognized in some mantle-derived gases[4,5,13]. Furthermore, given that isotopic fractionation during mantle processing is unlikely, these light Xe spectra must therefore reflect the presence of either solar or chondritic Xe (either average

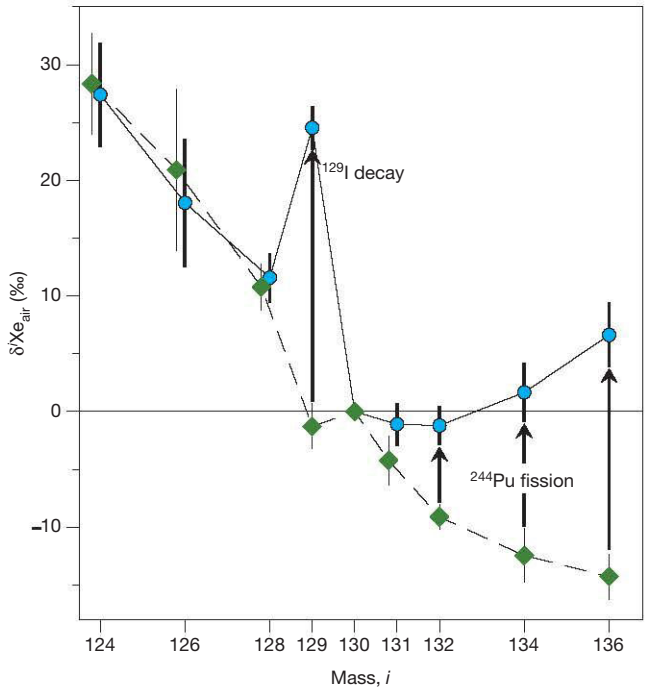

Figure 1 | Xe isotope composition of the Victoriaquelle gas. Data (blue filled circles) are normalized to the isotope composition of atmospheric Xe and to ^{130}Xe. Deviations from the atmospheric composition (Xe_{air}) are expressed in delta notation as parts per mil (‰). For comparison, we show the composition of a mixture composed of 84% atmospheric Xe and 16% chondritic (average carbonaceous chondrite) Xe (green diamonds; see Methods for the derivation of the component fractions). The excesses at masses $i = 129$ and $i = 131–136$ are the products of the extinct radioactivity of ^{129}I (half-life of 16 Myr) and ^{244}Pu (half-life of 82 Myr), respectively. Error bars indicate $\pm 1\sigma$.

[1]Instituto Nazionale di Geofisica e Vulcanologia, Sezione di Palermo, 90146 Palermo, Italy. [2]Centre de Recherches Pétrographiques et Géochimiques, UMR 7358, Université de Lorraine, CNRS, 54501 Vandoeuvre-lès-Nancy, France.
‡Deceased.

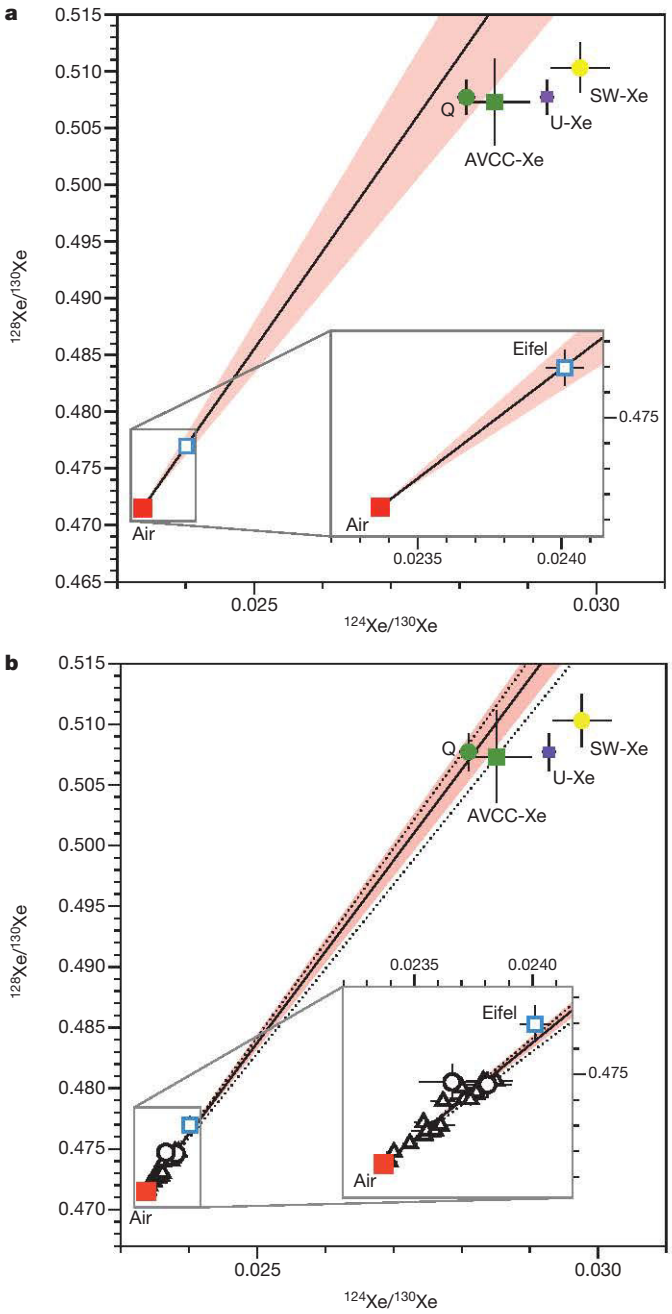

Figure 2 | Light Xe isotope correlations. a, The Eifel composition (open blue square) was derived from the mean of 15 measurements on three different aliquots of the same gas (see Methods). The solid black line is a best-fit line through the air (filled red square) and Eifel compositions; correlation errors were computed using the Isoplot code (courtesy of K. Ludwig, Berkeley Geochronology Center) (the light red envelope represents $\pm 1\sigma$ error). The compositions of phase-Q Xe ('Q', filled green circle; the major carrier of heavy noble gases trapped in primitive meteorites), average-carbonaceous-chondrite Xe ('AVCC-Xe', filled green square; ref. 9 and references therein), solar-wind Xe ('SW-Xe', filled yellow square; ref. 8) and the inferred progenitor of atmospheric Xe ('U-Xe', filled purple square; ref. 9) are also shown for comparison (with $\pm 1\sigma$ error bars). The correlation extrapolates to a chondritic, rather than solar or U-Xe, end-member in the mantle. Because of the overlap in the compositions of the 'Q'-type gases and average carbonaceous chondrites, it is not possible to distinguish the nature of the chondritic Xe carrier phase in the accreting Earth (in our discussion we use 'AVCC' without distinguishing 'Q' from the bulk chondritic composition). **b**, Comparison with other CO_2-rich well gases (Bravo Dome, black triangles; Harding County and Caroline, open circles; refs 5, 13, 19). The Eifel gas is seen either to contain the highest proportion of primordial Xe or to have been less affected by air contamination. The best-fit correlation for the Bravo Dome dataset (black dashed lines represent the upper and lower limit with $\pm 1\sigma$ error range) points to a chondritic composition for Xe in the upper mantle. The best-fit line obtained for the whole dataset (this study and the published well-gas data) also points to a chondritic Xe composition, demonstrating the ubiquitous presence of this component in the mantle.

carbonaceous chondrite or 'phase-Q', a ubiquitous noble gas component found in all classes of primitive meteorites; see, for example, ref. 9) in the Earth's mantle. Because the differences between the isotopic patterns of chondritic and solar-wind Xe are subtle[8,9], it has not previously been possible to differentiate between these two potential primordial sources of Xe. Given the nature of our sample, the high analytical precision of the present study and the recently improved precision on the isotope composition of solar-wind Xe (ref. 8), we are able to assign a chondritic rather than solar origin to the Eifel primordial Xe end-member (Fig. 2a, Methods, Extended Data Fig. 1). According to our calculations for the light isotopes, this chondritic Xe component represents 16% ± 2% of the Eifel gas, the remainder being atmospheric in origin (Methods, Extended Data Fig. 2). This is the highest proportion of primordial Xe identified in mantle-derived volatiles so far (Fig. 2b). Furthermore, the fact that all CO_2 well gases[4,5,13] analysed so far (from Bravo Dome (USA), Harding County (USA) and Caroline (Australia), and which have been ascribed an upper-mantle origin) also point to a chondritic Xe component and lie on a single correlation line with the Eifel gas (shown below to have a mantle plume origin; Fig. 2b), demonstrates the existence of a ubiquitous primordial Xe component in the Earth's mantle. Therefore, chondritic Xe was widely distributed in the proto-mantle during the Earth's accretion. Krypton isotopes also point to a chondritic source for Bravo Dome gases sampling the upper mantle[5], and, together with the present Xe data, support an asteroidal origin for heavy noble gases in the whole mantle.

This study points to several sources of volatile elements on Earth. The ancestor of atmospheric Xe was neither chondritic nor solar in origin because it had to have been relatively depleted in the heavy Xe isotopes (notably ^{134}Xe and ^{136}Xe) compared to documented primordial Xe components[19]. Known nuclear processes cannot resolve this issue because they can only contribute, not deplete, these isotopes. This problem, first recognized four decades ago[20], led to the definition of a primitive Xe component dubbed 'U-Xe' (not to be confused with Xe isotopes produced by ^{238}U fission), which was of solar composition for the light isotopes and depleted in both ^{134}Xe and ^{136}Xe relative to solar and chondritic Xe (ref. 19). Thus, two Xe components appear to co-exist on Earth: chondritic Xe preserved in the mantle and U-Xe found in the atmosphere. Consequently, the non-radiogenic, non-fissiogenic Xe in the atmosphere cannot have been derived from the mantle. To prevent mixing between the two components, the atmospheric Xe must have been added after growth of the Earth had largely been completed.

The heavy Xe isotope composition ($^{131,132,134,136}Xe$) of the mantle is more complex, being a mixture of four isotopically distinct end-members: (1) atmospheric Xe; (2) primordial Xe; (3) fissiogenic Xe produced from ^{244}Pu (^{Pu}Xe); and (4) fissiogenic Xe derived from ^{238}U (^{U}Xe). ^{244}Pu and ^{238}U each produce fissiogenic Xe isotopes in characteristic proportions, which differ from those of atmospheric or chondritic Xe. Excesses of fissiogenic or radiogenic $^{131-136}Xe$ and ^{129}Xe in natural samples can be used to distinguish between magmatic sources and to constrain the timing of mantle differentiation. Both ^{129}Xe and ^{136}Xe were produced in the early Earth by decay of extinct radiochronometers—^{129}I (half-life of 16 Myr) decaying to ^{129}Xe and ^{244}Pu (half-life of 80 Myr) producing $^{131-136}Xe$—while extant ^{238}U also produced $^{131-136}Xe$, but with different ratios to those produced by ^{244}Pu. Thus, the U-Xe system evolved over the entire history of the Earth, whereas the I-Xe and Pu-Xe systems reflect elemental fractionation that occurred during

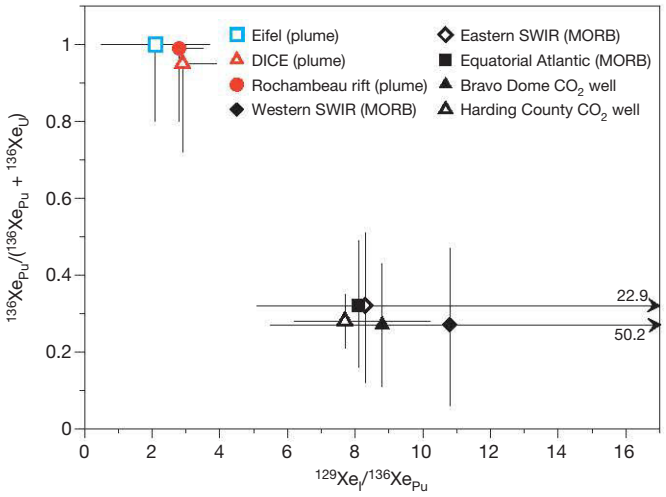

Figure 3 | Differences in the Xe isotopic compositions of the MORB and mantle plume reservoirs. The error-weighted ratios of iodine-derived Xe and plutonium-derived Xe ($^{129}Xe_I/^{136}Xe_{Pu}$) versus the fraction of fissiogenic Xe derived from plutonium ($^{136}Xe_{Pu}/(^{136}Xe_{Pu}+{}^{136}Xe_U)$) enable plume-type mantle sources to be resolved from MORB-type mantle sources[6,7] ($\pm1\sigma$ error bars). The $^{129}Xe_I/^{136}Xe_{Pu}$ and $^{136}Xe_{Pu}/(^{136}Xe_{Pu}+{}^{136}Xe_U)$ ratios of worldwide MORB, plume sources and CO_2 well gas (all data except Eifel) are from refs 6 and 7, computed assuming an average-carbonaceous-chondrite primordial component for all data. The data for the convective mantle (equatorial Atlantic MORB, filled black square; western Southwest Indian Ridge (SWIR), filled black diamond; eastern SWIR, open black diamond; Harding County gas, open black triangle; Bravo Dome gas, filled black triangle) and the mantle plume sources (Iceland (DICE), open red triangle; Rochambeau rift, filled red circle; Eifel gas, open blue square) define two distinct fields in this diagram, highlighting the different histories and compositions of their respective reservoirs.

only the first 100 Myr and 500 Myr, respectively. The fissiogenic Xe isotope composition, obtained after correction for the atmospheric Xe contribution and by assuming a chondritic Xe composition for primordial Xe (Methods, Extended Data Figs 3, 4), suggests that excesses of heavy Xe isotopes resulted from ^{244}Pu fission rather than ^{238}U fission (Methods, Extended Data Figs 5, 6). Quantitatively, the fissiogenic Xe contribution to the Eifel gases is 2.26% ± 0.28%, with the remainder being atmospheric or primordial (Methods). Previous estimates of the proportion of ^{238}U- versus ^{244}Pu-derived Xe in the mantle depended on the initial Xe isotope composition of the mantle[8] (chondritic or solar); the fact that we demonstrate that the light Xe isotopes are chondritic in origin (Fig. 2a, Extended Data Fig. 1) allows us to confidently establish a $^{Pu}Xe/(^{Pu}Xe+{}^{U}Xe)$ ratio of 0.8–1.0 ($\pm1\sigma$) for the Eifel mantle source (Fig. 3, Methods).

In comparison, the other CO_2-rich well gases (Bravo Dome and Harding County; refs 4, 5, 13) have significantly lower $^{Pu}Xe/(^{Pu}Xe+{}^{U}Xe)$ ratios of 0.06–0.51 ($\pm1\sigma$) (Fig. 3). Their mantle source has been identified as the convective upper mantle, which also supplies magmas to mid-ocean ridges worldwide. Mid-ocean ridge basalts (MORBs) that have been analysed with sufficient precision also display low $^{Pu}Xe/(^{Pu}Xe+{}^{U}Xe)$ ratios, comparable to the CO_2-rich well gases above, and define a well-homogenized convective mantle composition that is depleted in ^{Pu}Xe isotopes relative to ^{U}Xe (ref. 6). In a closed-system mantle with a chondritic Pu/U ratio[21], ^{Pu}Xe should dominate over ^{U}Xe ($^{Pu}Xe/(^{Pu}Xe+{}^{U}Xe)=0.97$). A mantle source degassed over geological timescales would see progressive depletion of ^{Pu}Xe and concurrent enrichment in ^{U}Xe still being produced. Therefore, the Eifel $^{Pu}Xe/(^{Pu}Xe+{}^{U}Xe)$ ratio—which is close to 1 and higher than the convective mantle ratio of 0.3 (Fig. 3)—suggests that the Eifel mantle source was much less degassed than the MORB mantle source and, hence, less affected by mantle convection through time. This observation is consistent with the source of the Eifel gas being a deep mantle plume. Two other samples associated with mantle plumes (Iceland plume and the Rochambeau rift in the western Pacific[6]) display comparable $^{Pu}Xe/(^{Pu}Xe+{}^{U}Xe)$ ratios (Fig. 3), also pointing to a mantle plume origin for the Eifel volcanism.

We also calculated a $^{129}Xe_I/^{136}Xe_{Pu}$ ratio of 2.1 ± 1.6 ($\pm1\sigma$) for the Eifel gas (Fig. 3, Methods), a value comparable to the other plume-like signatures (that is, Iceland and the Rochambeau rift[6]) and different from values characteristic of the convective mantle (>5.1; Fig. 3). Assuming a bulk silicate Earth iodine content of between 3 parts per billion (p.p.b.) and 13 p.p.b. (ref. 22 and references therein), we calculated a I-Pu-Xe 'closure age'[12] for the Eifel mantle of 82–139 Myr after the start of Solar System formation, that is, about 4.45 Gyr ago (Methods, Extended Data Fig. 7). Closure ages should be considered as discrete approximations of a continuous process: they assume that the reservoir was open to Xe loss before that time and that it quantitatively retained Xe isotopes produced by extinct radioactivities afterwards. The early closure age calculated here indicates that degassing of the mantle plume source must have been very efficient when the ^{129}I and ^{244}Pu extinct isotopes were still alive, that is, during the first 100 Myr of the history of the Earth. After this time, the Eifel mantle source became efficiently isolated from mantle convection, thus preserving a high $^{Pu}Xe/(^{Pu}Xe+{}^{U}Xe)$ ratio comparable within uncertainty to the closed-system value of 0.97. In contrast, the MORB source reservoir continued to lose ^{Pu}Xe while at the same time producing ^{U}Xe from long-lived ^{238}U fission, resulting in a $^{Pu}Xe/(^{Pu}Xe+{}^{U}Xe)$ ratio of only 0.3 (Fig. 3). Interestingly, a closure age range of 82–139 Myr is consistent with differentiation times of <150 Myr after the start of Solar System formation recorded by the ^{146}Sm–^{142}Nd (see, for example, ref. 11) and ^{182}Hf–^{182}W (see, for example, ref. 23) extinct radioactivity systems. Therefore, the Eifel closure ages might date the last large-scale melting events of the proto-Earth.

If the I/Pu ratio was homogenous during the Earth's accretion, then the higher $^{129}Xe/^{136}Xe_{Pu}$ ratio of the MORB-type sources (Fig. 3) would imply an earlier closure age for the upper mantle than for the plume-type mantle (Extended Data Fig. 7). However, noble gas isotope systematics indicate that the plume-type source is less degassed than the MORB reservoir. It would be paradoxical to suggest that the more-degassed MORB-type mantle became closed to the loss of volatiles before the less-degassed mantle plume source[7]. Thus, it seems more likely that the I/Pu ratio was heterogeneous[1,7] during accretion, with a higher I/Pu ratio in the MORB reservoir than in the plume source. The initial I/Pu ratio must have been at least 3.5 times higher in the MORB source (Extended Data Fig. 7) for the upper mantle to have a younger closure age than the lower mantle. Because iodine is a volatile element and plutonium is a refractory element, the increase in the I/Pu ratio from the deep mantle reservoir source of the Eifel gas to the shallow convective mantle can be viewed as a progressive contribution of volatile-rich material to an initially dry proto-Earth.

The results of this study, coupled with published data[4–7,13], indicate that Xe isotopes in the Eifel gas have preserved a chemical signature that is characteristic of other mantle plume sources (Fig. 3). This corroborates the presence of a deep mantle plume source for the Eifel volcanism, as has previously been suspected[16,17]. Although the helium isotopic signature of the Eifel gas (<6 Ra; refs 17, 18) lies within the field of 'low ^{3}He/^{4}He' mantle plumes (see, for example, ref. 24), the neon isotopes and neon–argon isotope systematics of the volcanic products point to a deep mantle source below the Eifel region[16,17]. The presence of a mantle plume is also supported by geophysical data[15,16,25,26]. Notably, tomographic images show a low-velocity structure at depths of 660–2,000 km, representing deep mantle upwelling under central Europe, that may feed smaller upper-mantle plumes (such as Eifel, Germany and Massif Central, France)[16].

Our results have implications for both the origin of terrestrial volatiles and the mechanisms and timing of their delivery. Neon, and presumably helium, has a solar-like origin[27], suggesting that these gases

were trapped early during terrestrial accretion, before dissipation of the nebular gas. The other mantle noble gases, krypton[5], Xe (this work) and presumably argon, were delivered together with major volatiles such as hydrogen and nitrogen (ref. 28) by asteroidal material before mantle 'closure' (<60 Myr after the start of Solar System formation). Although the non-radiogenic, non-fissiogenic isotope composition of Xe appears to be homogeneous between the deep mantle and the shallower convective mantle, the volatile/refractory (I/Pu) ratio increased during the Earth's accretion, as is independently suggested by palladium–silver isotope data[29]. This is consistent with the existence of a thermal gradient in the forming Solar System, with the innermost zones being too hot to allow condensation of volatile elements during the initial stages of the Earth's accretion. Dissipation of heat over time and/or contributions of volatile-rich bodies from larger heliocentric distances enabled more-efficient trapping of volatile elements in the shallower regions of the growing Earth[30]. The deepest regions of the mantle, now sampled by mantle plumes, have remained efficiently isolated from mantle convection since about 4.45 Gyr ago, thereby preserving a record of the early stages of terrestrial accretion. The origin of the progenitor of atmospheric Xe (U-Xe) remains enigmatic. It is possible that it was added only after the Earth's completion (>82–139 Myr after the start of Solar System formation), thus avoiding any mixing with mantle (chondritic) Xe. This exotic component may have been carried by volatile-rich bodies from the outer Solar System during late veneer episodes or the Late Heavy Bombardment.

Online Content Methods, along with any additional Extended Data display items and Source Data, are available in the online version of the paper; references unique to these sections appear only in the online paper.

Received 12 August 2015; accepted 8 February 2016.
Published online 25 April 2016.

1. Marty, B. Neon and xenon isotopes in MORB: implications for the Earth–atmosphere evolution. *Earth Planet. Sci. Lett.* **94,** 45–56 (1989).
2. Ballentine, C. J., Schoell, M., Coleman, D. & Cain, B. A. 300-Myr-old magmatic CO_2 in natural gas reservoirs of the west Texas Permian basin. *Nature* **409,** 327–331 (2001).
3. Ballentine, C. J., Marty, B., Sherwood Lollar, B. & Cassidy, M. Neon isotopes constrain convection and volatile origin in the Earth's mantle. *Nature* **433,** 33–38 (2005).
4. Holland, G. & Ballentine, C. J. Seawater subduction controls the heavy noble gases composition of the mantle. *Nature* **441,** 186–191 (2006).
5. Holland, G., Cassidy, M. & Ballentine, C. J. Meteorite Kr in the Earth's mantle suggests a late accretionary source for the atmosphere. *Science* **326,** 1522–1525 (2009).
6. Parai, R. & Mukhopadhyay, S. The evolution of MORB and plume mantle volatile budgets: constraints from fission Xe isotopes in Southwest Indian Ridge basalts. *Geochem. Geophys. Geosyst.* **16,** 719–735 (2015).
7. Mukhopadhyay, S. Early differentiation and volatile accretion recorded in deep-mantle neon and xenon. *Nature* **486,** 101–104 (2012).
8. Meshik, A., Hohenberg, C., Pravdivtsev, O. & Burnett, D. Heavy noble gases in solar wind delivered by Genesis mission. *Geochim. Cosmochim. Acta* **127,** 326–347 (2014).
9. Ott, U. Planetary and pre-solar noble gases in meteorites. *Chem. Erde* **74,** 519–544 (2014).
10. Harper, C. L. Jr & Jacobsen, S. B. Noble gases and Earth's accretion. *Science* **273,** 1814–1818 (1996).
11. Boyet, M. & Carlson, R. W. ^{142}Nd evidence for early (>4.53 Ga) global differentiation of the silicate Earth. *Science* **309,** 576–581 (2005).
12. Porcelli, D. & Ballentine, C. J. Models for distribution of terrestrial noble gases and evolution of the atmosphere. *Rev. Mineral. Geochem.* **47,** 411–480 (2002).
13. Caffee, M. W. *et al.* Primordial noble gases from Earth's mantle: identification of a primitive volatile component. *Science* **285,** 2115–2118 (1999).
14. Hoernle, K., Zhang, Y. S. & Graham, D. Seismic and geochemical evidence for large-scale mantle upwelling beneath the eastern Atlantic and western and central Europe. *Nature* **374,** 34–39 (1995).
15. Wedepohl, K. H. & Baumann, A. Central European Cenozoic plume volcanism with OIB characteristics and indications of a lower mantle source. *Contrib. Mineral. Petrol.* **136,** 225–239 (1999).
16. Goes, S., Spakman, W. & Bijwaard, H. A lower mantle source for central European volcanism. *Science* **286,** 1928–1931 (1999).
17. Buikin, A. *et al.* Noble gas isotopes suggest deep mantle plume source of late Cenozoic mafic alkaline volcanism in Europe. *Earth Planet. Sci. Lett.* **230,** 143–162 (2005).
18. Bräuer, K., Kämpf, H., Niedermann, S. & Strauch, G. Indications for the existence of different magmatic reservoirs beneath the Eifel area (Germany): a multi-isotope (C, N, He, Ne, Ar) approach. *Chem. Geol.* **356,** 193–208 (2013).
19. Pepin, R. O. & Porcelli, D. Xenon isotope systematic, giant impacts, and mantle degassing on the Earth. *Earth Planet. Sci. Lett.* **250,** 470–485 (2006).
20. Takaoka, N. An interpretation of general anomalies of xenon and the isotopic composition of primitive xenon. *J. Mass Spectrosc. Soc. Japan* **20,** 287–302 (1972).
21. Hudson, G. B., Kennedy, B. M., Podosek, F. A. & Hohenberg, C. M. The early Solar System abundance of ^{244}Pu as inferred from the St. Severin chondrite. *Proc. Lunar Planet. Sci. Conf.* **19,** 547–557 (1989).
22. Avice, G. & Marty, B. The iodine–plutonium–xenon age of the Moon–Earth system revisited. *Phil. Trans. R. Soc. A* **372,** 20130260 (2014).
23. Touboul, M., Puchtel, I. S. & Walker, R. J. ^{128}W evidence for long-term preservation of early mantle differentiation products. *Science* **335,** 1065–1069 (2012).
24. Graham, D. W. Noble gas isotope geochemistry of mid-ocean ridge and ocean island basalts: characterization of mantle source reservoirs. *Rev. Mineral. Geochem.* **47,** 247–317 (2002).
25. Budweg, M., Bock, G. & Weber, M. The Eifel plume—imaged with converted seismic waves. *Geophys. J. Int.* **166,** 579–589 (2006).
26. Ritter, J. R. R. in *Mantle Plumes: A Multidisciplinary Approach* (eds Ritter, J. R. R. & Christensen, U. R.) 379–404 (Springer-Verlag, 2007).
27. Honda, M. *et al.* Possible solar noble-gas component in Hawaiian basalts. *Nature* **349,** 149–151 (1991).
28. Marty, B. The origins and concentrations of water, carbon, nitrogen and noble gases on Earth. *Earth Planet. Sci. Lett.* **313–314,** 56–66 (2012).
29. Schönbächler, M., Carlson, R. W., Horan, M. F., Mock, T. D. & Hauri, E. H. Heterogeneous accretion and the moderately volatile element budget of Earth. *Science* **328,** 884–887 (2010).
30. Morbidelli, A. *et al.* Source regions and timescales for the delivery of water to the Earth. *Meteorit. Planet. Sci.* **35,** 1309–1320 (2000).

Acknowledgements This work is dedicated to Peter G. Burnard, who passed away after the submission of the manuscript. This study was supported by the Instituto Nazionale di Geofisica e Vulcanologia, by the European Research Council under the European Community's Seventh Framework Programme (FP7/2007-2013 grant agreement no. 267255) and by the Deep Carbon Observatory. D. L. Hamilton helped in setting up the new mass spectrometry system at CRPG. This is CRPG contribution #2413.

Author Contributions A.C., P.G.B. and B.M. designed the study. A.C. collected the samples, performed the experiments and analysed the data. G.A. processed the data and wrote the section on the processing procedure in Methods. A.C., P.G.B., G.A. and B.M. wrote the paper. E.F. collected the samples. All authors contributed to the interpretation and discussion of the data and provided comments on and input to the manuscript.

Author Information Data obtained in this study are available at the EarthChem library (http://dx.doi.org/10.1594/IEDA/100582). Reprints and permissions information is available at www.nature.com/reprints. The authors declare no competing financial interests. Readers are welcome to comment on the online version of the paper. Correspondence and requests for materials should be addressed to A.C. (antonio.caracausi@ingv.it).

METHODS

Analytical method. High-precision Xe isotopic ratios were determined in the Noble Gas Laboratory at the Centre de Recherches Pétrographiques et Géochimiques (Nancy, France) using multi-collection mass spectrometry. Xe isotopic compositions were determined in a sample of free gas collected from the Victoriaquelle well in the Eifel volcanic district (Germany). Gas samples were collected in pre-evacuated (10^{-5} Pa) steel bottles equipped with a high-vacuum valve at the end, after thorough flushing of connecting tubes with the well gas. We purified and analysed three aliquots of gas (Extended Data Table 1). Active gases were removed by sequential exposure to hot and cold SAES getters. Xe was condensed on a cold finger at liquid-nitrogen temperature and the abundances of all Xe isotopes were measured on a Thermofisher noble-gas multi-collector mass spectrometer (Helix MC Plus) operating in a combination of multi-collection and peak-jumping modes.

We carried out a total of 15 measurements on the three aliquots of the same gas (Extended Data Table 1; errors are $1\sigma/\sqrt{n}$, where n is the number of duplicate measurements). Procedural blanks were performed before and after each measurement. Xe blanks were typically 0.16% of the ^{130}Xe signal. Therefore, blank corrections were unnecessary and were not applied to the abundances or isotope ratios reported in Extended Data Table 1. Xenon standard runs were analysed before and during the Victoriaquelle analytical session (total of 30 standard runs with 5.37×10^{-15} mol of ^{132}Xe per aliquot).

We also purified a different aliquot of gas to measure the Ar isotopic ratio. Ar isotope compositions were measured on a GV-instruments multi-collector mass spectrometer. We determined a ^{40}Ar/^{36}Ar ratio of 1,780 for our Victoriaquelle sample, overlapping values reported in previous investigations[18].

Residuals of the fit on light isotopes. We performed a series of calculations to quantitatively identify the best candidate (Q-Xe, AVCC-Xe or SW-Xe) for the primordial Xe component measured in the Eifel gas. We first calculated the relative percentages of atmosphere and primordial component required to obtain the measured isotopic ratios (^{i}Xe/^{130}Xe, $i = 124$–128) for each potential primordial component. The calculated proportions were typically around 87% air mixed with 13% primordial Xe. By taking the mean percentages for each light isotope, we then determined the corresponding isotopic compositions of different mixtures of atmosphere and each primordial component. Extended Data Figure 1 depicts the residuals of this mixing for each case (Q-Xe, AVCC-Xe or SW-Xe). These residuals correspond to the differences between the isotopic ratios measured in the Eifel gas and the modelled isotopic ratios, divided by the corresponding Eifel isotopic ratios for normalization and representation purposes. SW-Xe is a poor candidate for the primordial component, largely owing to its high residual for ^{124}Xe. Q-Xe or AVCC-Xe are the best candidates.

Deconvolution of the Xe isotope spectrum. We assumed that the isotopic spectrum of Xe (excluding ^{129}Xe) was produced from a mixture of four end-members: (1) modern atmosphere; (2) a primordial component (in the following calculations we used Q-Xe as a proxy for present-day bulk chondrite because present-day bulk chondrite analyses (AVCC) probably contain fissiogenic Xe contributions); (3) fissiogenic Xe derived from ^{244}Pu (^{Pu}Xe); and (4) fissiogenic Xe derived from ^{238}U (^{U}Xe).

To estimate the contribution of each component, we divided the problem into two stages.

First, we used the light isotopes (^{124,126,128}Xe/^{130}Xe) to estimate the contribution of the primordial component relative to the atmosphere $\alpha_{\mathrm{prim/atm}}$

$$\alpha_{\mathrm{prim/atm}} = \frac{(^{i}\mathrm{Xe}/^{130}\mathrm{Xe})_{\mathrm{Eifel}} - (^{i}\mathrm{Xe}/^{130}\mathrm{Xe})_{\mathrm{atm}}}{(^{i}\mathrm{Xe}/^{130}\mathrm{Xe})_{\mathrm{Q}} - (^{i}\mathrm{Xe}/^{130}\mathrm{Xe})_{\mathrm{Eifel}}}$$

where $i = 124$, 126 or 128. We used a Monte Carlo method to propagate uncertainties in the isotopic ratios. As an example, the distribution of $\alpha_{\mathrm{prim/atm}}$ obtained using the isotopic ratio ^{124}Xe/^{130}Xe is shown in Extended Data Fig. 2. The average of all $\alpha_{\mathrm{prim/atm}}$ values obtained for $i = 124$, 126 and 128 is $16\% \pm 2\%$ ($\pm 1\sigma$). This value was then used to determine the isotopic composition of a mixture of Q-Xe and atmospheric Xe for the heavy isotopes. The uncertainty in this initial composition was calculated using a Monte Carlo propagation on the uncertainty in $\alpha_{\mathrm{prim/atm}}$ (see the normal distribution in Extended Data Fig. 2).

Second, this initial isotopic composition (renormalized to ^{136}Xe) was used to compute the relative contributions of the initial component (atmospheric Xe and Q-Xe), ^{Pu}Xe and ^{U}Xe required to match the isotopic ratios of the Eifel gases ($^{130–132}$Xe/^{136}Xe). We used ^{131}Xe and ^{132}Xe to constrain the nature of the fissiogenic component because these two isotopes are the most discriminant[31]. The linear system that was solved is

$$\left(\frac{^{i}\mathrm{Xe}}{^{136}\mathrm{Xe}}\right)_{\mathrm{Eifel}} = \beta_{\mathrm{initial}}\left(\frac{^{i}\mathrm{Xe}}{^{136}\mathrm{Xe}}\right)_{\mathrm{initial}} + \beta_{\mathrm{Pu_{Xe}}}\left(\frac{^{i}\mathrm{Xe}}{^{136}\mathrm{Xe}}\right)_{\mathrm{Pu_{Xe}}} + \beta_{\mathrm{U_{Xe}}}\left(\frac{^{i}\mathrm{Xe}}{^{136}\mathrm{Xe}}\right)_{\mathrm{U_{Xe}}}$$

where $i = 130$, 131 or 132 (3 equations), $\left(\frac{^{i}\mathrm{Xe}}{^{136}\mathrm{Xe}}\right)_{\mathrm{initial}}$ is the initial composition built during the first stage, $\left(\frac{^{i}\mathrm{Xe}}{^{136}\mathrm{Xe}}\right)_{\mathrm{Pu_{Xe}}}$ and $\left(\frac{^{i}\mathrm{Xe}}{^{136}\mathrm{Xe}}\right)_{\mathrm{U_{Xe}}}$ are the averages of the fissiogenic spectra from ref. 1, and β_{initial} $\beta_{\mathrm{Pu_{Xe}}}$ and $\beta_{\mathrm{U_{Xe}}}$ are the contributions of each component. We used the same approach as that adopted in ref. 6; that is, we used a MATLAB code with the *lsqlin* function, which minimizes the sum of the squared residuals. Because each component was normalized to the uncertainty in the isotopic composition of the Eifel gas, this sum corresponds to a χ^2 value. We used a Monte Carlo method to propagate the errors in the isotopic composition of the Eifel gas as well as in the initial composition determined during the first stage. A convergence of the results was achieved using 10^5 simulations. The χ^2 values computed for each simulation are shown in Extended Data Fig. 3. 75% of the χ^2 values are less than 3.

The final results are presented in Extended Data Fig. 4 (β_{initial}) and Extended Data Fig. 5 ($\beta_{\mathrm{Pu_{Xe}}}$). The fraction of the initial component (atmospheric Xe and Q-Xe) in the final composition is $97.7\% \pm 0.26\%$.

Virtually no simulation leads to a substantial contribution from ^{U}Xe; we demonstrate that $\beta_{\mathrm{U_{Xe}}} = {}^{136}\mathrm{Xe_U} = 0$. To fit a normal distribution to $\beta_{\mathrm{Pu_{Xe}}}$, we had to remove some of the very low values (Extended Data Fig. 5), which resulted in a ^{Pu}Xe contribution of $2.26\% \pm 0.28\%$.

Because $^{136}\mathrm{Xe_U} = 0$, the range for the $^{136}\mathrm{Xe_{Pu}}/(^{136}\mathrm{Xe_{Pu}} + {}^{136}\mathrm{Xe_U})$ ratio is 0.8–1.0 ($\pm 1\sigma$). The $^{129}\mathrm{Xe_I}/^{136}\mathrm{Xe_{Pu}}$ ratio was computed using

$$\frac{^{129}\mathrm{Xe_I}}{^{136}\mathrm{Xe_{Pu}}} = \frac{(^{129}\mathrm{Xe}/^{132}\mathrm{Xe})_{\mathrm{Eifel}} - \beta_{\mathrm{initial}}(^{129}\mathrm{Xe}/^{132}\mathrm{Xe})_{\mathrm{initial}}}{\beta_{\mathrm{Pu_{Xe}}}(^{136}\mathrm{Xe}/^{132}\mathrm{Xe})_{\mathrm{Pu_{Xe}}}}$$

and the errors in $(^{129}\mathrm{Xe}/^{132}\mathrm{Xe})_{\mathrm{Eifel}}$, β_{initial} and $\beta_{\mathrm{Pu_{Xe}}}$ were propagated using the Monte Carlo method. The value obtained for $^{129}\mathrm{Xe_I}/^{136}\mathrm{Xe_{Pu}}$ is 2.1 ± 1.6 ($\pm 1\sigma$), which was then used to compute the closure ages of the Eifel gas mantle source regions.

Code availability. The code for this Letter is available by contacting G.A. (gavice@crpg.cnrs-nancy.fr).

Sample size. No statistical methods were used to predetermine sample size.

Closure ages and I/Pu heterogeneity. The closure ages (in millions of years) of the Eifel gas mantle source regions were calculated using (see, for example, ref. 12)

$$t = \frac{1}{\lambda_{244} - \lambda_{129}} \ln\left[\left(\frac{^{129}\mathrm{Xe_I}}{^{136}\mathrm{Xe_{Pu}}}\right)\left(\frac{^{238}\mathrm{U}}{^{127}\mathrm{I}}\right)_0\left(\frac{^{244}\mathrm{Pu}}{^{238}\mathrm{U}}\right)_0\left(\frac{^{127}\mathrm{I}}{^{129}\mathrm{I}}\right)_0 {}^{136}\mathrm{Y}_{244}\right]$$

where $\lambda_{244} = 8.45 \times 10^{-3}\,\mathrm{Myr}^{-1}$ and $\lambda_{129} = 4.41 \times 10^{-2}\,\mathrm{Myr}^{-1}$ are the decay constants of ^{244}Pu and ^{129}I, respectively, $^{136}\mathrm{Y}_{244}$ is the yield of fission of ^{244}Pu for production of ^{136}Xe (ref. 1), and $^{238}\mathrm{U}_0$, $^{244}\mathrm{Pu}_0$, $^{129}\mathrm{I}_0$ and $^{127}\mathrm{I}_0$ are the initial abundances (in mol) of parent and stable nuclides. Using $\mathrm{U}_0 = 40$ p.p.b. and $\mathrm{I}_0 = 6.4$ p.p.b. (ref. 22), we obtained a closure age of 98^{+41}_{-16} Myr. This age is relatively insensitive to the initial uranium content (U_0) of the bulk-silicate Earth, whereas the initial iodine content (I_0) is important (see Extended Data Fig. 7 for the sensitivity of the closure age to variable initial I/Pu ratios).

31. Ozima, M. & Podosek, F. A. *Noble Gas Geochemistry* 2nd edn, 22 (Cambridge Univ. Press, 2002).

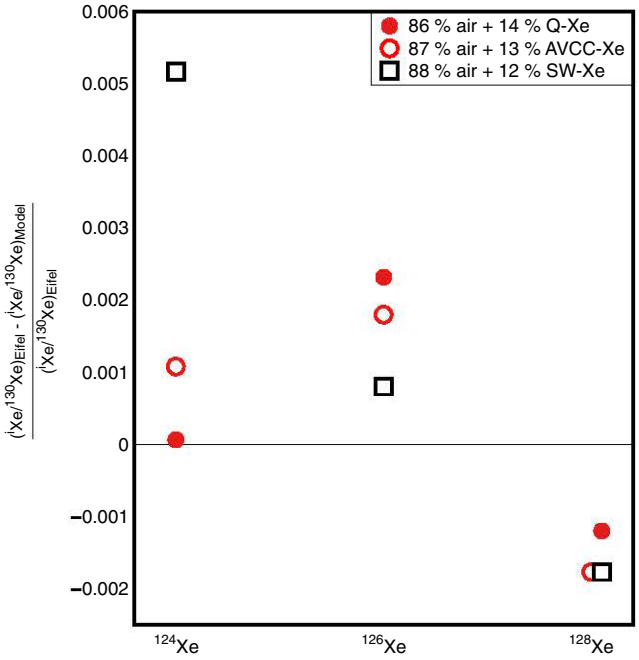

Extended Data Figure 1 | Residuals of the different mixing possibilities. Calculations were performed for the light isotopes ($^{124-128}$Xe) using the isotopic compositions of air (typically about 87%) and Q-Xe, AVCC-Xe or SW-Xe (typically about 13%). The best fit is achieved by taking either AVCC-Xe or Q-Xe as the primordial component. SW-Xe does not produce an adequate fit and therefore is not a suitable candidate for this component (as also shown in Fig. 1).

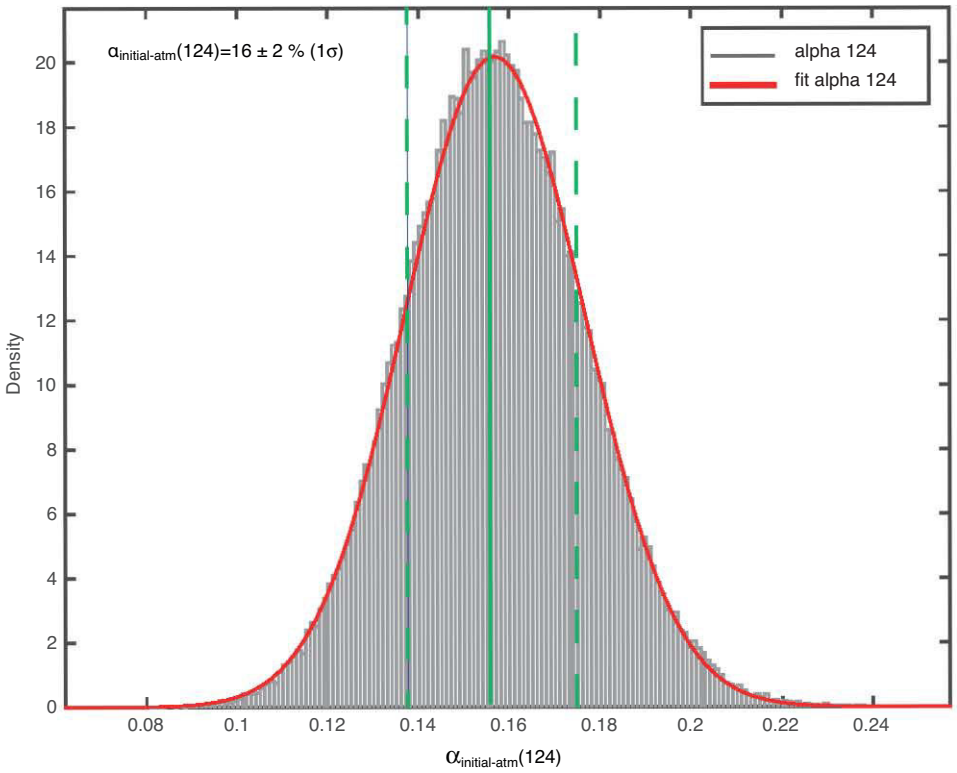

Extended Data Figure 2 | Deconvolution of the proportion of the primordial component (Q-Xe) relative to the atmosphere for $^{124}Xe/^{130}Xe$. The red line represents the result of the normal fit. The solid green line depicts the mean value and the dashed green lines depict the error range of $\pm 1\sigma$.

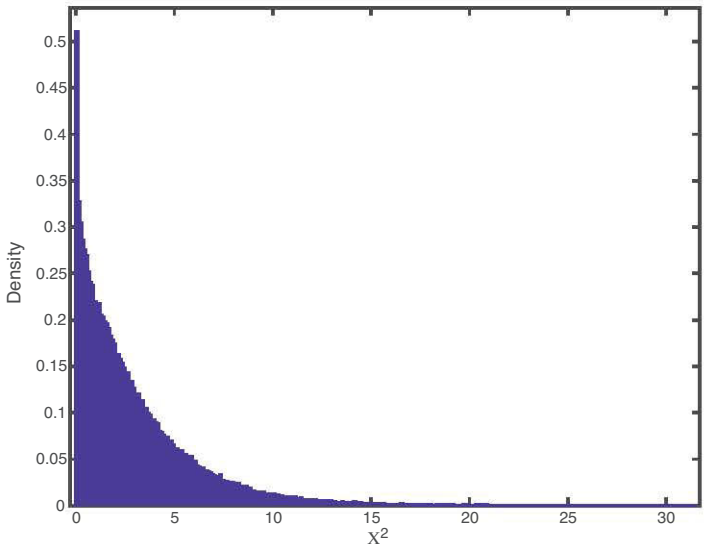

Extended Data Figure 3 | Range of χ^2 values obtained from the simulations. Approximately 75% of the values are less than 3.

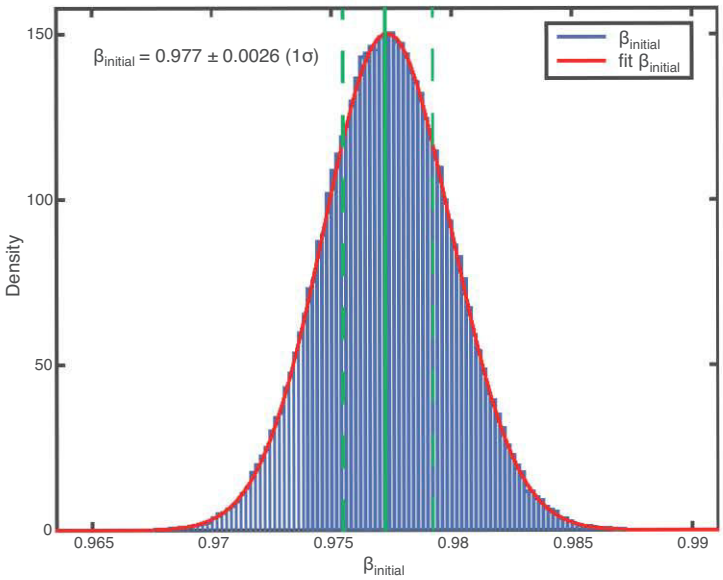

Extended Data Figure 4 | Fraction of initial component required to fit the isotopic composition of the Eifel gas. The solid green line depicts the mean value and the dashed green lines depict the error range of $\pm 1\sigma$.

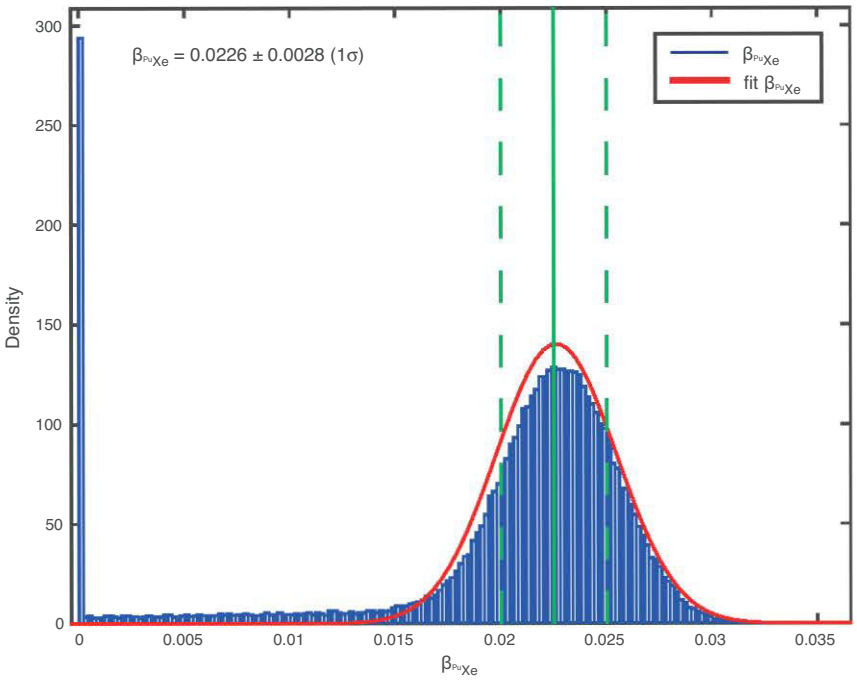

Extended Data Figure 5 | Fraction of Pu-Xe required to fit the isotopic composition of the Eifel gas. Some very low values (those less than 10^{-5}) were excluded from the calculations, resulting in a mean of 2.26% (green line) and a standard deviation of 0.28% (1σ).

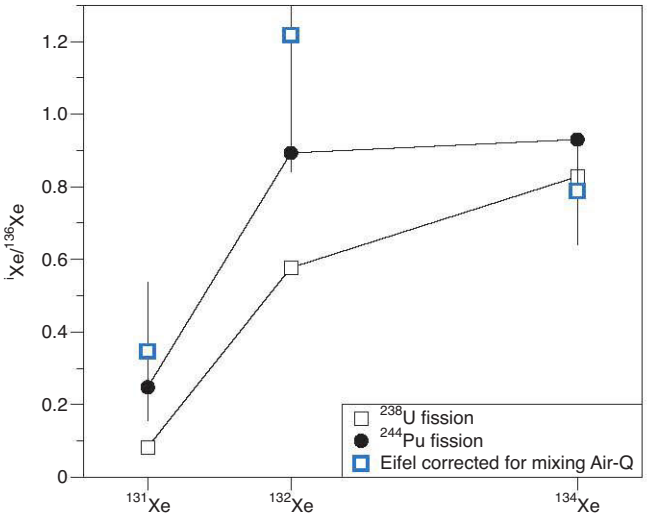

Extended Data Figure 6 | Isotopic composition of heavy isotopes ($^{131-134}$Xe). The data are normalized to ^{136}Xe of the Eifel gas after correction for atmospheric and primitive chondritic contributions, and compared to the fission spectrum of $^{131-136}$Xe produced by spontaneous fission of ^{238}U and ^{244}Pu. Excesses in heavy isotopes are compatible with spontaneous fission of ^{244}Pu.

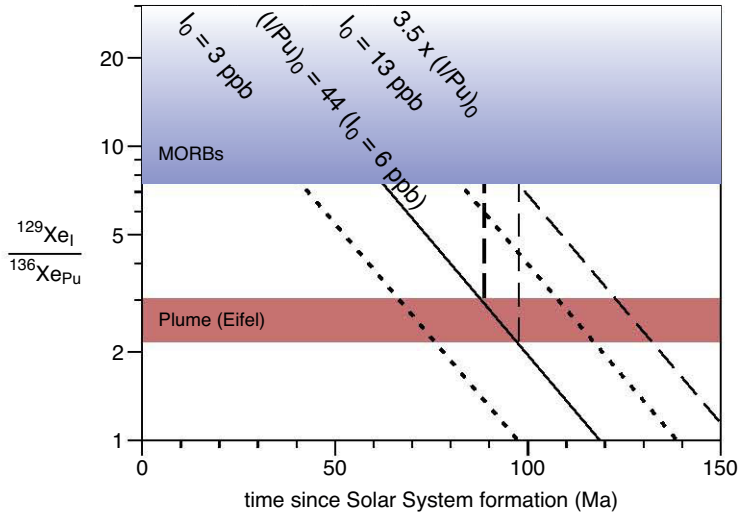

Extended Data Figure 7 | Closure ages calculated from the $^{129}Xe_I/^{136}Xe_{Pu}$ ratios. See Methods for details of the computation method. A younger closure age for the upper mantle is achieved only if the I/Pu ratio is at least 3.5 times higher than the lower-mantle source.

Extended Data Table 1 | Xenon isotopic ratios measured in aliquots of the Eifel gas

	^{130}Xe	$^{124}Xe/^{130}Xe$	$^{126}Xe/^{130}Xe$	$^{128}Xe/^{130}Xe$	$^{129}Xe/^{130}Xe$	$^{131}Xe/^{130}Xe$	$^{132}Xe/^{130}Xe$	$^{134}Xe/^{130}Xe$	$^{136}Xe/^{130}Xe$
Eif_1	7.9E-14	0.024225	0.022345	0.474745	6.654409	5.215284	6.618798	2.560233	2.187465
		0.000109	0.000078	0.000949	0.007304	0.005177	0.007846	0.002519	0.002158
Eif_2		0.023910	0.021997	0.474385	6.590819	5.159161	6.548295	2.532569	2.168481
		0.000130	0.000091	0.000948	0.009207	0.006145	0.008410	0.003489	0.002567
Eif_3		0.024502	0.022549	0.478018	6.681859	5.221782	6.655400	2.558332	2.245266
		0,000100	0.000156	0.001194	0.012001	0.008812	0.010520	0.005035	0.004652
Eif_4		0.024168	0.022220	0.474905	6.657195	5.198561	6.611074	2.553088	2.168967
		0.000291	0.000243	0.002040	0.014614	0.011353	0.013715	0.005527	0.006634
Eif_5		0.024139	0.022287	0.483613	6.646030	5.204344	6.622836	2.590335	2.191245
		0,000073	0.000071	0.000580	0.004642	0.004649	0.005234	0.002039	0.001730
Eif_6	4.8E-14	0.023824	0.021997	0.473584	6.643284	5.210670	6.574350	2.604929	2.205901
		0.000147	0.000093	0.000994	0.007954	0.005690	0.008443	0.003588	0.002612
Eif_7		0.024149	0.022200	0.478799	6.713198	5.209149	6.602612	2.552671	2.171623
		0.000172	0.000126	0.001052	0.013397	0.009307	0.013689	0.004772	0.004285
Eif_8		0.024435	0.022229	0.477518	6.664280	5.223837	6.607845	2.567031	2.193414
		0.000120	0.000129	0.000954	0.008644	0.006741	0.007181	0.003031	0.003246
Eif_9		0.023748	0.022094	0.476777	6.672970	5.199317	6.610295	2.587957	2.206022
		0.000309	0.000283	0.002715	0.021306	0.014451	0.019591	0.007130	0.007618
Eif_10		0.023691	0.022016	0.474975	6.597032	5.166969	6.544023	2.538413	2.165106
		0.000134	0.000089	0.001092	0.009874	0.008206	0.011637	0.003996	0.002991
Eif_11	3.2E-14	0.024006	0.022239	0.481571	6.667457	5.230183	6.637291	2.566452	2.178160
		0.000254	0.000232	0.001588	0.011310	0.008307	0.010491	0.005051	0.004298
Eif_12		0.023815	0.022016	0.475436	6.657245	5.221550	6.583217	2.569755	2.197417
		0.000130	0.000170	0.001235	0.009964	0.008811	0.010406	0.004551	0.003469
Eif_13		0.023881	0.022278	0.477177	6.673390	5.224593	6.648375	2.570202	2.197580
		0.000123	0.000127	0.000715	0.009322	0.006742	0.006568	0.004046	0.003036
Eif_14		0.023729	0.021977	0.477007	6.665152	5.215294	6.600769	2.594237	2.190850
		0.000152	0.000141	0.001239	0.009311	0.007765	0.007173	0.004340	0.003242
Eif_15		0.023939	0.022462	0.475946	6.648185	5.208323	6.582498	2.562519	2.188883
		0.000133	0.000158	0.000761	0.008624	0.006204	0.008454	0.003026	0.003239
Eifel		0.024011	0.022194	0.476964	6.655500	5.207268	6.603179	2.567248	2.190425
		0.000065	0.000046	0.000707	0.007827	0.005231	0.008213	0.005221	0.005209

Individual Xe isotopic ratio measurements ('Eif_*n*') for three different aliquots of the same gas. Errors (1σ) are reported in the cell below each ratio. The 'Eifel' ratios represent the average of 15 measurements ('Eif_1' to 'Eif_15') of three aliquots of the same gas. The amounts of ^{130}Xe are in mol and errors are 5%.

3.1.1 Additional Comments and Research Perspectives

Main results of this study are that Xe in the Earth's mantle has a Chondritic rather than Solar origin. The fissiogenic and radiogenic signatures are close to those found for xenon contained in plume-derived samples (Parai and Mukhopadhyay, 2015), suggesting a deep mantle influence for the Eifel magmatism. Furthermore, closure ages for the deep and upper mantle are coherent only if the deep mantle closed 4.45 Ga ago and if some iodine-rich "wet" material contributed significantly to the upper mantle.

Analyses of the isotopic composition of Kr in the same CO_2-rich gas from Eifel are planned in order to verify that, similarly to Holland et al. (2009), Kr isotopes point toward a chondritic component. Isotopic analyses of Ne are also envisaged since a previous study demonstrated that isotopic ratios of Ne in the Eifel gas fall on a mixing line parallel to the classical MORB-air mixing line (Bräuer et al., 2013). This translation above the MORB-air mixing line is maybe the evidence of the influence of the plume beneath Eifel.

The two reviewers that commented a first version of the paper presented above pointed out that the high contribution from a chondritic primordial component to Eifel Xe recorded may have two explanations: lower shallow-level air contamination or lower atmospheric contamination (by subduction) directly in the deep reservoir. During October 2015, a new sampling campaign permitted to recover gases from two wells in the Eifel region: Victoriaquelle and Schwefelquelle. Numerous samples were recovered in order to understand the process of shallow-level air contamination and to eventually correct the isotopic composition of Xe for this process. Sampling from two other gas sources in the Massif Central (France) have also been collected to decipher if magmatism in the Massif Central area has been influenced by a plume and maybe by the same plume than the Eifel region as proposed by geophysical studies (Goes et al., 1999). Unfortunately, samples recovered so far present very low $^{40}Ar/^{36}Ar$ ratios close the atmospheric value. Some air contamination probably happened during sampling. A new campaign with a better sampling equipment is planned to recover less contaminated samples.

3.2 Article Archean xenon reveals a possible cometary origin for the Earth's atmosphere

This article is in preparation for a submission to the Nature journal. It is divided into a short main text containing 3 figures and a "Methods and Extended Data" section containing additional details and figures.

In preparation for a submission to the Nature journal

Archean Xenon Reveals a Possible Cometary Origin for the Earth's Atmosphere

G. Avice[1], B. Marty[1], R. Burgess[2], A. Hofmann[3]

[1]CRPG-CNRS, Université de Lorraine, UMR 7358, 15 rue Notre-Dame des Pauvres, BP 20, 54501 Vandoeuvre-lès-Nancy Cedex, France.
[2]School of Earth and Atmospheric Sciences, University of Manchester, Oxford Rd, Manchester M13 9PL, UK.
[3]Department of Geology, University of Johannesburg, Auckland Park 2006, Johannesburg, South Africa.

Determining the origin of the atmosphere and early Earth's geodynamics are major issues in Earth sciences (Marty, 2012). Noble gases are exceptional geochemical tracers to achieve this goal. Xenon (Xe), the heaviest noble gas, is particularly relevant due to its large (9) number of isotopes having different nucleosynthetic origins, and to its ability to record isotopic fractionation processes (Ott, 2014). However, the initial isotopic composition of atmospheric Xe remains unknown as well as the mechanisms involved in its depletion in the Earth's atmosphere and its isotopic fractionation compared to other primordial reservoirs of the solar system (Marty, 2012). Our analyses of volatile elements (Xe, Ar, Kr) contained in fluid inclusions in Archean samples reveal the isotopic composition of the atmosphere ≈3.2 Ga ago. An archean atmospheric $^{40}Ar/^{36}Ar$ ratio of 202 ± 58 (2σ) confirms previous models of early and intensive crustal extraction during the Archean (Pujol et al., 2013). Here we also show that Archean atmospheric Xe has an isotopic composition intermediate between potential primordial components and the modern atmosphere with an isotopic fractionation of 13.2 ± 1.9 ‰.u^{-1} (2σ) relative to the latter. After correction for isotopic fractionation, ^{129}Xe excess measured in Barberton quartz is lower (6.07 ± 0.21 % (1σ)) than in the modern atmosphere (6.8 ± 0.3 %, (Porcelli and Ballentine, 2002)). It corresponds to a vigorous $^{129}Xe(I)$ degassing flux of 9 ± 5 mol.a^{-1} (1σ) during the last 3.2 Ga. Isotopic ratios of xenon measured at very high precision allow us to compute what was the isotopic composition of the primordial unfractionated Xe component brought to the Earth's atmosphere. Our study strengthens previous theoretical calculations (Pepin, 1991) that neither the solar nor the chondritic gases can be the carrying phases of initial atmospheric xenon. A different starting Xe component, similar to U-Xe (Pepin, 1991), depleted in ^{134}Xe and ^{136}Xe is necessary. Comets are objects in the solar system which may carry some nucleosynthetic anomalies necessary to explain this depletion (Levison et al., 2010). Furthermore, these objects are rich in noble gases compared to other volatile elements (Balsiger et al., 2015) and may have brought a significant part of the budget of heavy noble gases to the Earth's atmosphere during the final stages of the terrestrial accretion (Dauphas, 2003; Marty and Meibom, 2007).

The building blocks of the Earth originally accreted in the "dry zone" of the solar system, that is, beyond the so-called snow line at which temperatures were low enough to permit the condensation of volatile compounds (e.g. water and noble gases). The Earth has thus probably acquired its volatile elements (H, N, C, noble gases) later from more distant sources like Main Belt asteroids and/or comets. During the final stages of solar system formation, orbits of asteroids were disturbed by the migration of giant planets and, for some of them; their trajectories crossed Earth's orbit (O'Brien et al., 2014). Even if the isotopic composition of cometary water may prevent comets to be the source of terrestrial water (Altwegg et al., 2015), the high Ar/H_2O ratio measured in comet 67P/C-G by the Rosetta spacecraft (Balsiger et al., 2015) indicates that comets may have contributed significantly to the budget of heavy noble gases in the terrestrial atmosphere (Dauphas, 2003) specially during the terrestrial late heavy bombardment (Marty and Meibom, 2007; Morbidelli et al., 2000).

In search for the origin of volatile elements on Earth, studies of the noble gases in the terrestrial mantle demonstrate the presence of a solar-derived component for light noble gases such as neon (Honda et al., 1991) and helium (Honda et al., 1987). Contrary to light noble gases, krypton analyzed in mantle-derived gases presents an isotopic composition that tends toward a Chondritic (i.e. asteroidal) rather than Solar end-member (Holland et al., 2009). Similarly, xenon contained in the mantle seems to have a chondritic rather than solar origin (*see first paper in Chapter 3 (Results and Implications)*). These observations argue in favor of distinct cosmochemical sources for light (He, Ne) and heavy (Kr, Xe) noble gases in the Earth's mantle.

The terrestrial atmosphere is the main reservoir of noble gases on Earth. The presence of radiogenic noble gases in the atmosphere (^{40}Ar, $^{129,131\text{-}136}Xe$), produced by the radioactive decays of parent nuclides (^{40}K, ^{129}I, ^{244}Pu, ^{238}U) in the mantle and crust, certifies the existence of exchanges between the surface and the silicate Earth. However the ultimate origin of the Earth's atmosphere remains unknown, especially for xenon. Xenon in the Earth's atmosphere is depleted by a factor of 23 when compared to an estimated abundance if terrestrial noble gases were following the same depletion pattern than chondrites relative to the solar composition (Marty, 2012; Pepin and Porcelli, 2002). Furthermore atmospheric Xe is also enriched in heavy isotopes by 30-40 $‰.u^{-1}$ relative to Chondritic (Q-Xe) or Solar (SW-Xe) (Ott, 2014). These two features form the so-called "xenon paradox" (Ozima and Podosek, 2002). Furthermore, once mass-fractionated to match the light Xe isotopes of the atmosphere, both the chondritic and solar components appear to be too rich in heavy isotopes (^{134}Xe & ^{136}Xe) to be potential precursors of atmospheric xenon (Pepin, 1991; Takaoka, 1972). These observations led to the definition of a theoretical primordial component labeled "U-Xe" from multi-spatial correlations involving the isotopic composition of xenon in the solar gas, in the atmosphere and in carbonaceous chondrites (Pepin, 1991). This component closely resembles solar Xe for $^{124\text{-}132}Xe$ isotopes but is depleted in its heavy isotopes ^{134}Xe and ^{136}Xe. However, no study has ever demonstrated its presence in any terrestrial or extraterrestrial material and its hypothetical isotopic composition is ultimately based on the isotopic composition of the modern atmosphere.

Recent studies of Archean barite and quartz samples demonstrate that 3.5 to 3.0 Ga ago, atmospheric Xe had an isotopic composition intermediate, i.e. mass dependently fractionated, between any of the potential primordial components presented above (Solar, Chondritic or U-Xe) and the modern atmosphere (Extended Data Fig. S1) (Pujol et al., 2011; 2009). These preliminary results suggest a progressive long-term evolution of the isotopic composition of Xe that may be linked to an isotopic fractionation of Xe when ionization (Kuga et al., 2015) and trapping of Xe into organic hazes, abundant in the Archean atmosphere, together with a progressive escape of xenon atoms to the outer space (Avice and Marty, 2014; Hébrard and Marty, 2014). However, these studies did not elucidate the original composition of atmospheric xenon, which was then tentatively attributed to Solar or Chondritic (Marty, 2012; Pujol et al., 2011). To test this hypothesis of the evolution of the isotopic composition of the atmosphere and to search for its ultimate origin we selected and analyzed Archean quartz samples with a precision high enough to properly define the isotopic composition of volatile elements in the atmosphere 3.2 Ga-ago and to decipher the potential precursors of atmospheric Xe.

Samples are from one core (BARB 3) drilled in the 3.47 - 3.33 Ga-old Kromberg formation (Onverwacht Group) in the Barberton Greenstone Belt, South Africa. Rock samples are from cm-sized cross-cutting quartz veins (Extended Data Fig. S2) likely linked to early hydrothermal activity (Hofmann and Harris, 2008). The Barberton area underwent only low-grade metamorphism at the greenschist facies (Lowe and Byerly, 1999) ensuring a potential good preservation of volatile elements that have been trapped in fluid inclusions located in early-formed quartz veins. Detailed descriptions of the analytical techniques (Xe measurements and Ar-Ar dating method) as well as computation techniques are provided in the "Methods" section.

3D-correlations to correct for ^{40}Ar excess together with a Monte Carlo method to propagate errors on measurements (Methods, Fig. 1 & Extended Data Fig. S3) lead to an Ar-Ar age of 3.2 ± 0.2 Ga (2σ) for the Barberton quartz sample BMGA3-9 (Figure 1). Even if this range is identical within errors to ages of 3.33 - 3.47 Ga for the cross-cutted formation (Furnes et al., 2013), it may also correspond to some early hydrothermal fluid circulation events (Hofmann and Harris, 2008) linked to the intrusion of adjacent 3.22 Ga-old plutons (de Vries et al., 2006) and/or to the "D2" accretionary stage identified in the area (de Ronde and Wit, 1994). Application of this 3D correction leads to the determination of an initial ^{40}Ar/^{36}Ar of 460 ± 12 (2σ) for sample BMGA3-9 higher than the modern atmospheric ratio of 298.56 (Lee et al., 2006). Such a high value might be explained by the presence of some ^{40}Ar excess uncorrelated with the chlorine content in this computed atmospheric end-member.

A different approach, similar to a previous study (see Pujol et al. (2013), Methods), was used on sample BMGA3-13 to correct data (Table S1) for ^{40}Ar excess. It leads to a similar but less precise age of 3.5 ± 1.0 Ga (2σ, MSWD = 1.06). Initial atmospheric ^{40}Ar/^{36}Ar ratios for BMGA3-13, computed for ages varying between 2.9 and 3.1 Ga (Fig. 1), have values ranging from

191 to 214 with a mean value of 202 ± 58 (2σ) when fluid entrapment. This value for the Archean atmospheric $^{40}Ar/^{36}Ar$ ratio is in line with previous estimates and models calling for a peak in crustal extraction between 3.8 and 2.5 Ga (Pujol et al., 2013).

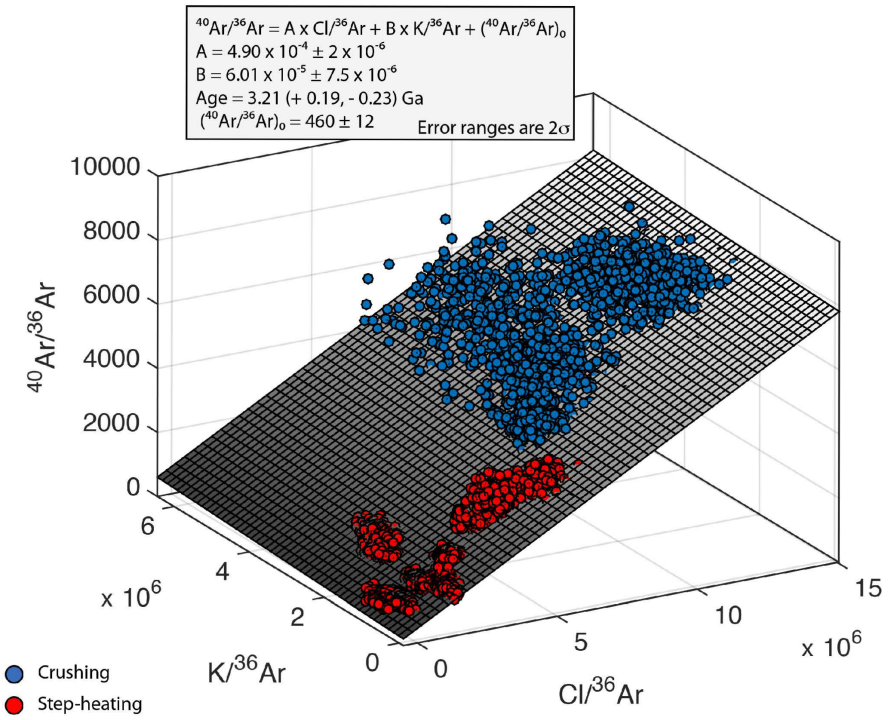

Figure 1: 3D ^{40}Ar-K-Cl-^{36}Ar multi-component diagram showing the results of the Monte Carlo error-propagation method (see Methods for details on the computation). The simulations for crushing steps are shown with blue-filled circles and those for step-heating steps are shown with red-filled circles. The fitted plane appears in grey colors. The projection of the plane on the 2D $^{40}Ar/^{36}Ar$ - $K/^{36}Ar$ space permits to compute an age of 3.2 ± 0.2 Ga (2σ) for fluid entrapment in Barberton quartz sample BMGA3-9.

For xenon, the excellent reproducibility of the results of crushing experiments on different samples and duplicates (Methods and Extended Data Fig. S4) permits to compute a precise error-weighted average for the isotopic ratios of xenon contained in Barberton quartz (Extended Data Table S2 and Fig. S4). The isotopic spectrum of xenon in Barberton quartz normalized to ^{130}Xe (Fig. 2) clearly identifies light isotopes ($^{124\text{-}129}Xe$) excesses together with depletions of heavy isotopes ($^{131\text{-}136}Xe$) relative to the modern atmospheric composition. The absence of mantle-originated ^{129}Xe excesses from the decay of now extinct ^{129}I ($T_{1/2}$=15.7 Ma) together with an isotopic composition of Kr in same samples that is similar to the modern atmosphere (Extended Data Fig. S5) argue against the presence of a mixture between a mantle-derived radiogenic component (Ballentine and Holland, 2008) and modern air in these samples. Xenon in Barberton quartz has thus an Archean atmospheric signature. The xenon isotopic pattern best corresponds to a mass-dependent isotopic fractionation of 13.2 ± 1.9 ‰.u^{-1} (2σ) for 3.2 ± 0.2 (2σ) Ga-old atmospheric xenon relative to the isotopic composition of the modern atmosphere together with $^{131\text{-}136}Xe$ excesses from the spontaneous fission of ^{238}U (Fig. 3 and Extended Data Figure S6). These observations confirm firmly and with greater precision than previous studies that, for light

isotopes ($^{124\text{-}130}$Xe), the isotopic fractionation of xenon in the Archean atmosphere was intermediate between isotopic fractionation recorded by potential primordial components (30 - 40 ‰.u^{-1}) and the modern atmosphere (Extended Data Figure S1).

Modern atmosphere contains a radiogenic ^{129}Xe excess (^{129}Xe(I) hereafter) produced in the silicate Earth by radioactive decay of extinct ^{129}I ($T_{1/2}$ = 15.7 Ma) (Katcoff et al., 1951) and subsequently degassed. Therefore, 6.8 ± 0.3 % (1σ) of atmospheric ^{129}Xe is radiogenic (Porcelli and Ballentine, 2002). The radiogenic ^{129}Xe(I) excess, computed for the 3.2 Ga-old atmosphere after correction for the isotopic fractionation described above, is lower than in the modern atmosphere with a value of 6.07 ± 0.22 % (1σ). This difference allows us to compute a lower limit rate of 9 ± 5 mol.a^{-1} for the degassing rate of ^{129}Xe(I) during the last 3.2 Ga assuming that there was no subsequent loss of atmospheric Xe. This degassing rate is 20 ± 11 (1σ) times higher than the modern ^{129}Xe(I) degassing rate of 0.45 ± 0.02 mol.a^{-1} degassed at mid-ocean spreading centers and estimated from the ^{3}He degassing rate (Bianchi et al., 2010) (see Methods for details on computation of modern and past degassing rates). Such a discrepancy is probably due to the fact that the low modern degassing rate was computed for degassing of the upper-mantle only (Bianchi et al., 2010) whereas our estimated value is for whole mantle degassing in the atmosphere. Degassing of the deep mantle, for example through plume-related magmatism, may thus have played a major role in transferring gases from the silicate Earth to the atmosphere. A higher degassing rate during the last 3.2 Ga may also sign the existence of a vigorous convection regime in the past sustained by a high heat flux produced by very active radioactive decay of parent nuclides (^{40}K, $^{238\text{-}235}$U, ^{232}Th) in the early silicate Earth (Korenaga, 2008).

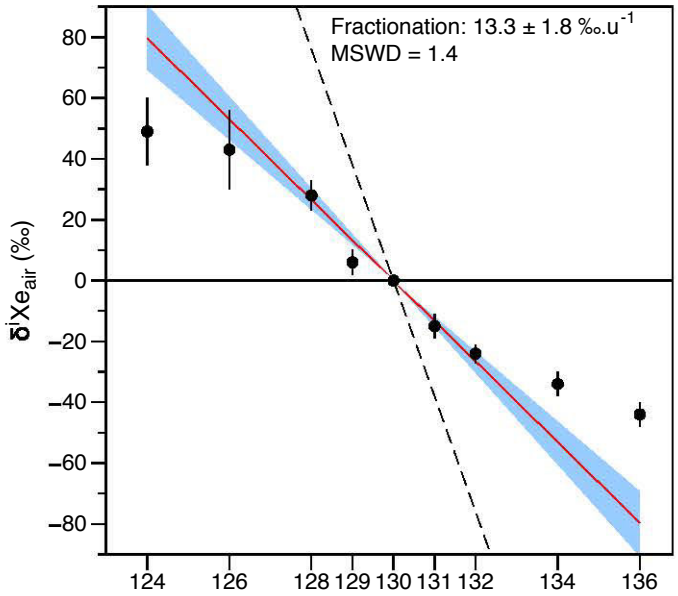

Figure 2: Isotope spectrum of xenon in Barberton quartz samples relative to the isotopic composition of the modern atmosphere and expressed with the delta notation ($\delta^{i}Xe_{air}=((^{i}Xe/^{130}Xe)_{Barb.}/(^{i}Xe/^{130}Xe)_{air}$-1)x1000. The computed isotopic fractionation (13.3 ± 1.8 ‰.u^{-1} (2σ)) appears in red line with its 2σ error envelope in blue color. The dashed line corresponds to the isotopic fractionation of SW-Xe relative to the air (38 ‰.u^{-1}). Note the depletion in ^{129}Xe relative to the mass fractionation corresponding to lower radiogenic ^{129}Xe excess in the Archean atmosphere. Errors at 2σ.

The three-isotope plot of xenon in Fig. 3 demonstrates by using a combination of the heavy isotopes ^{132,136}Xe and the stable isotope ^{130}Xe that, similarly to the modern atmosphere, past-atmospheric xenon trapped in Barberton quartz cannot be simply derived from Q-Xe (Chondritic) or SW-Xe (Solar) following mass-dependent isotope fractionation as these primordial components carry ^{136}Xe excesses (Pepin, 1991) relative to Archean atmospheric Xe. ^{134}Xe and ^{136}Xe excesses relative to the isotopic fractionation recorded by Barberton Xe correspond to addition of products of the spontaneous fission of ^{238}U (Extended Data Figure S6). For this reason Barberton Xe plots on the line of ^{238}U production. Furthermore, light isotopes excesses in the Barberton Xe isotopic spectrum (Fig. 2) correspond to an isotopic fractionation that can be propagated toward heavy isotopes to compute a theoretical primordial isotopic composition for the atmosphere, especially for ^{134}Xe and ^{136}Xe. Here we assume that the starting primordial component had a solar-like ^{132}Xe/^{130}Xe (= 6.061 ± 0.029) ratio (Meshik et al., 2014), that is, the lowest and probably the most pristine value ever measured for the isotopic composition of the solar system (see Methods and Extended Data Fig. S7 for details on the computation).

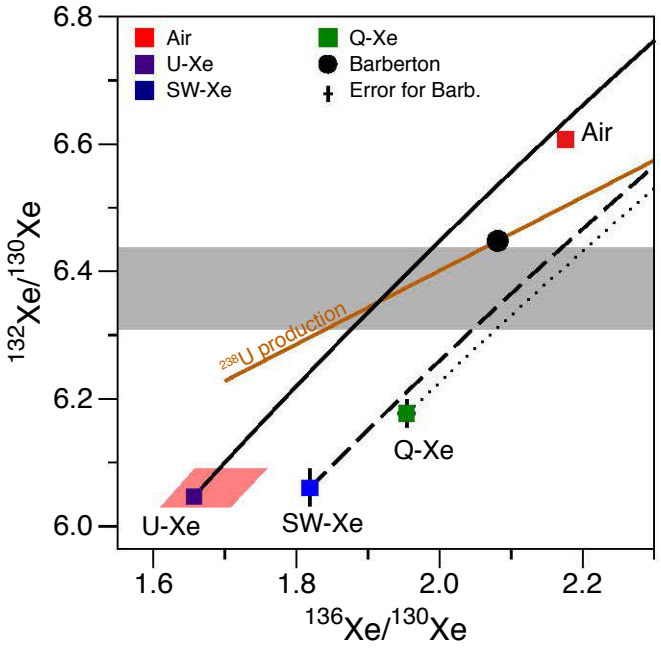

Figure 3: Three-isotope plot of Xe demonstrating that past-atmospheric xenon trapped in Barberton quartz can only be produced by mass-related isotopic fractionation (black line) of a starting isotopic composition (red area) similar to U-Xe (purple square) followed by the addition of xenon from the spontaneous fission of ^{238}U (brown line). Mass-dependent isotope fractionation (dashed and dotted lines) of SW-Xe (Solar Xe, blue square) and of Q-Xe (Chondritic Xe, green square) cannot lead to the isotopic compositions of Barberton or of the modern atmosphere. The grey area represents the range for the non-fissiogenic ^{132}Xe/^{130}Xe ratio of Barberton Xe obtained after propagation of the isotopic fractionation relative to SW-Xe measured on light Xe isotopes (Methods). Errors at 2σ.

The resulting space of possibilities for the starting isotopic composition (range at 2σ) appears in red color in Fig. 3 and in Extended Data Fig. S8 (for ^{134}Xe). It corresponds to ^{136}Xe/^{130}Xe = 1.685 ± 0.075 (2σ) and to ^{134}Xe/^{130}Xe = 2.14 ± 0.07 (2σ). The only known theoretical Xe component that may fit such a starting isotopic composition is U-Xe (Pepin, 1991). The mass-dependent isotopic fractionation of this starting isotopic composition followed by addition of $^{132\text{-}136}$Xe isotopes produced by spontaneous fission ^{238}U with constant and known ^{132}Xe/^{136}Xe and ^{134}Xe/^{136}Xe ratios (Ragettli et al., 1994) reproduce the isotopic spectrum measured in Barberton quartz. Hence, our results demonstrate that a starting isotopic composition similar to U-Xe must exist for the terrestrial ancient atmosphere without any correlation involving the isotopic composition of the modern atmosphere as it was done in previous studies (Pepin, 1991; Takaoka, 1972). It is worth noting that this conclusion relies on the assumption that the isotopic fractionation from the primitive component toward the atmosphere is mass dependent.

Depletions in ^{134}Xe and ^{136}Xe for the primordial component recorded by Barberton quartz sign the presence of a nucleosynthetic anomaly in the early atmosphere compared to other major components of the solar system (Chondritic or Solar Xe). This nucleosynthetic anomaly is problematic, as contribution from meteorites like the carbonaceous chondrites during the final stages of Earth's accretion was traditionally advocated to explain the abundances of volatile elements on Earth (Marty, 2012). However these meteorites and more differentiated ones do not carry such a U-Xe component (Pepin, 2006). Comets are primitive volatile-rich objects in the solar system that are susceptible to carry such an unusual primordial component maybe inherited from other stars formed in the vicinity of our Sun (Levison et al., 2010). Abundances of noble gases, and specially Xe, in comets are poorly known and highly depend on the physical state of the ice (amorphous vs. clathrates). However, a rough estimate of the composition of these objects can be drawn (Tables S4 & S5) based on experimental studies and on results of the Rosetta space mission (Balsiger et al., 2015) (Methods and Extended Data Fig. S9). Comets may have contributed significantly to the budget of atmospheric noble gases, and specially Xe, during the terrestrial late heavy bombardment for example (Extended Data Figure S9) (Marty and Meibom, 2007).

The dichotomy for Xe between the primitive components stored in the mantle and in the atmosphere may thus be explained by distinct mixing for the two reservoirs: Solar/Chondritic for the Earth's mantle and Chondritic/Cometary for the atmosphere. The latter was already present 3.2 Ga ago, and might have been contributed by outer solar system bodies.

Acknowledgments

N. Arndt is gratefully acknowledged for providing samples. L. Zimmermann is thanked for technical mentorship and assistance. Y. Marrocchi, M. Kuga, L. C. P. Martin and R. Belissont are thanked for insightful discussions. This project was funded by the European Research Council under the European Community's Seventh Framework Program (FP7/2007-2013 grant agreement no. 267255 to B.M.).

Contributions

G.A., B.M. and A.H. collected the samples. G.A., B.M. and R.B. performed the experiments. G.A. and B.M. analyzed the data and wrote the paper. All authors commented on the manuscript.

References

Altwegg, K., Balsiger, H., Bar-Nun, A., Berthelier, J.J., Bieler, A., Bochsler, P., Briois, C., Calmonte, U., Combi, M., De Keyser, J., Eberhardt, P., Fiethe, B., Fuselier, S., Gasc, S., Gombosi, T.I., Hansen, K.C., Hässig, M., Jackel, A., Kopp, E., Korth, A., LeRoy, L., Mall, U., Marty, B., Mousis, O., Neefs, E., Owen, T., Reme, H., Rubin, M., Semon, T., Tzou, C.Y., Waite, H., Wurz, P., 2015. 67P/Churyumov-Gerasimenko, a Jupiter family comet with a high D/H ratio. Science 347, 1–3. doi:10.1126/science.1261952

Avice, G., Marty, B., 2014. The iodine-plutonium-xenon age of the Moon-Earth system revisited. Phil. Trans. R. Soc. A 372, 1–16. doi:10.1126/science.1225542

Ballentine, C.J., Holland, G., 2008. What CO2 well gases tell us about the origin of noble gases in the mantle and their relationship to the atmosphere. Phil. Trans. R. Soc. A 366, 4183–4203. doi:10.1016/j.chemgeo.2005.09.030

Balsiger, H., Altwegg, K., Bar-Nun, A., Berthelier, J.J., Bieler, A., Bochsler, P., Briois, C., Calmonte, U., Combi, M., De Keyser, J., Eberhardt, P., Fiethe, B., Fuselier, S.A., Gasc, S., Gombosi, T.I., Hansen, K.C., Hässig, M., Jackel, A., Kopp, E., Korth, A., Le Roy, L., Mall, U., Marty, B., Mousis, O., Owen, T., Reme, H., Rubin, M., Semon, T., Tzou, C.Y., Waite, J.H., Wurz, P., 2015. Detection of argon in the coma of comet 67P/Churyumov-Gerasimenko. Science Advances 1, 1–4. doi:10.1126/sciadv.1500377

Bianchi, D., Sarmiento, J.L., Gnanadesikan, A., Key, R.M., Schlosser, P., Newton, R., 2010. Low helium flux from the mantle inferred from simulations of oceanic helium isotope data. EPSL 297, 379–386. doi:10.1016/j.epsl.2010.06.037

Dauphas, N., 2003. The dual origin of the terrestrial atmosphere. Icarus 165, 326–339. doi:10.1016/S0019-1035(03)00198-2

de Ronde, C.E.J., Wit, M.J., 1994. Tectonic history of the Barberton greenstone belt, South Africa: 490 million years of Archean crustal evolution. Tectonics 13, 983–1005.

de Vries, S.T., Nijman, W., Armstrong, R.A., 2006. Growth-fault structure and

stratigraphic architecture of the Buck Ridge volcano-sedimentary complex, upper Hooggenoeg Formation, Barberton Greenstone Belt, South Africa. Precambrian Research 149, 77–98. doi:10.1016/j.precamres.2006.04.005

Furnes, H., de Wit, M., Robins, B., 2013. A review of new interpretations of the tectonostratigraphy, geochemistry and evolution of the Onverwacht Suite, Barberton Greenstone Belt, South Africa. Gondwana Research 23, 403–428. doi:10.1016/j.gr.2012.05.007

Hébrard, E., Marty, B., 2014. Coupled noble gas-hydrocarbon evolution of the early Earth atmosphere upon solar UV irradiation. EPSL 385, 40–48. doi:10.1016/j.epsl.2013.10.022

Hofmann, A., Harris, C., 2008. Silica alteration zones in the Barberton greenstone belt: a window into subseafloor processes 3.5–3.3 Ga ago. Chemical Geology 257, 221–239. doi:10.1016/j.chemgeo.2008.09.015

Holland, G., Cassidy, M., Ballentine, C.J., 2009. Meteorite Kr in Earth's mantle suggests a late accretionary source for the atmosphere. Science. doi:10.1126/science.1131871)

Honda, M., McDougall, I., Patterson, D.B., Doulgeris, A., 1991. Possible solar noble-gas component in Hawaiian basalts. Nature 349, 149–151. doi:10.1038/349149a0

Honda, M., Reynolds, J.H., Roedder, E., 1987. Noble gases in diamonds: Occurences of solarlike helium and neon. J. Geophys. Res. 92, 507–522.

Katcoff, S., Schaeffer, O.A., Hastings, J.M., 1951. Half-Life of 129I and the Age of the Elements. Phys. Rev. 82, 688–690. doi:10.1103/PhysRev.82.688

Korenaga, J., 2008. Urey ratio and the structure and evolution of Earth's mantle. Rev. Geophys. 46, RG2007–32. doi:10.1029/2007RG000241

Kuga, M., Marty, B., Marrocchi, Y., Tissandier, L., 2015. Synthesis of refractory organic matter in the ionized gas phase of the solar nebula. PNAS 112, 7129–7134. doi:10.1073/pnas.1502796112

Lee, J.-Y., Marti, K., Severinghaus, J.P., Kawamura, K., Yoo, H.-S., Lee, J.B., Kim, J.S., 2006. A redetermination of the isotopic abundances of atmospheric Ar. Geochimica et Cosmochimica Acta 70, 4507–4512. doi:10.1016/j.gca.2006.06.1563

Levison, H.F., Duncan, M.J., Brasser, R., Kaufmann, D.E., 2010. Capture of the Sun's Oort Cloud from Stars in Its Birth Cluster. Science 329, 187–190. doi:10.1126/science.1187535

Lowe, D.R., Byerly, G.R., 1999. Geologic evolution of the Barberton Greenstone Belt and vicinity. Geological Society of America, Special Paper 287–312.

Marty, B., 2012. The origins and concentrations of water, carbon, nitrogen and noble gases on Earth. EPSL 313-314, 56–66. doi:10.1016/j.epsl.2011.10.040

Marty, B., Meibom, A., 2007. Noble gas signature of the late heavy bombardment in the Earth's atmosphere. EEarth 2, 43–49.

Meshik, A., Hohenberg, C., Pravdivtseva, O., Burnett, D., 2014. Heavy noble gases in solar

wind delivered by Genesis mission. Geochimica et Cosmochimica Acta 127, 326–347. doi:10.1016/j.gca.2013.11.030

Morbidelli, A., Chambers, J., Lunine, J.I., 2000. Source regions and time scales for the delivery of water to Earth. MAPS 35, 1309–1320.

Ott, U., 2014. Planetary and pre-solar noble gases in meteorites. Chemie der Erde - Geochemistry 74, 519–544. doi:10.1016/j.chemer.2014.01.003

Ozima, M., Podosek, F.A., 2002. Noble Gas Geochemistry, Second Edition. ed. Cambridge University Press, Cambridge.

O'Brien, D.P., Walsh, K.J., Morbidelli, A., Raymond, S.N., 2014. Water delivery and giant impacts in the "Grand Tack" scenario. Icarus 239, 74–84. doi:10.1016/j.icarus.2014.05.009

Pepin, R.O., 2006. Atmospheres on the terrestrial planets: Clues to origin and evolution. EPSL 252, 1–14. doi:10.1016/j.epsl.2006.09.014

Pepin, R.O., 1991. On the origin and early evolution of terrestrial planet atmospheres and meteoritic volatiles. Icarus 92, 2–79.

Pepin, R.O., Porcelli, D., 2002. Origin of Noble Gases in the Terrestrial Planets. RiMG 47, 191–246. doi:10.2138/rmg.2002.47.7

Porcelli, D., Ballentine, C.J., 2002. Models for Distribution of Terrestrial Noble Gases and Evolution of the Atmosphere. RiMG 47, 411–480. doi:10.2138/rmg.2002.47.11

Pujol, M., Marty, B., Burgess, R., 2011. Chondritic-like xenon trapped in Archean rocks: A possible signature of the ancient atmosphere. EPSL 308, 298–306. doi:10.1016/j.epsl.2011.05.053

Pujol, M., Marty, B., Burgess, R., Turner, G., Philippot, P., 2013. Argon isotopic composition of Archaean atmosphere probes early Earth geodynamics. Nature 498, 87–90. doi:10.1038/nature12152

Pujol, M., Marty, B., Burnard, P., Philippot, P., 2009. Xenon in Archean barite: Weak decay of 130Ba, mass-dependent isotopic fractionation and implication for barite formation. Geochimica et Cosmochimica Acta 73, 6834–6846. doi:10.1016/j.gca.2009.08.002

Ragettli, R.A., Hebeda, E.H., Signer, P., Wieler, R., 1994. Uranium-xenon chronology: precise determination of $\lambda sf*$ 136Ysf for spontaneous fission of 238 U. EPSL 128, 653–670.

Takaoka, N., 1972. An interpretation of general anomalies of xenon and the isotopic composition of primitive xenon. Mass Spectrometry 20, 287–302. doi:10.5702/massspec1953.20.287

Archean Xenon Reveals a Possible Cometary Origin for the Earth's Atmosphere

Methods - Extended Data Figures and Tables

G. Avice[1], B. Marty[1], R. Burgess[2], A. Hofmann[3]

[1]CRPG-CNRS, Université de Lorraine, UMR 7358, 15 rue Notre-Dame des Pauvres, BP 20, 54501 Vandoeuvre-lès-Nancy Cedex, France.

[2]School of Earth and Atmospheric Sciences, University of Manchester, Oxford Rd, Manchester M13 9PL, UK.

[3]Department of Geology, University of Johannesburg, Auckland Park 2006, Johannesburg, South Africa.

Geological setting and samples description

Samples are from one core (BARB 3) drilled in the Barberton Greenstone Belt (BGB) (South Africa). The drilling project is part of an ICDP Project ("Peering into the cradle of life", PI: N. Arndt). The BARB 3 core was drilled in rocks of the Kromberg formation (3.33 - 3.47 Ga) mainly made of a succession of white and black cherts and ultramafic rocks (Furnes et al., 2013). All samples of this study consist in macro-crystalline quartz with different modes of emplacement in rocks from the BGB. Some of the samples are from well-defined cm-sized bedded veins (Fig. S1) with sharp straight-lined (Fig. S1 (a)) or irregular (Fig. S1 (b)) transitions with the adjacent white chert and other samples are from meter-sized coarse quartz veins.

Ar-Ar experiment and determination of ages

Separated quartz fractions of the samples have been analyzed following the extended Ar-Ar method that permits to analyze the K and Cl contents and the isotopic composition of argon at the same time (Kelley, 2002a).

Prior to irradiation, each sample was wrapped in aluminum foil. Samples were placed in a quartz tube, evacuated and sealed to a maximum length of 6.5 cm using a flame. Hb3gr hornblendes were used as neutron monitors and were positioned in the bottom, and top of the tube. Samples were irradiated (irradiation designated "MN2014b") in the G-Ring In-Core Irradiation Tube (GRICIT) facility of the TRIGA Reactor, Oregon State University (OSU). As the halogen-derived noble gas isotopes are produced by low energy thermal neutrons and epithermal neutrons, the irradiation cans were not Cd-shielded. Samples were irradiated for a few hour intervals each day over several weeks (22/4/14 - 1/7/14) to give a total irradiation time of 205 hours for MN2014b.

The irradiation parameter J is determined from the measured $^{40}Ar/^{39}Ar$ ratio in the Hb3gr hornblende standards that were irradiated in the same tubes as the samples (Eq. S1).

$$J = \frac{\left(e^{\lambda t_m} - 1\right)}{{}^{40}Ar^{*}/{}^{39}Ar} \qquad \text{(Eq. S1)}$$

where t_m is the age of Hb3gr of 1074.9 ± 3.5 Ma (Schwarz and Trieloff, 2007) and λ is the total decay constant (5.531 x10^{-10} a^{-1}, (Steiger and Jäger, 1977)). Values of J are 0.01789 ± 0.00008 and 0.01773 ± 0.00008 for Hb3gr monitors place at the top and bottom of the tube, respectively.

The abundances of Ca and Cl in samples can also be determined from Hb3gr using additional irradiation parameters, α (Turner, 1972) and β (Kelley et al., 1986):

$$\frac{K}{Ca} = \alpha \frac{^{39}Ar_K}{^{37}Ar_{Ca}} \quad \text{(Eq. S2)}$$

$$\frac{K}{Cl} = \beta \frac{^{39}Ar_K}{^{38}Ar_{Cl}} \quad \text{(Eq. S3)}$$

The abundances (in wt.%) of K, Ca and Cl in Hb3gr are respectively 1.247 ± 0.008, 7.45 ± 0.09 and 0.2379 ± 0.0032 (Roddick, 1983). Analyses of the neutron monitors gave α values of 0.473 ± 0.002 (top) and 0.497 ± 0.002 (bottom). β values are 1.271 ± 0.018 (top) and 1.263 ± 0.019 (bottom).

Thus in units of moles/cm^3 STP:

$$K = (3.66 \pm 0.03) \times \frac{[^{39}Ar]}{J} \quad \text{(Eq. S4)}$$

$$Ca = (3.57 \pm 0.03) \times \frac{[^{37}Ar]}{J \times \alpha} \quad \text{(Eq. S5)}$$

$$Cl = (4.04 \pm 0.04) \times \frac{[^{38}Ar]}{J \times \beta} \quad \text{(Eq. S6)}$$

The thermal neutron fluence (φ_{th}) can also be calculated using the irradiation parameters determined from Hb3gr. The production of $^{38}Ar_{Cl}$ from ^{37}Cl is almost entirely from thermal neutrons:

$$^{38}Ar_{Cl} = [Cl] \cdot \sigma_{^{37}Cl} \cdot \left[\frac{^{37}Cl}{Cl}\right] \cdot \varphi_{th} \quad \text{(Eq. S7)}$$

where $^{37}Cl/Cl$=0.2424; σ_{th} is the thermal neutron cross-section for $^{37}Cl(n,\beta,\gamma)^{38}Ar$ (0.4330 barns); [Cl] is the chlorine abundance in Hb3gr. For MN2014b, φ_{th} = 2.48 x 10^{18} n.cm^{-2}.

The fast neutron flux (φ_f) is estimated from Hb3gr using:

$$\varphi_f = \frac{J\left(^{40}Ar_K/K\right)(\lambda_e/\lambda)}{\sigma_{^{39}K}\left(^{39}K/K\right)} \quad \text{(Eq. S8)}$$

where λ_e = 0.576 x10^{-10} a^{-1}, σ_{39K} = 2.1 barns; $^{39}K/K$ = 0.9326. For MN2014b, φ_f = 3.27 x 10^{18} n/cm^2.

Following irradiation, samples were analyzed in two successive steps: (1) step-crushing to release fluids trapped in fluid inclusions; (2) step-heating up to 1700°C to release K, Cl and Ar

trapped in small inclusions, and present in the quartz lattice. Extraction, purification, measurement and correction techniques are already described elsewhere (Kendrick et al., 2001).

Results obtained for samples BMGA3-9 and BMGA3-13 are listed in Table S1. The $^{40}Ar/^{36}Ar$ ratios measured during the crushing and step-heating experiments are very high (up to 7000) and cannot be explained by in-situ decay of ^{40}K even during 4.5 Ga. This ^{40}Ar excess, noted $^{40}Ar_E$ hereafter, is correlated to the chlorine content (Fig. S3) and probably linked to an hydrothermal fluid circulation through the samples (Kelley, 2002b). A way to correct the data for this $^{40}Ar_E$ contribution is to use the K-Cl-^{40}Ar space where crushing and step-heating data would lie on a plane with the following equation (Eq. S9):

$$\frac{^{40}Ar}{^{36}Ar} = \left(\frac{^{40}Ar}{^{36}Ar}\right)_0 + A\times\left(\frac{Cl}{^{36}Ar}\right) + B\times\left(\frac{K}{^{36}Ar}\right) \qquad \text{(Eq. S9)}$$

where $\frac{^{40}Ar}{^{36}Ar}, \frac{Cl}{^{36}Ar}$ and $\frac{K}{^{36}Ar}$ are obtained during measurements (Table S1), $\left(\frac{^{40}Ar}{^{36}Ar}\right)_0$ is the initial ratio trapped in the sample, A represents the correlation between $^{40}Ar_E$ and the chlorine content, and B (=$^{40}Ar^*/K$) reflects the relationship between in-situ produced ^{40}Ar ($^{40}Ar^*$) and the potassium content computed from the abundance of ^{39}Ar produced by neutron irradiation. The B value can thus be used to compute an age for the fluid entrapment following equation (Eq. S10):

$$t = \frac{1}{\lambda} ln\left[1 + J\times(4.59\times10^{-6})\times\frac{^{40}Ar^*}{K}\right] \qquad \text{(Eq. S10)}$$

where λ is the decay constant of ^{40}K (5.543×10^{-10} a^{-1}) and J (1.781×10^{-2}) is the dimension-less irradiation related parameter (Kelley, 2002a). The computed B value in the case of BMGA3-9 presented here is 6.01×10^{-5} and corresponds to an age of 3.21 Ga.

The errors on the parameters of the plane defined by the data points were determined by a Monte Carlo propagation method using a Matlab code. For each point a random-generated cloud of 5000 points was created in order to weight each point by its errors in the 3D space (Fig. 1 in the main text). The function "Fit" was applied to the 5000 points and led to a value of 6.01×10^{-5} ($\pm$ 8.5×10^{-6}) for B that corresponds to an age of 3.21 (+0.19; -0.22) Ga (2σ). The $(^{40}Ar/^{36}Ar)_0$, representative of the initial$^{40}Ar/^{36}Ar$ trapped in Barberton quartz, is 460 $\pm$ 12 (2σ) higher than the atmospheric value of 298.6. This higher value is certainly due to some remaining ^{40}Ar excess even after correction for $^{40}Ar_E$ linked to the chlorine content (Fig. S3) and radiogenic ^{40}Ar from in-situ decay of ^{40}K during 3.21 Ga.

A second method originally proposed by Pujol et al. (2013) has been applied to sample BMGA3-13 (see results in Table S1). Firstly, a $Cl\backslash^{40}Ar_E$ ratio of 6500 $\pm$ 949 was obtained from analysis of crushing results. Secondly, this ratio was used to correct step-heating data for the $^{40}Ar_E$ component by subtracting the chlorine content multiplied by $Cl\backslash^{40}Ar_E$ to the total ^{40}Ar. A set of initial $^{40}Ar/^{36}Ar$ ratios and times of fluid entrapments for in-situ decay of ^{40}K were then tested. A best solution was found for an initial atmospheric $^{40}Ar/^{36}Ar$ ratio of 202 $\pm$ 58 (2σ) for a fluid entrapment at 3.5 $\pm$ 1.0 Ga (2σ) with a Mean Standard Weighted Deviation (MSWD) of 1.06. This age, although imprecise, is in agreement with the age of 3.2 $\pm$ 0.2 Ga (2σ) determined with the 3D correlation method applied to sample BMGA3-9.

Detailed analytical procedure for Xe and Kr measurements

Xenon and krypton isotopic compositions (and abundance for Xe) in fluid inclusions in quartz were determined by stepwise crushing (Table S2 and S3). Before noble gas analysis, selected quartz fragments were gently crushed in a metal mortar to obtain granulometric fractions with a size comprised between 1 and 3 mm. This is the ideal range of sizes that minimizes adsorption of air on the surface of the grains and that permits to load up to 2 g of sample per crusher for noble gas analysis in order to get a significant Xe signal. Grains were subsequently cleaned with acetone in an ultrasonic bath, then rinsed with acetone and dried in an oven at 90°C during 30 mn. Quartz grains were subsequently hand-picked under a binocular microscope to ensure the absence of impurities on the surface of the grains and inside individual crystals. Each sample was then loaded in a stainless steel crusher. It consists in a modified valve where the valve's bellow has been replaced by a stainless tube moving downward when the modified valve is closed. Our samples were rich in fluid inclusions and their crushing released significant amounts of water and other inert or chemical reactive species (N_2, hydrocarbons...). Typical Ti-sponge getters, usually placed in a tube connected to the line and used to remove active species, were unable to remove all the water and to decrease its partial pressure in the purification system. A new system was designed that consists in an on-line Ti-sponge getter placed just after the crusher and heated at 700°C ensuring that all the gas recovered at the other end of the getter passed through the Ti-sponge. This new design solved the problem of the water purification, as demonstrated by the low pressure measured before the introduction in the mass spectrometer (*e.g.* 1-5 x 10^{-8} mbar). Xenon and a fraction of the krypton were condensed during 20 mn on a quartz tube held at liquid nitrogen temperature. This adsorption on the walls of the glass tube is unlikely to induce detectable isotopic fractionation (Marrocchi and Marty, 2013). The remaining part of the gas was pumped out. Archean quartz samples usually contain ^{40}Ar excess (Pujol et al., 2013), the remaining fraction of argon in the glass tube was so high that, during a preliminary study, its presence prevented an efficient ionization of Xe and thus reduced the sensitivity of the mass spectrometer for Xe. Ten dilutions of the volume of the glass tube (20 cm^3) into the whole line (1500 cm^3) dramatically decreased, by a factor of 750, the residual Ar partial pressure. Fractions rich in in Xe and Kr were then released and purified on three Ti-sponge getters at 550°C during 5 mn and at room temperature during 5 mn before the introduction into the noble gas multicollector mass spectrometer (Helix MC Plus, Thermo Fisher). Xe was the first gas to be analyzed using a peak jumping mode and an electron multiplier and Kr was subsequently analyzed using a similar procedure. Procedural Xe blanks were monitored before each crushing experiment and were very low, in the order of 10^{-18} mol of ^{132}Xe.

Error propagation and compilation of the results

27 crushing experiments on 7 samples were conducted in total. Isotopic ratios of Xe released during each crushing experiment are shown in Fig. S4. Very reproducible results permitted to compute an error-weighted average for each isotopic ratio (Table S2) with Mean Standard Weighted Deviation values comprised between 0.43 and 1.3.

Isotopic fractionation of Xe in Barberton quartz relative to the modern atmosphere

The isotopic fractionation (13.3 ± 1.8 ‰.u^{-1}) of xenon in Barberton quartz relative to the isotopic composition of the modern atmosphere was computed with the light stable, non-fissiogenic non-radiogenic isotopes of Xe (^{126,128,130}Xe) plus ^{131}Xe, which is little produced by the fission of ^{238}U (Ragettli et al., 1994) by using the Isoplot software (Ludwig, 1991). ^{124}Xe appears depleted relative to the fractionation computed on other light isotopes and has thus not been taken into account to compute the fractionation (*see next paper of Chapter 3 for a discussion on the origin of this ^{124}Xe depletion*).

Fissiogenic end-member from spontaneous fission of ^{238}U

The depletion of ^{134,136}Xe isotopes in the Barberton Xe spectrum (Fig. 2) demonstrates that neither Q-Xe nor SW-Xe can be the starting isotopic compositions for the Earth's atmosphere (see main text). Fractionating Q-Xe or SW-Xe would lead to excesses on ^{134}Xe and ^{136}Xe compared to Barberton. Once corrected for a mass fractionation of 25 ‰.u^{-1} relative to U-Xe, $^{131\text{-}136}$Xe excesses in Barberton quartz are fully compatible with the presence of products of spontaneous fission of ^{238}U (Extended Data Fig. S6).

Degassing rate over 3.2 Ga inferred from low ^{129}Xe(I) excess in Barberton quartz

All errors given in this section are at 1σ.

Modern atmosphere contains (4.06 ± 0.05) x 10^{12} mol of ^{129}Xe (Ozima and Podosek, 2002) and an excess of 6.8 ± 0.3 % of ^{129}Xe(I) (Porcelli and Ballentine, 2002a). This corresponds to 2.8 ± 0.1 x 10^{11} mol of ^{129}Xe(I). Barberton ^{129}Xe/^{130}Xe ratio has a $\delta^{129}Xe_{air}$ value of 6 ± 2 ‰ (Fig. 2 in the main text). Propagation of the isotopic fractionation computed on light isotopes (see above) toward ^{129}Xe leads to a theoretical non-radiogenic delta value ($\delta^{129}Xe_{theor.}$) of 13.3 ± 0.9 ‰ for ^{129}Xe. The difference of 7.3 ± 2.1 ‰ between theoretical and measured deviations relative to the isotopic composition of the atmosphere indicates that the 3.2 Ga-old atmosphere presented a ^{129}Xe(I) excess of 6.07 ± 0.44 % corresponding to (2.47 ± 0.09) x 10^{11} mol of ^{129}Xe(I) with the conservative assumption that no Xe was lost from the atmosphere. This result allows us to compute a lower limit of 9 ± 5 mol.a^{-1} for the degassing rate of ^{129}Xe(I) during the last 3.2 Ga.

Present degassing rate of ^{3}He from the upper-mantle producing Mid Ocean Ridge Basalts is estimated at 527 ± 102 mol.a^{-1}. Taking estimates for the ^{130}Xe/^{3}He ratio (0.00068 or 0.00049 depending on the ^{20}Ne/^{22}Ne ratio for the mantle) and for the ^{129}Xe(I)/^{130}Xe ratio in the MORB source (1.29 to 1.7) (Trieloff and Kunz, 2005), the degassing rate measured for helium corresponds to a degassing rate of 0.45 ± 0.02 mol.a^{-1} for ^{129}Xe(I).

Computation method for the starting isotopic composition of the Earth's atmosphere

The method used to compute the starting isotopic composition for the Earth's atmosphere is graphically explained in Fig. S7. The only starting hypothesis (Fig. S7(a)) is that the starting isotopic composition for Barberton quartz has a ^{132}Xe/^{130}Xe ratio in the range of the solar composition (Meshik et al., 2014). This hypothesis is reasonable because the other known

potential starting isotopic composition is Q-Xe that already carries ^{136}Xe excesses due to either in-situ fission or isotopic fractionation (Kuga et al., 2015; Marrocchi et al., 2015). The second step of the computation consisted in correcting the isotopic composition of Xe in Barberton quartz for contributions of ^{132}Xe and ^{136}Xe produced by the spontaneous fission of ^{238}U (black line in Fig. S7(b)). The pristine starting isotopic composition trapped in Barberton quartz must lie on this line. The green range in Fig. S7 (c) describes the result of the isotopic fractionation computed on light isotopes and applied to the heavy isotope ^{132}Xe. The intersection between the green range and the black line permitted to correct the pristine signal recorded in Barberton quartz for isotopic fractionation (Young et al., 2002) assuming a solar ^{132}Xe/^{130}Xe ratio and gave the blue range in Fig. S7 (d).

Potential contribution of comets to the budget of atmospheric Xe

Estimates of cometary bulk compositions containing amorphous ice or clathrates are listed in Table S4. C, N, water and ^{36}Ar contents do not depend on the modes of formation of ice (clathrates or amorphous ice) but ^{84}Kr and ^{130}Xe abundances highly depend on these parameters. Here we used experimental data obtained during amorphous ice deposition (Bar-Nun and Owen, 1998; Notesco, 2003) and theoretical data on the elemental composition of clathrates formed at 48 K (Mousis et al., 2010) to give estimates of the ^{36}Ar/^{130}Xe and ^{36}Ar/^{84}Kr (Table S5) trapped in cometary amorphous ices or clathrates formed from a gas with a protosolar composition (Lodders, 2003). The ^{36}Ar/H_2O ratio is from the measurement of gases emitted by comet 67P/C-G by the ROSINA mass spectrometer on board the Rosetta spacecraft (Balsiger et al., 2015) and the H_2O content is from Greenberg (1998). N and C contents are from a compilation of results (Le Roy et al., 2015; Rubin et al., 2015). In this study, we explored the effect of a cometary contribution of 10 % wt. in the Terrestrial Late Heavy Bombardment (TLHB) and took a total mass of 2 x 10^{23} g for this late accretionary event (Marty and Meibom, 2007). The contribution to the budget of volatile elements from the remaining 90 % wt. of chondrites is negligible (Marty and Meibom, 2007). The effect on C, N and H_2O abundances is small (Fig. S9) and ensures, for example, a preservation of the chondritic D/H value for Earth's oceans despite the elevated cometary D/H measured for comets (*e.g.* Altwegg et al. (2015)). Contrary to C, N and H_2O, the effect of a 10 % cometary contribution in the TLHB is significant for ^{36}Ar, ^{84}Kr and ^{130}Xe abundances (Fig. S9). Comets may bring the whole surficial budget of ^{36}Ar. The cometary contribution in the terrestrial late heavy bombardment is sufficient to bring the whole ^{84}Kr budget if it was trapped in amorphous ice but in that case ^{130}Xe would correspond to its actual budget in the Earth's atmosphere uncorrected for the 20 fold depletion (Avice and Marty, 2014). If noble gases were trapped in clathrates, a 10% cometary contribution would exceed by 2 to 3 orders of magnitude the surficial budget of Xe and Kr. In any case, a cometary contribution to the Earth's is tentative for ^{36}Ar and cannot be ruled out for ^{84}Kr and ^{130}Xe.

References

Altwegg, K., Balsiger, H., Bar-Nun, A., Berthelier, J.J., Bieler, A., Bochsler, P., Briois, C., Calmonte, U., Combi, M., De Keyser, J., Eberhardt, P., Fiethe, B., Fuselier, S., Gasc, S., Gombosi, T.I., Hansen, K.C., Hässig, M., Jackel, A., Kopp, E., Korth, A., LeRoy, L., Mall, U., Marty, B., Mousis, O., Neefs, E., Owen, T., Reme, H., Rubin, M., Semon, T., Tzou, C.Y., Waite, H., Wurz, P., 2015. 67P/Churyumov-Gerasimenko, a Jupiter family comet with a high D/H ratio. Science 347, 1–3. doi:10.1126/science.1261952

Avice, G., Marty, B., 2014. The iodine-plutonium-xenon age of the Moon-Earth system revisited. Phil. Trans. R. Soc. A 372, 1–16. doi:10.1126/science.1225542

Balsiger, H., Altwegg, K., Bar-Nun, A., Berthelier, J.J., Bieler, A., Bochsler, P., Briois, C., Calmonte, U., Combi, M., De Keyser, J., Eberhardt, P., Fiethe, B., Fuselier, S.A., Gasc, S., Gombosi, T.I., Hansen, K.C., Hässig, M., Jackel, A., Kopp, E., Korth, A., Le Roy, L., Mall, U., Marty, B., Mousis, O., Owen, T., Reme, H., Rubin, M., Semon, T., Tzou, C.Y., Waite, J.H., Wurz, P., 2015. Detection of argon in the coma of comet 67P/Churyumov-Gerasimenko. Science Advances 1, 1–4. doi:10.1126/sciadv.1500377

Bar-Nun, A., Owen, T., 1998. Trapping of Gases in Water Ice and Consequences to Comets and the Atmospheres of the Inner Planets, in: Schmitt, B. (Ed.), Solar System Ices. Springer Netherlands, Dordrecht, pp. 353–366. doi:10.1007/978-94-011-5252-5_15

Furnes, H., de Wit, M., Robins, B., 2013. Gondwana Research. Gondwana Research 23, 403–428. doi:10.1016/j.gr.2012.05.007

Greenberg, J.M., 1998. Making a comet nucleus. A&A 330, 375–380.

Holland, G., Lollar, B.S., Li, L., Lacrampe-Couloume, G., 2013. Deep fracture fluids isolated in the crust since the Precambrian era. Nature 497, 357–360. doi:10.1038/nature12127

Kelley, S., 2002a. K-Ar and Ar-Ar Dating. RiMG 47, 785–818. doi:10.2138/rmg.2002.47.17

Kelley, S., 2002b. Excess argon in K–Ar and Ar–Ar geochronology. Chemical Geology 188, 1–22.

Kelley, S., Turner, G., Butterfield, A.W., Shepherd, T.J., 1986. The source and significance of argon isotopes in fluid inclusions from areas of mineralization. EPSL 79, 303–318.

Kendrick, M.A., Burgess, R., Pattrick, R.A.D., Turner, G., 2001. Halogen and Ar–Ar age determinations of inclusions within quartz veins from porphyry copper deposits using complementary noble gas extraction techniques. Chemical Geology 177, 351–370.

Kerridge, J.F., 1985. Carbon, hydrogen and nitrogen in carbonaceous chondrites: Abundances and isotopic compositions in bulk samples. Geochimica et Cosmochimica Acta 49, 1707–1714. doi:10.1016/0016-7037(85)90141-3

Kuga, M., Marty, B., Marrocchi, Y., Tissandier, L., 2015. Synthesis of refractory organic matter in the ionized gas phase of the solar nebula. PNAS 112, 7129–7134.

doi:10.1073/pnas.1502796112

Le Roy, L., Altwegg, K., Balsiger, H., Berthelier, J.J., 2015. The inventory of the volatiles on comet 67P/Churyumov-Gerasimenko from Rosetta/ROSINA. Astronomy and Astrophysics 583 (A1), pp. 12.

Lodders, K., 2003. Solar system abundances and condensation temperatures of the elements. ApJ 591, 1220.

Ludwig, K.R., 1991. ISOPLOT; a plotting and regression program for radiogenic-isotope data; version 2.53. Open-File Report VL - USGS 91-445, 39.

Marrocchi, Y., Avice, G., Estrade, N., 2015. Multiple carriers of Q noble gases in primitive meteorites. GRL 42, 1–7. doi:10.1002/(ISSN)1944-8007

Marrocchi, Y., Marty, B., 2013. Experimental determination of the xenon isotopic fractionation during adsorption. GRL 40, 4165–4170. doi:10.1002/grl.50845

Marty, B., 2012. The origins and concentrations of water, carbon, nitrogen and noble gases on Earth. EPSL 313-314, 56–66. doi:10.1016/j.epsl.2011.10.040

Marty, B., Meibom, A., 2007. Noble gas signature of the late heavy bombardment in the Earth's atmosphere. EEarth 2, 43–49.

Mazor, E., Heymann, D., Anders, E., 1970. Noble gases in carbonaceous chondrites. Geochimica et Cosmochimica Acta 34, 781–824.

Meshik, A., Hohenberg, C., Pravdivtseva, O., Burnett, D., 2014. Heavy noble gases in solar wind delivered by Genesis mission. Geochimica et Cosmochimica Acta 127, 326–347. doi:10.1016/j.gca.2013.11.030

Mousis, O., Lunine, J.I., Picaud, S., Cordier, D., 2010. Volatile inventories in clathrate hydrates formed in the primordial nebula. Faraday Discuss. 147, 509–525. doi:10.1039/C003658G

Notesco, G., 2003. Gas trapping in water ice at very low deposition rates and implications for comets. Icarus 162, 183–189. doi:10.1016/S0019-1035(02)00059-3

Ott, U., 2014. Planetary and pre-solar noble gases in meteorites. Chemie der Erde - Geochemistry 74, 519–544. doi:10.1016/j.chemer.2014.01.003

Ozima, M., Podosek, F.A., 2002. Noble Gas Geochemistry, Second Edition. ed. Cambridge University Press, Cambridge.

Pepin, R.O., 1991. On the origin and early evolution of terrestrial planet atmospheres and meteoritic volatiles. Icarus 92, 2–79.

Porcelli, D., Ballentine, C.J., 2002a. Models for Distribution of Terrestrial Noble Gases and Evolution of the Atmosphere. RiMG 47, 411–480. doi:10.2138/rmg.2002.47.11

Porcelli, D., Ballentine, C.J., 2002b. An overview of noble gas geochemistry and cosmochemistry. RiMG 47, 1–19. doi:10.2138/rmg.2002.47.1

Pujol, M., Marty, B., Burgess, R., 2011. Chondritic-like xenon trapped in Archean rocks: A possible signature of the ancient atmosphere. EPSL 308, 298–306. doi:10.1016/j.epsl.2011.05.053

Pujol, M., Marty, B., Burgess, R., Turner, G., Philippot, P., 2013. Argon isotopic composition of Archaean atmosphere probes early Earth geodynamics. Nature 498, 87–90. doi:10.1038/nature12152

Pujol, M., Marty, B., Burnard, P., Philippot, P., 2009. Xenon in Archean barite: Weak decay of 130Ba, mass-dependent isotopic fractionation and implication for barite formation. Geochimica et Cosmochimica Acta 73, 6834–6846. doi:10.1016/j.gca.2009.08.002

Ragettli, R.A., Hebeda, E.H., Signer, P., Wieler, R., 1994. Uranium-xenon chronology: precise determination of $\lambda sf*$ 136Ysf for spontaneous fission of 238 U. EPSL 128, 653–670.

Roddick, J.C., 1983. High precision intercalibration of 40Ar-39 Ar standards. Geochimica et Cosmochimica Acta 47, 887–898. doi:10.1016/0016-7037(83)90154-0

Rubin, M., Altwegg, K., Balsiger, H., Bar-Nun, A., 2015. Molecular nitrogen in comet 67P/Churyumov-Gerasimenko indicates a low formation temperature. Science. doi:10.1126/science.aaa0193

Schultz, L., Franke, L., 2004. Helium, neon, and argon in meteorites: A data collection. Meteorit Planet Sci 39, 1889–1890. doi:10.1111/j.1945-5100.2004.tb00083.x

Schwarz, W.H., Trieloff, M., 2007. Intercalibration of 40Ar–39Ar age standards NL-25, HB3gr hornblende, GA1550, SB-3, HD-B1 biotite and BMus/2 muscovite. Chemical Geology 242, 218–231. doi:10.1016/j.chemgeo.2007.03.016

Srinivasan, B., 1976. Barites: anomalous xenon from spallation and neutron-induced reactions. EPSL 31, 129–141. doi:10.1016/0012-821X(76)90104-7

Steiger, R.H., Jäger, E., 1977. Subcommission on geochronology: convention on the use of decay constants in geo-and cosmochronology. EPSL 36, 359–362. doi:10.1016/0012-821X(77)90060-7

Trieloff, M., Kunz, J., 2005. Isotope systematics of noble gases in the Earth's mantle: possible sources of primordial isotopes and implications for mantle structure. Physics of the Earth and Planetary Interiors 148, 13–38. doi:10.1016/j.pepi.2004.07.007

Turner, G., 1972. 40Ar-39 Ar age and cosmic ray irradiation history of the Apollo 15 anorthosite, 15415. EPSL 14, 169–175. doi:10.1016/0012-821X(72)90002-7

Young, E.D., Galy, A., Nagahara, H., 2002. Kinetic and equilibrium mass-dependent isotope fractionation laws in nature and their geochemical and cosmochemical significance. Geochimica et Cosmochimica Acta 66, 1095–1104. doi:10.1016/S0016-7037(01)00832-8

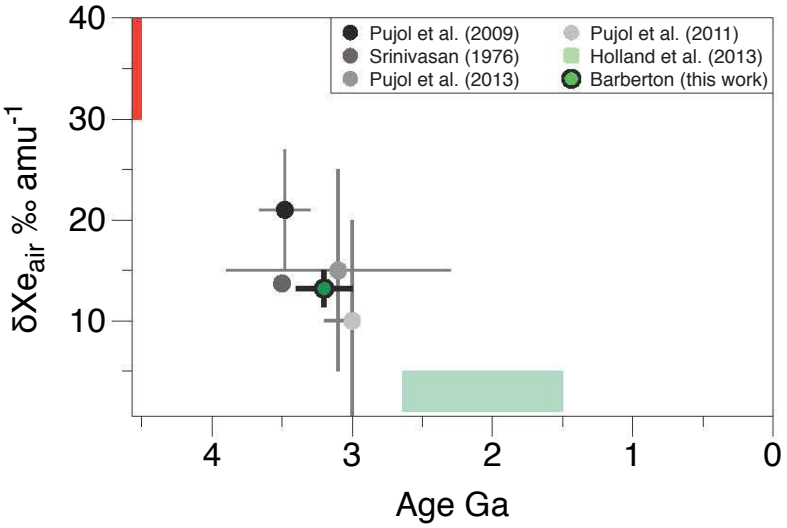

Figure S1: Isotopic fractionation (‰.u^{-1}) of atmospheric Xe with time. Data of fractionated Xe from the literature are indicated with black-filled to light grey-filled circles (Pujol et al., 2013; 2011; 2009; Srinivasan, 1976) and with a light green range (Holland et al., 2013). Starting isotopic fractionation (red range) varies between 30 and 40 ‰.u^{-1} depending if it is Solar (SW-Xe)/U-Xe or Chondritic (Q-Xe) (Ott, 2014). Errors at 2σ. No error is given for the fractionation described in Srinivasan (1976).

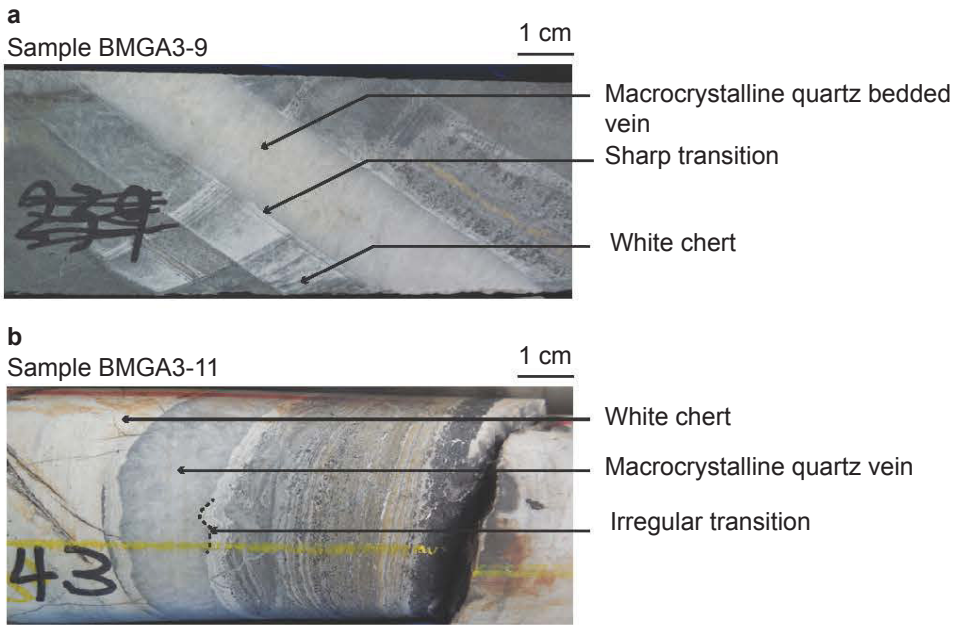

Figure S2: Photographs of two samples from the BARB3 core. (a) Samples BMGA3-9 is a vein cross-cutting white chert and filled with macro-crystalline quartz crystals. The transition between the two lithologies is sharp with two parallels straight lines. (b) Sample BMGA3-11 is a macro-crystalline quartz vein intruded in a lithology dominated by white chert and alternating black and white cherts. The transition between the vein and the intruded rock is irregular.

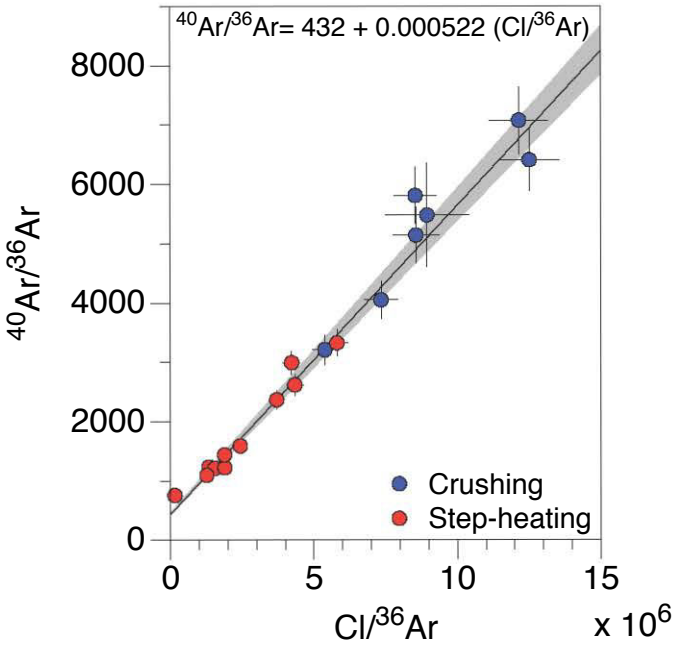

Figure S3: Ar-Cl correlation of results of crushing and step-heating experiments on sample BMGA3-9 demonstrating the presence of ^{40}Ar ($^{40}Ar_E$) excess related to the chlorine content. This ^{40}Ar excess prevents the direct determination of an age from ^{40}Ar-K correlation. The linear fitting (see equation) is shown with the black line and the grey area describes the error on the correlation at 1σ. Error bars at 1σ.

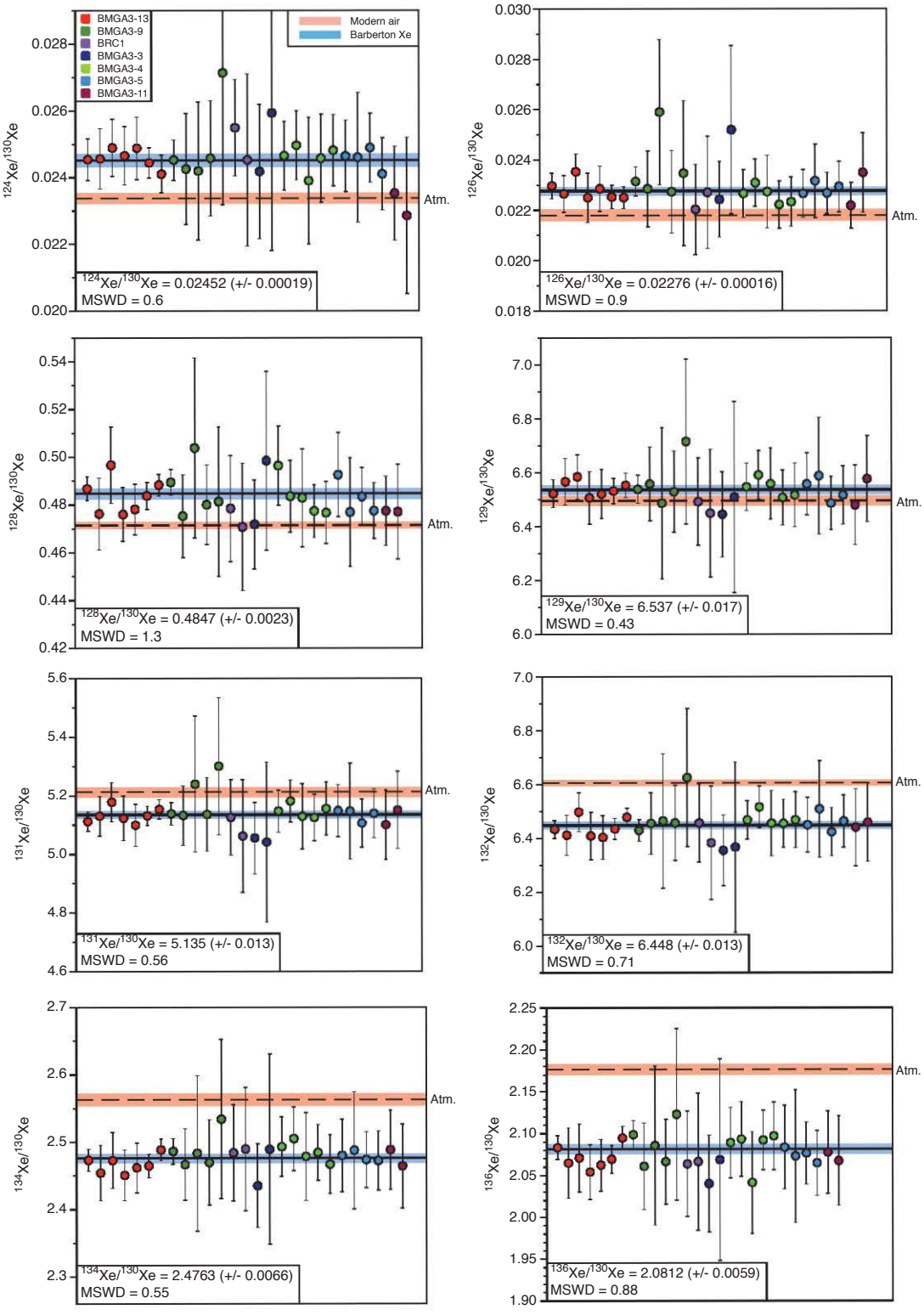

Figure S4: Isotopic ratios (27 measurements) of xenon (normalized to ^{130}Xe) released from fluid inclusions by crushing 7 different Barberton samples. The error-weighted mean for the xenon in Barberton appears with the solid black line and its error envelope with the blue area. The isotopic composition of modern air (dashed line) and its precision (red area) are shown for comparison. Error bars and ranges at 2σ.

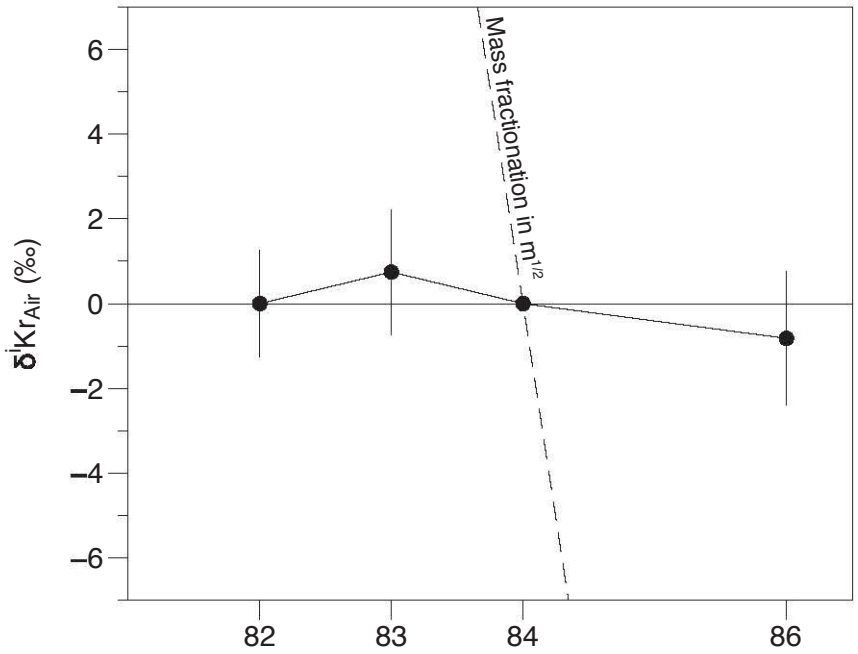

Figure S5: Isotopic ratios of krypton in fluid inclusions of Barberton quartz crystals expressed with the delta notation relative to ^{84}Kr and to the isotopic composition of the modern atmosphere. The dashed line represents the isotopic fractionation measured on Xe (13 ‰.u^{-1}) propagated toward Kr following a mass fractionation law in m$^{1/2}$. Errors at 2σ.

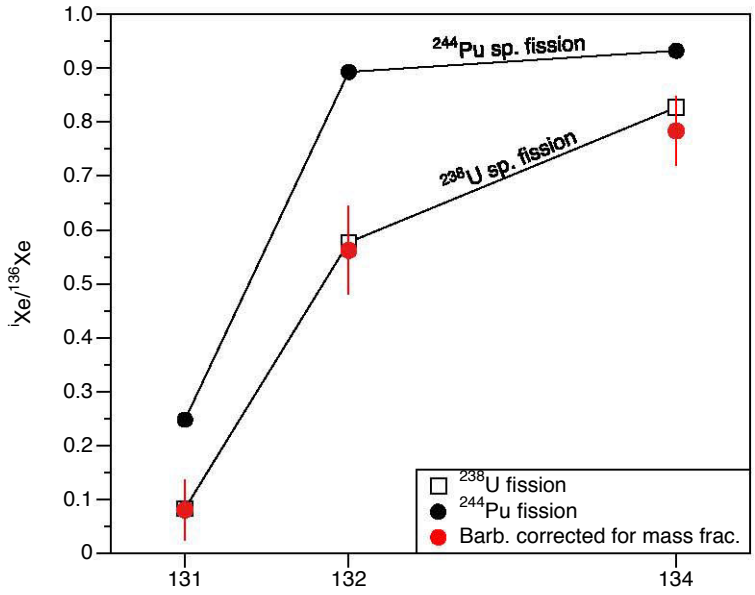

Figure S6: Fission spectrum of Barberton Xe corrected for mass-fractionation relative to a starting isotopic composition similar to U-Xe. It corresponds to spontaneous fission of ^{244}Pu. The fission spectra for fission of ^{238}U and ^{244}Pu are from a compilation in Porcelli and Ballentine (2002b).

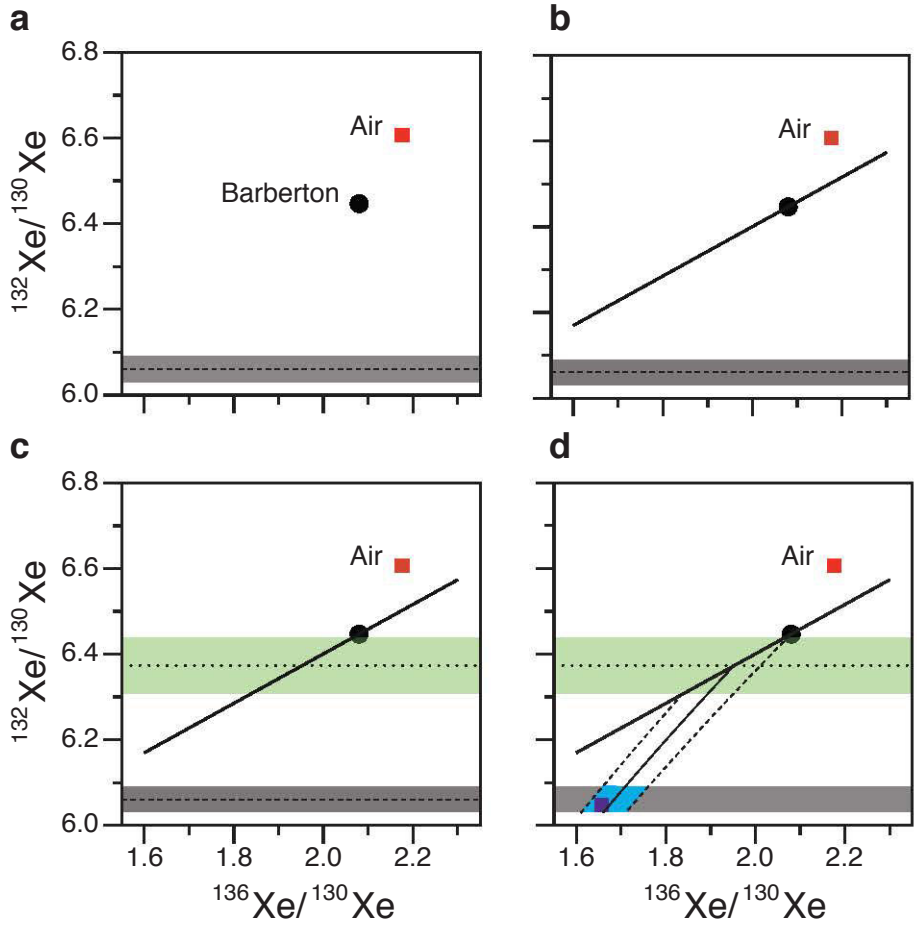

Figure S7: Schematic view of the successive steps leading to the determination of the initial $^{136}Xe/^{130}Xe$ for the ancient atmosphere trapped in Barberton quartz (see also text and "Methods") by using correlations in the three-isotope plot $^{132}Xe/^{136}Xe/^{130}Xe$. (a) The starting point uses only one data, the isotopic composition of Xe in Barberton quartz (the isotopic composition of the atmosphere is shown only for comparison) and makes the assumption that the starting $^{132}Xe/^{130}Xe$ is identical to SW-Xe. (b) The black line depicts the production of ^{132}Xe and ^{136}Xe by the spontaneous fission of ^{238}U. Barberton quartz samples carry these excesses (Fig. S6) and thus must lie on this line. (c) The green range represents the initial $^{132}Xe/^{130}Xe$ for Xe in Barberton quartz before addition of fission products. It was computed by using the mass fractionation recorded on stable isotopes ^{126}Xe and ^{128}Xe. (d) The intersection of the black line and the green range permits to compute what was the primordial $^{136}Xe/^{130}Xe$ ratio for the Earth's atmosphere before the progressive mass-dependent isotopic fractionation recorded in Barberton quartz. The resulting space of possibilities (range at 2σ) appears in blue. The purple square corresponds to the isotopic composition of U-Xe (Pepin, 1991).

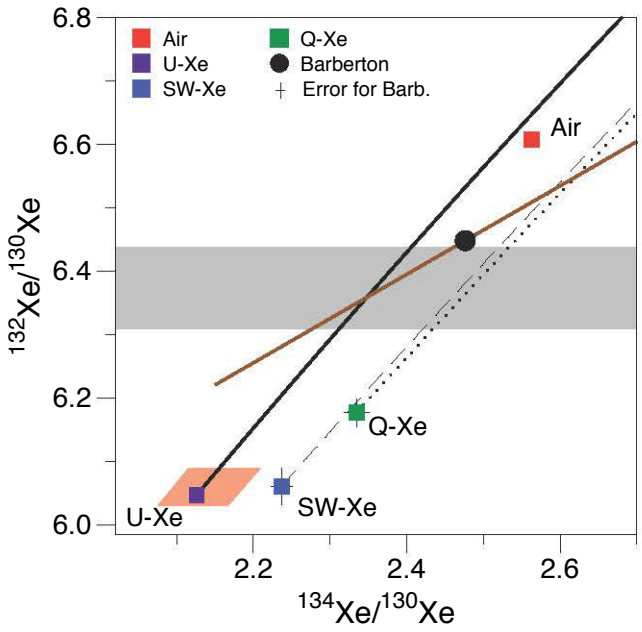

Figure S8: Three-isotope plot $^{132}Xe/^{130}Xe$ vs. $^{134}Xe/^{130}Xe$ similar to Fig. 3. Legend is the same as in Fig. 3. A starting isotopic composition depleted in ^{134}Xe is necessary to explain results obtained for Barberton quartz crystals. Errors at 2σ.

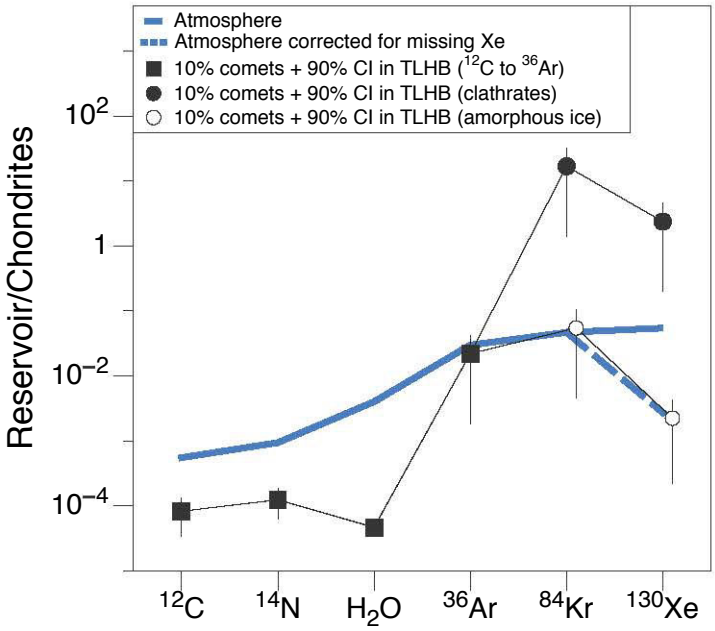

Figure S9: Abundances of C, N, H_2O, ^{36}Ar and ^{130}Xe in the atmosphere (air + oceans + sediments) (blue line), normalized to chondritic abundances and corrected for Xe loss (dashed line) (data from Table S4) and compared to the effect of a contribution of a Terrestrial Late Heavy Bombardment (TLHB) (2 x 10^{23} g) composed of 10% comets together with 90% CI chondrites. An atmospheric Xe partly brought by comets cannot be ruled out and depends highly on the mode of entrapment of Xe in comets (in clathrates or in amorphous ice).

Extended Tables captions

Table S1: Data for the Ar-Ar experiment (crushing and step-heating results) on BMGA3-9 and BMGA3-13 samples. Errors at 1σ.

Table S2: Isotopic ratios and abundances of Xe released from fluid inclusions during crushing experiments. Errors at 2σ.

Table S3: Isotopic ratios of krypton released from fluid inclusions during crushing experiments on Barberton quartz samples. Errors at 2σ.

Table S4: Abundances of volatile elements in chondrites (after a compilation of results (Kerridge, 1985; Mazor et al., 1970; Schultz and Franke, 2004)), in the atmosphere (air + oceans + sediments) (Marty, 2012) and in bulk comets composed of clathrates or amorphous ice (see text for details) all normalized to chondritic abundances. Not the differences in ^{84}Kr and ^{130}Xe abundances between clathrates and amorphous ices. Errors at 1σ.

Table S5: Elemental ratios of noble gases (Ar, Kr, Xe) in cometary ices depending if it is amorphous or in the form of clathrates. Starting solar abundances are from Lodders (2003). Data for amorphous ice from Notesco (2003) and for clathrates from Mousis et al. (2010).

Table S1

	^{36}Ar ($x10^{-14}$ mol.g^{-1})	±	$^{40}Ar/^{36}Ar$	±	$Cl/^{36}Ar$ ($x10^{6}$)	±	$K/^{36}Ar$ ($x10^{6}$)	±
Crushing								
BMGA3-9 C#1	2.05	0.13	5809	479	8.54	0.73	n.d.	
BMGA3-9 C#2	4.43	0.25	3207	250	5.39	0.43	n.d.	
BMGA3-9 C#3	5.02	0.28	4050	314	7.35	0.59	2.01	0.25
BMGA3-9 C#4	0.44	0.07	5479	875	8.95	1.45	4.36	0.70
BMGA3-9 C#5	1.74	0.13	5142	470	8.56	0.80	2.83	0.44
BMGA3-9 C#6	1.31	0.08	7077	571	12.15	1.02	2.56	0.33
BMGA3-9 C#7	0.81	0.05	6409	520	12.51	1.04	3.87	0.42
Step-heating A								
BMGA3-9 HA-600	9.58	0.45	2991	197	4.23	0.30	0.97	0.10
BMGA3-9 HA-1000	4.17	0.21	1236	84	1.35	0.14	1.88	0.15
BMGA3-9 HA-1200	4.16	0.23	757	55	0.16	0.26	0.72	0.15
BMGA3-9 HA-1400	8.39	0.39	2365	156	3.71	0.26	1.13	0.10
BMGA3-9 HA-1500	6.94	0.34	1212	82	1.54	0.12	0.30	0.13
BMGA3-9 HA-1600	9.39	0.48	1222	84	1.90	0.14	0.62	0.08
Step-heating B								
BMGA3-9 HB-600	9.66	0.46	3326	221	5.81	0.40	0.89	0.14
BMGA3-9 HB-1000	4.07	0.21	1441	100	1.89	0.18	2.31	0.23
BMGA3-9 HB-1200	3.55	0.19	1095	77	1.27	0.14	0.70	0.13
BMGA3-9 HB-1400	7.98	0.39	2617	176	4.34	0.30	1.13	0.10
BMGA3-9 HB-1600	10.83	0.52	1589	106	2.44	0.17	0.80	0.09
Crushing								
BMGA3-13 C#1	7.96	0.44	3611	57	17.01	1.34	2.17	0.20
BMGA3-13 C#2	3.72	0.21	4376	90	21.06	1.69	1.87	0.18
BMGA3-13 C#3	1.51	0.09	3607	83	21.46	1.74	2.50	0.27
BMGA3-13 C#4	1.10	0.07	3980	111	25.17	2.07	2.91	0.31
BMGA3-13 C#5	1.27	0.07	3294	72	20.20	1.62	2.62	0.31
BMGA3-13 C#6	2.83	0.16	2388	33	14.97	1.18	1.92	0.16
Step-heating								
BMGA3-13 600	6.84	0.33	1200	16	3.95	0.28	1.10	0.09
BMGA3-13 1000	4.85	0.25	512	11	0.85	0.09	4.30	0.30
BMGA3-13 1200	2.77	0.16	481	16	0.62	0.16	1.35	0.20
BMGA3-13 1400	6.02	0.29	909	12	3.42	0.24	1.04	0.08
BMGA3-13 1600	9.50	0.45	661	7	2.42	0.17	0.86	0.08
ASW			298.56		10-17			

Table S2

Barberton samples[1]	Location (m)	^{130}Xe ($x10^{-17}$ mol.g^{-1})	±	^{124}Xe	±	^{126}Xe	±	^{128}Xe	±	^{129}Xe	±	^{131}Xe	±	^{132}Xe	±	^{134}Xe	±	^{136}Xe	±
				$^{130}Xe = 1$															
BMGA3-13 A	555	17.44	0.16	0.0245	0.0006	0.0230	0.0005	0.4868	0.0049	6.52	0.05	5.11	0.03	6.43	0.03	2.47	0.02	2.08	0.01
BMGA3-13 B	-	21.85	0.34	0.0246	0.0009	0.0227	0.0007	0.4763	0.0150	6.57	0.09	5.13	0.07	6.41	0.07	2.45	0.04	2.06	0.04
BMGA3-13 C	-	16.05	0.24	0.0249	0.0009	0.0235	0.0007	0.4967	0.0160	6.59	0.08	5.18	0.07	6.50	0.07	2.47	0.04	2.07	0.04
BMGA3-13 D	-	14.41	0.17	0.0247	0.0009	0.0225	0.0010	0.4760	0.0112	6.51	0.10	5.12	0.08	6.41	0.09	2.45	0.04	2.05	0.03
BMGA3-13 E	-	19.18	0.21	0.0249	0.0009	0.0229	0.0009	0.4782	0.0106	6.52	0.09	5.10	0.07	6.40	0.08	2.46	0.04	2.06	0.03
BMGA3-13 F	-	15.91	0.20	0.0244	0.0005	0.0225	0.0005	0.4838	0.0056	6.53	0.05	5.13	0.03	6.44	0.04	2.46	0.02	2.07	0.02
BMGA3-13 G	-	17.10	0.16	0.0241	0.0006	0.0225	0.0004	0.4883	0.0045	6.55	0.05	5.15	0.03	6.48	0.03	2.49	0.02	2.09	0.01
BMGA3-9 A	238	6.32	0.06	0.0245	0.0006	0.0231	0.0006	0.4895	0.0053	6.54	0.05	5.14	0.04	6.43	0.04	2.49	0.02	2.10	0.02
BMGA3-9 B	-	3.38	0.08	0.0243	0.0017	0.0228	0.0015	0.4753	0.0173	6.56	0.14	5.13	0.10	6.46	0.12	2.47	0.05	2.06	0.05
BMGA3-9 B2	-	0.84	0.03	0.0242	0.0021	0.0259	0.0029	0.5038	0.0377	6.49	0.28	5.24	0.23	6.46	0.25	2.48	0.12	2.09	0.09
BMGA3-9 C	-	3.77	0.09	0.0246	0.0017	0.0227	0.0016	0.4801	0.0167	6.53	0.15	5.14	0.13	6.46	0.14	2.47	0.06	2.07	0.05
BMGA3-9 C2	-	0.94	0.03	0.0271	0.0040	0.0235	0.0029	0.4814	0.0312	6.72	0.31	5.30	0.23	6.63	0.26	2.53	0.12	2.12	0.10
BRC B	outcrop	2.54	0.10	0.0255	0.0014	0.0220	0.0018	0.4785	0.0223	6.49	0.16	5.13	0.13	6.46	0.15	2.48	0.07	2.06	0.06
BRC B2	-	2.08	0.05	0.0245	0.0026	0.0227	0.0022	0.4708	0.0267	6.45	0.24	5.06	0.19	6.38	0.21	2.49	0.09	2.07	0.08
BMGA3-3 A	717	2.48	0.06	0.0242	0.0020	0.0224	0.0015	0.4718	0.0187	6.45	0.16	5.06	0.12	6.35	0.13	2.44	0.06	2.04	0.06
BMGA3-3 A2	-	0.60	0.03	0.0259	0.0041	0.0252	0.0033	0.4985	0.0374	6.51	0.35	5.04	0.27	6.37	0.32	2.49	0.14	2.07	0.12
BMGA3-4 A	715	12.52	0.22	0.0247	0.0010	0.0227	0.0010	0.4965	0.0166	6.55	0.09	5.15	0.07	6.47	0.07	2.49	0.04	2.09	0.04
BMGA3-4 B	-	14.00	0.21	0.0250	0.0010	0.0231	0.0009	0.4836	0.0151	6.59	0.09	5.18	0.07	6.52	0.08	2.51	0.05	2.09	0.04
BMGA3-4 B2	-	2.60	0.09	0.0239	0.0019	0.0227	0.0014	0.4829	0.0205	6.56	0.13	5.13	0.11	6.46	0.12	2.48	0.07	2.04	0.06
BMGA3-4 C	-	9.53	0.13	0.0246	0.0013	0.0222	0.0009	0.4774	0.0110	6.51	0.10	5.13	0.08	6.45	0.09	2.48	0.04	2.09	0.04
BMGA3-4 D	-	8.23	0.12	0.0248	0.0011	0.0223	0.0010	0.4767	0.0130	6.52	0.12	5.16	0.09	6.47	0.10	2.47	0.04	2.10	0.04
BMGA3-5 A	784	11.02	0.22	0.0246	0.0011	0.0227	0.0009	0.4926	0.0176	6.56	0.12	5.15	0.09	6.45	0.10	2.48	0.05	2.08	0.05
BMGA3-5 A2	-	2.37	0.16	0.0246	0.0019	0.0232	0.0015	0.4770	0.0228	6.59	0.22	5.15	0.16	6.51	0.18	2.49	0.09	2.07	0.08
BMGA3-5 B	-	10.70	0.14	0.0249	0.0010	0.0227	0.0008	0.4834	0.0123	6.49	0.10	5.11	0.08	6.42	0.09	2.47	0.04	2.08	0.04
BMGA3-5 C	-	15.19	0.24	0.0241	0.0011	0.0229	0.0010	0.4775	0.0118	6.52	0.11	5.14	0.08	6.46	0.10	2.47	0.04	2.06	0.04
BMGA3-11 A	843	8.05	0.18	0.0235	0.0014	0.0222	0.0009	0.4774	0.0145	6.48	0.15	5.10	0.12	6.44	0.14	2.49	0.06	2.08	0.05
BMGA3-11 A2	-	2.14	0.05	0.0229	0.0023	0.0235	0.0016	0.4770	0.0199	6.58	0.16	5.15	0.13	6.46	0.15	2.46	0.06	2.07	0.05
BMGA3-12 A	-	0.31	0.02	0.0253	0.0050	0.0230	0.0046	0.4299	0.0518	6.47	0.54	5.03	0.43	6.39	0.50	2.45	0.22	2.03	0.20
Average				**0.0245**	**0.0002**	**0.0228**	**0.0002**	**0.4847**	**0.0023**	**6.537**	**0.017**	**5.135**	**0.013**	**6.448**	**0.014**	**2.476**	**0.007**	**2.081**	**0.006**
MSWD*				0.55		0.87		1.3		0.43		0.56		0.71		0.55		0.88	

[1]Barberton samples are labeled BMGA3-XX-YZ with XX the core samples, Y the 1-3 mm granulometric sub fraction and Z the crushing step excepted the "BRC" sample from one outcrop
*MSWD (for Mean Standard Weighted Deviation)

Table S3

Samples	Location (m)	^{80}Kr	±	^{82}Kr	±	^{83}Kr	±	^{86}Kr	±
					$^{84}Kr=1$				
BMGA3-13-G	555	0.0396	0.0004	0.2021	0.0018	0.2013	0.0016	0.3074	0.0017
BMGA3-13 B	555			0.2031	0.0015	0.2021	0.0013	0.3056	0.0025
BMGA3-13 C	-			0.2020	0.0017	0.2019	0.0016	0.3020	0.0027
BMGA3-13 D	-			0.2031	0.0015	0.2021	0.0013	0.3056	0.0025
BMGA3-13 E	-			0.2022	0.0009	0.2012	0.0007	0.3059	0.0028
BMGA3-4 A	715			0.1992	0.0021	0.1979	0.0024	0.3015	0.0041
BMGA3-4 B	-			0.2019	0.0020	0.2018	0.0015	0.3042	0.0024
BMGA3-4 B2	-			0.2021	0.0091	0.1995	0.0083	0.3034	0.0132
BMGA3-4 C	-			0.2023	0.0078	0.2016	0.0016	0.3042	0.0035
BMGA3-5 A	784			0.2017	0.0025	0.2015	0.0025	0.3028	0.0032
BMGA3-5 B	-			0.2012	0.0063	0.2015	0.0055	0.3058	0.0105
BMGA3-5 C	-			0.2024	0.0018	0.2021	0.0013	0.3044	0.0030
Average				**0.20217**	**0.0005**	**0.20151**	**0.00042**	**0.30499**	**0.00082**
MSWD*				1.05		1.2		1.7	

[1]Barberton samples are labeled BMGA3-XX-YZ with XX the core samples,
Y the 1-3 mm granulometric sub fraction and Z the crushing step.
*MSWD (for Mean Standard Weighted Deviation)

Table S4

Abundances (mol g^{-1} for Chondrites)	Chondrites		Atmosphere / Chondrites		Comets bulk (clathrate) / Chondrites		Comets bulk (amorphous ice) / Chondrites	
^{12}C	2.34E-03	1.17E-03	5.51E-04	2.75E-04	1.58E+01	1.45E+01	1.58E+01	1.45E+01
^{14}N	6.38E-05	2.48E-05	9.38E-04	3.65E-04	2.81E+01	1.84E+01	2.81E+01	1.84E+01
H_2O	3.70E-03	1.02E-03	4.00E-03	1.10E-03	4.91E+00	2.70E-01	4.91E+00	2.70E-01
^{36}Ar	3.13E-11	1.60E-11	2.98E-02	1.52E-02	6.60E+03	6.05E+03	6.60E+03	6.05E+03
^{84}Kr	4.09E-13	2.22E-13	4.68E-02	2.54E-02	5.06E+06	4.64E+06	1.64E+04	1.50E+04
^{130}Xe	3.84E-14	3.15E-14	2.72E-03	2.24E-03	7.10E+05	6.51E+05	6.57E+02	6.02E+02

Table S5

Elemental ratio	Protosolar nebula	Amorphous ice	Clathrates
$^{36}Ar/^{130}Xe$	3.28E+05	8.20E+03	7.57E+00
$^{36}Ar/^{84}Kr$	2.47E+03	3.09E+01	9.98E-02

3.3 Article Evolution of Atmospheric Xenon and other Noble Gases Inferred from the Study of Archean to Paleoproterozoic rocks

This article is in preparation for a submission to the journal *Geochimica et Cosmochimica Acta*. It is divided in a main text and a Supplementary Material that contains additional descriptions of methods and supplementary figures. This paper is focused on the characterization of the 3.2 Ga-old atmosphere and on the evolution of the isotopic composition of atmospheric Xe with time.

In preparation for a submission to Geochimica et Cosmochimica Acta

Evolution of atmospheric xenon and other noble gases inferred from the study of Archean to Paleoproterozoic rocks

G. Avice[1], B. Marty[1]

[1]CRPG-CNRS, Université de Lorraine, UMR 7358, 15 rue Notre-Dame des Pauvres, BP 20, 54501 Vandoeuvre-lès-Nancy Cedex, France.

Abstract

Our understanding of the origin and temporal evolution of the Earth's atmosphere is still very limited. We have analyzed ancient atmospheric gases (noble gases and nitrogen) trapped in Archean to Paleoproterozoic rocks in an attempt to document the evolution of the elemental composition and isotopic signature of the atmosphere with time. Doing so, we aimed at understanding how physical and chemical processes acted over geological time to shape the modern atmosphere.

In this study, we show that selected rocks and minerals with ages ranging from 3.2 Ga to 500 Ma have kept a record of the isotopic composition of the ancient atmosphere. The isotopic compositions of noble gases and nitrogen in the 3.2 Ga-old atmosphere were determined precisely by analyzing samples from the Barberton greenstone belt.

Ar-N_2 correlations are consistent with a partial pressure of nitrogen in the Archean atmosphere (p_{N2}) similar to, or lower than, the modern one, thus requiring other processes than a high p_{N2} to keep the Earth's surface warm despite a fainter Sun. The nitrogen isotope composition of the atmosphere at 3.2 Ga was already modern-like, attesting for inefficient nitrogen escape to space at that time.

3.2 Ga ago, atmospheric xenon was isotopically fractionated (enriched in the light isotopes) relative to the modern atmosphere, by 13 ± 1 (1σ) ‰.u^{-1} whereas krypton was isotopically identical to modern atmospheric Kr within ≈ 2 ‰. The specific and progressive isotopic fractionation of Xe during the Archean, proposed by Pujol et al. (2011), is now well established. Xe isotope fractionation marked a pause for at least 400 Ma between 3.2 Ga and 2.7 Ga, then evolved again to reach the modern-like atmospheric Xe composition around 2.1 Ga ago. Our results provide definitely an explanation for the long-standing paradox of xenon.

Xenon is the second atmospheric element, after sulfur, to show a secular isotope evolution during the Archean that ended up at the Archean-Proterozoic transition. We speculate that the Xe isotope evolution was the result of interactions between EUV photons from the young Sun and the electronic structure of xenon, in which the rise of atmospheric oxygen might have played a

role, either by killing organic haze, and/or by neutralizing xenon rapidly before Xe ions could reach the exobase.

Analyses of samples of various ages confirm that the starting isotopic composition of atmospheric Xe was specific to this reservoir - the U-Xe composition of Pepin (1991) - and was progressively isotopically fractionated over geological times. This composition appears different from that of mantle xenon, thus outlining the need for at least two cosmochemical sources - Chondritic and possibly Cometary - for this element on Earth.

1. Introduction

The origin of the volatile elements in the Earth's atmosphere and mechanisms responsible for its subsequent evolution remain poorly understood (Marty, 2012). The elemental and isotopic composition of the Earth's atmosphere has been shaped by numerous events in the history of our planet, such as contributions of diverse extraterrestrial sources, meteoritical impacts, mantle degassing, subduction with crustal recycling of volatile-rich lithologies, atmospheric escape etc. Furthermore, only little is known about the state of the atmosphere during the Archean (3.8 - 2.5 Ga), an epoch covering one third of Earth's history and during which early forms of life emerged and evolved (Mojzsis et al., 1996). Some isotopic signatures in ancient sediments are already pointing to major differences for the composition of the atmosphere in the Archean and early Paleoproterozoic. For example, sulfur isotopes measured in rocks older than ≈ 2.2 Ga carry a mass-independent fractionation signature (MIF) whose production and conservation in the rock record require the intervention of photochemical reactions involving UV photons in the atmosphere (Farquhar and Wing, 2003). Such photochemical reactions appear to be possible only in an O_2-poor atmosphere, ensuring low levels of ozone (O_3) that may have absorbed UV-light, and with abundant methane (CH_4) an important greenhouse gas (Catling (2014) and refs. therein). Furthermore, an atmospheric composition very different from the modern one seems to be required to keep a warm temperature at the Earth's surface despite a reduced solar luminosity in the past (Schwarzschild, 1958), the so-called "faint young sun paradox" (Ulrich, 1975).

Noble gases are chemically inert elements that are powerful tracers of the formation and subsequent evolution of the Earth's atmosphere. Xenon (Xe), the heaviest stable noble gas, has nine isotopes that present mass-dependent isotope variations. Some of its isotopes have also been contributed by extinct (^{129}I, $T_{1/2}$ = 15.7 Ma; ^{244}Pu; $T_{1/2}$ = 82 Ma) and extant (^{238}U; $T_{1/2}$ = 4.47 Ga) radioactivities. Terrestrial atmospheric Xe presents two unique features. Firstly, it is elementally depleted relative to other noble gases (Ne, Ar and Kr) and compared to Chondritic. This depletion factor is of about 23 (Marty, 2012). Secondly, atmospheric xenon is strongly enriched in the heavy isotopes relative to the light isotopes with a mass-dependent fractionation factor of 30 to 40 ‰.u^{-1} (computed on light isotopes) compared to other known solar system components such as AVCC-Xe (Average Carbonaceous Chondrite Xe) or SW-Xe (Solar Wind Xe) (Ott, 2014). These two features form the so-called "xenon paradox" (Ozima and Podosek, 2002).

An additional striking feature of atmospheric Xe is that it cannot be directly related neither to chondritic Xe nor to solar Xe. When corrected for mass-dependent isotope fractionation (using light Xe isotopes not contributed by radioactivities), the heavy Xe isotopes ^{134}Xe and ^{136}Xe are depleted relative to both Solar and Chondritic signatures (Pepin, 1991). This is a serious issue since no known nuclear process can selectively decrease the abundance of these isotopes in the atmosphere. Furthermore, spontaneous fission of extinct ^{244}Pu ($T_{1/2}$ = 82 Ma) and extant ^{238}U ($T_{1/2}$ = 4.47 Ga), which produce these isotopes in the silicate Earth, would have led to an increase of ^{134}Xe and ^{136}Xe abundances in the atmosphere with time due to mantle and crustal degassing, making the situation even worse. An alternative and mathematically-derived Xe component, labeled U-Xe, has thus been defined in previous studies (Pepin, 1991; Takaoka, 1972) and is considered as the starting isotopic composition for the Earth's atmosphere. To date, this exotic component has not been found elsewhere in the solar system.

Even assuming U-Xe as the starting isotopic composition for the atmosphere, solving the xenon paradox calls for complex models with episodes of mantle degassing and early isotopic fractionation of atmospheric noble gases driven by hydrodynamic escape of hydrogen (Pepin, 1991; Tolstikhin and O'Nions, 1994), and/or late addition of cometary gases to a residual, fractionated atmosphere (Dauphas, 2003). In these models, Xe processing and fractionation occurred during Earth's forming events (Dauphas and Morbidelli, 2014). Some recent studies call into question these models and propose instead that the depletion and isotopic fractionation of Xe took place progressively during geological eons. This model is based on the analysis of xenon in ancient rocks (Pujol et al., 2011; 2009; Srinivasan, 1976) that showed a stable isotope composition of xenon intermediate between those of the potential cosmochemical ancestors and of the modern atmosphere. Pujol et al. (2011) thus proposed that the isotope fractionation of atmospheric xenon was a long-term process that was still active during the Archean eon. This fractionation had to be specific to Xe, since other noble gases did not appear to be fractionated. Because xenon is the heaviest noble gas, only non-thermal (not mass-related) escape could be possible, possibly related to the specific electronic structure of this element, which makes it more prone to ionization by solar UV photons than other noble gases. These results have thus been subsequently interpreted as an evidence for a continuous escape of Xe during the Archean accompanied by an instantaneous isotopic fractionation (Marrocchi et al. (2011); Kuga et al. (2015)) when Xe is ionized and enters in contact with organic matter (Hébrard and Marty, 2014; Marty, 2012). Hébrard and Marty (2014) built a 1D photochemical model of the Archean atmosphere suggesting that the enhanced EUV flux from the young Sun (Ribas et al., 2005) ionized Xe atoms preferentially at altitudes between 90 and 110 km. This altitude range corresponds also to the maximum production of organic haze from photochemistry of H_2 - CH_4 mixtures (two species often advocated to have been present in the Archean atmosphere). Independently, laboratory experiments involving Xe ions trapped in forming organic matter (Kuga et al., 2015; Marrocchi et al., 2011) have shown a Xe mass-dependent instantaneous fractionation (α) of 1.0 ± 0.4 %.u^{-1} in favor of the heavy isotopes. Such a value is similar to the one needed to yield an integrated fractionation of 3 - 4 %.u^{-1} for a Xe depletion of a factor of 23 in a leaking atmosphere, assuming

a Rayleigh-type distillation during escape (Marty, 2012). Therefore Hébrard and Marty (2014) concluded that xenon in the Archean atmosphere was partly trapped and isotopically fractionated in organic haze, while other Xe ions were escaping to space.

Even if these studies provided a framework for understanding the xenon paradox described above, there are still some unresolved issues. (i) The above view is based on the analysis of only two samples from the same location (barite from North Pole, Pilbara craton, Australia, for Srinivasan (1976) and Pujol et al. (2009), fluid inclusions in quartz also from North Pole for Pujol et al. (2011)). (ii) The atmospheric origin of trapped Xe has been questioned (Pepin, 2013). (iii) Assuming that the model is correct, the physical processes behind the escape of Xe atoms and/or ions are still unknown. (iv) The similarity of Xe on Mars and on Earth is a major issue for the "haze-Xe" model (Hébrard and Marty, 2014) since there is no evidence for the existence of such haze production in the early Martian atmosphere (but it cannot be excluded either, since CH_4 has been detected there (Formisano et al., 2004)). (v) Finally, the exact timing of the evolution of the isotopic composition of atmospheric Xe remains unconstrained and it is up to now, difficult to link this evolution to other geochemical cycles such as progressive oxidation of the atmosphere for example. In order to document these issues, we present new high-precision analyses of Xe contained in fluid inclusions in quartz of different ages (3.2 Ga to 530 Ma) and from different geological areas (Table 1), A comprehensive study of noble gases (Ne, Ar, Kr, Xe) and nitrogen in 3.2 Ga-old samples from the Barberton area permits also to define the isotopic composition of the atmosphere at that time.

2. Samples and Analytical Methods

Brief descriptions of the analyzed samples, of geological age constraints and of analytical methods are presented in this section (*more details also appear in Chapter 2 "Samples and Analytical Methods").*

2.1 Geological Setting of the Samples and Age Constraints

Samples analyzed in this study consist of high-purity macro-crystalline quartz crystals containing numerous fluid inclusions, except for samples from Isua (Greenland) that are meta-carbonates consisting of a mixture of carbonate and quartz crystals. The high quantity of fluid inclusions ensured that quantities of gas released during crushing experiments were high enough to determine Xe isotopic ratios at high precision and that impurities did not pollute the Xe signal (for example by neutron capture on Ba or Te producing Xe isotopes (Pujol et al., 2009)). Geological provenances of the analyzed samples are listed in Table 1.

Samples from the Barberton greenstone belt were recovered from quartz veins cutting cores recovered during an ICDP drilling project (PI: N. Arndt (UJF Grenoble)) and are described in a previous publication *(see Chapter 2 "Samples and Analytical Methods" and the paper presented in the previous section of Chapter 3).* Ar-Ar dating permitted to define an age of 3.2 ± 0.1 (1σ)

Ga (*see previous paper in Chapter 3 "Results and Implications"*) in agreement with the age of the main deformation event "D_2" defined for this geological area that led to regional-scale fluid circulations (de Ronde and Wit, 1994).

Samples from the Boongal and Maddina formations (Fortescue Group, Hamersley Basin, Australia) are from quartz-bearing pods located in pillow-basalts. Comparable quartz pods in the North Pole 3.49 Ga-old area had already been considered as being derived from early hydrothermal circulations after lava emission (Foriel et al., 2004). Ar-Ar dating did not permit to constrain the age of these samples because of too low abundances of potassium and of ^{40}Ar excess that is not simply correlated with the chlorine content as usually seen in other studies (Kendrick et al., 2001). A maximum age of 2.74 Ga is thus inferred from U-Pb dating of the rocks (Trendall et al., 2004).

Some rocks from the Isua greenstone belt (West Greenland) are thought to be up to 3.8 Ga-old (Nutman and Friend, 2009). Samples analyzed in this study were collected in the southern part of the belt and consisted in quartz crystals mixed with carbonates probably of metasomatic origin (Rose et al., 1996). An early Archean age for these quartz is thus doubtful and the widespread resetting event at 2.3 ± 0.2 Ga identified by Sm-Nd dating on metamorphic garnets from the same area (Blichert-Toft and Frei, 2001) might be a more probable age for the fluid circulation in these samples (see Results and Implications sections for details on the choice of the age).

Quartz samples from the Quetico Belt are from veins intruded in meta-greywackes dated at ca. 2.7 Ga (Davis et al., 1990). The true age of the veins is unknown and could be 2.65 Ga, the age of the metamorphism almost synchronous to the onset of late plutonic intrusions (Card, 1990).

Quartz samples located in veins from the Gaoua mine district (Burkina Faso) are linked to the early stages of a porphyr deposit (Baratoux et al., 2015) and have an age of 2.10 ± 0.07 Ga (1σ) inferred from Re-Os dating of pristine pyrite minerals located in the same veins (Le Mignot et al., 2014).

Samples from Carnaíba (Brazil) are quartz crystals from emerald-hosting veins linked to the intrusion of Proterozoic leucogranites in volcano-sedimentary sequences (Giuliani et al., 1990). The age of the mineralization is bracketed between 1.98 Ga and 1.93 Ga based on Ar-Ar experiments on associated phlogopites (Cheilletz et al., 1993).

Samples from Caramal (Australia) are from quartz breccia zones located in the 1.8 - 1.7 Ga-old Kombolgie sandstones. Quartz formed probably slightly later than accompanying illites crystals dated at 1.6 - 1.7 Ga by the Ar-Ar method (Kyser et al. (2000) and refs. therein).

Table 1: Locations, types and ages of samples analyzed in this study. The corresponding isotopic fractionations of Xe relative to modern air (δXe_{air}) and to U-Xe ($\delta Xe_{U\text{-}Xe}$) are indicated together with Xe isotopes used to compute these fractionation factors (see text). The corresponding remaining atmospheric fractionations and depletion factors for the Rayleigh's distillation model (see text) are also indicated. Results from previous studies are also listed (Holland et al., 2013; Meshik et al., 2001; Pujol et al., 2013b; 2011; 2009; Srinivasan, 1976). Errors at 1σ.

Geological Area (Country)	Lithology	Age (Ga)	±	δXe_{air} (‰.u^{-1})	±	MSWD	Xe isotopes (/^{130}Xe) used to compute the fractionation	$\delta Xe_{U\text{-}Xe}$ (‰.u^{-1})	±	Remaining fraction	±	Depletion	±	Reference
Previous studies														
North Pole (Australia)	barites	3.48	0.09	21	3	n.d.	129,132,136	17	2	0.24	+0.05/-0.04	4.2	+0.9/-0.8	Pujol et al., 2009
North Pole (Australia)	barites	3.5	n.d.	13.7	n.d.	n.d.	134,136							Srinivasan, 1976
North Pole (Australia)	quartz	3.1	0.4	15	5	n.d.	128,129,132,134,136							Pujol et al., 2013
North Pole (Australia)	quartz	3.0	+0.2	10	5	n.d.	128,129,131							Pujol et al., 2011
Timmins (Canada)	fluids	see text	-	3	1	0.067	124,126,128,130	-	-					Holland et al., 2013
Belorechenskoe (Russia)	barites	0.170	0.015	0.5	n.d.	n.d.	124,126,128,129	-	-					Meshik et al. 2001
This study														
Barberton (South Africa)	quartz	3.2	0.1	13.27	0.92	1.4	126,128,130,131	25	1	0.11	0.01	8.2	0.7	**this study**
Fortescue (Australia)	-	2.7	n.d.	13.0	1.2	0.8	126,128,130,131	25	1	0.11	0.01	8.2	0.7	-
Quetico Belt (Canada)	-	2.55	0.15	3.8	2.5	0.42	124,126,128,129,130,131	35	2	0.05	0.01	19	+4/-3	-
Isua (Danemark)	-	2.3	0.3	5.8	1.5	0.3	124,126,128,129,130,131	30.5	1.4	0.07	0.01	13.2	+1.7/-1.5	-
Carnaiba (Brasil)	-	2.0	0.1	1.8	2.2	1.12	124,126,128,129,130,131	34	4	0.05	0.02	17	+7/-5	-
Gaoua (Burkina Faso)	-	2.10	0.07	2.1	1.6	0.94	124,126,128,129,131	36	2	0.05	0.01	21	+4/-3	-
Caramal (Australia)	-	1.7	??	0.32	0.78	0.89	124-136	-	-					-
Avranches (France)	-	0.53	0.01	1.5	1.6	0.12	124-136	-	-					-
Rhynie (Scotland)	-	0.396	0.012	0.1	1.9	0.28	124-136	-	-					-

The sample from Avranches (France) is from quartz veins intruded in the western part of the Mancellian batholith. This geological area underwent several orogenic episodes but radiometric dating results in the sampling area permit to estimate an age of 530 ± 10 Ma (1σ) for this sample ((Chantraine et al., 1994) and refs therein).

The sample from Rhynie (Scotland) is a cherty (microcrystalline quartz) sample that already provided information about the ancient atmosphere with a trapped paleo-atmospheric $^{40}Ar/^{36}Ar$ ratio of 294.1 ± 1.5 (1σ) (renormalized to the revised value of 298.56 for the modern atmospheric ratio (Lee et al., 2006)) and an age of 396 ± 12 Ma (1σ) obtained with the Ar-Ar dating method (see Rice et al. (1995) and refs. therein).

2.2 Analytical methods

Descriptions of the N_2-Ar-Ne measurements are given in the Supplementary Material.

For Xe-Kr measurements, gases were extracted from fluid inclusions contained in 2-3 mm-sized grains by using a modified VAT® valve. The below was replaced by a cylinder crushing grains (up to 1 g), placed on a stainless steel pastille, when the valve is closed. Online Ti-sponge getters ensured the removal of reactive gases and especially water, the major constituent of fluid inclusions. Xenon was condensed on walls of a glass tube plunged in liquid N_2 (77 K) during 20 mn. Part of the krypton also condensed on this tube. The remaining fraction was then pumped out during 10 mn. Around 10 dilutions of the volume of the glass tube into the whole line and under static vacuum followed by pumping were necessary to decrease the partial pressure of Ar (mainly ^{40}Ar usually found in excess in fluid inclusions) before introduction of the gas in the mass spectrometer. The Xe analysis was carried out on a Helix MC Plus Thermofisher® noble gas mass spectrometer operated in peak jumping mode for abundances and Xe isotopic ratios measurements. The high stability of the mass spectrometer ensured a very good reproducibility of the standards measured during crushing experiments and permitted to obtain the high precision on the data presented here. Xe blanks were typically around 10^{-18} mol of ^{130}Xe and thus had a negligible contribution (usually < 1 %) on the Xe abundance measured during crushing (10^{-16} to 10^{-15} mol ^{130}Xe). Kr blanks were also negligible. All isotopic ratios presented in the Results section are corrected for blank contribution and mass discrimination of the mass spectrometer. A full propagation of the errors on the internal precision, the sensitivity of the mass spectrometer, the reproducibility of the standards and the blank contribution has been applied in order to take into account all potential sources of variability. Mass spectrometer sensitivity was calibrated with known amounts of atmospheric noble gases following the same procedure as reported by Marty and Zimmermann (1999). Recent quartz samples (0 to 35 Ma) have been analyzed to check that there was no isotopic fractionation during gas extraction and purification.

3. Results

3.1 Xenon and the Isotopic Fractionation of Ancient Atmospheres

Results for Xe isotopic ratios and abundances released during each extraction step are presented in Table S1 (Supplementary Material). The error-weighted mean for each isotopic ratio and the corresponding Mean Standard Weighted Deviation (MSWD) appear in bold. MSWD values are usually close to or lower than 1, meaning that sometimes errors may have been overestimated. Mean values were not computed for some $^{131\text{-}136}Xe/^{130}Xe$ ratios that are presenting various fissiogenic excesses. Mean isotopic ratios of Xe in Barberton quartz appear in the first line of Table S1 (Supplementary Material).

Except for some fissiogenic $^{131\text{-}136}Xe$ excesses, isotopic spectra of Xe released from recent quartz samples do not show any resolvable isotopic fractionation relative to the isotopic composition of the modern atmosphere with a maximum isotopic fractionation of 1.4 ± 1.6 ‰.u^{-1} (1σ).

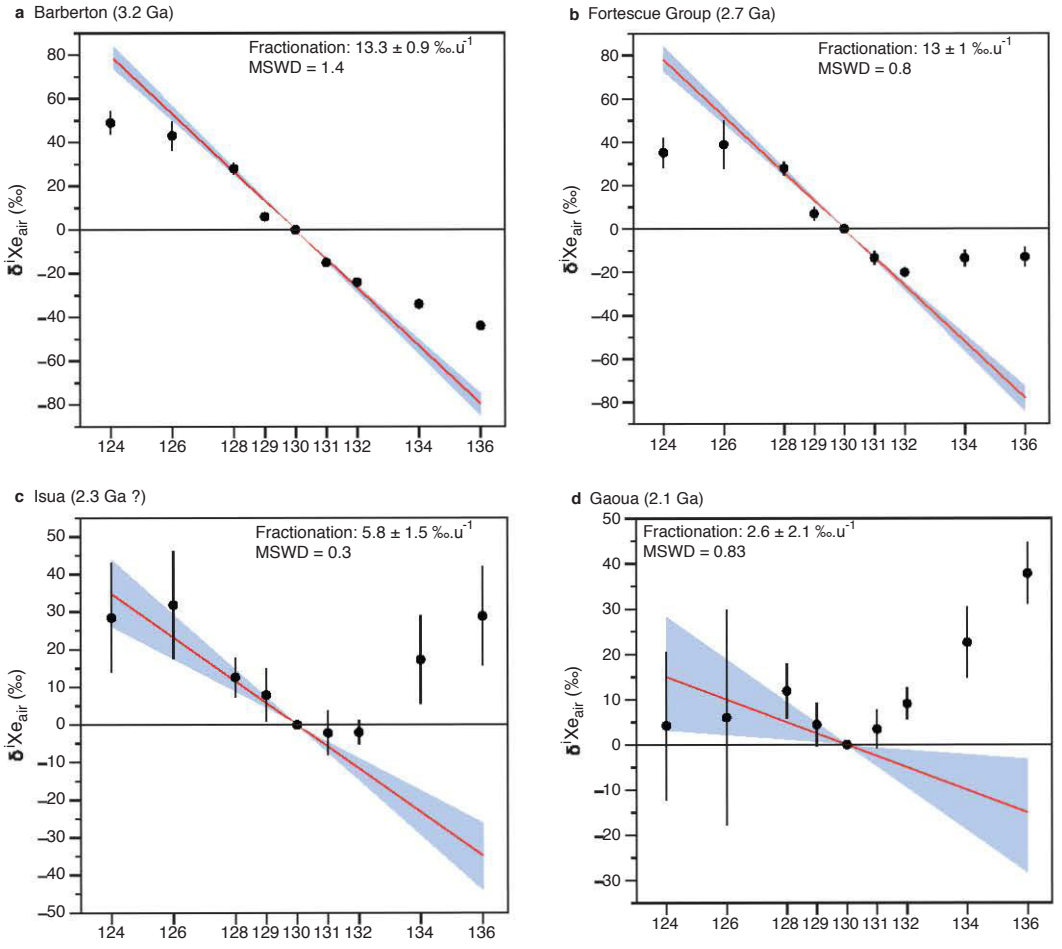

Figure 1: Isotopic spectra of Xe released from fluid inclusions of Barberton (a), Fortescue Group (b), Isua (c) and Gaoua (d) samples (see Table S1 in Supplementary Material). Isotopic compositions are given with the delta notation normalized to ^{130}Xe and to the isotopic composition of the modern atmosphere (δ^iXe_{air} = 0 ‰): $\delta^i Xe_{air} = 1000\times(\frac{(^{i}Xe/_{^{130}Xe})_{sample}}{(^{i}Xe/_{^{130}Xe})_{air}} - 1)$. Red lines correspond to the isotopic fractionation and blue areas correspond to 1σ error ranges. Errors at 1σ.

Isotopic spectra normalized to the isotopic composition of the modern atmosphere for xenon in Barberton, Fortescue Group, Isua and Gaoua samples are presented in Fig. 1a, b, c and d, respectively. Note the differences in scale in Fig. 1a-b compared to Fig. 1c-d. Isotopic spectra, without $^{132\text{-}136}Xe/^{130}Xe$ ratios altered by fissiogenic excesses, for Quetico Belt (2.7 - 2.65 Ga) and Carnaíba (2.1 Ga) samples are displayed in Fig. S1 and S2 (Supplementary Material), respectively.

For each spectrum in Fig. 1, light isotopes ($^{124\text{-}129}Xe$) released from fluid inclusions are enriched relative to the isotopic composition of the modern atmosphere except for the Gaoua spectrum (2.1 Ga, Fig. 1d) where only some ^{128}Xe excess is definitely present and where $^{124}Xe/^{130}Xe$ and $^{126}Xe/^{130}Xe$ ratios are higher than the atmosphere although imprecise. For Barberton (Fig. 1a) and Fortescue Gp. (Fig. 1b) samples, heavy isotopes ($^{131\text{-}136}Xe$) are also depleted relative to the isotopic composition of the modern atmosphere. Isua (Fig. 1c) and Gaoua (Fig. 1d) samples present $^{131\text{-}136}Xe$ excesses, which might be attributed to the spontaneous fission of ^{238}U although fission spectra are imprecise (Fig. S3 & S4, respectively, in Supplementary Information). Such light isotopes excesses and depletions on heavy isotopes are consistent with a mass-dependent isotopic fractionation recorded in these quartz of different ages in a similar manner to what was measured in previous studies of ancient atmosphere trapped in fluid inclusions in quartz and barite samples (e.g. Pujol et al. (2011)). Results presented here cannot be interpreted in terms of mixing between an atmospheric and a mantle-derived component (Pepin, 2013) since no analysis revealed the presence of significant ^{129}Xe excess relative to the modern atmosphere (6.8 % of radiogenic $^{129}Xe^*$ excess from the decay of extinct ^{129}I in the modern atmosphere). Such radiogenic excess would be expected if a mantle-derived component was present (Caffee et al., 1999). In fact, after correction for isotopic fractionation relative to U-Xe, there is a $^{129}Xe^*$ excess of 6.0 ± 0.4% (1σ) in Barberton quartz relative to total ^{129}Xe. This observation demonstrates that Barberton samples are records of an ancient atmosphere containing lower amounts of radiogenic gases 3.2 Ga ago, which were subsequently degassed by the mantle and ended in the modern atmosphere. N_2-Ne-Kr isotope systematics on Barberton samples also argues against any significant mantle influence on fluids trapped in these samples (see next section). Analyses presented here appear to be records of the isotopic composition of xenon in ancient atmospheres.

The isotopic fractionation of Xe (δXe_{air}) of 13.3 ± 0.9 ‰.u^{-1} (1σ) measured in Barberton (3.2 ± 0.1 Ga) samples is obtained by computation on $^{126,128,130,131}Xe$ isotopes (Table 1). This very precise value is in agreement with previous data obtained for 3.0 - 3.1 Ga-old quartz from North Pole (Australia) (Pujol et al., 2011; 2013b). More interestingly, it confirms that the isotopic fractionation of the atmosphere 3.2 Ga ago was lower than the isotopic fractionation of 21 ± 3 ‰.u^{-1} measured in 3.5 Ga-old barite samples (Pujol et al., 2009) suggesting an evolution of the isotopic composition of atmospheric Xe with time. Fortescue Gp. quartz samples (≈ 2.7 Ga) gave Xe results compatible with an isotopic fractionation of 13 ± 1 ‰.u^{-1} (1σ) identical within

errors to the fractionation measured in Barberton samples plus some addition of $^{131-136}$Xe from the spontaneous fission of ^{238}U (see Fig. S5 in Supplementary Material). Furthermore, Xe results for Fortescue Gp. samples confirm that the only possible starting isotopic composition for the Earth's atmosphere is similar to U-Xe (see the three-isotope plot in Fig. S6 in Supplementary Material). Mass-dependent fractionation of this component and addition of products of the spontaneous fission of ^{238}U are the only ways to reproduce the measured ^{136}Xe/^{130}Xe ratio.

^{124}Xe depletion, relative to any plausible mass-dependent fractionation computed by using other light non-radiogenic/fissiogenic isotopes, is observed in the case of Barberton (3.2 Ga) and Fortescue Group (2.7 Ga) samples. This depletion is unlikely to be due to an isotopic fractionation phenomenon during extraction, purification and analysis of the gas since crushing experiments of more recent quartz crystals (Tables S1) did not reproduce such depletion and gave atmospheric ^{124}Xe/^{130}Xe ratios (e.g. results for samples from Avranches (500 Ma) in Fig. S8 in Supplementary Material). These mono-isotopic depletions for Barberton and Fortescue Group samples remain hard to explain since there are only few processes (radioactive decay or neutron capture) able to selectively decrease the abundance of this isotope. Radioactive decay of ^{124}Xe may occur by double electron capture. However the half-life ($t_{1/2}$) of ^{124}Xe is higher than 4.10^{20} a (Suhonen, 2013) and there is no reason to expect that this process occurred only in-situ and not in all cosmochemical or terrestrial reservoirs including the terrestrial atmosphere that is used here to normalize isotopic spectra. Thermal neutron capture on ^{124}Xe leads to the production of ^{125}Xe decaying rapidly ($t_{1/2}$ = 18 hr) in ^{125}I that is also unstable and decays ($t_{1/2}$ = 60 days) in ^{125}Te (Bresesti et al., 1964). Because the modern atmosphere, after correction for mass-dependent isotopic fractionation, does not carry such depletion in ^{124}Xe relative to potential primordial components, neutron capture might have taken place in-situ. However, average thermal neutron flux in the crust is not sufficient to explain this observation (see details on the computation in Supplementary Material). Because the origin of the depletion in ^{124}Xe remains unknown, mass-dependent fractionations computed for Barberton and Fortescue Group samples (Table 1) did not take into account the measured ^{124}Xe/^{130}Xe ratios. It must be noticed here that, in the case of Fortescue Group Xe for example, propagation of mass fractionation computed with ^{124}Xe toward heavy isotopes ($^{131-136}$Xe) leads to $^{131-136}$Xe excesses that are not compatible with neither spontaneous fission of ^{238}U nor with fission of ^{244}Pu (see the mismatch for ^{132}Xe in the fission spectrum in Fig. S5 in Supplementary Material). This observation argues in favor of an abnormally low ^{124}Xe rather than overestimated ^{126}Xe and ^{128}Xe excesses.

Samples from Isua present an isotopic fractionation of 5.8 ± 1.5 ‰.u^{-1} (Table 1, Fig. 1c) and late additions of products of the spontaneous fission of ^{238}U (Fig. S3). This isotopic fractionation is lower than the fractionation recorded in Barberton (3.2 Ga) and Fortescue Group (2.7 Ga) samples (≈13 ‰.u^{-1}).

Samples from the Quetico Belt (2.7 - 2.65 Ga) display small ^{128}Xe excesses relative to the modern atmosphere but uncertain ^{124,126}Xe/^{130}Xe ratios prevent any precise determination of the possible isotopic fractionation (Fig. S1 in Supplementary Material). The small ^{128}Xe excess is not due to double-beta decay of ^{128}Te (λ = 9 x 10^{-26} a^{-1}) since concomitant double-beta decay of ^{130}Te (λ = 2.6x10^{-22} a^{-1}) would have produced significant ^{130}Xe excess that is not observed here (Pujol et

al., 2009). Neutron capture on ^{127}I followed by beta decay of ^{128}I ($^{127}I(n, \gamma)^{128}I(\beta^-)$) is another way to produce mono-isotopic ^{128}Xe excesses (Srinivasan et al., 1971). However, the abundance of iodine in Quetico Belt samples is unknown preventing us to check this hypothesis. A slight isotopic fractionation of 3.8 ± 2.5 ‰.u^{-1} is still possible even if it only relies on this ^{128}Xe excess of doubtful origin. Similarly, the isotopic fractionation of 2.5 ± 1.6 ‰.u^{-1} recorded in Gaoua ≈2.1 Ga-old quartz samples (Table 1, Fig. 1(d)) is mainly carried by the $^{128}Xe/^{130}Xe$ ratio that is higher than the modern one. Even if $^{124}Xe/^{130}Xe$ and $^{126}Xe/^{130}Xe$ ratios are imprecise, they are also compatible with an isotopic fractionation of this magnitude.

Carnaíba samples (2.0 - 1.9 Ga) do not show any resolvable isotopic fractionation (1.8 ± 2.2 ‰.u^{-1}) and present only a ^{126}Xe excess of unknown origin (Fig. S2 in Supplementary Material) since possible cosmogenic productions would have led to comparable ^{124}Xe excesses (Pujol et al., 2009) not present in that case.

Samples from Caramal (1.7 Ga) (Fig. S7 in Supplementary Material) present only some ^{128}Xe excess maybe due to neutron capture on ^{127}I (similarly to Quetico Belt samples). All other isotopes are compatible with a modern-like isotopic composition. The maximum isotopic fractionation is 0.32 ± 0.78 ‰.u^{-1} (Table 1).

Xe in sample from Avranches (530 Ma) (Fig. S8 in Supplementary Material) does not show any resolvable deviation relative to the isotopic composition of the modern atmosphere.

Sample from Rhynie (396 Ma) does not present any deviation from the isotopic composition of the modern atmosphere on light isotopes, apart from slight, but very imprecise, $^{124\text{-}126}Xe$ excesses, and can thus be considered as having an isotopic composition of Xe identical to the modern atmosphere. Maximum fractionations and their associated errors for Caramal, Avranches and Rhynie samples are listed in Table 1.

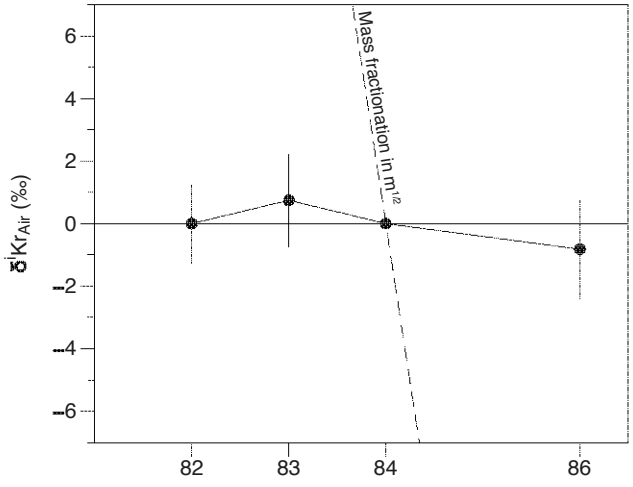

Figure 2: Isotopic composition of Kr released from fluid inclusions in Barberton samples (Table S2). Isotopic ratios are normalized to ^{84}Kr and to the isotopic composition of the modern atmosphere and expressed with the delta notation (in permil): $\delta^i Kr_{air} = 1000 \times \left(\frac{(^{i}Kr/_{^{84}Kr})_{sample}}{(^{i}Kr/_{^{84}Kr})_{air}} - 1\right)$. The isotopic composition does not show any deviation from the isotopic composition of the atmosphere. Propagation for Kr of the isotopic fractionation measured for Xe in Barberton quartz and following a mass fractionation law in m$^{1/2}$ is given as the dashed line.

3.2 Neon, Argon and Krypton Isotopes

Isotopic compositions of krypton in Barberton samples are reported in Table S2 (Supplementary Material) and displayed in Fig. 2 where isotopic ratios are normalized to ^{84}Kr and expressed with the delta notation relative to the isotopic composition of the modern atmosphere. The isotopic composition of krypton in Barberton quartz samples is identical to the atmospheric one, and very different from what would be expected if the mass fractionation recorded by Xe (13 ‰.u^{-1}) was extended to Kr considering a fractionation law proportional to the square root of the masses (($^{i}Kr/^{i+1}Kr)^{1/2}$). Therefore, the isotopic fractionation recorded by Xe is specific to this noble gas and does not affect other noble gases. It also indicates the absence of mantle-derived fluids since mantle-derived CO_2 well-gases carry a Kr signature that is intermediate between air and a Chondritic component (AVCC-Kr) (Holland et al., 2009).

Results for abundances and isotopic compositions of nitrogen, argon and neon in fluid inclusions in sample BMGA3-9 (Barberton) are listed in Table 2. All results are given in the table and in the text with 1σ error ranges. $^{40}Ar/^{36}Ar$ ratios are elevated with a maximum value of 978 ± 82 (crushing step #5 for sample BMGA3-9 B) and a reproducible mean value around 700 with also very reproducible ^{36}Ar contents of 1.16 x 10^{-13} mol.g^{-1}. This elevated $^{40}Ar/^{36}Ar$ ratio relative to the modern atmospheric ratio of 298.56 (Lee et al., 2006) cannot be explained by simple addition of ^{40}Ar produced in-situ by the radioactive decay of ^{40}K *(see previous paper in Chapter 3 "Results and Implications").* This demonstrates that fluids trapped in these quartz samples do not correspond directly to seawater equilibrated with the atmosphere. If the initial fluid was derived from seawater, its isotopic and elemental compositions were modified when it leached the crust and enriched in radiogenic ^{40}Ar, fissiogenic $^{131\text{-}136}Xe$ etc. Hopefully, the isotopic composition of non-radiogenic/fissiogenic isotopes of xenon did not change since crustal noble gases are dominated by the atmospheric component (Drescher et al., 1998). Similarly to Kr, $^{38}Ar/^{36}Ar$ ratios of 0.190 ± 0.004 and 0.188 ± 0.009 for samples BMGA3-9 B and BMGA3-9 A, respectively, do not show any resolvable deviation from the isotopic composition of the modern atmosphere (0.1885 ± 0.0003, Lee et al. (2006)).

Ne/Ar ratios (0.03-0.04) are intermediate between seawater (0.015) and air (0.053) values (Holland and Ballentine, 2006). This difference may be explained by the mixing between air or seawater and another crustal component of unknown elemental composition. However, it must be noticed that several processes such as boiling of water, salinity, separation of a gas phase in inclusions are also known to fractionate elemental compositions of noble gases (Ballentine et al., 2002). Elemental ratios are thus poor tools here to decipher the origin of gases trapped in these fluid inclusions.

Neon isotopic ratios are displayed in a three-isotope plot and compared to the mantle component ($^{20}Ne/^{22}Ne$ = 12.7 - 13.4, (Marty, 2012)) and to the modern (Kennedy et al., 1990) and Archean crustal mixing lines (Holland et al., 2013; Lippmann-Pipke et al., 2011) (Fig. 3). Crushing steps and bulk results are close to the atmospheric composition. Some data points present $^{20}Ne/^{22}Ne$ and $^{21}Ne/^{22}Ne$ ratios that are lower than the atmosphere's. This is probably due to some underestimation of the correction on ^{22}Ne for $^{44}CO_2^{++}$ contribution (see Supplementary Material).

One may consider that one result ($^{20}Ne/^{22}Ne$ = 10.35 ± 0.35, crushing step #7 for BMGA3-9 A) seems to tend toward a mantle component. However this represents only 7.5 % of the total ^{22}Ne released from fluid inclusions during the crushing experiment and bulk neon isotopic ratios for sample BMGA3-9 A ($^{20}Ne/^{22}Ne$ = 9.79 ± 0.008, $^{21}Ne/^{22}Ne$ = 0.032 ± 0.002) are, similarly to the $^{38}Ar/^{36}Ar$ ratio, very close to atmospheric values.

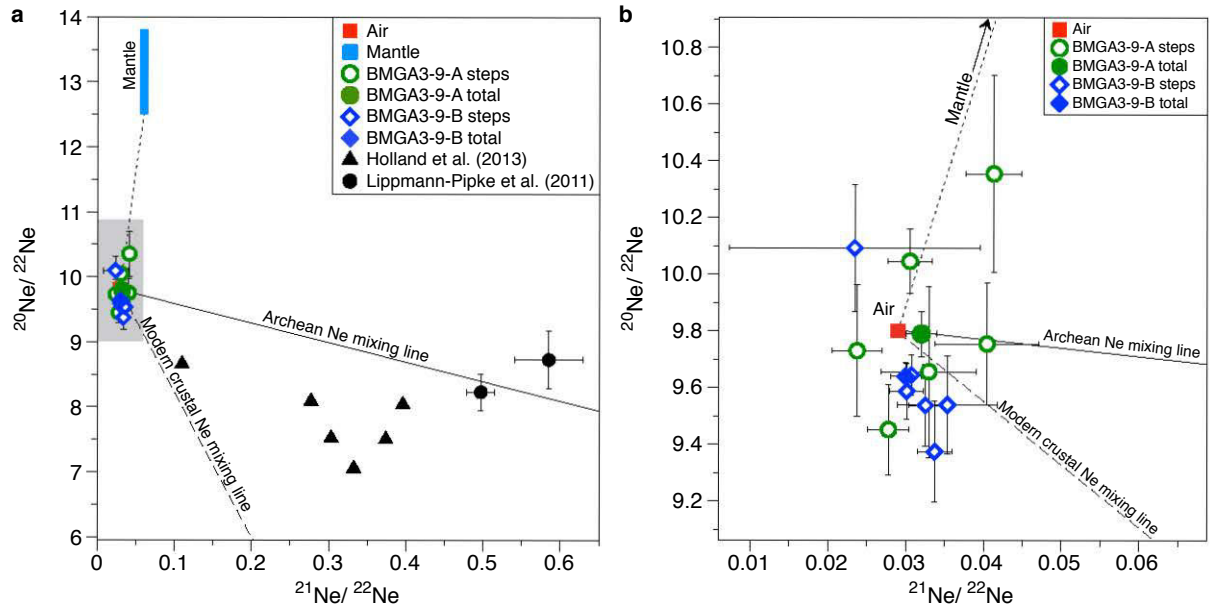

Figure 3: Three-isotope plot of Ne for crushing experiment on BMGA3-9 subsamples (green (A) and blue (B)) (see data in Table 2). Empty symbols correspond to crushing steps and filled symbols to total extractions. The blue range corresponds to possible mantle $^{20}Ne/^{22}Ne$ ratios (12.5 to 13.7) (Yokochi and Marty, 2004). Modern crustal Ne mixing line corresponds to addition of crustal nucleogenic Ne (Kennedy et al., 1990). The Archean mixing line and associated black-filled circles are from analyses by Lippmann-Pipke et al. (2011). Data obtained on Precambrian fluids by Holland et al. (2013) are indicated with black-filled triangles. Grey range in (a) corresponds to the zoom in sub-panel (b). Errors at 1σ.

3.3 Nitrogen

Marty et al. (2013) already demonstrated by using N_2-Ar isotope systematics on 3.5 Ga old quartz samples (Australia) that, at this epoch, the partial pressure of atmospheric nitrogen (p_{N2}) was modern-like and thus unlikely to be 2-3 times higher than the modern one as it was originally advocated to partially solve the faint young Sun paradox (Goldblatt et al., 2009). Here we used the same approach on results obtained on the 3.2 Ga old samples from Barberton (Table 2). $^{40}Ar/^{36}Ar$ isotopic ratios versus $N_2/^{36}Ar$ elemental ratios are displayed in the argon-mixing diagram in Fig. 4 (a). Crushing steps define a linear correlation compatible with a mixing between two end-members. The first end-member would be a crustal/hydrothermal component with elevated $N_2/^{36}Ar$ and $^{40}Ar/^{36}Ar$ ratios (Marty et al., 2013). The second end-member would be from the 3.2 Ga-old atmosphere with a $^{40}Ar/^{36}Ar$ lower than modern air (≤ 298.56) and a $N_2/^{36}Ar$ ratio similar or even lower than the modern atmosphere ($(N_2/^{36}Ar)_{air}$ = 1.02 - 1.31 x 10^4 for ocean temperatures between 2°C and 70°C (Marty et al., 2013) and refs. therein). In details, the

correlation defined by measurements in Fig. 4 (a) only permits to define an upper limit of 6.6 x 10^3 for the $N_2/^{36}Ar$ ratio (considering a maximum value of 298.56 for the atmospheric end-member) since the $^{40}Ar/^{36}Ar$ ratio of the atmospheric component is not well known. In any case this upper limit for the atmospheric-derived $N_2/^{36}Ar$ ratio recorded in Barberton quartz suggests that the partial pressure of nitrogen in the 3.2 Ga-old atmosphere might have been lower than the modern one, possibly by a factor of about 2.

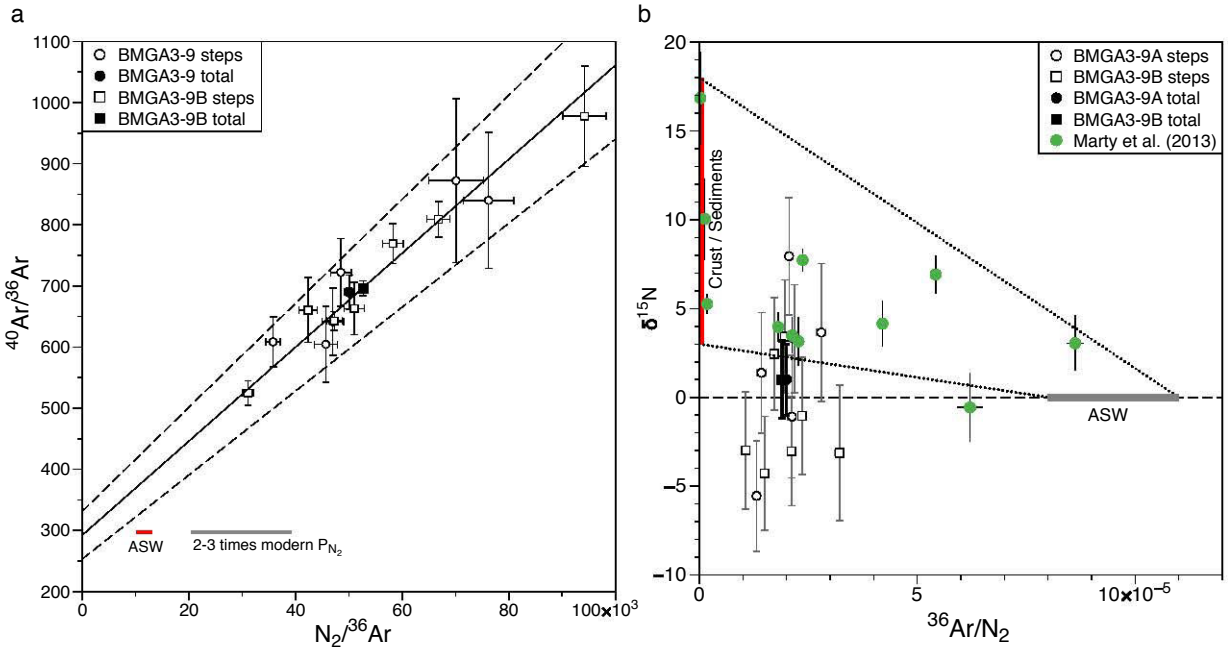

Figure 4: Nitrogen-Argon mixing diagrams. (a) Argon-mixing diagram for crushing experiments on BMGA3-9 sub-samples (see data in Table 2). Crushing steps define a linear correlation (black line and 1σ error range defined by dashed lines) between a modern-like atmospheric end-member and a hydrothermal component. An atmospheric end-member with a maximum $N_2/^{36}Ar$ ratio of 6.6 x 10^3 is envisaged (see text). (b) Nitrogen-mixing diagram. Data are compatible with a mixing between a modern-like component (air or ASW) and a crustal/sedimentary-derived component. Green-filled circles correspond to data from Marty et al. (2013). Range for $\delta^{15}N$ in crust or sediments are from Cartigny and Marty (2013) and refs. therein.

Nitrogen isotopic compositions are displayed in a nitrogen-mixing diagram ($\delta^{15}N$ vs. $^{36}Ar/N_2$) in Fig. 4b. Nitrogen isotopic compositions are expressed with the delta notation ($\delta^{15}N$) relative to the isotopic composition of the air ($\delta^{15}N_{air}$=0 ‰). Values for crust and sediments ($3< \delta^{15}N <18$) are from Cartigny and Marty (2013) and refs. therein. Crushing steps and total extractions are clustered on $^{36}Ar/N_2$ values around 2 x 10^{-5} with a total $\delta^{15}N$ of 1 ± 2 ‰ (1σ). Similarly to Marty et al. (2013) (green-filled circles in Fig. 4 (b)), our results are consistent with a mixing between an ancient atmospheric component with $\delta^{15}N \approx 0$ ‰ and a crustal/sedimentary end-member. This modern-like isotopic composition of nitrogen for the Archean atmosphere argues for the presence of a magnetic field 3.2 Ga ago preventing erosion and isotopic fractionation of atmospheric nitrogen through electron impacts, charge exchanges and photoionization (Lichtenegger et al., 2010).

Table 2: Results for the N_2-Ar-Ne crushing experiment on two subsamples of Barberton (BMGA3-9 A & B). Bolds values correspond to total gas released from fluid inclusions. Errors at 1σ.

Sample	Crush	$^{28}N_2$	+/-	$\delta^{15}N$	+/-	^{36}Ar	+/-	$^{40}Ar/^{36}Ar$	+/-	$^{38}Ar/^{36}Ar$	+/-	^{22}Ne	+/-	$^{20}Ne/^{22}Ne$	+/-	$^{21}Ne/^{22}Ne$	+/-
		mol g^{-1}		‰		mol g^{-1}						mol g^{-1}					
BMGA3-9-A	#2*	1.139E-09	3.2E-11	8	3	2.35E-14	7E-16	722	56	0.187	0.019	1.24E-15	2E-17	10.05	0.11	0.031	0.003
	#3	8.30E-10	2.3E-11	3	3	1.82E-14	7E-16	604	62	0.197	0.025	8.7E-16	2E-17	9.75	0.22	0.040	0.007
	#4	9.95E-10	2.8E-11	4	4	2.78E-14	7E-16	609	41	0.188	0.016	1.09E-15	2E-17	9.45	0.16	0.028	0.003
	#5	1.007E-09	2.8E-11	-1	3	2.14E-14	7E-16	641	55	0.185	0.021	8.5E-16	2E-17	9.73	0.23	0.024	0.003
	#6	1.019E-09	2.8E-11	-6	3	1.34E-14	7E-16	840	111	0.187	0.033	4.2E-16	1E-17	9.66	0.30	0.033	0.006
	#7	8.06E-10	2.2E-11	1	3	1.15E-14	8E-16	872	134	0.188	0.039	3.6E-16	1E-17	10.35	0.35	0.041	0.004
Total		**5.797E-09**	**6.6E-11**	**1**	**2**	**1.16E-13**	**2E-15**	**690**	**28**	**0.188**	**0.009**	**4.82E-15**	**4E-17**	**9.79**	**0.08**	**0.032**	**0.002**
BMGA3-9-B	#1	1.444E-09	4.0E-11	-3	3	3.06E-14	4E-16	643	15	0.186	0.006	1.40E-15	2E-17	9.64	0.07	0.031	0.001
	#2	6.27E-10	1.7E-11	-3	4	2.02E-14	3E-16	525	20	0.191	0.009	4.6E-16	1E-17	10.09	0.22	0.023	0.016
	#3	1.318E-09	3.7E-11	-4	3	1.97E-14	3E-16	809	29	0.190	0.009	9.4E-16	1E-17	9.59	0.10	0.030	0.002
	#4	9.80E-10	2.7E-11	2	3	1.68E-14	3E-16	769	32	0.191	0.011	5.8E-16	9E-18	9.54	0.14	0.033	0.002
	#5	7.76E-10	2.2E-11	-3	3	8.24E-15	3E-16	978	82	0.193	0.022	3.6E-16	6E-18	9.37	0.18	0.034	0.002
	#6	5.73E-10	1.6E-11	3	3	1.12E-14	3E-16	663	43	0.190	0.016	1.0E-16	2E-18	9.54	0.17	0.035	0.006
	#7	3.84E-10	1.1E-11	-1	3	9.05E-15	3E-16	660	53	0.190	0.020	4.1E-17	1E-18	9.58	0.30	0.039	0.005
Total		**6.103E-09**	**6.9E-11**	**1**	**2**	**1.158E-13**	**9E-16**	**696**	**12**	**0.190**	**0.004**	**3.89E-15**	**3E-17**	**9.64**	**0.05**	**0.030**	**0.002**
Air[a]				0				298.56		0.188				9.8		0.029	

*Analysis of the first cruch had to be aborted because of high water content

a Values are from Ozima and Podosek (2002) for noble gases and air is the reference for $\delta^{15}N$ so $\delta^{15}N_{air}$=0‰

4. Discussion

Overall N_2-Ar-Ne measurements demonstrate that fluids trapped in the analyzed quartz samples correspond to fluids derived from the atmosphere and modified by the interaction with surrounding crustal rocks. Neon and krypton isotopic results do not show any hint of a mantle-derived component (Pujol et al., 2013a) as already demonstrated by the absence of ^{129}Xe excesses from the decay of extinct ^{129}I (see previous section). The unique element showing large isotope differences with respect to modern atmospheric composition is therefore xenon.

4.1 Evolution of the Isotopic Composition of Atmospheric Xe

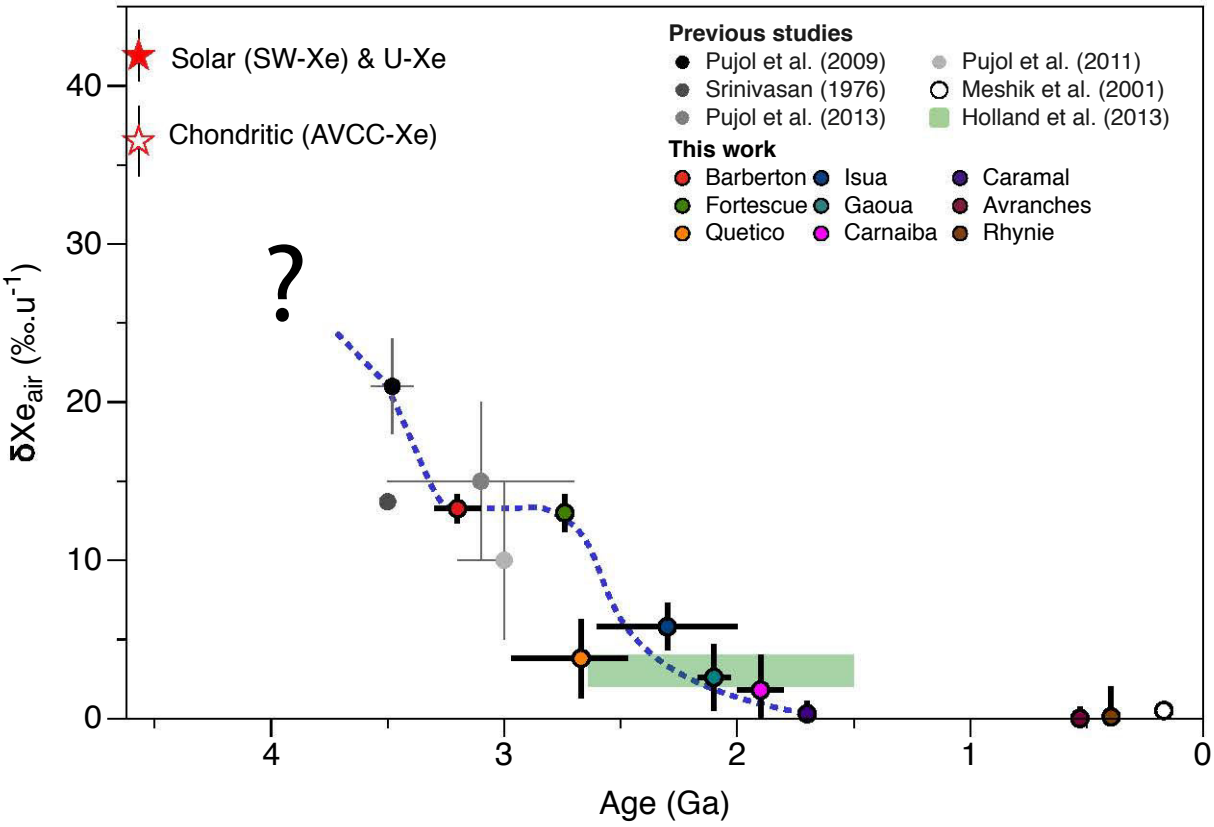

Figure 5: Evolution of the isotopic fractionation of atmospheric Xe with time. Red-filled and empty red stars represent the isotopic fractionation computed on light isotopes of Solar-/U-Xe and Chondritic Xe, respectively, relative to the modern atmosphere (Ott, 2014). Black-filled to white-filled circles and the green range are results from previous studies (see text and refs. therein). Color-filled circles are results from the present study (see Table 1). The blue dashed curve is a schematic view of the evolution of the isotopic fractionation of Xe with time. The question mark symbolizes the fact that, up to now, the mode of transition from primordial components toward Archean Xe is unknown.

Xe results obtained in this study are summarized in Fig. 5 with the values of isotopic fractionation (δXe_{air} in ‰.u^{-1}) computed for Xe released from fluid inclusions in samples of different ages. These values are also listed in Table 1. Results from previous studies (Holland et al., 2013; Meshik et al., 2001; Pujol et al., 2013b; 2011; 2009; Srinivasan, 1976) are also displayed. Results obtained in this study permit to precisely define the evolution (schematically represented with the blue dashed curve) of the isotopic composition of atmospheric Xe with time. Interestingly, samples from Barberton (South Africa) dated at 3.2 ± 0.1 Ga display a similar fractionation (13.3 ± 0.9 ‰.u^{-1}) than samples from the Fortescue Group (Australia) (13.0 ± 1.2 ‰.u^{-1}) that are younger than 2.74 Ga. This observation suggests that the isotopic evolution of atmospheric Xe marked a stop during at least 400 Ma. The isotopic fractionation of 5.8 ± 1.5 ‰.u^{-1} recorded in samples from Isua is intermediate between the isotopic fractionation recorded at 2.7 Ga (≈13 ‰.u^{-1}) and 2.1 Ga (≈2.1 ‰.u^{-1}). In a model of a progressive decrease of this isotopic fractionation with time (see next section), this observation tends to confirm that Isua metacarbonate samples are more likely ca. 2.3 Ga old than >3.7 Ga old. This age of 2.3 Ga may correspond to the resetting event recorded by Sm-Nd dating of rocks from this area (Blichert-Toft and Frei, 2001). Isotopic fractionation of atmospheric Xe may have reached its present value and stopped between 2.1 Ga (δXe_{air} = 2.1 ± 1.6 ‰.u^{-1} for samples from Gaoua) and 1.7 Ga (0.32 ± 0.89 ‰.u^{-1} for samples from Caramal). Because of the scarcity of well-preserved rocks formed during the Hadean, there is, up to now, no constraints on the early isotopic evolution of atmospheric Xe (represented by the question mark in Fig. 5).

A possible analogy to interpret the evolution represented in Fig. 5 is a Rayleigh's distillation (Hébrard and Marty, 2014; Marty, 2012). During this process, the progressive escape of Xe atoms from the atmosphere to space is accompanied by an instantaneous isotopic fractionation α (Hébrard and Marty, 2014; Marty, 2012; Pujol et al., 2011). Fractionation could occur during Xe ion trapping in forming organic haze (Hébrard and Marty, 2014; Kuga et al., 2015; Marrocchi et al., 2011) or directly during the escape mechanism (Zahnle and Kasting, 1986). The Rayleigh distillation's equation writes:

$$\frac{(^{i}Xe/^{130}Xe)_{t}}{(^{i}Xe/^{130}Xe)_{initial,4.56\ Ga\ ago}} = f^{(130-i)\alpha} \qquad \text{[Eqn. 1]}$$

where f is the depletion factor of the reservoir (the atmosphere), α is the instantaneous fractionation factor (‰.u^{-1}), and $(^{i}Xe/^{130}Xe)_{t}$ and $(^{i}Xe/^{130}Xe)_{initial,4.56\ Ga\ ago}$ are the isotopic ratios of Xe normalized to ^{130}Xe for the atmosphere at age t and for the initial composition, that is U-Xe, 4.56 Ga ago, respectively.

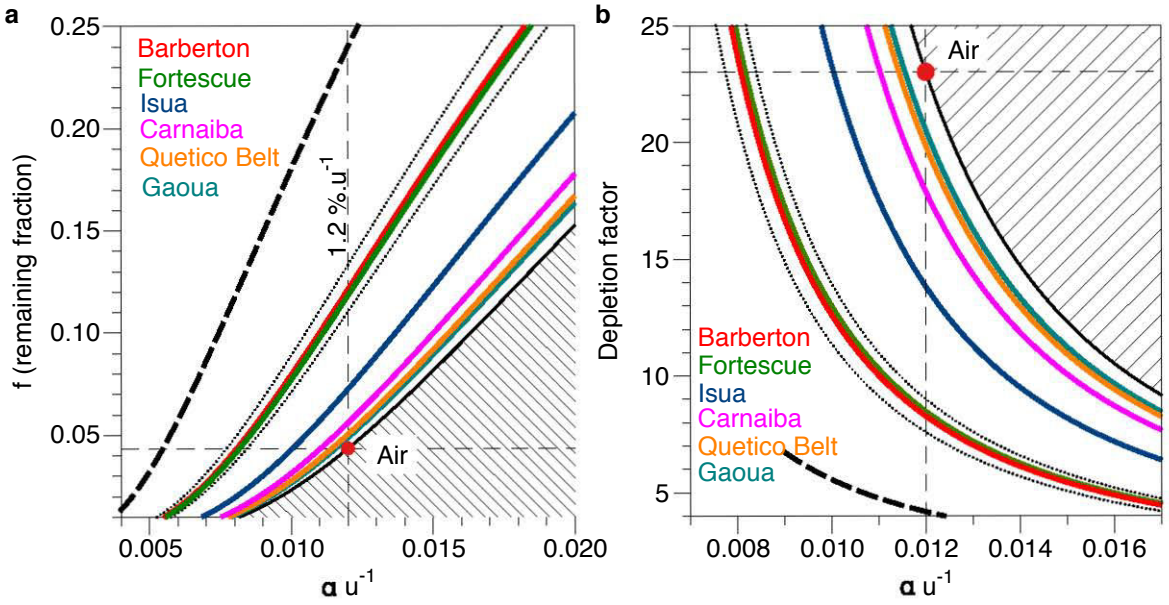

Figure 6: Remaining fractions (a) and depletion factors (b) for isotopic fractionations of Xe measured in this study if the atmosphere evolved following a Rayleigh's distillation process (see Table 1). Dotted lines correspond to the 1σ error on the fractionation measured for Barberton Xe (Table 1). A result from a previous study (Pujol et al., 2011) is shown for comparison (thick black dashed line).

Remarkably the isotopic composition of Xe in the modern atmosphere together with its 23 fold depletion (f = 0.043) (Pepin, 1991) are compatible with a Rayleigh distillation evolution with an instantaneous fractionation factor α around 1.2 ‰.u^{-1} (Fig. 6 (a) and (b)). This value perfectly matches the range of isotopic fractionation (1.0 ± 0.4 ‰.u^{-1}) observed in laboratory experiments when ionized Xe is trapped in organic matter (Kuga et al., 2015; Marrocchi et al., 2011). It is worth mentioning that Eqn. (1) assumes a constant instantaneous fractionation factor, which may not be the case since the physico-chemical process(es) behind selective atmospheric escape of Xe might have varied (see next section). The instantaneous fractionation factor of 1.2 ‰.u^{-1} computed for the modern atmosphere must thus be considered as an integrated isotopic fractionation over the whole depletion. Furthermore this simple model makes the assumption that the original Earth's atmosphere contained chondrite-like abundances of noble gases. However, a cometary contribution for the Earth's atmosphere during late stages of planetary accretion (*e.g.* during the Late Heavy Bombardment) appears possible (Marty and Meibom, 2007) and heavy noble gas elemental abundances in this possible cometary contribution are unknown. By using the generalized notation $\delta Xe_{U\text{-}Xe}$, which is the measured isotopic fractionation relative to U-Xe, a plausible starting composition (Pepin, 1991), the remaining fraction f can also be expressed following Eqn. (2):

$$f = \left(1 - \frac{\delta Xe_{U-Xe}}{1000}\right)^{\frac{1}{\alpha}} \qquad \text{[Eqn. 2]}$$

Figure 6 (a) depicts the remaining fraction of Xe in the atmosphere (the depletion factor (1/f) appears in Fig. 6 (b)) versus the instantaneous fractionation factor (α) for each set of samples analyzed in this study. Error ranges at 1σ are shown for Barberton in both sub-panels.

Remaining fractions and depletion factors of the atmosphere for $\alpha = 1.2$ %.u^{-1} are listed in Table 1 with an error bar at 1σ corresponding to the propagation of the incertitude on the isotopic fractionation relative to the starting U-Xe composition. Xe in Barberton and Fortescue Group samples present identical isotopic fractionations corresponding to a remaining fraction of the original atmosphere of 11 ± 1 %. Such a value means that, in this simple model, 3.2 Ga ago, ≈ 89 % of atmospheric Xe was already lost through this process. This would also mean that escape and isotopic fractionation of Xe marked a pause during at least 400 Ma between 3.2 Ga and 2.7 Ga. The depletion factors computed for Xe in Quetico Belt, Isua, Carnaíba, Gaoua samples (2.1 Ga) are indistinguishable within their errors (Table 1) and vary between 12 and 25.

The existence of an isotopic fractionation of Xe in the atmosphere still present ca. 2 Ga ago has also important implications for interactions between the Earth's mantle and the atmosphere. Parai and Mukhopadhyay (2015) noted that including a fractionated Archean air component in the mantle fails to explain the isotopic composition of mantle-derived gases. Even if the presence of a recycled fractionated ancient air in the present mantle appears unlikely, this component might have been initially subducted in the early Earth's mantle and thus re-degassed in the atmosphere during mantle overturn (Coltice et al., 2009). Furthermore, Parai and Mukhopadhyay (2015) considered only the replacement of the atmospheric component by a fractionated component similar to what was measured by Pujol et al. (2011). There is maybe still some space for a progressive addition of a subducted component with an evolving isotopic composition going toward modern values.

4.2 Possibilities of Escape and Relation to the Evolution of the Atmosphere

Results presented in this study call for a long-term escape of Xe from the atmosphere to the outer space. However, the simple model of Rayleigh's distillation presented in the previous section does not take into account the mechanism responsible for Xe escape.

Early models of xenon-hydrogen escape built to solve the xenon paradox required a very high EUV flux (e.g. Hunten et al. (1987)) indicating that such a process was only possible early in Earth's history (Zahnle and Kasting, 1986). Furthermore complex models of differential degassing and/or Xe retention in the silicate Earth were necessary to selectively deplete and isotopically fractionate Xe (Pepin, 1991; Tolstikhin and O'Nions, 1994). In a hydrodynamic escape model, the escape flux of heavier species (i = Xe) lifted up by escaping hydrogen is governing by Eqn. (4):

$$\phi_i = \left(\phi_H - \frac{(m_i - m_H) g b(i,H)}{kT}\right) f_i \qquad \text{[Eqn. 4]}$$

where f_H, m_H and f_i, m_i are the escape fluxes (cm^{-2} s^{-1}) and masses of hydrogen and of specie i respectively, g the gravity (980.65 cm^2 s^{-1}), k the Boltzmann constant, T the temperature of the exobase (K) and $b(i,H)$ the binary diffusion coefficient (cm^{-1} s^{-1}) equal to 4.5 x 10^{17} T$^{0.71}$ (Zahnle and Kasting, 1986) in the case of ^{130}Xe escaping with H_2. Such a high value and the high mass of ^{130}Xe lead to extreme f_H values required for Xe escape. Zahnle (2015) concludes that Xe escape in its neutral form was possible only in the first 100 Ma of Earth's history when EUV flux from the

young Sun was high enough (>300 times the modern one) to drive a significant hydrogen-driven escape of neutral Xe. However, our results demonstrate that, if the escape and fractionation hypothesis is true, then a mechanism for Xe escape, still ongoing ca. 2.1 Ga ago, has yet to be found.

In 2015, K. Zahnle provided a theoretical framework explaining the progressive escape of Xe from a hydrogen-rich early atmosphere (Zahnle, 2015). In his model, Xe is no more neutral but easily ionized due to enhanced EUV flux from the young Sun (Claire et al., 2012). Furthermore Xe^+ radiative recombination in neutral Xe is presented as a slow process. When ionized, Xe is prone to interact with H^+ via Coulomb interactions decreasing the binary diffusion coefficient $b(Xe^+,H^+)$ by several orders of magnitude compared to the case where Xe is in its neutral form. In these conditions a hydrogen escape flux similar to the modern one may have been sufficient to escape Xe^+ ions. The presence of a strong magnetic field in the past (Tarduno et al., 2014) may have also favored this escape. Indeed, Zahnle (2015) advocated than Xe^+ ions could migrate toward Earth's magnetic poles where open magnetic lines would allow the escape of ions. However, most of the parameters governing this coupled hydrogen/xenon escape model that are hydrogen mixing ratio in the atmosphere, Xe^+ scale height, ionization efficiency, magnetic field strength etc., are still poorly constrained and require further modeling (*see the discussion on these parameters following the Supplementary Material of this paper*).

Zahnle et al. (2013) argued that hydrogen-escape is the main mechanism that drove the oxidation of the Earth's atmosphere. Even if oxygenic photosynthesis may have taken place before the great oxygenation event (e.g. Eigenbrode and Freeman (2006)), H_2 oxidized the surface reservoirs later, until O_2 was stable in the atmosphere. If it is true, progressive isotopic fractionation of Xe in the past might have had an evolution that was concomitant with the progressive oxidation of surficial reservoirs of the Earth.

Figure 7 depicts the evolution of the isotopic composition of Xe determined in this study (cf. Figure 5) compared to: (a) the record of $\Delta^{33}S$ in sedimentary rocks (Johnston, 2011); (b) recent models of the progressive oxygenation of the Earth's atmosphere (Lyons et al., 2015) and; (c) impact and superplume events occurring over Earth's geological history (Abbott and Isley, 2002; Reimold and Koeberl, 2014). Sulfur mass-independent isotopic fractionation (S-MIF) stopped around 2.45 Ga whereas the isotopic fractionation of Xe seems to have continued to evolve until 2 Ga. Disappearance of S-MIFs is usually linked to the very beginning of the oxygenation of the Earth's atmosphere (Fig. 7(b)) because only minute amounts of oxygen in the air prevented the efficient separation of sulfur-bearing species required to preserve a $\Delta^{33}S$ record in sedimentary rocks (Farquhar and Wing, 2003). Sulfur isotopes are thus powerful tracers of the very beginning of the oxygenation. If hydrogen escape was driving xenon escape and isotopic fractionation as proposed above, stop of the isotopic fractionation of Xe around 2.0 Ga may sign the end of hydrogen escape and the onset of moderate oxygen levels (between 10^{-4} and 10^{-2} the present atmospheric level, Fig. 7(b)). It is worth noting that these moderate oxygen levels would also have prevented the development of organic hazes that might be necessary to fractionate Xe isotopes (Hébrard and Marty, 2014). In this context, the quiescent time between 3.2 Ga and 2.7 Ga for Xe isotopic fractionation (Fig. 5), also present for the S-MIF signatures (Fig. 7(a)), might

be linked to whiffs of oxygen (Anbar et al. (2007), blue arrows in Fig. 7(b)) causing brief stops of the production of organic hazes and preventing the penetration of UV photons in the atmosphere responsible for ionization of Xe and photolysis of sulfur.

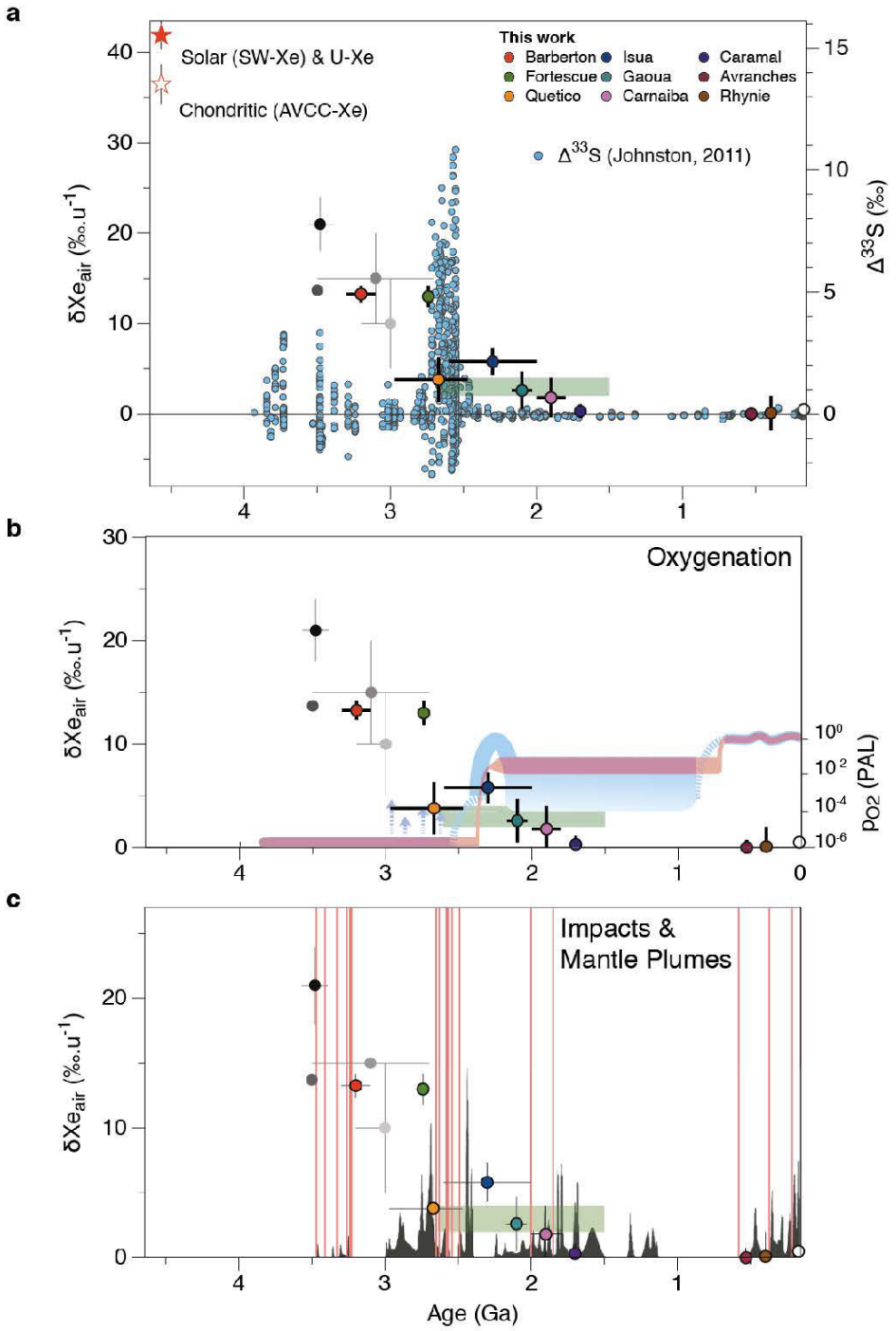

Figure 7: Evolution of the isotopic composition of xenon (in a, b & c) compared to other isotopic signatures and significant events over Earth's geological history: (a) $\Delta^{33}S$ measured in the geological record (data are from Johnston (2011)). A mass-independent fractionation signal is present prior to 2.45 Ga. (b) Evolution of the oxygen level in the Earth's atmosphere. Figure adapted from Lyons et al. (2015). Blue arrows indicate possible whiffs of oxygen (Anbar et al., 2007). The blue range depicts a classical two-step view of the evolution whereas the blue range depicts the model presented by Lyons et al. (2015). (c) Occurrences of spherule beds (compiled by Reimold and Koeberl (2014)) indicative of major impacts (vertical red lines) and time series of superplume events compiled by Abbott and Isley (2002).

4.3 Mars-Xe and Alternative Models

The case of Xe in the Martian atmosphere is interesting here since it seems to present an isotopic fractionation relative to the solar composition that is similar to the Earth's modern atmosphere (≈40 ‰.u^{-1} relative to the solar composition) (Bogard et al., 2001). A hydrogen-Xe^+ escape mechanism might have also been operative on Mars since some H_2 may have been present in its early atmosphere and later escaped through hydrodynamic escape mechanisms (Ramirez, 2013).

However, it is very surprising to measure a comparable value for the isotopic fractionation of modern atmospheric Xe on both planets since parameters governing the escape (hydrogen escape flux, EUV flux to ionize Xe, magnetic field strength, initial abundances of Xe) were probably very different due to the differences in position relative to the Sun and to the very different geological histories of both planets. One may thus expect to measure different isotopic fractionations of Xe for both planetary atmospheres. The similarity for Xe in the atmosphere of Mars and Earth leaves the possibility that the evolution of the isotopic signature of atmospheric Xe presented here is linked to a progressive contribution of volatile-rich bodies to the terrestrial atmospheres. In this model, these atmospheres started with chondritic or solar Xe signatures. Volatile-rich bodies may have carried a U-Xe (or solar for Mars) component that was already isotopically fractionated like modern atmospheric xenon but with a process that took place in the solar nebula for example (Kuga et al., 2015). Progressive contribution of these bodies to the atmosphere would have shifted the isotopic fractionation from chondritic/solar to modern values. It must be noticed here that, in that case, the starting isotopic composition for the Martian atmosphere might have been closer to solar Xe than to U-Xe as a solar-like component has been measured in the Martian meteorite Chassigny (Mathew and Marti, 2001). If this progressive contribution of fractionated Xe is true, major impacts events inferred from the presence of spherule beds (Reimold and Koeberl, 2014) potentially releasing fractionated U-Xe in the Earth's atmosphere and mantle degassing episodes of chondritic-derived Xe are two important parameters to scrutinize (Fig. 7 (c)). Interestingly, important shifts in the isotopic composition of atmospheric Xe seem to be temporally correlated with major impact events present in the 3.5 Ga to 3.2 Ga and 2.7 to ca. 2 Ga intervals, for example. In this scenario the isotopic plateau for Xe between 3.2 Ga and 2.7 Ga would be explained by a stop in the delivery of fractionated Xe to the Earth's atmosphere. It is worth noting here that the absence of spherule beds between 3.5 Ga and 3.2 Ga might be simply due to a sampling bias. For mantle activity, there is no straightforward correlation between the evolution of the isotopic composition of atmospheric xenon and the occurrence of super-plume events (Abbott and Isley, 2002).

Measuring the isotopic composition and the abundance of Xe (and Kr) in the Venusian atmosphere would be of great interest here since a comparison with Earth and Mars would help to constrain what are the physical processes behind this progressive isotopic fractionation. The three planets present very different characteristics (mass, distance from the Sun, degassing history, atmospheric composition, magnetic field) so that a similar composition of Xe on these three terrestrial planets would favor the model of a progressive isotopic evolution of planetary

atmospheres due to a progressive contribution of wet-rich material carrying a fractionated Xe component to an originally chondritic or solar atmosphere.

5. Conclusions

Results presented in this study confirm that the isotopic composition of xenon in the Earth's atmosphere is well recorded in fluid inclusions of ancient quartz samples.

The isotopic composition of xenon had a long-term evolution from a primordial composition similar to U-Xe, as shown by Barberton and Fortescue Gp. Xe, toward the isotopic fractionation of the modern atmosphere. Isotopic fractionation of Xe marked a stop between 3.2 and 2.7 Ga and the present-day isotopic composition was probably acquired between 2.1 and 1.7 Ga. Such a long-term evolution calls for a modification of models built to solve the xenon paradox (elemental depletion and isotopic fractionation) and originally based on an early atmospheric escape of Xe. An escape mechanism based on hydrogen escape coupled with the ionization of Xe is proposed. The end of the isotopic fractionation of Xe might be due to the end of the hydrogen escape also advocated to explain the progressive oxygenation of the Earth's atmosphere (Zahnle et al., 2013). Atmospheric Xe might thus be an indirect proxy of this progressive oxidation.

A modeling effort of coupled Xe^{+}-H^{+} escape may provide important keys to estimate if this is a viable mechanism for long-term escape and isotopic fractionation of Xe. In addition, measuring the isotopic composition of Xe in Venus atmosphere is essential as it would provide, in addition to Martian Xe, a third element of comparison to understand what are the processes and acting factors necessary to progressively fractionate atmospheric Xe.

References

Abbott, D.H., Isley, A.E., 2002. The intensity, occurrence, and duration of superplume events and eras over geological time. Journal of Geodynamics 34, 265–307. doi:10.1016/S0264-3707(02)00024-8

Anbar, A.D., Duan, Y., Lyons, T.W., Arnold, G.L., Kendall, B., Creaser, R.A., Kaufman, A.J., Gordon, G.W., Scott, C.T., Garvin, J., Buick, R., 2007. A whiff of oxygen before the great oxidation event? Science 317, 1903–1906. doi:10.1126/science.1138700

Ballentine, C.J., Burgess, R., Marty, B., 2002. Tracing Fluid Origin, Transport and Interaction in the Crust. RiMG 47, 539–614. doi:10.2138/rmg.2002.47.13

Baratoux, L., Metelka, V., Naba, S., Ouiya, P., Siebenaller, L., Jessell, M.W., Naré, A., Salvi, S., Béziat, D., Franceschi, G., 2015. Tectonic evolution of the Gaoua region, Burkina Faso: Implications for mineralization. Journal of African Earth Sciences 112, 419–439. doi:10.1016/j.jafrearsci.2015.10.004

Blichert-Toft, J., Frei, R., 2001. Complex Sm-Nd and Lu-Hf isotope systematics in metamorphic garnets from the Isua supracrustal belt, West Greenland. Geochimica et Cosmochimica Acta 65, 3177–3189. doi:10.1016/S0016-7037(01)00680-9

Bogard, D.D., Clayton, R.N., Marti, K., Owen, T., Turner, G., 2001. Martian volatiles: Isotopic composition, origin, and evolution, in: Chronology and Evolution of Mars. Chronology and

Evolution of Mars, Netherlands, pp. 425–458.

Bresesti, M., Cappellani, F., Del Turco, A.M., Orvini, E., 1964. The thermal neutron capture cross-section and the resonance capture integral of 124Xe. J. Inorg. Nucl. Chem. 26, 9–14. doi:10.1016/0022-1902(64)80225-6

Caffee, M.W., Hudson, G.B., Velsko, C., Huss, G.R., Alexander, E.C., Jr, Chivas, A.R., 1999. Primordial Noble Gases from Earth's Mantle: Identification of a Primitive Volatile Component. Science 285, 2115–2118. doi:10.1126/science.285.5436.2115

Card, K.D., 1990. A review of the Superior Province of the Canadian Shield, a product of Archean accretion. Precambrian Research 48, 99–156. doi:10.1016/0301-9268(90)90059-Y

Cartigny, P., Marty, B., 2013. Nitrogen Isotopes and Mantle Geodynamics: The Emergence of Life and the Atmosphere-Crust-Mantle Connection. Elements 9, 359–366. doi:10.2113/gselements.9.5.359

Catling, D.C., 2014. The Great Oxidation Event transition, in: Treatise on Geochemistry (Second Edition). Elsevier, Oxford, pp. 177–195. doi:10.1016/B978-0-08-095975-7.01307-3

Chantraine, J., Auvray, B., Brun, J.P., Chauvel, J.J., Rabu, D., 1994. Introduction, in: Chantraine, J., Rolet, J., Santallier, D.S., Piqué, A. (Eds.), Pre-Mesozoic Geology in France and Related Areas. pp. 75–80.

Cheilletz, A., Féraud, G., Giuliani, G., and Ruffet, G. (1993). Emerald dating through 40Ar/39Ar step- heating and laser spot analysis of syngenetic phlogopite. Earth and Planetary Science Letters, 120(3- 4):473–485.

Claire, M.W., Sheets, J., Cohen, M., Ribas, I., Meadows, V.S., Catling, D.C., 2012. The evolution of solar flux from 0.1 nm to 160 um: Quantitative estimates for planetary studies. ApJ 757, 1–12. doi:10.1088/0004-637X/757/1/95

Coltice, N., Marty, B., Yokochi, R., 2009. Chemical Geology. Chemical Geology 266, 4–9. doi:10.1016/j.chemgeo.2009.04.017

Dauphas, N., 2003. The dual origin of the terrestrial atmosphere. Icarus 165, 326–339. doi:10.1016/S0019-1035(03)00198-2

Dauphas, N., Morbidelli, A., 2014. Geochemical and Planetary Dynamical Views on the Origin of Earth's Atmosphere and Oceans, in: Turekian, H.D.H.K. (Ed.), Treatise on Geochemistry (Second Edition), Treatise on Geochemistry (Second Edition). Elsevier, Oxford, pp. 1–35.

Davis, D.W., Pezzutto, F., Ojakangas, R.W., 1990. The age and provenance of metasedimentary rocks in the Quetico Subprovince, Ontario, from single zircon analyses: implications for Archean sedimentation and tectonics in the Superior Province. EPSL 99, 195–205. doi:10.1016/0012-821X(90)90110-J

de Ronde, C.E.J., Wit, M.J., 1994. Tectonic history of the Barberton greenstone belt, South Africa: 490 million years of Archean crustal evolution. Tectonics 13, 983–1005.

Drescher, J., Kirsten, T., Schäfer, K., 1998. The rare gas inventory of the continental crust, recovered by the KTB Continental Deep Drilling Project. EPSL 154, 247–263.

Eigenbrode, J.L., Freeman, K.H., 2006. Late Archean rise of aerobic microbial ecosystems. PNAS 103(43), 15759-15764.

Farquhar, J., Wing, B.A., 2003. Multiple sulfur isotopes and the evolution of the atmosphere.

EPSL 213, 1–13. doi:10.1016/S0012-821X(03)00296-6

Foriel, J., Philippot, P., Rey, P., Somogyi, A., Banks, D., Ménez, B., 2004. Biological control of Cl/Br and low sulfate concentration in a 3.5-Gyr-old seawater from North Pole, Western Australia. EPSL 228, 451–463. doi:10.1016/j.epsl.2004.09.034

Formisano, V., Atreya, S., Encrenaz, T., Ignatiev, N., Giuranna, M., 2004. Detection of methane in the atmosphere of Mars. Science 306, 1758–1761. doi:10.1126/science.1101732

Giuliani, G., Silva, L.J.H.D., Couto, P., 1990. Origin of emerald deposits of Brazil. Mineral. Deposita 25, 57–64. doi:10.1007/BF03326384

Goldblatt, C., Claire, M.W., Lenton, T.M., Matthews, A.J., Watson, A.J., Zahnle, K.J., 2009. Nitrogen-enhanced greenhouse warming on early Earth. Nature Geoscience 2, 891–896. doi:10.1038/ngeo692

Hébrard, E., Marty, B., 2014. Coupled noble gas-hydrocarbon evolution of the early Earth atmosphere upon solar UV irradiation. EPSL 385, 40–48. doi:10.1016/j.epsl.2013.10.022

Holland, G., Ballentine, C.J., 2006. Seawater subduction controls the heavy noble gas composition of the mantle. Nature 441, 186–191. doi:10.1038/nature04761

Holland, G., Cassidy, M., Ballentine, C.J., 2009. Meteorite Kr in Earth's mantle suggests a late accretionary source for the atmosphere. Science. doi:10.1126/science.1131871)

Holland, G., Lollar, B.S., Li, L., Lacrampe-Couloume, G., Slater G. F., Ballentine C. J., 2013. Deep fracture fluids isolated in the crust since the Precambrian era. Nature 497, 357–360. doi:10.1038/nature12127

Hunten, D.M., Pepin, R.O., Walker, J.C., 1987. Mass fractionation in hydrodynamic escape. Icarus 69, 532–549.

Johnston, D.T., 2011. Multiple sulfur isotopes and the evolution of Earth's surface sulfur cycle. Earth Science Reviews 106, 161–183. doi:10.1016/j.earscirev.2011.02.003

Kendrick, M.A., Burgess, R., Pattrick, R.A.D., Turner, G., 2001. Halogen and Ar–Ar age determinations of inclusions within quartz veins from porphyry copper deposits using complementary noble gas extraction techniques. Chemical Geology 177, 351–370.

Kennedy, B.M., Hiyagon, H., Reynolds, J.H., 1990. Crustal neon: a striking uniformity. EPSL 98, 277–286.

Kuga, M., Marty, B., Marrocchi, Y., Tissandier, L., 2015. Synthesis of refractory organic matter in the ionized gas phase of the solar nebula. PNAS 112, 7129–7134. doi:10.1073/pnas.1502796112

Kyser, K., Hiatt, E., Renac, C., Durocher, K., Holk, G., Deckart, K., 2000. Diagenetic fluids in Paleo-and Meso-Proterozoic sedimentary basins and their implications for long protracted fluid histories, in: Kyser, K. (Ed.), Fluids and Basin Evolution. Fluids and basin evolution, pp. 73–506.

Le Mignot, E., Siebenaller, L., Béziat, D., Salvi, S., André-Mayer, A.S., Reisberg, L., Velasquez, G., Zimmermann, C., Franceschi, G., 2014. The Paleoproterozoic Copper-Gold Deposit of Gaoua, Burkina Faso: Evidence for A Polyphased Mineralization. Acta Geologica Sinica (English Edition) 88, 970–972. doi:10.1111/1755-6724.12378_5

Lee, J.-Y., Marti, K., Severinghaus, J.P., Kawamura, K., Yoo, H.-S., Lee, J.B., Kim, J.S., 2006. A

redetermination of the isotopic abundances of atmospheric Ar. Geochimica et Cosmochimica Acta 70, 4507–4512. doi:10.1016/j.gca.2006.06.1563

Lichtenegger, H.I.M., Lammer, H., Grießmeier, J.M., Kulikov, Y.N., Paris, von, P., Hausleitner, W., Krauss, S., Rauer, H., 2010. Aeronomical evidence for higher CO2 levels during Earth's Hadean epoch. Icarus 210, 1–7. doi:10.1016/j.icarus.2010.06.042

Lippmann-Pipke, J., Lollar, B.S., Niedermann, S., Stroncik, N.A., Naumann, R., van Heerden, E., Onstott, T.C., 2011. Chemical Geology. Chemical Geology 283, 287–296. doi:10.1016/j.chemgeo.2011.01.028

Lyons, T.W., Reinhard, C.T., Planavsky, N.J., 2015. The rise of oxygen in Earth's early ocean and atmosphere. Nature 506, 307–315. doi:10.1038/nature13068

Marrocchi, Y., Marty, B., Reinhardt, P., Robert, F., 2011. Adsorption of xenon ions onto defects in organic surfaces: Implications for the origin and the nature of organics in primitive meteorites. Geochimica et Cosmochimica Acta 75, 6255–6266. doi:10.1016/j.gca.2011.07.048

Marty, B., 2012. The origins and concentrations of water, carbon, nitrogen and noble gases on Earth. EPSL 313-314, 56–66. doi:10.1016/j.epsl.2011.10.040

Marty, B., Meibom, A., 2007. Noble gas signature of the late heavy bombardment in the Earth's atmosphere. EEarth 2, 43–49.

Marty, B., Zimmermann, L., 1999. Volatiles (He, C, N, Ar) in mid-ocean ridge basalts: Assesment of shallow-level fractionation and characterization of source composition. Geochimica et Cosmochimica Acta 63, 3619–3633.

Marty, B., Zimmermann, L., Pujol, M., Burgess, R., Philippot, P., 2013. Nitrogen Isotopic Composition and Density of the Archean Atmosphere. Science 342, 101–104. doi:10.1126/science.1240971

Mathew, K.J., Marti, K., 2001. Early evolution of Martian volatiles: Nitrogen and noble gas components in ALH84001 and Chassigny. Journal of Geophysical Research: Planets 106, 1401–1422. doi:10.1029/2000JE001255

Meshik, A.P., Hohenberg, C.M., Pravdivtseva, O.V., Kapusta, Y.S., 2001. Weak decay of 130Ba and 132Ba: Geochemical measurements. Phys. Rev. C 64, 035205. doi:10.1103/PhysRevC.64.035205

Mojzsis, S.J., Arrhenius, G., McKeegan, K.D., Harrison, T.M., 1996. Evidence for life on Earth before 3,800 million years ago. Nature 384, 55–59.

Nutman, A.P., Friend, C.R.L., 2009. New 1:20,000 scale geological maps, synthesis and history of investigation of the Isua supracrustal belt and adjacent orthogneisses, southern West Greenland: A glimpse of Eoarchaean crust formation and orogeny. Precambrian Research 172, 189–211. doi:10.1016/j.precamres.2009.03.017

Ott, U., 2014. Planetary and pre-solar noble gases in meteorites. Chemie der Erde - Geochemistry 74, 519–544. doi:10.1016/j.chemer.2014.01.003

Ozima, M., Podosek, F.A., 2002. Noble Gas Geochemistry, Second Edition. ed. Cambridge University Press, Cambridge.

Parai, R., Mukhopadhyay, S., 2015. The evolution of MORB and plume mantle volatile budgets: Constraints from fission Xe isotopes in Southwest Indian Ridge basalts. Geochem. Geophys.

Geosyst. 16, 1–17. doi:10.1002/2014GC005566

Pepin, R.O., 2013. Comment on "Chondritic-like xenon trapped in Archean rocks: A possible signature of the ancient atmosphere" by M. Pujol, B. Marty, R. Burgess [Earth Planet. Sci. Lett. 308 (2011) 298–306]. EPSL 371-372, 294–295. doi:10.1016/j.epsl.2013.03.027

Pepin, R.O., 1991. On the origin and early evolution of terrestrial planet atmospheres and meteoritic volatiles. Icarus 92, 2–79.

Pujol, M., Marty, B., Burgess, R., 2013a. Reply to comment on "Chondritic-like xenon trapped in Archean rocks: A possible signature of the ancient atmosphere" by Pujol, M., Marty, B., Burgess, R., Earth and Planetary Science Letters 308 (2011) 298-306 by Pepin, R. O. EPSL 371-372, 296–298. doi:10.1016/j.epsl.2013.03.029

Pujol, M., Marty, B., Burgess, R., 2011. Chondritic-like xenon trapped in Archean rocks: A possible signature of the ancient atmosphere. EPSL 308, 298–306. doi:10.1016/j.epsl.2011.05.053

Pujol, M., Marty, B., Burgess, R., Turner, G., Philippot, P., 2013b. Argon isotopic composition of Archaean atmosphere probes early Earth geodynamics. Nature 498, 87–90. doi:10.1038/nature12152

Pujol, M., Marty, B., Burnard, P., Philippot, P., 2009. Xenon in Archean barite: Weak decay of 130Ba, mass-dependent isotopic fractionation and implication for barite formation. Geochimica et Cosmochimica Acta 73, 6834–6846. doi:10.1016/j.gca.2009.08.002

Ramirez, R.M., 2013. Warming early Mars with CO2 and H2. Nature Geoscience 7, 59–63. doi:10.1038/ngeo2000

Reimold, W.U., Koeberl, C., 2014. Impact structures in Africa: A review. Journal of African Earth Sciences 93, 57–175. doi:10.1016/j.jafrearsci.2014.01.008

Ribas, I., Guinan, E.F., Gudel, M., Audard, M., 2005. Evolution of the Solar Activity over Time and Effects on Planetary Atmospheres. I. High-Energy Irradiances (1-1700 Å). ApJ 622, 680–694. doi:10.1086/427977

Rice, C.M., Ashcroft, W.A., Batten, D.J., Boyce, A.J., Caulfield, J.B.D., Fallick, A.E., Hole, M.J., Jones, E., Pearson, M.J., Rogers, G., Saxton, J.M., Stuart, F.M., Trewin, N.H., Turner, G., 1995. A Devonian auriferous hot spring system, Rhynie, Scotland. Journal of the Geological Society, London 152, 229–250.

Rose, N.M., Rosing, M.T., Bridgwater, D., 1996. The origin of metacarbonate rocks in the Archaean Isua supracrustal belt, West Greenland. American Journal of Science 296, 1004–1044. doi:10.2475/ajs.296.9.1004

Schwarzschild, M., 1958. Structure and Evolution of the Stars, Princeton University Press. ed. Dover Publications Inc., Princeton.

Srinivasan, B., 1976. Barites: anomalous xenon from spallation and neutron-induced reactions. EPSL 31, 129–141. doi:10.1016/0012-821X(76)90104-7

Srinivasan, B., Alexander, E.C., Jr, Manuel, O.K., 1971. Iodine-129 in Terrestrial Ores. Science 173, 327–328. doi:10.1126/science.173.3994.327

Suhonen, J., 2013. Double beta decays of 124Xe investigated in the QRPA framework. J. Phys. G: Nucl. Part. Phys. 40, 1–14. doi:10.1088/0954-3899/40/7/075102

Takaoka, N., 1972. An interpretation of general anomalies of xenon and the isotopic composition of primitive xenon. Mass Spectrometry 20, 287–302.

Tarduno, J.A., Blackman, E.G., Mamajek, E.E., 2014. Detecting the oldest geodynamo and attendant shielding from the solar wind: Implications for habitability. Physics of the Earth and Planetary Interiors 233, 68–87. doi:10.1016/j.pepi.2014.05.007

Tolstikhin, I.N., O'Nions, R.K., 1994. The Earth's missing xenon: A combination of early degassing and of rare gas loss from the atmosphere. Chemical Geology 115, 1–6.

Trendall, A.F., Compston, W., Nelson, D.R., De Laeter, J.R., Bennett, V.C., 2004. SHRIMP zircon ages constraining the depositional chronology of the Hamersley Group, Western Australia. Australian Journal of Earth Sciences 51, 621–644. doi:10.1111/j.1400-0952.2004.01082.x

Ulrich, R.K., 1975. Solar neutrinos and variations in the solar luminosity. Science 190, 619–624.

Yokochi, R., Marty, B., 2004. A determination of the neon isotopic composition of the deep mantle. EPSL 225, 77–88. doi:10.1016/j.epsl.2004.06.010

Zahnle, K.J., 2015. Xenon fractionation and Archean hydrogen escape, in:. Presented at the 46th Lunar and Planetary Science Conference, The Woodlands (Texas), pp. 1–2.

Zahnle, K.J., Catling, D.C., Claire, M.W., 2013. The rise of oxygen and the hydrogen hourglass. Chemical Geology 362, 26–34. doi:10.1016/j.chemgeo.2013.08.004

Zahnle, K.J., Kasting, J.F., 1986. Mass fractionation during transonic escape and implications for loss of water from Mars and Venus. Icarus 68, 462–480. doi:10.1016/0019-1035(86)90051-5

Acknowledgments

This study was funded in Nancy (France) by the European Research Council under the European Community's Seventh Framework Programme (FP7/2007-2013 grant agreement No. 267255 to B.M.). Nick Arndt, Pascal Philippot, Francis & Isabelle Avice, Elodie Le Mignot, Antonin Richard, Marie-Christine Boiron and Ray Burgess are acknowledged for providing samples analyzed in this study. Laurent Zimmermann is gratefully acknowledged for technical mentorship and assistance.

Evolution of atmospheric xenon and other noble gases inferred from the study of Archean to Paleoproterozoic rocks

Supplementary Material

G. Avice[1], B. Marty[1]

[1]CRPG-CNRS, Université de Lorraine, UMR 7358, 15 rue Notre-Dame des Pauvres, BP 20, 54501 Vandoeuvre-lès-Nancy Cedex, France.

Description of the N_2-Ar-Ne Experiment

Samples were crushed with the same crushers than for Xe-Kr gas extractions. Crusher volume was directly in contact with a double-walled glass tube system plunged in liquid nitrogen in order to condense water and a major part of other reactive gases (except nitrogen, T≈100 K) on the walls of the tube. After waiting for gas equilibration, the original aliquot was divided in two sub-aliquots by closing a valve. One aliquot was dedicated to Ne-Ar measurements and the other aliquot to N_2 measurement. In the first aliquot, Ar was trapped on a charcoal held at liquid nitrogen temperature (77 K) ensuring no trapping of Ne. Neon was then analyzed on a VG 5400 mass spectrometer. After monitoring of $CO2^+$ (m=44) quantities at the beginning and the end of each analysis, some corrections on ^{22}Ne (m=21.991) were applied for double ionization of CO_2^{++} (m=21.995) following Eqn. (S1), for the ^{20}Ne/^{22}Ne ratio for example,

$$\frac{^{20}Ne}{^{22}Ne} = \frac{[^{20}Ne]}{[^{22}Ne]-\beta\times CO_2^+} \qquad \text{[Eqn. S1]}$$

where CO_2^+ is the signal of CO_2^+ in the mass spectrometer during the analysis, [^{20}Ne] and [^{22}Ne] are the signals detected on the electron multiplier and β is the double ionization ratio (CO_2^{2+}/CO_2^+) with a value of 0.5 % determined during the experiment. Corrections for $^{40}Ar^{++}$ (m=19.981) were not necessary because of an efficient separation of Ar and a sufficient resolution allowing shifting of the mass where measurement was done in order to prevent any contribution of $^{40}Ar^{++}$ to the ^{20}Ne (m=19.992) signal.

During Ne measurement, Ar was released from the charcoal and analyzed in a subsequent run. Separation and purification of nitrogen were made following the method described in a previous study (Zimmermann et al., 2009). It consisted in dissociation and oxidation of all impurities into CO_2, H_2O, SO_2 and NO_x species with a high partial pressure of oxygen (p_{O2}) produced by heating a CuO to 800°C. After oxidation, all oxides except NO_x were trapped in a cold trap held at -183°C. The p_{O2} was then reduced by cooling the CuO to 300°C a temperature sufficient for the complete transition from NO_x to N_2. N_2 was then introduced in the mass

spectrometer. Results were corrected for CO^+ and HC^+ contribution following the method described by Hashizume and Marty (2004).

Computation of the Depletion in ^{124}Xe by Thermal Neutron Capture

The rate of depletion in ^{124}Xe depends on both the thermal neutron capture cross-section of ^{124}Xe and on the crustal neutron flux. Interestingly, the thermal neutron capture cross-section of ^{124}Xe is high (165 ± 11 barns) compared to other Xe isotopes (0.26 to 85 barns) (Bresesti et al., 1964). Following the rationale presented in Ballentine and Burnard (2002), the depletion in ^{124}Xe by thermal neutron capture is given by Eqn. (S2):

$$^{124}Xe_{nc} = P_{th} \times N \times F_{^{124}Xe} \qquad \text{[Eqn. S2]}$$

where P_{th} is the probability for neutrons to be thermalized (0.8), N is the neutron flux in the crust (11.2 neutrons.g^{-1}.a^{-1}), F_{124Xe} is the probability that ^{124}Xe will capture a thermal neutron. It corresponds to the neutron capture probability of ^{124}Xe (abundance in quartz (≈10^{-16} mol.g^{-1} cf. Table 1) multiplied by the thermal neutron capture cross-section (165 barns)) divided by the total neutron capture probability in the crust (0.00979 mol.barns). All values, except the thermal neutron capture cross-section of ^{124}Xe, are from Ballentine and Burnard (2002). Calculations led to a rate of removal of ^{124}Xe atoms by thermal neutron capture of 7.10^{-37} mol.g^{-1}.a^{-1} corresponding to only 2.10^{-27} mol.g^{-1} of ^{124}Xe removed by this process during 3.2 Ga (time of fluid-entrapment). This first-order estimate demonstrates that thermal neutron capture on ^{124}Xe is unlikely to be the process responsible for the depletion in ^{124}Xe recorded in Barberton and Fortescue Group quartz samples.

References

Ballentine, C.J., Burnard, P.G., 2002. Production, Release and Transport of Noble Gases in the Continental Crust. RiMG 47, 481–538. doi:10.2138/rmg.2002.47.12

Basford, J.R., Dragon, J.C., Pepin, R.O., Coscio, M. R., Murthy, V. R., 1973. Krypton and xenon in lunar fines. Proceedings of the fourth Lunar and Planetary Science Conference 2, 1915-1955.

Bresesti, M., Cappellani, F., Del Turco, A.M., Orvini, E., 1964. The thermal neutron capture cross-section and the resonance capture integral of 124Xe. J. Inorg. Nucl. Chem. 26, 9–14. doi:10.1016/0022-1902(64)80225-6

Busemann, H., Baur, H., Wieler, R., 2000. Primordial noble gases in "phase Q" in carbonaceous and ordinary chondrites studied by closed-system stepped etching. Meteorit Planet Sci 35, 949–973.

Hashizume, K., Marty, B., 2004. Nitrogen Isotopic Analyses at the Sub-Picomole Level Using an Ultralow Blank Laser Extraction Technique, in: Groot, P.A. de (Ed.), Handbook of Stable

Isotope Analytical Techniques, Handbook of Stable Isotope Analytical Techniques. Elsevier, Amsterdam, pp. 361–374.

Meshik, A., Hohenberg, C., Pravdivtseva, O., Burnett, D., 2014. Heavy noble gases in solar wind delivered by Genesis mission. Geochimica et Cosmochimica Acta 127, 326–347. doi:10.1016/j.gca.2013.11.030

Pepin, R.O., 1991. On the origin and early evolution of terrestrial planet atmospheres and meteoritic volatiles. Icarus 92, 2–79.

Porcelli, D., Ballentine, C.J., 2002. An overview of noble gas geochemistry and cosmochemistry. RiMG 47, 1–19. doi:10.2138/rmg.2002.47.1

Zimmermann, L., Burnard, P., Marty, B., Gaboriaud, F., 2009. Laser Ablation (193 nm), Purification and Determination of Very Low Concentrations of Solar Wind Nitrogen Implanted in Targets from the GENESIS Spacecraft. Geostandards and Geoanalytical Research 33, 183–194.

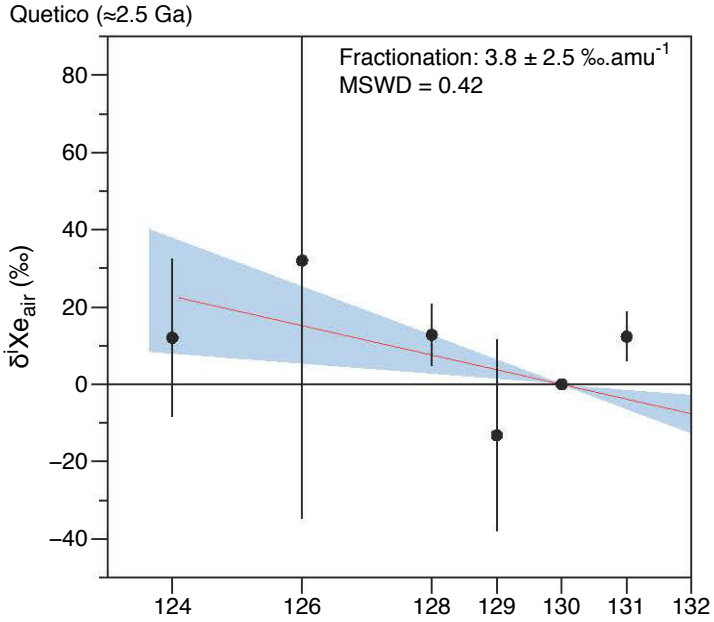

Figure S1: Isotopic spectrum of xenon released during crushing experiment on quartz samples from the Quetico Belt (error bars and range at 1σ). Isotopic ratios ($^{124\text{-}131}Xe/^{130}Xe$) are expressed with the delta notation and normalized to ^{130}Xe and to the isotopic composition of the modern atmosphere.

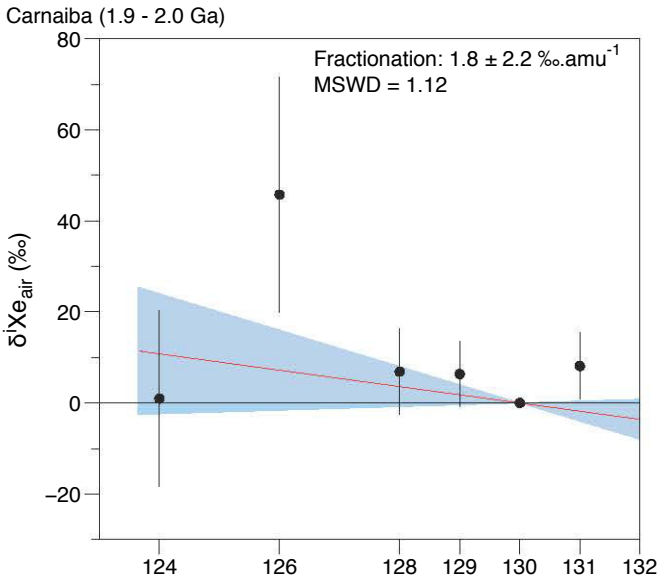

Figure S2: Isotopic spectrum of xenon released during crushing experiment on quartz samples from Carnaíba (error bars and range at 1σ). Isotopic ratios ($^{124\text{-}131}Xe/^{130}Xe$) are expressed with the delta notation and normalized to ^{130}Xe and to the isotopic composition of the modern atmosphere.

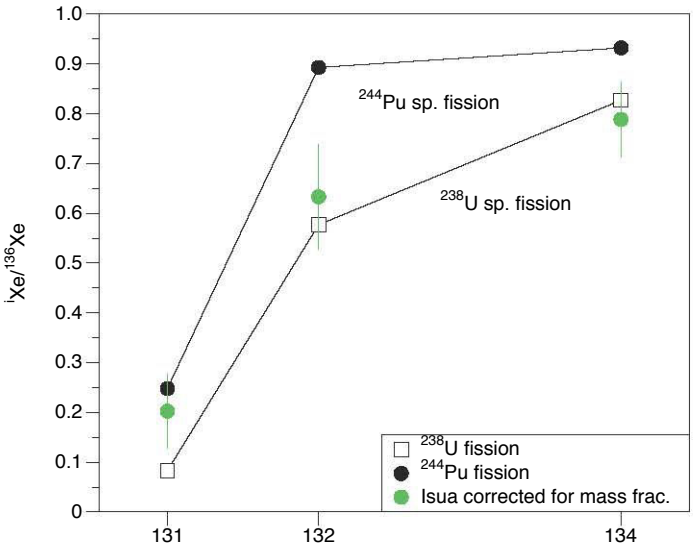

Figure S3: Fission spectrum for xenon in Isua samples once corrected for isotopic fractionation (Errors at 1σ). Except for some ^{131}Xe excess, the fission spectrum is compatible with the spontaneous fission of ^{238}U. Fission spectra for ^{238}U and ^{244}Pu are from Porcelli and Ballentine (2002).

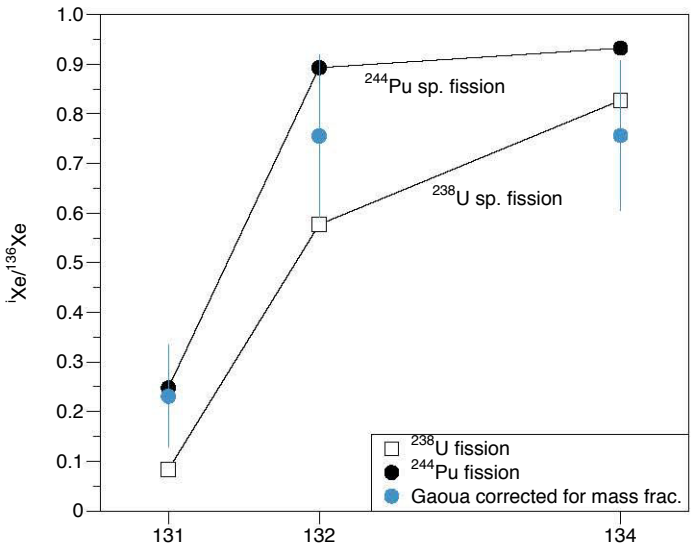

Figure S4: Fission spectrum for xenon in Gaoua samples once corrected for isotopic fractionation (errors at 1σ). Uncertainties are too large to decipher between spontaneous fission of ^{238}U or ^{244}Pu. Fission spectra are from Porcelli and Ballentine (2002).

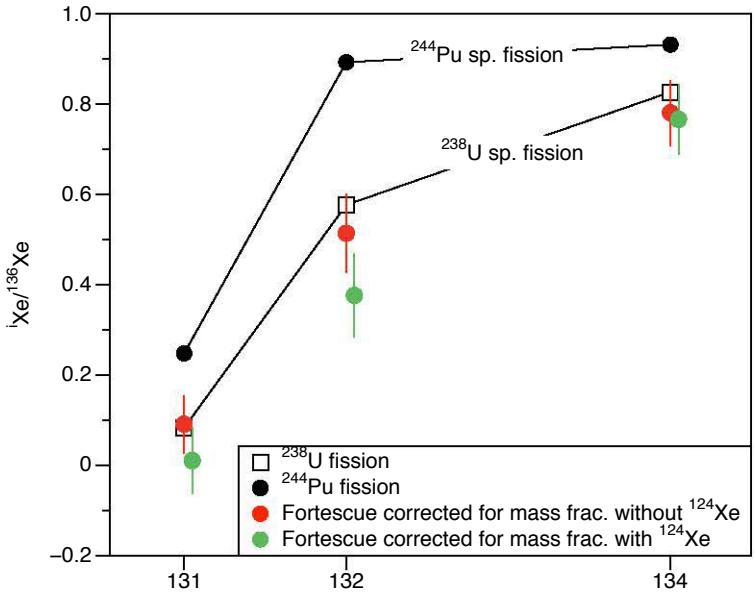

Figure S5: Fission spectra of Xe extracted from Fortescue Group samples once corrected for the mass-fractionation relative to U-Xe computed with ^{124}Xe (green dots) or without (red dots) ^{124}Xe. When ^{124}Xe is used to compute the isotopic fractionation, the fission spectrum does not correspond neither to spontaneous fission of ^{238}U nor to spontaneous fission of ^{244}Pu. Fission spectra are from Porcelli and Ballentine (2002). Errors at 1σ.

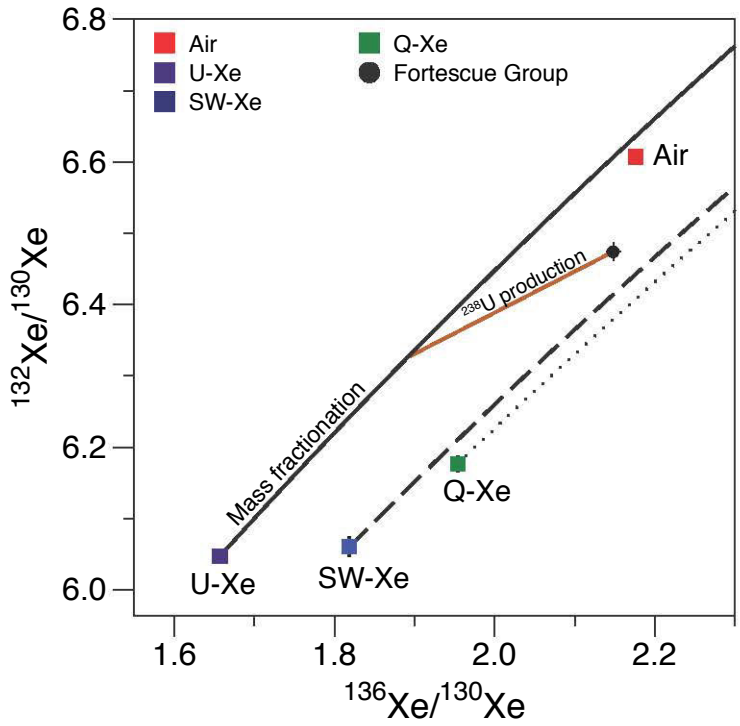

Figure S6: Three-isotope plot of Xe demonstrating that ancient atmospheric xenon trapped in Fortescue Group quartz samples can only be reproduced by mass-related isotopic fractionation (black plain line) of a starting isotopic composition similar to U-Xe (purple square) followed by the addition of xenon from the fission of ^{238}U (brown line). Mass-dependent isotope fractionation (dashed and dotted lines) of SW-Xe (Solar Xe, blue square) and of Q-Xe (chondritic Xe, green square) cannot lead to the isotopic compositions of Fortescue Group or of the modern atmosphere. Error bars at 1σ.

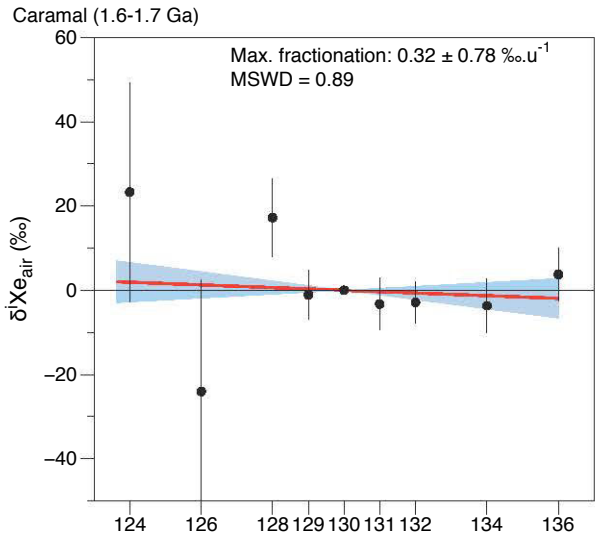

Figure S7: Isotopic spectrum of xenon released during crushing experiment on quartz samples from Caramal (error bars and range at 1σ). Isotopic ratios ($^{124\text{-}136}$Xe/^{130}Xe) are expressed with the delta notation and normalized to ^{130}Xe and to the isotopic composition of the modern atmosphere (δXe_{air}=0 ‰).

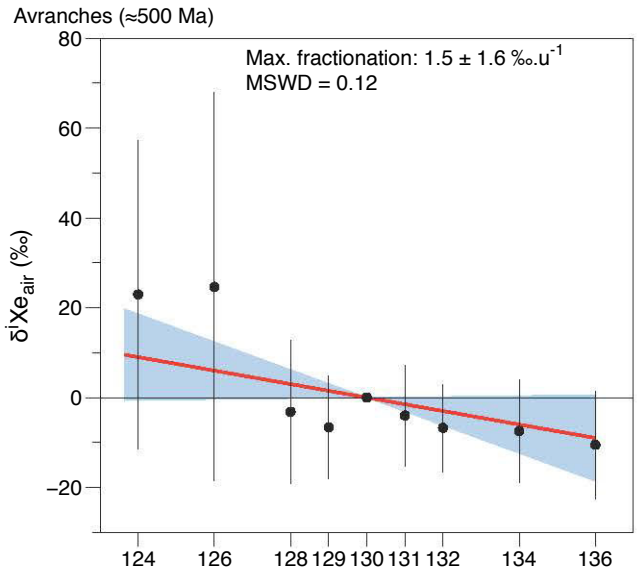

Figure S8: Isotopic spectrum of xenon released during crushing experiment on the quartz sample from Avranches (error bars and range at 1σ). Isotopic ratios ($^{124\text{-}136}Xe/^{130}Xe$) are expressed with the delta notation and normalized to ^{130}Xe and to the isotopic composition of the modern atmosphere (δXe_{air}=0 ‰).

Table S1: Abundances and isotopic ratios of Xe released during crushing experiments on samples (Table 1) analyzed during this study. The mean isotopic ratios for Barberton Xe (*from previous paper in Chapter 3*) are indicated in the first line. Mean values for the isotopic ratios are in **bold** together with their respective Mean Standard Weighted Deviation values. Isotopic ratios for the atmosphere and cosmochemical components are from Basford et al. (1973); Busemann et al. (2000); Meshik et al. (2014) and Pepin (1991). Errors at 2σ.

Samples	^{130}Xe ($x10^{-17}$ mol.g^{-1})	±	^{124}Xe		^{126}Xe		^{128}Xe		^{129}Xe		^{131}Xe		^{132}Xe		^{134}Xe		^{136}Xe	
			^{130}Xe = 1															
Barberton			**0.0245**	**0.0002**	**0.0228**	**0.0002**	**0.4847**	**0.0020**	**6.537**	**0.017**	**5.135**	**0.013**	**6.448**	**0.014**	**2.476**	**0.007**	**2.081**	**0.006**
Fortescue Gp (Australia) [1]																		
Pi03-17 A	1.72	0.07	0.0250	0.0020	0.0225	0.0017	0.4736	0.0202	6.49	0.18	5.19	0.14	6.52	0.16	2.56	0.08	2.18	0.07
Pi03-17 B	2.05	0.05	0.0240	0.0012	0.0225	0.0010	0.4789	0.0092	6.45	0.09	5.10	0.07	6.45	0.08	2.52	0.03	2.16	0.03
Pi03-44 A	18.27	0.17	0.0244	0.0006	0.0230	0.0004	0.4854	0.0048	6.58	0.05	5.14	0.03	6.48	0.04	2.52	0.02	2.15	0.01
Pi03-44 B	12.45	0.13	0.0242	0.0006	0.0228	0.0007	0.4867	0.0052	6.57	0.05	5.17	0.04	6.50	0.05	2.54	0.02	2.15	0.02
Pi03-17 C	2.69	0.03	0.0238	0.0008	0.0219	0.0008	0.4880	0.0069	6.55	0.06	5.17	0.05	6.49	0.05	2.56	0.02	2.18	0.02
Pi03-44 C	6.11	0.14	0.0246	0.0015	0.0228	0.0010	0.4830	0.0134	6.46	0.10	5.06	0.08	6.42	0.09	2.50	0.04	2.11	0.04
Pi03-44 C2	3.74	0.09	0.0244	0.0019	0.0223	0.0011	0.4793	0.0155	6.46	0.11	5.08	0.09	6.38	0.10	2.47	0.05	2.12	0.04
Pi03-44 C3	1.66	0.05	0.0224	0.0021	0.0203	0.0014	0.4789	0.0199	6.40	0.17	5.05	0.13	6.34	0.14	2.45	0.07	2.06	0.06
Pi03-44 D	9.07	0.12	0.0242	0.0005	0.0228	0.0005	0.4827	0.0060	6.55	0.05	5.15	0.04	6.48	0.04	2.52	0.02	2.13	0.02
Average			**0.0242**	**0.0003**	**0.0227**	**0.0004**	**0.4846**	**0.0025**	**6.541**	**0.038**	**5.143**	**0.026**	**6.474**	**0.026**	**2.528**	**0.017**	**2.148**	**0.018**
MSWD*			0.64		2.3		0.71		1.9		1.7		1.4		2.7		3.5	
Isua (Greenland)																		
BM0406-DE	2.18	0.03	0.0242	0.0008	0.0225	0.0007	0.4790	0.0061	6.55	0.07	5.21	0.05	6.618	0.056	2.600	0.028	2.233	0.023
BM0406-A	1.28	0.03	0.0235	0.0018	0.0224	0.0015	0.4734	0.0135	6.55	0.12	5.21	0.10	6.557	0.103	2.621	0.049	2.256	0.041
BM0406-BC	1.59	0.04	0.0240	0.0016	0.0226	0.0015	0.4771	0.0102	6.53	0.08	5.19	0.08	6.566	0.076	2.609	0.039	2.243	0.033
Average			**0.02406**	**0.0007**	**0.02252**	**0.0006**	**0.4779**	**0.0048**	**6.543**	**0.047**	**5.205**	**0.037**	**6.593**	**0.041**	**2.606**	**0.02**	**2.24**	**0.017**
MSWD*			0.25		0.016		0.3		0.091		0.12		0.89		0.28		0.5	
Quetico Belt (Canada)																		
QTBM-01-A	0.30	0.01	0.0236	0.0020	0.0221	0.0015	0.4768	0.0178	6.57	0.20	5.27	0.16	7.04	0.16	3.16	0.09	2.89	0.09
QTBM-01-B	3.30	0.09	0.0235	0.0015	0.0217	0.0012	0.4723	0.0120	6.47	0.14	5.31	0.11	7.47	0.12	3.85	0.12	3.76	0.14
BGBBM2	1.69	0.05	0.0239	0.0016	0.0239	0.0014	0.4825	0.0113	6.31	0.12	5.26	0.09	6.90	0.10	3.19	0.07	2.95	0.07
Average			**0.0237**	**0.0009**	**0.0225**	**0.0029**	**0.4775**	**0.0073**	**6.41**	**0.32**	**5.28**	**0.06**	-	-	-	-	-	-
MSWD*			0.057		3		0.77		3.1		0.29							
Gaoua (West Africa)																		
DF087-B	1.09	0.03	0.0242	0.0021	0.0218	0.0016	0.4826	0.0155	6.62	0.13	5.24	0.11	6.72	0.12	2.64	0.05	2.26	0.05
DF087-A	1.11	0.03	0.0240	0.0021	0.0247	0.0024	0.4749	0.0136	6.51	0.13	5.23	0.11	6.65	0.12	2.59	0.06	2.23	0.05
DF087-C	0.53	0.01	0.0235	0.0018	0.0212	0.0016	0.4738	0.0139	6.52	0.13	5.25	0.11	6.66	0.12	2.67	0.06	2.31	0.05
DF086-A	0.48	0.02	0.0248	0.0025	0.0224	0.0025	0.4775	0.0169	6.53	0.17	5.27	0.14	6.68	0.15	2.64	0.07	2.26	0.06
DF088 A	0.50	0.02	0.0217	0.0022	0.0223	0.0021	0.4725	0.0202	6.51	0.16	5.20	0.14	6.57	0.14	2.57	0.07	2.20	0.06
DF087D	0.55	0.02	0.0225	0.0028	0.0227	0.0023	0.4884	0.0205	6.58	0.19	5.33	0.15	6.81	0.17	2.72	0.08	2.35	0.07
DF085-A	1.06	0.03	0.0235	0.0016	0.0212	0.0014	0.4772	0.0122	6.48	0.10	5.19	0.08	6.64	0.09	2.56	0.04	2.25	0.03
Average			**0.0235**	**0.0008**	**0.0220**	**0.0010**	**0.4775**	**0.0057**	**6.53**	**0.05**	**5.23**	**0.04**	**6.67**	**0.05**	**2.62**	**0.05**	**2.26**	**0.04**
MSWD*			0.81		1.4		0.37		0.6		0.57		0.95		3.4		2.6	
Carnaiba (Brasil)																		
G2Ga-A	0.60	0.01	0.0237	0.0011	0.0226	0.0014	0.4718	0.0107	6.57	0.11	5.26	0.09	6.92	0.10	2.97	0.05	2.67	0.05
G2Ga-B	1.33	0.07	0.0227	0.0016	0.0232	0.0018	0.4813	0.0161	6.46	0.17	5.23	0.14	6.84	0.17	2.92	0.08	2.64	0.07
Average			**0.02339**	**0.0009**	**0.0228**	**0.0011**	**0.4747**	**0.0087**	**6.537**	**0.092**	**5.255**	**0.074**	-	-	-	-	-	-
Caramal (Australia)																		
QAnt-1	2.63	0.06	0.02412	0.0016	0.02108	0.0014	0.47608	0.0109	6.48326	0.0915	5.1623	0.0795	6.5569	0.0812	2.54493	0.0398	2.18	0.0332
QAnt-2	1.58	0.04	0.02358	0.0019	0.02151	0.0019	0.48435	0.0135	6.50755	0.1156	5.24393	0.0979	6.6361	0.1052	2.56763	0.0504	2.19	0.0441
Average			**0.02391**	**0.0012**	**0.02128**	**0.0011**	**0.47958**	**0.0087**	**6.4888**	**0.0724**	**5.19565**	**0.0617**	**6.5876**	**0.0651**	**2.55336**	**0.0313**	**2.1845**	**0.0264**
Avranches (France)																		
GM-B	1.33	0.04	0.0239	0.0016	0.0223	0.0019	0.470	0.015	6.45	0.15	5.19	0.12	6.56	0.13	2.54	0.06	2.15	0.05
Rhynie (Scotland)																		
R115B-A	0.51	0.01	0.0253	0.0031	0.0231	0.0022	0.477	0.023	6.55	0.18	5.17	0.15	6.66	0.16	2.58	0.08	2.19	0.07
Modern quartz (0-35 Ma)																		
G35-A (Colombie)	2.10	0.04	0.0238	0.0010	0.0218	0.0009	0.4743	0.0086	6.52	0.08	5.22	0.07	6.60	0.07	2.55	0.03	2.20	0.03
LG3-A (Alpes, France)	0.84	0.06	0.0227	0.0026	0.0233	0.0025	0.4679	0.0469	6.45	0.61	5.17	0.49	6.85	0.47	3.09	0.28	2.92	0.26
K1-A (Rhine graben, France)	15.46	0.46	0.0233	0.0011	0.0220	0.0010	0.4687	0.0203	6.49	0.26	5.21	0.21	6.61	0.19	2.57	0.10	2.18	0.09
Average			**0.0235**	**0.0007**	**0.0220**	**0.0006**	**0.4733**	**0.0077**	**6.516**	**0.074**	**5.21**	**0.06**	-	-	-	-	-	-
Air[a]			0.0234	0.0001	0.0218	0.0002	0.4715	0.0014	6.496	0.019	5.213	0.017	6.607	0.010	2.563	0.009	2.176	0.006
Q-Xe[b]			0.0281	0.0003	0.0251	0.0002	0.5077	0.0031	6.436	0.034	5.056	0.022	6.177	0.023	2.335	0.016	1.954	0.014
SW-Xe[c]			0.0298	0.0009	0.0252	0.0011	0.5103	0.0044	6.306	0.033	5.004	0.028	6.061	0.029	2.237	0.014	1.819	0.011
U-Xe[d]			0.0293	0.0001	0.0253	0.0001	0.5083	0.0006	6.286	0.006	4.996	0.006	6.047	0.006	2.126	0.004	1.657	0.003

[1]Fortescue Gp samples are labeled Pi03-17 XY and Pi03-44 XY with X the 1-3 mm granulometric sub fraction and Y the crushing step.
[a]Basford et al. (1973)
[b]Busemann et al. (2000)
[c]Meshik et al. (2014)
[d]Pepin (1991)
*MSWD (for Mean Standard Weighted Deviation)

Table S2: Isotopic composition of krypton (normalized to ^{84}Kr) released during crushing experiments on quartz samples from the Barberton greenstone belt. Locations of samples in the BARB3 core are indicated. Errors at 2σ.

Samples	**Location (m)**	^{80}Kr	±	^{82}Kr	±	^{83}Kr	±	^{86}Kr	±
						$^{84}Kr=1$			
BMGA3-13-G	555	0.0396	0.0004	0.2021	0.0018	0.2013	0.0016	0.3074	0.0017
BMGA3-13 B	555			0.2031	0.0015	0.2021	0.0013	0.3056	0.0025
BMGA3-13 C	-			0.2020	0.0017	0.2019	0.0016	0.3020	0.0027
BMGA3-13 D	-			0.2031	0.0015	0.2021	0.0013	0.3056	0.0025
BMGA3-13 E	-			0.2022	0.0009	0.2012	0.0007	0.3059	0.0028
BMGA3-4 A	715			0.1992	0.0021	0.1979	0.0024	0.3015	0.0041
BMGA3-4 B	-			0.2019	0.0020	0.2018	0.0015	0.3042	0.0024
BMGA3-4 B2	-			0.2021	0.0091	0.1995	0.0083	0.3034	0.0132
BMGA3-4 C	-			0.2023	0.0078	0.2016	0.0016	0.3042	0.0035
BMGA3-5 A	784			0.2017	0.0025	0.2015	0.0025	0.3028	0.0032
BMGA3-5 B	-			0.2012	0.0063	0.2015	0.0055	0.3058	0.0105
BMGA3-5 C	-			0.2024	0.0018	0.2021	0.0013	0.3044	0.0030
Average				**0.20217**	**0.0005**	**0.20151**	**0.00042**	**0.30499**	**0.00082**
MSWD*				1.05		1.2		1.7	

[1]Barberton samples are labeled BMGA3-XX-YZ with XX the core samples,
Y the 1-3 mm granulometric sub fraction and Z the crushing step.
*MSWD (for Mean Standard Weighted Deviation)

3.3.1 Additional Comments and Research Perspectives

The article presented above demonstrates the need for a long-term mechanism of Xe escape operating at least until 2.1 Ga and the end of the discussion is focused on the possibility for xenon to escape under an ionized form together with hydrogen ions (Zahnle, 2015). This section is focused on the evaluation of parameters that probably control this escape mechanism.

Parameters controlling Xe escape

The escape mechanism proposed in the discussion of the third paper (section 3.3) in chapter 3 (Results and Implications) is schematically represented in Fig. 3.1 adapted from Zahnle (2015). In this model, Xe ions are dragged by hydrogen ions in the upper atmosphere and can escape along open magnetic field lines. Even if numerical simulations are necessary to evaluate if this is a viable mechanism to escape Xe, some of the key parameters controlling this escape can be listed:

- solar EUV flux at the top of Earth's atmosphere ;
- presence and intensity of a the magnetosphere ;
- ability of Xe to be and stay ionized ;

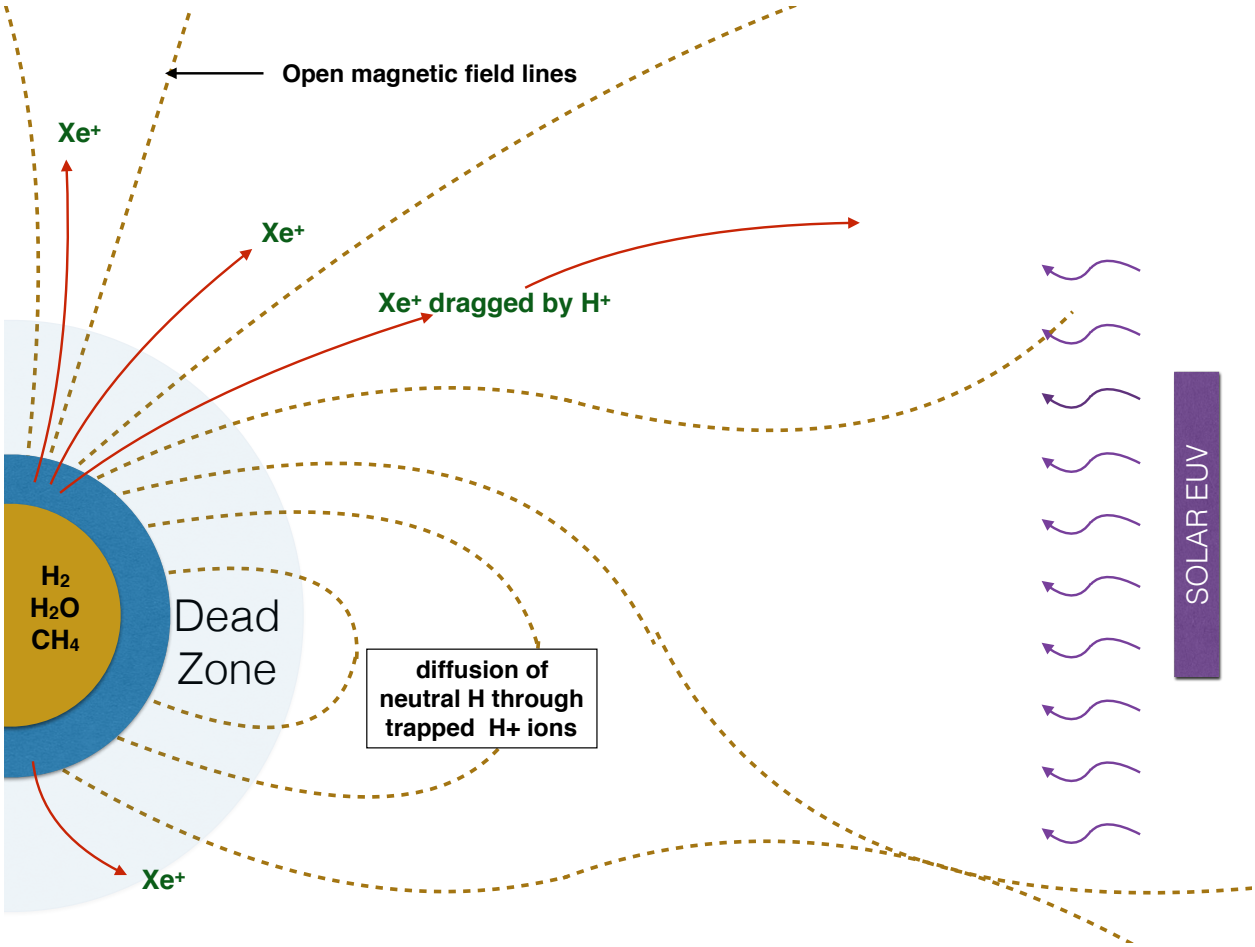

Fig. 3.1: Schematic view of the H-Xe escape process. Brown dashed lines represent magnetic field lines from the terrestrial magnetosphere. The H-bearing species in the atmosphere may be H_2, H_2O or CH_4. In the dead zone, only H ions/neutrals can escape by diffusion and successive recombinations. Open magnetic field lines at the Earth's magnetic poles provide pathways for escape of Xe^+ ions. Adapted from Zahnle (2015).

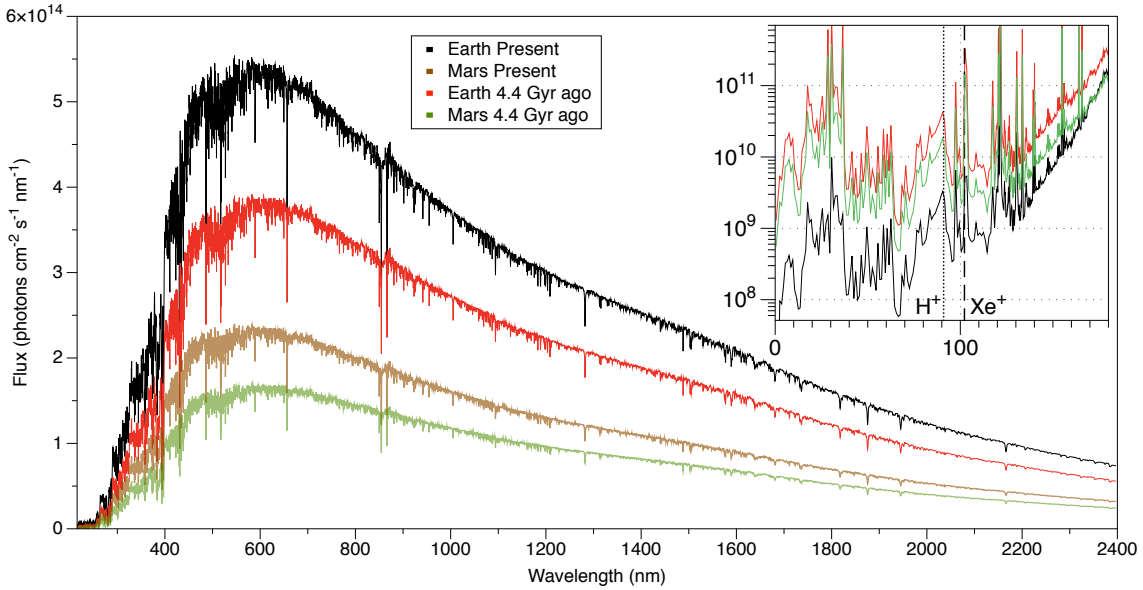

Fig. 3.2: Solar irradiance spectra (0 to 2400 nm) for the modern and 4.4 Gyr-old Earth and Mars. The subpanel depicts the irradiance spectra between 0 and 200 nm with the dashed and dotted lines representing the wavelength for ionization of Xe (102.23 nm) and H (91 nm), respectively. Data are from Claire et al. (2012).

Informations on these parameters over Earth's geological history are listed in the next paragraphs.

Solar irradiance

The evolution of solar irradiance with time is of primordial importance here since this parameter controls the nature and extent of the terrestrial ionosphere. Solar irradiance may thus have a severe impact on ionization rate of Xe and on its escape from the atmosphere. The young Sun is often described as a weaker source of luminosity (Ulrich, 1975). This is true but only for wavelengths higher than ca. 200 nm corresponding to near-UV, visible and infra-red bands. This progressive increase in the luminosity with time for high wavelengths is due to the nuclear reaction of hydrogen burning which is producing helium in our star. This nuclear process is releasing large amounts of heat favoring the H burning activity that, in turns, produces more heat etc. Far/Extreme UV (FUV/EUV) bands intensities depend on different factors. Their emission is controlled by the magnetic activity of the star. The intensity of the solar magnetosphere directly depends on its rotational speed that is decreasing with time in order to keep the same angular momentum despite the energy released by the emission of solar winds (Claire et al., 2012). The emission of EUV radiations is thus decreasing since Sun's formation.

Observations of luminosities of stars considered as solar analogs of different ages permitted to follow the evolution fo the irradiance spectrum with time. Ribas et al. (2005) confirmed that EUV flux were higher in the past than today by several orders of magnitudes. Claire et al. (2012) modeled a full irradiance spectrum of the Sun with time based on observational data and on statistical analyses. Figure 3.2 represents the full spectrum of solar irradiance at the top of the terrestrial atmosphere. The subpanel (note the log scale) represents the solar irradiance spectrum between 0 and 200 nm i.e. in the EUV region with the dashed line indicating the wavelength at which Xe is ionized (λ = 102.23 nm). The EUV solar flux, impacting Earth's upper atmosphere, was 2 orders of magnitude higher 4.4 Ga ago compared to the present flux. It must be noticed here that, for all times considered, the flux impacting the martian atmosphere (F_{Mars}) is linked to the solar flux impacting the Earth (F_{Earth}) by the relation $F_{Mars} = F_{Earth}/1.5^2$ where 1.5 is the distance (in astronomical units) of Mars from the Sun. This means that, 4.4 Ga ago, the EUV flux received by Mars was also two orders of magnitude higher than the present one.

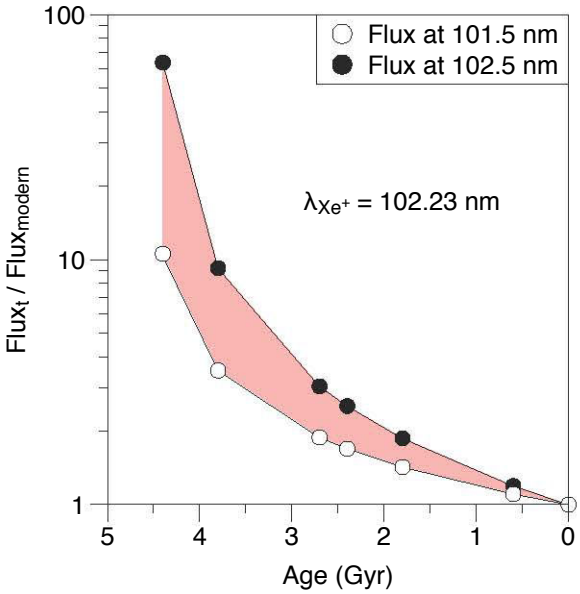

Fig. 3.3: Evolution of the solar flux with time for two wavelengths (λ = 101.5 nm and 102.5 nm). The enhancement of the solar flux in the past highly depends on the considered wavelength. See emission peaks in Figure 3.2. Data are from Claire et al. (2012).

About xenon, its energy of ionisation of 12.15 eV corresponds to a wavelength of 102.23 nm. Claire et al. (2012) provided estimations of the solar irradiance spectrum in the past with a resolution of 1 nm. Figure 3.3 depicts the enhancement of the solar flux with time compared to the present solar flux. For example for a range of λ between 101.5 and 102.5 nm, the solar flux at the top of Earth's atmosphere 3.2 Ga ago was 2.5 to 5 times higher than the present flux. At 4.4 Ga the EUV flux was 10 to 63 times higher.

These observations suggest that the EUV flux at the top of the atmosphere was indeed very high during the Archean eon. Such a high flux promoted an extension of the atmosphere together with its heating and probably favored ionization of H and Xe and their efficient escapes (Zahnle et al., 1988).

Magnetic field on the early Earth

The intensity of the terrestrial magnetic field plays a major role in the potential escape of Xe^+ ions because escape would have been restricted to the polar regions where magnetic field open lines are present. Recently, Tarduno et al. (2014) provided a comprehensive review of the intensity of the paleo-magnetic field for the early Earth (Fig. 3.4). Even if data are scarce, a magnetic field seems to have been present as early as 3.5 Ga ago even if the magnetosphere was probably generated uniquely by intense mantle convection rather than core-induced dynamo since the solid-core nucleation probably occurred later (Tarduno et al., 2014). Biggin et al. (2015) analyzed a wide set of paleo-magnetic data and concluded that there was a decrease in magnetic field strength until 1.3-2.4 Ga ago due to progressive decrease of the originally vigorous convection. This observation is in favor of an intense atmospheric escape of ions before 2.4 Ga. About 1.3 Ga ago, the magnetic field strength increased, possibly due to inner-core nucleation and the beginning of very efficient decoupled convection alimenting the geodynamo.

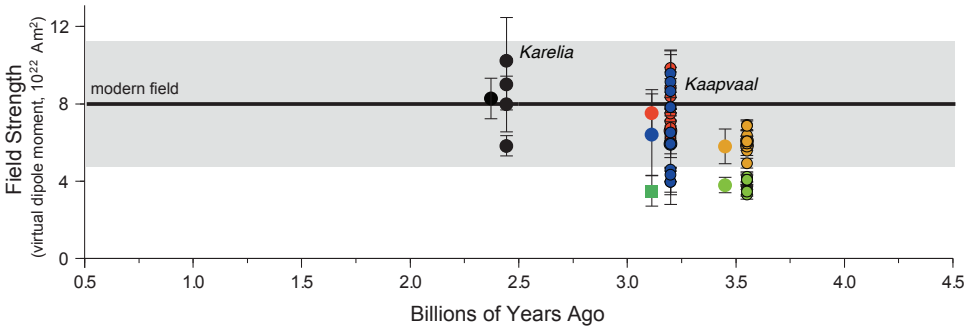

Fig. 3.4: Evolution of the magnetic field strength with time. Data obtained on single crystals suggest the presence of a magnetic field similar to the modern one 3.2 Ga ago. The grey range represents modern variations of the magnetic field strength ($\simeq$5 to 11 $\times$ 10^{22} Amp.m^2, Muscheler et al. (2005)). Modified after Tarduno et al. (2014) and see references therein.

Ionization of Xe in the Earth's atmosphere

An enhanced EUV flux in the past is not sufficient to guarantee efficient ionization of Xe in the Earth's atmosphere. Indeed, xenon had to be ionized but more importantly it had to *stay* ionized despite radiative recombination and interactions with other possible ions or neutrals (dissociative recombination). Zahnle (2015) notes that, contrary to Kr, Xe^+ do not interact with H_2. This means that Xe would not be too much concerned by the following dissociative recombination process:

$$Xe^+ + H_2 \rightarrow HXe^+ + H$$
$$HXe^+ + e^- \rightarrow H + Xe$$

Most of the loss of Xe^+ would thus be due to the radiative recombination presented as a slow process by Zahnle (2015):

$$Xe^+ + e^- \rightarrow Xe + h\nu$$

All parameters governing Xe escape seem to have been in favor of a vigorous Xe ionization and escape in the past. However, a thorough numerical model is required here to quantitatively estimate if ionization of Xe in the Archean atmosphere and its escape through interactions with escaping hydrogen is a viable mechanism for long-term escape.

3.4 Article The iodine-plutonium-xenon age of the Moon-Earth system revisited, *published in 2014 in Phil. Trans. Roy. Soc. A, Vol. 372, p.2024*

PHILOSOPHICAL TRANSACTIONS OF THE ROYAL SOCIETY A

rsta.royalsocietypublishing.org

Research

Cite this article: Avice G, Marty B. 2014 The iodine–plutonium–xenon age of the Moon–Earth system revisited. *Phil. Trans. R. Soc. A* **372**: 20130260.
http://dx.doi.org/10.1098/rsta.2013.0260

One contribution of 18 to a Discussion Meeting Issue 'Origin of the Moon'.

Subject Areas:
Solar System, geochemistry

Keywords:
Moon, xenon, age, atmosphere

Author for correspondence:
G. Avice
e-mail: gavice@crpg.cnrs-nancy.fr

Royal Society Publishing

The iodine–plutonium–xenon age of the Moon–Earth system revisited

G. Avice and B. Marty

CRPG-CNRS, Université de Lorraine, 15 rue Notre-Dame des Pauvres, BP 20, 54501 Vandoeuvre-lès-Nancy Cedex, France

Iodine–plutonium–xenon isotope systematics have been used to re-evaluate time constraints on the early evolution of the Earth–atmosphere system and, by inference, on the Moon-forming event. Two extinct radionuclides (^{129}I, $T_{1/2} = 15.6$ Ma and ^{244}Pu, $T_{1/2} = 80$ Ma) have produced radiogenic ^{129}Xe and fissiogenic $^{131-136}$Xe, respectively, within the Earth, the related isotope fingerprints of which are seen in the compositions of mantle and atmospheric Xe. Recent studies of Archaean rocks suggest that xenon atoms have been lost from the Earth's atmosphere and isotopically fractionated during long periods of geological time, until at least the end of the Archaean eon. Here, we build a model that takes into account these results. Correction for Xe loss permits the computation of new closure ages for the Earth's atmosphere that are in agreement with those computed for mantle Xe. The corrected Xe formation interval for the Earth–atmosphere system is 40^{+20}_{-10} Ma after the beginning of Solar System formation. This time interval may represent a lower limit for the age of the Moon-forming impact.

1. Introduction

The age of the Solar System is well established at 4.568 Ga [1–3]. Extant and extinct radioactive series indicate that not only primitive bodies but also differentiated planetesimals and planetary embryos, including Mars, formed within a few million years after the beginning of condensation in the Solar System (inferred from the age of calcium–aluminium-rich inclusions, CAIs, in primitive meteorites). By contrast, the formation age of the Earth–Moon system is uncertain and is presently debated within a time interval of 30–200 Ma after CAI (this issue). Deciphering the details of the early chronology of

the Earth requires the development of adequate extinct radioactivity chronometers. Because the Earth's interior has been well mixed by mantle convection over 4.5 Ga, most of the early reservoirs have been rehomogenized, even if some remnants of past heterogeneities might still be present [4–7]. However, information on ancient reservoirs is still held at the Earth's surface, in old terranes, and, in the case of noble gases, in the terrestrial atmosphere.

Xenon, the heaviest noble gas, has a large number (nine) of isotopes, and extant and extinct radioactivity products have contributed several of them. Iodine-129 decays with a half-life of 15.7 Ma into ^{129}Xe [8], resulting in ^{129}Xe excesses in primitive meteorites relative to the potential primordial Xe isotopic compositions [9]. Atmospheric Xe presents a monoisotopic excess of ^{129}Xe (compared with adjacent ^{128}Xe and ^{130}Xe isotopes) of about 7% [10] attributed to the decay of extinct ^{129}I. Some natural gases and mantle-derived rocks [11–13] have ^{129}Xe/^{130}Xe ratios (where ^{130}Xe is a stable isotope of xenon that is used for normalization) higher than the atmospheric value. Altogether, these observations demonstrate that the Earth formed and differentiated while ^{129}I was still present, thus within a few tens of millions of years. Most (more than 80% of) terrestrial Xe is now in the atmosphere ([11] but see [14] for an alternative view), so that atmospheric Xe is to first order representative of total terrestrial Xe. Consequently, a ^{129}I–^{129}Xe age of the Earth can be constrained from estimates of the initial abundance of iodine, inferred from the present-day abundance of the stable isotope ^{127}I [15]. Although the latter is not well known (probably no better than a factor of 2, see below), the exponential nature of radioactive decay makes the result less sensitive to this uncertainty. Thus, the I–Xe age of the Earth's atmosphere, which is in fact the time interval Δt_{129} of reservoir closure, can be expressed as

$$\Delta t_{129} = \frac{1}{\lambda_{129}} \ln\left(\frac{^{129}\mathrm{I}_{\mathrm{INI}}}{^{129}\mathrm{Xe(I)}}\right), \tag{1.1}$$

where λ_{129} is the decay constant of ^{129}I (4.41×10^{-2} Ma^{-1}), and $^{129}\mathrm{I}_{\mathrm{INI}}$ is the initial ^{129}I abundance in the reservoir. The latter is computed from the $(^{129}\mathrm{I}/^{127}\mathrm{I})_{\mathrm{INI}}$ initial ratio from meteorite data (1.1×10^{-4}) [16] and estimates of terrestrial ^{127}I abundance (greater than 3 ppb, up to 13 ppb, see §2). ^{129}Xe(I) represents the ^{129}Xe excess resulting from the decay of ^{129}I in the atmosphere (2.8×10^{11} mol of ^{129}Xe(I) [10]). Within these assumptions, the Earth would have become closed for Xe isotope loss at 100–120 Ma after CAI, this range depending mostly on the initial abundance of iodine (for further discussion of these parameters, see reviews [10,15,17–19]). This is the classical 'age' of the atmosphere found in textbooks.

The other short-lived nuclide of interest here is ^{244}Pu (half-life of 80 Ma [20]) which, in addition to α-decay, presents a weak (0.125%) branch for spontaneous fission and produces ^{131,132,134,136}Xe isotopes (represented hereafter by ^{136}Xe(Pu)). These heavy Xe isotopes are also produced in the Earth by the spontaneous fission of extant ^{238}U. However, the contribution of ^{238}U fission to Xe isotopes was minor compared with that of ^{244}Pu during the periods of time characterizing the Earth's formation and its early evolution. Contrary to iodine, plutonium has no stable isotope, so that the initial abundance of ^{244}Pu is inferred from comparison with U in meteorites and the Earth [21], because both are refractory and lithophile elements. Fissiogenic Xe from ^{244}Pu has been found in the Earth's interior [4,12,22]. The detection of fissiogenic Xe in the atmosphere is, however, not straightforward, as the original composition of atmospheric xenon is not directly measurable. In fact, atmospheric xenon is isotopically fractionated by 3–4% per atomic mass unit relative to potential primordial candidates [23]. Furthermore, even after correction for such mass-dependent isotope fractionation, neither chondritic nor solar Xe can be directly related to atmospheric Xe, because both chondritic and solar Xe are rich in the heavy Xe isotopes (^{134}Xe and ^{136}Xe) compared with 'unfractionated' atmospheric Xe [24]. Takaoka [25] and Pepin & Phinney [26] extrapolated, from meteorite data, a primordial Xe component (labelled Xe–U by Pepin & Phinney [26]), from which atmospheric Xe could be derived by mass-dependent isotopic fractionation. Xe–U has an isotope composition close to solar Xe for its light masses but is depleted in ^{134}Xe and ^{136}Xe. This U–Xe component has still not been found in meteorites, possibly because of the presence of superimposed components of nucleosynthetic origin. Indeed, xenon

trapped in different meteoritic phases presents variations in its s-, p- and r-process isotopes (e.g. the P3, P6 and HL components trapped in nanodiamonds [27,28]). Thus, the heavy Xe isotope difference between potential Xe ancestors and solar Xe could be the result of different mixes of nucleosynthetic Xe isotopes in primitive reservoirs, with the possibility that solar Xe was contributed more by s-process isotopes than by other Xe primordial progenitors [29]. Whatever the composition of the progenitor of atmospheric Xe, this reservoir appears poor in ^{244}Pu-derived Xe isotopes.

Estimates of ^{136}Xe excess in the atmosphere due to the contribution of extinct ^{244}Pu vary between 4.6% and 2.8%, according to Pepin & Phinney [26] and Igarashi [30], respectively. ^{136}Xe(Pu) gives another possibility to estimate closure ages for the Earth–atmosphere system. Both the I–Xe and Pu–Xe systems can be combined, yielding an I–Pu–Xe time interval $\Delta t_{129\text{–}244}$ of

$$\Delta t_{129\text{–}244} = \frac{1}{\lambda_{244} - \lambda_{129}} \ln \left[\frac{^{129}\mathrm{Xe(I)}/^{136}\mathrm{Xe(Pu)}}{(^{129}\mathrm{I}/^{244}\mathrm{Pu})_{\mathrm{INI}}} {}^{136}Y_{244} \right], \tag{1.2}$$

where λ_{244} is the decay constant of ^{244}Pu (8.45×10^{-3} Ma^{-1}), and $^{136}Y_{244}$ is the production yield of ^{136}Xe from ^{244}Pu fission (7×10^{-5}) [31]. The ^{129}Xe(I)/^{136}Xe(Pu) ratio of the atmosphere has been estimated to be 4.6 [32], which yields an atmospheric $\Delta t_{129\text{–}244}$ closure time of about 100 Ma after CAI, consistent with the I–Xe age. The fact that these two closure ages are comparable is not merely a coincidence, because $\Delta t_{129\text{–}244}$ depends in large part on the residual amount of ^{129}Xe(I) in the Earth's atmosphere (of the order of 1%) rather than on that of ^{136}Xe(Pu) in this time interval, given the much shorter half-life of ^{129}I compared with that of ^{244}Pu. A more interesting constraint arises from a direct comparison of the amount of ^{136}Xe(Pu) left in the Earth (atmosphere) with that potentially produced by initial ^{244}Pu. Although the latter also has a significant uncertainty, it appears that a large fraction of ^{136}Xe(Pu) (greater than or equal to 70%) is missing in the present-day Earth's atmosphere [17,32–34]. Given the half-life of ^{244}Pu of 80 Ma, this discrepancy suggests that Xe was lost from the atmosphere after the giant impact phase of the Earth's accretion [17,33].

Atmospheric xenon not only is isotopically fractionated (enriched in heavy isotopes by 3–4% per atomic mass unit) compared with potential primordial Xe, but also is elementally depleted by one order of magnitude relative to other noble gases (e.g. Kr) compared with the abundance pattern of meteoritic noble gases. These dual characteristics, known for a long time as the 'xenon paradox' (elementally depleted in heavy elements, isotopically enriched in heavy isotopes), have not yet found a satisfactory explanation. The Xe depletion and the lack of Pu-produced Xe isotopes in the atmosphere suggest that, after a last giant impact event, there might have been more xenon in the atmosphere, which would have been lost through a process that fractionated Xe isotopes (if both features were related). Therefore, the I–Pu–Xe ages should be corrected for Xe loss, and the scope of the correction would depend on the timing of loss relative to I and Pu decays. The apparent deficiency of ^{136}Xe(Pu) in the atmosphere (see previous paragraph) may indeed be a consequence of prolonged selective loss of atmospheric Xe.

Recent studies of noble gases in Archaean (3.5–3.0 Ga old) rocks may provide a solution to the xenon paradox. Isotopically fractionated Xe has been found in Archaean barite [35,36] and hydrothermal quartz [37,38]. The Xe isotopic spectrum is intermediate between the primordial and the modern atmospheric Xe isotope patterns, and the isotopic fractionation (relative to the modern composition) tends to decrease with decreasing age (figure 1). Together with Xe data from ancient basement fluids of presumed Proterozoic age [40], the evolution of Xe isotopic fractionation with time is consistent with a Rayleigh distillation in which Xe has been lost from the atmosphere with an instantaneous fractionation factor of about 1.1% per atomic mass unit [38]. The magnitude of the latter is in agreement with experimental studies of Xe isotope fractionation upon ionization [41]. The exponential decrease of Xe isotope fractionation with time is qualitatively consistent with that of the far-UV light (FUV) flux from the evolving Sun with time ([39]; figure 1), suggesting that Xe was selectively ionized and lost from the atmosphere to space through time [42,43] at a rate that followed the declining FUV flux.

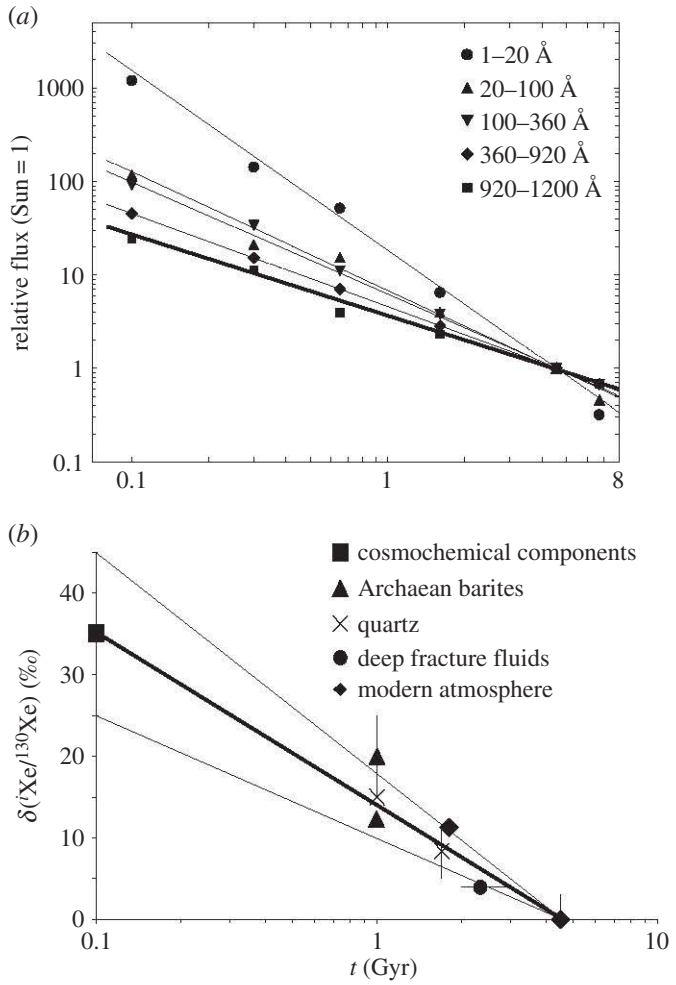

Figure 1. Relationship between the evolution of the solar EUV flux with time and the progressive isotopic fractionation of atmospheric xenon. (*a*) Evolution of the solar flux with time. Figure and data are from [39]. The wavelength of ionization of Xe atoms corresponds to the range 920–1200 Å. (*b*) Progressive isotopic fractionation of atmospheric Xe from cosmochemical components [10] to modern atmosphere [31]. Ancient rocks record intermediate isotopic compositions: 3.5 Ga-old barites [35,36]; quartz samples [37,38]; Proterozoic deep fracture fluids [40].

In this study, we investigate the possibility to reproduce the current features of atmospheric Xe (elemental and isotopic compositions), taking into account this long-term escape. We develop a three-box model (solid Earth, atmosphere, space) that allows us to correct the abundances of radiogenic/fissiogenic Xe isotopes for Xe loss. Previous computed ages are therefore not valid any more and their values and meaning have to be revisited. Doing so, we follow Podosek & Ozima [17], who predicted that 'if allowance is made for the possibility that most of the Xe, including radiogenic Xe, that should be in the atmosphere, has somehow be removed or hidden, the I–Xe and Pu–Xe formation interval could be reduced to perhaps 60 Ma'. We now have observational evidence for such Xe loss through geological time. Because the atmosphere is probably very sensitive to impact-driven erosion [44,45], corrected closure ages may be related to the end of the giant impact epoch that led to the formation of the Moon [46].

2. Building of the model

The model consists of three reservoirs: the silicate Earth, the atmosphere and outer space (figure 2). We aim to estimate the closure time of the atmosphere Δt, defined here as the time after CAI when the atmosphere became closed to volatile loss (except for Xe preferentially lost during the Hadean and Archaean eons). Between time 0 (CAI) and Δt, volatile elements

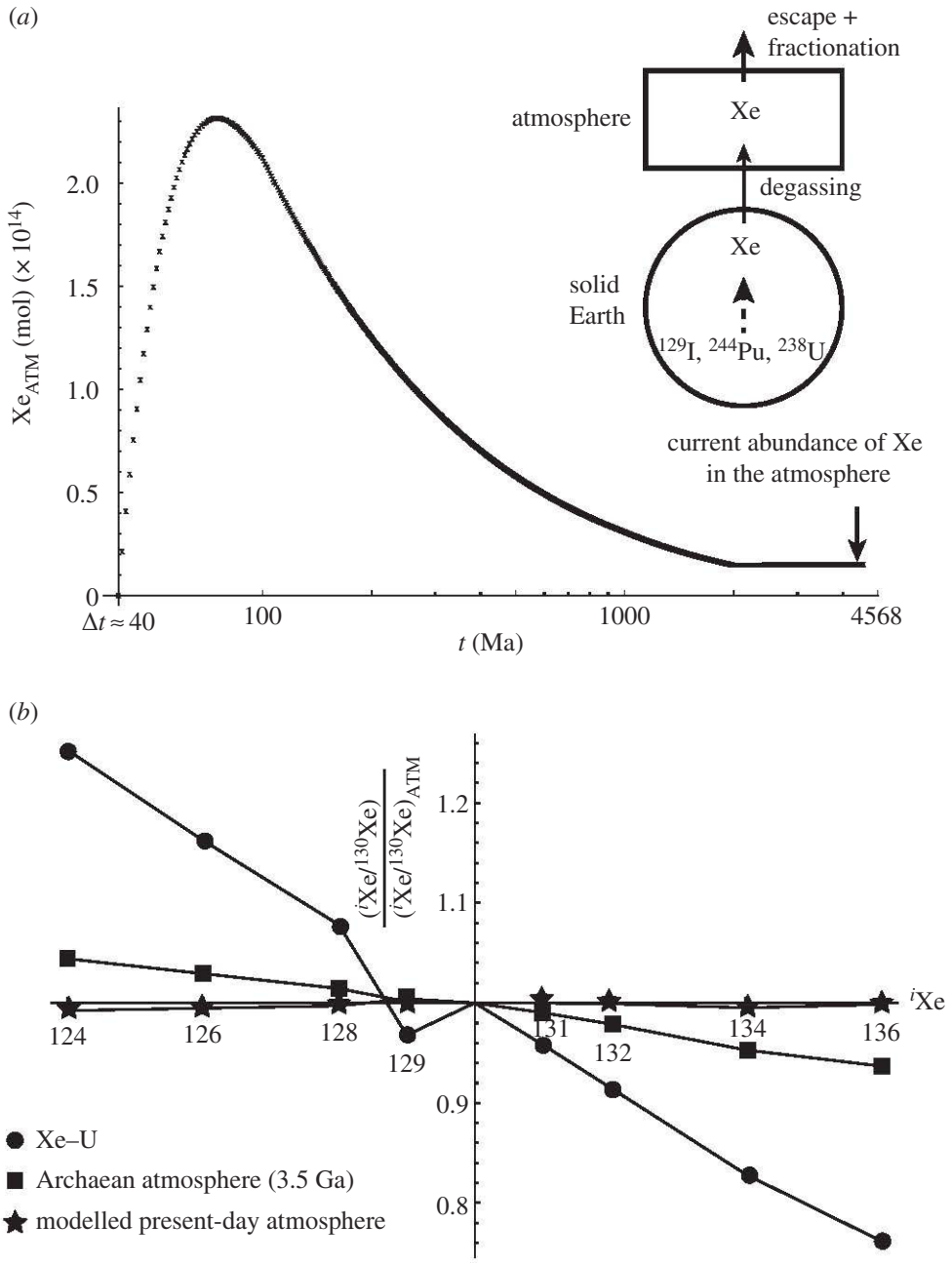

Figure 2. (*a*) Schematic explanation of the model and evolution of the budget of atmospheric Xe over time. The model is built with three boxes: solid Earth, atmosphere and space. Some Xe isotopes are produced by radioactive decay of ^{129}I, ^{244}Pu and ^{238}U (see text). After a time interval Δt (40 Ma, one outcome of the model), the Earth begins to retain its volatile elements and accumulates xenon degassed from the solid Earth to the atmosphere without isotopic fractionation. Xenon atoms escape from the atmosphere to outer space with isotopic fractionation. The evolution of the budget of atmospheric xenon shows the progressive escape of Xe atoms with time. The escape lasts until the end of the Archaean eon ($t = 2$ Ga). At this time, the abundance has almost reached the current abundance of xenon in the atmosphere. The process is completed by further degassing of the xenon atoms. (*b*) Isotopic spectrum of xenon relative to the current isotopic composition of the Earth's atmosphere using ^{130}Xe as a reference isotope. Xe–U is the starting isotopic composition (circles). The fractionated Archaean atmosphere (around 1% amu^{-1}) is shown with squares and the 'artificial' current isotopic composition of the reference solution is shown with stars. The current isotopic composition is reproduced within 0.7% or better.

are contributed to the proto-Earth by accreting bodies, and partially lost through collision and atmospheric erosion. Between Δt and present, only Xe is lost to space, the other volatile elements being conservative in the atmosphere. We correct for this secondary Xe loss using the depletion of xenon relative to other noble gases in the atmosphere.

Xenon is degassed without isotopic fractionation from the Earth's interior to the atmosphere through magmatism. Between Δt and the end of the Archaean eon, xenon escapes from the atmosphere to outer space, and is isotopically fractionated during this escape. Three radioactive series are involved: ^{129}Xe produced by the β-decay of ^{129}I ($T_{1/2} = 15.6$ Ma), and ^{131,132,134,136}Xe from the fission of ^{244}Pu ($T_{1/2} = 80$ Ma) and ^{238}U ($T_{1/2} = 4.47$ Ga). As ^{136}Xe, compared with other xenon isotopes (^{131,132,134}Xe), is a major product from the fission of ^{244}Pu, it will be considered as a proxy for the entire fission component in the following discussion.

The following mass balance exemplifies the evolution of the atmospheric $^{129}Xe_{ATM}$ (mol) with time:

$$\frac{d^{129}Xe_{ATM}(t)}{dt} = \varphi(t)^{129}Xe_{MANT}(t) - \beta(t)(1+\alpha_{esc})^{129}Xe_{ATM}(t). \tag{2.1}$$

Here $^{129}Xe_{ATM}(t)$ is the abundance of ^{129}Xe in the atmosphere at time t; $^{129}Xe_{MANT}(t)$ represents the abundance of ^{129}Xe atoms in the mantle at time t; $\varphi(t)$ and $\beta(t)$ are the degassing and escape parameters, respectively; and α_{esc} is the isotopic fractionation factor described below (equation (2.4)). The evolution of the mantle $^{129}Xe_{MANT}$ (mol) with time is expressed by

$$\frac{d^{129}Xe_{MANT}(t)}{dt} = -\varphi(t)^{129}Xe_{MANT}(t) + \lambda_{129}{}^{129}I(t), \tag{2.2}$$

where $\varphi(t)$ is the degassing parameter at time t, λ_{129} is the decay constant of ^{129}I into ^{129}Xe, and ^{129}I(t) is the abundance of iodine-129 in the mantle at time t. Similarly, equations for $^{124-136}$Xe are defined taking into account the decays of the different radioactive nuclides (^{244}Pu, ^{238}U). For example, for $^{136}Xe_{MANT}$, the equation is

$$\frac{d^{136}Xe_{MANT}(t)}{dt} = -\varphi(t)^{136}Xe_{MANT}(t) + \lambda_{244}B_{244}{}^{136}Y_{244}{}^{244}Pu(t) + \lambda_{238}B_{238}{}^{136}Y_{238}{}^{238}U(t), \tag{2.3}$$

where $^{136}Xe_{MANT}(t)$ is the abundance of ^{136}Xe in the mantle at time t, ^{244}Pu(t) and ^{238}U(t) are the abundances of parent nuclides in the mantle at time t, B_{244} (1.25×10^{-3}) and B_{238} (5.45×10^{-7}) are the branching ratios for ^{244}Pu and ^{238}U, respectively, and $^{136}Y_{244}$ (6.3%) and $^{136}Y_{238}$ (5.6%) are the yields of fission [31].

Equations are resolved with 1 Ma step using an original code written with the MATHEMATICA programming language. Results of the model comprise, for each temporal step, the amount of each stable isotope in each reservoir plus the amount of each radiogenic/fissiogenic isotope (e.g. ^{136}Xe in the atmosphere coming from the fission of ^{244}Pu).

(a) Degassing from the Earth's interior

The rate of Xe degassing ($\varphi(t)$ in equations (2.1)–(2.3)) from the Earth's interior through time can be anticipated from thermal and geochemical considerations. Having a constant degassing parameter $\varphi(t)$ through Earth's history would result in a too severe Xe loss from the mantle. We have tested different functions for $\varphi(t)$, and the model results that best fit the data are those obtained using three different values ($\varphi_1 > \varphi_2 > \varphi_3$) for the respective intervals of time [Δt, 100 Ma], [100 Ma, 1000 Ma], [1000 Ma, 4500 Ma] (table 1). An exponential decrease of $\varphi(t)$ could also fit the data but not as well as this stepped function.

The choices of these steps and of the related time intervals have some physical grounds. Owing to a higher thermal regime of the solid Earth, the degassing rate during the Hadean eon was probably an order of magnitude higher than the modern one [18,47–49]. During the Archaean eon, the degassing rate was also probably higher than at present, as indicated for example by the ubiquitous presence of komatiitic lavas, presumably originating from a mantle hotter than today (although some authors argue that a hotter mantle does not necessarily imply a higher convection rate [14,50]). Isotopic fractionation of xenon during magma generation and degassing could only be kinetic, if any, and is neglected here. The model is built in such a way that the mantle is degassing Xe into the atmosphere from the time of Earth's accretion, which is mathematically

Table 1. Input parameters of the model. Italicized values are adjusted parameters using multiple runs of the model.

parameter		literature	see	adjusted value
I_{INI}	ppb	3–13	§3*a*	*6.4*
$(^{129}I/^{127}I)_{INI}$	mol mol^{-1}	1.1×10^{-4}	§3*a*	1.1×10^{-4}
$^{238}U_{INI}$	ppb	33–41	§3*b*	*40*
$(^{244}Pu/^{238}U)_{INI}$	mol mol^{-1}	6.8×10^{-3}	§3*b*	6.8×10^{-3}
$^{244}Pu_{INI}$	mol		§3*b*	3.2×10^{15}
$^{130}Xe_{INI}$	mol	n.d.	§3*c*	1.44×10^{13}
$(^{124}Xe/^{130}Xe)_{INI}$	mol mol^{-1}	0.02928	§3*c*	0.02928
$(^{126}Xe/^{130}Xe)_{INI}$	—	0.02534	—	0.02534
$(^{128}Xe/^{130}Xe)_{INI}$	—	0.5083	—	0.5083
$(^{129}Xe/^{130}Xe)_{INI}$	—	6.286	—	6.286
$(^{131}Xe/^{130}Xe)_{INI}$	—	4.996	—	4.996
$(^{132}Xe/^{130}Xe)_{INI}$	—	6.047	—	6.047
$(^{134}Xe/^{130}Xe)_{INI}$	—	2.126	—	2.126
$(^{136}Xe/^{130}Xe)_{INI}$	—	1.657	—	1.657
degassing parameters				
φ_1	Ma^{-1}	n.d.	§3*d*	*0.065*
φ_2	—	n.d.	—	*0.0011*
φ_3	—	n.d.	—	*0.000073*
escape parameters				
b	Ma^{-1}	2.53	§3*d*	2.53
c	—	0.85	—	0.85
d	—	n.d.		*1.2270*
instantaneous fractionation	% amu^{-1}	1.0–1.5	§3*d*	*1.3*

equivalent, during the short time interval of a few tens of millions of years, to adding Xe from impacting bodies directly to the atmosphere.

(b) Loss of xenon to outer space

As introduced above, Archaean rocks of surficial origin contain mass-fractionated Xe isotopically intermediate between chondritic/solar and modern atmospheric (figure 2). Data are scarce because they are extremely difficult to obtain (owing to the need to date confidently the host phases). Available data are consistent with a time evolution of the Xe isotopic fractionation, presumably in the ancient atmosphere. This evolution can be fitted with a Rayleigh distillation model in which Xe isotopes are escaping from the atmosphere through time with mass-dependent instantaneous isotopic fractionation. The exponential evolution of the isotopic composition of atmospheric xenon with time predicted by Rayleigh distillation is consistent with the decline of FUV light flux from the ancient Sun (figure 1), suggesting that interactions between atmospheric Xe and FUV light from the Sun played a role in Xe escape. The Rayleigh distillation equation can be

written as

$$\frac{(^{i+1}\mathrm{Xe}/^{i}\mathrm{Xe})_{t=4.56\,\mathrm{Ga,\,today}}}{(^{i+1}\mathrm{Xe}/^{i}\mathrm{Xe})_{t=0}} = f^{\alpha_{\mathrm{esc}}-1} \sim 1.035, \tag{2.4}$$

where the factor 1.035 relates to the isotopic difference between solar/chondritic and modern air and f is the depletion factor of Xe in modern air corresponding to a factor of ≈20 relative to carbonaceous chondrites (CCs) [23]. The instantaneous fractionation factor α_{esc} is then ≈1.011% per atomic mass unit. This isotope fractionation is large for an inert gas with such a high mass. Thus, either Xe isotopic fractionation resulted from a specific process during atmospheric escape, which is not yet documented, or it involved ionization of xenon, which, from laboratory experiments, has been shown to yield isotopic fractionation of the order of 0.8–1.6% per atomic mass unit [41,51–55]. Among most volatile species that were potentially present in the ancient atmosphere (e.g. noble gases, CO, CO_2, N_2, CH_4, ...), xenon has the lowest ionization potential. Hébrard & Marty [42] have investigated the possible behaviour of atmospheric Xe, taking into account the inferred distribution of FUV light wavelengths of the ancient Sun. Hébrard & Marty proposed that Xe was ionized at an atmospheric height comparable to that of organic haze formation in the Archaean atmosphere, so that ionized heavy Xe isotopes were preferentially retained in the lower atmosphere, whereas ionized light Xe isotopes could escape from the upper atmosphere. This possibility is certainly not unique, and other processes may be explored, but, whatever the origin of this isotopically fractionating Xe loss, it remains firm that Xe isotopically intermediate between primordial Xe and modern atmospheric Xe has been found trapped in Archaean rocks.

In our model, we use an instantaneous fractionation factor α_{esc} allowed to vary within 1.0–1.5% per atomic mass unit. The rate of escape of xenon atoms is scaled using FUV decay curves corresponding to the wavelength at which xenon atoms are ionized (102.3 nm) [39]. The intensity of escape ($\beta(t)$ in Ma^{-1}) with time t is given by

$$\beta(t) = \frac{1}{d}(b \times t)^{c}, \tag{2.5}$$

where b and c are constant parameters from [39] and d is an adjusted constant. Parameter values are shown in table 1, and the decay of atmospheric Xe with time is shown in figure 2.

3. Key parameters

The key parameters of the model are either taken directly from the literature (e.g. $(^{129}\mathrm{I}/^{127}\mathrm{I})_{\mathrm{INI}}$) when the value is widely accepted or are adjusted testing a range of values when the value is badly known (e.g. $\mathrm{I}_{\mathrm{INI}}$). Table 1 contains canonical values for parameters of the model and adjusted values.

(a) Iodine content of the Earth

Because of its volatility, the precise iodine content of the Earth, and thus $^{129}\mathrm{I}_{\mathrm{INI}}$, is not well known. A large range between 3 and 13 ppb is proposed in the literature [56–58]. The lower value of 3 ppb is computed with iodine data from the depleted mantle [58], which, by definition, is poor in incompatible elements such as iodine. Thus, it represents a lower limit of the iodine budget of the Earth. Here, we use a value of 6.4 ppb in our reference solution, which gives model results consistent with observed Xe data, and permits a good match between the two chronometers

(I–Xe and I–Pu–Xe). The range of I_{INI} values is used as an uncertainty and is propagated in the age calculation. An abundance of 6.4 ppb for ^{127}I together with the initial $^{129}I/^{127}I$ ratio of 1.1×10^{-4} obtained from meteorite data [16] yields an initial amount of terrestrial ^{129}I ($^{129}I_{INI}$) of 3.8×10^{12} mol.

(b) U–Pu content of the Earth

The range of present-day abundances for ^{238}U is between 16 and 20 ppb [18], corresponding to initial values, 4.57 Ga ago, between 33 and 41 ppb. Here, we take a value of 38 ppb for the initial ^{238}U content as in [18]. The average value of 6.8×10^{-3} for $(^{244}Pu/^{238}U)_{INI}$ is derived from the analysis of meteorites [21,59] and is consistent with data obtained from ancient terrestrial zircons [18,60–62].

(c) Initial amount and isotopic composition of xenon

Xenon is under-abundant in the terrestrial atmosphere relative to other noble gases by a factor of 23 ± 5 relative to Kr [23]. Thus, the present-day atmospheric inventory (6.15×10^{11} mol of ^{130}Xe [31]) can be corrected for selective escape of xenon atoms by multiplying the current abundance by this factor, which leads to an initial ^{130}Xe amount of $1.41(\pm 0.36) \times 10^{13}$ mol. It is beyond the scope of this study to evaluate the starting isotopic composition of primordial xenon and we refer to discussions elsewhere [17,26,32]. The U–Xe [23] is, so far, the only initial isotopic composition that permits the reproduction of the current isotopic composition of atmospheric Xe, including fissiogenic and radiogenic contributions [63], and its composition is adopted as a starting isotopic composition for the model.

(d) Optimization of the parameters

The model is constrained using the initial Xe amount for the Earth and the U–Xe composition, on the one hand, and the present-day amount and composition of atmospheric Xe and, for some of the isotopic ratios, of mantle Xe, on the other. The silicate Earth contents of parent elements (I and Pu) are additional parameters that can be adjusted within a plausible range of values. The model must yield ancient Xe isotopic compositions that are consistent with data from Archaean rocks.

Key parameters from the literature are $^{130}Xe_{INI}$, $(^{129}I/^{127}I)_{INI}$, $^{238}U_{INI}$, $(^{244}Pu/^{238}U)_{INI}$ and the starting isotopic composition (U–Xe). Other parameters are adjusted following multiple runs. ^{130}Xe, the stable isotope of reference, is used to scale the degassing and escape rates over time. The different degassing rates φ_1, φ_2 and φ_3 (table 1) are fitted in order to respect the ^{130}Xe depletion over time and to take into account variations in the degassing rate of the mantle. The φ_1, φ_2 and φ_3 values that best fit the data are 890, 15 and 1 times the modern rate between Δt and 100 Ma, 100 Ma and 1 Ga, and 1 Ga and present, respectively. The variation of the atmospheric Xe escape rate (equation (2.5)) is scaled to the variation of the FUV light flux over time. Once the degassing and escape rates of ^{130}Xe are scaled, it is possible to optimize other key parameters, such as the instantaneous fractionation factor α_{esc} and the initial iodine abundance I_{INI}. The aim of this final step of optimization is to reproduce the modern and the Archaean isotopic compositions of atmospheric Xe to better than 1% (figure 2).

(e) Outcomes of the model

In addition to optimization of the degassing and escape parameters, the model allows one to determine the atmospheric closure time Δt that best fits the observations. Time Δt corresponds to the time after CAI when the atmosphere became closed (except for Xe, whose escape to space continued over eons).

Table 2. Reference solution of the model compared to values from the literature.

parameter	dimension	literature	note	reference solution
Xe_{ATM}	mol	1.537×10^{13}	[a]	1.5184×10^{13}
$(^{124}Xe/^{130}Xe)_{ATM}$	mol mol^{-1}	0.02337	—	0.0232
$(^{126}Xe/^{130}Xe)_{ATM}$	—	0.0218	—	0.0217
$(^{128}Xe/^{130}Xe)_{ATM}$	—	0.4715	—	0.470
$(^{129}Xe/^{130}Xe)_{ATM}$	—	6.496	—	6.522
$(^{131}Xe/^{130}Xe)_{ATM}$	—	5.213	—	5.21
$(^{132}Xe/^{130}Xe)_{ATM}$	—	6.607	—	6.60
$(^{134}Xe/^{130}Xe)_{ATM}$	—	2.563	—	2.55
$(^{136}Xe/^{130}Xe)_{ATM}$	—	2.176	—	2.17
$^{129}Xe(I)_{ATM,CORR}$	mol		[b]	3.71×10^{12}
$(^{129}Xe(I)/^{136}Xe(Pu))_{ATM}$	mol mol^{-1}	6.5–7.1	[c]	6.99
$(^{129}Xe(I)/^{136}Xe(Pu))_{ATM,CORR}$	—	—	[d]	21.75
Xe_{MANT}	mol			2.0356×10^{12}
$(^{124}Xe/^{130}Xe)_{MANT}$	mol mol^{-1}			0.0293
$(^{126}Xe/^{130}Xe)_{MANT}$	—			0.0253
$(^{128}Xe/^{130}Xe)_{MANT}$	—			0.508
$(^{129}Xe/^{130}Xe)_{MANT}$	—			9.00
$(^{131}Xe/^{130}Xe)_{MANT}$	—			5.18
$(^{132}Xe/^{130}Xe)_{MANT}$	—			6.73
$(^{134}Xe/^{130}Xe)_{MANT}$	—			2.86
$(^{136}Xe/^{130}Xe)_{MANT}$	—			2.50

[a] The total inventory and isotopic ratios of Xe are from [31].
[b] Amount of ^{129}Xe in the atmosphere coming from the decay of ^{129}I and corrected for loss.
[c] Ratio of radioactivity products uncorrected for loss from [64].
[d] Ratio corrected for loss.

4. Discussion

The long-term escape affects the global budget of xenon atoms in the Earth's atmosphere and therefore the amount of radioactive products, which have to be corrected as shown in table 2.

(a) Corrected I–Xe age of the Earth–atmosphere system

The I–Xe closure age of the atmosphere, corrected for long-term escape of atmospheric Xe, becomes 41 Ma after CAI, instead of 110 Ma, with our reference I content of 6.4 ppb. For a possible range of 3–13 ppb for terrestrial iodine [56–58], the range of closure age becomes 21–62 Ma (see ranges of solutions in figure 3). It must be noted that the I abundance of 3 ppb [57] and the corresponding closure age of 21 Ma after CAI are likely to be lower limits, so that a possible range of ≈30–60 Ma, corresponding to a terrestrial I content of 6–13 ppb, is preferred.

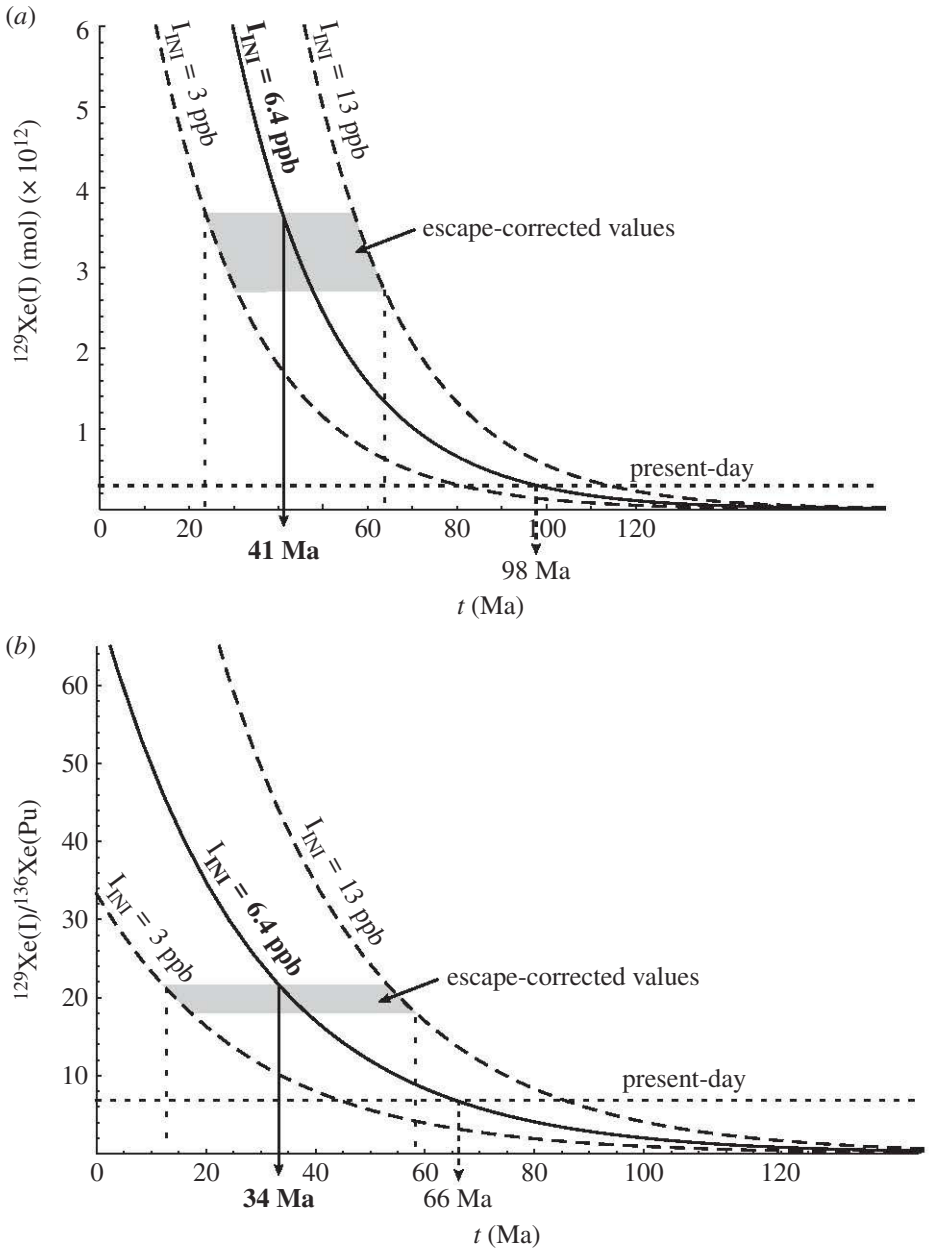

Figure 3. (*a*) Evolution of the atmospheric content of ^{129}Xe derived from the decay of ^{129}I with time. The non-corrected amount gave a closure age of 98 Ma for the I–Xe system. After correction for subsequent loss, the age becomes 41 Ma. (*b*) Evolution with time of the ratio of radioactive products in the atmosphere (^{129}Xe(I) and ^{136}Xe(Pu)). The non-corrected ratio gave a closure age of 66 Ma for the I–Pu–Xe system. After correction, the age becomes 34 Ma, in agreement with the time of closure of the I–Xe system and with the closure age of the mantle given by the mantle samples [4,32].

(b) I–Pu–Xe closure age

The I–Xe closure age given above is in fact a mass balance between the residual amount of radiogenic ^{129}Xe in the atmosphere and the amount of initial ^{129}I, with the underlying assumption that the former derived from the latter. In fact, the whole amount of ^{129}Xe(I) could have been added to a 'dead' Earth (i.e. an Earth closed after the complete decay of ^{129}I) by an accreting primitive body formed just after CAIs and having therefore a high ^{129}Xe(I)/I ratio. In such an extreme case, the 'closure' age based on I–Xe would not have any chronological meaning for the Earth. Here, it becomes interesting to make use of the I–Pu–Xe system in addition to the

I–Xe system. The $(^{129}Xe(I)/^{136}Xe(Pu))_{ATM,CORR}$ ratio depends on two decay constants having contrasting values. Thus, this ratio is time-dependent and decreases with age. In the example given above, the $(^{129}Xe(I)/^{136}Xe(Pu))_{ATM,CORR}$ ratio should yield a very young age, contrary to the I–Xe chronometer. In other words, the two chronometers all together have the faculty to give, or not, 'concordant' closure ages.

The atmospheric $^{129}Xe(I)/^{136}Xe(Pu)$ ratio, corrected for Xe escape, becomes 21.7 instead of 4.6 (table 2), yielding a closure age of 34 Ma using equation (1.2), with a possible range of 13–58 Ma. However, the lower time limit is based again on an unrealistically low terrestrial amount of iodine. This range is 'concordant' with the I–Xe range of 30–60 Ma and both methods converge to a revised closure age of $\approx 40^{+20}_{-10}$ Ma for the atmosphere, instead of about 100 Ma previously thought (figure 3). Interestingly, the $^{129}Xe(I)/^{136}Xe(Pu)$ ratio has also been estimated for the mantle from the precise Xe isotope analysis of mantle-derived CO_2-rich gases [32]. Estimates of this ratio vary between 20 and 64, depending on the parameters (e.g. I/Pu/U ratios, primordial Xe isotopic composition) chosen to derive them. This range of values leads to a possible interval of 20–50 Ma for a major episode of mantle degassing [32]. Thus, it is tempting to link such an event to a major catastrophic impact that affected the interior of the proto-Earth and its atmosphere and that led to the formation of the Moon. However, it must also be noted that Xe isotope data for mid-ocean ridge basalts (MORBs) seem to define lower $^{129}Xe(I)/^{136}Xe(Pu)$ ratios around 6–10 [4,5], which could represent another giant event [32], or, in our opinion, fractionation of volatile iodine with respect to refractory plutonium/uranium for the mantle source of MORBs, during Earth's building episodes.

The range of closure ages (30–60 Ma after CAI) is consistent with hafnium–tungsten (Hf–W) model ages for the Moon's formation predicting an ancient fractionation (25–50 Ma) from the W isotope difference between chondrites and the Earth [65–68]. However, it is only marginally consistent with those based on the similarity of the W isotope ratios between the Earth and the Moon, which requires the Moon formation event to have taken place 60 Ma or more after CAIs [69]. The former case would reinforce the link between the last episode of major loss of the atmosphere and the formation of the Moon.

(c) Physical significance of closure ages and the epoch of the formation of the Earth–Moon system

The model presented here permits the xenon budget of the Earth's atmosphere to be corrected for long-term escape to space. This correction leads to a reconstruction of the xenon isotopic composition of the atmosphere just after the last episode of major loss. After correction, the I–Xe and the I–Pu–Xe systems converge towards a common range of closure ages within 30–60 Ma after CAI, suggesting that they have indeed recorded common catastrophic event(s). In fact, the closure ages estimated here probably result from the integration of a suite of events occurring during the accretion and where primitive and differentiated bodies with variable volatile contents contributed to the building of the proto-Earth.

The fraction of the proto-atmosphere removed during a giant impact is debated [45,70]. New modelling results based on the Moon-forming scenario with a fast-spinning Earth [71] suggest that a large part (if not the whole) of the atmosphere could have been removed during this major event [72]. Our reconstructed Xe budget indicates that about 23% of the total $^{129}Xe(I)$ produced by terrestrial ^{129}I was left in the atmosphere after completion of the Earth. The possibility that ≈77% of initial volatile elements would have been lost before the atmosphere's closure is not unreasonable in regard to possible atmospheric erosion during terrestrial accretion [45]. This mass balance implies that the proto-Earth could have hosted a factor of ≈4 more volatiles than at present, if these volatiles were supplied before the last giant impact event. Because the present-day terrestrial inventory of volatile elements is estimated to be equivalent to about $2 \pm 1\%$ of CC material [73], this mass balance suggests that the proto-Earth could have been contributed by up to ≈10% CC material before the last giant impact. Alternatively, terrestrial volatiles could

have been supplied from bodies having Xe/I ratios higher than those observed presently in CC (e.g. cometary material?).

The conclusions drawn here have to be taken carefully, as there all still too many shady areas in the early accretional history of the Earth. Our model does not pretend to describe such accretional processes, which will require a continuous accretion/degassing simulation. The main result of this study is nevertheless that the age of the terrestrial atmosphere appears closer to ≈40 Ma rather than to 100 Ma as previously thought.

5. Conclusion

The I–Pu–Xe system gives useful, yet not fully understood, time constraints 'on establishment of global chemical inventories' [17] for the Earth and, presumably, for the Moon. After geological loss of Xe from the atmosphere, the closure ages derived from the I–Xe and I–Pu–Xe systematics are more ancient than previously proposed and suggest major forming events around 40 Ma (range 30–60 Ma) after CAI. A more comprehensive approach of this chronology will need to integrate the I–Pu–Xe system into *n*-body simulations of terrestrial accretion, parametrized with gain and loss of volatiles, especially during the giant impact epoch.

Acknowledgements. David Stevenson and Alex Halliday, organizers of the 'Origin of the Moon' Discussion Meeting, are gratefully acknowledged, as well as other participants of the meeting, for fruitful discussions. Remarks from Maïa Kuga and Eric Hébrard helped to build this model. We are grateful to Allessandro Morbidelli, Seth Jacobson and Patrick Michel for sharing exciting ideas on the accretion of terrestrial planets, and to Jamie Gilmour and Sujoy Mukhopadhyay for constructive reviews.

Funding statement. This work was supported by the European Research Council under the European Community's Seventh Framework Programme (FP7/2007–2013 grant agreement no. 267255 to B.M.). This is CRPG contribution no. 2308.

References

1. Patterson C. 1956 Age of meteorites and the Earth. *Geochim. Cosmochim. Acta* **10**, 230–237. (doi:10.1016/0016-7037(56)90036-9)
2. Amelin Y, Krot AN, Hutcheon ID, Ulyanov AA. 2002 Lead isotopic ages of chondrules and calcium–aluminum-rich inclusions. *Science* **297**, 1678–1683. (doi:10.1126/science.1073950)
3. Bouvier A, Wadhwa M. 2010 The age of the Solar System redefined by the oldest Pb–Pb age of a meteoritic inclusion. *Nat. Geosci.* **3**, 637–641. (doi:10.1038/ngeo941)
4. Mukhopadhyay S. 2012 Early differentiation and volatile accretion recorded in deep-mantle neon and xenon. *Nature* **486**, 101–104. (doi:10.1038/nature11141)
5. Tucker JM, Mukhopadhyay S, Schilling J-G. 2012 The heavy noble gas composition of the depleted MORB mantle (DMM) and its implications for the preservation of heterogeneities in the mantle. *Earth Planet. Sci. Lett.* **355–356**, 244–254. (doi:10.1016/j.epsl.2012.08.025)
6. Parai R, Mukhopadhyay S, Standish JJ. 2012 Heterogeneous upper mantle Ne, Ar and Xe isotopic compositions and a possible Dupal noble gas signature recorded in basalts from the Southwest Indian Ridge. *Earth Planet. Sci. Lett.* **359–360**, 227–239. (doi:10.1016/j.epsl.2012.10.017)
7. Pető MK, Mukhopadhyay S, Kelley KA. 2013 Heterogeneities from the first 100 million years recorded in deep mantle noble gases from the Northern Lau Back-arc Basin. *Earth Planet. Sci. Lett.* **369–370**, 13–23. (doi:10.1016/j.epsl.2013.02.012)
8. Katcoff S, Schaeffer OA, Hastings JM. 1951 Half-life of iodine-129 and the age of the elements. *Phys. Rev.* **82**, 688–690. (doi:10.1103/PhysRev.82.688)
9. Reynolds JH. 1960 Determination of the age of the elements. *Phys. Rev. Lett.* **4**, 8–10. (doi:10.1103/PhysRevLett.4.8)
10. Porcelli D, Ballentine CJ. 2002 Models for distribution of terrestrial noble gases and evolution of the atmosphere. *Rev. Mineral. Geochem.* **47**, 411–480. (doi:10.2138/rmg.2002.47.11)
11. Staudacher T, Allègre CJ. 1982 Terrestrial xenology. *Earth Planet. Sci. Lett.* **60**, 389–406. (doi:10.1016/0012-821X(82)90075-9)

12. Caffee MW, Hudson GB, Velsko C, Huss GR, Alexander EC, Chivas AR. 1999 Primordial noble gases from Earth's mantle: identification of a primitive volatile component. *Science* **285**, 2115–2118. (doi:10.1126/science.285.5436.2115)
13. Marty B. 1989 Neon and xenon isotopes in MORB: implications for the Earth–atmosphere evolution. *Earth Planet. Sci. Lett.* **94**, 45–56. (doi:10.1016/0012-821X(89)90082-4)
14. Padhi CM, Korenaga J, Ozima M. 2012 Thermal evolution of Earth with xenon degassing: a self-consistent approach. *Earth Planet. Sci. Lett.* **341–344**, 1–9. (doi:10.1016/j.epsl.2012.06.013)
15. Wetherill GW. 1975 Radiometric chronology of the early solar system. *Annu. Rev. Nucl. Sci.* **25**, 283–328. (doi:10.1146/annurev.ns.25.120175.001435)
16. Hohenberg CM, Podosek FA, Reynolds JH. 1967 Xenon–iodine dating: sharp isochronism in chondrites. *Science* **156**, 233–236. (doi:10.1126/science.156.3772.233)
17. Podosek FA, Ozima M. 2000 The xenon age of the Earth. In *Origin of the Earth and Moon* (eds RM Canup, K Righter), pp. 63–72. Tucson, AZ: University of Arizona Press.
18. Tolstikhin I, Marty B, Porcelli D, Hofmann A. 2014 Evolution of volatile species in the Earth's mantle: a view from xenology. *Geochim. Cosmochim. Acta* **136**, 229–246. (doi:10.1016/j.gca.2013.08.034)
19. Allègre CJ, Staudacher T, Sarda P, Kurz MD. 1983 Constraints on evolution of Earth's mantle from rare gas systematics. *Nature* **303**, 762–766. (doi:10.1038/303762a0)
20. Alexander EC, Lewis RS, Reynolds JH, Michel MC. 1971 Plutonium-244: confirmation as an extinct radioactivity. *Science* **172**, 837–840. (doi:10.1126/science.172.3985.837)
21. Hudson GB, Kennedy BM, Podosek FA, Hohenberg CM. 1989 The early solar system abundance of ^{244}Pu as inferred from the St. Severin chondrite. In *Proc. 19th Lunar and Planetary Science Conf., Houston, TX, 14–18 March 1988* (eds G Ryder, VL Sharpton), pp. 547–557. Cambridge, UK: Cambridge University Press.
22. Kunz J, Staudacher T, Allègre CJ. 1998 Plutonium-fission xenon found in Earth's mantle. *Science* **280**, 877–880. (doi:10.1126/science.280.5365.877)
23. Pepin RO. 1991 On the origin and early evolution of terrestrial planet atmospheres and meteoritic volatiles. *Icarus* **92**, 2–79. (doi:10.1016/0019-1035(91)90036-S)
24. Pepin RO. 2000 On the isotopic composition of primordial xenon in terrestrial planet atmospheres. *Space Sci. Rev.* **92**, 371–395. (doi:10.1023/A:1005236405730)
25. Takaoka N. 1972 An interpretation of general anomalies of xenon and the isotopic composition of primitive xenon. *Mass Spectrosc.* **20**, 287–302. (doi:10.5702/massspec1953.20.287)
26. Pepin RO, Phinney D. 1978 Components of xenon in the solar system (unpublished preprint).
27. Huss GR, Lewis RS. 1995 Presolar diamond, SiC, and graphite in primitive chondrites: abundances as a function of meteorite class and petrologic type. *Geochim. Cosmochim. Acta* **59**, 115–160. (doi:10.1016/0016-7037(94)00376-W)
28. Gilmour JD. 2010 'Planetary' noble gas components and the nucleosynthetic history of solar system material. *Geochim. Cosmochim. Acta* **74**, 380–393. (doi:10.1016/j.gca.2009.09.015)
29. Crowther SA, Gilmour JD. 2013 The genesis solar xenon composition and its relationship to planetary xenon signatures. *Geochim. Cosmochim. Acta* **123**, 17–34. (doi:10.1016/j.gca.2013.09.007)
30. Igarashi G. 1995 Primitive xenon in the Earth. *AIP Conf. Proc.* **341**, 70–80. (doi:10.1063/1.48751)
31. Ozima M, Podosek FA. 2002 *Noble gas geochemistry*, 2nd edn. Cambridge, UK: Cambridge University Press.
32. Pepin RO, Porcelli D. 2006 Xenon isotope systematics, giant impacts, and mantle degassing on the early Earth. *Earth Planet. Sci. Lett.* **250**, 470–485. (doi:10.1016/j.epsl.2006.08.014)
33. Tolstikhin IN, Marty B. 1998 The evolution of terrestrial volatiles: a view from helium, neon, argon and nitrogen isotope modelling. *Chem. Geol.* **147**, 27–52. (doi:10.1016/S0009-2541(97)00170-8)
34. Yokochi R, Marty B. 2005 Geochemical constraints on mantle dynamics in the Hadean. *Earth Planet. Sci. Lett.* **238**, 17–30. (doi:10.1016/j.epsl.2005.07.020)
35. Srinivasan B. 1976 Barites: anomalous xenon from spallation and neutron-induced reactions. *Earth Planet. Sci. Lett.* **31**, 129–141. (doi:10.1016/0012-821X(76)90104-7)
36. Pujol M, Marty B, Burnard P, Philippot P. 2009 Xenon in Archean barite: weak decay of ^{130}Ba, mass-dependent isotopic fractionation and implication for barite formation. *Geochim. Cosmochim. Acta* **73**, 6834–6846. (doi:10.1016/j.gca.2009.08.002)
37. Pujol M, Marty B, Burgess R, Turner G, Philippot P. 2013 Argon isotopic composition of Archaean atmosphere probes early Earth geodynamics. *Nature* **498**, 87–90. (doi:10.1038/nature12152)

38. Pujol M, Marty B, Burgess R. 2011 Chondritic-like xenon trapped in Archean rocks: a possible signature of the ancient atmosphere. *Earth Planet. Sci. Lett.* **308**, 298–306. (doi:10.1016/j.epsl.2011.05.053)
39. Ribas I, Guinan EF, Güdel M, Audard M. 2005 Evolution of the solar activity over time and effects on planetary atmospheres. I. High-energy irradiances (1–1700 Å). *Astrophys. J.* **622**, 680–694. (doi:10.1086/427977)
40. Holland G, Lollar BS, Li L, Lacrampe-Couloume G, Slater GF, Ballentine CJ. 2013 Deep fracture fluids isolated in the crust since the Precambrian era. *Nature* **497**, 357–60. (doi:10.1038/nature12127)
41. Marrocchi Y, Marty B, Reinhardt P, Robert F. 2011 Adsorption of xenon ions onto defects in organic surfaces: implications for the origin and the nature of organics in primitive meteorites. *Geochim. Cosmochim. Acta* **75**, 6255–6266. (doi:10.1016/j.gca.2011.07.048)
42. Hébrard E, Marty B. 2014 Coupled noble gas–hydrocarbon evolution of the early Earth atmosphere upon solar UV irradiation. *Earth Planet. Sci. Lett.* **385**, 40–48. (doi:10.1016/j.epsl.2013.10.022)
43. Zahnle K, Arndt N, Cockell C, Halliday A, Nisbet E, Selsis F, Sleep NH. 2007 Emergence of a habitable planet. *Space Sci. Rev.* **129**, 35–78. (doi:10.1007/s11214-007-9225-z)
44. Chen GQ, Ahrens TJ. 1997 Erosion of terrestrial planet atmosphere by surface motion after a large impact. *Phys. Earth Planet. Inter.* **100**, 21–26. (doi:10.1016/S0031-9201(96)03228-1)
45. Genda H, Abe Y. 2005 Enhanced atmospheric loss on protoplanets at the giant impact phase in the presence of oceans. *Nature* **433**, 842–844. (doi:10.1038/nature03360)
46. Canup RM, Agnor CB. 2000 Accretion of the terrestrial planets and the Earth–Moon system. In *Origin of the Earth and Moon* (eds RM Canup, K Righter), pp. 113–130. Tucson, AZ: University of Arizona Press.
47. Blichert-Toft J, Albarède F. 1994 Short-lived chemical heterogeneities in the Archean mantle with implications for mantle convection. *Science* **263**, 1593–1596. (doi:10.1126/science.263.5153.1593)
48. Coltice N. 2005 The role of convective mixing in degassing the Earth's mantle. *Earth Planet. Sci. Lett.* **234**, 15–25. (doi:10.1016/j.epsl.2005.02.041)
49. Gonnermann HM, Mukhopadhyay S. 2009 Preserving noble gases in a convecting mantle. *Nature* **459**, 560–563. (doi:10.1038/nature08018)
50. Korenaga J. 2003 Energetics of mantle convection and the fate of fossil heat. *Geophys. Res. Lett.* **30**, 1437. (doi:10.1029/2003GL016982)
51. Frick U, Mack R, Chang S. 1979 Noble gas trapping and fractionation during synthesis of carbonaceous matter. In *Proc. 10th Lunar and Planetary Science Conf., Houston, TX, 19–23 March 1979* (ed. RB Merrill), pp. 1961–1972. New York, NY: Pergamon.
52. Bernatowicz TJ, Fahey AJ. 1986 Xe isotopic fractionation in a cathodeless glow discharge. *Geochim. Cosmochim. Acta* **50**, 445–452. (doi:10.1016/0016-7037(86)90197-3)
53. Bernatowicz TJ, Hagee BE. 1987 Isotopic fractionation of Kr and Xe implanted in solids at very low energies. *Geochim. Cosmochim. Acta* **51**, 1599–1611. (doi:10.1016/0016-7037(87)90341-3)
54. Ponganis K, Graf T, Marti K. 1997 Isotopic fractionation in low-energy ion implantation. *J. Geophys. Res.* **102**, 19 335–19 343. (doi:10.1029/97JE01686)
55. Hohenberg CM, Thonnard N, Meshik A. 2002 Active capture and anomalous adsorption: new mechanisms for the incorporation of heavy noble gases. *Meteorit. Planet. Sci.* **37**, 257–267. (doi:10.1111/j.1945-5100.2002.tb01108.x)
56. Déruelle B, Dreibus G, Jambon A. 1992 Iodine abundances in oceanic basalts: implications for Earth dynamics. *Earth Planet. Sci. Lett.* **108**, 217–227. (doi:10.1016/0012-821X(92)90024-P)
57. Armytage RMG, Jephcoat AP, Bouhifd MA, Porcelli D. 2013 Metal–silicate partitioning of iodine at high pressures and temperatures: implications for the Earth's core and ^{129*}Xe budgets. *Earth Planet. Sci. Lett.* **373**, 140–149. (doi:10.1016/j.epsl.2013.04.031)
58. Wänke H, Dreibus G, Jagoutz E. 1984 Mantle chemistry and accretion history of the Earth. In *Archaean geochemistry* (eds A Kröner, GN Hanson, AM Goodwin), pp. 1–24. Berlin, Germany: Springer. (doi:10.1007/978-3-642-70001-9_1)
59. Lugmair GW, Marti K. 1977 Sm–Nd–Pu timepieces in the Angra dos Reis meteorite. *Earth Planet. Sci. Lett.* **35**, 272–284. (doi:10.1016/0012-821X(77)90131-5)
60. Honda M, Nutman AP, Bennett VC. 2003 Xenon compositions of magmatic zircons in 3.64 and 3.81 Ga meta-granitoids from Greenland – a search for extinct ^{244}Pu in ancient terrestrial rocks. *Earth Planet. Sci. Lett.* **207**, 69–82. (doi:10.1016/S0012-821X(02)01147-0)

61. Turner G, Harrison TM, Holland G, Mojzsis SJ, Gilmour J. 2004 Extinct ^{244}Pu in ancient zircons. *Science* **306**, 89–91. (doi:10.1126/science.1101014)
62. Turner G, Busfield A, Crowther SA, Harrison M, Mojzsis SJ, Gilmour J. 2007 Pu–Xe, U–Xe, U–Pb chronology and isotope systematics of ancient zircons from Western Australia. *Earth Planet. Sci. Lett.* **261**, 491–499. (doi:10.1016/j.epsl.2007.07.014)
63. Porcelli D, Pepin RO. 2000 Rare gas constraints on early Earth history. In *Origin of the Earth and Moon* (eds RM Canup, K Righter), pp. 435–458. Tucson, AZ: University of Arizona Press.
64. Porcelli D, Turekian KK. 2003 The history of planetary degassing as recorded by noble gases. In *Treatise on geochemistry* (eds HD Holland, KK Turekian), vol. 4, *The atmosphere* (ed. RF Keeling), pp. 281–318. Amsterdam, The Netherlands: Elsevier. (doi:10.1016/B0-08-043751-6/04181-5)
65. Yin Q, Jacobsen SB, Yamashita K, Blichert-Toft J, Télouk P, Albarède F. 2002 A short timescale for terrestrial planet formation from Hf–W chronometry of meteorites. *Nature* **418**, 949–952. (doi:10.1038/nature00995)
66. Righter K, Shearer CK. 2003 Magmatic fractionation of Hf and W: constraints on the timing of core formation and differentiation in the Moon and Mars. *Geochim. Cosmochim. Acta* **67**, 2497–2507. (doi:10.1016/S0016-7037(02)01349-2)
67. Halliday AN. 2004 Mixing, volatile loss and compositional change during impact-driven accretion of the Earth. *Nature* **427**, 505–509. (doi:10.1038/nature02275)
68. Kleine T, Palme H, Mezger K, Halliday AN. 2005 Hf–W chronometry of lunar metals and the age and early differentiation of the Moon. *Science* **310**, 1671–1674. (doi:10.1126/science.1118842)
69. Touboul M, Kleine T, Bourdon B, Palme H, Wieler R. 2007 Late formation and prolonged differentiation of the Moon inferred from W isotopes in lunar metals. *Nature* **450**, 1206–1209. (doi:10.1038/nature06428)
70. Genda H, Abe Y. 2003 Survival of a proto-atmosphere through the stage of giant impacts: the mechanical aspects. *Icarus* **164**, 149–162. (doi:10.1016/S0019-1035(03)00101-5)
71. Ćuk M, Stewart ST. 2012 Making the Moon from a fast-spinning Earth: a giant impact followed by resonant despinning. *Science* **338**, 1047–1052. (doi:10.1126/science.1225542)
72. Lock SJ, Stewart ST. 2013 Atmospheric loss during high angular momentum giant impacts. In *Proc. 44th Lunar and Planetary Science Conf., The Woodlands, TX, 18–22 March 2013*, Abstract 2608. See http://www.lpi.usra.edu/meetings/lpsc2013/pdf/2608.pdf.
73. Marty B. 2012 The origins and concentrations of water, carbon, nitrogen and noble gases on Earth. *Earth Planet. Sci. Lett.* **313–314**, 56–66. (doi:10.1016/j.epsl.2011.10.040)

3.4.1 Additional Results and Research Perspectives

The model published in 2014 needs some modifications and refinements because of recent discoveries and investigations even if the conceptual basis and main results (correction of closure ages) remain the same.

Scientific discussions with the authors (S. Jacobson and A. Morbidelli) of a recent publication on the age of the Moon-forming impact inferred from dynamical simulations of the terrestrial planets and estimations of the late veneer on Earth (Jacobson et al., 2015), led to a refinement of the model. First, a partial removal of the atmosphere during the giant impact that led to the formation of the Moon is possible even if the exact amount of atmospheric loss is uncertain (Genda and Abe, 2003, 2005; Schlichting et al., 2015). Secondly the chondritic late veneer (2.92 ± 0.98 x10^{25}g, see estimates by Jacobson et al. (2015) and refs. therein) inferred from the abundances of siderophile elements in the Earth's mantle might have added some Xe in the atmosphere during its delivery to the Earth. A simple additional model with three degrees of freedom and two constraints has thus been constructed to take into account these two important parameters. The three free parameters are t_{GI}, D and F. t_{GI} is the time of the last giant impact. D is the dilution factor of the Earth's originally degassed atmosphere prior to/during the last giant impact D, that is $D = \frac{\text{Mol of atmosphere before impact}}{\text{Mol of atmosphere after impact}}$. F is the fraction of carbonaceous chondritic material in the late veneer. The two constraints are estimates of the radiogenic isotope abundance to parent element abundance ratio of $^{129}Xe^*_{corr}/^{129}I_{init}$ and $^{136}Xe^*_{corr}/^{244}Pu_{init}$. The two relevant equations (Eq. 3.1 & 3.2) are:

$$0.17 = \frac{^{129}Xe^*_{corr}}{^{129}I_{init}} = \frac{1 - e^{-\lambda_{129} t_{GI}}}{D} + e^{-\lambda_{129} t_{GI}} + \frac{^{129}Xe^*_{LV}}{^{129}I_{init}} \tag{3.1}$$

$$0.56 = \frac{^{136}Xe^*_{corr}}{^{244}PuB_{244}{}^{136}Y_{244}} = \frac{1 - e^{-\lambda_{244} t_{GI}}}{D} + e^{-\lambda_{244} t_{GI}} + \frac{^{136}Xe^*_{LV}}{^{244}PuB_{244}{}^{136}Y_{244}} \tag{3.2}$$

where the left-hand side for equation 3.1 is the radiogenic ionization/escape-loss-corrected abundance $^{129}Xe^*_{corr}$ relative to the initial abundance of parent isotope $^{129}I_{init}$. The left-hand side for equation 3.2 is the abundance of $^{136}Xe^*_{corr}$ relative to the initial abundance of parent isotope $^{244}Pu_{init}$ multiplied by the branching ratio for spontaneous fission of ^{244}Pu (B_{244}=1.25 x 10^{-3}) and by the yield of fission of ^{244}Pu producing ^{136}Xe atoms ($^{136}Y_{244}$=6.3 %) (Ozima and Podosek, 2002). Values of 0.166 and 0.556 are used for the $^{129}Xe^*_{corr}/^{129}I_{init}$ and $^{136}Xe^*_{corr}/^{244}Pu_{init}$ ratios and are from Avice and Marty (2014). These values highly depend on the initial amounts of parent nuclides in the silicate Earth and on the model used to correct the abundance of isotopes of xenon in the atmosphere for subsequent selective loss. However, the model built here aims to explore the effect of partial removal of the atmosphere during the giant impact and/or the addition of late accreting material on the Xe chronologies whatever the model considered. The first term on the right-hand side of equations 3.1 and 3.2 is the xenon produced from radioactive decay of the respective parent nuclides on the Earth before the last giant impact and diluted by a factor D during this giant impact relative to the initial parent abundance. D depicts the dilution of the abundance of radiogenic xenon atoms induced by the successive impacts that ended up with the Moon's formation. The process of atmospheric escape following giant impacts does not concern only radiogenic isotopes. D is thus identical to the dilution of bulk atmospheric Xe (all isotopes) during to the giant impact phase. The second term is the xenon atoms produced from radioactive decay of the parent nuclide in the Earth after the last giant impact relative to the initial parent abundances. The third term is the contribution of radiogenic/fissiogenic xenon from the late accretion relative to the initial parent concentrations on Earth.

If the late veneer consists of a fraction F of AVCC material (bearing Q noble gases plus a radiogenic fraction (Pepin, 1991)) and a fraction 1-F of U-Xe gas bearing material (i.e. depleted in radiogenic isotopes), then the third terms of equations 3.1 and 3.2 can be rewritten in:

$$\frac{^{129}Xe^*_{LV}}{^{129}I_{init}} = F \times \frac{^{129}Xe^*_{AVCC}}{^{129}Xe^*_{corr}} \times \frac{^{129}Xe^*_{corr}}{^{129}I_{init}} \tag{3.3}$$

$$\frac{^{136}Xe^*_{LV}}{^{244}PuB_{244}{}^{136}Y_{244}} = F \times \frac{^{136}Xe^*_{AVCC}}{^{136}Xe^*_{corr}} \times \frac{^{136}Xe^*_{corr}}{^{244}PuB_{244}{}^{136}Y_{244}} \tag{3.4}$$

The other fraction made of U-Xe gas bearing material does not contribute significantly to the abundance of radiogenic xenon atoms as it matches the isotopic composition Xe in Solar Wind for light isotopes and it is depleted in heavy isotopes (Pepin, 1991). The last terms in equations 3.3 and 3.4 are the same as the left-hand sides ones of equations 3.1 and 3.2. For the same quantity of total xenon gas, the proportions of radiogenic xenon in AVCC material are different from those of the corrected Earth's atmosphere (Avice and Marty, 2014; Pepin, 1991). Numbers in equations 3.5 and 3.6 are estimated by computing the excess of ^{129}Xe and ^{136}Xe in each component (AVCC and corrected atmosphere) relative to the isotopic composition of Xe in Solar Wind (Meshik et al., 2014) after correction for the isotopic fractionation of the chondritic and atmospheric components relative to the SW composition (Marrocchi et al., 2011).

$$^{129}Xe^*_{AVCC} = 0.87 \times ^{129}Xe^*_{corr} \tag{3.5}$$

$$^{136}Xe^*_{AVCC} = 5.9 \times ^{136}Xe^*_{corr} \tag{3.6}$$

Using the above relationships, the third term in the constraint equations is re-written as a function of F only:

$$\frac{1 - e^{-\lambda_{129} t_{GI}}}{D} + e^{-\lambda_{129} t_{GI}} + 0.14 \times F = 0.17 \tag{3.7}$$

$$\frac{1 - e^{-\lambda_{244} t_{GI}}}{D} + e^{-\lambda_{244} t_{GI}} + 3.3 \times F = 0.56 \tag{3.8}$$

Figure 3.5 describes the relations between the three parameters of the model (t_{GI}, D and F). Of course, it is not possible to evaluate the exact timing of the giant impact by using only these two equations governing the three parameters. Interestingly, Fig. 3.5(a) demonstrates that only a minor fraction of the late veneer had an AVCC-Xe composition otherwise the time of last giant impact would have switched rapidly to very high values >120 Ma in disagreement with other estimations of the age of the giant impact (Jacobson et al., 2015). This result means that, if the late veneer delivered matter to the Earth, it was enriched in Xe and depleted in iodine (producing ^{129}Xe). This may correspond to a cometary delivery since these objects have high gas/silicate ratios. Figure 3.5(b) demonstrates that, if the atmosphere was only partially removed (Genda and Abe, 2003) during the final giant impacts, the age of 40 (+20/-10) Ma was underestimated.

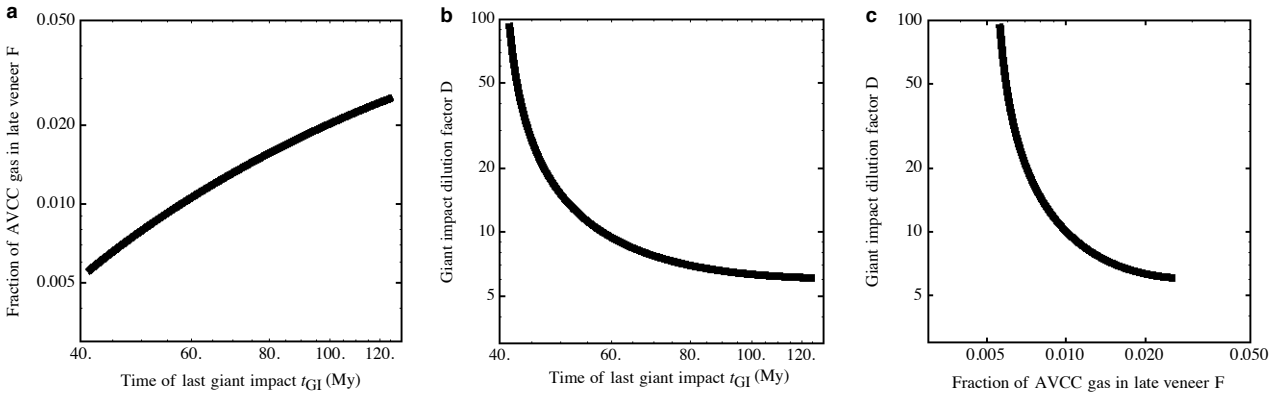

Fig. 3.5: Influence of the mass of the late veneer accreted on Earth and of the dilution factor induced by the giant impact on the time of the giant impact recorded in I-Pu-Xe systematics.

Even if this is a first-order simple model, it demonstrates that correct I-Pu-Xe closure ages can be estimated only if the amount of atmosphere removed during giant impacts and the composition and amount of the matter accreted by the Earth during the final stages of accretion are known. However, it must be noticed that the model presented in the previous section (Avice and Marty, 2014) was focused on taking into account the progressive escape of Xe atoms from the atmosphere to the outer space. Some modifications are now needed to consider partial removal of the atmosphere during impacts and effects of the addition of the late veneer to the Earth's atmosphere/mantle system.

A second important and recent observation is that the study presented in section 3.1 demonstrates that mantle Xe has a chondritic origin and is different from the atmosphere probably derived from U-Xe (section 3.2). In the previous version of the model, U-Xe was first incorporated in the silicate Earth during accretion and subsequently vigorously degassed into the atmosphere. Because of the dichotomy between the mantle and the atmosphere (chondritic vs. U-Xe), the model needs to be modified in order to incorporate U-Xe in the atmosphere and Q-Xe or AVCC-Xe in the silicate Earth. Subsequent degassing of radiogenic (^{129}Xe) and fissiogenic ($^{131-136}$Xe) products from the silicate Earth would also have carried an AVCC-Xe component. This may create a major issue since mixing AVCC-Xe with U-Xe (depleted in ^{136}Xe relative to SW-Xe) in the atmosphere may have enhanced the abundance of non-fissiogenic atmospheric ^{136}Xe. One way to circumvent this issue would be to escape a major part of a primitive atmosphere degassed by the mantle and, then, to bring a volatile-rich body with a U-Xe like composition to the Earth's atmosphere.

Chapter 4

Conclusions and Perspectives

Results of this study, and described in papers listed in Chapter 3, deal with the different origins of xenon and volatile elements in both the mantle and the atmosphere. They also put important constraints on the elemental and isotopic composition of noble gases and nitrogen in the Archean atmosphere and on the long-term evolution of atmospheric xenon. This final Chapter aims to summarize and detail these findings in order to build a coherent picture of the origin(s) and evolution of volatile elements on Earth. Some research opportunities relevant to solve the remaining issues are presented at the end of the Chapter.

Contents

4.1 Main Results of this Study

The outstanding issues which orientated this study were: What is/are the origin(s) of Xe on Earth? What is the isotopic composition of the ancient atmosphere? and what is the evolution this isotopic composition with time?

High-precision analyses of nitrogen and noble gases, specially xenon, contained in ancient quartz samples (3.2 Ga to 500 Ma) permit to answer, at least partially, these three questions.

Isotopic ratios of Xe contained in samples from Barberton (3.2 Ga) and determined with a precision at the permil level demonstrate that the precursor of Archean atmospheric xenon had an isotopic composition similar to the theoretical U-Xe (Pepin, 1991). This result is illustrated in Fig. 4.1(a) (extracted from paper in section 3.2 of Chapter 3) where only the mass-related fractionation of U-Xe followed by the addition of products of the spontaneous fission of ^{238}U can reproduce the isotopic composition of Xe measured in Barberton quartz samples. However, U-Xe has never been measured in any extraterrestrial material. Such an unusual starting composition might reflect a different nucleosynthetic mix for this component compared to other known Solar System components and comets could be the carrier phase of this composition. Conversely, isotope systematics on mantle-derived gases demonstrates that mantle Xe has a Chondritic, not Solar nor U-Xe, precursor. There is thus a dual origin of Xe on Earth: Chondritic Xe in the silicate Earth and U-Xe

in the atmosphere. This dichotomy for the origin of terrestrial Xe probably reflects the contribution of at least two cosmochemical sources (chondrites and maybe comets) to the budget of terrestrial heavy noble gases (Ar, Kr, Xe).

Precise results for Xe in Barberton samples permit also to compute a degassing rate of the mantle of 9 $\pm$ 5 mol.a^{-1} (1σ) of $^{129}Xe_I$ during the last 3.2 Ga. This degassing rate is far higher than the modern one (0.45 $\pm$ 0.02 mol.a^{-1}), maybe for two reasons. Firstly, the modern degassing rate is computed for the upper mantle only (Bianchi et al., 2010). However, the long-term degassing rate, determined for the first time in this study, takes into account the total input from the Earth's mantle during the last 3.2 Ga. Plume-related magmatism, degassing the deep mantle, might thus have contributed significantly to this high degassing rate. Secondly, the high heat flux produced by radioactivities in the early silicate Earth (Korenaga, 2008) may have maintained a higher convection regime in the past compared to Present promoting degassing of Xe from the Earth's interior.

This study permitted also to precisely define the elemental and isotopic compositions of other noble gases (Ar, Kr) and nitrogen in the 3.2 Ga-old atmosphere. Firstly, the partial pressure of N_2 in the Archean atmosphere was at least similar or maybe even lower than in the modern atmosphere. This results is in agreement with previous studies (Marty et al., 2013) excluding a higher partial pressure of N_2 as a solution to the faint young Sun paradox. Furthermore, the isotopic composition of nitrogen in the Archean atmosphere was probably similar to the modern one ($\delta^{15}N = 0$ ‰) demonstrating the presence of a magnetic field protecting atmospheric nitrogen from ionization and escape as such an escape would have modified the isotopic composition of atmospheric nitrogen. An Archean atmospheric $^{40}Ar/^{36}Ar$ ratio of 200 $\pm$ 58 (2σ) is in agreement with models calling for an intense crustal extraction between 3.8 and 2.5 Ga (Pujol et al., 2013b). Finally, krypton has an isotopic composition similar to the modern atmosphere demonstrating that the isotopic fractionation recorded for Xe is specific to this noble gas.

Xe contained in samples of ages comprised between 3.2 Ga and 2.1 Ga presents an isotopic composition intermediate between those of U-Xe and of the modern atmosphere. This evolution is reported in Fig. 4.1(b) (extracted from the paper in section 3.3 of Chapter 3). New results from this study (color-filled circles) constrain the evolution of the isotopic fractionation of atmospheric Xe (blue dashed-line) with a much higher precision than in previous studies. Xe isotope fractionation marked a pause for at least 400 Ma between 3.2 Ga and 2.7 Ga with an isotopic fractionation of 13 $\pm$ 2 ‰.u^{-1} (2σ) relative to the modern atmosphere, then evolved again to reach the modern-like atmospheric Xe composition around 2.0 Ga.

Xenon, similarly to sulfur (Farquhar and Wing, 2003), shows a secular isotope evolution during the Archean that ended up at the Archean-Proterozoic transition. The Xe isotope evolution was maybe the result of interactions between EUV photons from the young Sun and the electronic structure of xenon (through ionization), in which the rise of atmospheric oxygen might have played a role, either by killing organic haze able to trap fractionated Xe (Hébrard and Marty, 2014), and/or by neutralizing xenon rapidly before Xe ions could reach the exobase. As hydrogen escape might have driven the progressive oxygenation of the Earth's atmosphere (Zahnle et al., 2013), the evolution of the fractionation of Xe might be an indirect tracer of this major change in Earth's geological history. A theoretical framework for escape and isotopic fractionation of Xe is proposed during which escaping hydrogen ions are lifting xenon ions. Even if it requires further modeling, it appears promising to explain the unique isotopic evolution of atmospheric xenon among other volatile elements.

Most of the results obtained during this study call for a contribution of volatile-rich material during the last stages of Earth's accretion and the two papers in sections 3.2 and 3.3 of Chapter 3 propose a cometary contribution to the Earth's atmosphere to explain the peculiar starting isotopic composition of atmospheric Xe (U-Xe) and the dichotomy between mantle Chondritic Xe and atmospheric Xe. The next section is focused on the test of this hypothesis.

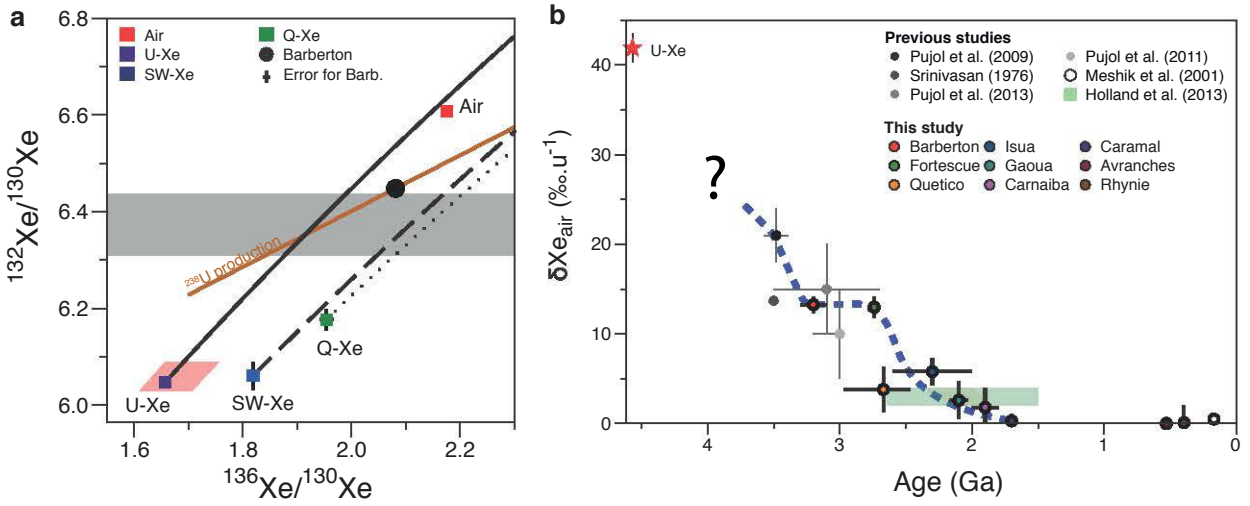

Fig. 4.1: Main results of this study. (a) Three-isotope plot demonstrating the need for U-Xe as the starting isotopic composition of the Earth's ancient (3.2 Ga-old) and modern atmosphere. Errors at 2σ. (b) Evolution of the isotopic fractionation of atmospheric Xe with time. The question mark indicates the uncertainty on the mode of transition from U-Xe to an isotopically fractionated 3.5 Ga-old atmospheric Xe. Errors at 1σ.

4.2 The Potential Contribution from Comets

The paper presented in section 3.2 of Chapter 3 demonstrates that atmospheric Xe cannot be derived from Chondritic or Solar sources. The starting isotopic composition of the Earth's atmosphere was similar to the theoretical U-Xe component (Pepin, 1991). This isotopic composition, depleted in the r-process nuclides ^{134}Xe and ^{136}Xe, probably originated from a different nucleosynthetic mix compared to the Chondritic or Solar components. Comets are objects from the outer regions of our solar system that might carry such an unusual starting isotopic composition since some of them may have formed nearby other stars in the Sun's birth cluster and have been subsequently captured by our Sun (Levison et al., 2010). But how does a cometary contribution to the Earth's atmosphere fit with the abundance and isotopic composition of volatile elements on Earth?

Marty and Meibom (2007) partly answered this question by using a simple mass balance model and concluded that 0.5 % of cometary objects in the Terrestrial Late Heavy Bombardment (TLHB) (2×10^{23} g) is sufficient to bring all noble gases (Ne, Ar, Kr, Xe) in the Earth's atmosphere (Fig. 4.2) without altering the terrestrial D/H and ^{15}N/^{14}N ratios (elevated in comets compared to the Earth's atmosphere, see section 1.1.1). However, this study was based on estimates of the Ar/H_2O ratio in comets inferred from experiments during which noble gases were trapped in growing amorphous ice. The absence of a direct measurement of this ratio in comets prevented to confirm the cometary origin of terrestrial noble gases.

The ESA Rosetta space probe orbiting around comet 67P/Churyumov-Gerasimenko (67P/C-G) provides an unique opportunity to further explore this hypothesis of a cometary contribution to the Earth's atmosphere. Recently, the ROSINA mass spectrometer on-board the Rosetta spacecraft measured a D/H ratio of $(5.3 \pm 0.7) \times 10^{-4}$ (Altwegg et al., 2015) as well as a Ar/H_2O ratio of (0.1 to 2.3) $\times 10^{-5}$ (Balsiger et al., 2015) for gases emitted by the coma. These in-situ measurements of cometary D/H and Ar/H_2O ratios permit to put constraints on the amount of cometary matter potentially delivered to the Earth's atmosphere. Results of this mass balance are presented in a co-authored paper (Marty et al., 2016) published in 2016 in *Earth and Planetary Science Letters* and placed in Annexe 5.4. Main results of this study are presented below.

One of the major outcomes of this study is that, based on isotope compositions, any cometary contribution to the Earth's water, carbon and nitrogen inventories must have been minor. Figure 4.3 (Marty et al. (2016);

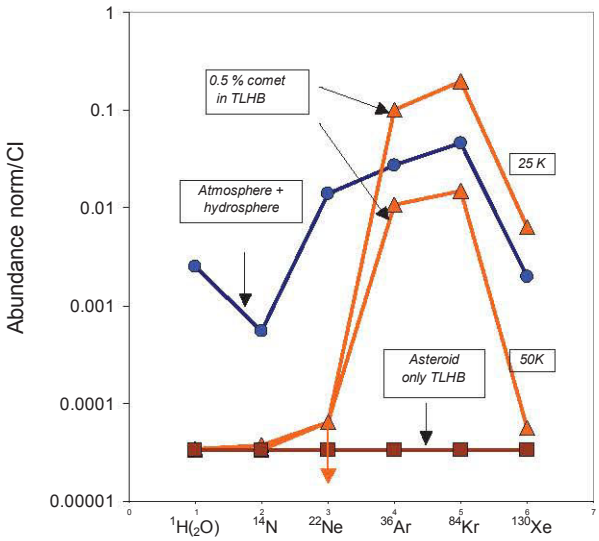

Fig. 4.2: Effect of the Terrestrial Late Heavy Bombardment (2×10^{23} g) containing 0.5 % comet on the volatile abundances of the atmosphere normalized to Chondritic. Two different formation temperatures for cometary material are considered (25 K and 50 K). Note that a pure asteroidal contribution during the late heavy bombardment has a negligible contribution to the Earth's atmosphere and hydrosphere. Adapted from Marty and Meibom (2007).

Annexe 5.4) represents the percent of cometary contribution to explain the Ar/H_2O (a) and Ar/N (b) ratios of the Earth's atmosphere by a mixing between Chondritic and cometary material. In this model, less than 1 % of water and maximum few percent of nitrogen can have been delivered by comets.

However, a cometary contribution to the terrestrial atmosphere might have been significant, at least for argon and maybe for all noble gases, since the Rosetta space probe measured a high Ar/H_2O ratio of 0.1 to 2.3×10^{-5} for gases emitted by comet 67P/C-G (Balsiger et al., 2015). Figure 4.4(a) (Marty et al. (2016); Annexe 5.4) represents the effect on terrestrial reservoirs of a Terrestrial Late Heavy Bombardment (2×10^{23} g) composed of 10 % comets and 90 % primitive meteorites (carbonaceous chondrites). This late addition has only a negligible effect on terrestrial C, N and water abundances but the whole amount of atmospheric argon might have been contributed to the Earth's atmosphere during this final stage of accretion. The absence of measurements of the Xe/Kr/Ar ratios in comets prevents a clear estimation of the amount of Xe delivered to the Earth during the final stages of terrestrial accretion. However, rough estimates have been computed during this study based on experimental results of Xe trapping in amorphous ice (e.g. Notesco (2003)) and on numerical models of clathrates formation (Mousis et al., 2010). Results are presented in Fig. 4.4(b) and tables with abundances of noble gases in comets appear at the end of the paper in section 3.2 of Chapter 3. If cometary ices are composed of clathrates, the TLHB would have overwhelmed by a factor of 40 the whole atmospheric budget of Xe corrected for subsequent escape. This not too much an issue here since there is no certainty on the starting abundance of atmospheric Xe. If Xe is trapped in amorphous ice, the TLHB would not have been sufficient to deliver all atmospheric Xe. Based on these estimates, a cometary contribution to the budget of atmospheric Xe cannot be ruled out. This possible cometary contribution to the whole budget of atmospheric noble gases may explain one major result of this study, that is, the dichotomy for the origin of terrestrial Xe (Chondritic Xe in the mantle and U-Xe in the atmosphere). The exotic component for the Earth's atmosphere could have been carried out by icy bodies initially located in the outer regions of the solar system. The dichotomy between mantle Chondritic Xe and atmospheric fractionated U-Xe would thus be a record of the change in the nature of extraterrestrial matter contributed to the growing Earth. The proto-Earth would have started accreting Chondritic-like material and its surface would have been subsequently contributed by volatile-rich cometary bodies carrying U-Xe.

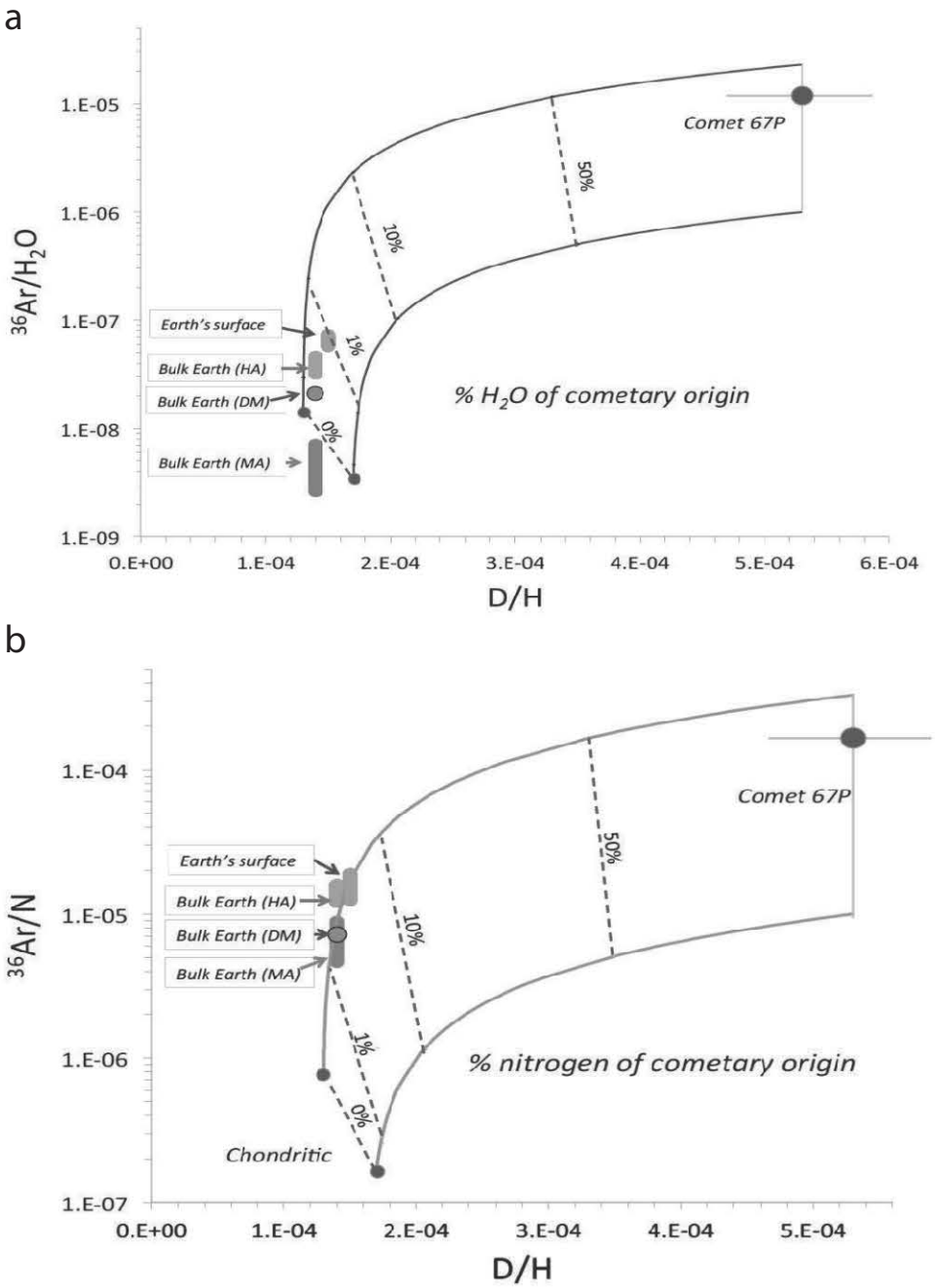

Fig. 4.3: $^{36}Ar/H_2O$ (a) and $^{36}Ar/N$ (b) versus D/H mixing diagrams bewteen cometary and Chondritic end-members. HA, DM and MA are the bulk Earth estimates from Halliday (2013), Dauphas and Morbidelli (2014) and Marty (2012), respectively. a: Dotted lines indicate the percentage of Terrestrial water of cometary origin. b: Dotted lines indicate the percentage of Terrestrial nitrogen of cometary origin. See details on the reservoir inventories in Marty et al. (2016) (Annexe 5.4).

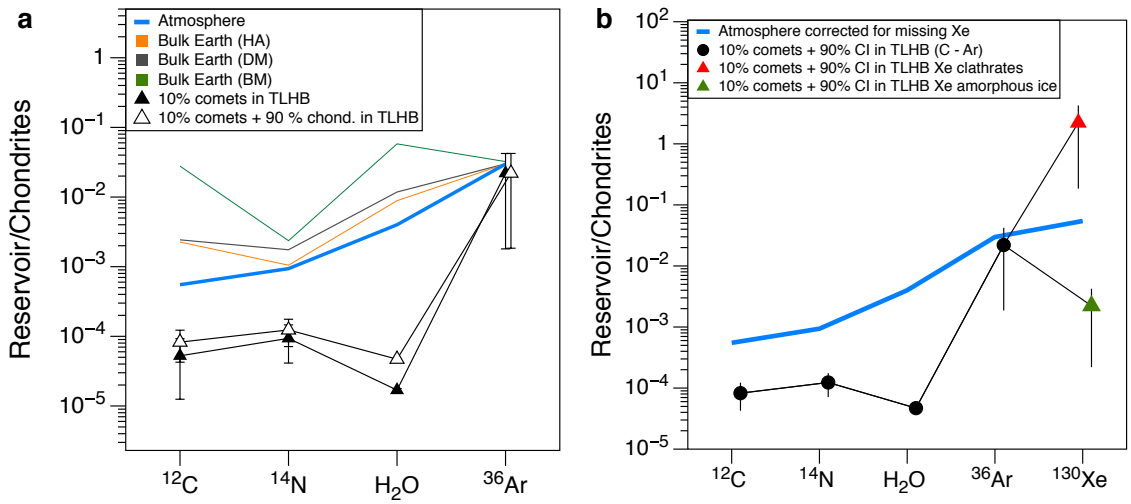

Fig. 4.4: Effect of a cometary contribution to the budget of volatile elements on Earth. (a) Abundances of C, N, H_2O and ^{36}Ar in the atmosphere sensu largo (air + oceans + sediments), normalized to Chondritic. For comparison bulk Earth inventories from Halliday (2013), Dauphas and Morbidelli (2014) and Marty (2012) are represented. A $\simeq$10% comet contribution in the TLHB fits well the ^{36}Ar inventory of the atmosphere, without impacting the isotope compositions of C, N and H. Adapted from Marty et al. (2016). (b) Effect of a $\simeq$10% cometary contribution in the TLHB for the budget of atmospheric ^{130}Xe once corrected ($\times$20) for subsequent long-term escape. If cometary ice is in the form of clathrates, this cometary contribution would have overwhelmed the budget of atmospheric Xe. Conversely, if cometary ices are composed of amorphous ice, such a cometary contribution would have not been sufficient to bring all terrestrial Xe. See papers in section 3.2 of Chapter 3 and in section 5.4 (Annexes) for details on the budget of volatile elements in terrestrial reservoirs and on the effect of this late addition.

4.3 An Emerging Picture for the Origin and Evolution of Terrestrial Xenon

Major outcomes of this PhD work and data from the literature can be used to build a scenario for the origins and evolution of terrestrial Xe. This scenario is schematically represented in Fig. 4.5 and can be divided in 5 major steps:

- A: Initial state. The Earth system started with Chondritic Xe in the undifferentiated mantle (see paper in section 3.1 of Chapter 3). Some ^{129}Xe(I) was probably transferred early to the Earth's atmosphere during vigorous degassing of the magma ocean following giant impacts;

- B: The giant impact phase ended with the Moon-forming event that removed most of the Earth's atmosphere. I-Pu-Xe systematics (Avice and Marty, 2014) corrected for subsequent selective Xe escape (step D) dates this event at 4.54 to 4.47 Ga (30 to 100 Ma after the solar system formation). Estimates of the age depend on the amount of loss during the giant impact phase and on the amount of Chondritic Xe delivered during the late veneer (see Avice and Marty (2014) and discussion in section 3.4.1 of Chapter 3).

- C: A late contribution, potentially containing cometary material, might have delivered the whole budget of atmospheric Ar (Marty et al. (2016); Annexe 5.4) and maybe Xe with a starting isotopic composition similar to U-Xe (paper 3.2 in Chapter 3). This cometary contribution might have taken place as late as 3.8 Ga when the Terrestrial Late Heavy Bombardment ended. This time corresponds to the establishment of the dichotomy for the origin of Xe on Earth: Chondritic Xe in the Earth's mantle and U-Xe in the Earth's atmosphere. For the mantle, two reservoirs isolated from each other at least for Xe. The time of isolation might be around 4.45 Ga even if it highly depends on the initial iodine content of the mantle. Isotope systematics also demonstrates that the air component dominating Xe

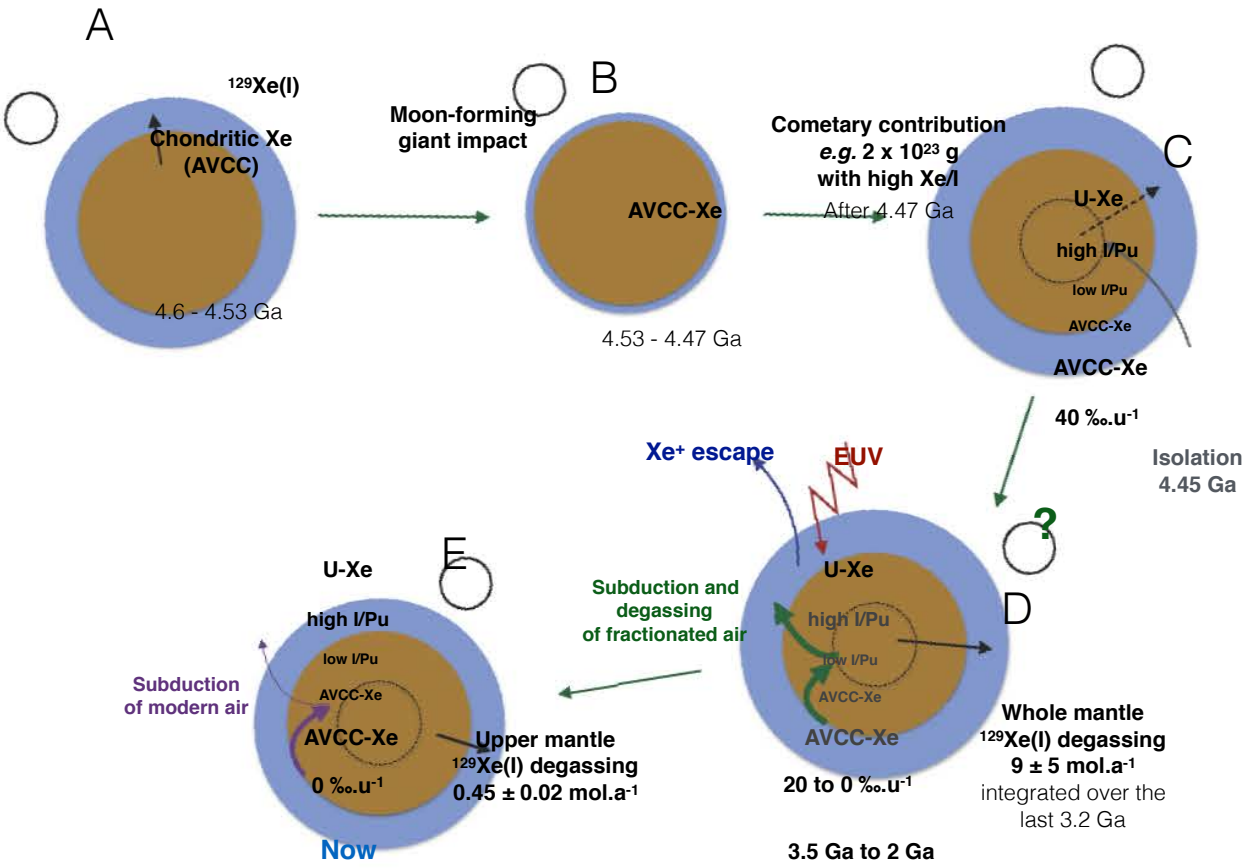

Fig. 4.5: Schematic view of the scenario proposed for the origin and evolution of terrestrial xenon. See text for details on steps A, B, C , D and E. The Earth's core is not represented. Brown: mantle. Blue: atmosphere. Not to scale.

in mantle-derived samples has an isotopic composition similar to the modern atmosphere (see paper in section 3.1, Parai and Mukhopadhyay (2015)). It means that if ancient air with fractionated Xe had been introduced in the upper mantle by early onset of subduction (e.g. Smart et al. (2016)), it was subsequently degassed (green arrows) suggesting several mantle overturns as shown, for example, by the low $^{136}Xe_{Pu}/^{136}Xe_{U}$ ratio of this reservoir. Whatever the iodine content, the upper mantle presents a I (volatile)/Pu (refractory) ratio higher than the lower mantle suggesting a more important contribution from volatile-rich material to the upper mantle during the final stages of Earth's accretion.

- D: The mode of transition from an atmosphere with an unfractionated U-Xe to an isotopic fractionation around 20 ‰.u^{-1} at 3.5 Ga is not known (green question mark in Fig. 4.5). Analyses of Xe contained in samples of various ages permit to define the evolution of the isotopic composition of atmospheric Xe. Details on the isotopic fractionation mechanism are still missing but an hydrogen escape mechanism coupled with ionization of Xe by the high EUV flux from the young Sun is tentative (paper 3.3 in Chapter 3). The mechanism responsible for the isotopic fractionation marked apparently a pause between 3.2 and 2.7 Ga and ended around 2 Ga. This is roughly the epoch of oxidation of the Earth's atmosphere and it is tempting to see a link between the evolution of the isotopic composition of atmospheric Xe and the onset of high oxygen levels in the atmosphere since hydrogen escape might have driven both processes (Zahnle et al., 2013; Zahnle, 2015). A low ^{129}Xe(I) excess for the 3.2 Ga atmosphere compared to the modern one indicates a much more vigorous degassing rate of ^{129}Xe(I) from the mantle for the last 3.2 Ga (9 ± 5 mol.a^{-1}) than at Present (0.42 ± 0.05 mol.a^{-1}).

- E: The modern Earth system is an integration of all events and processes described in steps A to D. Atmospheric Xe originates from U-Xe, isotopically fractionated by 40 ‰.u^{-1}. The Earth's mantle contains Chondritic gases and is contaminated by modern atmospheric Xe (purple arrow) through subduction (Parai and Mukhopadhyay, 2015) and continues to degas radiogenic ^{129}Xe(I).

Results obtained during this PhD work are thus useful to refine our views on the origins and evolution of terrestrial volatile elements. They demonstrate the need for U-Xe to build the Earth's atmosphere. Some volatile elements on Earth, for example Xe in the mantle, might have been brought by Chondritic material during Earth's accretion (Marty, 2012). However, a cometary input, already proposed by several authors (Marty and Meibom, 2007; Dauphas, 2003; Marty et al., 2016), with a starting isotopic composition similar to U-Xe appears necessary. A long-term isotopic evolution of atmospheric Xe demonstrates that the isotopic fractionation of atmospheric Xe cannot have been established during the first hundreds of Ma of Earth's history as originally proposed (Pepin, 1991; Dauphas, 2003; Tolstikhin and O'Nions, 1994). Hydrogen escape that might have lasted for long, driving Earth's oxygenation (Zahnle et al., 2013), appears to be viable process for escaping Xe ions to space (Zahnle, 2015).

4.4 Open Issues and Research Perspectives

Although our knowledge on the origin and evolution of terrestrial volatile elements is progressing through the study of Earth's xenon, some shadow zones remain. This section presents some remaining questions and research opportunities that would probably help to solve these issues.

The exact time of the end of the isotopic fraction of atmospheric xenon remains unknown because of the difficulty to precisely date the quartz samples containing Xe by the Ar-Ar method. Indeed, such samples generally have low potassium contents and high quantities of ^{40}Ar excess. Analyses of barite samples are promising here since these crystals contain significant amounts of Xe and can be dated by using a combined U-Ba-Xe dating technique (Pujol et al., 2009). A collection of barite samples of various ages has been collected by A. Hofmann (Univ. of Johannesburg, South Africa) and is readily available for step-heating

experiments. A new induction furnace has been recently developed at CRPG and can easily heat these samples to temperatures higher than 1600°C, the temperature of barite dissociation. Purification issues due to the large amount of sulfur that transformed into corrosive H_2S in the purification line may be solved by using the on-line getter described in section 2.2 of Chapter 2 and already successfully tested on gases released during step-heating experiment on meteoritic sulfides.

On major remaining issue for *Xenology* is that the origin of U-Xe remains enigmatic. Estimates of ^{134,136}Xe depletions are only based on the hypothesis of starting solar $^{124-132}$Xe/^{130}Xe ratios for this component. This leaves space for a totally different nucleosynthetic mix for the starting isotopic composition of Xe. Comets are ideal candidates for carrying this unusual isotopic composition since some of these objects might have formed close to other stars and have subsequently been captured by our Sun (Levison et al., 2010). Is there a way to measure this starting isotopic composition free of all these isotopic fractionation and radiogenic/fissiogenic effects observed in the modern and ancient atmosphere? A preliminary study by Michel and Eugster (1994) demonstrated the presence of a trapped component in the Tatahouine diogenite, maybe originating from asteroid (4) Vesta (e.g. Mittlefehldt (2015)), released at 1200°C and very similar to U-Xe. A new step-heating experiment on 5 g of the same meteorite will be conducted in order to precisely determine the isotopic composition of this component.

The genetic relationship between Chondritic Xe (Q-Xe) and Solar Xe (SW-Xe) is still debated (e.g. Marrocchi et al. (2015); Meshik et al. (2014); Crowther and Gilmour (2013)). For light Xe isotopes ($^{124-130}$Xe) the only resolvable difference between the two components seems to rely on a ^{124}Xe depletion of Q-Xe relative to SW-Xe (Busemann et al., 2000; Meshik et al., 2014) even if an isotopic fractionation of Q-Xe relative to SW-Xe cannot be excluded (Kuga et al., 2015; Marrocchi et al., 2011). Furthermore, Q gases are ubiquitous in Chondritic meteorites but also in differentiated meteorites such as iron meteorites (Matsuda et al., 2005) and even in "Hypatia" a diamond-rich extraterrestrial pebble of unknown origin (Avice et al. (2015), Annexe 5.1). Much more work is needed here to understand the conditions of formation of Q gases from a gas of solar composition and to constrain the mode of survival of this Q component in melted differentiated bodies.

If one assumes that U-Xe has been delivered to the Earth's atmosphere by cometary objects, a precise determination of the relative abundances of heavy noble gases, Kr & Xe, relative to Ar and water in these objects is necessary. At this time, evaluation of Xe quantities brought by comets only relies on trapping ice experiments or on theoretical models of clathrates formation. Evaluation of these abundances in gases released by comet 67P/C-G would be possible by using the ROSINA mass spectrometer on-board of the Rosetta spacecraft. It is worth noting that, up to now, corrections of the abundance of atmospheric Xe rely on the assumption that there is a twenty fold depletion of Xe in the Earth's atmosphere. This is based on the comparison between the abundance pattern of noble gases in the Earth's atmosphere and in Chondritic meteorites. However, if atmospheric Xe has been brought by comets, there is space for a much higher initial abundance of Xe in the early atmosphere (see Fig. 4.4(b)). In that case, a moderate instantaneous fractionation during long-term escape of these large amounts of Xe would be sufficient to end up with the isotopic composition of the modern atmosphere.

Similarities between Martian and terrestrial xenon (comparable Kr / Xe ratios and isotopically fractionated Xe) are still intriguing. Measurements of the abundance and isotopic composition of xenon in the Venusian atmosphere would be decisive to definitively understand what are the mechanisms that built the peculiar abundance and isotopic composition of xenon in planetary atmospheres. There is, up to now, only an upper limit of 120 ppb for the abundance of Xe in the Venusian atmosphere and no data on its isotopic composition (Donahue et al., 1981). Measuring abundances and isotope compositions of atmospheric gases in the atmosphere of Venus has already been identified as the highest scientific priority for forthcoming spatial missions (Crisp et al., 2002).

Chapter 5

Annexes

Main work of this study and side-projects led to the publication or preparation of several articles listed in this chapter.

Contents

5.1 Article A comprehensive study of noble gases and nitrogen in "Hypatia", a diamond-rich pebble from SW Egypt, *published in 2015 in Earth and Planetary Science Letters, Vol. 432C, pp. 243-253.*

Earth and Planetary Science Letters 432 (2015) 243–253

Contents lists available at ScienceDirect

Earth and Planetary Science Letters

www.elsevier.com/locate/epsl

A comprehensive study of noble gases and nitrogen in "Hypatia", a diamond-rich pebble from SW Egypt

Guillaume Avice [a,*], Matthias M.M. Meier [b,a], Bernard Marty [a], Rainer Wieler [b], Jan D. Kramers [c], Falko Langenhorst [d], Pierre Cartigny [e], Colin Maden [b], Laurent Zimmermann [a], Marco A.G. Andreoli [f]

[a] CRPG-CNRS, Université de Lorraine, UMR 7358, 15 rue Notre-Dame des Pauvres, BP 20, 54501 Vandoeuvre-lès-Nancy Cedex, France
[b] Department of Earth Sciences, ETH Zürich, Clausiusstrasse 25, CH-8092 Zürich, Switzerland
[c] Department of Geology, University of Johannesburg, Auckland Park 2006, Johannesburg, South Africa
[d] Institut für Geowissenschaften, Friedrich-Schiller-Universität Jena, Carl-Zeiss-Promenade 10, D-07745 Jena, Germany
[e] Équipe de Géochimie des Isotopes Stables, Institut de Physique du Globe de Paris, Sorbonne Paris Cité, Univ. Paris Diderot, UMR 7154 CNRS, F-75005 Paris, France
[f] School of Geosciences, University of the Witwatersrand, PO Box 3, Wits 2050, South Africa

ARTICLE INFO

Article history:
Received 23 June 2015
Received in revised form 16 August 2015
Accepted 6 October 2015
Available online xxxx
Editor: C. Sotin

Keywords:
meteorites
noble gases
nitrogen
phase Q
graphite

ABSTRACT

This is a follow-up study of a work by Kramers et al. (2013) on a very unusual diamond-rich rock fragment found in the area of south west Egypt in the south-western side of the Libyan Desert Glass strewn field. This pebble, called Hypatia, is composed of almost pure carbon. Transmission Electron Microscopy (TEM) and X-ray diffraction (XRD) results reveal that Hypatia is mainly made of defect-rich diamond containing lonsdaleite and multiple deformation bands. These characteristics are compatible with an impact origin on Earth and/or in space. We also analyzed concentrations and isotopic compositions of all five noble gases and nitrogen in several ~mg sized Hypatia samples. These data confirm the conclusion by Kramers et al. (2013) that Hypatia is extra-terrestrial. The sample is relatively rich in trapped noble gases with an isotopic composition being close to the Q component found in many types of meteorites. $^{40}Ar/^{36}Ar$ ratios in individual steps are as low as 0.4 ± 0.3. Cosmic-ray produced "cosmogenic" ^{21}Ne is present in concentrations corresponding to a nominal cosmic-ray exposure (CRE) age of roughly 0.1 Myr if produced in a typical meter-sized meteoroid. Such an atypically low nominal CRE age suggests high shielding in a considerably larger body. In addition to the Xe–Q composition, an excess of radiogenic ^{129}Xe (from the decay of short-lived radioactive ^{129}I) is observed ($^{129}Xe/^{132}Xe = 1.18+/-0.03$). Two isotopically distinct N components are present, an isotopically heavy component ($\delta^{15}N \sim +20‰$) released at low temperatures and a major isotopically light component ($\delta^{15}N \sim -110‰$) at higher temperatures. This disequilibrium in N suggests that the diamonds in Hypatia were formed in space rather than upon impact on Earth ($\delta^{15}N_{atm} = 0‰$). All our data are broadly consistent with concentrations and isotopic compositions of noble gases in at least three different types of carbon-rich meteoritic materials: carbon-rich veins in ureilites, graphite in acapulcoites/lodranites and graphite nodules in iron meteorites. However, Hypatia does not seem to be directly related to any of these materials, but may have sampled a similar cosmochemical reservoir. Our study does not confirm the presence of exotic noble gases (e.g. G component) that led Kramers et al. (2013) to propose that Hypatia is a remnant of a comet nucleus that impacted the Earth.

1. Introduction

In 1996 a very unusual ~30 g sized pebble was found in the Libyan Desert Glass strewn field where abundant fragments of impact-related silica-rich glass are found (Barakat, 2012; Reimold and Koeberl, 2014). This brittle black stone (Fig. S1) consists of ~70 wt% carbon, and has a hardness comparable to diamond, reminiscent of carbonados. Kramers et al. (2013) named the stone "Hypatia" in honor of a 4th century female philosopher from Alexandria (Egypt). These authors performed an exploratory analytical study on Hypatia, including XRD, SEM, Raman spectroscopy, TEM, and analyses of C and noble gas isotopes motivated by the fact that this stone was found in the area of the Libyan Desert Glass (LDG), the origin of which remains enigmatic (Reimold and Koeberl, 2014). Noble gas isotope analysis is central to the study of

* Corresponding author. Tel.: +33 3 83 59 42 46.
E-mail address: gavice@crpg.cnrs-nancy.fr (G. Avice).

http://dx.doi.org/10.1016/j.epsl.2015.10.013
0012-821X/

meteorites because these rocks formed from multiple components with distinct noble gas isotopic signatures that help to constrain their origin and evolution. Among these components, the so-called Q phase dominates the budget of heavy noble gases (Ar, Kr Xe) in chondrites originating from the asteroid belt. Although the chemical nature (Marrocchi et al., 2015) and mode of formation (Kuga et al., 2015; Ott, 2014) of Q are debated, this component is chemically and isotopically fractionated relative to the isotopic composition of the Solar Wind (Meshik et al., 2014) possibly due to ionization processes (Marrocchi et al., 2011) and is ubiquitous in pristine to moderately metamorphosed chondrites (Busemann et al., 2000). Other minor noble gas components (e.g. the P3 and G components) are found in presolar materials (for example SiC) trapped in meteorites (Ott, 2014). These components are derived from sources external to the solar system and carry isotopic signatures characteristic of nucleosynthesis in stars. Kramers et al. (2013) concluded that Hypatia is extra-terrestrial, based on $^{40}Ar/^{36}Ar$ ratios as low as about 40. They noted that O/C ratios (0.19–0.51) in Hypatia are higher than in chondritic Insoluble Organic Matter (IOM). In addition, they reported that the trapped Ne, Kr, and Xe in Hypatia indicate the occurrence of the nucleosynthetic P3 and G components of presolar origin known from meteorites (Ott, 2014), while the Q (and HL) components ubiquitous in chondrites were absent in Hypatia. The combined evidence led them to conclude that Hypatia did not originate in the asteroid belt where chondrites likely formed. They suggested instead that it formed in a more external region of the solar accretion disk, such as the Kuiper Belt, where presolar components might be more abundant, i.e., that Hypatia could be of cometary origin. They further proposed that the airburst of the parent comet of Hypatia resulted in the formation of the Libyan Desert Glass. This interpretation was subsequently criticized by Reimold and Koeberl (2014), although a cometary origin for the Libyan Desert Glass has been advocated many times, starting with Urey's seminal paper (Urey, 1957).

In this work we extend the study by Kramers et al. (2013) with isotopic analyses of all five noble gases in several mg-sized fragments of Hypatia in two different laboratories (CRPG Nancy, France and ETH Zürich, Switzerland) and with a nitrogen isotope investigation performed both at CRPG (Nancy) and IPG-Paris. We also describe results from X-ray diffraction (XRD) experiments and transmission electron microscopy (TEM) observations performed at the University of Jena (Germany). An attempt to determine the oxygen isotopic composition in Hypatia by the Nancy Cameca 1280 ion probe failed because of the reduced size of oxygen-bearing phases and because of the presence of contaminants and important amounts of water. This new study confirms and provides new evidence for the earlier conclusion that Hypatia is a fascinating new type of extra-terrestrial material. In contrast to the exploratory work reported by Kramers et al. (2013), we did find noble gases with isotopic signatures closely resembling the Q component. We also found nitrogen with an isotopic signature clearly distinct from primitive chondrites and closely resembling those of various differentiated meteoritic materials. In particular, we compare our data with noble gas and nitrogen signatures in three known types of carbon-rich extraterrestrial materials: carbon-rich veins in ureilite meteorites, graphite nodules in iron meteorites, and carbon-rich lithologies in acapulcoites and lodranites, and we discuss a possible link of Hypatia with each of these materials.

2. Samples and methods

X-ray diffraction and Transmission Electron Microscopy (TEM) techniques used in this study are described in the supplementary material.

Table 1
Analytical techniques and list of chemical species analyzed in Hypatia samples during this study.

Samples Id.	Mass (mg)	Analyzed species	Extraction method
H-N1	8.52	N_2, Ne, Ar	stepwise CO_2 laser extraction
H-N2	1.07	–	–
H-N3	2.35	–	–
H-N4	8.4	Ar, Kr, Xe	stepwise induction furnace extraction (400–2200 °C)
H-Z1	1.0	He, Ne, Ar	single step IR laser extraction
H-Z2	2.9	–	–
H-Z3	2.9	–	single step furnace extraction
H-Z4	1.0	–	–
H-Z5	2.8	–	–
H-P1	1.6	N_2, C	on-line combustion
H-P2	1.6	N_2, C	–

Samples analyzed in Nancy labeled "H-N…", samples analyzed in Zürich labeled "H-Z…", samples analyzed in Paris labeled "H-P…". In all cases, all stable isotopes of the listed species were analyzed, although in some cases large blank corrections inhibited a meaningful determination of gas amounts and/or isotopic ratios (see Results section).

2.1. Noble gas and nitrogen analyses

Table 1 indicates the samples analyzed and the analytical techniques used in Nancy, Zürich and Paris. Samples are from the same group of samples (≈1 g) as used by Kramers et al. (2013). In Nancy, noble gases and nitrogen were extracted conjointly in samples H-N1, H-N2 and H-N3 upon heating in high-vacuum with an infra-red (IR) CO_2 laser (Humbert et al., 2000). Extracted gases were subsequently split into an aliquot for nitrogen analysis and another one for noble gas analysis. The nitrogen was purified in a glass line and analyzed using a VG 5400 mass spectrometer following the procedure reported in Zimmermann et al. (2009). The noble gas aliquot was purified using Ti-sponge getters and Ar was trapped on charcoal held at liquid N_2 temperature. Following N analysis, Ne and Ar were sequentially analyzed using the same mass spectrometer. Sample H-N4 was heated in five extraction steps (400, 850, 1400, 1800 and 2200 °C) in a Ta crucible using an induction furnace. Extracted gases were purified on three Ti-sponge getters. Xe and Kr were trapped on a quartz tube cooled to 77 K. Xe and Kr were then sequentially analyzed on a Helix MC Plus mass spectrometer. Mass spectrometer sensitivity was calibrated with known amounts of atmospheric noble gases following the same procedure as reported in Marty and Zimmermann (1999).

In Paris, the nitrogen content and isotope composition of two Hypatia diamond samples were investigated following methods described previously (Boyd et al., 1995). Importantly, the two analyzed Hypatia pieces (about 1.5 mg) were pre-combusted, over 6 h at 600 °C in order to remove any organic matter and/or graphite and, therefore, ensuring that the analyzed carbon phase consisted essentially of pure diamonds. The two samples were weighed before their analysis and CO_2 yield was used to determined the abundance of carbon.

In Zürich, noble gases were extracted from samples Z1 and Z2 with a 30 W continuous-wave IR laser ($\lambda = 1064$ nm) heating the samples for about 60 s (Vogel et al., 2003). Noble gases in samples Z3, Z4, and Z5 were extracted at ∼1800 °C during 30 min in a Mo crucible heated by electron bombardment. For all analyses, the respective sample chamber had been preheated at 100 °C for ∼24 h to remove adsorbed atmospheric gases. Extracted gases were cleaned by various getters before Ar was frozen onto charcoal at liquid nitrogen temperature. The He–Ne and the Ar fractions were sequentially analyzed in a custom-built sector-field noble gas mass spectrometer equipped with an ion counting multiplier and a Faraday detector. Additional details of the analytical procedure are given in Wieler et al. (1989). An additional step after the main

extraction was done for samples H-Z1, H-Z2, and H-Z3 and demonstrated complete gas extraction during the main step. Blank gas amounts for the laser extractions (H-Z1 and H-Z2) were determined by firing the laser at an empty spot of the sample holder for 60 s. For the furnace extractions (for H-Z3 to H-Z5) a piece of Al foil of the same mass as used to wrap samples was melted at the same temperature and for the same duration as the samples. Mass spectrometer sensitivity was calibrated with known amounts of pure standard gases as described in Heber et al. (2009).

3. Results

3.1. XRD results and TEM observations

The X-ray diffraction pattern of Hypatia is characterized by broad, low-intensity peaks (Fig. S2) indicating the poor crystallinity of the material. A comparison with the pattern of well-crystallized synthetic diamond shows that the main X-ray reflections in the pattern of the Hypatia sample are fully compatible with the diamond structure. X-ray diffraction tails on both sides of the 111 diamond peak were also observed and can be interpreted as the $10\bar{1}0$ and $10\bar{1}1$ peaks of the hexagonal high-pressure polymorph lonsdaleite. The position of the 0002 peak of lonsdaleite would thereby coincide with the 111 peak of diamond. The lattice parameter a refined from the X-ray diffraction pattern of the Hypatia diamond is 3.57 Å, identical to the lattice constant of normal diamond. Besides diamond and lonsdaleite no other phase could be identified on the basis of X-ray diffraction.

X-ray line broadening analysis of Hypatia was additionally used to obtain clues to the causes for the poor crystallinity. This analysis revealed that the limited long-range order of Hypatia diamond is not only due to small crystallite size, but is also partly attributable to considerable internal strain, indicative of numerous lattice defects.

The defect microstructure was, therefore, examined by TEM. Conventional TEM imaging shows that Hypatia is composed of numerous diamond grains with sizes on the order of a few micrometers. Some grains exhibit multiple 100 nm wide bands with alternating diffraction contrast (Fig. S3). Although this alternating contrast suggests a twin configuration, electron diffraction disproves this possibility for the diamond structure. Similar multiple bands have only been found in impact diamonds from various craters and could be attributed to shock-induced mechanical twins of the graphite precursor (Langenhorst et al., 1999). The multiple twinning must have occurred just before the solid-state transformation when the shock wave entered into graphite (Langenhorst and Deutsch, 2012).

High-resolution TEM images reveal that diamond is associated with some graphite discernible by the typical 0001 spacing of 3.35 Å. The graphite can be onion-shaped and covers the surface of diamond (see Fig. S4 in supplementary material). The graphite-like areas are mostly <10 nm in size explaining why they were not detected by X-ray diffraction.

The coating of diamond surfaces with graphite and the absence of an epitactic orientation relationship between the two phases (e.g. $(0001)_{\text{graphite}}$ does not coincide with $(111)_{\text{diamond}}$) suggest that the graphite flakes are probably a result of retrograde annealing of diamond.

3.2. Noble gas and nitrogen results

Concentrations and isotopic compositions of noble gases and nitrogen extracted in Nancy, Zürich and Paris are shown in Tables 2, 3 and S1 (supplementary material) respectively. Abundances and isotopic composition of nitrogen and carbon extracted in Paris are shown in supplementary material (Table S1). In this section we will first discuss isotopic compositions and then gas abundances and elemental ratios.

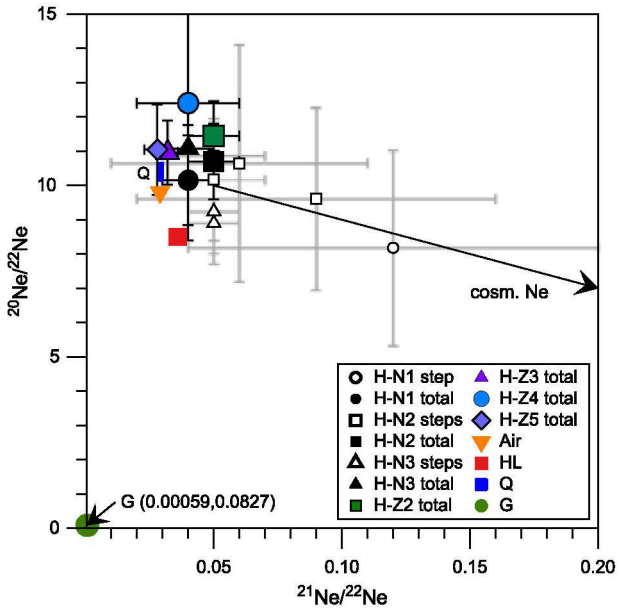

Fig. 1. Isotopic composition of neon in Hypatia samples. Empty symbols are for individual heating steps and filled symbols for bulk samples. The isotopic compositions of Ne in Earth's atmosphere, Ne–HL, Ne–Q and Ne–G are shown as references (Ott, 2014). Arrow shows the tendency toward the cosmogenic component ($^{21}Ne/^{22}Ne \approx 0.9$; Leya et al., 2001). Errors at 1σ.

3.2.1. Helium

The $^{3}He/^{4}He$ ratios in all five Hypatia "Z" samples are very similar to values observed for He-Q, with a weighted average of $(1.55 \pm 0.11) \times 10^{-4}$. While this value is slightly higher than the "canonical value" of He-Q of $\sim 1.23 \times 10^{-4}$ (Busemann et al., 2000; Ott, 2014) values around $\sim 1.6 \times 10^{-4}$ for He-Q-rich samples have also been reported (Wieler et al., 1991). Remarkably, the measured $^{3}He/^{4}He$ ratios do not vary systematically with ^{4}He concentration (the somewhat higher value of sample H-Z1 of 2.1×10^{-4} has an untypically large uncertainty). This also suggests that He in Hypatia is essentially trapped and of Q origin, as otherwise contributions from cosmic-ray produced (^{3}He-rich) and radiogenic ^{4}He in each of the samples would have to add up fortuitously to a Q-like ratio. This seems very unlikely, although it needs to be noted that the $^{4}He/^{36}Ar$ ratios in Hypatia ($\sim$15–20) are higher than the mean value of $\approx$5 for Q (Ott, 2014). However, $^{4}He/^{36}Ar$ ratios in Q vary over a wide range of values (1–11; Busemann et al., 2000). To explain this latter observation by variable concentrations of radiogenic ^{4}He in different pieces of Hypatia would require U and Th concentrations of roughly half the values in ordinary chondrites (assuming an age of Hypatia of 4.56 Ga). This is unlikely given that only a few percent of Hypatia is non-carbonaceous material. Together with the fact that all analyzed samples show similar $^{3}He/^{4}He$ ratios, we can thus exclude that the Q-like value of He in Hypatia is due to radiogenic and cosmogenic He fortuitously adding up. The majority of the He in Hypatia must be trapped with an isotopic composition close to that of He-Q. This means that a reliable concentration of cosmogenic ^{3}He cannot be easily derived in any of our samples, as the exact isotopic composition of the trapped Q-like He remains unknown. See next section for a discussion about the abundance of cosmogenic ^{3}He.

3.2.2. Neon

All temperature steps and total extractions are listed in Tables 2 and 3, and the totals and some selected data from individual steps

Table 2
Data of Ne, Ar, and N_2 measured in Hypatia samples H-N1 to H-N3. Errors at 1σ.

Sample	Extraction step	^{22}Ne (mol/g)	±	^{20}Ne/^{22}Ne	±	^{21}Ne/^{22}Ne	±	^{36}Ar (mol/g)	±	^{40}Ar/^{36}Ar	±	^{38}Ar/^{36}Ar	±	N_2 (mol/g)	±	δ^{15}N (‰)	±
H-N1 (8.52 mg)	#1	1.4E−14	3.E−15	9.7	0.8	0.071	0.011	< blk		n.d.		n.d.		2.23E−08	2.E−10	−9	57
	#2	< blk		n.d.		n.d.		4.32E−13	9.4E−14	178.3	151.5	0.244	0.085	2.97E−08	2.E−10	14	8
	#3	1.3E−14	3.E−15	n.d.		0.084	0.015	< blk		n.d.		n.d.		5.19E−09	2.E−10	2	40
	#4	1.1E−14	2.E−15	9.9	0.9	0.015	0.009	1.95E−12	5.7E−14	8.9	30.8	0.205	0.016	1.48E−08	2.E−10	9	14
	#5	4.9E−14	1.E−14	9.1	0.6	0.033	0.011	8.32E−12	5.1E−14	2.4	0.6	0.187	0.001	8.00E−08	3.E−10	−111	3
	#6	4.0E−14	5.E−15	8.2	0.6	0.011	0.008	1.45E−11	8.7E−14	0.4	0.3	0.185	0.001	2.16E−07	8.E−10	−112	1
	#7	2.1E−14	3.E−15	10.5	0.6	0.037	0.019	4.42E−12	3.3E−14	8.2	1.1	0.185	0.002	5.75E−08	3.E−10	−107	5
	#8	3.9E−14	2.E−15	8.9	0.3	0.010	0.008	1.26E−11	8.6E−14	0.2	0.4	0.185	0.002	2.08E−07	7.E−10	−105	2
	#9	1.1E−14	2.E−15	9.7	0.9	0.056	0.013	1.35E−12	2.0E−14	1.2	3.5	0.194	0.005	1.09E−08	2.E−10	−65	23
	#10	1.6E−14	2.E−15	8.2	0.6	0.116	0.023	1.41E−13	7.7E−15	n.d.		0.173	0.024	1.48E−09	2.E−10	116	145
	Total	2.1E−13	3.E−14	10.1	1.3	0.041	0.011	4.37E−11	1.8E−13	3.5	1.7	0.187	0.001	6.46E−07	1.E−09	−95	2
H-N2 (1.07 mg)	#1	6.2E−15	2.E−15	n.d.		n.d.		6.90E−13	1.0E−14	198.7	6.3	0.180	0.006	7.23E−08	3.E−10	−29	46
	#2	1.11E−13	3.E−15	n.d.		n.d.		1.47E−13	5.1E−15	5.8	25.9	0.169	0.019	6.37E−09	2.E−10	40	25
	#3	2.06E−13	4.E−15	n.d.		n.d.		1.45E−12	1.6E−14	n.d.		0.188	0.004	1.70E−08	2.E−10	1	11
	#4	3.6E−14	2.E−15	9.8	0.4	0.037	0.005	6.39E−12	5.2E−14	22.8	0.6	0.183	0.001	4.04E−08	2.E−10	−107	4
	#5	2.8E−14	2.E−15	10.9	0.5	0.048	0.005	2.13E−11	1.4E−13	n.d.		0.188	0.001	2.17E−07	8.E−10	−111	2
	#6	2.3E−14	2.E−15	7.3	0.4	0.031	0.004	3.03E−12	2.0E−14	n.d.		0.183	0.003	6.78E−08	3.E−10	−108	3
	#7	1.4E−14	2.E−15	9.6	0.6	0.090	0.015	3.11E−12	2.6E−14	15.1	1.2	0.186	0.002	5.57E−08	3.E−10	−104	3
	#8	1.2E−14	2.E−15	10.6	0.7	0.059	0.010	9.57E−13	9.7E−15	1.0	4.0	0.175	0.005	1.62E−08	2.E−10	−66	9
	#9	2.3E−14	2.E−15	10.2	0.4	0.054	0.005	8.17E−13	1.4E−14	2.7	4.7	0.179	0.006	1.03E−08	2.E−10	−64	16
	#10	2.6E−14	2.E−15	9.7	0.4	0.035	0.006	5.33E−13	1.0E−14	8.2	7.2	0.193	0.012	6.83E−09	2.E−10	−48	28
	Total	1.6E−13	2.E−14	10.7	1.1	0.047	0.007	3.84E−11	1.6E−13	8.7	0.2	0.186	0.001	5.10E−07	1.E−09	−89	7
H-N3 (2.35 mg)	#1	2.7E−15	6.E−16	14.2	1.5	0.073	0.020	1.59E−13	2.4E−15	121.2	11.4	0.189	0.009	3.60E−08	1.E−10	25	3
	#2	3.2E−15	1.E−15	13.5	1.3	0.068	0.022	3.95E−13	8.0E−15	n.d.		0.196	0.007	1.43E−08	9.E−11	9	6
	#3	6.0E−15	6.E−16	13.0	0.7	n.d.		1.14E−12	9.2E−15	n.d.		0.192	0.002	5.20E−09	8.E−11	18	14
	#4	3.0E−15	9.E−16	11.0	1.1	0.210	0.042	3.82E−13	4.6E−15	4.9	4.5	0.180	0.005	2.29E−08	1.E−10	−9	48
	#5	3.4E−15	6.E−16	9.9	0.8	0.026	0.015	2.05E−13	3.6E−15	n.d.		0.192	0.009	8.86E−10	8.E−11	−117	138
	#6	4.6E−15	1.E−15	8.5	0.7	0.060	0.013	3.21E−13	4.2E−15	183.6	6.0	0.180	0.005	9.28E−10	8.E−11	25	72
	#7	1.5E−14	1.E−15	9.2	0.4	0.035	0.006	2.47E−12	1.9E−14	n.d.		0.188	0.002	1.77E−08	1.E−10	−96	5
	#8	2.5E−14	1.E−15	10.1	0.3	0.034	0.003	6.19E−12	3.9E−14	0.6	0.3	0.191	0.001	5.66E−08	2.E−10	−111	1
	#9	4.16E−14	9.E−16	9.5	0.2	0.031	0.007	1.58E−11	9.4E−14	0.9	0.1	0.187	0.001	1.53E−07	5.E−10	−113	3
	#10	2.2E−14	1.E−15	10.3	0.4	0.030	0.004	6.81E−12	4.3E−14	0.9	0.3	0.189	0.002	7.87E−08	3.E−10	−108	3
	#11	2.2E−14	1.E−15	8.7	0.3	0.025	0.006	1.14E−12	1.0E−14	3.0	1.5	0.188	0.002	2.43E−08	1.E−10	−101	4
	#12	1.47E−14	9.E−16	8.9	0.4	0.045	0.004	< blk		n.d.		n.d.		4.67E−10	8.E−11	−166	122
	Total	1.57E−13	9.E−15	11.1	0.7	0.040	0.005	3.50E−11	1.1E−13	3.0	0.1	0.188	0.001	4.11E−07	7.E−10	−86	1

Table 3
Data of He, Ne, and Ar measured in Hypatia samples H-Z1 to H-Z5. Errors at 1σ.

Sample	Extraction step	^{4}He (mol/g)	±	^{3}He/^{4}He	±	^{22}Ne (mol/g)	±	^{20}Ne/^{22}Ne	±	^{21}Ne/^{22}Ne	±	^{36}Ar (mol/g)	±	^{40}Ar/^{36}Ar	±	^{36}Ar/^{38}Ar	±
H-Z1 (0.5 mg)	total	2.5E−10	4.9E−011	2.1E−04	7.E−05	< blk		n.d.				1.8E−11	8.E−12	n.d.		0.2	0.1
H-Z2 (2.9 mg)	total	2.9E−10	1E−011	1.39E−04	1.E−05	3.3E−14	3.E−15	11	1	0.05	0.01	2.2E−11	1.E−12	n.d.		0.20	0.01
H-Z3 (2.9 mg)	total	6.8E−10	3.5E−011	1.65E−04	9.E−06	4.3E−14	3.E−15	11.0	0.9	0.032	0.004	3.27E−11	8.E−13	2	2	0.19	0.01
H-Z4 (1.0 mg)	total	5.0E−10	3.5E−011	1.7E−04	2.E−05	3.3E−14	9.E−15	12	4	0.04	0.02	3.0E−11	2.E−12	0.1	7.6	0.19	0.02
H-Z5 (2.8 mg)	1000 °C	1.55E−11	2.9E−013			< blk						1.10E−13	4.E−13				
	1800 °C	6.2E−10	3.2E−011			3.6E−14	3.E−15					3.47E−11	9.E−13				
	total	6.4E−10	3.2E−011	1.65E−04	9.E−06	3.6E−14	3.E−15	11	1	0.028	0.005	3.48E−11	1.E−12	n.d.		0.19	0.01

are shown in Fig. 1. The ^{20}Ne/^{22}Ne ratios of the total gas measured in all three Nancy samples and the ratios of the three Zürich samples all vary between 10 and 11, with a weighted average of 11.0 ± 0.8. This average value is within the range of ^{20}Ne/^{22}Ne ratios of 10.1–10.7 reported for Ne–Q in many meteorite classes (Busemann et al., 2000; Ott, 2014). Although some individual temperature steps (Table 2, Fig. 1) likely indicate the release of some atmospheric Ne and one individual step in sample H-N2 gives a low value of 7.3 ± 0.4 for ^{20}Ne/^{22}Ne (Table 2), we conclude that the major portion of the Ne in Hypatia represents Ne–Q. We find no clear evidence for the presence of Ne–HL or "exotic" Ne–G (essentially pure ^{22}Ne) in Hypatia, as Kramers et al. (2013) reported.

A contribution of excess ^{21}Ne is visible in individual data points located at the right side of pure potential end-members (Fig. 1) and pointing towards the cosmogenic component (^{21}Ne/^{22}Ne = 0.93, Leya et al., 2001). Concentrations of excess ^{21}Ne in the bulk individual samples range between 5×10^{-16} and 4×10^{-15} mol g^{-1}. This excess ^{21}Ne cannot be nucleogenic, as can be estimated by conservatively assuming all measured ^{4}He to be radiogenic (see previous Subsection 3.2.1) and a $^{21}Ne_{nuc}/^4He_{rad}$ ratio of $\sim 2.8 \times 10^{-8}$ for an O-content of ca. 30% (Cox et al., 2015). Furthermore, the excess ^{21}Ne cannot have been produced on Earth by cosmic rays, as this would require an unreasonably long exposure age of 100 Ma at the find site using a production rate of 21 atoms of ^{21}Ne per g of SiO_2 per year (Niedermann, 2000), corrected for latitude and altitude of the find site (Stone, 2000) and a concentration of ^{21}Ne-producing target elements (Na, Al, Si, Mg) at the upper end of the range given by Kramers et al. (2013). Lower concentrations of these elements result in even higher terrestrial exposure ages. The ^{21}Ne excess is thus interpreted to have been produced uniquely by cosmic-rays in an extra-terrestrial environment. It corresponds to nominal cosmic-ray exposure (CRE) ages of 0.004 to 0.09 Ma. This age is a rough estimate based on the production rate model given in Leya and Masarik (2009), assuming a meteoroid radius <3 m, and a concentration of ^{21}Ne-producing target elements (Na, Al, Si, Mg) at the upper end of the range given by Kramers et al. (2013), and no terrestrial contamination in any of these elements.

The original concentration of ^{21}Ne-producing target elements in Hypatia is, however, difficult to assess. Kramers et al. (2013) suggested that most of the oxygen and magnesium in Hypatia might be the result of secondary (i.e. terrestrial) encrustations and fracture fillings. Such terrestrial contamination would imply that the above range of ^{21}Ne exposure ages would be a lower limit to the real exposure age of Hypatia. In contrast to ^{21}Ne, cosmogenic ^{3}He is produced directly from C, the major element in Hypatia, essentially not affected by terrestrial contamination. A very conservative upper limit to the exposure age of Hypatia can therefore be calculated by assuming all measured ^{3}He is cosmogenic, in contrast to what we concluded in Section 3.2.1. Again using the model calculations by Leya and Masarik (2009) with appropriate target element concentrations (dominated by C in this case), and no loss of cosmogenic ^{3}He, the measured concentrations of ^{3}He (~ 4–11×10^{-14} mol/g) correspond to CRE ages of 0.05 to 0.25 Ma in meteoroids with a radius <3 m. This range is also low, similar to the nominal ^{21}Ne age range found above, in particular if we consider that likely in none of our samples more than perhaps 25% of the measured ^{3}He is actually cosmogenic (Section 3.2.1). This suggests that Hypatia was either exposed to cosmic-rays in space for only a very short time, or was instead part of a significantly larger object. The slight excess of ^{3}He/^{4}He relative to He-Q could, thus, easily be explained by the addition of some cosmogenic ^{3}He.

3.2.3. Argon

Except for some very low temperature steps, ^{40}Ar/^{36}Ar ratios in all Hypatia samples are significantly lower than the atmospheric

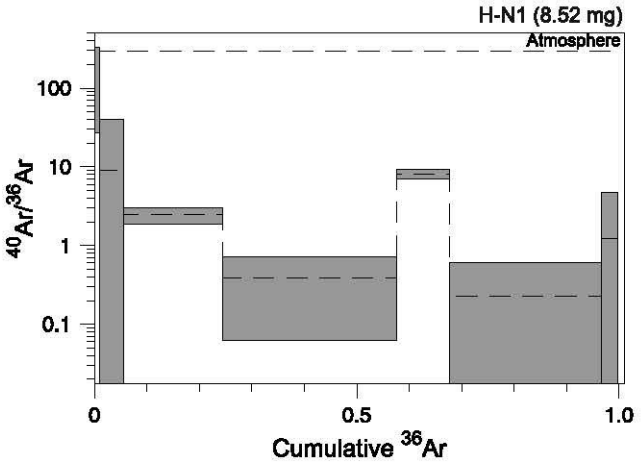

Fig. 2. Evolution of the $^{40}Ar/^{36}Ar$ ratio during step-heating of the H-N1 sample. Note the log-scale for the y axis showing very low ratios well below the atmospheric value of 298.56 (Lee et al., 2006). Ranges correspond to 1σ.

ratio with values as low as 0.23 ± 0.38 measured in each of the three CO_2 laser extractions (H-N1, H-N2 & H-N3). Fig. 2 shows the evolution of $^{40}Ar/^{36}Ar$ as a function of ^{36}Ar released in sample H-N1. Table 2 and Fig. S5 (in supplementary material) show that $^{40}Ar/^{36}Ar$ ratios as low as 1 ± 4 and 0.6 ± 0.3 in individual steps were also observed in samples H-N2 and H-N3 respectively. $^{40}Ar/^{36}Ar$ ratios of the total gas released during the CO_2 laser extractions are also very low with values of 3.5 ± 1.7, 8.7 ± 0.2 and 3.0 ± 0.1 for samples H-N1, H-N2, and H-N3, respectively. For the samples analyzed in Zürich, $^{40}Ar/^{36}Ar$ ratios are less well constrained due to sizeable blank corrections, but in samples H-Z3 and H-Z4 the values are clearly much below the atmospheric ratio with an upper limit of 4 in sample H-Z4.

As already noted by Kramers et al. (2013), $^{40}Ar/^{36}Ar$ ratios below the atmospheric value provide clear evidence that Hypatia is extra-terrestrial. Values for the $^{38}Ar/^{36}Ar$ ratio are consistent both with the isotopic composition of Ar in phase Q (0.1873, Busemann et al., 2000) and with the atmospheric ratio. However, the very low $^{40}Ar/^{36}Ar$ values demonstrate that atmospheric Ar can only be a minor component.

3.2.4. Xenon and krypton

Xe and Kr were measured in sample H-N4 (8.4 mg) by stepwise extraction in an induction furnace. Data are shown in Table S1. Fig. 3 shows the isotopic spectra of Xe released in the lowest temperature (400 °C) and the highest temperature (1800–2200 °C) steps, respectively. Xe released at low temperature is very similar to present-day atmospheric Xe and, therefore likely results from adsorbed atmospheric Xe. In contrast, the highest temperature step (Fig. 3b) released essentially pure Xe–Q (note that scales in Fig. 3a and 3b are distinct) plus a clear excess of radiogenic ^{129}Xe. Xe data presented here are in stark contrast to those reported by Kramers et al. (2013) where no excess radiogenic ^{129}Xe was found and large errors on isotopic ratios prevented any clear distinction between an extra-terrestrial component (e.g. Xe–Q) and the atmosphere. This is also illustrated in the three-isotope diagram in Fig. 4. Our data are plotted together with a selection of extreme data reported by Kramers et al. (2013) characterized by particularly low $^{129}Xe/^{132}Xe$ and $^{136}Xe/^{132}Xe$ values. These data were used to propose the presence of the exotic Xe-G component, which falls near the origin in Fig. 4. Our data, however, do not show any hint for the presence of this Xe-G component in Hypatia.

The Kr data from analysis of H-N4 allow a less clear distinction between atmospheric Kr and Kr-Q. However, the Kr released in the

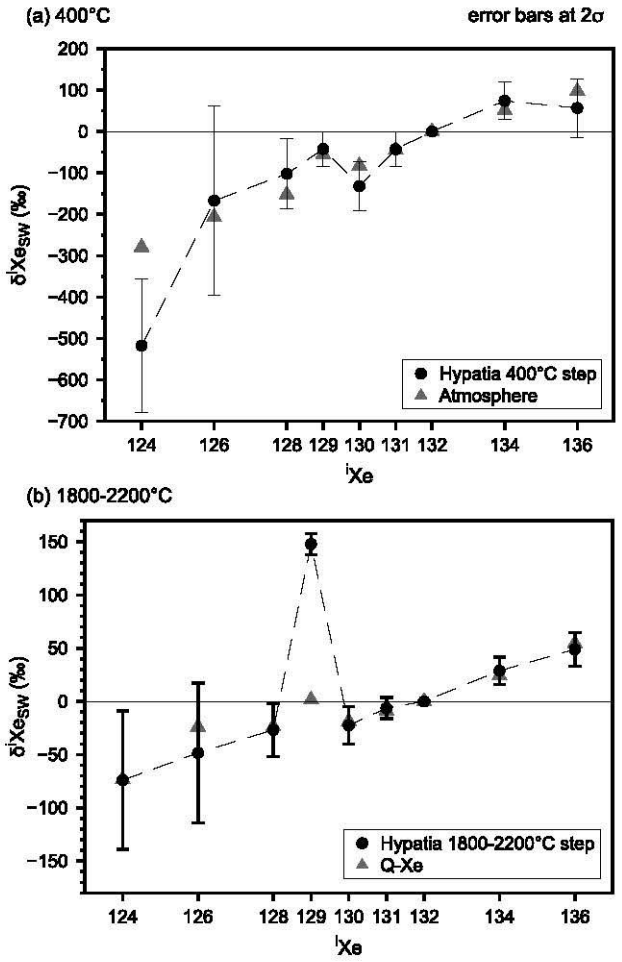

Fig. 3. Isotopic spectra of Xe released at 400 °C (a) and between 1800 and 2200 °C (b) during the induction furnace experiment. The isotopic composition is expressed with the delta notation relative to the isotopic composition of Xe in Solar Wind (Meshik et al., 2014) ($\delta^{i}Xe = ((^{i}Xe/^{132}Xe)_{mes}/(^{i}Xe/^{132}Xe)_{SW} - 1) \times 1000$). Grey triangles in (a) represent the isotopic composition of Earth's atmosphere and grey triangles in (b) represent the isotopic composition of Xe in phase Q (Busemann et al., 2000). Errors at 2σ.

high temperature steps is also fully consistent with the Kr-Q composition. Fig. S6 (see supplementary material) is a three-isotope plot ($^{83}Kr/^{84}Kr$ vs. $^{82}Kr/^{84}Kr$) showing some data from our study together with a selection of extreme data points from Kramers et al. (2013). Again, there is no evidence from our data for the presence of exotic Kr-G in Hypatia.

3.2.5. Nitrogen and carbon

Results for the two bulk samples analyzed in Paris are very reproducible, showing that these pre-combusted carbon-rich samples were composed of ca. 95% diamond, with identical $\delta^{15}N$-values of $-100 \pm 1‰(2\sigma)$ and low N-content (i.e. N/C-ratio) of 18 ppm. $\delta^{13}C$-values have an error-weighted mean of $-3.44 \pm 0.14‰(2\sigma)$, a value in agreement with the result for the least contaminated samples of Kramers et al. (2013). Nitrogen data in all 3 stepwise CO_2 laser extractions conducted in Nancy are listed in Table 2. The evolution of the isotopic composition of nitrogen released during stepwise extraction of H-N3 is shown in Fig. 5 and is also representative for the two other extractions (see Fig. S7 in supplementary material for the isotopic composition of N_2 in H-N1 and H-N2). In all samples, the major fraction (>85%) of nitrogen is released at mid- to high temperature. Remarkably, all three Hy-

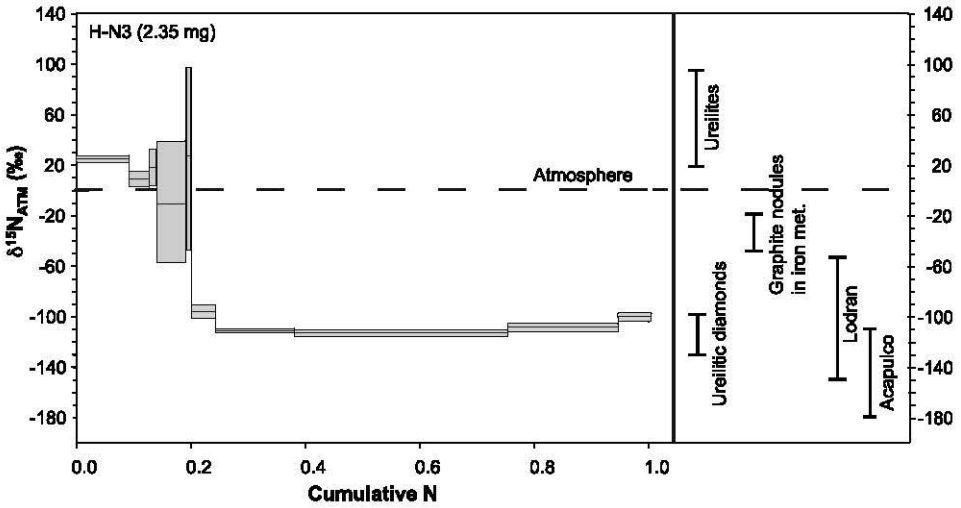

Fig. 5. Ranges of isotopic compositions of nitrogen released during step-heating of the H-N3 sample. Ranges for individual steps correspond to errors at 1σ.

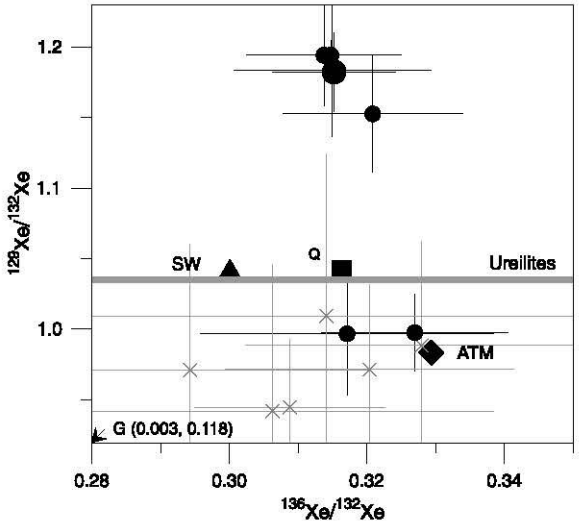

Fig. 4. Three-isotope plot of xenon. Small black-filled circles are for individual heating steps, the large black-filled circle corresponds to the total of all extraction steps. Reference values of Solar Wind (SW) xenon, Xe–Q, G-Xe, and atmospheric Xe are shown for comparison (Ott, 2014) as well as the mean value of the $^{129}Xe/^{132}Xe$ ratio measured in ureilites (Rai et al., 2003a). A representative set of data by Kramers et al. (2013) are shown with small grey axes and error bars. Error bars are at 2σ.

patia samples released a very light component with an essentially constant $\delta^{15}N$ around $-110‰$ over up to five high temperature steps. At lower temperatures, presumably some adsorbed atmospheric N ($\delta^{15}N = 0‰$) was released, but it seems very likely that in at least some of these steps a second indigenous component with a positive $\delta^{15}N$ is also present. This component most clearly reveals itself in the first step of H-N3 (Fig. 5) with a $\delta^{15}N$ value of $+25 \pm 3‰$ and in the second steps of H-N1 and H-N2. Since these steps may also have been affected by some adsorbed atmospheric nitrogen, we conclude that the indigenous low-T component in Hypatia has a $\delta^{15}N$ ratio around $+25‰$ or higher. As discussed below, such high $\delta^{15}N$ values are common in meteorites and rare on Earth. Remarkably, total $\delta^{15}N$ values of nitrogen extracted from samples in Nancy (e.g. $-95 \pm 4‰(2\sigma)$ in sample H-N1; Table 2) agree well with values obtained in Paris on Hypatia diamonds ($\delta^{15}N = -100 \pm 1‰(2\sigma)$). The slightly higher $\delta^{15}N$ value of $-86 \pm 1‰(1\sigma)$ for sample H-N3 (Table 2) is likely due to the presence of the heavy component released during the first heating step in Nancy and probably removed by the pre-combustion at 600 °C in Paris. For the subsequent detailed discussion, Fig. 5 shows ranges of $\delta^{15}N$ values observed in different meteoritic materials. We note that nitrogen components similar to both the heavy and the light nitrogen found in Hypatia have been detected in various extra-terrestrial samples.

3.2.6. Concentrations and elemental ratios

The relative elemental abundances of noble gases and nitrogen can be diagnostic of their carrier phases (Ott, 2014). Fig. 6 shows the mean (thick black line) and the ranges (grey area) of total concentrations of noble gases and nitrogen extracted from Hypatia samples analyzed in this study. Concentrations in the different samples are quite uniform, e.g. vary by less than a factor of 2.5 for ^{36}Ar (3.2×10^{-11} mol/g). Volatile element abundances in bulk ureilites, a bulk Almahata Sitta ureilitic fragment (Murty et al., 2010) and bulk Goalpara (Göbel et al., 1978) ureilite, in carbon-rich residues extracted from ureilites (Rai et al., 2003a), in a graphite inclusion from the Canyon Diablo iron meteorite (Matsuda et al., 2005), in bulk Monument Draw acapulcoite (McCoy et al., 1996) and in the Earth's atmosphere (in mol per g of atmosphere) are also shown for comparison. In our study and in references listed above all abundances are the results of total extractions and may include in some cases an atmospheric component. Concentrations of noble gases and nitrogen in Hypatia samples are considerably lower than the high values measured in phase Q. For example, ^{132}Xe concentrations in phase Q reach values up to 1.5×10^{-11} mol/g (Busemann et al., 2000) versus 4.3×10^{-14} mol/g in Hypatia. By contrast, the abundance levels and elemental pattern in Hypatia is similar to that of bulk ureilites and also of the Canyon Diablo graphite nodule, apart from He that seems enriched relative to the graphite nodule with a mean value of 4.7×10^{-10} mol/g. The abundance pattern in the Monument Draw acapulcoite is also broadly compatible with that of Hypatia for He, Ne, and Xe. Hypatia shows much lower volatile concentrations than carbon-rich residues extracted from ureilites despite the fact that Hypatia is mainly composed of carbon. These low concentrations prevent us from directly linking Hypatia to the carbon-rich part of ureilites (see discussion Section 4.2).

4. Discussion

The data presented here undoubtedly confirm and strengthen the conclusion by Kramers et al. (2013) that Hypatia is an extraterrestrial material. Apart from the confirmation of very low $^{40}Ar/^{36}Ar$

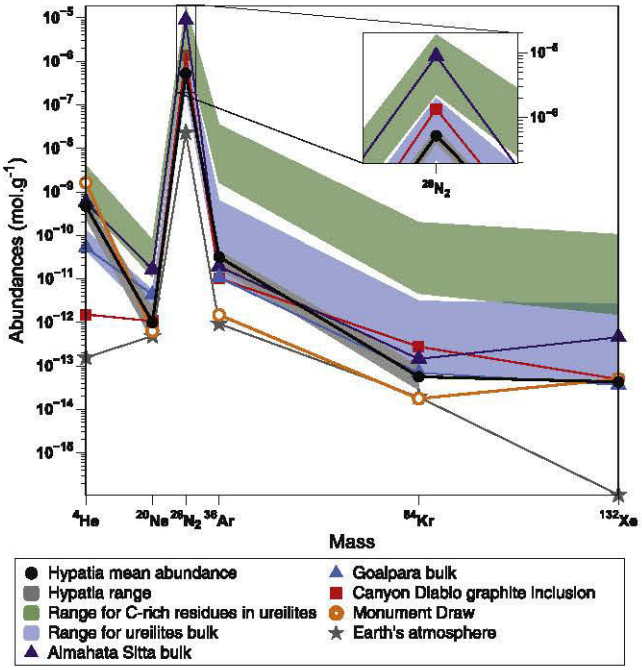

Fig. 6. Range of elemental abundances (in mol/g) of volatile elements in Hypatia compared to several types of meteorites. The range for ^{4}He abundances is from the analysis of H-Z1 to H-Z5 assuming that all ^{4}He is trapped. The range for ^{20}Ne (trapped) abundances is from H-Z2 to H-Z5 and from H-N1 to H-N3. Value from H-Z1 analysis is rejected because it is unrealistically low due to high corrections due to the presence of water. Range for ^{36}Ar is from H-Z1 to H-Z5 and from H-N1 to H-N3. Range for N_2 is from H-N1 to H-N3. Range for ^{84}Kr is from the unique analysis on sample H-N4 and the range corresponds to a relative high uncertainty due to a perfectible calibration of the Kr content of the standard bottle. However, it does not change any conclusion of this study. Only the value of ^{132}Xe amount obtained during analysis of sample H-N4 is shown. See text for details about references.

ratios, this is also clearly shown by the isotopic composition of He, Ne, and Xe, which in many extraction steps and bulk samples is essentially identical to the Q component, ubiquitous in many meteorite classes. Furthermore, given that values of δ^{15}N below -40‰ have never been reported in terrestrial samples and that the nitrogen isotopic composition in Hypatia is similar to values found in different type of meteoritic materials, a δ^{15}N value of -110‰ for more than 85% of the N budget (Table 2) is a new convincing piece of evidence for the extraterrestrial nature of Hypatia. Elemental abundances of the ultravolatile elements analyzed here are also very different from the terrestrial atmospheric pattern and are in the range observed for different meteoritic samples (Fig. 6). Furthermore terrestrial impact diamonds occur in a geological context where graphite-bearing target rocks are present such as gneisses in the Ries, Popigai, and Lappajärvi craters (Langenhorst et al., 1999). In case of Hypatia, the potential target is made of Nubian sandstone. The absence of graphite-bearing target rock in this area further supports the conclusions that Hypatia must be extraterrestrial.

Although the indications for 'exotic' extrasolar components reported by Kramers et al. (2013), discussed below, are tenuous, there are further, quite robust differences between the noble gas data obtained by these authors and the present dataset, and also one marked similarity. (i) Their data for Ar, Kr, and Xe are dominated by terrestrial atmospheric contamination, which persisted to high temperatures in the degassing experiments. (ii) They found no excess ^{129}Xe. (iii) While their inferred abundances of the extraterrestrial noble gas components for He, Ar, and Xe are 5 to 10 times lower than those determined in the present study, their corresponding He/Xe and Ar/Xe ratios are very similar to our data (and significantly higher than those in typical Q gas). The grains analyzed by Kramers et al. (2013) came from a different subsample of Hypatia to ours, and it is thus likely that the stone is heterogeneous on a mm to cm scale with regard to its iodine and trapped noble gas abundances, but homogeneous with regard to the composition of its dominant extraterrestrial noble gas component.

In the following discussion we will explore possible links between Hypatia and extra-terrestrial objects from which it may originate based on the findings presented above.

4.1. A cometary origin for Hypatia?

Our study does not confirm the presence of any G noble gas component as reported by Kramers et al. (2013). The presence of "exotic" G-gases, normally found in presolar SiC grains, could have been a clue to a cometary origin of Hypatia under the premise that cometary matter should be rich in primordial noble gas components produced by nucleosynthesis in stars. In further contrast to Kramers et al. (2013) we unequivocally show that the analyzed fragments of Hypatia are rich in isotopically "normal" Q gases, a major primordial noble gas component in many different meteorite classes originating from the asteroid belt. Furthermore, only little is known about volatile elements in comets and for example Ne isotopically similar to Ne–Q in chondrites has been measured in Stardust samples (Marty et al., 2008).

4.2. Possible links of Hypatia with known carbon-rich meteoritic materials

Because phase-Q noble gases are ubiquitous in many meteorite classes (Ott, 2014), nitrogen isotopic composition may be more useful for exploring possible links between Hypatia and known extraterrestrial objects, as N isotopic compositions are very variable in different extraterrestrial samples (Füri and Marty, 2015). On the right hand side of Fig. 5, δ^{15}N ranges of various C-rich phases in meteorites are shown. The very light (δ^{15}N ≈ -110‰) and reproducible nitrogen released from all three analyzed Hypatia samples at high temperature is reminiscent of a main component measured in ureilitic diamonds (δ^{15}N < -100‰; Rai et al., 2003b). In addition, the likely minor N component released at low to mid temperatures, with δ^{15}N > 25‰, is reminiscent of an isotopic signature of a component with δ^{15}N higher than 19‰ and reaching values up to 100‰ (Rai et al., 2003b; Yamamoto et al., 1998) released at low temperature from graphite in ureilites. It is worth noting that such values are released at low temperatures which is again consistent with our observations (Rai et al., 2003b). Additionally, trapped noble gases with an isotopic composition similar to the Q component and with elemental abundances ratios more similar to those in Hypatia than in phase Q are present in ureilites (Rai et al., 2003a). Note here that the bulk δ^{13}C value of -3.4 ± 0.1‰ measured in diamond is also in the range of values measured in ureilites (Grady and Wright, 2003). Unlike in Hypatia, however, despite an active search, no excess ^{129}Xe from the decay of ^{129}I has ever been reported in ureilites (Göbel et al., 1978; Rai et al., 2003a) (Fig. 4). This latter observation suggests that Hypatia may not be connected to ureilites after all.

Grady and Wright (2003) found isotopically light N in the range of δ^{15}N $= -50$ to -20‰ in graphite nodules of iron meteorites. Such nodules are mainly found in IAB and IIICD types of meteorites (Benedix et al., 2000). While this range of δ^{15}N is not overlapping with that of the main N component in Hypatia (Fig. 5), C-rich samples of iron meteorites appear to contain nitrogen with quite heterogeneous δ^{15}N values. For example, isotopically very light nitrogen with δ^{15}N < -82‰ has been reported in Copiapo (IAB) (Ponganis and Marti, 2007). Notably, radiogenic ^{129}Xe as well as

Table 4
C-rich meteoritic lithologies that partially match the features observed in Hypatia. The "✓" symbol denotes a match with a feature, "×" a dismatch and "–" the difficulty to conclude. See text for details and references.

Hypatia (this study)	Ureilites	Iron meteorites	Acapulcoites
Size: cm	mm	cm	µm
Diamonds	✓	✓	×
Q noble gases	✓	✓	✓
Excess ^{129}Xe	×	✓	✓
$\delta^{13}C \approx -3.4$‰	✓	–	×
Main $\delta^{15}N \approx -110$‰	✓	–	–

trapped noble gases similar to Q have also been found in graphite nodules of Canyon Diablo (IAB) (Matsuda et al., 2005). Furthermore Kramers et al. (2013) reported the presence in Hypatia of bright inclusions composed of a Fe–Ni–Cr alloy and troilite reminiscent of the major constituents of iron meteorites. The IAB iron meteorite ALH 77283 contains also troilite–graphite–schreibersite–cohenite inclusions rich in diamond-lonsdaleite nodules that may be similar to Hypatia (Clarke et al., 1981). Finally the bulk $\delta^{13}C$ value of -3.4 ± 0.1‰ measured in this study is also in the range of -30 to $+4$‰ measured in graphite nodules in iron meteorites even if this value, given the large range measured among different samples, is not diagnostic of this type of extra-terrestrial material (Grady and Wright, 2003). Graphite rich parts of iron meteorites may thus appear linked to Hypatia, although the heterogeneity of the N isotopic composition in such samples prevents us to unequivocally interpret Hypatia as a graphite nodule from an iron meteorite.

Acapulco and Lodran, the type specimens of the primitive achondrite groups of acapulcoites and lodranites contain small µm-sized graphite nodules or carbonized veins with isotopically often very light nitrogen ($\delta^{15}N$ as low as -166‰ in Acapulco Charon et al., 2014). Furthermore, acapulcoites and lodranites also carry noble gases of Q-composition as well as excess ^{129}Xe (McCoy et al., 1997; Palme et al., 1981). Acapulcoites and lodranites may, therefore, also share a genetic link with Hypatia.

Hypatia is cm-sized (Barakat, 2012). Only graphite nodules in iron meteorites typically reach this size. Carbon-rich phases in other known meteoritic classes discussed here (ureilites, acapulcoites and lodranites) are much smaller (µm- to mm-sized) except in one case where a large cm-sized carbon-rich nodule, maybe containing diamonds, has been found in the Portales Valley (H6) chondrite (Ruzicka et al., 2000). If size matters to establish a link between Hypatia and other know extraterrestrial objects none of the candidates discussed here, except graphite nodules from iron meteorites, match this feature (Table 4).

In summary, while Hypatia clearly is a different type of material than any of the carbon-rich phases discussed in this section, its noble gas and nitrogen signatures share many characteristics with some of these phases, although none matches perfectly (see Table 4 for a comparison between the features met in Hypatia and those in known extraterrestrial carbon-rich phases). Therefore, it seems possible that the volatile inventory of Hypatia or its parent material is related to the volatiles in these carbon-rich phases of known meteorite classes and that all these carbon-rich lithologies may have sampled the same geochemical reservoir.

4.3. A link between Hypatia and the Libyan Desert Glass?

Kramers et al. (2013) suggested that Hypatia is a remnant of the impactor that created the Libyan Desert Glass. Irrespective of whether Hypatia is of cometary or asteroidal origin, their main argument for a causal relation between Hypatia and LDG was that a large object was required to generate diamonds by impact. The shock pressures required to produce impact diamonds from graphite must generally exceed about 25–30 GPa. In case of a terrestrial impact the projectile should be at least some meters in diameter. This would be consistent with the likely minimum size of Hypatia inferred from the cosmogenic noble gases as discussed further down in this paragraph. A crater or a crater strewn field would also result (Collins et al., 2005). Such pressures are indeed recorded in bedrocks of LDG, however a crater or a crater strewn field related to Hypatia is not known. It should also be noted that so far some 40 meteorites of different classes (named "Great Sand Sea n°XX"), including ordinary chondrites, iron meteorites and lodranites, have been found near the LDG area. The find location is thus not a compelling argument for a causal relationship. The XRD and TEM studies presented here also do not allow us to directly decide whether the diamonds in Hypatia formed upon impact on Earth or by an earlier collision in space, for example during the event which ejected the Hypatia-bearing meteoroid from its parent body. However, nitrogen in Hypatia is not isotopically equilibrated between the low-to-medium temperature release of N with a $\delta^{15}N$ component around $+25$‰ or higher, and a medium-to-high temperature component depleted in ^{15}N ($\delta^{15}N$ values close to -110‰). Part of the nitrogen released in the first heating steps is probably of terrestrial origin, but likely not all since $\delta^{15}N$ values above 20‰ are extremely rare on Earth but common in extraterrestrial carbon-rich material, e.g. insoluble organic matter in carbonaceous chondrites or low to medium heating steps of ureilites (Rai et al., 2003b). The high temperature extraction of isotopically light N is consistent with its occurrence in diamond as N is the most abundant impurity found in diamonds and its substitution in the place of carbon explains the difficulty, and thus the high-temperature required, to release it from the diamond structure (Kaiser and Bond, 1959). Hence, the isotopic disequilibrium of N among different carbon-rich phases implies that, in Hypatia, diamonds are unlikely to have formed by shock of the C-rich material during atmospheric entry. In the parent meteoroid, diamonds hosting light N likely co-existed with non-diamond, C-rich phases hosting heavy N before encounter with Earth, as observed for instance in ureilitic C-rich veins. Whatever the processes involved, the dichotomy in $\delta^{15}N$ between diamond-rich and amorphous carbon-rich lithologies must have developed in space otherwise the impact and the production of diamond would have homogenized the isotopic composition of nitrogen. Thus, the disequilibrium in nitrogen isotopic compositions argues against production upon impact on Earth. The very low nominal noble gas exposure ages of Hypatia may also be considered in this context. Because the $^{22}Ne/^{21}Ne$ ratio of the cosmogenic component could not be determined due to the dominant presence of trapped Ne and because so far no cosmogenic radionuclide data for Hypatia is available, information about the shielding of Hypatia during its journey towards Earth (i.e. the size of the Hypatia parent meteoroid and the preatmospheric depth of Hypatia within that meteoroid) is unconstrained. The exposure age of Hypatia on the order of a mere 100,000 years was therefore estimated by assuming a production rate valid for a "typical" meteoroid size <3 m. Hence, the qualification of this number as "nominal exposure age". True meteorite exposure ages considerably less than a million years are very rare. If Hypatia had been brought to Earth as part of an iron meteorite, its exposure age would be expected to be at least 10–20 Ma, but more likely to be longer than 100 Ma (Herzog and Caffee, 2014). Also among stony meteorites, exposure ages of less than 1 Ma are only found for some types of carbonaceous chondrites (Nishiizumi and Welten, 2005), with most other ages being at least a few Ma and ranging up to some 100 Ma. Thus, it seems likely that the low nominal exposure age of Hypatia actually is the result of a much larger shielding, and, hence, larger meteoroid size, than assumed above.

While no clear-cut conclusion on the size of the Hypatia parent meteorite can be drawn from these considerations, it seems rather likely that it was a body of at least a few meters in diameter. On the other hand, if the parent meteorite/asteroid had been even considerably larger, as would be implied by a supposed connection with the LDG event, then Hypatia would have to originate from the outermost few meters of this body. Otherwise, the low but measurable concentrations of cosmogenic ^{21}Ne could not have been produced even during billions of years of cosmic ray exposure. The example of the Canyon Diablo iron meteorite shows that surviving large chunks of a large bolide are indeed likely to originate from the rear near-surface portions of the impacting projectile (Bjork, 1961). In summary, the concentration of cosmogenic ^{21}Ne in Hypatia hints at a parent object of at least a few meters in diameter, but not necessarily large enough to have been able to create the LDG or to produce the shock-diamonds upon impact on Earth. Nevertheless, the suggestion by Kramers et al. (2013), that more fragments similar to the Hypatia stone might be found near the site, is further supported by the low cosmogenic ^{21}Ne concentration.

5. Summary and conclusions

The analyses presented here confirm conclusions by Kramers et al. (2013) that the enigmatic pebble Hypatia represents an unusual type of extraterrestrial material. In addition to the clear cut evidence pointed out by Kramers et al. (2013) (e.g. ^{40}Ar/^{36}Ar ratios below the atmospheric value), our study shows: ^{3}He/^{4}He, ^{20}Ne/^{22}Ne, Xe isotopes, and likely Kr and Ar close to the isotopic composition of the ubiquitous component phase Q in meteorites, isotopic composition of nitrogen similar to components found in ureilites and maybe in graphite inclusions of iron meteorites or acapulcoites, and finally small concentrations of cosmogenic ^{21}Ne produced in space. We also found significant differences from data previously published on Hypatia. In particular we found no evidence for the presence of any presolar signature (e.g. the G component) that was used to infer a cometary origin for Hypatia. At this time, we cannot definitively associate Hypatia with any known type of meteorites as each candidate considered here (ureilites, graphite nodules in iron meteorites or in acapulcoites/lodranites) fails to reproduce all features of the ultravolatile elements determined in this study (Table 4). However, from our comparisons it appears that Hypatia may be related to differentiated cosmochemical objects and thus might present a great opportunity to understand the origin and mode of survival of primordial noble gases and nitrogen in such objects (Wieler et al., 2006).

Acknowledgements

Yves Marrocchi, David Bekaert, Marc Chaussidon and Léo Martin are gratefully acknowledged for fruitful discussions. We appreciate the constructive comments by two anonymous reviewers. This study was funded in Nancy (France) by the European Research Council under the European Community's Seventh Framework Programme (FP7/2007-2013 grant agreement No. 267255 to B.M.). M.M. is supported by an Ambizione grant (project PZ00P2_154874) from the Swiss National Science Foundation. Further financial support was provided by the Deutsche Forschungsgemeinschaft (LA 830/14-1 to FL). This is CRPG contribution #2377.

Appendix A. Supplementary material

Supplementary material related to this article can be found online at http://dx.doi.org/10.1016/j.epsl.2015.10.013.

References

Barakat, A.A., 2012. The Precious Gift of Meteorites and Meteorite Impact Processes. Nova Science Publishers.
Benedix, G.K., McCoy, T.J., Keil, K., Love, S.G., 2000. A petrologic study of the IAB iron meteorites: constraints on the formation of the IAB–Winonaite parent body. Meteorit. Planet. Sci. 35, 1127–1141.
Bjork, R.L., 1961. Analysis of the formation of Meteor Crater, Arizona: a preliminary report. J. Geophys. Res. 66, 3379–3387.
Boyd, S.R., Rejou-Michel, A., Javoy, M., 1995. Improved techniques for the extraction, purification and quantification of nanomole quantities of nitrogen gas: the nitrogen content of diamond. Meas. Sci. Technol. 6, 297–305. http://dx.doi.org/10.1088/0957-0233/6/3/007.
Busemann, H., Baur, H., Wieler, R., 2000. Primordial noble gases in "phase Q" in carbonaceous and ordinary chondrites studied by closed-system stepped etching. Meteorit. Planet. Sci. 35, 949–973.
Charon, E., Aléon, J., Rouzaud, J.N., 2014. Impact delivery of organic matter on the acapulcoite–lodranite parent-body deduced from C, N isotopes and nanostructures of carbon phases in Acapulco and Lodran. Geochim. Cosmochim. Acta 142, 224–239. http://dx.doi.org/10.1016/j.gca.2014.07.009.
Clarke, R.S., Appleman, D.E., Ross, D.R., 1981. An Antarctic iron meteorite contains preterrestrial impact-produced diamond and lonsdaleite. Nature 291, 396–398.
Collins, G.S., Melosh, H.J., Marcus, R.A., 2005. Earth impact effects program: a web-based computer program for calculating the regional environmental consequences of a meteoroid impact on Earth. Meteorit. Planet. Sci. 40, 817–840. http://dx.doi.org/10.1111/j.1945-5100.2005.tb00157.x.
Cox, S.E., Farley, K.A., Cherniak, D.J., 2015. Direct measurement of neon production rates by (a, n) reactions in minerals. Geochim. Cosmochim. Acta 148, 130–144. http://dx.doi.org/10.1016/j.gca.2014.08.036.
Füri, E., Marty, B., 2015. Nitrogen isotope variations in the Solar System. Nat. Geosci., 1–8. http://dx.doi.org/10.1038/ngeo2451.
Göbel, R., Ott, U., Begemann, F., 1978. On trapped noble gases in ureilites. J. Geophys. Res. 83, 855–867.
Grady, M.M., Wright, I.P., 2003. Elemental and isotopic abundances of carbon and nitrogen in meteorites. Space Sci. Rev. 106, 231–248.
Heber, V.S., Wieler, R., Baur, H., Olinger, C., Friedmann, T.A., Burnett, D.S., 2009. Noble gas composition of the solar wind as collected by the Genesis mission. Geochim. Cosmochim. Acta 73, 7414–7432. http://dx.doi.org/10.1016/j.gca.2009.09.013.
Herzog, G.F., Caffee, M.W., 2014. Cosmic-ray exposure ages of meteorites. In: Turekian, H.D.H.K. (Ed.), Treatise on Geochemistry, second edition. Elsevier, Oxford, pp. 419–454.
Humbert, F., Libourel, G., France-Lanord, C., Zimmermann, L., Marty, B., 2000. CO_2-laser extraction-static mass spectrometry analysis of ultra-low concentrations of nitrogen in silicates. Geostand. Newsl. 24, 255–260.
Kaiser, W., Bond, W.L., 1959. Nitrogen, a major impurity in common type I diamond. Phys. Rev. 115, 857–863. http://dx.doi.org/10.1103/PhysRev.115.857.
Kramers, J.D., Andreoli, M.A.G., Atanasova, M., Belyanin, G.A., Block, D.L., Franklyn, C., Harris, C., Lekgoathi, M., Montross, C.S., Ntsoane, T., Pischedda, V., Segonyane, P., Viljoen, K.S.F., Westraadt, J.E., 2013. Unique chemistry of a diamond-bearing pebble from the Libyan Desert Glass strewnfield, SW Egypt: evidence for a shocked comet fragment. Earth Planet. Sci. Lett. 382, 21–31. http://dx.doi.org/10.1016/j.epsl.2013.09.003.
Kuga, M., Marty, B., Marrocchi, Y., Tissandier, L., 2015. Synthesis of refractory organic matter in the ionized gas phase of the solar nebula. Proc. Natl. Acad. Sci. http://dx.doi.org/10.1073/pnas.1502796112, 201502796-6.
Langenhorst, F., Deutsch, A., 2012. Shock metamorphism of minerals. Elements 8, 31–36. http://dx.doi.org/10.2113/gselements.8.1.31.
Langenhorst, F., Shafranovsky, G.I., Masaitis, V.L., Koivisto, M., 1999. Discovery of impact diamonds in a Fennoscandian crater and evidence for their genesis by solid-state transformation. Geology 27, 747–750.
Lee, J.-Y., Marti, K., Severinghaus, J.P., Kawamura, K., Yoo, H.-S., Lee, J.B., Kim, J.S., 2006. A redetermination of the isotopic abundances of atmospheric Ar. Geochim. Cosmochim. Acta 70, 4507–4512. http://dx.doi.org/10.1016/j.gca.2006.06.1563.
Leya, I., Masarik, J., 2009. Cosmogenic nuclides in stony meteorites revisited. Meteorit. Planet. Sci. 44, 1061–1086.
Leya, I., Neumann, S., Wieler, R., Michel, R., 2001. The production of cosmogenic nuclides by galactic cosmic-ray particles for 2π exposure geometries. Meteorit. Planet. Sci. 36, 1547–1561.
Marrocchi, Y., Avice, G., Estrade, N., 2015. Multiple carriers of Q noble gases in primitive meteorites. Geophys. Res. Lett. 42 (7), 2093–2099. http://dx.doi.org/10.1002/2015GL063198.
Marrocchi, Y., Marty, B., Reinhardt, P., Robert, F., 2011. Adsorption of xenon ions onto defects in organic surfaces: implications for the origin and the nature of organics inprimitive meteorites. Geochim. Cosmochim. Acta 75, 6255–6266. http://dx.doi.org/10.1016/j.gca.2011.07.048.
Marty, B., Palma, R.L., Pepin, R.O., Zimmermann, L., Schlutter, D.J., Burnard, P.G., Westphal, A.J., Snead, C.J., Bajt, S., Becker, R.H., Simones, J.E., 2008. Helium and neon abundances and compositions in cometary matter. Science 319, 75–78. http://dx.doi.org/10.1126/science.1148001.

Marty, B., Zimmermann, L., 1999. Volatiles (He, C, N, Ar) in mid-ocean ridge basalts: assessment of shallow-level fractionation and characterization of source composition. Geochim. Cosmochim. Acta 63, 3619–3633.
Matsuda, J.-I., Namba, M., Maruoka, T., Matsumoto, T., Kurat, G., 2005. Primordial noble gases in a graphite–metal inclusion from the Canyon Diablo IAB iron meteorite and their implications. Meteorit. Planet. Sci. 40, 431–443.
McCoy, T.J., Keil, K., Clayton, R.N., Mayeda, T.K., Bogard, D.D., Garrison, D.H., Huss, G.R., Hutcheon, I.D., Wieler, R., 1996. A petrologic, chemical, and isotopic study of Monument Draw and comparison with other acapulcoites: evidence for formation by incipient partial melting. Geochim. Cosmochim. Acta 60, 2681–2708.
McCoy, T.J., Keil, K., Clayton, R.N., Mayeda, T.K., Bogard, D.D., Garrison, D.H., Wieler, R., 1997. A petrologic and isotopic study of lodranites: evidence for early formation as partial melt residues from heterogeneous precursors. Geochim. Cosmochim. Acta 61, 623–637.
Meshik, A., Hohenberg, C., Pravdivtseva, O., Burnett, D., 2014. Heavy noble gases in solar wind delivered by Genesis mission. Geochim. Cosmochim. Acta 127, 326–347. http://dx.doi.org/10.1016/j.gca.2013.11.030.
Murty, S.V.S., Mahajan, R.R., Jenniskens, P., Shaddad, M.H., Eldien, B., 2010. Noble gases and nitrogen in the Almahata Sitta ureilite. Meteorit. Planet. Sci. 45, 1751–1764. http://dx.doi.org/10.1111/j.1945-5100.2010.01095.x.
Niedermann, S., 2000. The ^{21}Ne production rate in quartz revisited. Earth Planet. Sci. Lett. 183 (3–4), 361–364. http://dx.doi.org/10.1016/S0012-821X(00)00302-2.
Nishiizumi, K., Welten, K.C., 2005. Kalahari 008/009–the shortest exposure age of all meteorites. In: Meteoritics and Planetary Science, vol. 40, p. 5270.
Ott, U., 2014. Planetary and pre-solar noble gases in meteorites. Chem. Erde 74, 519–544. http://dx.doi.org/10.1016/j.chemer.2014.01.003.
Palme, H., Schultz, L., Spettel, B., Weber, H.W., Wänke, H., Michel-Levy, M.C., Lorin, J.C., 1981. The Acapulco meteorite: chemistry, mineralogy and irradiation effects. Geochim. Cosmochim. Acta 45, 727–752.
Ponganis, K.V., Marti, K., 2007. Nitrogen components in IAB/IIICD iron meteorites. Meteorit. Planet. Sci. 42, 331–346.
Rai, V.K., Murty, S.V.S., Ott, U., 2003a. Noble gases in ureilites: cosmogenic, radiogenic, and trapped components. Geochim. Cosmochim. Acta 67, 4435–4456. http://dx.doi.org/10.1016/S0016-7037(03)00379-X.
Rai, V.K., Murty, S.V.S., Ott, U., 2003b. Nitrogen components in ureilites. Geochim. Cosmochim. Acta 67, 2213–2237. http://dx.doi.org/10.1016/S0016-7037(02)01373-X.
Reimold, W.U., Koeberl, C., 2014. J. Afr. Earth Sci. 93, 57–175. http://dx.doi.org/10.1016/j.jafrearsci.2014.01.008.
Ruzicka, A., McHone, J.F., Killgore, M., 2000. Portales Valley: discovery of a large graphite nodule. Meteorit. Planet. Sci. Suppl. 35, 140.
Stone, J.O., 2000. Air pressure and cosmogenic isotope production. J. Geophys. Res. 105, 23753–23759.
Urey, H.C., 1957. Origin of tektites. Nature 179, 556–557.
Vogel, N., Wieler, R., Bischoff, A., Baur, H., 2003. Microdistribution of primordial Ne and Ar in fine-grained rims, matrices, and dark inclusions of unequilibrated chondrites—clues on nebular processes. Meteorit. Planet. Sci. 38, 1399–1418.
Wieler, R., Anders, E., Baur, H., Lewis, R.S., Signer, P., 1991. Noble gases in "phase Q": closed-system etching of an Allende residue. Geochim. Cosmochim. Acta 55, 1709–1722.
Wieler, R., Baur, H., Pedroni, A., Signer, P., Pellas, P., 1989. Exposure history of the regolithic chondrite Fayetteville: I. Solar-gas-rich matrix. Geochim. Cosmochim. Acta 53, 1441–1448.
Wieler, R., Busemann, H., Franchi, I.A., 2006. Trapping and modification processes of noble gases and nitrogen in meteorites and their parent bodies. In: Meteorites and the Early Solar System II, pp. 499–521.
Yamamoto, T., Hashizume, K.O., Matsuda, J.-I., Kase, T., 1998. Multiple nitrogen isotopic components coexisting in ureilites. Meteorit. Planet. Sci. 33, 857–870.
Zimmermann, L., Burnard, P., Marty, B., Gaboriaud, F., 2009. Laser ablation (193 nm), purification and determination of very low concentrations of solar wind nitrogen implanted in targets from the GENESIS spacecraft. Geostand. Geoanal. Res. 33, 183–194.

A comprehensive study of noble gases and nitrogen in "Hypatia", a diamond-rich pebble from SW Egypt

Supplementary information

G. Avice[a*], M. M. M. Meier[b, a], B. Marty[a], R. Wieler[b], J. D. Kramers[c], F. Langenhorst[d], P. Cartigny[e], C. Maden[b], L. Zimmermann[a], M. A. G. Andreoli[f]

*corresponding author. E-mail: gavice@crpg.cnrs-nancy.fr

[a]CRPG-CNRS, Université de Lorraine, 15 rue Notre-Dame des Pauvres, BP 20, 54501 Vandoeuvre-lès-Nancy Cedex, France.

[b]Department of Earth Sciences, ETH Zürich, Clausiusstrasse 25, CH-8092 Zürich, Switzerland.

[c]Department of Geology, University of Johannesburg, Auckland Park 2006, South Africa.

[d]Institut für Geowissenschaften, Friedrich-Schiller-Universität Jena, Carl-Zeiss-Promenade 10, D-07745 Jena, Germany.

[e]Laboratoire de Géochimie des Isotopes Stables de l'Institut de Physique du Globe de Paris, UMR 7154, Université Paris Denis-Diderot, 1 rue Jussieu, 75005 Paris, France.

[f]School of Geosciences, University of the Witwatersrand, PO Box 3, Wits 2050, South Africa.

Methods: X-ray diffraction and Transmission Electron Microscopy (TEM)

Mineralogical characterization of Hypatia fragments was done by X-ray powder diffraction and TEM, using a Seifert-FPM XRD7 diffractometer (Cu-K_α radiation) and a 200 kV ZEISS LEO922 TEM at the University of Jena (Germany). For comparison, we applied the same techniques on impact diamonds from the Popigai crater (Koeberl et al., 1997), where impact diamonds were first discovered in terrestrial impact rocks (Masaitis et al., 1972). Samples were crushed in liquid nitrogen to obtain a powder for the X-ray diffraction experiment. The powder X-ray diffraction experiment on Hypatia was conducted for three days in order to obtain a pattern with a signal to noise ratio higher than 50 for the 111 reflection of diamond. Small fractions of the crushed samples were loaded on perforated carbon grids for TEM observations. Conventional bright-field/dark-field and high-resolution TEM imaging were used to characterize the micro-structure of Hypatia, which in turn provides clues to its deformation and transformation effects (Langenhorst and Deutsch, 2012; Langenhorst et al., 1999).

Supplementary figures

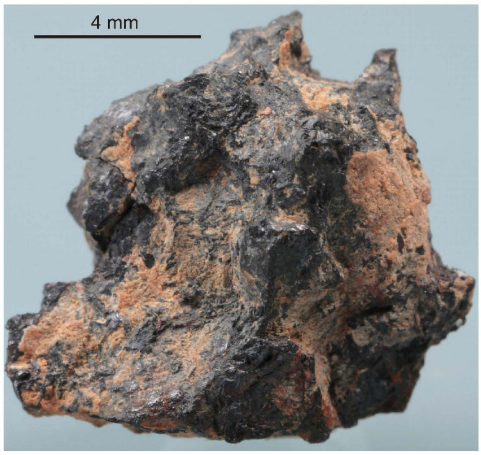

Supplementary Figure S1: Photography of Hypatia (Kramers et al., 2013)

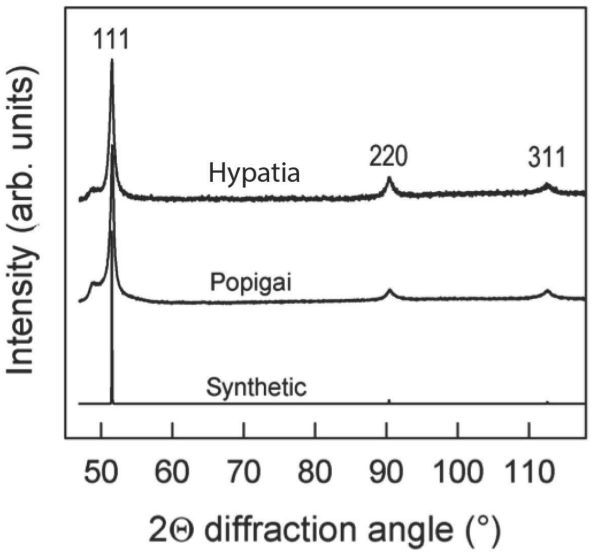

Supplementary Figure S2: X-ray diffraction pattern of Hypatia in comparison to synthetic diamonds and impact diamonds from the Popigai structure.

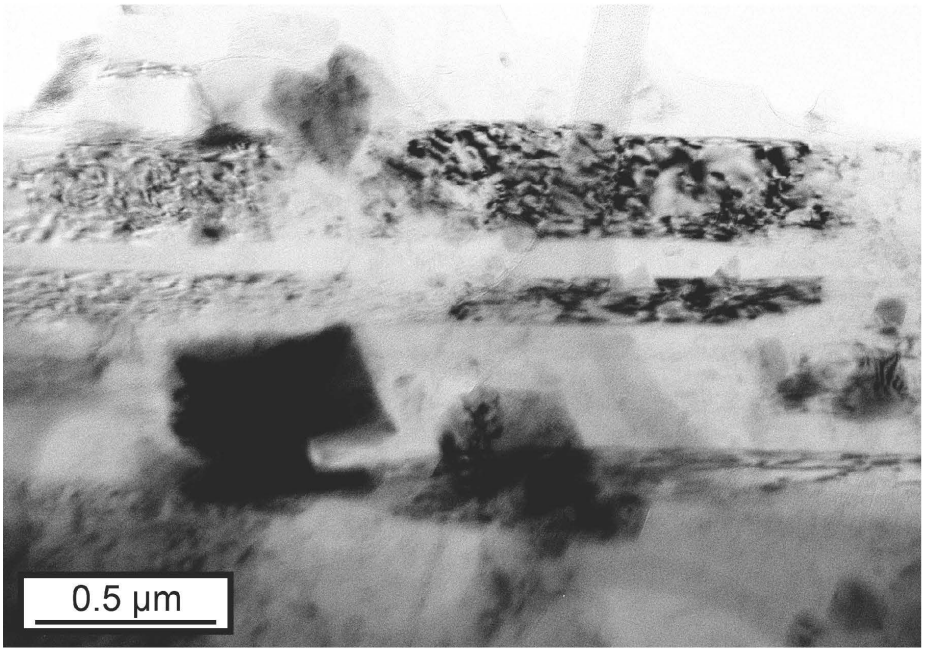

Supplementary Figure S3: Bright-field TEM image of multiple deformation bands in Hyptia.

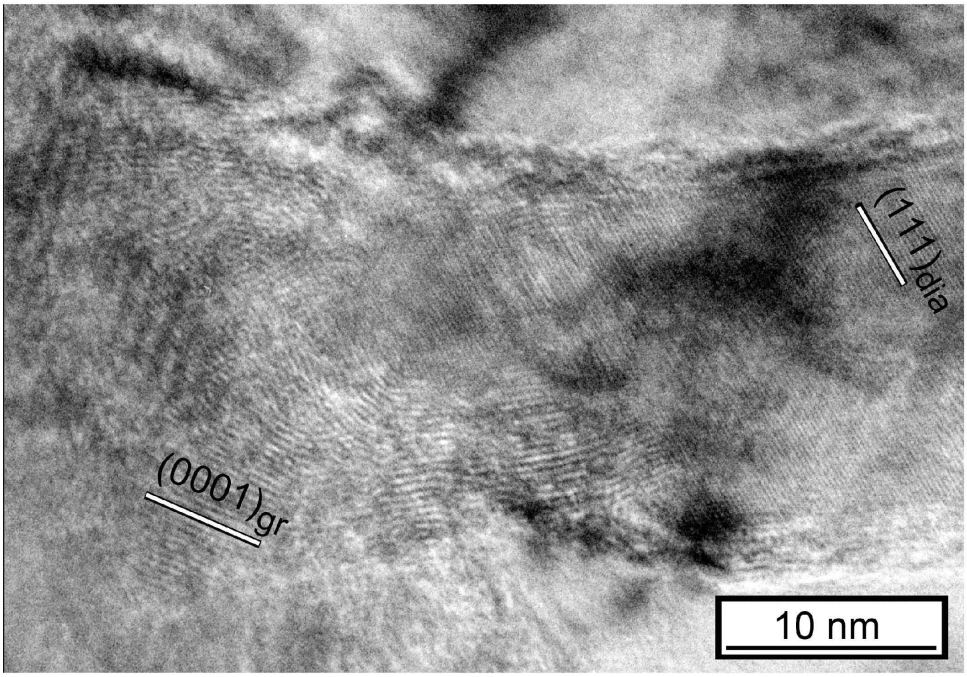

Supplementary Figure S4: High resolution TEM image showing the onion-shaped graphite $(0001)_{gr}$ in the surface of diamond $(111)_{dia}$. The absence of orientation relationship suggests that graphite is here a product of retrograde annealing of diamond.

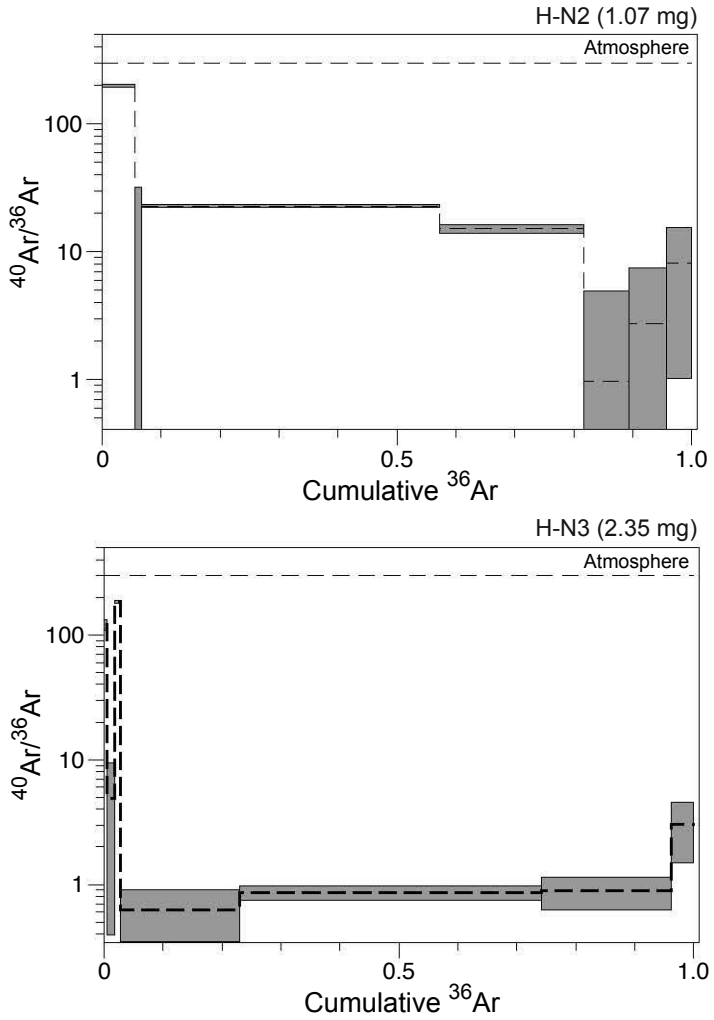

Supplementary Figure S5: Evolution of the $^{40}Ar/^{36}Ar$ ratio during step-heating of the H-N2 and H-N3 samples. Ranges are at 1σ.

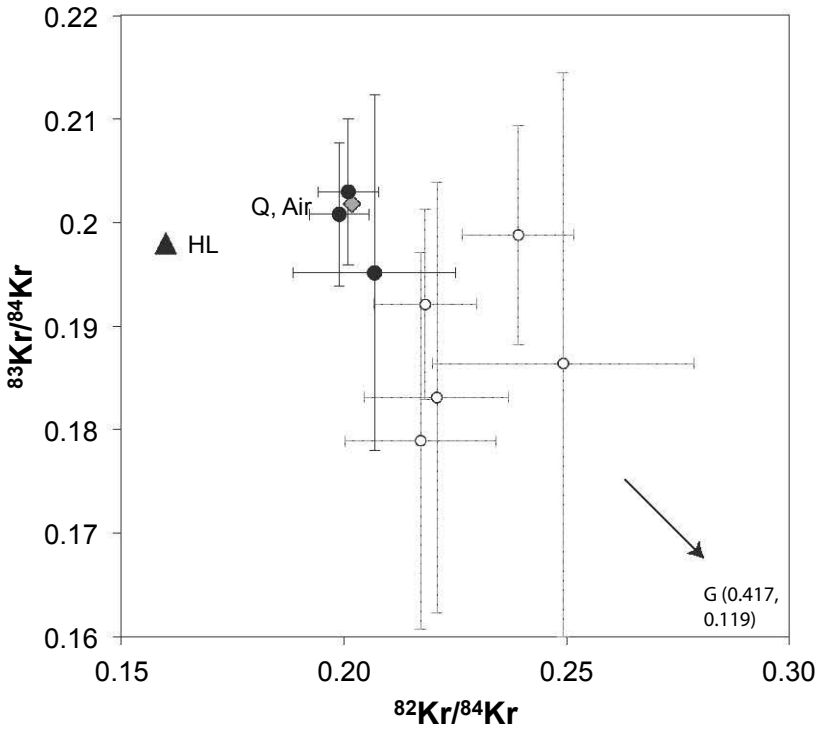

Supplementary Figure S6: Three-isotope diagram of krypton. Heating steps of H-N4 are shown with black dots and Q, Air and HL isotopic compositions are from (Ott, 2014). **Withe dots with dotted error bars are extreme data taken from** (Kramers et al., 2013). **Error bars are 2σ.**

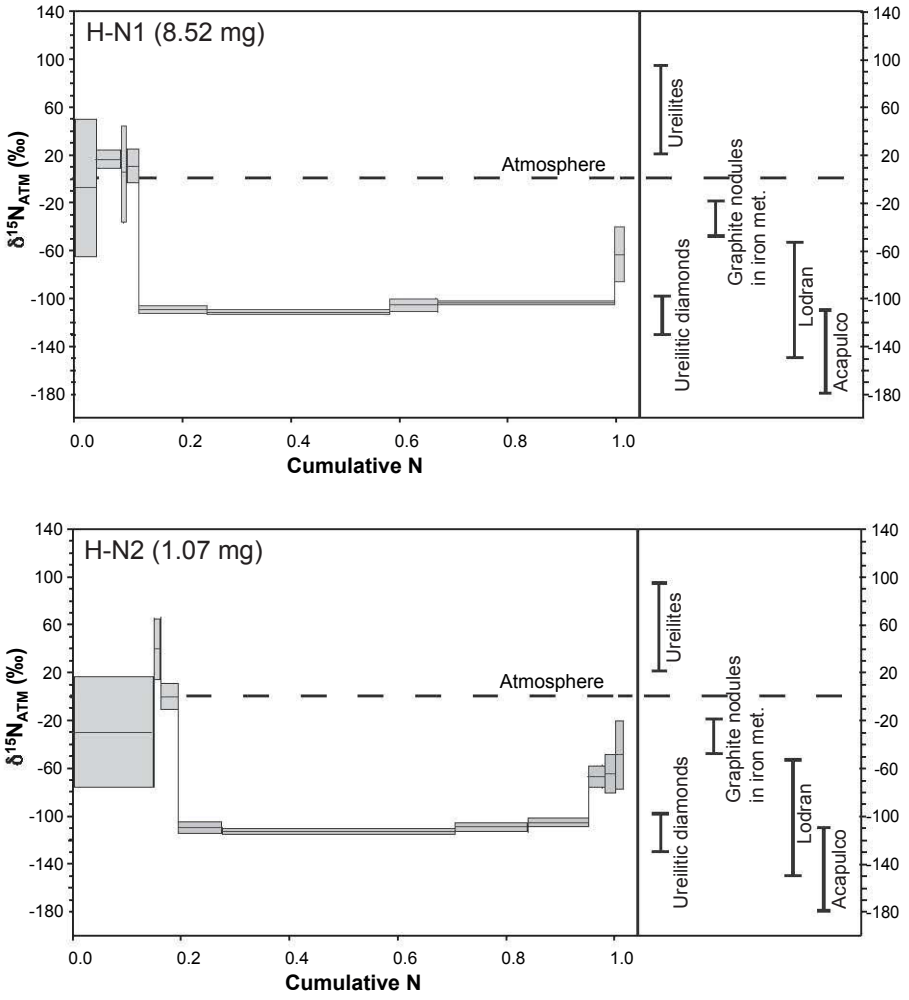

Supplementary Figure S7: Ranges of isotopic compositions of nitrogen released during step-heating of the H-N1 (a) and H-N2 (b) samples. Ranges for individual steps correspond to errors at 1σ. Ranges of isotopic composition of N in C-rich meteoritic materials are shown for comparison. See main text for references.

Supplementary Table S1: Data of bulk N and C isotope measurements conducted in IPG-Paris. Errors at 2σ.

Sample	Weight (mg)	$\delta^{15}N$ (‰)	±	N (ppm)	±	$\delta^{13}C$	±	% C
H-P1	1.57	-99.6	1	17.1	1.71	-3.54	0.14	93
H-P2	1.61	-99.9	1	19.3	1.93	-3.33	0.14	95

Supplementary Table S2: Data of Kr and Xe measured in Hypatia sample H-N4. Errors at 2σ.

H-N4 (8.4 mg)

T (°C)	^{132}Xe (mol/g)	±	^{124}Xe/^{132}Xe	±	^{126}Xe/^{132}Xe	±	^{128}Xe/^{132}Xe	±	^{129}Xe/^{132}Xe	±	^{130}Xe/^{132}Xe	±	^{131}Xe/^{132}Xe	±	^{134}Xe/^{132}Xe	±	^{136}Xe/^{132}Xe	±
400	8.05E-16	3.E-17	0.0024	0.0008	0.0035	0.0009	0.076	0.007	1.00	0.04	0.143	0.010	0.790	0.035	0.396	0.017	0.317	0.021
850	9.67E-16	3.E-17	0.0040	0.0008	0.0032	0.0008	0.071	0.005	1.00	0.03	0.157	0.011	0.778	0.031	0.375	0.013	0.327	0.014
1400	1.24E-14	2.E-16	0.0047	0.0003	0.0039	0.0003	0.083	0.003	1.19	0.04	0.162	0.006	0.819	0.027	0.382	0.013	0.314	0.011
1800	3.35E-15	1.E-16	0.0042	0.0006	0.0040	0.0005	0.083	0.005	1.18	0.05	0.160	0.008	0.805	0.034	0.373	0.016	0.315	0.014
2200	2.22E-14	3.E-16	0.0045	0.0003	0.0040	0.0003	0.082	0.002	1.19	0.01	0.161	0.003	0.820	0.008	0.380	0.005	0.315	0.005
2200 bis	2.96E-15	7.E-17	0.0047	0.0007	0.0035	0.0006	0.083	0.005	1.15	0.04	0.162	0.007	0.809	0.033	0.384	0.015	0.321	0.013
Total	4.27E-14	4.E-16	0.0045	0.0003	0.0039	0.0003	0.082	0.003	1.18	0.03	0.161	0.005	0.816	0.021	0.380	0.010	0.315	0.009

T (°C)	^{84}Kr (mol/g)	±	^{80}Kr/^{84}Kr	±	^{82}Kr/^{84}Kr	±	^{83}Kr/^{84}Kr	±	^{86}Kr/^{84}Kr	±
400	8.6E-16	1.E-16	0.048	0.010	0.207	0.018	0.195	0.017	0.31	0.03
850	7.2E-16	2.E-16	0.043	0.041	0.204	0.135	0.200	0.117	0.30	0.18
1400	5.10E-15	3.E-16	0.037	0.004	0.201	0.007	0.203	0.007	0.31	0.01
1800	4.61E-15	1.E-15	0.030	0.053	0.194	0.266	0.202	0.260	0.31	0.40
2200	3.7E-14	2.E-15	0.036	0.004	0.199	0.007	0.201	0.007	0.31	0.01
2200 bis	7.72E-15	3.E-15	0.037	0.116	0.184	0.579	0.203	0.572	0.31	0.87
Total	5.6E-14	4.E-15	0.036	0.018	0.198	0.087	0.201	0.085	0.31	0.13

References

Koeberl, C., Masaitis, V.L., Shafranovsky, G.I., Gilmour, I., Langenhorst, F., Schrauder, M., 1997. Diamonds from the Popigai impact structure, Russia. Geology 25, 967–970.

Kramers, J.D., Andreoli, M.A.G., Atanasova, M., Belyanin, G.A., Block, D.L., Franklyn, C., Harris, C., Lekgoathi, M., Montross, C.S., Ntsoane, T., Pischedda, V., Segonyane, P., Viljoen, K.S.F., Westraadt, J.E., 2013. Unique chemistry of a diamond-bearing pebble from the Libyan Desert Glass strewnfield, SW Egypt: Evidence for a shocked comet fragment. Earth and Planetary Science Letters 382, 21–31. doi:10.1016/j.epsl.2013.09.003

Langenhorst, F., Deutsch, A., 2012. Shock Metamorphism of Minerals. Elements 8, 31–36. doi:10.2113/gselements.8.1.31

Langenhorst, F., Shafranovsky, G.I., Masaitis, V.L., Koivisto, M., 1999. Discovery of impact diamonds in a Fennoscandian crater and evidence for their genesis by solid-state transformation. Geology 27, 747–750.

Masaitis, V.L., Mikhailov, M.V., Selivanovskaya, T.V., 1972. Popigai basin—an explosion meteorite crater. Meteoritics 7, 39–46.

Ott, U., 2014. Planetary and pre-solar noble gases in meteorites. Chemie der Erde - Geochemistry 74, 519–544. doi:10.1016/j.chemer.2014.01.003

5.2 Article Multiple carriers of Q noble gases in primitive chondrites, *published in 2015 in Geophysical Research Letters, Vol. 42, pp. 1-7.*

AGU PUBLICATIONS

Geophysical Research Letters

RESEARCH LETTER
10.1002/2015GL063198

Key Points:
- Noble gas isotopic fractionation
- Origin of meteoritic noble gases
- Evolution of the accretion disk

Correspondence to:
Y. Marrocchi,
yvesm@crpg.cnrs-nancy.fr

Citation:
Marrocchi, Y., G. Avice, and N. Estrade (2015), Multiple carriers of Q noble gases in primitive meteorites, *Geophys. Res. Lett.*, *42*, doi:10.1002/2015GL063198.

Received 31 JAN 2015
Accepted 5 MAR 2015
Accepted article online 9 MAR 2015

Multiple carriers of Q noble gases in primitive meteorites

Yves Marrocchi[1,2], Guillaume Avice[1,2], and Nicolas Estrade[1,2,3]

[1]OTELo Department, Université de Lorraine, Vandoeuvre-lès-Nancy, France, [2]CNRS, CRPG, UMR 7358, Vandoeuvre-lès-Nancy, France, [3]PCIGR, EOS, University of British Columbia, Vancouver, British Columbia, Canada

Abstract The main carrier of primordial heavy noble gases in chondrites is thought to be an organic phase, known as phase Q, whose precise characterization has resisted decades of investigation. Indirect techniques have revealed that phase Q might be composed of two subphases, one of them associated with sulfide. Here we provide experimental evidence that noble gases trapped within meteoritic sulfides present chemically and thermally driven behavior patterns that are similar to Q gases. We therefore suggest that phase Q is likely composed of two subcomponents: carbonaceous phases and sulfides. In situ decay of iodine at concentration levels consistent with those reported for meteoritic sulfides can reproduce the ^{129}Xe excess observed for Q gases relative to fractionated solar wind. We suggest that the Q-bearing sulfides formed at high temperature and could have recorded the conditions that prevailed in the chondrule-forming region(s).

1. Introduction

Primordial noble gases trapped in chondrites are concentrated in residues obtained after demineralization by HF/HCl of the respective bulk meteorites [*Lewis et al.*, 1975]. Most of the heavy noble gases (Ar, Kr, and Xe) and a small amount of He and Ne are readily released from the original HF/HCl residues by HNO_3 oxidation. This discovery led to the operational definition of phase Q, the oxidizable carrier of primordial noble gases (hereafter Q gases), which has been found to be ubiquitous in different classes of chondrites [*Busemann et al.*, 2000; *Huss et al.*, 1996]. The nature of phase Q is still under debate, but it likely corresponds to carbonaceous structures as noble gas abundances released from acid residues by stepped combustion correlate with those of carbon [*Ott et al.*, 1981]. However, despite the consensus on the carbonaceous nature of phase Q, the phase has not yet been isolated from acid residues [*Amari et al.*, 2013]. Nevertheless, indirect techniques have enabled characterization of Q gases and have revealed (i) a high noble gas concentration [*Huss et al.*, 1996], (ii) a significant fractionation relative to the solar composition in favor of heavy elements and isotopes [*Busemann et al.*, 2000], and (iii) a common high gas-release temperature for all noble gases in the range 1000–1200°C for unaltered chondrites [*Huss et al.*, 1996]. In addition, several studies indicated that phase Q may consist of two subcomponents: Q_1 which is readily soluble in HNO_3 and contains most of the heavy noble gases; and Q_2 which dissolves slowly in hot concentrated HNO_3 [*Busemann et al.*, 2000; *Gros and Anders*, 1977; *Marrocchi et al.*, 2005a]. It has been proposed that at least one of these subcomponents might be related to sulfides [*Gros and Anders*, 1977], but no study has specifically investigated this possibility. However, recent studies report striking results that also suggest that sulfides may have been underestimated as a potential subcarrier of Q gases. Troilite (FeS) from iron meteorites reproduces the thermal behavior of phase Q well, with a common release temperature of 1000–1200°C for all noble gases [*Nishimura et al.*, 2008]. In addition, stepped combustion measurements on Renazzo-type chondrites have revealed that very little carbon is associated with Q gases, suggesting that phase Q might not be solely carbonaceous [*Verchovsky et al.*, 2012]. Furthermore, study of the microdistribution of noble gases within ordinary chondrites has revealed that the sulfide coatings surrounding chondrules exhibit Ne and Ar concentrations at the Q level as well as Q-like elemental (^{36}Ar/^{20}Ne) and isotopic (^{38}Ar/^{36}Ar) ratios [*Vogel et al.*, 2004]. Here we report results from an experimental study in which the same chemical treatments as those used for the isolation of phase Q (HF/HCl treatment) and the release of Q gases (HNO_3 oxidation) were applied to iron sulfides separated from the Mundrabilla iron meteorite (IAB). We also test the possibility that sulfides could contribute significantly to the ^{129}Xe and ^{131,132,134,136}Xe excesses observed for Xe-Q relative to fractionated solar wind.

Table 1. ^{84}Kr and ^{132}Xe Concentrations and $^{86}Kr/^{84}Kr$ and $^{129}Xe/^{132}Xe$ Isotopic Ratios Determined by Stepwise Heating of Original Pyrrhotite (FeS), HF/HCl-Treated Pyrrhotite (FeS-HCl), and Nitric-Etched Pyrrhotite (FeS-HNO_3)[a]

Samples	Mass (g)	Temperature (°C)	^{84}Kr (10^{-10} cc g^{-1})	$^{86}Kr/^{84}Kr$	^{132}Xe (10^{-10} cc g^{-1})	$^{129}Xe/^{132}Xe$
FeS	0.0149	295	bdl	-	bdl	-
		591	bdl	-	bdl	-
		887	1.37	30.6 ± 0.4	0.76	194.6 ± 0.5
		1183	4.32	29.8 ± 0.3	1.82	245.5 ± 0.4
		1478	3.52	28.9 ± 0.3	0.68	173.3 ± 0.5
		1770	1.18	30.5 ± 0.4	0.21	103.6 ± 0.8
		Total	9.21	29.6 ± 0.3	3.27	218.5 ± 0.4
FeS-HCl	0.0173	291	bdl	-	bdl	-
		583	bdl	-	bdl	-
		875	1.18	30.2 ± 0.4	0.78	164.6 ± 0.6
		1166	2.07	29.9 ± 0.4	1.06	241.4 ± 0.4
		1458	1.08	29.8 ± 0.4	0.17	134.4 ± 0.8
		1770	0.82	30.5 ± 0.5	0.009	113.1 ± 1.1
		Total	4.33	30.0 ± 0.4	2.01	202.4 ± 0.5
FeS-HNO_3	0.0126	291	bdl	-	bdl	-
		583	bdl	-	bdl	-
		875	0.61	30.9 ± 0.6	0.21	129.4 ± 1.8
		1166	0.48	30.4 ± 0.6	0.21	141.2 ± 1.1
		1458	0.43	30.0 ± 0.6	0.20	116.6 ± 1.2
		1770	0.16	30.5 ± 0.7	0.16	106.4 ± 1.3
		Total	1.52	30.5 ± 0.6	0.62	129.2 ± 1.3

[a]Isotopic ratios × 100; bdl = below detection limit.

2. Experimental Details

Pyrrhotite (2.6 g, $Fe_{0.98}S$) extracted from a fragment of the Mundrabilla iron meteorite (Naturmuseum Senckenberg, Frankfurt, Germany) was ground and separated into two fractions. The first fraction (FeS) was set aside (without undergoing chemical treatment) in order to determine the noble gas content of the Mundrabilla's pyrrhotites. The second fraction was immersed for 24 h in a HF/HCl, 0.1/1, vol/vol mixture at 70°C and under nitrogen flow [*Piani et al.*, 2012]. After HF/HCl treatment, the sample was washed with water, thoroughly dried at 50°C and then separated into two equal aliquots. One aliquot was retained for noble gas analysis (hereafter FeS-HCl), while the other was etched with 14 M HNO_3 for 24 h at 70°C and under nitrogen flow [*Lewis et al.*, 1975]. The resulting etched residue (FeS-HNO_3) was washed with water and dried at 50°C before analysis. The FeS-HNO_3 fraction exhibits a reddish color that is distinct from the gray color of both the starting material and the HF/HCl residue.

Ar, Kr, and Xe were measured in the raw sample, HF/HCl residue, and nitric-etched residue. Samples were weighed, wrapped in platinum foil, and then loaded into a glass sample tree. The samples were gently baked at 150°C for 3 days in order to remove adsorbed atmospheric gases. Noble gases were extracted by stepped pyrolysis in the temperature range 300–1768°C using a tungsten coil. The linear current-temperature calibration curve for the coil was obtained using an optical pyrometer with a precision of ±25°C for temperatures above 800°C. The calibration curve was extrapolated to temperatures lower than 800°C. Extraction times were adjusted as function of temperature: (i) 15 min for the four low-temperature steps (i.e., 300–1300°C), (ii) 12 min for the 1500°C step, and (iii) 5 min for the final step (at the platinum melting point: 1768°C). The released gases were exposed to three consecutive pellet getters containing SAES St172 getter alloy in order to remove active gases (10 min at 450°C and 10 min at room temperature). Ar, Kr, and Xe were held on a charcoal finger at liquid nitrogen temperature for 45 min, then the residual light noble gases were pumped out over 5 min. Active charcoal immersed in liquid nitrogen was then heated to −105°C using an electric wire that surrounds the charcoal. Calibration curves determined from air standards showed that Kr and Xe are not affected at this temperature while 70% of the Ar is released. This procedure reduces the amount of Ar in the mass spectrometer, which has a considerable effect on the mass discrimination of krypton and xenon. Argon released from the charcoal finger was then pumped out for 5 min. The liquid nitrogen was then removed, and the charcoal finger was heated to 250°C for 25 min to release Xe, Kr, and the residual fraction of Ar. Heavy noble gases were then introduced into high-sensitivity pulse-counting static mass spectrometer

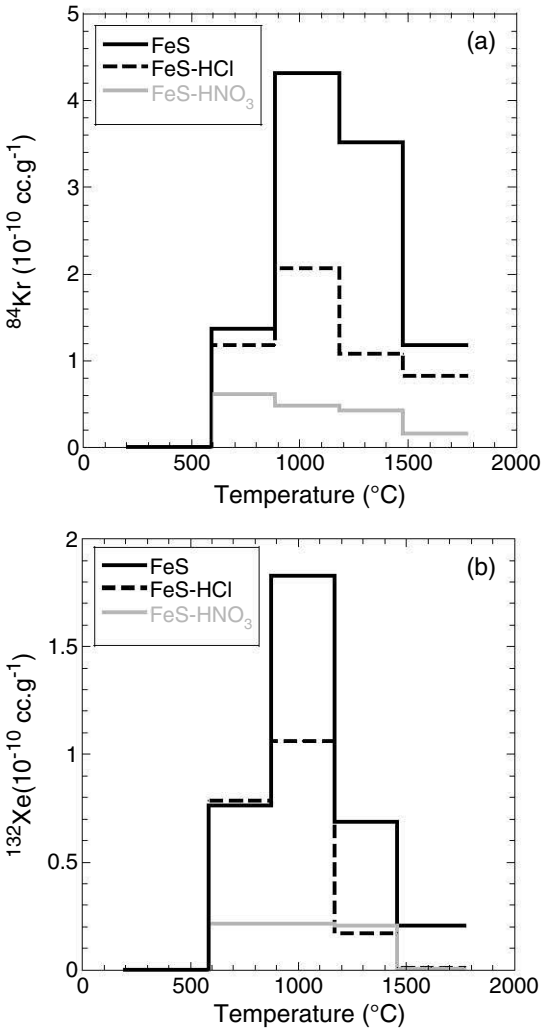

Figure 1. (a) ^{84}Kr elemental abundances determined by stepwise heating in the range 300–1768°C for original pyrrhotite (FeS), pyrrhotite that has undergone HF/HCl treatment (FeS-HCl), and etched pyrrhotite (FeS-HNO_3). (b) ^{132}Xe elemental abundances determined by stepwise heating in the range 300–1768°C for original pyrrhotite (FeS), HF/HCl residue (FeS-HCl), and pyrrhotite oxidized by HNO_3 (FeS-HNO_3).

(Washington University, Saint Louis, USA) [*Mabry et al*., 2007; *Meshik et al*., 2007] for determination of Ar, Kr, and Xe abundances and ^{38}Ar/^{36}Ar, ^{86}Kr/^{84}Kr, and ^{129}Xe/^{132}Xe isotopic ratios.

Hot blanks (1200°C) were performed several times during each analytical session. The Kr and Xe concentrations within Pt foils were also measured and appeared to be negligible. The measured Kr and Xe abundances are typically accurate to better than 5%, whereas the Ar concentrations present a lower precision of ≈25% and are not presented here. The uncertainties in the ^{86}Kr/^{84}Kr and ^{129}Xe/^{132}Xe isotopic ratios (1σ) include hot blank, standard, and sample uncertainties (Table 1).

3. Results

The stepwise-heating analysis shows that pyrrhotite releases Kr and Xe at temperatures between 900 and 1768°C, with a maximum release occurring in the range 900–1175°C (Figure 1 and Table 1). The total concentration of ^{132}Xe measured in the Mundrabilla's pyrrhotite was 3.27×10^{-10} cm^3 STP g^{-1}, while the ^{84}Kr concentration was slightly higher (9.21×10^{-10} cm^3 STP g^{-1}). ^{86}Kr/^{84}Kr ratios measured for each temperature step present homogeneous values close to the atmospheric composition (Table 1). ^{129}Xe/^{132}Xe ratios show more important variations with a clear excess of radiogenic ^{129}Xe in all except the final extraction steps that lies close to the atmospheric composition (Table 1). These results are consistent with previous reports of Kr and Xe concentrations within troilites from iron meteorites [*Mathew and Marti*, 2009; *Nishimura et al*., 2008]. No significant mass variation was observed following the HF/HCl treatment, but the FeS-HCl residues displayed a significant gas loss compared to the initial material, both for Kr (≈53%) and Xe (≈38%; Figure 1 and Table 1). However, Kr and Xe did present the same thermal release patterns as the original sample, with the maximum noble gas release occurring in the range 1000–1200°C (Figure 1). ^{86}Kr/^{84}Kr and ^{129}Xe/^{132}Xe ratios are similar to the original sample (Table 1). The FeS-HNO_3 residue displayed a reddish color that was distinct from the gray color of the starting material and the HF/HCl residue, but no mass variation was observed compared to the initial material. The amounts of Kr and Xe released from the FeS-HNO_3 residue are much lower than those from the FeS-HCl fraction, with gas losses of 65% and 69% recorded for Kr and Xe, respectively (Figure 1 and Table 1). Stepwise-heating analyses revealed that all of the temperature steps were affected by the degassing of Kr and Xe (Figure 1). ^{129}Xe/^{132}Xe ratios show resolvable but lower excess of radiogenic ^{129}Xe comparing to the other residues (Table 1).

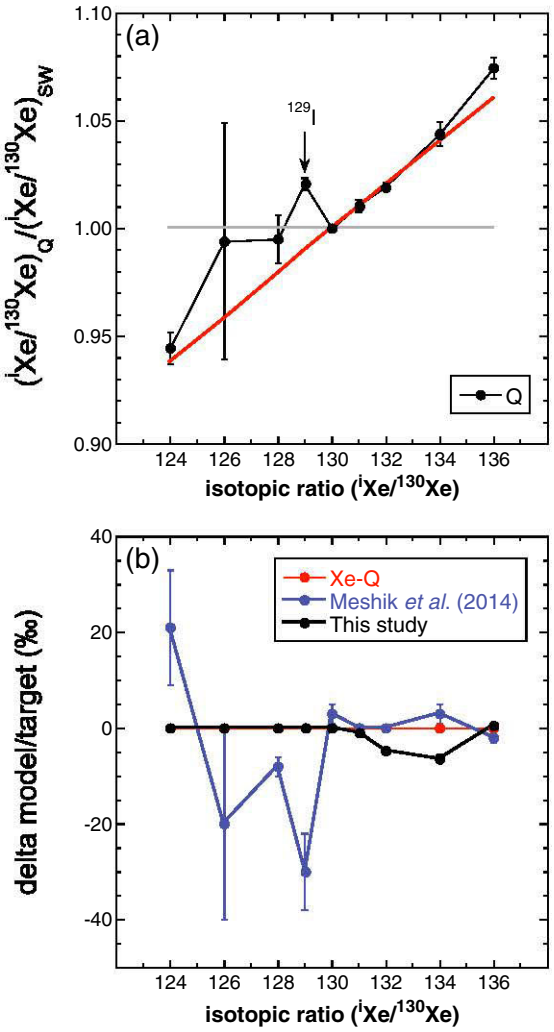

Figure 2. (a) Xe-Q composition normalized to the SW-Xe. Clear excesses of ^{129}Xe and ^{134,136}Xe are observed relative to a ≈ 10.1‰ amu^{-1} mass-fractionated SW-Xe calculated from nonradiogenic/nonfissiogenic xenon isotopes (red line). These excesses are generally attributed to ^{129}I decay and to a contribution from an unidentified carrier with the same Xe-HL isotopic composition as HL-bearing nanodiamonds. (b) Modeled composition of Xe-Q corrected for the radiogenic and fissiogenic contributions of 0.21 ppm of ^{129}I and 9.63 ppm of ^{238}U, respectively. This model is compared to a recent model based on the mixing of fractionated SW-Xe with Xe-HL and Xe-S [*Meshik et al.*, 2014].

4. Discussion

Significant degassing was observed upon HF/HCl treatment, suggesting that sulfides are sensitive to chemical digestion (Figure 1). However, HF/HCl-treated pyrrhotite still contains a significant amount of Kr and Xe and could thus be considered as an acid-resistant mineral. This is confirmed by transmission electron microscopy observations of meteoritic acid residues that contain an important amount of inorganic material such as sulfides and oxides [*Derenne and Robert*, 2010]. In addition, our results indicate that pyrrhotite has a strong susceptibility to HNO_3 oxidation (Table 1). This feature has also been reported for pentlandite (i.e., $(Fe,Ni)_9S_8$), but pentlandite differs from phase Q in its thermal stability with decomposition starting at 610°C [*Kerridge et al.*, 1979]. In contrast, the release pattern of noble gases trapped within pyrrhotite closely resembles that of the Q gases, with a major release of Kr and Xe occurring between 900 and 1200°C (Figure 1). Similar results were obtained for each of the five noble gases released from troilite from the Saint Aubin iron meteorite (ungrouped) [*Nishimura et al.*, 2008], demonstrating that nickel-poor iron sulfides match the thermal characteristics of phase Q. The high-temperature release is directly linked to the incongruent dissociation of pyrrhotite, which occurs in the range 1000–1200°C, depending on the stoichiometry [*Kellerud*, 1963]. Hence, our results suggest that chondritic sulfides could (i) represent a plausible subcarrier of Q gases and could (ii) contribute to the Q gas budget at the maximum-release temperature of Q gases (i.e., 1000–1200°C) [*Huss et al.*, 1996]. This is in good agreement with sulfides separated from Allende (CV3) that show typical Xe-Q isotopic compositions at high temperature (i.e., $>$ 900°C), representing few percent of the total Xe-Q reported for this chondrite [*Busemann et al.*, 2000; *Lewis et al.*, 1977]. It might be argued that the amounts of Kr and Xe measured in iron sulfides from the Mundrabilla iron meteorite are 3 orders of magnitude lower than those reported in phase Q [*Busemann et al.*, 2000; *Huss et al.*, 1996]. However, the goal of this study was not to isolate phase Q as iron meteorites do not show this noble gas component (except in rare graphite nodules) [*Matsuda et al.*, 2005] but rather to test the chemical sensitivity and the thermal behavior of noble gas-bearing sulfides. Consequently, we suggest that phase Q likely corresponds to complex Q gas subcarriers of different natures: carbonaceous phases and iron sulfides.

Table 2. Amounts of Initial ^{238}U and ^{129}I Required for Correcting Observed Excesses of ^{129}Xe and $^{131,132,134,136}Xe$ in the Xe-Q of Different Chondrites and in the Average Q Composition Relative to Mass-Fractionated SW-Xe (Data Are From *Busemann et al.* [2000] and *Wieler et al.* [1992])[a]

	Allende	Chainpur	Cold Bokkeveld	Dimmit	Grosnaja	Isna	Lance	Murchison	Q
	CV3	LL3.4	CM2	H3.7	CV3	CO3.7	CO3.4	CM2	
I (ppm)	0.445	0.057	0.294	0.031	0.152	0.402	0.035	0.395	0.21
U (ppm)	50.07	2.06	0.02	0.56	5.53	33.98	2.55	43.29	9.63
^{129}Xe from I decay (cc/g)	8.64 (−9)	1.03 (−9)	5.71 (−9)	6.13 (−10)	2.97 (−9)	7.80 (−9)	6.90 (−10)	7.67 (−9)	4.08 (−9)
^{131}Xe from U fission (cc/g)	6.25 (−12)	2.57 (−13)	2.49 (−15)	7.04 (−14)	6.90 (−13)	4.24 (−12)	3.19 (−13)	5.40 (−12)	1.20 (−12)
^{132}Xe from U fission (cc/g)	4.89 (−11)	2.01 (−12)	1.95 (−14)	5.51 (−13)	5.40 (−12)	3.32 (−11)	2.49 (−12)	4.23 (−11)	9.41 (−12)
^{134}Xe from U fission (cc/g)	6.84 (−11)	2.81 (−12)	2.73 (−14)	7.71 (−13)	7.55 (−12)	4.64 (−11)	3.49 (−12)	5.91 (−11)	1.32 (−11)
^{136}Xe from U fission (cc/g)	8.22 (−11)	3.38 (−12)	3.28 (−14)	9.26 (−13)	9.08 (−12)	5.58 (−11)	4.19 (−12)	7.11 (−11)	1.58 (−11)
^{129}Xe from Pu fission (cc/g)	1.08 (−10)	4.43 (−12)	4.30 (−14)	1.21 (−12)	1.19 (−11)	7.30 (−11)	5.49 (−12)	9.30 (−11)	2.07 (−11)
^{131}Xe from Pu fission (cc/g)	5.56 (−10)	2.29 (−11)	2.22 (−13)	6.27 (−12)	6.14 (−11)	3.77 (−10)	2.84 (−11)	4.81 (−10)	1.07 (−10)
^{132}Xe from Pu fission (cc/g)	2.00 (−9)	8.24 (−11)	8.00 (−13)	2.26 (−11)	2.21 (−10)	1.36 (−9)	1.02 (−10)	1.73 (−9)	3.85 (−10)
^{134}Xe from Pu fission (cc/g)	2.08 (−9)	8.58 (−11)	8.33 (−13)	2.35 (−11)	2.30 (−10)	1.42 (−9)	1.06 (−10)	1.80 (−9)	4.01 (−10)
^{136}Xe from Pu fission (cc/g)	2.24 (−9)	9.23 (−11)	8.95 (−13)	2.53 (−11)	2.48 (−10)	1.52 (−9)	1.14 (−10)	1.94 (−9)	4.31 (−10)

[a]Amounts of ^{129}Xe produced by the decay of ^{129}I at the concentrations required for correcting ^{129}Xe excesses observed relative to fractionated SW calculated from nonradiogenic/nonfissiogenic xenon isotopes. $^{131,132,134,136}Xe$ concentrations produced by the fission of ^{238}U and ^{244}Pu concentrations required to correct the observed excesses of $^{131,132,134,136}Xe$ in phase Q relative to mass-fractionated SW calculated from nonradiogenic/nonfissiogenic xenon isotopes and iodine-corrected ^{129}Xe (i.e., $^{124,126,128,129}Xe/^{130}Xe$). The numbers in parentheses correspond to the power.

Among the meteoritic noble gases, Xe-Q in different classes of chondrite is characterized by mass-dependent fractionation relative to solar wind (SW), favoring the heavy isotopes [*Marrocchi and Marty*, 2013; *Meshik et al.*, 2014]. However, clear excesses of ^{129}Xe and $^{131,132,134,136}Xe$ are also observed together with the mass-fractionated SW (Figure 2a). These features are generally explained by a mixing model in which 98.4% of ≈8‰ amu^{-1} mass-fractionated SW-Xe is mixed with 1.6% Xe-HL from nanodiamonds and monoisotopic ^{129}Xe from ^{129}I decay [*Gilmour*, 2010]. However, Xe-HL cannot contribute to Xe-Q release generated by online nitric oxidation of acid residues [*Busemann et al.*, 2000] because nanodiamonds are unaffected by etching [*Crowther and Gilmour*, 2013]. Hence, the $^{131,132,34,136}Xe$ excesses have been attributed to a gas carrier that presents the same enrichment in the light and heavy xenon isotopes as nanodiamonds but which has not yet been isolated [*Gilmour*, 2010]. Given our results, we can test an alternative explanation based on in situ fission and decay of $^{238}U + ^{244}Pu$ and ^{129}I within sulfides. The mass fractionation of Xe-Q relative to SW-Xe and its associated uncertainty were determined for eight chondrites and for the average Q composition [*Busemann et al.*, 2000] using only the nonradiogenic/fissiogenic Xe-Q isotopic ratios (i.e., $^{124,126,128}Xe/^{130}Xe$). According to the abundance of ^{129}Xe in phase Q [*Busemann et al.*, 2000] and assuming an initial solar system ratio of 1.1×10^{-4} for $^{129}I/^{127}I$ [*Gilmour et al.*, 2006], we thus determined the iodine content required to correct the ^{129}Xe excess relative to the fractionated SW (Table 2). Then on the basis of the abundances of $^{131,132,134,136}Xe$ in phase Q [*Busemann et al.*, 2000], we calculated the ^{238}U concentrations required to correct the excesses of $^{131,132,134,136}Xe$ relative to fractionated SW using the fission yields reported for ^{238}U and ^{244}Pu [*Ragettli et al.*, 1994], the branching ratio for ^{238}U and ^{244}Pu [*Ozima and Podosek*, 2002], the initial solar system ratios of $(^{244}Pu/^{238}U)_0 = 6.8 \times 10^{-3}$ and $(^{238}U/^{235}U)_0 = 137.88$ [*Ozima and Podosek*, 2002], and a start of radioactive decay 4.57 Gyr ago. Our results show that the respective ^{129}I and ^{238}U initial concentrations required to correct the ^{129}Xe and $^{131,132,134,136}Xe$ excesses relative to fractionated SW observed for Xe-Q across different chondrites [*Busemann et al.*, 2000] fall in the range of 0.03–0.45 ppm ^{129}I and 0–50 ppm ^{238}U (Table 2). The resulting iodine contents are in good agreement with the concentrations of 0.1–3.5 ppm reported for sulfides from different types of meteorites [*Clark et al.*, 1967; *Goles and Anders*, 1962]. Consequently, we propose that Q gases trapped within sulfides could be responsible for the ^{129}Xe excess observed during the release of Q gases. In contrast, the uranium contents required within sulfides to explain the $^{131,132,134,136}Xe$ excess relative to fractionated SW are generally too high compared to the sub-ppm concentrations reported for meteoritic sulfides [*Crozaz*, 1979]. Moreover, the Xe-Q corrected for $^{238}U + ^{244}Pu$ contributions does not produce a better fit for heavy xenon isotopes than the canonical model involving mixing of different Xe reservoirs [*Meshik et al.*, 2014] (Figure 2b). Consequently, the excesses of ^{129}Xe could be attributed to the in situ decay of ^{129}I within sulfides, while fission of $^{238}U + ^{244}Pu$ would play a negligible role in generating the excess of $^{131,132,134,136}Xe$ relative to fractionated SW observed for Q gases (Figure 2a).

Q gases are ubiquitous among the different types of chondrites, despite the fact that they experienced diverse secondary alteration processes such as fluid percolation and/or metamorphism [*Bourot-Denise et al*., 2010; *Brearley*, 2006; *Hewins et al*., 2014; *Huss et al*., 2006; *Marrocchi et al*., 2014]. This suggests that the formation of the S-rich subcarrier of Q gases is linked to primary high-temperature processes rather than to parent body alteration. Recent reports have revealed that chondrule formation took place under high partial pressure of sulfur, leading to the formation of iron sulfide from the chondrule melts by solubility/saturation processes [*Marrocchi and Libourel*, 2013] and/or condensation at the surface of chondrules [*Tachibana and Huss*, 2005]. The formation of Q-bearing sulfides would be directly related to the chondrule-forming event. Such a view supports models which postulate that the formation of chondrules took place in an environment characterized by volatile-enriched gas that interacts at high temperature with chondrule precursor [*Marrocchi and Libourel*, 2013]. Thus, formation of Q-bearing sulfides can be achieved in regions characterized by enhancement of the respective noble gas partial pressures and under ionizing conditions that allow the isotopic fractionation observed for Q gases relative to SW to be reproduced [*Hohenberg et al*., 2002; *Marrocchi et al*., 2005b, 2011].

5. Concluding Remarks

We have performed an experiment to test whether iron sulfides might represent a plausible subcomponent of the main noble gas carriers in primitive meteorites—phase Q. Although significant noble gas degassing was observed upon HF-HCL treatment, our results show that noble gases trapped within sulfides present similar chemical susceptibility and thermal behavior than Q gases. Hence, we propose that sulfides likely represent a plausible subcomponent of phase Q. Under this hypothesis, phase Q represents a mix of multiple primordial noble gas carriers of different natures such as carbonaceous phases and iron sulfide minerals. This suggests that Q gases may represent a ubiquitous noble gas reservoir outside the Sun at the time of the formation and accretion of the first solids in the protosolar nebula.

Acknowledgments
We are grateful to Maïa Kuga, Laurette Piani, Pete Burnard, Pierre-Henri Blard, Bernard Marty, Alice Williams, Barbara Marie, Laurent Rémusat, and Matthias M.M. Meier for helpful discussions. The data for this paper are available by contacting Yves Marrocchi (yvesm@crpg.cnrs-nancy.fr). This is CRPG contribution 2333.

The Editor thanks two anonymous reviewers for their assistance in evaluating this paper.

References

Amari, S., J.-I. Matsuda, R. M. Stroud, and M. F. Chisholm (2013), Highly concentrated nebular noble gases in porous nanocarbon separates from the Saratov (L4) meteorite, *Astrophys. J.*, *778*, 37–45.

Bourot-Denise, M., B. Zanda, Y. Marrocchi, R. C. Greenwood, S. Pont, R. H. Hewins, I. A. Franchi, and G. Cornen (2010), Paris: The slightly altered, slightly metamorphosed CM that bridges the gap between CMs and COs, *Lunar and Planetary Science Conference XXXXI*, Lunar Planet. Inst., Houston, Tex., Abstract 1683.

Brearley, A. J. (2006), The action of water, in *Meteorites and Early Solar System II*, edited by D. S. Lauretta and H. Y. McSween, pp. 587–624, Ariz. Univ. Press, Tucson.

Busemann, H., H. Baur, and R. Wieler (2000), Primordial noble gases in "phase Q" in carbonaceous and ordinary chondrites studied by closed system etching, *Meteorit. Planet. Sci.*, *35*, 949–973.

Clark, R. S., M. W. Rowe, R. Ganapathy, and P. K. Kuroda (1967), Iodine, uranium and tellurium contents in meteorites, *Geochim. Cosmochim. Acta*, *31*, 1605–1613.

Crowther, S. A., and J. D. Gilmour (2013), The Genesis solar xenon composition and its relationship to planetary xenon signatures, *Geochim. Cosmochim. Acta*, *123*, 17–34.

Crozaz, G. (1979), Uranium and thorium microdistributions in stony meteorites, *Geochim. Cosmochim. Acta*, *43*, 127–133.

Derenne, S., and F. Robert (2010), Model of molecular structure of the insoluble organic matter isolated from Murchison meteorite, *Meteorit. Planet. Sci.*, *45*, 1461–1475.

Gilmour, J. D. (2010), "Planetary" noble gas components and the nucleosynthesis history of solar system material, *Geochim. Cosmochim. Acta*, *74*, 380–393.

Gilmour, J. D., O. V. Pravdivtseva, A. Busfield, and C. M. Hohenberg (2006), The I-Xe chronometer and the early solar system, *Meteorit. Planet. Sci.*, *41*, 19–31.

Goles, G. G., and E. Anders (1962), Abundances of iodine, uranium and tellurium in meteorites, *Geochim. Cosmochim. Acta*, *26*, 723–737.

Gros, J., and E. Anders (1977), Gas-rich minerals in the Allende meteorite: Attempted chemical characterization, *Earth Planet. Sci. Lett.*, *33*, 401–406.

Hewins, R. H., et al. (2014), The Paris meteorite, the least altered CM chondrite so far, *Geochim. Cosmochim. Acta*, *124*, 190–222.

Hohenberg, C. M., N. Thonnard, and A. Meshik (2002), Active capture and anomalous adsorption: New mechanisms for the incorporation of heavy noble gases, *Meteorit. Planet. Sci.*, *37*, 257–267.

Huss, G. R., R. S. Lewis, and S. Hemkin (1996), The "normal planetary" noble gas component in primitive chondrites: Compositions, carrier, and metamorphic history, *Geochim. Cosmochim. Acta*, *60*, 3311–3340.

Huss, G. R., et al. (2006), Thermal metamorphism in chondrites, in *Meteorites and Early Solar System II*, edited by D. S. Lauretta and H. Y. McSween, pp. 567–586, Ariz. Univ. Press, Tucson.

Kellerud, G. (1963), The Fe-Ni-S system, in *Carnegie Institution Washington Yearbook*, vol. 62, pp. 175–189, Carnegie Science.

Kerridge, J. F., J. D. Macdougall, and J. Carlson (1979), Iron-nickel sulfides in the Murchison meteorite and their relationship to phase Q1, *Earth Planet. Sci. Lett.*, *43*, 1–4.

Lewis, R. S., B. Srinivasan, and E. Anders (1975), Host phase of a strange xenon component in Allende, *Science*, *190*, 1251–1262.

Lewis, R. S., J. Hertogen, and L. Alaerts (1977), Xenon in Allende sulfides and other recent studies, *Meteoritics*, *12*, 292–297.

Mabry, J., et al. (2007), Refinement and implications of noble gas measurements from Genesis, *Lunar and Planetary Science Conference XXXVIII*, Lunar. Planet. Inst., Houston, Tex., Abstract 1338.

Marrocchi, Y., and G. Libourel (2013), Sulfur and sulfides in chondrules, *Geochim. Cosmochim. Acta*, *119*, 117–136.
Marrocchi, Y., and B. Marty (2013), Experimental determination of the xenon isotopic fractionation during adsorption, *Geophys. Res. Lett.*, *40*, 4165–4170, doi:10.1002/grl.50845.
Marrocchi, Y., S. Derenne, B. Marty, and F. Robert (2005a), Interlayer trapping of noble gases in insoluble organic matter of primitive meteorites, *Earth Planet. Sci. Lett.*, *236*, 569–578.
Marrocchi, Y., A. Razafitianamaharavo, L. J. Michot, and B. Marty (2005b), Low-pressure adsorption of Ar, Kr, and Xe on carbonaceous materials (kerogen and carbon blacks), ferrihydrite, and montmorillonite: Implications for the trapping of noble gases onto meteoritic matter, *Geochim. Cosmochim. Acta*, *69*, 2419–2430.
Marrocchi, Y., B. Marty, P. Reinhardt, and F. Robert (2011), Adsorption of xenon ions onto defects in organic surfaces: Implications for the origin and the nature of organics in primitive meteorites, *Geochim. Cosmochim. Acta*, *75*, 6255–6266.
Marrocchi, Y., M. Gounelle, I. Blanchard, F. Caste, and A. T. Kearsley (2014), The Paris CM chondrite: Secondary minerals and asteroidal processing, *Meteorit. Planet. Sci.*, *49*, 1232–1249.
Mathew, K. J., and K. Marti (2009), Galactic cosmic ray-produced ^{129}Xe and ^{131}Xe excesses in troilites of the Cape York iron meteorite, *Meteorit. Planet. Sci.*, *44*, 107–114.
Matsuda, J.-I., M. Namba, T. Maruoka, T. Matsumoto, and G. Kurat (2005), Primordial noble gases in a graphite-metal inclusion from the Canyon Diablo IAB iron meteorite and their implications, *Meteorit. Planet. Sci.*, *40*, 431–443.
Meshik, A. P., et al. (2007), Constraints on neon and argon isotopic fractionation in solar wind, *Science*, *318*, 433–435.
Meshik, A. P., C. Hohenberg, O. Pravdivtseva, and D. Burnett (2014), Heavy noble gases in solar wind delivered by Genesis mission, *Geochim. Cosmochim. Acta*, *127*, 326–347.
Nishimura, C., J.-I. Matsuda, and G. Kurat (2008), Noble gas content and isotope abundances in phases of the Saint-Aubin (UNGR) iron meteorite, *Meteorit. Planet. Sci.*, *43*, 1333–1350.
Ott, U., R. Mack, and C. Sherwood (1981), Noble-gas-rich separates from the Allende meteorite, *Geochim. Cosmochim. Acta*, *45*, 1751–1788.
Ozima, M., and F. A. Podosek (2002), *Noble Gas Geochemistry*, 286 pp., Cambridge Univ. Press, Cambridge, U. K.
Piani, L., et al. (2012), Structure, composition, and location of organic matter in the enstatite chondrite Sahara 97096 (EH3), *Meteorit. Planet. Sci.*, *47*(1), 8–29.
Ragettli, R. A., E. H. Hebeda, P. Signer, and R. Wieler (1994), Uranium-xenon chronology: Precise determination of λsf*136Ysf for spontaneous fission of 238U, *Earth Planet. Sci. Lett.*, *128*, 653–670.
Tachibana, S., and G. R. Huss (2005), Sulfur isotope composition of putative primary troilite in chondrules from Bishunpur and Semarkona, *Geochim. Cosmochim. Acta*, *69*, 3075–3097.
Verchovsky, A. B., V. K. Pearson, A. V. Fisenko, L. F. Semjonova, M. A. Sephton, and I. P. Wright (2012), Separation of Q from carbon in CR meteorites during stepped combustion, in *Lunar and Planetary Science Conference*, Lunar Planet. Inst., Houston, Tex.
Vogel, N., I. Leya, A. Bischoff, H. Baur, and R. Wieler (2004), Noble gases in chondrules and associated metal-sulfide-rich samples: Clues on chondrule formation and the behavior of noble gas carrier phases, *Meteorit. Planet. Sci.*, *39*, 117–135.
Wieler, R., E. Anders, H. Baur, R. S. Lewis, and P. Signer (1992), Characterisation of Q gases and other noble gas components in the Murchison meteorite, *Geochim. Cosmochim. Acta*, *56*, 2907–2921.

5.3 Article Tissint Martian Meteorite: A Fresh Look at the Interior, Surface, and Atmosphere of Mars, *published in 2012 in Science, Vol. 338, pp. 785-788.*

The supplementary material of this paper is available through the following link: http://www.sciencemag.org/content/338/6108/785/suppl/DC1.

stages of oxidation and show the conversion of the less stable macrocycles into the knot, which is presumably the smallest oligomer that can maximize hydrophobic stabilization. Although other pathways may be involved, the kinetic profile shown in Fig. 3 suggests that knot formation predominantly occurs via the formation and folding of the open trimer. Once formed, the open trimer folds into condensed structures that bury the hydrophobic NDI surfaces. Presumably only one of the structures places the terminal thiols in sufficiently close proximity to allow the ring closure that results in a knot. If the ring were opened by cleavage of a disulfide link, closure would be rapid, whereas unfolding would require unfavorable and slow reexposure of hydrophobic surfaces. The formation of the trefoil knot is, therefore, kinetically and thermodynamically favored and closely mimics the mechanism of knot formation in naturally occurring α/β methyl transferases (*18*).

The conclusions drawn from the experimental results were corroborated by molecular modeling calculations, which showed that the knot was relatively more stable and has a smaller surface area and volume than its topological isomers (the closed trimer and the [2]catenane) (*19*).

Although the cyclic monomer and dimer are transiently formed in the library, the reversible nature of the disulfide bond allows their reorganization into the more ordered, but more stable, trimeric knot, highlighting the dual conflicting role of entropy at the different stages of the folding process: On one hand, the formation of small molecules is preferred, whereas the formation and stability of the larger knot result from the necessity of burying hydrophobic surfaces. Overall, the design of the building block offers an efficient way to access purely organic knotted macrocycles in aqueous media. First, the alternation of rigid hydrophobic NDIs, which can stack and form the core of the knot and bury most hydrophobic surfaces, and flexible hydrophilic loops supplies an ideal scaffold for the knitting of organic oligomers into complex knots. Second, the choice of the amino acid chirality is crucial: The all-L and all-D building blocks induce the directionality of the knot; whereas in the D/L building block, the mismatch of chiralities prevents knot formation. The folding of a linear species into a knot, driven by the hydrophobic effect, may provide a simple model for the formation of knots in proteins.

References and Notes

1. L. F. Liu, L. Perkocha, R. Calendar, J. C. Wang, *Proc. Natl. Acad. Sci. U.S.A.* **78**, 5498 (1981).
2. C. Z. Liang, K. Mislow, *J. Am. Chem. Soc.* **116**, 11189 (1994).
3. P. Virnau, A. L. Mallam, S. E. Jackson, *J. Phys. Condens. Matter* **23**, 033101 (2011).
4. J.-P. Sauvage, D. B. Amabilino, *Supramol. Chem.* (2012).
5. J. Guo, P. C. Mayers, G. A. Breault, C. A. Hunter, *Nat. Chem.* **2**, 218 (2010).
6. C. O. Dietrich-Buchecker, J.-P. Sauvage, *Angew. Chem. Int. Ed. Engl.* **28**, 189 (1989).
7. J.-F. Ayme *et al.*, *Nat. Chem.* **4**, 15 (2012).
8. P. E. Barran *et al.*, *Angew. Chem. Int. Ed. Engl.* **50**, 12280 (2011).
9. K. I. Arias, E. Zysman-Colman, J. C. Loren, A. Linden, J. S. Siegel, *Chem. Commun. (Camb.)* **47**, 9588 (2011).
10. L.-E. Perret-Aebi, A. von Zelewsky, C. Dietrich-Buchecker, J.-P. Sauvage, *Angew. Chem. Int. Ed.* **43**, 4482 (2004).
11. O. Safarowsky, M. Nieger, R. Fröhlich, F. Vögtle, *Angew. Chem. Int. Ed. Engl.* **39**, 1616 (2000).
12. M. Feigel, R. Ladberg, S. Engels, R. Herbst-Irmer, R. Fröhlich, *Angew. Chem. Int. Ed.* **45**, 5698 (2006).
13. P. T. Corbett *et al.*, *Chem. Rev.* **106**, 3652 (2006).
14. S. Wallin, K. B. Zeldovich, E. I. Shakhnovich, *J. Mol. Biol.* **368**, 884 (2007).
15. F. B. L. Cougnon, N. A. Jenkins, G. D. Pantoş, J. K. M. Sanders, *Angew. Chem. Int. Ed. Engl.* **51**, 1443 (2012).
16. N. Ponnuswamy, G. D. Pantoş, M. M. J. Smulders, J. K. M. Sanders, *J. Am. Chem. Soc.* **134**, 566 (2012).
17. S. Anderson, H. L. Anderson, J. K. M. Sanders, *Acc. Chem. Res.* **26**, 469 (1993).
18. A. L. Mallam, E. R. Morris, S. E. Jackson, *Proc. Natl. Acad. Sci. U.S.A.* **105**, 18740 (2008).
19. The lower stability of the cyclic monomer and dimer was apparent when, during our attempt to isolate these macrocycles, they rapidly reequilibrated into a library dominated by the knot.
20. J. J. P. Stewart, *J. Mol. Model.* **13**, 1173 (2007).
21. M. Korth, *J. Chem. Theory Comput.* **6**, 3808 (2010).
22. A. Klamt, G. Schüürmann, *J. Chem. Soc., Perkin Trans. 2* **2**, 799 (1993).

Acknowledgments: We are grateful to Gates Cambridge (N.P.), Engineering and Physical Sciences Research Council (F.B.L.C., J.K.M.S.), and the University of Bath (G.D.P.) for financial support. We thank S. Jackson for helpful discussions, N. Jenkins for his contribution in the early stage on the project, and A. Belenguer for maintaining the LC-MS facility.

Supplementary Materials

www.sciencemag.org/cgi/content/full/338/6108/783/DC1
Materials and Methods
Figs. S1 to S22
Tables S1 to S4
References

5 July 2012; accepted 11 September 2012
10.1126/science.1227032

Tissint Martian Meteorite: A Fresh Look at the Interior, Surface, and Atmosphere of Mars

H. Chennaoui Aoudjehane,[1,2]* G. Avice,[3] J.-A. Barrat,[4] O. Boudouma,[2] G. Chen,[5] M. J .M. Duke,[6] I. A. Franchi,[7] J. Gattacceca,[8] M. M Grady,[7,9] R. C. Greenwood,[7] C. D. K. Herd,[5] R. Hewins,[10] A. Jambon,[2] B. Marty,[3] P. Rochette,[8] C. L Smith,[9,11,12] V. Sautter,[10] A. Verchovsky,[7] P. Weber,[13] B. Zanda[10]

Tissint (Morocco) is the fifth martian meteorite collected after it was witnessed falling to Earth. Our integrated mineralogical, petrological, and geochemical study shows that it is a depleted picritic shergottite similar to EETA79001A. Highly magnesian olivine and abundant glass containing martian atmosphere are present in Tissint. Refractory trace element, sulfur, and fluorine data for the matrix and glass veins in the meteorite indicate the presence of a martian surface component. Thus, the influence of in situ martian weathering can be unambiguously distinguished from terrestrial contamination in this meteorite. Martian weathering features in Tissint are compatible with the results of spacecraft observations of Mars. Tissint has a cosmic-ray exposure age of 0.7 ± 0.3 million years, consistent with those of many other shergottites, notably EETA79001, suggesting that they were ejected from Mars during the same event.

Demonstration in the early 1980s that an important group of meteorites was of martian origin represented a breakthrough in attempts to understand the geological evolution of Mars (*1*–*3*). Unfortunately, most of the samples were collected long after their arrival on Earth and thus have experienced variable degrees of terrestrial weathering (*4*). Even the few martian meteorites that were collected shortly after their observed fall to Earth have been exposed to organic and other potential contaminants during storage. Here, we report on the Tissint martian meteorite, which fell on 18 July 2011 in Morocco (figs. S1 and S2). This is only the fifth witnessed fall of a meteorite from Mars and therefore provides an opportunity to improve our understanding of processes that operated on that planet at the time the meteorite was ejected from its surface.

The largest recovered stones from the Tissint fall are almost fully covered with a shiny black fusion crust (Fig. 1). Internally the meteorite consists of olivine macrocrysts set in a fine-grained matrix of pyroxene and feldspathic glass (maskelynite) (*5*) (figs. S3 to S6 and tables S1 to S6). The matrix is highly fractured and penetrated by numerous dark shock veins and patches filled with black glassy material enclosing bubbles (fig. S7). The petrology of Tissint shows similarities to that of other picritic shergottites (an important group of olivine-rich martian basaltic rocks), in particular, lithologies A and C of EETA79001 (*2*). The grain density and magnetic properties of Tissint (fig. S8) also match previous results from basaltic and picritic shergottites (*6*).

Tissint is an Al-poor ferroan basaltic rock, rich in MgO and other compatible elements (Ni,

Cr, Co). Its major element abundances are similar to those of the other picritic shergottites, especially EETA79001. Furthermore, key element weight (wt) ratios (wt %/wt %) such as FeO/MnO (39.7), Al/Ti (7.2), Na/Ti (1.41), Ga/Al (3.9 10^{-3}), Na/Al (0.20) (*3*, *4*, *7*), and $\Delta^{17}O$ [+0.301 per mil (‰)] (fig. S9) (*8*) are also typical of martian meteorites. The average composition of the black glass (tables S7 and S8) is identical to a mixture of the major phases of the rock (augite, maskelynite, and olivine: 50:20:30) with compositional variations reflecting incomplete dissolution of one phase or another (fig. S7). Among minor elements in the black glass, chlorine is always below the detection level of electron microprobe analysis [100 parts per million (ppm)], whereas fluorine and sulfur exhibit variations in the range 0 to 4000 ppm and 0 to 6000 ppm, respectively (*5*).

Like most other picritic shergottites, bulk Tissint displays a marked depletion in light rare earth elements (LREEs) and other highly incompatible elements, such as Rb, Li, Be, Nb, Ta, Th, and U (Fig. 2). Its Lu/Hf ratio (0.2) is in the range of values measured for EETA79001 and other basaltic shergottites [0.1 to 0.2; e.g., (*9*)], and lower than those of the picritic shergottites DaG 476/489, SaU 005, and Dhofar 019 [about 0.3 (*10*–*12*)]. Although the sizes of the two samples analyzed here are somewhat limited (0.49 and 1.25 g), their trace-element abundances are very similar and so are likely to be representative of the whole rock composition, despite the irregular distribution of olivine megacrysts.

To evaluate the possible heterogeneity of this stone, we analyzed two additional samples: a groundmass-rich sample (devoid of large olivine crystals and weighing 181 mg) and a fragment of the same glassy pocket selected for volatile analysis (40 mg). Both samples display markedly higher LREE abundances, with REE patterns generally similar to those of the enriched shergottites, as exemplified by Zagami. However, there is a minor, but analytically valid, positive Ce anomaly (Ce/Ce* = 1.1) (Fig. 2), and the La/Nd, La/Nb, and Th/La ratios are higher than those of other enriched shergottites (fig. S10). These two samples indicate that an LREE-enriched component, different from those previously recorded in other shergottites, is heterogeneously dispersed throughout the matrix of Tissint.

The presence of short-lived ^{48}V (half-life = 16 days), among other cosmogenic isotopes, demonstrates that the stones we analyzed are from the fall of 18 July (table S10). We measured stable cosmogenic isotopes of He, Ne, and Ar in three aliquots, consisting of matrix-rich, glass-matrix mixed, and glass-rich separates (table S11). The cosmic-ray exposure (CRE) ages computed for $^{3}He_c$, $^{21}Ne_c$, and $^{38}Ar_c$ are 1.2 ± 0.4, 0.6 ± 0.2, and 0.9 ± 0.4 million years (My), respectively, resulting in an average CRE age of 0.7 ± 0.3 My for Tissint. This age is in the range of CRE ages of other shergottites, notably that of EETA79001 [0.73 ± 0.15 My (*2*)], suggesting that Tissint and other shergottites were ejected during a single event. Nitrogen isotopes were analyzed together with the noble gases. The glass aliquot displayed a well-defined excess of ^{15}N, which persisted after correction for contribution of cosmogenic $^{15}N_c$ (assuming a production rate of 6.7 ± 2.6 × 10^{-13} mol ^{15}N/gMa) (*13*). This excess ^{15}N is best explained by trapping of a martian atmospheric component (*2*). Using a $\delta^{15}N$ versus $^{40}Ar/N$ correlation and taking a martian atmospheric value from the Viking measurements of 0.33 ± 0.03 (*14*), we obtain a $\delta^{15}N$ value of 634 ± 60‰ (1σ), which agrees well with the Viking measurement of 620 ± 160‰ (*7*) (Fig. 3).

Simultaneous measurement of carbon and nitrogen was carried out by stepped combustion–mass spectrometry on a small chip (21 mg) from the same sample that we used for oxygen isotopic analysis (*5*). The sample had a total carbon abundance of 173 ppm and $\delta^{13}C$ of –26.6 ‰ and contained 12.7 ppm nitrogen with total $\delta^{15}N$ of –4.5‰. At temperatures above 600°C, both carbon and nitrogen were distributed among three discrete martian components (fig. S11 and table S12). Below 600°C, readily resolvable components of organic material combusted; although these may have been introduced during postfall collection and sample storage and are an unavoidable consequence of sample handling procedures, we cannot yet rule out the presence of small quantities of indigenous martian organic matter (*5*). At the highest temperatures of the extraction, there was a clear indication of the presence of trapped martian atmosphere, with elevated $\delta^{13}C$ and $\delta^{15}N$ (even allowing for a cosmogenic component, blank-corrected $\delta^{13}C$ reaches +16‰ and $\delta^{15}N$ reaches +298 ± 25‰). At intermediate temperatures (600° to 800°C), there were maxima in both $\delta^{13}C$ (–14‰) and $\delta^{15}N$ (+110‰), suggesting that the component bears some relationship to the martian atmosphere. In addition, there was clear analytical evidence for a simultaneous release of sulfur (~19 ppm), presumably from either sulfide or sulfate decomposition. This intermediate component probably corresponds to a surface-derived weathering component, as identified in Tissint glass on the basis of REE, S, and

Fig. 1. The Natural History Museum (London) stone. This 1.1-kg stone (BM.2012,M1) exhibits a black fusion crust with glossy olivines. The olivine macrocrysts (pale green) and the numerous black glass pockets and veins are characteristics of this shergottite. The scale is in centimeters.

[1]Hassan II University Casablanca, Faculty of Sciences, Géosciences Appliquées à l'Ingénierie et l'Aménagement (GAIA) Laboratory, BP 5366 Maârif, Casablanca Morocco. [2]Université Pierre et Marie Curie Paris 6, Institut de la Terre de Paris (UMR 7193) 4 Place Jussieu, 75005 Paris France. [3]Centre de Recherches Pétrographiques et Géochimiques-CNRS, Université de Lorraine, 15 rue Notre Dame des Pauvres, BP 20, F-54501 Vandoeuvre-lès-Nancy, France. [4]Université de Bretagne Occidentale–Institut Universitaire Européen de la Mer, UMR 6538, Place Nicolas Copernic, 29280 Plouzané Cedex, France. [5]Department of Earth and Atmospheric Sciences, University of Alberta, Edmonton, AB, T6G 2E3, Canada. [6]SLOWPOKE Nuclear Reactor Facility, 1-20 University Hall, University of Alberta, Edmonton, AB, T6G 2J9, Canada. [7]Planetary and Space Sciences, The Open University, Walton Hall, Milton Keynes, MK7 6AA, UK. [8]Centre Européen de Recherche et d'Enseignement des Géosciences de l'Environnement, CNRS Aix-Marseille University, BP80 13545 Aix en Provence, Cedex 4, France. [9]Department of Mineralogy, Natural History Museum, Cromwell Road London SW7 5BD, UK. [10]Laboratoire d'Etudes de la Matière Extraterrestre, Muséum National d'Histoire Naturelle and CNRS-UMS2679, 61 rue Buffon, 75005 Paris, France. [11]ESA (European Space Agency) European Space Research and Technology Center, Keplerlaan 1, 2200 AG Noordwijk, Netherlands. [12]UK Space Agency, ESA Harwell Centre, Atlas Building, Harwell Oxford, Didcot, Oxfordshire OX11 0QX, UK. [13]University of Bern, Albert Einstein Center for Fundamental Physics, Sidlerstrasse 5, CH-3012 Bern, Switzerland.

*To whom correspondence should be addressed. E-mail: chennaoui_h@yahoo.fr, h.chennaoui@fsac.ac.ma

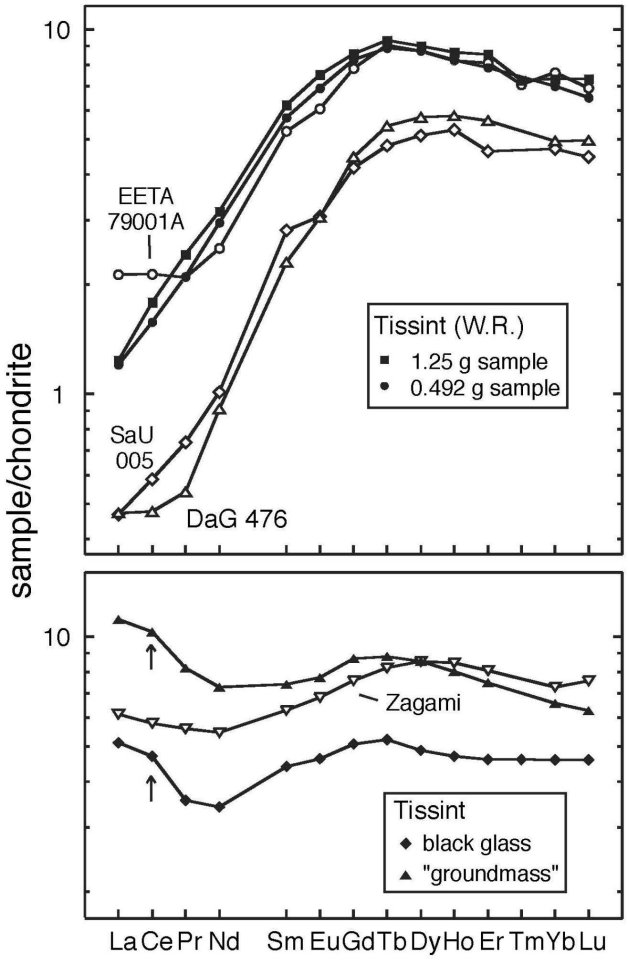

Fig. 2. REE patterns. (**Top**) Tissint in comparison with other depleted picritic shergottites. (**Bottom**) Black glass and groundmass-rich fraction in comparison with enriched shergottite Zagami. Data from (*10*–*12*). CI chondrite normalization values are from (*24*).

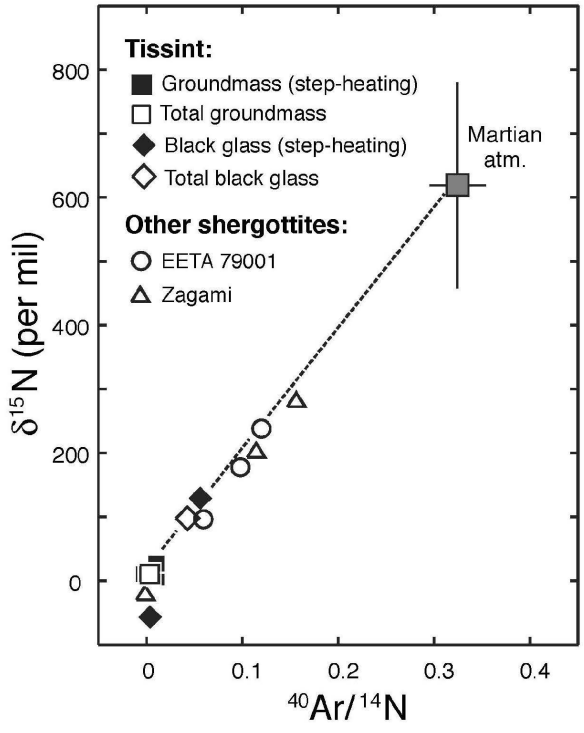

Fig. 3. Gas analyses of the black glass. Both bulk analyses and step-heating analyses plot on a single mixing line between terrestrial atmospheric gas (at left) and Mars atmospheric gas (*14*). Zagami data from (*25*).

F data (see below). The third martian component represents magmatic carbon, which is present in low abundance (1.4 ppm with $\delta^{13}C$ of –26.3‰) and is associated with isotopically light nitrogen ($\delta^{15}N < +10‰$).

Our study demonstrates that Tissint is a picritic shergottite comparable in many respects to EETA79001. The black shock glass resembles lithology C of EETA79001, as well as shock melt pockets commonly found in other shergottites (*15*). Major elements and oxygen isotope data indicate that this glass represents a melted mixture of the surrounding bulk rock, composed of olivine, maskelynite, and clinopyroxene (*5*). However, this glass is substantially different from the bulk meteorite and igneous groundmass in that it has a variable but generally high S and F content; a distinct LREE-enriched composition; and a high $\delta^{15}N$ value indicative of trapped martian atmosphere.

The LREE-enriched composition of the glass is somewhat enigmatic. Phosphates are often invoked as a carrier of REE. However, the P content of the black glass relative to bulk rock is not consistent with enrichment in phosphates. One possibility to explain the LREE composition of the glass might be selective crustal contamination before final emplacement of the Tissint magma. Although LREE-enriched magmatic rocks have been generated on Mars, as exemplified by the Nakhlites and Chassignites, these do not exhibit anomalous Ce abundances (*16*, *17*). In addition, crustal contamination of magma is unlikely to result in REE ratio variations at the subcentimeter scale, as observed here. Decoupling of Ce from the other REE indicates partial oxidation to Ce^{4+}, a process that requires oxidizing conditions, such as those that prevail in the near-surface environment of Mars. Surface weathering caused by leaching of phosphates by acid aqueous fluids, the process that is responsible for terrestrial alteration of eucritic meteorites in Antarctica (*18*), would also explain the LREE-enriched composition of the Tissint glass. The high $\delta^{15}N$ value of the Tissint glass, as well as its enrichment in S and F, demonstrates that it has been contaminated by martian surface components. In view of this evidence, the most likely explanation for the relatively LREE-enriched composition of the glass, and the origin of the Ce anomaly, is that these features also reflect the presence of a near-surface martian component in Tissint. A martian soil component was previously suggested for EETA79001 lithology C, which also contains martian atmospheric gases (*19*). However, because this meteorite is a find, rather than a fresh fall like Tissint, there's the possibility of terrestrial contamination, which complicates the interpretation (*20*).

We propose the following scenario to explain the composite nature of Tissint. A picritic basalt was emplaced at or near the surface of Mars. After some period, the rock was weathered by fluids, which had leached elements from the martian regolith. Subsequently, these fluids

deposited mineral phases within fissures and cracks. The martian weathering products are the most likely source of the required LREE, incompatible, and volatile elements. Upon impact, preferential, shock-induced melting occurred in the target rock along fractures where weathering products were concentrated. This melting produced the black glass and retained in it chemical signatures characteristic of the martian surface. Shock melting also trapped a component derived from the martian atmosphere, as revealed by stepped combustion–mass spectrometry. About 0.7 My ago, the sample was ejected from Mars and eventually landed on Earth in July 2011. The martian weathering features in Tissint described here are compatible with spacecraft observations on Mars, including those made by the NASA Viking landers, MER Spirit rover, and ESA's Mars Express orbiter (*5*, *21*–*23*).

References and Notes

1. D. D. Bogard, P. Johnson, *Science* **221**, 651 (1983).
2. R. H. Becker, R. O. Pepin, *Earth Planet. Sci. Lett.* **69**, 225 (1984).
3. A. H. Treiman, J. D. Gleason, D. D. Bogard, *Planet. Space Sci.* **48**, 1213 (2000).
4. G. Crozaz, M. Wadhwa, *Geochim. Cosmochim. Acta* **65**, 971 (2001).
5. Supplementary materials are available on *Science* Online.
6. P. Rochette *et al*., *Meteorit. Planet. Sci.* **40**, 529 (2005).
7. A. O. Nier, M. B. McElroy, *J. Geophys. Res.* **82**, 4341 (1977).
8. I. A. Franchi, I. P. Wright, A. S. Sexton, C. T. Pillinger, *Meteorit. Planet. Sci.* **34**, 657 (1999).
9. J. Blichert-Toft, J. D. Gleason, P. Télouk, F. Albarède, *Earth Planet. Sci. Lett.* **173**, 25 (1999).
10. G. Dreibus *et al*., *Meteorit. Planet. Sci.* **35**, A49 (2000).
11. J. A. Barrat, J. Blichert-Toft, R. W. Nesbitt, F. Keller, *Meteorit. Planet. Sci.* **36**, 23 (2001).
12. C. R. Neal, L. A. Taylor, J. C. Ely, J. C. Jain, M. A. Nazarov, *Lunar Planet. Sci.* **32**, 1671 (2001).
13. B. Marty, K. Hashizume, M. Chaussidon, R. Wieler, *Space Sci. Rev.* **106**, 175 (2003).
14. T. Owen *et al*., *J. Geophys. Res.* **82**, 4635 (1977).
15. J.-A. Barrat *et al*., *Geochim. Cosmochim. Acta* **66**, 3505 (2002).
16. V. Sautter *et al*., *Earth Planet. Sci. Lett.* **195**, 223 (2002).
17. P. Beck *et al*., *Geochim. Cosmochim. Acta* **70**, 2127 (2006).
18. D. W. Mittlefehldt, M. M. Lindstrom, *Geochim. Cosmochim. Acta* **67**, 1911 (2003).
19. M. N. Rao, L. E. Borg, D. S. McKay, S. J. Wentworth, *Geophys. Res. Lett.* **26**, 3265 (1999).
20. E. L. Walton, P. J. Jugo, C. D. K. Herd, M. Wilke, *Geochim. Cosmochim. Acta* **74**, 4829 (2010).
21. R. E. Arvidson, J. L. Gooding, H. J. Moore, *Rev. Geophys.* **27**, 39 (1989).
22. L. A. Haskin *et al*., *Nature* **436**, 66 (2005).
23. A. Gendrin *et al*., *Science* **307**, 1587 (2005).
24. J. A. Barrat *et al*., *Geochim. Cosmochim. Acta* **83**, 79 (2012).
25. K. Marti, J. S. Kim, A. N. Thakur, T. J. McCoy, K. Keil, *Science* **267**, 1981 (1995).

Acknowledgments: We acknowledge D. N. Menegas and family for their generous donation enabling the acquisition of Tissint (BM.2012,M1), M. Aoudjehane for fieldwork, A. Aaranson for field information, J. Gibson for assistance with oxygen isotope analysis, L. Labenne for loan of a sample, and A. Irving for 400 mg of powdered sample. This study was funded at Hassan II University Casablanca, Faculté des Sciences Ain Chock, by Centre de Recherches Scientifiques et Techniques Morocco and CNRS France (Projet International de Coopération Scientifique, Sciences de l'Univers 01/10), and by Comité Mixte Inter Universitaire Franco-Marocain Volubilis (MA/11/252); CRPG Nancy, France, by the CNES, CNRS, and European Research Council under the European Community's Seventh Framework Programme (FP7/2007-2013 no. 267255); Université de Bretagne Occidentale–Institut Universitaire Européen de la Mer, Plouzané, France, by the Programme National de Planétologie, Institut National des Sciences de l'Univers; Open University, by Science and Technology Facilities Council grant to the Planetary and Space Sciences Discipline; and University of Alberta, by the Natural Sciences and Engineering Research Council of Canada (grant 261740-03).

Supplementary Materials

www.sciencemag.org/cgi/content/full/science.1224514/DC1
Materials and Methods
Supplementary Text
Figs. S1 to S11
Tables S1 to S13
References (*26*–*35*)

9 May 2012; accepted 25 September 2012
Published online 11 October 2012;
10.1126/science.1224514

Development and Disintegration of Maya Political Systems in Response to Climate Change

Douglas J. Kennett,[1]*† Sebastian F. M. Breitenbach,[2]* Valorie V. Aquino,[3] Yemane Asmerom,[4] Jaime Awe,[5] James U.L. Baldini,[6] Patrick Bartlein,[7] Brendan J. Culleton,[1] Claire Ebert,[1] Christopher Jazwa,[1] Martha J. Macri,[8] Norbert Marwan,[9] Victor Polyak,[4] Keith M. Prufer,[3] Harriet E. Ridley,[6] Harald Sodemann,[10] Bruce Winterhalder,[11] Gerald H. Haug[2]

The role of climate change in the development and demise of Classic Maya civilization (300 to 1000 C.E.) remains controversial because of the absence of well-dated climate and archaeological sequences. We present a precisely dated subannual climate record for the past 2000 years from Yok Balum Cave, Belize. From comparison of this record with historical events compiled from well-dated stone monuments, we propose that anomalously high rainfall favored unprecedented population expansion and the proliferation of political centers between 440 and 660 C.E. This was followed by a drying trend between 660 and 1000 C.E. that triggered the balkanization of polities, increased warfare, and the asynchronous disintegration of polities, followed by population collapse in the context of an extended drought between 1020 and 1100 C.E.

The Classic Maya (300 to 1000 C.E.) left a remarkable historical record inscribed on well-dated stone monuments. Wars, marriages, and accessions of kings and queens are tied to long count calendar dates and correlate with specific days in the Christian calendar (Goodman-Thompson-Martinez correlation). The termination of this tradition between 800 and 1000 C.E. marks the widespread collapse of Classic Maya political systems. Multidecadal drought has been implicated, but remains controversial because of dating uncertainties and insufficient temporal resolution in paleoclimatic records. Lake sediments from the Yucatan Peninsula provided the first evidence of substantial drying in the Terminal Classic (*1*). However, disturbances to lake sediment sequences caused by prehistoric deforestation and agricultural expansion during the Classic Period complicate reproducing these results near the largest and most politically important Maya centers (such as Tikal and Caracol). Several studies more distant from the Maya lowlands (ML) support either relatively dry conditions or a series of droughts during the Terminal Classic (*2*–*5*), but the relevance of these records for the ML remains unclear (*6*).

Cave deposits in the ML show great promise for paleoclimatic reconstruction (*7*–*9*). The challenge lies in developing long, continuous records from rapidly growing stalagmites that can be dated precisely by using ^{234}U-^{230}Th (U-Th). Here, we present a subannually resolved rainfall record from an exceptionally well-dated stalagmite collected from Yok Balum (YB) Cave in Belize (16°12'30.780" N, 89°4'24.420" W, 366 m above sea level) (*10*). YB cave is located 1.5 km from the Classic Period Maya site of Uxbenká. Three other important Maya centers (Pusilha, Lubaantun, Nim Li Punit) are within 30 km (fig. S1); Tikal and other major Classic Period population centers (such as Caracol, Copan, and Calakmul) are

[1]Department of Anthropology, Pennsylvania State University, University Park, PA 16802, USA. [2]Department of Earth Science, Eidgenössische Technische Hochschule (ETH), CH-8092 Zürich, Switzerland. [3]Department of Anthropology, University of New Mexico, Albuquerque, NM 87131, USA. [4]Department of Earth and Planetary Sciences, University of New Mexico, Albuquerque, NM 87131, USA. [5]Institute of Archaeology, National Institute of Culture and History, Belmopan, Belize. [6]Department of Earth Sciences, University of Durham, Durham DH1 3LE, UK. [7]Department of Geography, University of Oregon, Eugene, OR 97403, USA. [8]Department of Native American Studies, University of California, Davis, Davis, CA 95616, USA. [9]Potsdam Institute for Climate Impact Research, Post Office Box 60 12 03, 14412 Potsdam, Germany. [10]Institute for Atmospheric and Climate Science, ETH, CH-8092 Zürich, Switzerland. [11]Department of Anthropology, University of California, Davis, Davis, CA 95616, USA.

*These authors contributed equally to this work.
†To whom correspondence should be addressed. E-mail: djk23@psu.edu

5.4 Article Origins of volatile elements (H, C, N, noble gases) on Earth and Mars in light of recent results from the ROSETTA cometary mission, *published in 2016 in Earth and Planetary Science Letters, Vol. 441, 91-102.*

Earth and Planetary Science Letters 441 (2016) 91–102

Contents lists available at ScienceDirect

Earth and Planetary Science Letters

www.elsevier.com/locate/epsl

Origins of volatile elements (H, C, N, noble gases) on Earth and Mars in light of recent results from the ROSETTA cometary mission

Bernard Marty [a,*], Guillaume Avice [a], Yuji Sano [b], Kathrin Altwegg [c], Hans Balsiger [c], Myrtha Hässig [c], Alessandro Morbidelli [d], Olivier Mousis [e], Martin Rubin [c]

[a] Centre de Recherches Pétrographiques et Géochimiques, CRPG-CNRS, Université de Lorraine, UMR 7358, 15 rue Notre Dame des Pauvres, BP 20, 54501 Vandoeuvre lès Nancy, France
[b] Ocean and Atmosphere Research Institute, The University of Tokyo, 5-1-5, Kashiwanoha, Kashiwa-shi, Chiba 277-8564, Japan
[c] Physikalisches Institut, University of Bern, Sidlerstr. 5, CH-3012 Bern, Switzerland
[d] Laboratoire Lagrange, Université Côte d'Azur, CNRS, Observatoire de la Côte d'Azur, Boulevard de l'Observatoire, BP 4229, 06304 Nice Cedex 4, France
[e] Aix Marseille Université, CNRS, LAM (Laboratoire d'Astrophysique de Marseille) UMR 7326, 13388 Marseille, France

ARTICLE INFO

Article history:
Received 28 September 2015
Received in revised form 9 February 2016
Accepted 15 February 2016
Editor: C. Sotin

Keywords:
ROSETTA
argon
origins
terrestrial volatiles
Martian atmosphere

ABSTRACT

Recent measurements of the volatile composition of the coma of Comet 67P/Churyumov–Gerasimenko (hereafter 67P) allow constraints to be set on the origin of volatile elements (water, carbon, nitrogen, noble gases) in inner planets' atmospheres. Analyses by the ROSINA mass spectrometry system onboard the Rosetta spacecraft indicate that 67P ice has a D/H ratio three times that of the ocean value (Altwegg et al., 2015) and contains significant amounts of N_2, CO, CO_2, and importantly, argon (Balsiger et al., 2015). Here we establish a model of cometary composition based on literature data and the ROSINA measurements. From mass balance calculations, and provided that 67P is representative of the cometary ice reservoir, we conclude that the contribution of cometary volatiles to the Earth's inventory was minor for water ($\leq$1%), carbon ($\leq$1%), and nitrogen species (a few % at most). However, cometary contributions to the terrestrial atmosphere may have been significant for the noble gases. They could have taken place towards the end of the main building stages of the Earth, after the Moon-forming impact and during either a late veneer episode or, more probably, the Terrestrial Late Heavy Bombardment around 4.0–3.8 billion years (Ga) ago. Contributions from the outer solar system via cometary bodies could account for the dichotomy of the noble gas isotope compositions, in particular xenon, between the mantle and the atmosphere. A mass balance based on ^{36}Ar and organics suggests that the amount of prebiotic material delivered by comets could have been quite considerable – equivalent to the present-day mass of the biosphere. On Mars, several of the isotopic signatures of surface volatiles (notably the high D/H ratios) are clearly indicative of atmospheric escape processes. Nevertheless, we suggest that cometary contributions after the major atmospheric escape events, e.g., during a Martian Late Heavy Bombardment towards the end of the Noachian era, could account for the Martian elemental C/N/^{36}Ar ratios, solar-like krypton isotope composition and high ^{15}N/^{14}N ratios. Taken together, these observations are consistent with the volatiles of Earth and Mars being trapped initially from the nebular gas and local accreting material, then progressively added to by contributions from wet bodies from increasing heliocentric distances. Overall, no unified scenario can account for all of the characteristics of the inner planet atmospheres. Advances in this domain will require precise analysis of the elemental and isotopic compositions of comets and therefore await a cometary sample return mission.

1. Introduction

According to cosmochemical constraints and simulations, the inner planets grew first "dry", and water and atmophile elements were contributed later on by volatile-rich objects originating from larger heliocentric distances (Morbidelli et al., 2000; Raymond et al., 2004; Albarède et al., 2013; Marty, 2012). A cometary origin for the Terrestrial oceans, the atmosphere and the organics is often advocated (Oro, 1961; Anders and Owen, 1977; Safronov, 1972) because (i) comets are volatile-rich as they contain abundant organics and ices (30–50 wt.% H_2O), and (ii) their high eccentricities and hyperbolic trajectories increase their probability to encounter inner solar system bodies. Other potential sources of

* Corresponding author.
E-mail address: bmarty@crpg.cnrs-nancy.fr (B. Marty).

http://dx.doi.org/10.1016/j.epsl.2016.02.031
0012-821X/

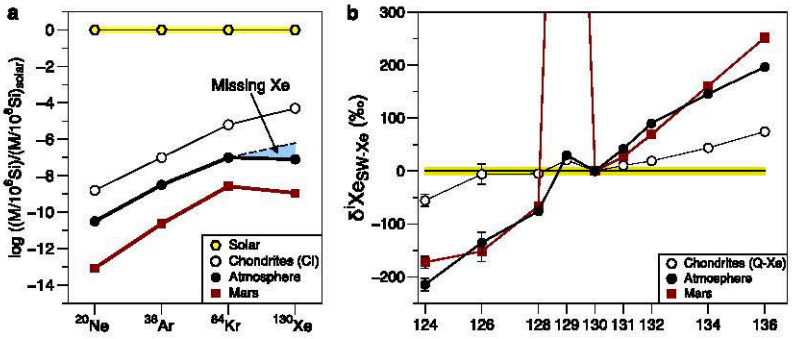

Fig. 1. (a) Comparison of the abundance patterns of noble gases in the Sun ("Solar", yellow hexagons), in volatile-rich primitive meteorites ("CI", empty circles) and in the atmospheres of Earth (black-filled circles) and Mars (red squares). Note that the latter are depleted in xenon relative to krypton and meteorites by about a factor of 20, and that the Kr/Xe is close to the solar abundance (the "missing" Xe for Earth's atmosphere is represented by the blue area, see text). Modified after Porcelli and Ballentine (2002), Mars data from Dauphas and Morbidelli (2014). (b) Comparison of the Xe isotope compositions of meteoritic Xe (empty circles, "Q–Xe"), atmospheric Xe ("Atmosphere", black-filled circles), and Martian atmosphere Xe ("Mars–Xe", red squares), expressed in deviations in parts per mil (‰) relative to the solar composition (derived from solar wind measurements, yellow bar). In this format, the solar composition gives a flat spectrum at 0‰. The meteoritic composition is slightly different from Solar, whereas Martian and Terrestrial Xe are clearly fractionated (enriched in heavy isotopes) compared to solar, prohibiting direct derivation from the protosolar nebula and, by inference, from cometary ice (see text). Data from Ott (2014). (For interpretation of the references to color in this figure legend, the reader is referred to the web version of this article.)

water are "wet" asteroids. Meteorites are generally dry, although some of them, the carbonaceous chondrite clan, can contain up to 15 wt.% equivalent H_2O as hydrated phases. Because these phases are remnant of water–rock interactions on asteroids, the original water content could have been significantly higher, possibly matching those of comets. This would argue in favor of a continuum between meteoritic and cometary compositions in the past. The Terrestrial oceans (1.5×10^{24} g) correspond to 0.025% of the Earth's mass. Taking into account water in the deep Earth may raise the Terrestrial H_2O inventory to a maximum of 0.2 wt.% (Marty, 2012). Assuming conservation of volatile elements during impacts, that is, no loss of volatiles to space (an assumption discussed later on), Terrestrial water could have been supplied by a few wt. per mil to a few wt. percent of cometary, or asteroidal, material to a dry proto-Earth, leaving the bulk chemical composition of Earth little affected.

Dynamical models suggest that, during its formation, the Earth accreted water and other volatile elements predominantly from planetesimals parented to primitive asteroids, i.e. with composition similar to carbonaceous chondrites (Morbidelli et al., 2000; Raymond et al., 2004, 2007; O'Brien et al., 2006, 2014). Comets, intended as planetesimals of trans-Neptunian origin, should have had a negligible contribution during Earth's accretion. Instead, once the Earth's formation was completed, possibly several hundreds of million years (Ma) afterwards, the Earth should have accreted non-negligible amounts of mass from asteroids and/or from icy bodies of trans-Neptunian origin, during a dynamical instability event that re-structured the orbital configuration of the giant planets (the so-called "Nice model"; Gomes et al., 2005). These models predict contributions of icy bodies in proportions comparable to those of asteroids. From the lunar impact crater record, Chyba (1990) argued that the Earth could have acquired an exogenous ocean around 4 Ga ago if comets comprised $\geq$10 wt.% of the impacting population. Marty and Meibom (2007) made the point that, if comets contain noble gases in amount predicted by laboratory ice trapping experiments (see below), then the fraction of cometary material in the late heavy bombardment on Earth could not have been more than 0.5%, as constrained by the noble gas inventory of the atmosphere.

Cometary contributions might have left an imprint in the composition of the ocean–atmosphere. Owen and Bar-Nun (1995) noted that the noble gas elemental composition of the atmospheres of Mars and Earth (which are different from those of chondrites by having a one order of magnitude lower Xe/Kr ratio, Fig. 1), are consistent with a cometary origin. Experiments of noble gas trapping in growing amorphous ice have shown that the absolute amounts and their relative proportions depend on the trapping kinetics, pressure and, importantly, temperature (Bar-Nun et al., 1985). Owen and Bar-Nun (1995) proposed a cometary ice formation temperature of 50 K to account for the Martian and Terrestrial Ar/Kr/Xe ratios. Other works questioned the relevance of these experimental conditions to those of the protosolar nebula (Notesco and Bar-Nun, 2005; Yokochi et al., 2012) or preferred trapping of cometary noble gases in clathrates rather than in amorphous ice (Mousis et al., 2010). Importantly, because Xe from the protosolar nebula is expected to be quantitatively trapped in cometary ice (Notesco and Bar-Nun, 2005; Yokochi et al., 2012; Mousis et al., 2010) and because physical adsorption does not induce significant Xe isotope fractionation (Marrocchi and Marty, 2013), cometary Xe should have a solar-like isotopic composition. However, the xenon isotopic compositions of the atmospheres of Earth and Mars are not solar (nor chondritic), being enriched in the heavy isotopes relative to the light ones by 3–4% par atomic mass unit (Fig. 1). Taking into account this discrepancy, Dauphas (2003) proposed a dual origin for the Terrestrial atmosphere. In his model, a primary atmosphere of solar composition was lost to space, leaving residual gases mostly made of isotopically fractionated Xe. Then comet-like bodies contributed noble gases depleted in Xe (following the same argument as Owen and Bar-Nun, 1995, that cometary ice should depleted in Xe compared to Chondritic and other noble gases, Fig. 1). This model accounts successfully for the elemental and isotopic compositions of atmospheric noble gases and for the "xenon paradox": Atmospheric xenon is depleted relative to Chondritic Xe but also relative to atmospheric Kr, and enriched in its heavy isotopes relative to any known cosmochemical composition (Fig. 1), both properties being paradoxical if xenon depletion was due atmospheric escape. However, the Xe paradox might be related to a different process and may not be a diagnostic of source composition. Indeed, from the analysis of ancient (>2.7 Ga-old) minerals, Pujol et al. (2011) argued for continuous loss and isotopic fractionation of atmospheric xenon to space through geological time as a cause of the peculiar composition of atmospheric Xe. Therefore the xenon paradox might be due to secondary long-term processing and not to a source effect.

The hydrogen and nitrogen isotopes give independent insight into the origin(s) of planetary volatiles (e.g. Alexander et al., 2012; Marty, 2012; Füri and Marty, 2015; Fig. 2). Taken together, they suggest an asteroidal, rather than cometary, origin for nitrogen

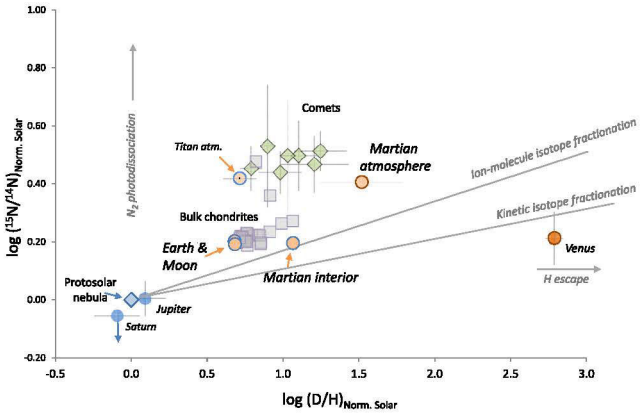

Fig. 2. Nitrogen vs. hydrogen isotope variations among solar system reservoirs (modified after Aléon, 2010, and Füri and Marty, 2015). The H and N isotopic ratios are normalized to the respective protosolar values. Fractionation trajectories are displayed for illustration. "Ion-molecule" is from Aléon (2010), representing isotope fractionation during ion molecule exchange. "Kinetic" illustrates the case of isotope fractionation proportional to the inverse square root of masses and is only one of the possibilities (others involve reduced masses, molecular masses instead of atomic masses etc.). Light blue dots: Giant planets; beige dots: inner planets and Titan; grey squares: bulk primitive meteorites; light green diamonds: comets. (For interpretation of the references to color in this figure legend, the reader is referred to the web version of this article.)

and water in the Terrestrial atmosphere and the oceans. The D/H ratios of comets are generally higher by a factor of 2–3 relative to the ocean's value and to most of the chondritic values, prohibiting a genetic relationship between cometary ice and Terrestrial water. Available data are mostly from long-period comets thought to originate from the Oort cloud. The measurement of an ocean-like D/H ratio for a Jupiter family comet (Hartogh et al., 2011), presumably originating from the Kuiper belt, suggests a D/H heterogeneity among comet families. Recently, a D/H value three times the ocean's has been measured in the coma from Comet 67P/Churyumov–Gerasimenko (thereafter 67P), also a Jupiter family member (Altwegg et al., 2015). The nitrogen isotopes give a similar story. Chondrites have variable N isotope ratios which distribution coincides with the Terrestrial composition. In contrast, comets have $^{15}N/^{14}N$ ratios about two times the Terrestrial and bulk chondritic values (Fig. 2). One possible caveat is that only HCN, CN, and NH_2^+ could be measured at distance by spectroscopy (there is no in-situ measurement on a comet), and it is not clear if these nitrogen species are representative of bulk cometary N.

In this contribution we use the recent compositional data of the 67P coma obtained by the ROSINA mass spectrometer on board of the ROSETTA spacecraft to set constraints on the origin(s) of volatile elements on Earth and Mars. Importantly, this instrument measured for the first time a noble gas – argon – in cometary gases (Balsiger et al., 2015). We present first a model composition for cometary matter using literature data and assuming that 67P is representative of the cometary reservoir. We then attempt a mass balance to infer the possible contribution of the outer solar system to the Terrestrial and Martian inventory of water, carbon, nitrogen and noble gases.

2. Reservoir inventories

2.1. Comets

2.1.1. Elemental abundances

The chemical and isotopic compositions of comets is constrained by (i) in-situ measurements by spacecrafts (e.g., A'Hearn et al., 2011; Le Roy et al., 2015; Jessberger et al., 1988; Kissel and Krueger, 1987), (ii) spectroscopic observations of comae (e.g., Bockelée-Morvan, 2011; Mumma and Charnley, 2011), and (iii) laboratory analysis of cometary grains recovered by the Stardust mission (Brownlee et al., 2006) and of interplanetary dust particles presumably of cometary in origin (e.g., Duprat et al., 2010).

Table 1
Coma composition. *1*: Species and elements are molar fractions normalized to water (=100). *2*: The range of C- and N-bearing species concentrations are for all comets analyzed so far (compiled from Bockelée-Morvan, 2011; Mumma and Charnley, 2011; Le Roy et al., 2015). *3*: The N_2 content is derived from the comet 67P measurement by Rubin et al. (2015), the good correlation between CO and N_2, and the cometary CO content given above. *4*: Ar/H_2O ratio from Balsiger et al. (2015).

	Lower	Upper	Mean	+/−	
Water			100		*1*
Carbon					
CO_2	2.5	80	41	39	*2*
CO	1	30	16	15	*2*
CH_4	0.6	1.5	1.05	0.45	*2*
C_2H_2	0.1	0.46	0.28	0.18	*2*
C_2H_6	0.4	10.5	5.45	5.05	*2*
others	0.4	2.4	1.40	1.00	*2*
ΣC			71	65	
Nitrogen					
NH_3	0.3	1.5	0.90	0.60	*2*
HCN	0.1	0.6	0.35	0.25	*2*
N_2			0.088	0.083	*3*
ΣN			1.43	1.02	
$N_2/\Sigma N$			0.06	0.07	
Argon					
^{36}Ar			1.20E−03	1.10E−03	*4*

Comets are made of refractory silicates and metal, refractory and non-refractory organics, and ices (Jessberger et al., 1988; Kissel and Krueger, 1987; Mumma and Charnley, 2011; Bockelée-Morvan, 2011). The analysis of cometary grains recovered by the Stardust mission revealed the occurrence of several high temperature phases reminiscent of chondritic material. These are calcium–aluminum rich inclusions, chondrules and refractory olivines. Stable isotope compositions of these phases indicate an inner solar system origin for this material (Brownlee et al., 2006). From mass balance, silicate + metal (Si, Mg, Fe) grains make about 25–30 wt.% (Jessberger et al., 1988). Refractory organics constitute a significant fraction of C and, to a lesser extent, of N and H, and must be taken into account in the bulk composition of cometary matter (Greenberg, 1998). This is confirmed by a refractory organics/silicate + metal ratio close to 1 for dust emitted by comet Halley (Kissel and Krueger, 1987). Therefore, organic refractory particles (the so-called CHON grains, Jessberger et al., 1988) could make another 25–30 wt.%, and non-refractory carbon-bearing species could contribute about 4–8 wt.% (Greenberg, 1998). The proportion of ice amounts for 30–50 wt.%. The composition of comae (Table 1) gives insight into the ice composition (~80 wt.% H_2O with CO, CO_2, CH_3OH, CH_4, H_2S, and N-compounds including CN, HCN, NH_3 and N; Bockelée-Morvan, 2011; Hässig et al., 2015; Rubin et al., 2015).

Noble gases are able to set stringent constraints on the origin of planetary volatiles on one hand, and on processes and conditions of comet formation on another hand. Unfortunately the abundances of noble gases in comets are essentially unknown as these elements are extremely difficult to detect by spectroscopy. Stern et al. (2000) proposed an Ar/O ratio of $1.8 \pm 1.0 \times 10^{-4}$ for Comet Hale Bopp, lower than the solar value of 46×10^{-4} (Weaver et al., 2002, and refs. therein), but this estimate has not been confirmed. Weaver et al. (2002) suggested that the cometary Ar/O ratios are lower than 42×10^{-4}, based on three comet observations. The only reliable set of measurements are those done on 67P coma using the ROSINA mass spectrometer which directly the 67P coma composition (Balsiger et al., 2015). They indicate a

Table 2
Cometary bulk composition. Abundances are computed with data from cometary composition (see text), Table 1 and refs. therein. The ^{36}Ar content is for 30% water ice.

	Coma (mole/g)	+/−	Bulk (mole/g)	+/−
^{12}C	0.012	0.011	0.037	0.028
^{14}N	0.00025	0.00018	0.0018	0.0010
H_2O	0.017	0.0010	0.019	0.0010
^{36}Ar	2.07E−07	1.89E−07	2.07E−07	1.89E−07

$^{36}Ar/H_2O$ varying between 0.1×10^{-5} and 2.3×10^{-5} during the 3 days measurement period. Considering that Ar/O ∼1.3 Ar/H_2O (Weaver et al., 2002), and taking into account a solar isotope composition for argon ($^{40}Ar \sim 0$, $^{38}Ar/^{36}Ar = 0.183$), the corresponding Ar/O range of 67P is $0.01–0.35 \times 10^{-4}$, thus lower than the upper limits given above, and 2–3 orders of magnitude lower than the solar ratio of 46×10^{-4}. It is worth mentioning that even if noble gases are mostly hosted in ices, refractory grains may also contain large amounts of these elements, as suggested by the discovery of high He and Ne abundances in grains of comet Wild2 recovered by the Stardust spacecraft (Marty et al., 2008). However, a mass balance is not possible due to the lack of relevant Ar data, and we adopt here the 67P coma composition.

2.1.2. Isotopes

The stable isotope ratios relevant to this study are the D/H ratios of comets, with special reference to the 67P value ($[5.3 \pm 0.7] \times 10^{-4}$, ∼3 times the ocean water ratio; Altwegg et al., 2015), and N isotope variations depicted in Fig. 2, although no data are yet available for 67P. For noble gases, only the $^{36}Ar/^{38}Ar$ ratio has been measured in the coma of 67P (5.4 ± 1.6; Balsiger et al., 2015), consistent with a solar system composition, but with a precision too low to permit identification of a specific cosmochemical component. Models of ice formation from a protosolar nebula gas predict that the isotopic composition of noble gases are solar. However, there is considerable uncertainty arises for the mode of trapping (i.e., neutral versus ionized) which may fractionate, or not, noble gas isotopes, and for the local composition of the gas during ice formation. Furthermore, the analysis of Stardust refractory grains revealed a high abundance of light noble gases and has shown that the neon isotope composition is closer to a meteoritic signature than to a solar one, precluding to establish a definite composition for cometary noble gases. Measurements of noble gas isotopes in comets should be a given a high priority in future space programmes. In the absence of such, we only discuss here the case of argon. The model cometary composition is given in Table 2. The uncertainties represent the range of values observed in comets, unless a single set of values is available.

2.2. Carbonaceous chondrites

For noble gases, we use a literature survey of 87 noble gas analyses of CI and CM (Schultz and Franke, 2004). The H, C and N data are from 40 analyses compiled by Kerridge (1985). The respective mean chondritic abundances of C, N, H_2O and ^{36}Ar are, in mol/g: $2.3 \pm 1.2 \times 10^{-3}$, $6.4 \pm 2.5 \times 10^{-5}$, $3.7 \pm 1.0 \times 10^{-3}$ and $3.1 \pm 1.6 \times 10^{-11}$, respectively.

2.3. Earth

The inventory of volatile elements at the Earth's surface (the atmosphere, the oceans and the crust) is reasonably well known. The problem is to estimate the amount of volatiles in the mantle, since magmas tend to degas readily upon eruption, and the inferred source compositions are model-dependent. Recent estimates

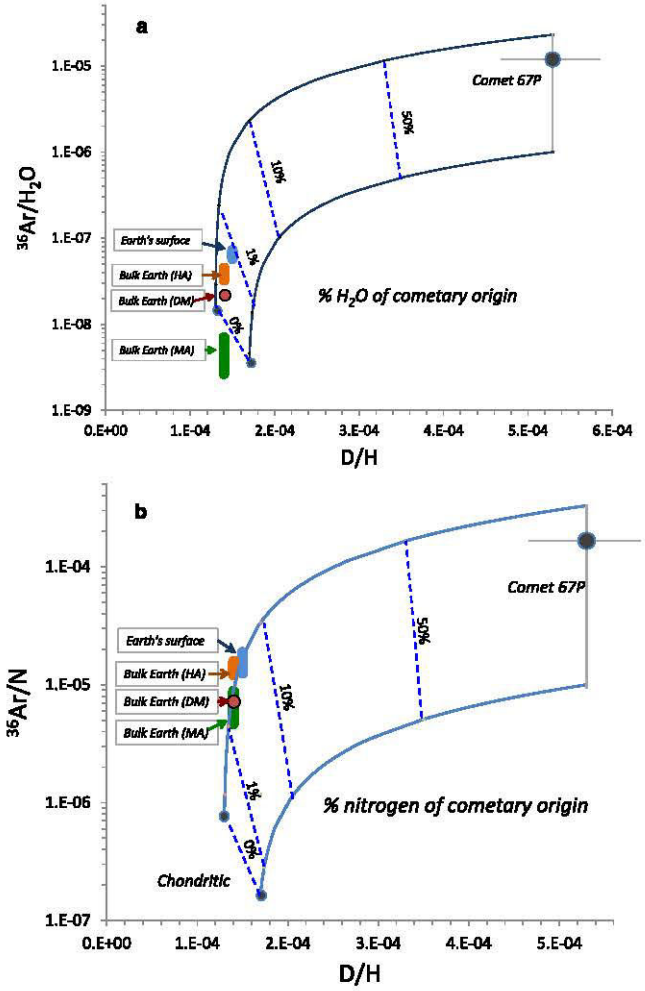

Fig. 3. $^{36}Ar/H_2O$ (a) and $^{36}Ar/N$ (b) versus D/H mixing diagrams between cometary and chondritic (asteroidal) end-members. The mixing curves are constructed as $[X/Y]_{observed} = \alpha \times [X/Y]_1 + (1 - \alpha) \times [X/Y]_2$ for two end-members having cometary/chondritic elemental/isotopic compositions. Coefficients α are computed in each case using the end-member compositions (Tables 1 and 2). Terrestrial reservoir compositions from Table 3: HA, DM and MA are the bulk Earth estimates from Halliday (2013), Dauphas and Morbidelli (2014) and Marty (2012), respectively. Dotted lines indicate the percentage of cometary water (a) and of cometary nitrogen (b), respectively, on Earth.

of the bulk Earth (mantle plus surface) volatile inventories have been given by Marty (2012), Halliday (2013) and Dauphas and Morbidelli (2014). We adopt here two limiting cases. The lower limit is based on the reconstruction of the initial volatile inventory of the mantle regions sampled by volcanism. The initial contents of water, C, N and noble gases in the mantle source of mid-ocean ridge basalts (MORB; volumetrically the main source of lavas at the Earth's surface) is derived from a combination of lava fluxes and calibration to relevant tracers like ^{3}He or refractory elements like Ce, Nb. Halliday (2013) considered also the source of Ocean Island basalts (another important source of volcanism thought to tap deep regions of the mantle), ("HA" in Figs. 3 and 4). Dauphas and Morbidelli (2014; "DM") obtained an inventory comparable to the one of Halliday (2013) from global calibration of volatiles to refractory (Ce, Nb) elements, and obtained a total bulk Earth water content of about 3 ocean masses (M_{Ocean} equivalent to 230 ppm H_2O for bulk Earth). The isotopic compositions of helium, neon, argon and xenon suggest that deep mantle regions could be richer in volatiles than the convective mantle sampled by mid-ocean ridges.

Table 3
Earth's volatile composition. Data are in mol/g for bulk Earth (mass = 5.98×10^{27} g). "Atmosphere" refers to the atmosphere *sensu stricto*, the oceans and crustal and sedimentary rocks (data are from Ozima and Podosek, 2002; Dauphas and Morbidelli, 2014, and refs. therein). Uncertainties on the C and N contents of the "atmosphere" are ~20%. Halliday (2013; HA) considered the mantle sources of MORBs and of ocean basalt islands (note that the listed abundances differ from those given by Halliday, 2013, in which some of the numbers could not be reproduced). Marty (2012; MA) computed volatile element abundances from K–Ar systematics which predicts that, for a K content of 280 ± 60 ppm (1σ; Arevalo et al., 2009), half of radiogenic ^{40}Ar produced by the decay of ^{40}K ($T_{1/2}$ = 1.25 Ga) over 4.5 Ga is still trapped in the mantle. The other volatile contents are computed from ^{40}Ar/N/C/H_2O ratio estimates for OIBs and MORBs. Dauphas and Morbidelli (2014; DM) published recently estimates for volatile content of inner planets and other cosmochemical reservoirs, which are intermediate between HA and MA abundances, although closer to the former. HA and BM are assumed to represent two limiting cases for the Terrestrial inventory of volatile elements in the silicate Earth + surface.

	Atmosphere (mol/g)	Halliday, 2013 – HA				Marty, 2012 – MA				Dauphas and Morbidelli, 2014
		Mantle		atm. + mantle		Mantle		atm. + mantle		DM (mol/g)
		(mol/g)	+/−	(mol/g)	+/−	(mol/g)	+/−	(mol/g)	+/−	
^{12}C	1.29E−06	4.00E−06	1.89E−06	5.29E−06	1.89E−06	6.38E−05	2.50E−05	6.51E−05	2.50E−05	5.60E−06
^{14}N	5.98E−08	7.48E−09	4.71E−09	6.73E−08	8.97E−09	9.08E−08	4.60E−08	1.51E−07	4.60E−08	1.12E−07
H_2O	1.48E−05	1.80E−05	6.00E−06	3.28E−05	6.00E−06	2.00E−04	9.60E−05	2.15E−04	9.60E−05	4.35E−05
^{36}Ar	9.33E−13	3.03E−15	1.59E−15	9.36E−13	1.59E−15	7.83E−14	4.30E−14	1.01E−12	4.30E−14	9.29E−13

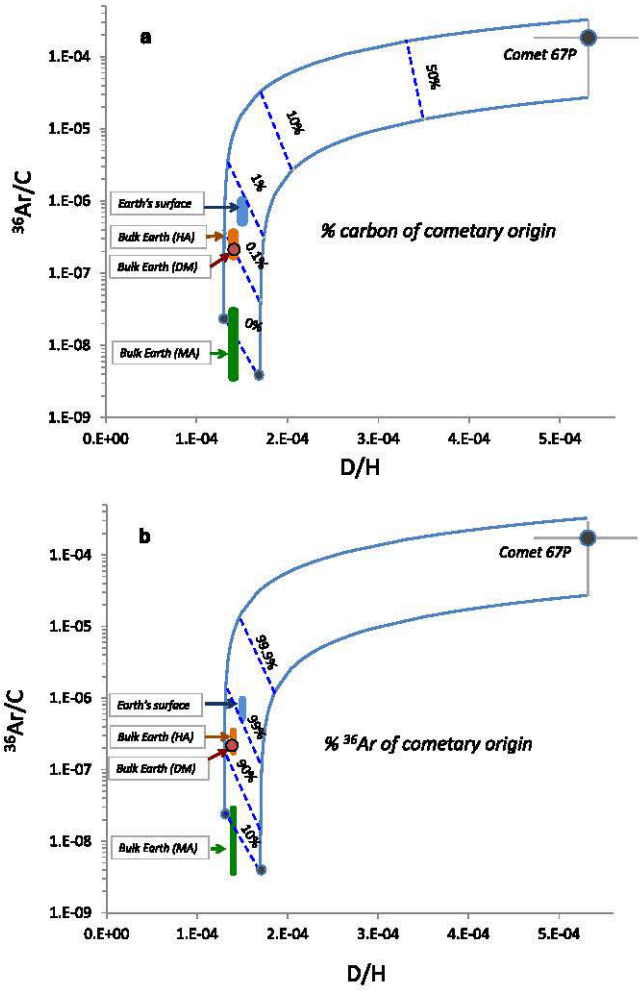

Fig. 4. D/H versus ^{36}Ar/C mixing diagram between cometary and chondritic (asteroidal) end-members. HA, DM and MA are the bulk Earth estimates from Halliday (2013), Dauphas and Morbidelli (2014) and Marty (2012), respectively. (a) Dotted lines indicate the percentage of Terrestrial carbon of cometary origin. (b) Dotted lines indicate the percentage of cometary ^{36}Ar on Earth.

K–Ar systematics indicate that about half of radiogenic ^{40}Ar produced in Earth over 4.5 Ga is still trapped in the solid Earth, the rest having been degassed into the atmosphere (Allègre et al., 1996). Calibrating volatile elements to ^{40}Ar trapped in the mantle led Marty (2012) to propose a bulk mantle ("MA") higher than the above estimates, corresponding to 4–10 ocean masses. This approach does not rely on models of the structure and the composition of mantle domains. However, it assumes a chondritic composition for Terrestrial refractory elements. This is because the potassium content of the Earth (Arevalo et al., 2009) is calibrated against refractory uranium as potassium is semi-volatile and its abundance cannot be retrieved from meteoritic analogs. A chondritic Earth composition for refractory elements has been recently questioned on the basis of sub-chondritic Terrestrial Nd isotope ratios, with the possibility that up to half of U, and therefore K, could have been stripped off by impacts on a differentiated Earth (e.g., Jellinek and Jackson, 2015; and refs. therein). This would reduce the ^{40}Ar inventory and therefore allow much lower volatile contents. For this reason, we consider that the MA inventory of Table 4 gives an upper limit for the Terrestrial volatile budget.

Table 4
Volatile element composition of the Martian atmosphere (sensu lato, including estimates for surface reservoirs). Elemental abundance data are from Bogard et al. (2001), Dauphas and Morbidelli (2014), and refs. therein. Key elemental ratios and isotope data are also given, referenced in Bogard et al. (2001), Dauphas and Morbidelli (2014), Mahaffy et al. (2013), Atreya et al. (2013) and Wong et al. (2013). The δ^{15}N values are given in parts per mil (‰) relative to terrestrial atmospheric nitrogen. The δD values are global estimates from Montmessin et al. (2005), given as deviations in ‰ relative to terrestrial ocean water. The F_X values (where X is a noble gas isotope ratio), represent deviations (in ‰ per atomic mass unit) from the solar composition (Dauphas and Morbidelli, 2014). Note that Ar and Xe appear highly fractionated relative to Solar and compared to Kr, the latter being close to Solar. Ar, Kr and Xe are assumed to be isotopically solar in comets, as cometary ice should have trapped quantitatively these elements from the protosolar nebula. Neon is unlikely to have been trapped in comets, given the inferred formation temperature of these objects, and its abundance and isotopic composition cannot be inferred.

	Mars atm. (mol/g)	Carb. chondr. (mol/g)	Comets (mol/g)
^{12}C	8.6×10^{-10}	2.3×10^{-3}	3.7×10^{-2}
^{14}N	3.4×10^{-11}	6.4×10^{-5}	1.8×10^{-3}
^{36}Ar	9.1×10^{-15}	3.9×10^{-11}	2.1×10^{-7}
C/N	25	36	21
C/^{36}Ar, 10^4	9.5	5900	17.9
N/^{36}Ar, 10^3	3.7	1640	8.7
^{20}Ne/^{22}Ne	7–10	8.5–12.5	?
δ^{15}N‰	572 (±82)	−30 to +150	+600 to +1000
δD‰	+5500	−300 to +1000	0 to 2000
F_{Ne}‰/u	246	173	?
F_{Ar}‰/u	151	6	0
F_{Kr}‰/u	±10	10	0
F_{Xe}‰/u	33	3	0

3. Discussion

3.1. How representative are cometary data?

We assume here that 67P data on one hand, and available cometary data on another hand, are representative of the compo-

sition of icy bodies that scattered in the inner solar system. This assumption is certainly fragile in the sense that key species measured in 67P coma are likely to vary from comet to comet. However, comets formed probably from comparable building material, water and other ice species making ~30–50% of total mass. For most volatile species given in Tables 2 and 3, measurements were done spectroscopically on several comets (Mumma and Charnley, 2011; Bockelée-Morvan, 2011; Le Roy et al., 2015) so the large range of observed values is considered to be representative of the natural variability.

For noble gases, the Ar measurement of Balsiger et al. (2015) is the only available set of data, but we propose below that the range of observed values is representative of the coma composition. Fractionation of a minor, low temperature species/element like argon relative to H_2O can range over 1–2 order(s) of magnitude, depending on its sublimation temperature relative to that of H_2O ice. Marboeuf and Schmitt (2014) modeled fractional degassing of cometary volatiles as a function of the distance to the perihelion, under a range of different assumptions concerning the thermal inertia of a comet, the nature of ice, and the abundance and distribution of the different volatile species. Argon was not considered in their study, so we take as a proxy CO which has a comparable condensation/sublimation temperature. Results of their modeling indicate that, at a distance between 3 and 4 AU from the perihelion, the CO/H_2O ratio of the coma is comparable to that of the bulk comet. Argon measurements by the ROSINA mass spectrometer were done on October 19, 20, 22, and 23, 2014 when Comet 67P was at ~3.1 AU from the Sun, thus possibly minimizing fractionation of minor species like Ar relative to H_2O. The 67P $^{36}Ar/H_2O$ ratio of $0.1–2.3 \times 10^{-5}$ is also comparable to, although lower than, ratios predicted from modeling of ice trapping experiment data ($2–40 \times 10^{-5}$ in the 30–45 K range according to Dauphas, 2003; $8–75 \times 10^{-5}$ according to Marty and Meibom, 2007, based on experimental data from Notesco and Bar-Nun, 2005). Models and experiments of noble gas trapping into cometary ice indicate that the main controlling factors on the abundance of trapped noble gases are the temperature and the partial pressures of gases (Bar-Nun et al., 1985; Yokochi et al., 2012), so that other parameters of comet formation being equal, we assume that the Ar content of cometary matter is represented by 67P data. Although the above assumptions may constitute the main weak point of the present approach, we note that uncertainty range covers one order of magnitude of the stated values (the $^{36}Ar/H_2O$ ratio) whereas the present conclusions here are based on variations of key parameters over several orders of magnitude.

3.2. Impact driven atmospheric loss

The present approach assumes that impacts are conservative, that is, contributed volatiles and target volatiles are not lost into space. This was likely not the case since giant impacts probably led to significant atmospheric loss (e.g., Genda and Abe, 2005). Recent models argue for a steady state regime between replenishment and atmospheric escape, depending on velocities, atmospheric entry angles, and sizes of impacting bodies (De Niem et al., 2012; Schlichting et al., 2014), but modeling the overall budget of volatile loss/gain is presently out of reach. Instead, we turn to a mass balance approach involving radiogenic ^{129}Xe, produced from the extinct radioactivity of iodine-129 ($T_{1/2} = 16$ Ma). Iodine was present when the Earth formed, as shown by the occurrence on Earth of the stable isotope ^{127}I. From meteoritic studies, it is possible to derive the solar system initial $^{129}I/^{127}I$ (1.0×10^{-4}). If the Earth formed when ^{129}I was still alive, then terrestrial reservoirs should present excesses of ^{129}Xe produced by the decay of ^{129}I. This is the case as an excess of 7% ^{129}Xe (the main reservoir of terrestrial xenon) is present in air. This excess corresponds to about 1–2% of ^{129}Xe that could have been present if the Earth formed at the start of solar system formation. Assuming that produced ^{129}Xe was lost before the atmosphere became closed for volatile escape, one obtains a I–Xe closure age of ~100 Ma after start of Solar System formation for the terrestrial system (Wetherhill, 1980). Atmospheric xenon including ^{129}Xe might have been escaping from the terrestrial atmosphere for prolongated periods of time, possibly during about 2 Ga (Pujol et al., 2011), so that the ^{129}Xe excess has to be corrected for subsequent loss of atmospheric Xe. After correction, the closure age of the atmosphere becomes 30–60 Ma (Avice and Marty, 2014). A comparable budget arises when combining extinct radioactivities of ^{129}I and ^{244}Pu ($T_{1/2} = 82$ Ma), implying that Xe loss was early, within a few tens of Ma after start of Solar System formation. Thus, according to I–Pu–Xe mass balance, early atmospheric loss, presumably during the proto-Earth building epoch, might not have exceeded 60–80% of atmospheric Xe, and probably less after the Moon-forming impact which occurred within 40–90 Ma after start of Solar System formation. We tentatively conclude that the atmosphere was grossly conservative, within a factor of two, after the Moon-forming impact (the period of time relevant to cometary contributions, see next sub-sections).

3.3. Origin of major volatile species on Earth

The Ar content of cometary material inferred from the analysis of argon in 67P coma is 3–4 orders of magnitude higher than the one of chondritic material, which makes Ar, and by inference other heavy noble gases, a key tracer of cometary contribution to Earth. Together with the D/H ratio, the ratio between argon and H_2O, C and N permits to establish firm constraints on the contribution of 67P-like material to Terrestrial volatiles. Swindle and Kring (2001) considered the ratio between ^{36}Ar and H_2O in comets (they took the Hale Bopp's $^{36}Ar/O$ ratio from Stern et al., 2000, which has been questioned since then) to infer an extremely low contribution of cometary material to the surfaces of Earth and Mars. Dauphas (2003) noted that the low Xe/H_2O ratio of the Earth compared to other cosmochemical end-members could set stringent constraints on the maximum amount of cometary water on Earth. Since then, it has been proposed that the low terrestrial Xe/H_2O ratio could be secondary (Pujol et al., 2011), making the argument less constraining. Figs. 3 and 4 represent mixing curves between chondritic and cometary end-members using the $^{36}Ar/X$ (where X represents water, nitrogen or carbon) ratio versus the D/H ratio. In fact the ^{36}Ar concentration is more sensitive than the D/H ratio alone, because contribution of 67P-like material can strongly impact the atmospheric inventory of argon. For water, a cometary contribution of the order of 1% or less is allowed depending on the bulk silicate Earth + surface composition (Fig. 3a), confirming that Terrestrial water is mostly non-cometary. A comparable conclusion arises for nitrogen (Fig. 3b), although a larger cometary contribution up to a few percent is allowed, due to the depletion of N in Earth (Marty, 2012). Nitrogen isotopes may permit to get independent constraints because spectroscopic measurements on comets indicate that the measured N-bearing species, CN, HCN and NH_2 (the latter presumably from NH_3) are all enriched by a factor of 2 in ^{15}N relative to ^{14}N (e.g., Füri and Marty, 2015, for a review). However, other N species like N_2 (Rubin et al., 2015) and refractory organics are present in comets with unknown N isotope composition, preventing to establish an isotope budget for the cometary reservoir.

Based on the same approach, Terrestrial carbon appears to originate from chondrite-like material (Fig. 4a), with a possible cometary contribution being lower than ~1%. This conclusion stands even when considering that cometary carbon may be

hosted not only in ice but also in refractory organics from the nucleus.

3.4. Possible cometary origin for atmospheric noble gases

Contrary to major volatiles, the mixing diagram of Fig. 4b suggests that atmospheric argon, and by extension other heavy noble gases, could originate from a cometary reservoir, a possibility already proposed by Anders and Owen (1977) and Owen and Bar-Nun (1995) based on the noble gas abundance pattern of the atmosphere, and by Marty and Meibom (2007) from mass balance considerations. For the bulk silicate Earth inventory, the conclusion depends on the adopted composition. For the HA and DM inventories, a major cometary origin for argon is clearly possible (Fig. 4b). The MA inventory does not require contribution of cometary noble gases to the bulk Earth (Fig. 4b). In this model, noble gases are mostly in the atmosphere, and major volatiles (H_2O, C) are in the mantle, the sum of which being consistent with the addition of ~2 wt.% of carbonaceous chondrite type material.

3.5. Potential cometary contribution during the major bombardment periods

Here we examine possibilities of a cometary contribution from the dynamical point of view. From solar system dynamics and isotope cosmochemistry, the major events that contributed potentially wet material to the building of Earth are:

1. Contribution of wet bodies to the growing proto-Earth (Morbidelli et al., 2000; Raymond et al., 2004; O'Brien et al., 2006, 2014). Dry material in the Terrestrial region became scarce as a result of accretion to larger bodies, leaving space to wet contributions from larger heliocentric distances. These late contributions should have consisted of volatile-rich asteroids, rather than comets. In line with this, krypton (Holland et al., 2009), hydrogen and nitrogen isotopes (Alexander et al., 2012; Marty, 2012) point to a chondritic, rather than cometary, source for contributed volatiles that are now stored in the Terrestrial mantle (Fig. 2).

2. The giant impact that led to the Moon formation. It is not clear if this event resulted or not in a major loss of volatile elements the proto-Earth. Already existing atmosphere and oceans could have survived the event (Genda and Abe, 2005), and/or the impactor could have contributed volatiles to the Earth–Moon system. From key isotope signatures (e.g., oxygen), the impactor was likely to originate from the iner solar system, and a cometary contribution is not considered further.

3. A late veneer (LV) might have supplied chondritic material after the last equilibration of mantle material with the core, presumably after the Moon forming impact (Kimura et al., 1974). Its contribution is estimated to be 0.3 wt.% (range 0.1–0.8%) of the Terrestrial mass (Righter, 2003), that is, $\sim 2 \times 10^{25}$ g. According to dynamical models, the LV was made of planetesimal leftover from the Terrestrial planet formation, without contribution of comets (Bottke et al., 2010; Raymond et al., 2013; Morbidelli et al., 2012; Jacobson et al., 2014). In line with this view, a 100% cometary LV (Fig. 5a) contributing 0.3% of the Terrestrial mass would supply too much atmospheric ^{36}Ar by 2–3 orders of magnitude, and would have dominated the H, C and N inventory, which is unlikely. A cometary contribution of 1% or less could account for atmospheric Ar without impacting the stable isotope signatures (Fig. 5b).

4. The Terrestrial late heavy bombardment (TLHB) is an extrapolation of the late heavy bombardment thought to have occurred on the Moon from the size-age distribution of lunar craters (Tera et al., 1974). Estimates of the mass contribution to Earth during the TLHB, based on the Lunar cratering record, range from 2.2×10^{23} g (Hartmann et al., 2002) down to 4×10^{22} g (assuming that the TLHB started at the time of formation of Nectaris basin; Morbidelli et al., 2012). From a modeling approach, Levison et al. (2001) proposed a mass contribution of 8×10^{22} g. Gomes et al. (2005) estimated a TLHB of 4×10^{23} g, about half of which being cometary. The newest version of the Nice model, however, reduces the mass flux to the Earth to about 4×10^{22} g of asteroidal material (Bottke et al., 2012) and $2–4 \times 10^{22}$ g of cometary material (depending on the dynamical state of the trans-Neptunian disk before the dynamical instability). For the calculations presented here, a conservative value of 2.0×10^{23} g is adopted. Marty and Meibom (2007) concluded that less than 1% comets were present in the TLHB, the rest being asteroidal material, and proposed that atmospheric noble gases could constitute the only remaining evidence for the TLHB. Their mass balance was based on noble gas cometary concentration from ice trapping experiments, which are higher than the one constrained by Ar in 67P. With the ROSINA ^{36}Ar measurement, a 100% cometary TLHB would supply too much ^{36}Ar to the atmosphere (Fig. 5c). It would also supply most major volatiles at the Earth's surface, which is not allowed by the D/H and ^{15}N/^{14}N ratios of the atmosphere and oceans. A cometary fraction of ~10% in the TLHB accounts reasonably well for atmospheric ^{36}Ar without impacting the stable isotope budget (Fig. 5d). Thus a cometary contribution of $\sim 2.0 \times 10^{22}$ g respects our mass balance and is in excellent agreement with the latest model results.

5. The post TLHB continuous flux of interplanetary dust particles (IDPs), and micrometeorites is estimated at $\sim 2 \times 10^{20}$ g, assuming a constant flux comparable to modern one (about 30,000 tons/yr, Love and Brownlee, 1993). A near-constant flux (with a possible factor of 5 increase in the last 0.5 Ga) is consistent with the lunar soil record of extraterrestrial material (Culler et al., 2000; Hashizume et al., 2002). From the analysis of IDPs, this flux consists of both cometary and asteroidal materials. A 100% continuous IDP flux would not impact the volatile inventory of the Earth's surface including noble gases, even when this flux is increased by a factor of 5 (Fig. 5e).

3.6. Further evidence for heterogeneous sources of noble gases on Earth

From isotope geochemistry considerations, several distinct cosmochemical sources contributed noble gases to the growing Earth:

(i) Solar neon has been identified in the mantle (Honda et al., 1991). It does not necessarily imply a solar origin for heavier noble gases because the solar component is rich in light noble gases compared to Chondritic, so that mixing between Solar and Chondritic may impact light noble gases only. Neon is unlikely to have been trapped in cometary ice given its elevated condensation temperature.

(ii) The isotopic compositions of H, N and mantle Kr isotopes are consistent with a chondritic source.

(iii) Atmospheric xenon is unique in the solar system and cannot be derived directly from Solar or Chondritic. The light Xe isotopes are isotopically fractionated (depleted) by 3–4%/amu relative to cosmochemical Xe (either Solar or Chondritic). However this mass fractionation may be secondary and may not be a source signature (Pujol et al., 2011; Avice and Marty, 2014). Even when corrected for mass-dependent fractionation, the atmospheric Xe isotope composition cannot be derived from either Solar or Chondritic, because it is depleted in the heavy isotopes ^{134}Xe and ^{136}Xe relative to the latter. Secondary (nuclear) processes such as fission of heavy radionuclides can only enrich, and not deplete, these isotopes. This observation led Takaoka (1972) and Pepin (1991) to postulate the existence of a distinct primordial Xe having sourced the Terrestrial atmosphere (the Xe–U component of Pepin, 1991). This mass-independent isotope fractionation of Xe isotopes might have resulted from an unknown nuclear effect, or from a different

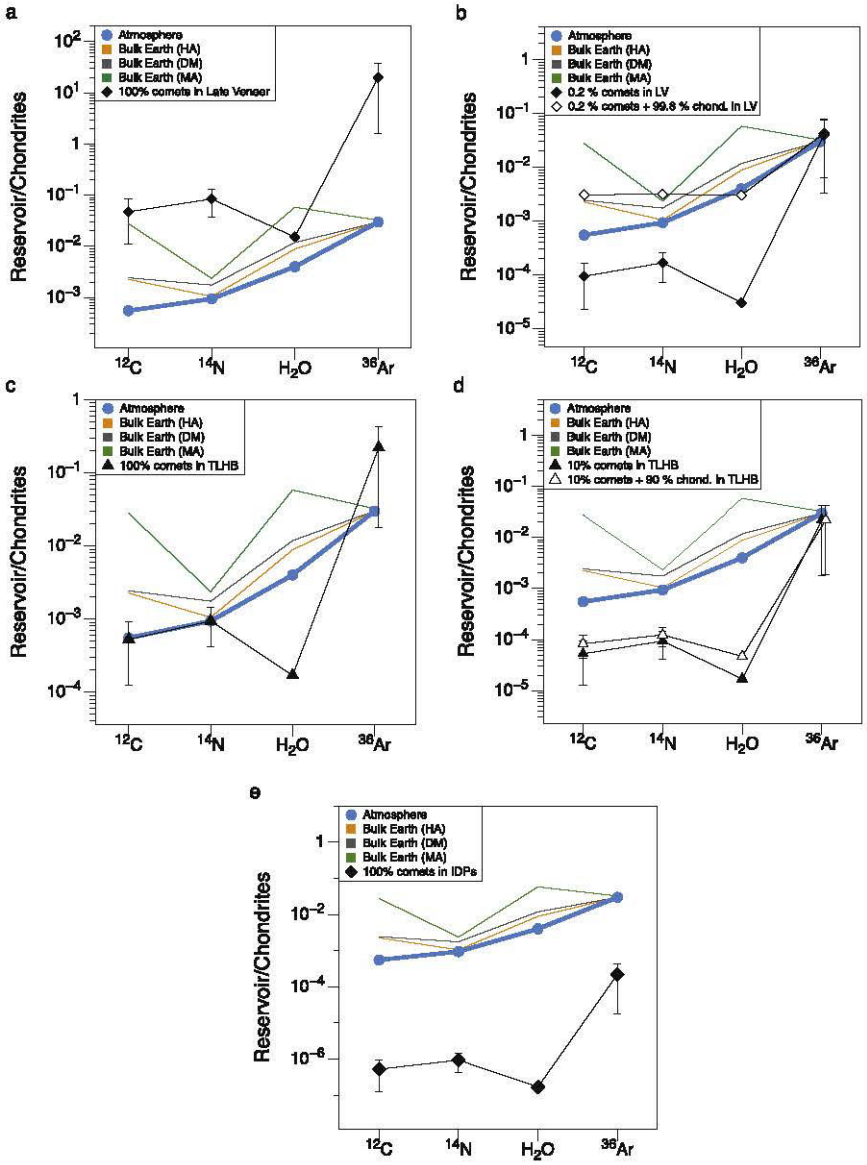

Fig. 5. Abundances of C, N, H_2O and ^{36}Ar in the atmosphere *sensu largo* (air + oceans + sediments), normalized to Chondritic (data from Tables 2 and 3). For comparison bulk Earth inventories from Table 4 are also represented. (a) Effect of addition of a late veneer (0.3% of the Terrestrial mass) made of 100% comet. The ^{36}Ar inventory of the atmosphere (the main reservoir of noble gases) is overabundant by several orders of magnitude, and major volatiles are also dominated by cometary material. (b) Same as 3a but for a tiny contribution of cometary material in the late Veneer, arbitrarily chosen as 0.2% to fit the Terrestrial abundances. (c) Effect of contribution of a Terrestrial Late Heavy Bombardment (2×10^{23} g) made of 100% comet. Given the uncertainties, the ^{36}Ar content of the atmosphere can be matched, but the major volatiles at the Earth's surface are dominated by a cometary component. (d) A ~10% cometary contribution in the TLHB fits well the ^{36}Ar inventory of the atmosphere, without impacting the isotope compositions of C, N and H. (e) Effect of addition of a continuous IDP flux since 3.5 Ga ago. This flux has no impact on the Terrestrial inventory of H, C, N and ^{36}Ar.

mix of nucleosynthetic components that were not fully homogenized during solar system formation.

Given the possible cometary origin of atmospheric noble gases, we speculate that this exotic Xe component could have been carried out from the outer solar system to its inner region by icy bodies. The dichotomy between mantle chondritic Xe and surface Xe would then be a record of Terrestrial growth, with the Proto-Earth being built from chondritic-like material, and its surface having been subsequently contributed by cometary bodies. In order to supply all atmospheric ^{36}Ar (5.55×10^{15} moles, Ozima and Podosek, 2002), a cometary contribution between 3×10^{21} and 6.5×10^{23} g would have been necessary (computed with a ^{36}Ar cometary concentration of $2.1 \pm 1.9 \times 10^{-7}$ mol/g, and a cometary density of 0.5 from the 67P measurements). This is in great agreement with the most recent estimates of the cometary flux to the Earth during the TLHB. Thus, there is no "missing comet bombardment" unlike the earlier conclusions of Marty and Meibom (2007) based on a higher ^{36}Ar content of comets. The impact of a single cometary body with a radius of 100–300 km, or of a limited number of smaller bodies, could have sufficient to supply all atmospheric argon. Therefore, it may be possible that the supply of atmospheric volatiles to the Terrestrial planets was a stochastic process involving a small population of objects, which might have resulted in a heterogeneous distribution of outer solar system

isotopic signatures. In this respect, the high abundance of ^{36}Ar in the atmosphere of Venus could effectively be the result of random contribution of cometary material ton inner planets.

3.7. Origin of prebiotic material on Earth constrained from atmospheric argon

Peptide synthesis from amino-acids appears a necessary step for the development of prebiotic material on Earth. Although a number of possible scenarios invoking catalytic reactions in specific Terrestrial environments have been advanced, it has also been proposed that impacts could have favored peptide synthesis from ET amino-acids (Blank et al., 2001). Sugahara and Mimura (2014) simulated comet impacts by shock experiments at low temperature in the range 5–26 GPa and found that linear peptide synthesis up to tripeptide forms could be achieved only with initially low temperature. As formation of linear peptide appears a key process for further elongation of peptide chains, these authors argued that comet impacts might have played a key role in the formation of prebiotic material on Earth. An upper limit for the total delivery of potential prebiotic material to Earth by comets can be set by considering that all atmospheric ^{36}Ar was delivered by icy bodies to the Earth's surface. Carbonaceous chondrites contain about 80 different amino-acids (Ehrenfreund and Charnley, 2000), with their total concentration amounting for 250 ppm (e.g., Martins et al., 2007). Their concentration in cometary matter is unknown. Studies of Stardust cometary grains suggest similarities with stratospheric IDPs and carbonaceous chondrites (Brownlee et al., 2006). Thus, for the purpose of illustration, we consider that the carbonaceous chondrite concentration is representative of cometary matter. The mass of cometary material having the ^{36}Ar content of 67P ($2.1 \pm 1.9 \times 10^{-7}$ mol/g) that would have delivered atmospheric ^{36}Ar (5.55×10^{15} moles) is $0.2–5 \times 10^{22}$ g, leading to the delivery of $0.6–13 \times 10^{18}$ g of amino acid-rich material. This amount is comparable to the present-day mass of the biosphere ($\sim 2 \times 10^{18}$ g). With the present-day mass of the oceans, comets could have delivered up to 10–40 ppm prebiotic material to seawater. Thus depending on the efficiency of survival and of peptide synthesis upon impact, comets might have contributed non-negligible prebiotic material during the TLHB.

3.8. The case of the Martian atmosphere

The composition of the atmosphere of Mars (Table 4) is reasonably known from the in-situ analyses by the Viking and the Mars Science Laboratory (MSL) landers, and from the analysis of some of the Martian meteorites which contain atmospheric volatiles trapped in impact glasses (see Bogard et al., 2001, for a comprehensive review, and Wong et al., 2013, and refs. therein, for recent Curiosity MSL data). Compared to Earth and bulk meteorites, the Martian atmosphere is rich in ^{15}N ($\delta^{15}N = 572 \pm 82‰$ relative to the Terrestrial atmosphere, Wong et al., 2013) and in deuterium ($\delta D = 5500‰$ relative to the oceans; Bogard et al., 2001; Montmessin et al., 2005, and refs. therein; Fig. 2). Likewise, neon, argon (^{36}Ar, ^{38}Ar) and xenon isotopic signatures are enriched in their heavy isotopes by 246, 151, and 33‰, respectively, relative to the solar compositions (Table 4). In contrast, volatiles in the Mars interior, also analyzed in Martian meteorites, have isotopic ratios comparable to inner solar system signatures (Fig. 2).

The atmospheric signatures have been interpreted as resulting from isotope fractionation during atmospheric escape processes. Possibilities include solar wind-induced photochemical reactions producing electrons able to dissociate N_2 for nitrogen (McElroy et al., 1977), and sputtering for the noble gases (Jakosky et al., 1994). Chassefière and Leblanc (2004) reviewed potential escape mechanisms that might have affected the atmosphere of Mars and concluded that (i) not a single process can account for the observations; and (ii) non-thermal processes are required and therefore might have affected different atoms/species at variable levels independently of their masses. Atmospheric loss is attested by morphological evidence on Mars indicating past water flows (Carr and Head, 2003), and major escape processes might have taken towards the end of the Noachian period 4.0–3.7 Ga ago. Thus escape-related fractionation of Martian volatiles is likely to have played a key role in fractionating elemental abundances and isotopic compositions. Nevertheless, we suggest here that possible source effects, namely cometary contributions, should be also considered, especially after the major escape events that resulted in a tenuous atmosphere on Mars.

Several key observations are not entirely consistent with atmospheric escape as a cause of isotopic enrichments. (i) The noble gas elemental abundance of the Martian atmosphere and the C/N ratio (Pepin, 1991) are comparable to those of Venus and Earth (for which similar escape fractionations are unlikely). (ii) The krypton isotopic composition of the Martian atmosphere is close to the solar composition (Bogard et al., 2001, and refs. therein), contrary to those of Ne, Ar and Xe (Table 4). Because the mass of Kr is intermediate between those of Ne, Ar and Xe, this difference points to other processes than escape-related fractionation. We note that the Martian Ne isotopic composition is within the range of chondritic values, e.g., the so-called Ne–A (planetary) component of carbonaceous chondrites. Neon is not expected to be trapped in comets, so that Martian atmospheric Ne could have been sourced by an another cosmochemical reservoir. The high ^{38}Ar/^{36}Ar ratio (0.238 ± 0.005; Atreya et al., 2013) is indeed a good diagnostic of escape-related fractionation, but cosmic-ray production of noble gas isotopes (which also increases this ratio) could have been significant for the tenuous Martian atmosphere. Such effects need to be assessed. The Xe isotope fractionation could have arisen from a Xe-specific non-thermal escape process, like the one proposed for Terrestrial atmospheric Xe (Pujol et al., 2011). (iv) The isotopes of C, O, S in the Martian surface and crust are little fractionated. CO_2 is enriched in ^{13}C relative to Terrestrial ($\delta^{13}C = 46 \pm 4‰$; Mahaffy et al., 2013) but to a much lesser extent than ^{15}N in nitrogen ($\delta^{15}N = 572 \pm 82‰$, Wong et al., 2013). However this argument is not carved in stone since C, O, S isotope compositions might have been buffered by crustal reservoirs.

We suggest that some of the Martian atmospheric characteristics are consistent with a cometary origin. This possibility was proposed by Owen and Bar-Nun (1995) who noted ^{36}Ar/^{84}Kr/^{132}Xe similarities between the Earth and Mars despite large differences in atmospheric pressures, suggesting that a non-fractionating process supplied atmospheric noble gases to both planets. They argued that the Martian ^{36}Ar/^{84}Kr/^{132}Xe ratios resemble to those obtained in experimentally grown ice, and proposed impacts of icy planetesimals as the source of Martian surface volatiles. Although we do not think that the Xe abundance pattern and its isotopic composition are cometary (the Martian Xe fractionation could result from Xe-specific non-thermal processing like on Earth, Pujol et al., 2011), we test below a possible cometary contribution by using other volatile element signatures.

First, in a N vs. H isotope diagram, the atmosphere of Mars plots close to the field of comets (Fig. 2). Second, the Martian C/N, C/^{36}Ar and N/^{36}Ar ratios are all close within a factor of 2 to our estimate for cometary composition (and to Earth's surface inventory, Table 4, Fig. 6), whereas the C/^{36}Ar and N/^{36}Ar ratios are markedly different from the chondritic values (Table 4). The δ^{15}N vs. ^{36}Ar/N_2 isotope variations are consistent with a two-component mixing (Fig. 7). In this format, mixings define straight lines (curves in the semi-log diagram of Fig. 7). Both the Martian atmosphere's δ^{15}N and ^{36}Ar/N_2 values are within the estimated range of cometary ratios, and variations observed in Martian meteorites define an-

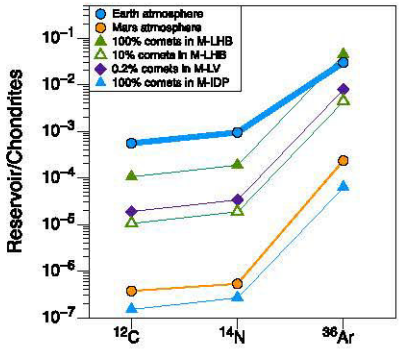

Fig. 6. Elemental composition of the Martian atmosphere, compared to Earth's atmosphere and comets. Data sources: Pepin (1991), Bogard et al. (2001), Dauphas and Morbidelli (2014). Water is not represented here since its Martian inventory is unknown. The effects of a Martian late veneer (M–LV), a Martian Late Heavy Bombardment (M–LHB) and continuous IDP flux are also represented.

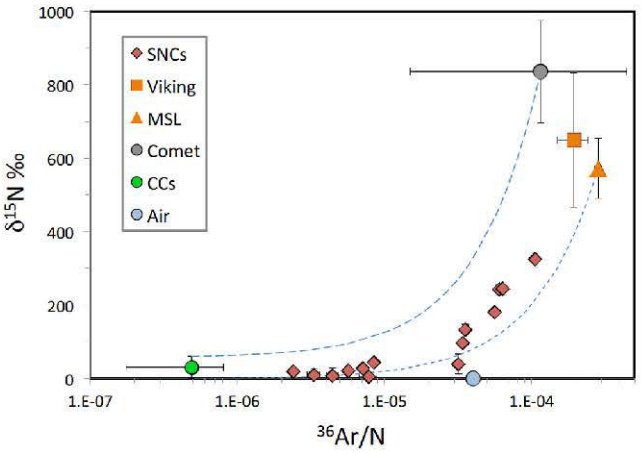

Fig. 7. N isotope vs. $^{36}Ar/N$ ratio mixing diagram between carbonaceous chondrite (CCs) and comet end-members. The dotted curves represent mixing trajectories between Comet and CCs on one hand, and between MSL measured Martian atmospheric composition on another hand. Between Viking and Martian meteorite data are from Bogard et al. (2001) and refs. therein, and Chennaoui Aoudjehane et al. (2012). MSL data are from Wong et al. (2013) and Mahaffy et al. (2013).

other end-member having lower $\delta^{15}N$ and higher $^{36}Ar/N_2$ ratios, that could be chondritic and/or terrestrial contamination (preferential adsorption of nitrogen relative to argon). The Kr isotope composition is solar-like, as expected for a cometary origin. After correction for mass-dependent fractionation, Xe is also isotopically solar (Pepin, 1991).

We then explore the possibility of a cometary contribution by scaling potential cometary fluxes on Earth to the dimensions of Mars. In Fig. 6, the impacting fluxes on Earth have been adapted to the Martian dimensions by dividing them by a factor of ∼5. This factor is obtained from the ratio of planetary surfaces (3.5 for Earth/Mars) plus a gravitational focusing effect of ∼1.5. It comes out that a Martian late veneer would supply far too much cometary volatiles to Mars (Fig. 6). For a TLHB total (asteroidal+cometary) flux of $\sim 2 \times 10^{23}$ g, the total Martian LHB (M–LHB) flux would be $\sim 5 \times 10^{22}$ g. Ten % comet in the M–LHB as on Earth gives a cometary flux on Mars of $\sim 5 \times 10^{21}$ g, which is remarkably comparable to the range of $7–14 \times 10^{21}$ g obtained from recent simulations. However, a 10% cometary M–LHB would add too much volatiles to Mars by ∼1 order of magnitude (Fig. 6). Thus either the LHB flux was heterogeneous between Earth and Mars, or part of the Martian atmosphere was subsequently lost after M–LHB by atmospheric escape processes. In line with the second possibility, the D/H values of the Martian interior and Martian atmosphere are shifted towards D-enrichments (right-hand side in Fig. 2) relative to inner solar system values defined by Earth and chondrites on one hand, and by comets on another hand. Thus the Martian D/H value is too high to be solely cometary, and it is likely that atmospheric escape processes played a role in fractionating hydrogen isotopes, and, possibly, other light species (neon ?). Finally, the continuous flux of IPDs on Mars could constitute a non-negligible source of cometary volatiles (Fig. 6), if made predominantly of cometary material. In line with this possibility, Fries et al. (2016) proposed recently that "meteor showers" made of cometary debris could account for the presence of methane in the Martian atmosphere.

4. Conclusions and outlook

The in-situ analysis of coma from comet 67P together with remote sensing data from other comets gives semi-quantitative constraints on the origin of volatile elements in Terrestrial planets. Particularly important is the discovery of significant amounts of primordial argon in the coma of 67P, well above the level observed in primitive meteorites.

For Earth, the major volatiles documented here – H_2O, C, N – were sourced mostly by material akin of wet asteroids. Only a few percents at most of water, carbon and nitrogen could have originated from comet-like bodies. However the terrestrial atmosphere could contain a significant, possibly dominant, fraction of cometary noble gases, which might have been delivered during the Terrestrial Late Heavy Bombardment around 4 Ga ago. This possibility is in line with dynamical models of solar system evolution, which predict a significant fraction of icy bodies in the TLHB. Resolving this question will require a better estimate of the volatile element inventory of the Earth. Models that ascribe a "low" volatile content of our planet (Halliday, 2013; Dauphas and Morbidelli, 2014) imply that atmospheric noble gases are cometary, whereas the "high" volatile content model (Marty, 2012) does not require comets and is consistent with a predominantly asteroidal (chondritic) source (see Fig. 4b). A chondritic, rather than cometary, origin for atmospheric noble gases is independently consistent with Ne–Ar isotope variations among the major terrestrial reservoirs including the atmosphere (Marty, 2012). This problem may appear too specialized for a non-specialist audience, but there are outstanding issues beyond it, such as the origin of prebiotic material on Earth (which could be traced with noble gases), the early processes of volatile delivery and escape, the timing of volatile delivery (which can be addressed with noble gas radiogenic isotopes), and the composition and mode of transfer of material from the outskirts of the Solar System. For example, the isotopic composition of atmospheric xenon cannot be simply related to either the solar nebula or asteroidal material. It requires a specific composition (U–Xe; Pepin, 1991) that could trace nucleosynthetic heterogeneities in outer solar system bodies. Resolving these important issues will require a better estimate of the volatile content of the mantle on the one hand, as well as precise cometary noble gas data including isotopes on the other hand.

A cometary contribution to Martian surface volatiles (nitrogen and noble gases) appears clearly possible, given our present state of knowledge, and is consistent with solar system dynamical models. However, the strong deuterium enrichment of the Martian surface can hardly be the result of a cometary contribution, and requires isotope fractionation during escape processes at least for these light species. Resolving source effects versus processing is a major challenge that will require, as for the Earth, a better knowledge of the Martian and cometary signatures for major and minor volatile species.

The volatile characteristics of the inner planets are consistent with trapping of protosolar nebula gas during early stages on accretion, and contributions from wet bodies from increasing heliocentric distance during the sequence of planetary building and late accretion. However no unified picture emerges for the origin(s) and processes of delivery of inner planets' atmospheric volatiles. What are now highly needed are measurements of the noble gas abundances in comets and the isotopic ratios of neon, krypton and most importantly xenon. Such measurements should be given a high priority in future cometary missions. The requested level of precision (better than percent for noble gas isotopic ratios, and per mil for stable isotopes including the three isotopes of oxygen) will require a cometary sample return mission to permit laboratory analysis.

Acknowledgements

Exchanges with the members of the ROSINA Science Team helped in shaping the ideas presented here. Work at UoB was funded by the State of Bern, the Swiss National Science Foundation, and by the European Space Agency PRODEX Program. This work was also supported by CNES and by the European Research Council (grant no. 267255). Rosetta is an ESA mission with contributions from its member states and NASA. We acknowledge herewith the work of the ESA Rosetta team. BM is grateful to the University of Tokyo for supporting his visit. This work has been partly carried out thanks to the support of the A*MIDEX project (no. ANR-11-IDEX-0001-02) funded by the "Investissements d'Avenir" French Government program, managed by the French National Research Agency (ANR). Discussions with D. Nesvorny, D. Bocquelée-Morvan, K. Mandt, E. Fueri, A. Le Roy, U. Calmonte, P. Bochsler, Tobias Owen, A. Bar-Nun and members of the ROSINA Science Team, helped us to shape our ideas. Constructive reviews by an anonymous reviewer, K. Mandt and N. Dauphas, and efficient edition by C. Sotin are gratefully acknowledged. This is CRPG contribution 2417.

References

A'Hearn, M., et al., 2011. EPOXI at Comet Hartley 2. Science 332, 1396–1400.
Albarède, F., et al., 2013. Asteroidal impacts and the origin of terrestrial and lunar volatiles. Icarus 222, 44–52.
Aléon, J., 2010. Multiple origins of nitrogen isotopic anomalies in meteorites and comets. Astrophys. J. 722, 1342–1351.
Alexander, C.M.O'D., et al., 2012. The provenances of asteroids, and their contributions to the volatile inventories of the terrestrial planets. Science 337, 721–723.
Allègre, C.J., Hofmann, A.W., O'Nions, R.K., 1996. The argon constraints on mantle structure. Geophys. Res. Lett. 23, 3555–3557.
Altwegg, K., et al., 2015. 67P/Churyumov–Gerasimenko, a Jupiter family comet with a high D/H ratio. Science 347, 1261952-1.
Anders, E., Owen, T., 1977. Mars and Earth origin and abundance of volatiles. Science 198, 453–465.
Arevalo, R., McDonough, W.F., Luong, M., 2009. The K/U ratio of the silicate Earth: insights into mantle composition, structure and thermal evolution. Earth Planet. Sci. Lett. 278, 361–369.
Atreya, S., et al., 2013. Primordial argon isotope fractionation in the atmosphere of Mars measured by the SAM instrument on *Curiosity* and implications for atmospheric loss. Geophys. Res. Lett. 40, 5605–5609.
Avice, G., Marty, B., 2014. The iodine–plutonium–xenon age of the Moon–Earth system revisited. Philos. Trans. R. Soc., Math. Phys. Eng. Sci. 372, 20130260.
Balsiger, H., et al., 2015. Detection of argon in the coma of comet 67P/Churyumov–Gerasimenko. In: Science Advances, vol. 1.
Bar-Nun, A., Herman, G., Laufer, D., Rappaport, M.L., 1985. Trapping and release of gases by water ice and implications for icy bodies. Icarus 63, 317–332.
Blank, J.G., Miller, G.H., Ahrens, M.J., Winans, R.E., 2001. Experimental shock chemistry of aqueous amino acid solutions and the cometary delivery of prebiotic compounds. Orig. Life Evol. Biosph. 31, 15–51.
Bockelée-Morvan, D., 2011. An overview of comet composition. In: Proceed. Intern. Astron. Union, vol. 7, pp. 261–274.
Bogard, D.D., Clayton, R.N., Marti, K., Owen, T., Turner, T., 2001. Martian volatiles: isotopic composition, origin and evolution. Space Sci. Rev. 96, 425–458.
Bottke, W.F., et al., 2012. An Achaean heavy bombardment from a destabilized extension of the asteroid belt. Nature 485, 78–81.
Bottke, W.F., Walker, R.J., Day, J.M.D., Nesvorny, D., Elkins-Tanton, L., 2010. Stochastic late accretion to Earth, the Moon, and Mars. Science 330, 1527.
Brownlee, D.L., et al., 2006. Comet 81P/Wild 2 under a microscope. Science 314, 1711–1716.
Carr, M.H., Head, J.W., 2003. Oceans on Mars: an assessment of the observational evidence and possible fate. J. Geophys. Res. 108. http://dx.doi.org/10.1029/2002JE001963.
Chassefière, E., Leblanc, F., 2004. Mars atmospheric escape and evolution: interaction with the solar wind. Planet. Space Sci. 52, 1039–1058.
Chennaoui Aoudjehane, H., et al., 2012. Tissint Martian meteorite: a fresh look at the interior, surface, and atmosphere of Mars. Science 738, 785–788.
Chyba, C.F., 1990. Impact delivery and erosion of planetary oceans in the inner solar system. Nature 343, 129–133.
Culler, T.S., Becker, T.A., Muller, R.A., Renne, P.R., 2000. Lunar impact history from ^{40}Ar–^{39}Ar dating of glass spherules. Science 287, 1785–1788.
Dauphas, N., 2003. The dual origin of the terrestrial atmosphere. Icarus 165, 326–339.
Dauphas, N., Morbidelli, A., 2014. Geochemical and planetary dynamical views on the origin of Earth' atmosphere and oceans. In: Treatise Geochem., vol. 6, 2nd ed., pp. 1–35.
De Niem, D., Kührt, E., Morbidelli, A., Motschmann, U., 2012. Atmospheric erosion and replenishment induced by impacts upon the Earth and Mars during a heavy bombardment. Icarus 221, 495–507.
Duprat, J., et al., 2010. Extreme deuterium excesses in ultracarbonaceous micrometeorites from central Antarctic snow. Science 328, 742–745.
Ehrenfreund, P., Charnley, S.B., 2000. Organic molecules in the interstellar medium, comets, and meteorites: a voyage from dark clouds to the early Earth. Annu. Rev. Astron. Astrophys. 38, 427–483.
Fries, M., et al., 2016. A cometary origin for Martian atmospheric methane. Geochem. Perspect. Lett. 2, 10–23.
Füri, E., Marty, B., 2015. Nitrogen isotope variations in the solar system. Nat. Geosci. 8, 515–522.
Genda, H., Abe, Y., 2005. Enhanced atmospheric loss on protoplanets at the giant impact phase in the presence of oceans. Nature 433, 842–844.
Gomes, R., Levison, H.F., Tsiganis, K., Morbidelli, A., 2005. Origin of the cataclysmic late heavy bombardment period of the terrestrial planets. Nature 435, 466–469.
Greenberg, J.M., 1998. Making a comet nucleus. Astron. Astrophys. 330, 375–380.
Halliday, A.N., 2013. The origins of volatiles in the terrestrial planets. Geochim. Cosmochim. Acta 105, 146–171.
Hartmann, W.K., Ryder, G., Dones, L., Grinspoon, D., 2002. The time-dependent intense bombardment of the primordial Earth/Moon system. In: Canup, R.M., Righter, K. (Eds.), Origin of the Earth and Moon. Univ. Arizona Press, pp. 451–493.
Hartogh, P., et al., 2011. Ocean-like water in the Jupiter-family comet 103P/Hartley 2. Nature 478, 218–220.
Hashizume, K., Marty, B., Wieler, R., 2002. Analyses of nitrogen and argon in single lunar grains: towards a quantification of the asteroidal contribution to planetary surfaces. Earth Planet. Sci. Lett. 202, 201–216.
Hässig, M., et al., 2015. Time variability and heterogeneity in the coma of 67P/Churyumov–Gerasimenko. Science 347 (6220). aaa0276-1.
Holland, G., Cassidy, M., Ballentine, C.J., 2009. Meteorite Kr in Earth's mantle suggests a late accretionary source for the atmosphere. Science 326, 1522–1525.
Honda, M., McDougall, I.A., Patterson, D.B., Doulgeris, A., Clague, D.A., 1991. Possible solar noble-gas component in Hawaiian basalts. Nature 349, 149–151.
Jacobson, S.A., Morbidelli, A., Raymond, S.N., O'Brien, D.P., Walsh, K.J., Rubie, D.C., 2014. Highly siderophile elements in Earth's mantle as a clock for the Moon-forming impact. Nature 508, 84–87.
Jakosky, B.M., Pepin, R.O., Johnson, R.E., Fox, J.L., 1994. Mars atmospheric loss and isotopic fractionation by solar-wind-induced sputtering and photochemical escape. Icarus 111, 271–281.
Jellinek, A.M., Jackson, M.G., 2015. Connections between the bulk composition, geodynamics and habitability of Earth. Nat. Geosci. 8, 587–593.
Jessberger, E.K., Cristoforidis, E.A., Kissel, J., 1988. Aspects of the major elemental composition of Halley's dust. Nature 332, 691–695.
Kerridge, F., 1985. Carbon, hydrogen and nitrogen in carbonaceous chondrites: abundances and isotopic compositions in bulk samples. Geochim. Cosmochim. Acta 49, 1707–1714.
Kimura, K., Lewis, R.S., Anders, E., 1974. Distribution of gold and rhenium between nickel–iron and silicate melts – implications for the abundance of siderophile elements on Earth and Moon. Geochim. Cosmochim. Acta 38, 683–701.
Kissel, J., Krueger, F.R., 1987. The organic component in dust from comet Halley as measured by the PUMA mass spectrometer on board Vega 1. Nature 326, 755–760.
Le Roy, L., et al., 2015. The volatile inventory of comet 67P/Churyumov–Gerasimenko from Rosetta/Rosina. Astron. Astrophys. 9. http://dx.doi.org/10.1051/0004-6361/201526450.
Levison, H.F., Dones, L., Chapman, C.R., Stern, A., 2001. Could the lunar 'Late Heavy Bombardment' have been triggered by the formation of Uranus and Neptune? Icarus 151, 286–306.
Love, S., Brownlee, D.E., 1993. A direct measurement of the terrestrial mass accretion rate of cosmic dust. Science 262, 550–553.

Mahaffy, P.R., et al., 2013. Abundance and isotopic composition of gases in the Martian atmosphere from the curiosity Rovber. Science 341, 263–266.
Marboeuf, U., Schmitt, B., 2014. How to link the relative abundances of gas species in coma of comets to their initial chemical composition? Icarus 242, 225–248.
Marrocchi, Y., Marty, B., 2013. Experimental determination of the xenon isotopic fractionation during adsorption. Geophys. Res. Lett. 40, 4165–4170.
Martins, Z., Botta, O., Ehrenfreund, P., 2007. Amino acids in antarctic CM1 meteorites and their relationship to other carbonaceous chondrites. Meteorit. Planet. Sci. 92, 81–92.
Marty, B., 2012. The origins and concentrations of water, carbon, nitrogen and noble gases on Earth. Earth Planet. Sci. Lett. 313–314, 56–66.
Marty, B., et al., 2008. Helium and neon abundances and compositions in cometary matter. Science 319, 75–78.
Marty, B., Meibom, A., 2007. Noble gas signature of the late heavy bombardment in the Earth's atmosphere. eEarth 2, 43–49.
McElroy, M.B., Kong, T.Y., Yung, Y.L., 1977. Photochemistry and evolution of Mars' atmosphere: a Viking perspective. J. Geophys. Res. 82, 4379–4388.
Montmessin, F., Fouchet, T., Forget, F., 2005. Modeling the annual cycle of HDO in the Martian atmosphere. J. Geophys. Res. 110, E03006.
Morbidelli, A., et al., 2000. Source regions and timescales for the delivery of water to the Earth. Meteorit. Planet. Sci. 35, 1309–1320.
Morbidelli, A., Marchi, S., Bottke, W.F., Kring, D.A., 2012. A sawtooth-like timeline for the first billion years of lunar bombardment. Earth Planet. Sci. Lett. 355, 144–151.
Mousis, O., et al., 2010. Impact regimes and post-formation sequestration processes: implications for the origin of heavy noble gases in terrestrial planets. Astrophys. J. 714, 1418–1423.
Mumma, M.J., Charnley, S.B., 2011. The chemical composition of comets – emerging taxonomies and Natal heritage. Annu. Rev. Astron. Astrophys. 49, 471–524.
Notesco, G., Bar-Nun, A., 2005. A ∼25 K temperature Fo formation for the submicron ice grains which formed comets. Icarus 175, 546–550.
O'Brien, D.P., Morbidelli, A., Levison, H.F., 2006. Terrestrial planet formation with strong dynamical friction. Icarus 184, 39–58.
O'Brien, D.P., Walsh, K.J., Morbidelli, A., Raymond, S.N., Mandell, A.M., 2014. Water delivery and giant impacts in the "Grand Tack" scenario. Icarus 239, 74–84.
Oro, J., 1961. Comets and the formation of biochemical compounds on the primitive Earth. Nature 190, 389–390.
Ott, U., 2014. Planetary and pre-solar noble gases in meteorites. Chem. Erde 74, 519–544.
Owen, T., Bar-Nun, A., 1995. Comets, impacts and atmospheres. Icarus 116, 215–226.
Ozima, M., Podosek, F.A., 2002. Noble Gas Geochemistry. Cambridge University Press. 286 pp.
Pepin, R.O., 1991. On the origin and early evolution of terrestrial planet atmospheres and meteoritic volatiles. Icarus 92, 2–79.
Porcelli, D., Ballentine, C.J., 2002. Models for the distribution of terrestrial noble gases and evolution of the atmosphere. Rev. Mineral. Geochem. 47, 411–480.
Pujol, M., Marty, B., Burgess, R., 2011. Chondritic-like xenon trapped in Archean rocks: a possible signature of the ancient atmosphere. Earth Planet. Sci. Lett. 308, 298–306.
Raymond, S.N., Quinn, T., Lunine, J.I., 2004. Making other earths: dynamical simulations of terrestrial planet formation and water delivery. Icarus 168, 1–17.
Raymond, S.N., Quinn, T., Lunine, J.I., 2007. High-resolution simulations of the final assembly of Earth-like planets. 2. Water delivery and planetary habitability. Astrobiology 7, 66–84.
Raymond, S.N., Schlichting, H.E., Hersant, F., Selsis, F., 2013. Dynamical and collisional constraints on a stochastic late veneer on the Terrestrial planets. Icarus 226, 671–681.
Righter, K., 2003. Metal-silicate partitioning of siderophile elements and core formation in the early Earth. Annu. Rev. Earth Planet. Sci. 31, 135–174.
Rubin, M., et al., 2015. Molecular nitrogen in comet 67P/Churyumov–Gerasimenko indicates a low formation temperature. Science 348, 232–235.
Safronov, V.S., 1972. The motion, evolution and origin of comets. In: Chebotarev, G.A. (Ed.), The Motion, Evolution and Origin of Comets. Springer-Verlag, pp. 329–334.
Schlichting, H.E., Sari, R., Yalinewich, A., 2014. Atmospheric mass loss during planet formation: the importance of planetesimal impacts. Icarus 247, 81–94.
Schultz, L., Franke, L., 2004. Helium, neon, and argon in meteorites: a data collection. Meteorit. Planet. Sci. 39, 1889–1890.
Stern, S.A., et al., 2000. The discovery of argon in comet C/1995 O1 (Hale Bopp). Astrophys. J. 544, L169–L172.
Sugahara, H., Mimura, K., 2014. Glycine oligomerization up to triglycine by shock experiments simulating comet impacts. Geochem. J. 48, 51–62.
Swindle, T.D., Kring, A., 2001. Implications of the noble gas budgets for the origin of water on Earth and Mars. In: Lunar Planet. Sci. Conf. Abstr. #3785.
Takaoka, N., 1972. An interpretation of general anomalies of xenon and the isotopic composition of primitive xenon. Mass Spectrom. 20, 287–302.
Tera, F., Papanastassiou, D.A., Wasserburg, G.J., 1974. Isotopic evidence for a terminal lunar cataclysm. Earth Planet. Sci. Lett. 22, 1–21.
Weaver, H.A., Feldman, P.D., Combi, M.R., Krasnopolsky, V., Lisse, C.M., Shemansky, D.E., 2002. A search for argon and O_{VI} in three comets using the far ultraviolet spectroscopic explorer. Astrophys. J. 576, L95–L98.
Wetherhill, G.W., 1980. Formation of the terrestrial planets. Annu. Rev. Astron. Astrophys. 18, 77–113.
Wong, M.H., et al., 2013. Isotopes of nitrogen on Mars: atmospheric measurements by curiosity's mass spectrometer. Geophys. Res. Lett. 40, 6033–6037.
Yokochi, R., Marboeuf, U., Quirico, E., Schmitt, B., 2012. Pressure dependent trace gas trapping in amorphous water ice at 77 K: implications for determining conditions of comet formation. Icarus 218, 760–770.

List of Figures

List of Tables

Bibliography

Altwegg, K., Balsiger, H., Bar-Nun, A., Berthelier, J. J., Bieler, A., Bochsler, P., Briois, C., Calmonte, U., Combi, M., De Keyser, J., Eberhardt, P., Fiethe, B., Fuselier, S., Gasc, S., Gombosi, T. I., Hansen, K. C., Hässig, M., Jackel, A., Kopp, E., Korth, A., LeRoy, L., Mall, U., Marty, B., Mousis, O., Neefs, E., Owen, T., Reme, H., Rubin, M., Semon, T., Tzou, C. Y., Waite, H., and Wurz, P. (2015). 67P/Churyumov-Gerasimenko, a Jupiter family comet with a high D/H ratio. *Science*, 347(6220):1–3.

Anbar, A. D., Duan, Y., Lyons, T. W., Arnold, G. L., Kendall, B., Creaser, R. A., Kaufman, A. J., Gordon, G. W., Scott, C. T., Garvin, J., and Buick, R. (2007). A whiff of oxygen before the great oxidation event? *Science*, 317:1903–1906.

Aoudjehane, H. C., Avice, G., Barrat, J. A., Boudouma, O., Chen, G., Duke, M. J. M., Franchi, I. A., Gattacceca, J., Grady, M. M., Greenwood, R. C., Herd, C. D. K., Hewins, R., Jambon, A., Marty, B., Rochette, P., Smith, C. L., Sautter, V., Verchovsky, A., Weber, P., and Zanda, B. (2012). Tissint Martian Meteorite: A Fresh Look at the Interior, Surface, and Atmosphere of Mars. *Science*, 338(6108):785–788.

Arndt, N. T., Nelson, D. R., Compston, W., Trendall, A. F., and Thorne, A. M. (1991). The age of the Fortescue Group, Hamersley Basin, Western Australia, from ion microprobe zircon U-Pb results. *Australian Journal of Earth Sciences*, 38:261–281.

Arndt, N. T. and Nisbet, E. G. (2012). Processes on the Young Earth and the Habitats of Early Life. *Annual Review of Earth and Planetary Sciences*, 40(1):521–549.

Avice, G. and Marty, B. (2014). The iodine-plutonium-xenon age of the Moon-Earth system revisited. *Philosophical Transactions of the Royal Society A: Mathematical, Physical and Engineering Sciences*, 372(20130260):1–16.

Avice, G., Meier, M. M. M., Marty, B., Wieler, R., Kramers, J. D., Langenhorst, F., Cartigny, P., Maden, C., Zimmermann, L., and Andreoli, M. A. G. (2015). A comprehensive study of noble gases and nitrogen in "Hypatia", a diamond-rich pebble from SW Egypt. *Earth and Planetary Science Letters*, 432(C):243–253.

Ballentine, C. J. and Burnard, P. G. (2002). Production, Release and Transport of Noble Gases in the Continental Crust. *Reviews in Mineralogy and Geochemistry*, 47(1):481–538.

Ballentine, C. J. and Holland, G. (2008). What CO2 well gases tell us about the origin of noble gases in the mantle and their relationship to the atmosphere. *Philosophical Transactions of the Royal Society A: Mathematical, Physical and Engineering Sciences*, 366:4183–4203.

Ballentine, C. J., Marty, B., Lollar, B. S., and Cassidy, M. (2005). Neon isotopes constrain convection and volatile origin in the Earth's mantle. *Nature*, 433(7021):33–38.

Balsiger, H., Altwegg, K., Bar-Nun, A., Berthelier, J. J., Bieler, A., Bochsler, P., Briois, C., Calmonte, U., Combi, M., De Keyser, J., Eberhardt, P., Fiethe, B., Fuselier, S. A., Gasc, S., Gombosi, T. I., Hansen,

K. C., Hässig, M., Jackel, A., Kopp, E., Korth, A., Le Roy, L., Mall, U., Marty, B., Mousis, O., Owen, T., Reme, H., Rubin, M., Semon, T., Tzou, C. Y., Waite, J. H., and Wurz, P. (2015). Detection of argon in the coma of comet 67P/Churyumov-Gerasimenko. *Science Advances*, 1(8):1–4.

Bar-Nun, A. and Owen, T. (1998). Trapping of Gases in Water Ice and Consequences to Comets and the Atmospheres of the Inner Planets. In Schmitt, B., editor, *Solar System Ices*, pages 353–366. Springer Netherlands, Dordrecht.

Baratoux, L., Metelka, V., Naba, S., Ouiya, P., Siebenaller, L., Jessell, M. W., Naré, A., Salvi, S., Béziat, D., and Franceschi, G. (2015). Tectonic evolution of the Gaoua region, Burkina Faso: Implications for mineralization. *Journal of African Earth Sciences*, 112(B):419–439.

Bianchi, D., Sarmiento, J. L., Gnanadesikan, A., Key, R. M., Schlosser, P., and Newton, R. (2010). Low helium flux from the mantle inferred from simulations of oceanic helium isotope data. *Earth and Planetary Science Letters*, 297(3-4):379–386.

Biggin, A. J., Piispa, E. J., Pesonen, L. J., Holme, R., Paterson, G. A., Veikkolainen, T., and Tauxe, L. (2015). Palaeomagnetic field intensity variations suggest Mesoproterozoic inner-core nucleation. *Nature*, 526(7572):245–248.

Blichert-Toft, J. and Albarède, F. (2008). Hafnium isotopes in Jack Hills zircons and the formation of the Hadean crust. *Earth and Planetary Science Letters*, 265(3-4):686–702.

Blichert-Toft, J. and Frei, R. (2001). Complex Sm-Nd and Lu-Hf isotope systematics in metamorphic garnets from the Isua supracrustal belt, West Greenland. *Geochimica et Cosmochimica Acta*, 65(18):3177–3189.

Bogard, D. D., Clayton, R. N., Marti, K., Owen, T., and Turner, G. (2001). Martian volatiles: Isotopic composition, origin, and evolution. In *Chronology and Evolution of Mars*, pages 425–458. Chronology and Evolution of Mars, Netherlands.

Böhlke, J. K. and Irwin, J. J. (1992). Laser microprobe analyses of noble gas isotopes and halogens in fluid inclusions: Analyses of microstandards and synthetic inclusions in quartz. *Geochimica et Cosmochimica Acta*, 56(1):187–201.

Bräuer, K., Kämpf, H., Niedermann, S., and Strauch, G. (2013). Indications for the existence of different magmatic reservoirs beneath the Eifel area (Germany): A multi-isotope (C, N, He, Ne, Ar) approach. *Chemical Geology*, 356(C):193–208.

Britvin, S. N., Kashtanov, S. A., Krzhizhanovskaya, M. G., Gurinov, A. A., Glumov, O. V., Strekopytov, S., Kretser, Y. L., Zaitsev, A. N., Chukanov, N. V., and Krivovichev, S. V. (2015). Perovskites with the Framework-Forming Xenon. *Angewandte Chemie International Edition*, 54(48):14340–14344.

Buick, R. and Dunlop, J. S. R. (1990). Evaporitic sediments of Early Archaean age from the Warrawoona Group, North Pole, Western Australia. *Sedimentology*, 37(2):247–277.

Burgess, R., Layzelle, E., Turner, G., and Harris, J. W. (2002). Constraints on the age and halogen composition of mantle fluids in Siberian coated diamonds. *Earth and Planetary Science Letters*, 197:193–203.

Busemann, H., Baur, H., and Wieler, R. (2000). Primordial noble gases in "phase Q" in carbonaceous and ordinary chondrites studied by closed-system stepped etching. *Meteoritics & Planetary Science*, 35(5):949–973.

Cadogan, P. H. (1977). Palaeoatmospheric argon in Rhynie chert. *Nature*, 268(5615):38–41.

Caffee, M. W., Hudson, G. B., Velsko, C., Huss, G. R., Alexander Jr, E. C., and Chivas, A. R. (1999). Primordial Noble Gases from Earth's Mantle: Identification of a Primitive Volatile Component. *Science*, 285(5436):2115–2118.

Card, K. D. (1990). A review of the Superior Province of the Canadian Shield, a product of Archean accretion. *Precambrian Research*, 48(1-2):99–156.

Caro, G., Bourdon, B., Birck, J. L., and Moorbath, S. (2003). 146Sm–142Nd evidence from Isua metamorphosed sediments for early differentiation of the Earth's mantle. *Nature*, 423:428–432.

Catling, D. C. (2014). The Great Oxidation Event transition. In *Treatise on Geochemistry (Second Edition)*, pages 177–195. Elsevier, Oxford.

Chambers, J. (2014). Forming Terrestrial Planets. *Science*, 344(6183):479–480.

Chan, W. F., Cooper, G., Guo, X., Burton, G. R., and Brion, C. E. (1992). Absolute optical oscillator strengths for the electronic excitation of atoms at high resolution. III. The photoabsorption of argon, krypton, and xenon. *Physical Review A*, 46(1):149–171.

Chantraine, J., Auvray, B., Brun, J. P., Chauvel, J. J., and Rabu, D. (1994). Introduction. In Chantraine, J., Rolet, J., Santallier, D. S., and Piqué, A., editors, *Pre-Mesozoic Geology in France and related areas*, pages 75–80.

Cheilletz, A., Féraud, G., Giuliani, G., and Ruffet, G. (1993). Emerald dating through 40Ar/39Ar step-heating and laser spot analysis of syngenetic phlogopite. *Earth and Planetary Science Letters*, 120(3-4):473–485.

Ciborowski, T. J. R. and Kerr, A. C. (2016). Did mantle plume magmatism help trigger the Great Oxidation Event? *Lithos*, pages 1–25.

Claire, M. W., Sheets, J., Cohen, M., Ribas, I., Meadows, V. S., and Catling, D. C. (2012). The evolution of solar flux from 0.1 nm to 160 um: Quantitative estimates for planetary studies. *The Astrophysical Journal*, 757(95):1–12.

Clayton, D. D. and Ward, R. A. (1978). S-process studies-Xenon and krypton isotopic abundances. *The Astrophysical Journal*, 224:1000–1006.

Clayton, R. N., O'Neil, J. R., and Mayeda, T. K. (1972). Oxygen isotope exchange between quartz and water. *Journal of Geophysical Research: Planets*, 77(17):3057–3067.

Crisp, D., Allen, M. A., Anicich, V. G., Arvidson, R. E., Atreya, S. K., Baines, K. H., Banerdt, W. B., Bjoraker, G. L., Bougher, S. W., Campbell, B. A., Carlson, R. W., Chin, G., Chutjian, A., Clancy, R. T., Clark, B. C., Cravens, T. E., Del Genio, A. D., Esposito, L. W., Fegley, B., Flasar, M., Fox, J. L., Gierash, P. J., Goody, R. M., Grinspoon, D. H., Gulkis, S., Hansen, V. L., Herrick, R. R., Huestis, D. L., Hunten, D. M., Janssen, M. A., Jenkins, J., Johnson, C. L., Keating, G. M., Kliore, A. J., Limaye, S. S., Luhmann, J. G., Lunine, J. I., Mahaffy, P., McGovern, P. J., Meadows, V. S., Mills, F. P., Niemann, H. B., Owen, T. C., Oyama, K. I., Pepin, R. O., Plaut, J. J., Reuter, D. C., Richardson, M. I., Russell, C. T., Saunders, R. S., Schofield, J. T., Schubert, G., Senske, D. A., Shepard, M. K., Slanger, T. G., Smrekar, S. E., Stevenson, D. J., Titov, D. V., Ustinov, E. A., Young, R. E., and Yung, Y. L. (2002). Divergent evolution among Earth-like planets: the case for Venus exploration. *The Future of Solar System Exploration (ASP Conference Series)*, 272:5–34.

Crowther, S. A. and Gilmour, J. D. (2013). The Genesis solar xenon composition and its relationship to planetary xenon signatures. *Geochimica et Cosmochimica Acta*, 123(C):17–34.

Dauphas, N. (2003). The dual origin of the terrestrial atmosphere. *Icarus*, 165(2):326–339.

Dauphas, N. and Morbidelli, A. (2014). Geochemical and Planetary Dynamical Views on the Origin of Earth's Atmosphere and Oceans. In Turekian, H. D. H. K., editor, *Treatise on Geochemistry (Second Edition)*, pages 1–35. Elsevier, Oxford.

Dauphas, N. and Pourmand, A. (2011). Hf–W–Th evidence for rapid growth of Mars and its status as a planetary embryo. *Nature*, 473(7348):489–492.

Dauphas, N., van Zuilen, M., Busigny, V., Lepland, A., Wadhwa, M., and Janney, P. E. (2007). Iron isotope, major and trace element characterization of early Archean supracrustal rocks from SW Greenland: Protolith identification and metamorphic overprint. *Geochimica et Cosmochimica Acta*, 71(19):4745–4770.

Davis, D. W., Pezzutto, F., and Ojakangas, R. W. (1990). The age and provenance of metasedimentary rocks in the Quetico Subprovince, Ontario, from single zircon analyses: implications for Archean sedimentation and tectonics in the Superior Province. *Earth and Planetary Science Letters*, 99(3):195–205.

de Niem, D., Kührt, E., Morbidelli, A., and Motschmann, U. (2012). Atmospheric erosion and replenishment induced by impacts upon the Earth and Mars during a heavy bombardment. *Icarus*, 221(2):495–507.

de Wit, M. J., Furnes, H., and Robins, B. (2011). Geology and tectonostratigraphy of the Onverwacht Suite, Barberton Greenstone Belt, South Africa. *Precambrian Research*, 186:1–27.

Derome, D., Cuney, M., Cathelineau, M., Fabre, C., Dubessy, J., Bruneton, P., and Hubert, A. (2003). A detailed fluid inclusion study in silicified breccias from the Kombolgie sandstones (Northern Territory, Australia): inferences for the genesis of middle-Proterozoic unconformity-type uranium deposits. *Journal of Geochemical Exploration*, 80(2-3):259–275.

Domagal-Goldman, S. D., Kasting, J. F., Johnston, D. T., and Farquhar, J. (2008). Organic haze, glaciations and multiple sulfur isotopes in the Mid-Archean Era. *Earth and Planetary Science Letters*, 269(1-2):29–40.

Donahue, T. M., Hoffman, J. H., and Hodges, R. R. (1981). Krypton and xenon in the atmosphere of Venus. *Geophysical Research Letters*, 8(5):513–516.

Drescher, J., Kirsten, T., and Schäfer, K. (1998). The rare gas inventory of the continental crust, recovered by the KTB Continental Deep Drilling Project. *Earth and Planetary Science Letters*, 154:247–263.

Farber, K., Dziggel, A., Meyer, F. M., Prochaska, W., Hofmann, A., and Harris, C. (2015). Fluid inclusion analysis of silicified Palaeoarchaean oceanic crust – A record of Archaean seawater? *Precambrian Research*, 266:150–164.

Farquhar, J., Savarino, J., Airieau, S., and Thiemens, M. H. (2001). Observation of wavelength-sensitive mass-independent sulfur isotope effects during SO2 photolysis: Implications for the early atmosphere. *Journal of Geophysical Research: Planets*, 106(E12):32829–32839.

Farquhar, J. and Wing, B. A. (2003). Multiple sulfur isotopes and the evolution of the atmosphere. *Earth and Planetary Science Letters*, 213(1-2):1–13.

Feulner, G. (2012). The faint young Sun problem. *Reviews of Geophysics*, 50(2):RG2006.

Furnes, H., de Wit, M., and Robins, B. (2013). A review of new interpretations of the tectonostratigraphy, geochemistry and evolution of the Onverwacht Suite, Barberton Greenstone Belt, South Africa. *Gondwana Research*, 23(2):403–428.

Gaillard, F., Scaillet, B., and Arndt, N. T. (2011). Atmospheric oxygenation caused by a change in volcanic degassing pressure. *Nature*, 478(7368):229–232.

Genda, H. and Abe, Y. (2003). Survival of a proto-atmosphere through the stage of giant impacts: the mechanical aspects. *Icarus*, 164(1):149–162.

Genda, H. and Abe, Y. (2005). Enhanced atmospheric loss on protoplanets at the giant impact phase in the presence of oceans. *Nature*, 433(7028):842–844.

Giuliani, G., Silva, L. J. H. D., and Couto, P. (1990). Origin of emerald deposits of Brazil. *Mineralium Deposita*, 25(1):57–64.

Goes, S., Spakman, W., and Bijwaard, H. (1999). A Lower Mantle Source for Central European Volcanism. *Science*, 286(5446):1928–1931.

Goldblatt, C., Claire, M. W., Lenton, T. M., Matthews, A. J., Watson, A. J., and Zahnle, K. J. (2009). Nitrogen-enhanced greenhouse warming on early Earth. *Nature Geoscience*, 2(12):891–896.

Gomes, R., Levison, H. F., Tsiganis, K., and Morbidelli, A. (2005). Origin of the cataclysmic Late Heavy Bombardment period of the terrestrial planets. *Nature*, 435(7041):466–469.

Gounelle, M. (2011). The Asteroid-Comet Continuum: In Search of Lost Primitivity. *Elements*, 7(1):29–34.

Halliday, A. N. (2013). The origins of volatiles in the terrestrial planets. *Geochimica et Cosmochimica Acta*, 105(C):146–171.

Haner, J. and Schrobilgen, G. J. (2015). The Chemistry of Xenon(IV). *Chemical Reviews*, 115(2):1255–1295.

Hanes, J. A., Archibald, D. A., and Hodgson, C. J. (1992). Dating of Archean auriferous quartz vein deposits in the Abitibi greenstone belt, Canada; 40Ar/39Ar evidence for a 70-to 100-my-time gap between plutonism-metamorphism and mineralization. *Economic Geology*, 87:1849–1861.

Harrison, T. M. (2009). The Hadean Crust: Evidence from >4 Ga Zircons. *Annual Review of Earth and Planetary Sciences*, 37(1):479–505.

Hartogh, P., Lis, D. C., Bockelée-Morvan, D., de Val-Borro, M., Biver, N., Küppers, M., Emprechtinger, M., Bergin, E. A., Crovisier, J., Rengel, M., Moreno, R., Szutowicz, S., and Blake, G. A. (2011). Ocean-like water in the Jupiter-family comet 103P/Hartley 2. *Nature*, 478:218–220.

Heber, V. S., Baur, H., Bochsler, P., McKeegan, K. D., Neugebauer, M., Reisenfeld, D. B., Wieler, R., and Wiens, R. C. (2012). Isotopic Mass Fractionation of Solar Wind: Evidence from Fast and Slow Solar Wind Collected by the Genesis Mission. *The Astrophysical Journal*, 759(121):1–13.

Heber, V. S., Wieler, R., Baur, H., Olinger, C., Friedmann, T. A., and Burnett, D. S. (2009). Noble gas composition of the solar wind as collected by the Genesis mission. *Geochimica et Cosmochimica Acta*, 73(24):7414–7432.

Hébrard, E. and Marty, B. (2014). Coupled noble gas-hydrocarbon evolution of the early Earth atmosphere upon solar UV irradiation. *Earth and Planetary Science Letters*, 385(C):40–48.

Heymann, D. and Dziczkaniec, M. (1979). Xenon from intermediate zones of supernovae. *Proceedings of the 10th Lunar and Planetary Science Conference*, pages 1943–1959.

Hickman, A. H. and van Kranendonk, M. J. (2012). Early Earth evolution: evidence from the 3.5-1.8 Ga geological history of the Pilbara region of Western Australia. *Episodes*, 35(1):283–297.

Hofmann, A. (2005). The geochemistry of sedimentary rocks from the Fig Tree Group, Barberton greenstone belt: Implications for tectonic, hydrothermal and surface processes during mid-Archaean times. *Precambrian Research*, 143(1-4):23–49.

Hofmann, A., Bolhar, R., Orberger, B., and Foucher, F. (2014). Cherts of the Barberton Greenstone Belt, South Africa: Petrology and Trace-Element Geochemistry of 3.5 to 3.3 Ga Old Silicified Volcaniclastic Sediments. *South African Journal of Geology*, 116(2):297–322.

Hofmann, A. and Harris, C. (2008). Silica alteration zones in the Barberton greenstone belt: a window into subseafloor processes 3.5–3.3 Ga ago. *Chemical Geology*, 257:221–239.

Holland, G. and Ballentine, C. J. (2006). Seawater subduction controls the heavy noble gas composition of the mantle. *Nature*, 441(7090):186–191.

Holland, G., Cassidy, M., and Ballentine, C. J. (2009). Meteorite Kr in Earth's Mantle Suggests a Late Accretionary Source for the Atmosphere. *Science*, 326(5959):1522–1525.

Holland, G., Lollar, B. S., Li, L., Lacrampe-Couloume, G., Slater, G. F., and Ballentine, C. J. (2013). Deep fracture fluids isolated in the crust since the Precambrian era. *Nature*, 497:357–360.

Holland, H. D. (2006). The oxygenation of the atmosphere and oceans. *Philosophical Transactions of the Royal Society B: Biological Sciences*, 361(1470):903–915.

Honda, M., McDougall, I., Patterson, D. B., and Doulgeris, A. (1991). Possible solar noble-gas component in Hawaiian basalts. *Nature*, 349(6305):149–151.

Honda, M., Reynolds, J. H., and Roedder, E. (1987). Noble gases in diamonds: Occurences of solar-like helium and neon. *Journal of Geophysical Research*, 92(B12):507–522.

Hutsemékers, D., Manfroid, J., Jehin, E., and Arpigny, C. (2009). New constraints on the delivery of cometary water and nitrogen to Earth from the 15N/14N isotopic ratio. *Icarus*, 204(1):346–348.

Igarashi, G. (1995). Primitive xenon in the Earth. *AIP Conference Proceedings*, 341(70):70–80.

Jacobson, S. A., Morbidelli, A., Raymond, S. N., O'Brien, D. P., Walsh, K. J., and Rubie, D. C. (2015). Highly siderophile elements in Earth's mantle as a clock for the Moon-forming impact. *Nature*, 508(7494):84–87.

Jakosky, B. M. and Pepin, R. O. (1994). Mars atmospheric loss and isotopic fractionation by solar-wind-induced sputtering and photochemical escape. *Icarus*, 111:271–288.

Johnston, D. T. (2011). Multiple sulfur isotopes and the evolution of Earth's surface sulfur cycle. *Earth Science Reviews*, 106(1-2):161–183.

Kamo, S. L. and Davis, D. W. (1994). Reassessment of Archean crustal development in the Barberton Mountain Land, South Africa, based on U-Pb dating. *Tectonics*, 13(1):167–192.

Kasting, J. F. (2014). Atmospheric composition of Hadean–early Archean Earth: The importance of CO. *Geological Society of America Special Papers*, 504:19–28.

Katcoff, S., Schaeffer, O. A., and Hastings, J. M. (1951). Half-Life of 129I and the Age of the Elements. *Physical Review*, 82(5):688–690.

Kelley, S. (2002). Excess argon in K–Ar and Ar–Ar geochronology. *Chemical Geology*, 188(1):1–22.

Kelley, S., Turner, G., Butterfield, A. W., and Shepherd, T. J. (1986). The source and significance of argon isotopes in fluid inclusions from areas of mineralization. *Earth and Planetary Science Letters*, 79(3):303–318.

Kemp, A. I. S., Hickman, A. H., Kirkland, C. L., and Vervoort, J. D. (2015). Hf isotopes in detrital and inherited zircons of the Pilbara Craton provide no evidence for Hadean continents. *Precambrian Research*, 261:112–126.

Kendrick, M. A. (2012). High precision Cl, Br and I determinations in mineral standards using the noble gas method. *Chemical Geology*, 292-293(C):116–126.

Kendrick, M. A., Miller, J. M., and Phillips, D. (2006). Part II. Evaluation of 40Ar–39Ar quartz ages: Implications for fluid inclusion retentivity and determination of initial 40Ar/36Ar values in Proterozoic samples. *Geochimica et Cosmochimica Acta*, 70(10):2562–2576.

Korenaga, J. (2008). Urey ratio and the structure and evolution of Earth's mantle. *Reviews of Geophysics*, 46(2):RG2007–32.

Kramers, J. D., Andreoli, M. A. G., Atanasova, M., Belyanin, G. A., Block, D. L., Franklyn, C., Harris, C., Lekgoathi, M., Montross, C. S., Ntsoane, T., Pischedda, V., Segonyane, P., Viljoen, K. S. F., and Westraadt, J. E. (2013). Unique chemistry of a diamond-bearing pebble from the Libyan Desert Glass strewnfield, SW Egypt: Evidence for a shocked comet fragment. *Earth and Planetary Science Letters*, 382(C):21–31.

Krummenacher, D., Merrihue, C. M., Pepin, R. O., and Reynolds, J. H. (1962). Meteoritic krypton and barium versus the general isotopic anomalies in meteoritic xenon. *Geochimica et Cosmochimica Acta*, 26(2):231–249.

Kuga, M., Marty, B., Marrocchi, Y., and Tissandier, L. (2015). Synthesis of refractory organic matter in the ionized gas phase of the solar nebula. *Proceedings of the National Academy of Sciences*, 112(23):7129–7134.

Kunz, J. (1999). Is there solar argon in the Earth's mantle? *Nature*, 399(6737):649–650.

Kunz, J., Staudacher, T., and Allègre, C. J. (1998). Plutonium-Fission Xenon Found in Earth's Mantle. *Science*, 280:877–880.

Kyser, K., Hiatt, E., Renac, C., Durocher, K., Holk, G., and Deckart, K. (2000). Diagenetic fluids in Paleo- and Meso-Proterozoic sedimentary basins and their implications for long protracted fluid histories. In Kyser, K., editor, *Fluids and basin evolution*, pages 73–506. Fluids and basin evolution.

Le Mignot, E., Siebenaller, L., Béziat, D., Salvi, S., André-Mayer, A. S., Reisberg, L., Velasquez, G., Zimmermann, C., and Franceschi, G. (2014). The Paleoproterozoic Copper-Gold Deposit of Gaoua, Burkina Faso: Evidence for A Polyphased Mineralization. *Acta Geologica Sinica (English Edition)*, 88(s2):970–972.

Lee, J.-Y., Marti, K., Severinghaus, J. P., Kawamura, K., Yoo, H.-S., Lee, J. B., and Kim, J. S. (2006). A redetermination of the isotopic abundances of atmospheric Ar. *Geochimica et Cosmochimica Acta*, 70(17):4507–4512.

Levison, H. F., Duncan, M. J., Brasser, R., and Kaufmann, D. E. (2010). Capture of the Sun's Oort Cloud from Stars in Its Birth Cluster. *Science*, 329(5988):187–190.

Lewis, R. S., AMARI, S., and Anders, E. (1994). Interstellar grains in meteorites: II. SiC and its noble gases. *Geochimica et Cosmochimica Acta*, 58(1):471–494.

Ludwig, K. R. (1991). ISOPLOT; a plotting and regression program for radiogenic-isotope data; version 2.53. *Open-File Report VL - USGS*, 91-445:39.

Lyons, T. W., Reinhard, C. T., and Planavsky, N. J. (2015). The rise of oxygen in Earth's early ocean and atmosphere. *Nature*, 506:307–315.

Marin-Carbonne, J., Faure, F., Chaussidon, M., Jacob, D., and Robert, F. (2013). A petrographic and isotopic criterion of the state of preservation of Precambrian cherts based on the characterization of the quartz veins. *Precambrian Research*, 231:290–300.

Marrocchi, Y., Avice, G., and Estrade, N. (2015). Multiple carriers of Q noble gases in primitive meteorites. *Geophysical Research Letters*, 42:1–7.

Marrocchi, Y. and Marty, B. (2013). Experimental determination of the xenon isotopic fractionation during adsorption. *Geophysical Research Letters*, 40(16):4165–4170.

Marrocchi, Y., Marty, B., Reinhardt, P., and Robert, F. (2011). Adsorption of xenon ions onto defects in organic surfaces: Implications for the origin and the nature of organics in primitive meteorites. *Geochimica et Cosmochimica Acta*, 75(20):6255–6266.

Marti, K. and Mathew, K. J. (2015). Xenon in the Protoplanetary Disk (PPD-Xe). *The Astrophysical Journal*, 806(L30):1–5.

Marty, B. (1989). Neon and xenon isotopes in MORB: implications for the earth-atmosphere evolution. *Earth and Planetary Science Letters*, 94(1):45–56.

Marty, B. (2012). The origins and concentrations of water, carbon, nitrogen and noble gases on Earth. *Earth and Planetary Science Letters*, 313-314:56–66.

Marty, B., Avice, G., Sano, Y., Altwegg, K., Balsiger, H., Hässig, M., Morbidelli, A., Mousis, O., and Rubin, M. (2016). Origins of volatile elements (H, C, N, noble gases) on Earth and Mars in light of recent results from the ROSETTA cometary mission. *Earth and Planetary Science Letters*, 441:91–102.

Marty, B. and Meibom, A. (2007). Noble gas signature of the late heavy bombardment in the Earth's atmosphere. *EEarth*, 2(2):43–49.

Marty, B., Palma, R. L., Pepin, R. O., Zimmermann, L., Schlutter, D. J., Burnard, P. G., Westphal, A. J., Snead, C. J., Bajt, S., Becker, R. H., and Simones, J. E. (2008). Helium and Neon Abundances and Compositions in Cometary Matter. *Science*, 319(5859):75–78.

Marty, B., Zimmermann, L., Pujol, M., Burgess, R., and Philippot, P. (2013). Nitrogen Isotopic Composition and Density of the Archean Atmosphere. *Science*, 342(6154):101–104.

Mathew, K. J. and Marti, K. (2001). Early evolution of Martian volatiles: Nitrogen and noble gas components in ALH84001 and Chassigny. *Journal of Geophysical Research: Planets*, 106(E1):1401–1422.

Matsuda, J.-i., Namba, M., Maruoka, T., Matsumoto, T., and Kurat, G. (2005). Primordial noble gases in a graphite-metal inclusion from the Canyon Diablo IAB iron meteorite and their implications. *Meteoritics & Planetary Science*, 40(3):431–443.

Meech, K. J., A'Hearn, M. F., Adams, J. A., Bacci, P., Bai, J., Barrera, L., Battelino, M., Bauer, J. M., Becklin, E., Bhatt, B., Biver, N., Bockelee-Morvan, D., Bodewits, D., Böhnhardt, H., Boissier, J., Bonev, B. P., Borghini, W., Brucato, J. R., Bryssinck, E., Buie, M. W., Canovas, H., Castellano, D., Charnley, S. B., Chen, W. P., Chiang, P., Choi, Y. J., Christian, D. J., Chuang, Y. L., Cochran, A. L., Colom,

P., Combi, M. R., Coulson, I. M., Crovisier, J., Dello Russo, N., Dennerl, K., DeWahl, K., DiSanti, M. A., Facchini, M., Farnham, T. L., Fernández, Y., Florén, H. G., Frisk, U., Fujiyoshi, T., Furusho, R., Fuse, T., Galli, G., García-Hernández, D. A., Gersch, A., Getu, Z., Gibb, E. L., Gillon, M., Guido, E., Guillermo, R. A., Hadamcik, E., Hainaut, O., Hammel, H. B., Harker, D. E., Harmon, J. K., Harris, W. M., Hartogh, P., Hashimoto, M., Häusler, B., Herter, T., Hjalmarson, A., Holland, S. T., Honda, M., Hosseini, S., Howell, E. S., Howes, N., Hsieh, H. H., Hsiao, H. Y., Hutsemékers, D., Immler, S. M., Jackson, W. M., Jeffers, S. V., Jehin, E., Jones, T. J., de Juan Ovelar, M., Kaluna, H. M., Karlsson, T., Kawakita, H., Keane, J. V., Keller, L. D., Kelley, M. S., Kinoshita, D., Kiselev, N. N., Kleyna, J., Knight, M. M., Kobayashi, H., Kobulnicky, H. A., Kolokolova, L., Kreiny, M., Kuan, Y. J., Küppers, M., Lacruz, J. M., Landsman, W. B., Lara, L. M., Lecacheux, A., Levasseur-Regourd, A. C., Li, B., Licandro, J., Ligustri, R., Lin, Z. Y., Lippi, M., Lis, D. C., Lisse, C. M., Lovell, A. J., Lowry, S. C., Lu, H., Lundin, S., Magee-Sauer, K., Magain, P., Manfroid, J., Mazzotta Epifani, E., McKay, A., Melita, M. D., Mikuz, H., Milam, S. N., Milani, G., Min, M., Moreno, R., Mueller, B. E. A., Mumma, M. J., Nicolini, M., Nolan, M. C., Nordh, H. L., Nowajewski, P. B., Team, O., Ootsubo, T., Paganini, L., Perrella, C., Pittichová, J., Prosperi, E., Radeva, Y. L., Reach, W. T., Remijan, A. J., Rengel, M., Riesen, T. E., Rodenhuis, M., Rodríguez, D. P., Russell, R. W., Sahu, D. K., Samarasinha, N. H., Sánchez Caso, A., Sandqvist, A., Sarid, G., Sato, M., Schleicher, D. G., Schwieterman, E. W., Sen, A. K., Shenoy, D., Shi, J. C., Shinnaka, Y., Skvarc, J., Snodgrass, C., Sitko, M. L., Sonnett, S., Sosseini, S., Sostero, G., Sugita, S., Swinyard, B. M., Szutowicz, S., Takato, N., Tanga, P., Taylor, P. A., Tozzi, G. P., Trabatti, R., Trigo-Rodríguez, J. M., Tubiana, C., de Val-Borro, M., Vacca, W., Vandenbussche, B., Vaubaillion, J., Velichko, F. P., Velichko, S. F., Vervack Jr, R. J., Vidal-Nunez, M. J., Villanueva, G. L., Vinante, C., Vincent, J. B., Wang, M., Wasserman, L. H., Watanabe, J., Weaver, H. A., Weissman, P. R., Wolk, S., Wooden, D. H., Woodward, C. E., Yamaguchi, M., Yamashita, T., Yanamandra-Fischer, P. A., Yang, B., Yao, J. S., Yeomans, D. K., Zenn, T., Zhao, H., and Ziffer, J. E. (2011). EPOXI: Comet 103P/Hartley 2 Observations from a worldwide campaign. *The Astrophysical Journal*, 734(1):L1–9.

Meshik, A., Hohenberg, C., Pravdivtseva, O., and Burnett, D. (2014). Heavy noble gases in solar wind delivered by Genesis mission. *Geochimica et Cosmochimica Acta*, 127(C):326–347.

Meshik, A. P., Hohenberg, C. M., Pravdivtseva, O. V., and Kapusta, Y. S. (2001). Weak decay of 130Ba and 132Ba:Geochemical measurements. *Physical Review C*, 64(3):035205.

Meshik, A. P., Kehm, K., and Hohenberg, C. M. (2000). Anomalous xenon in zone 13 Okelobondo. *Geochimica et Cosmochimica Acta*, 64(9):1651–1661.

Meshik, A. P., Pravdivtseva, O. V., and Burnett, D. S. (2015). Primitive Terrestrial Xenon: A Relation to Refined Composition of Solar Wind. *Proceedings of the 78th Annual Meeting of the Meteoritical Society*, page 5371.

Michel, T. and Eugster, O. (1994). Primitive xenon in diogenites and plutonium-244-fission xenon ages of a diogenite, a howardite, and eucrites. *Meteoritics*, 29:593–606.

Mittlefehldt, D. W. (2015). Asteroid (4) Vesta: I. The howardite-eucrite-diogenite (HED) clan of meteorites. *Chemie der Erde - Geochemistry*, 75(2):155–183.

Mojzsis, S. J., Arrhenius, G., McKeegan, K. D., and Harrison, T. M. (1996). Evidence for life on Earth before 3,800 million years ago. *Nature*, 384:55–59.

Mojzsis, S. J., Harrison, T. M., and Pidgeon, R. T. (2001). Oxygen-isotope evidence from ancient zircons for liquid water at the Earth's surface 4,300 Myr ago. *Nature*, 409:178–181.

Morbidelli, A., Bitsch, B., Crida, A., Gounelle, M., Guillot, T., Jacobson, S., Johansen, A., Lambrechts, M., and Lega, E. (2015). Fossilized condensation lines in the Solar System protoplanetary disk. *Icarus*, pages 1–31.

Moreira, M. (2013). Noble gas constraints on the origin and evolution of Earth's volatiles. *Geochemical Perspectives*, 2(2):229–403.

Moreira, M. and Charnoz, S. (2015). The origin of the neon isotopes in chondrites and on Earth. *Earth and Planetary Science Letters*, 433:1–8.

Mousis, O., Lunine, J. I., Picaud, S., and Cordier, D. (2010). Volatile inventories in clathrate hydrates formed in the primordial nebula. *Faraday Discuss.*, 147:509–525.

Mukhopadhyay, S. (2012). Early differentiation and volatile accretion recorded in deep-mantle neon and xenon. *Nature*, 486(7401):101–104.

Muscheler, R., Beer, J., Kubik, P. W., and Synal, H. A. (2005). Geomagnetic field intensity during the last 60,000 years based on 10Be and 36Cl from the Summit ice cores and 14C. *Quaternary Science Reviews*, 24(16-17):1849–1860.

Myers, J. S. (2001). Protoliths of the 3.8–3.7 Ga Isua greenstone belt, West Greenland. *Precambrian Research*, 105(2-4):129–141.

Notesco, G. (2003). Gas trapping in water ice at very low deposition rates and implications for comets. *Icarus*, 162:183–189.

Nutman, A. P. and Friend, C. R. L. (2009). New 1:20,000 scale geological maps, synthesis and history of investigation of the Isua supracrustal belt and adjacent orthogneisses, southern West Greenland: A glimpse of Eoarchaean crust formation and orogeny. *Precambrian Research*, 172(3-4):189–211.

Ohmoto, H., Watanabe, Y., Lasaga, A. C., Naraoka, H., Johnson, I., Brainard, J., and Chorney, A. (2014). Oxygen, iron, and sulfur geochemical cycles on early Earth: Paradigms and contradictions. *Geological Society of America Special Papers*, 504:55–95.

Ott, U. (2014). Planetary and pre-solar noble gases in meteorites. *Chemie der Erde - Geochemistry*, 74(4):519–544.

Ott, U., Mack, R., and Sherwood, C. (1981). Noble-gas-rich separates from the Allende meteorite. *Geochimica et Cosmochimica Acta*, 45(10):1751–1788.

Owen, T., Bar-Nun, A., and Kleinfeld, I. (1992). Possible cometary origin of heavy noble gases in the atmospheres of Venus, Earth and Mars. *Nature*, 358:43–46.

Owen, T., Biemann, K., Rushneck, D. R., Biller, J. E., Howarth, D. W., and Lafleur, A. L. (1977). The composition of the atmosphere at the surface of Mars. *Journal of Geophysical Research: Planets*, 82(28):4635–4639.

Ozima, M. and Podosek, F. A. (2002). *Noble Gas Geochemistry*. Cambridge University Press, Cambridge, second edition edition.

Page, R. W. (1988). Geochronology of early to middle Proterozoic fold belts in northern Australia: a review. *Precambrian Research*, 40-41:1–19.

Parai, R. and Mukhopadhyay, S. (2015). The evolution of MORB and plume mantle volatile budgets: Constraints from fission Xe isotopes in Southwest Indian Ridge basalts. *Geochemistry, Geophysics, Geosystems*, 16:1–17.

Patterson, C. (1956). Age of meteorites and the earth. *Geochimica et Cosmochimica Acta*, 10(4):230–237.

Pepin, R. O. (1991). On the origin and early evolution of terrestrial planet atmospheres and meteoritic volatiles. *Icarus*, 92(1):2–79.

Pepin, R. O. (1994). The hunt for U-Xenon. *Meteoritics*, 29:568–569.

Pepin, R. O. (1997). Evolution of Earth's Noble Gases: Consequences of Assuming Hydrodynamic Loss Driven by Giant Impact. *Icarus*, 126:148–156.

Pepin, R. O. (2013). Comment on "Chondritic-like xenon trapped in Archean rocks: A possible signature of the ancient atmosphere" by M. Pujol, B. Marty, R. Burgess [Earth Planet. Sci. Lett. 308 (2011) 298–306]. *Earth and Planetary Science Letters*, 371-372(C):294–295.

Pepin, R. O. and Porcelli, D. (2002). Origin of Noble Gases in the Terrestrial Planets. *Reviews in Mineralogy and Geochemistry*, 47(1):191–246.

Philippot, P., Van Kranendonk, M., van Zuilen, M., Lepot, K., Rividi, N., Teitler, Y., Thomazo, C., Blanc-Valleron, M.-M., Rouchy, J.-M., Grosch, E., and de Wit, M. (2009). Early traces of life investigations in drilling Archean hydrothermal and sedimentary rocks of the Pilbara Craton, Western Australia and Barberton Greenstone Belt, South Africa. *Comptes Rendus Palevol*, 8(7):649–663.

Pinti, D. L. (2005). The Origin and Evolution of the Oceans. In Gargaud, M., editor, *Lectures in Astrobiology*, pages 83–112. Berlin Heidelberg.

Porcelli, D. and Ballentine, C. J. (2002). Models for Distribution of Terrestrial Noble Gases and Evolution of the Atmosphere. *Reviews in Mineralogy and Geochemistry*, 47(1):411–480.

Pujol, M., Marty, B., and Burgess, R. (2011). Chondritic-like xenon trapped in Archean rocks: A possible signature of the ancient atmosphere. *Earth and Planetary Science Letters*, 308(3-4):298–306.

Pujol, M., Marty, B., and Burgess, R. (2013a). Reply to comment on "Chondritic-like xenon trapped in Archean rocks: A possible signature of the ancient atmosphere" by Pujol, M., Marty, B., Burgess, R., Earth and Planetary Science Letters 308 (2011) 298-306 by Pepin, R. O. *Earth and Planetary Science Letters*, 371-372:296–298.

Pujol, M., Marty, B., Burgess, R., Turner, G., and Philippot, P. (2013b). Argon isotopic composition of Archaean atmosphere probes early Earth geodynamics. *Nature*, 498(7452):87–90.

Pujol, M., Marty, B., Burnard, P., and Philippot, P. (2009). Xenon in Archean barite: Weak decay of 130Ba, mass-dependent isotopic fractionation and implication for barite formation. *Geochimica et Cosmochimica Acta*, 73(22):6834–6846.

Ragettli, R. A., Hebeda, E. H., Signer, P., and Wieler, R. (1994). Uranium-xenon chronology: precise determination of λsf$*$ 136Ysf for spontaneous fission of 238 U. *Earth and Planetary Science Letters*, 128(3):653–670.

Raquin, A. and Moreira, M. (2009). Atmospheric 38Ar/36Ar in the mantle: Implications for the nature of the terrestrial parent bodies. *Earth and Planetary Science Letters*, 287(3-4):551–558.

Reimold, W. U. and Koeberl, C. (2014). Impact structures in Africa: A review. *Journal of African Earth Sciences*, 93(C):57–175.

Reynolds, J. H. (1960). Determination of the age of the elements. *Phys. Rev. Letters*, 4:8–10.

Ribas, I., Guinan, E. F., Gudel, M., and Audard, M. (2005). Evolution of the Solar Activity over Time and Effects on Planetary Atmospheres. I. High-Energy Irradiances (1-1700 Å). *The Astrophysical Journal*, 622(1):680–694.

Rice, C. M., Ashcroft, W. A., Batten, D. J., Boyce, A. J., Caulfield, J. B. D., Fallick, A. E., Hole, M. J., Jones, E., Pearson, M. J., Rogers, G., Saxton, J. M., Stuart, F. M., Trewin, N. H., and Turner, G. (1995). A Devonian auriferous hot spring system, Rhynie, Scotland. *Journal of the Geological Society, London*, 152:229–250.

Robert, F. and Chaussidon, M. (2006). A palaeotemperature curve for the Precambrian oceans based on silicon isotopes in cherts. *Nature*, 443(7114):969–972.

Rose, N. M., Rosing, M. T., and Bridgwater, D. (1996). The origin of metacarbonate rocks in the Archaean Isua supracrustal belt, West Greenland. *American Journal of Science*, 296(9):1004–1044.

Rosing, M. T., Rose, N. M., Bridgwater, D., and Thomsen, H. S. (1996). Earliest part of Earth's stratigraphic record: A reappraisal of the >3.7 Ga Isua (Greenland) supracrustal sequence. *Geology*, 24(1):43–46.

Sagan, C. and Chyba, C. (1997). The early faint sun paradox: organic shielding of ultraviolet-labile greenhouse gases. *Science*, 276(5316):1217–1221.

Sanloup, C., Schmidt, B. C., Perez, E., Jambon, A., Gregoryanz, E., and Mezouar, M. (2005). Retention of xenon in quartz and Earth's missing xenon. *Science*, 310:1174–1177.

Schatz, G. (1986). The s-process of stellar nucleosynthesis. *Progress in Particle and Nuclear Physics*, 17:393–417.

Schlichting, H. E., Sari, R., and Yalinewich, A. (2015). Atmospheric mass loss during planet formation: The importance of planetesimal impacts. *Icarus*, 247(C):81–94.

Shaw, G. H. (2014). Evidence and arguments for methane and ammonia in Earth's earliest atmosphere and an organic compound–rich early ocean. *Geological Society of America Special Papers*, 504:1–10.

Shcheka, S. S. and Keppler, H. (2012). The origin of the terrestrial noble-gas signature. *Nature*, 490(7421):531–534.

Smart, K. A., Tappe, S., Stern, R. A., Webb, S. J., and Ashwal, L. D. (2016). Early Archaean tectonics and mantle redox recorded in Witwatersrand diamonds. *Nature Geoscience*, pages 1–6.

Srinivasan, B. (1976). Barites: anomalous xenon from spallation and neutron-induced reactions. *Earth and Planetary Science Letters*, 31(1):129–141.

Staudacher, T. and Allegre, C. J. (1982). Terrestrial xenology. *Earth and Planetary Science Letters*, 60(3):389–406.

Strutz, T. (2010). *Data fitting and uncertainty.* A practical introduction to weighted least squares and beyond. Springer Fachmedien Wiesbaden GmbH 2011, Wiesbaden.

Swindle, T. D. (2002). Martian Noble Gases. *Reviews in Mineralogy and Geochemistry*, 47(1):171–190.

Swindle, T. D., Caffee, M. W., and Hohenberg, C. M. (1986). Xenon and other noble gases in shergottites. *Geochimica et Cosmochimica*, 50(6):1001–1015.

Takaoka, N. (1972). An interpretation of general anomalies of xenon and the isotopic composition of primitive xenon. *Mass Spectrometry*, 20(4):287–302.

Tarduno, J. A., Blackman, E. G., and Mamajek, E. E. (2014). Detecting the oldest geodynamo and attendant shielding from the solar wind: Implications for habitability. *Physics of the Earth and Planetary Interiors*, 233(C):68–87.

Thorne, A. M. and Trendall, A. F. (2001). Geology of the Fortescue Group, Pilbara Craton, Western Australia. Geological Survey of Western Australia, Perth.

Tice, M. M., Bostick, B. C., and Lowe, D. R. (2004). Thermal history of the 3.5–3.2 Ga Onverwacht and Fig Tree Groups, Barberton greenstone belt, South Africa, inferred by Raman microspectroscopy of carbonaceous material. *Geology*, 32(1):37.

Tolstikhin, I. N. and O'Nions, R. K. (1994). The Earth's missing xenon: A combination of early degassing and of rare gas loss from the atmosphere. *Chemical Geology*, 115(1):1–6.

Touboul, M., Puchtel, I. S., and Walker, R. J. (2012). 182W Evidence for Long-Term Preservation of Early Mantle Differentiation Products. *Science*, 335(6072):1065–1069.

Toulkeridis, T., Clauer, N., Kröner, A., and Todt, W. (2015). A Mineralogical, Chemical and Isotopic Investigation of Shales from the Barberton Greenstone Belt, South Africa, To Constrain Source Materials and Post-Deposition Evolution. *South African Journal of Geology*, 118(4):389–410.

Touret, J. (2001). Fluids in metamorphic rocks. *Lithos*, 55:1–25.

Treiman, A. H., Gleason, J. D., and Bogard, D. D. (2000). The SNC meteorites are from Mars. *Planetary and Space Science*, 48(12-14):1213–1230.

Trendall, A. F., Compston, W., Nelson, D. R., De Laeter, J. R., and Bennett, V. C. (2004). SHRIMP zircon ages constraining the depositional chronology of the Hamersley Group, Western Australia. *Australian Journal of Earth Sciences*, 51(5):621–644.

Turner, G. and Bannon, M. P. (1992). Argon isotope geochemistry of inclusion fluids from granite-associated mineral veins in southwest and northeast England. *Geochimica et Cosmochimica Acta*, 56(1):227–243.

Ulrich, R. K. (1975). Solar neutrinos and variations in the solar luminosity. *Science*, 190(4215):619–624.

Valbracht, P. J., Staudacher, T., and Malahoff, A. (1997). Noble gas systematics of deep rift zone glasses from Loihi Seamount, Hawaii. *Earth and Planetary Science Letters*, 150(3-4):399–411.

Verchovsky, A. B., Pearson, V. K., and Fisenko, A. V. (2012). Separation of Q from carbon in CR meteorites during stepped combustion. In *Proceedings of the 43rd Lunar and Planetary Science Conference*, The Woodlands, TX, US.

Vogel, N., Leya, I., Bischoff, A., Baur, H., and Wieler, R. (2004). Noble gases in chondrules and associated metal-sulfide-rich samples: Clues on chondrule formation and the behavior of noble gas carrier phases. *Meteoritics & Planetary Science*, 39(1):117–135.

Walsh, K. J., Morbidelli, A., Raymond, S. N., O'Brien, D. P., and Mandell, A. M. (2011). A low mass for Mars from Jupiter's early gas-driven migration. *Nature*, 475(7355):206–209.

White, W. M. (2015). Isotopes, DUPAL, LLSVPs, and Anekantavada. *Chemical Geology*, 419(C):10–28.

Wieler, R. (2002). Noble Gases in the Solar System. *Reviews in Mineralogy and Geochemistry*, 47(1):21–70.

Wieler, R. (2014). Noble Gas Mass Spectrometry. In *Treatise on Geochemistry (Second Edition)*, pages 355–373. Elsevier, Oxford.

Wiens, R. C., Becker, R. H., and Pepin, R. O. (1986). The case for a Martian origin of the shergottites, II. Trapped and indigenous gas components in EETA 79001 glass. *Earth and Planetary Science Letters*, 77(2):149–158.

Wong, M. H., Atreya, S. K., Mahaffy, P. N., Franz, H. B., Malespin, C., Trainer, M. G., Stern, J. C., Conrad, P. G., Manning, H. L. K., Pepin, R. O., Becker, R. H., McKay, C. P., Owen, T. C., Navarro-González, R., Jones, J. H., Jakosky, B. M., and Steele, A. (2013). Isotopes of nitrogen on Mars: Atmospheric measurements by Curiosity's mass spectrometer. *Geophysical Research Letters*, 40(23):6033–6037.

Yokochi, R. and Marty, B. (2004). A determination of the neon isotopic composition of the deep mantle. *Earth and Planetary Science Letters*, 225(1-2):77–88.

Zahnle, K. J. (2015). Xenon fractionation and Archean hydrogen escape. In *46th Lunar and Planetary Science Conference*, pages 1–2, The Woodlands (Texas).

Zahnle, K. J., Catling, D. C., and Claire, M. W. (2013). The rise of oxygen and the hydrogen hourglass. *Chemical Geology*, 362(C):26–34.

Zahnle, K. J., Kasting, J. F., and Pollack, J. B. (1988). Evolution of a steam atmosphere during Earth's accretion. *Icarus*, 74(1):62–97.

Zhu, L., Liu, H., Pickard, C. J., Zou, G., and Ma, Y. (2014). Reactions of xenon with iron and nickel are predicted in the Earth's inner core. *Nature Chemistry*, 6(7):644–648.

Zimmermann, L. (2014). Méthode d'extraction des gaz rares sous ultravide. *Techniques de l'ingénieur*, J6632:1–21.

Zimmermann, L., Burnard, P., Marty, B., and Gaboriaud, F. (2009). Laser Ablation (193 nm), Purification and Determination of Very Low Concentrations of Solar Wind Nitrogen Implanted in Targets from the GENESIS Spacecraft. *Geostandards and Geoanalytical Research*, 33(2):183–194.

Zimmermann, L., Füri, E., and Burnard, P. (2015). Purification des gaz rares sous ultravide - Méthodes de purification. *Techniques de l'ingénieur*, (J6635):1–23.

Origine et évolution du xénon et des autres gaz rares atmosphériques: implications géodynamiques et atmosphériques

L'origine de l'atmosphère terrestre demeure énigmatique. De plus, de nombreux évènements tels que les contributions de matière extraterrestre, le dégazage de la Terre solide ou encore les fuites de l'atmosphère vers l'espace ont modifié la composition de l'atmosphère au cours du temps. Ces travaux de thèse visaient à analyser précisément la composition de l'atmosphère ancienne piégée dans des roches âgées de plusieurs milliards d'années afin de mieux contraindre son origine et son évolution. L'analyse des isotopes du xénon, un gaz rare, démontre qu'une fraction de l'atmosphère terrestre ne peut avoir été apportée par les météorites mais plutôt par des corps riches en eau et en éléments volatils tels que les comètes. De plus, la composition isotopique de l'atmosphère a évolué au cours du temps jusqu'à il y a deux milliards d'années environ. Cette évolution du fractionnement est peut-être concomitante à celle l'oxygénation progressive de l'atmosphère qui a permis le développement de la vie telle que nous la connaissons aujourd'hui.

mots-clés : atmosphère, gaz rares, xénon, géodynamique

Origin and evolution of atmospheric xenon and other noble gases: geodynamical and atmospheric implications

The origin of the Earth's atmosphere remains poorly understood. Its elemental and isotopic compositions have been shaped by numerous events in the history of our planet, such as extraterrestrial contributions, mantle degassing, atmospheric escape etc. This study aimed to analyze the composition of atmospheric gases trapped in several billion years old samples in order to better understand the origin and evolution of the Earth's atmosphere. Isotope analyses of xenon, a noble gas, demonstrate that part of the atmosphere was not brought by meteorites but might have been delivered to the Earth's atmosphere by volatile-rich bodies such as comets. Furthermore, the isotopic composition of atmospheric Xe evolved over geological ages and can be linked to the progressive oxidation of the atmosphere that permitted the emergence and development of modern forms of life.

keywords : atmosphere, noble gases, xenon, geodynamics